

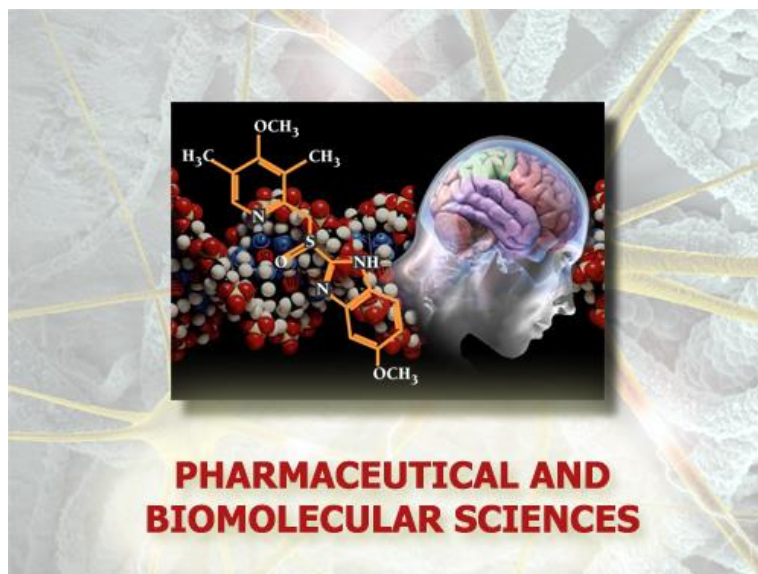
Università degli Studi di Torino



Scuola di Dottorato in
Scienze della Natura e Tecnologie Innovative

Dottorato in Scienze Farmaceutiche e Biomolecolari

CICLO: XXXII



COMBINING ULTRASOUND AND MICROWAVES IN CHEMICAL PROCESSES

Candidata: María Jesús Morán Plata

Tutor: Prof. Katia Martina

Handwritten signature of María Jesús Morán Plata.

Handwritten signature of Prof. Katia Martina.

Università degli Studi di Torino



**Dottorato in
Scienze Farmaceutiche e Biomolecolari**

Tesi svolta presso il Dipartimento di Scienza e Tecnologia del Farmaco

CICLO: XXXII

TITOLO DELLA TESI: COMBINING ULTRASOUND AND MICROWAVES IN CHEMICAL PROCESSES

TESI PRESENTATA DA: María Jesús Morán Plata

TUTOR: Prof. Katia Martina

COORDINATORE DEL DOTTORATO: Prof. Gianmario Martra

ANNO ACCADEMICO: 2016-2019

SETTORE SCIENTIFICO-DISCIPLINARE DI AFFERENZA: Chimica Organica (06/C1)



This project has received funding from the European Union's Horizon 2020 research and innovation programme under the Marie Skłodowska-Curie grant agreement No 721290. This publication reflects only the author's view, exempting the Community from any liability. Project website: <http://cosmic-etn.eu/>

Index

Preface. COSMIC Project	1
Chapter 1: Introduction	5
1.1 Green chemistry.....	7
1.2 Reduction reactions.....	8
1.2.1 Hydrogen transfer (HT)	11
1.2.2 Hydrogen borrowing (HB). Glycerol as hydrogen source	12
1.2.3 Nitroarenes	16
1.2.4 Alkynes.....	21
1.3 Copper catalysis	24
1.3.1 Nanoparticles	25
1.3.2 Copper catalysis in reduction reactions.....	27
1.4 Enabling technologies in heterogeneous catalysis.....	31
1.4.1 Microwave irradiation.	31
1.4.1.1 Technique	31
1.4.1.2 Microwave in heterogeneous catalysis	36
1.4.2 Ultrasound irradiation	37
1.4.2.1 Technique	37
1.4.2.2 Ultrasound in heterogeneous catalysis	40
1.4.3 Combined microwave and ultrasound irradiation. Synergic effects.	41
1.4.3.1 Technique	41
1.4.3.2 Combined MW and US in heterogeneous catalysis	42
1.4.4 Mechanochemistry.....	43
1.4.4.1 Technique	43
1.4.4.2 Mechanochemistry in heterogeneous catalysis	45
1.4.5 Ultrasonic and microwave-assisted synthesis of metal nanoparticles	46
Chapter 2: Non-conventional energy sources for nitro compounds and alkynes reduction	49
2.1 Introduction	51
2.2 Mechanochemical reduction of nitroarenes and alkyl/aryl azides without catalyst addition	51
2.3 Copper catalysed reduction of aromatic nitrocompounds. Glycerol: an optimal hydrogen source.....	61
2.4 MW-assisted copper-catalysed transfer hydrogenation reduction of nitrobenzene. Industrial MW-assisted scale-up.	72

2.5 A simple set up for transfer hydrogenation in flow chemistry. Reduction of nitrobenzene over copper supported catalyst (Cu/Celite).	80
2.5 Cu-catalysed TH of nitroarenes to amino or azo derivative <i>via</i> controllable transfer hydrogenation sources.....	93
2.6 Copper catalysed selective semihydrogenation of alkynes to cis alkenes	103
2.7 Conclusion	112
Chapter 3: Sonochemically-promoted preparation of Cu-β-CD grafted silica	115
3.1 Introduction	117
3.2 Organic-Inorganic hybrid material and its application in click chemistry	118
3.2.1 Synthesis of copper supported on Si-NH-CD and Si-DETA-CD	118
3.2.2. Characterisation of copper supported on Si-NH-CD and Si-DETA-CD	124
3.2.3. Test of catalytic activity of copper supported systems	126
3.3 Conclusion	130
Chapter 4: Experimental details	131
4.1 Non-conventional, non-contact energy sources for nitroarenes and alkynes reduction. ...	133
4.1.1 Mechanochemical reduction of nitroarenes and alkyl/aryl azides without catalyst addition.....	133
4.1.1.1 Materials and methods.....	133
4.1.1.2 General procedures	133
4.1.2 Copper catalysed reduction of aromatic nitrocompounds. Glycerol: an optimal hydrogen source	134
4.1.2.1 Materials and methods.....	134
4.1.2.2 General procedures	134
4.1.3 MW-assisted copper-catalysed transfer hydrogenation reduction of nitrobenzene. Industrial MW-assisted scale-up.....	136
4.1.3.1 Materials and methods.....	136
4.1.3.2 General procedures	136
4.1.4 A simple set up for transfer hydrogenation in flow chemistry. Reduction of nitrobenzene over copper supported catalyst (Cu/Celite).....	138
4.1.4.1 Materials and methods.....	138
4.1.4.2 General procedures	138
4.1.4 Cu-catalysed TH of nitroarenes to amino or azo derivative <i>via</i> controllable transfer hydrogenation sources.....	140
4.1.4.1 Material and methods	140
4.1.4.2 General procedures	140
4.1.5 Copper catalysed selective semihydrogenation of alkynes to cis alkenes	142
4.1.5.1 Materiall and methods	142

4.1.5.2 General procedures	142
4.2 Sonochemically-promoted preparation of Cu- β -CD grafted silica	143
4.2.1 Material and methods	143
4.2.2 General procedures	144
Supporting information	SI-1
S-1. NMR Amino-derivatives	SI-3
S-2. NMR Alkyl amines derivatives	SI-25
S-3. NMR Azo-derivatives	SI-35
S-4. NMR alkynes-derivatives	SI-45
S-5. NMR (Z)-alkenes-derivatives	SI-52
Appendix: Achievements	A-1
Papers	A-1
Conferences Communications	A-1
Secondments	A-2
Acknowledgement	A-5
Bibliography	B-1

Preface. COSMIC Project.

The PhD Thesis herein described has been funded with a Marie Skłodowska-Curie Actions (MSCAs) award. It has been elaborated as outcome of one of the fifteen individual projects belonging to the MSCA EU-H2020 COSMIC, the European Training Network (ETN) (Grant Agreement No 721290) for Continuous Sonication and Microwave Reactors.

MSCA is currently financed through the eighth Framework Programme for Research and Technological Development, the so-called Horizon 2020. This programme is the biggest EU Research and Innovation programme ever with nearly €80 billion of funding available over 7 years (2014 to 2020) – in addition to the private investment that this money attracts. In this way, Horizon 2020 promises more breakthroughs, discoveries and world-firsts by taking great ideas from the lab to the market.

The Marie Skłodowska-Curie actions were established in 1996 by the European Commission as tools to fund research in the European Research Area (ERA) and provide grants for all stages of researchers' careers; encouraging transnational, intersectoral and interdisciplinary mobility. In this way, through MSCAs, universities, companies as well as academic and non-academic research centres can host talented foreign researchers and create strategic partnerships and networking with leading institutions all over the world. These actions are open to all areas of research and novelty, from fundamental research to market take-up and innovation services, responding to actual challenges that are chosen freely by the applicants (individuals and/or organisations) in a fully 'bottom-up' manner. Since 1996, more than 100,000 researchers have been awarded with a MSCAs fellowship.

Currently, the conventional technologies in the chemical process industry - and in particular the fine chemicals and pharmaceuticals industries - tend to be batch-type, combined with mechanical mixing and conduction-based heat transfer, inherently leading to poor process control. Thus, COSMIC Project, a four years project started in October 2016, is a key instrument for supporting and training these sectors in their transition from batch to continuous production.

The European share of the global chemical market has halved during the period 1996 to 2013 (from ~31% in 1996 to ~17 % in 2013) and, as a result, the number of EU citizens directly employed by this sector has also dramatically fallen (from 1.6 million in 1996 to 1.2 million in 2013). A key root cause of this decline has been the advent of lower-labour-cost markets in the emerging global economies, and as this labour-cost differential is unlikely to be redressed in the near future, one of the key strategies for halting this decline and subsequently re-establishing European growth is to develop competitive technologies that deliver performance – in terms of resource efficiency and product quality – beyond that of Europe's rivals, in particular those new industries in Asia and the Near East. In order to design and operate these new technologies, new competencies and different skills from scientists and engineers are required. The introduction of revolutionary technologies can indeed only succeed if sufficient professionals trained in these novel technologies are available on the market. Innovative milli-reaction technology – central to COSMIC's activities – offers the potential to address all these issues.

In this context, COSMIC trains 15 ESRs (Early Stage Researchers) in the transition from chemical reactions with poor resource – both material and energy – efficiency and poor

product quality to processes with high resource efficiency and excellent product properties. The training of 15 ESRs – through responsible research and innovation – leads to further understanding of the knowledge gaps described earlier, disseminates the potential of flow processes actuated by alternative energy sources for the chemical industry and transfers developed technologies into real applications via the involved industrial participants (both technology suppliers and end-users). COSMIC’s vision is that of intensified processes, where continuous technologies use alternative energy sources to achieve the localized ultrasound and microwave actuation of multiphase and milliflow reactors for the purpose of high-value product synthesis. COSMIC focuses on the synthesis of organic molecules and nanoparticles for use in organic syntheses, catalyst preparation and health applications, all of which are important domains in the fine-chemicals and pharmaceuticals industries today and into the future (Figure 1).

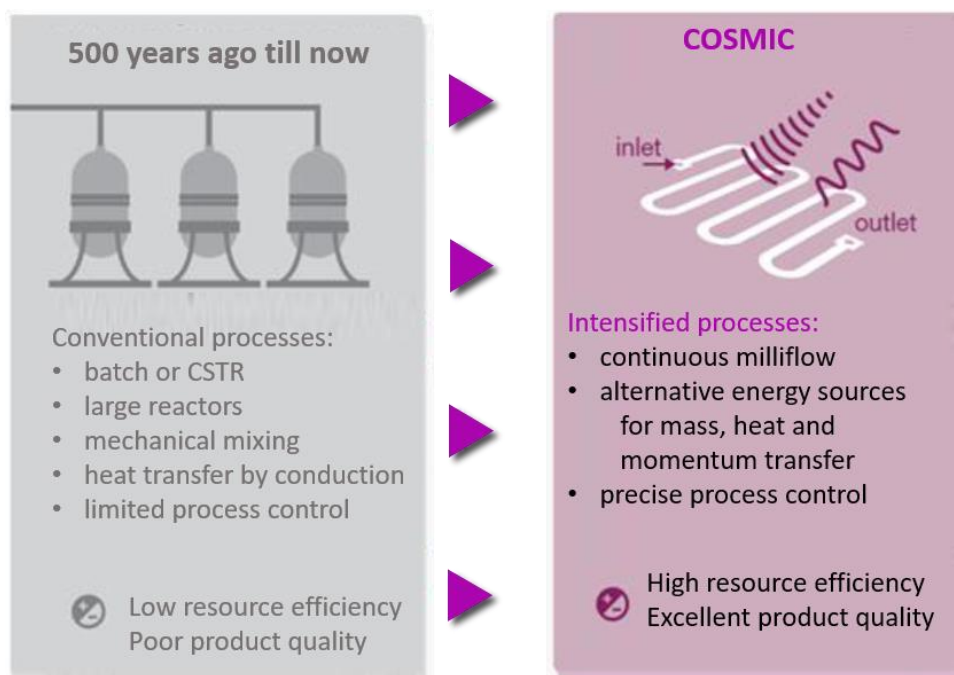


Figure 1: COSMIC's foreseen transition for chemical processes.

In particular, the main goals of my PhD research inside COSMIC project were:

- ❖ Optimization of heat and mass transfer as well as catalytic effects for selected reactions by a combination of ultrasound and microwaves.
- ❖ Development of sequential and integrated configurations for the hybrid reactor.
- ❖ To carry out reactions in the hybrid reactor.

Based on these premises, the research conducted during my PhD and described in this thesis concerns the development of new environmentally friendly, efficient and atom-economic synthetic methodologies for precious target molecules. Clean energy sources such as microwave and ultrasound irradiations have been crucial tools to successfully pursue those goals.

The actual environmental concern and the desire of facing the current planetary emergency has opened a door for an extensive number of green research procedures¹. Conventional protocols are replaced with new efficient processes where safer chemicals,

solvent free conditions, natural abundant solvents, atom economy and alternative energy sources are used to achieve sustainability and scalability. Aiming to develop selective catalysts that are able to suppress the undesired noble metals such as Pd and Pt, copper (Cu) as heterogeneous catalyst can be considered a “perfect” candidate for being inexpensive, readily available and easily handled. Herein, by applying transfer hydrogenation strategy, Cu catalyst has been successfully employed in presence of different alcohols as “sacrificial” hydrogen sources, for the synthesis of important target and industrially valuable molecules.

Being part of important building blocks in organic synthesis, the selective reduction of aromatic nitrocompounds represents a fundamental procedure in organic synthesis and many synthetic routes have been described *via* the catalytic hydrogenation. Herein, we report a mechanochemical reduction of aromatic nitro compounds in a stainless steel jar with formate salts without catalyst addition.² Moreover, a new efficient and hydride free Cu-catalysed procedure for the selective reduction of nitroarenes to anilines and azocompounds has also been developed, using glycerol and ethanolamine as excellent hydrogen sources. In this way, the reaction can be preferably selective to different reduction products when changing the hydrogen donor. US has been shown to play an important role in the process *via* its ability to enhance copper nanoparticles (CuNPs) dispersion, favouring mechanical depassivation and increasing catalytic active surface area; while MW irradiation shortened the reaction time from some hours to a few minutes. In addition, since recovery and reuse of catalysts is an important factor for sustainable process management, heterogeneous copper supported catalysts has been deeply studied and analyzed. Copper nanoparticles supported over celite proved to be an ideal material for the transfer hydrogenation reaction of nitrobenzene in continuous flow. In the same manner, a new hybrid organic-inorganic material based on copper catalyst on an efficient grafting of β -CD onto the inorganic silica surface has showed to behave as an excellent catalyst in the Cu(II)-catalysed alkyne azide reactions in absence of a reducing agent.

Moreover, following the same transfer hydrogenation strategy, in presence of ethylen glycol as efficient and eco-base hydrogen source, a wide range of aliphatic and aromatic alkynes has been selectively reduced to Z-alkynes, what constitute an important step in the synthesis of natural products.

Chapter 1: Introduction

1.1 Green chemistry

The ideology of Green Chemistry^{3,4} calls for the development of new reaction conditions that can potentially provide benefits for chemical synthesis in terms of efficiency, selectivity, operational simplicity, health and environmental safety. In this context, the aim of Green Chemistry is the design of safer chemicals and processes in order to reduce or, if possible, eliminate hazards across all the life-cycle stages and limit the risk of accident and damage.

Going beyond research, this concept of Green Chemistry has touched industry, education, environment and public. This new field has demonstrated how next generation products and processes can be profitable and, at the same time, be good for human health and the environment.

The concept of Green and Sustainable Chemistry was first formulated at the beginning of the 1990s, nearly 30 years ago, and in 1998, Anastas⁵ and Warner defined a list of Twelve Principles (Table 1) outlining an early conception of what would make a greener chemical, process or product.

Table 1. The Twelve Principles of Green Chemistry³

1. Prevention	It is better to prevent waste, than to treat it or clean up after it has been created
2. Atom Economy	Synthetic methods should be designed to maximize the incorporation of all materials used in the process into the final product
3. Less Hazardous Chemical Syntheses	Wherever practicable, synthetic methods should be designed to use and generate substances that possess little or no toxicity to human health and the environment
4. Designing Safer Chemicals:	Chemical products should be tailored ad-hoc to affect their desired function while minimizing toxicity
5. Safer Solvents and Auxiliaries:	The use of auxiliary substances (e.g. solvents, separation agents, etc.) should be made unnecessary wherever possible and innocuous when used
6. Design for Energy Efficiency:	Energy requirements of chemical processes should be recognized for their environmental and economic impacts and should be minimized. If possible, synthetic methods should be conducted at room temperature and pressure

7. Use of Renewable Feedstocks	Raw material or feedstock should be renewable rather than depleting whenever technically and economically practicable
8. Reduce Derivatives	Unnecessary derivatization (use of blocking groups, protection/deprotection, temporary modification of physical/chemical processes) should be minimized or avoided if possible, because such steps require additional reagents and can generate waste
9. Catalysis	Catalytic reagents (as selective as possible) are superior to stoichiometric reagents
10. Design for Degradation	Chemical products should be designed so that at the end of their function they break down into innocuous degradation products and do not persist in the environment
11. Real-time analysis for Pollution Prevention	Analytical methodologies need to be further developed to allow for real-time, in-process monitoring and control prior to the formation of hazardous substances
12. Inherently Safer Chemistry for Accident Prevention	Substances used in a chemical process should be chosen to minimize the potential for chemical accidents, including releases, explosions, and fires

1.2 Reduction reactions

Redox reactions are a vital class of chemical reactions confronted in daily processes and taking place all around us. In general chemistry, reduction reactions refers to processes in which a compound or atom is reduced by gaining electrons, while when losing electrons it is called oxidation. These two processes occur always in pairs: if one species is oxidized, another must be reduced at the same time - thus the term 'redox reaction'.

In organic chemistry, redox reactions look a bit different (Figure 2). When a carbon atom gains a bond to hydrogen and loses a bond to a heteroatom (or to another carbon atom), it is considered to be a reduction process because hydrogen, of all the elements, is the least electronegative. Thus, in the process, the carbon atom undergoes an overall gain of electron density; and gains of electrons is reduction.

Conversely, when a carbon atom in an organic compound loses a bond to hydrogen and gains a bond to a heteroatom (or to another carbon atom), we say that the compound has been oxidised.

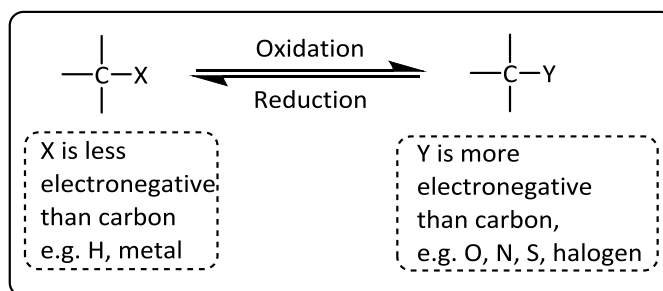


Figure 2: Redox transformations in organic compounds

In 2009, W. Hoffmann et al.⁶ published a review in which highlighted the importance of pursuing redox economy when performing organic synthesis. The economics of synthesis planning and analysis can be simultaneously examined from the vantage point of atom, step, and redox manipulations.

- In atom economy, the aim is to minimize wasteful steps and encourage the use of catalysis to efficiently generate molecular frameworks. It is refer to the conversion efficiency of a chemical process in terms of all atoms involved and the desired products produced.
- In step economy, a more “macroscopic” view of the entire synthesis is considered and a general reduction in the number of steps is encouraged with powerful reactions and strategies that build up complexity as rapidly as possible.

In redox economic synthesis (

- *Figure 3*), the goals are to minimize unnecessary non-strategic redox manipulations within a synthesis. When the oxidation state of intermediates changes, it should do so in a linear (or exponential) fashion and steadily increase or decrease throughout the course of the synthesis without overshooting the goal and requiring an extra redox step.

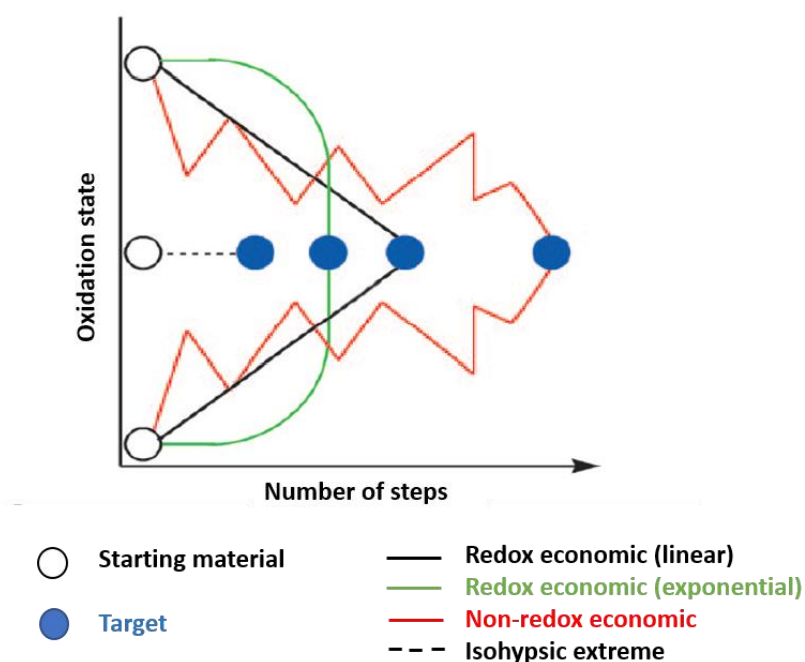


Figure 3: A schematic view of redox economy in a synthetic sequence inspired by Evans' lectures on the topic.

The benefit of applying the concepts of redox economy is to streamline syntheses of complex target molecules to an optimal point, approaching the ideal synthesis as defined by Hendrickson already in 1975.⁷ “The ideal synthesis creates a complex skeleton in a sequence only of successive construction reactions involving no intermediary refunctionalizations, and leading directly to the structure of the target, not only its skeleton but also its correctly placed functionality”.

Synthetic organic chemists have a wide range of reagents at their disposal for the reduction or oxidation of functional groups in organic compounds. The reagent must be chosen carefully for any given transformation, in order to ensure that only the desired functional group or groups are affected.

In particular, the reduction of organic compounds is one of the most common reaction types in chemical organic synthesis today. The development in this field has been tremendous, progressing from the use of stoichiometric reagents to the modern reactions that use cheaper and “more sustainable” catalytic methods.

A wide range of reducing agents have been used for this catalytic transformation. Three of the most common one are sodium borohydride (NaBH_4), lithium aluminum hydride (LiAlH_4), and diisobutyl aluminum hydride (DIBAH) (Figure 4).

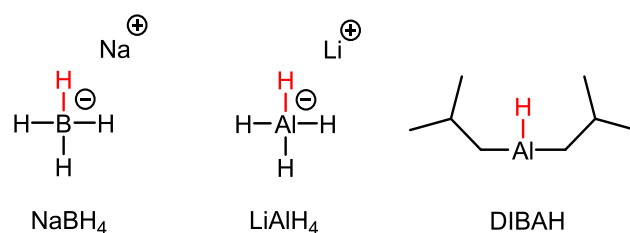


Figure 4: Common reducing agents.

Hydrogenation, being one of the most fundamental transformations in organic synthesis, is present in lot of different industrial applications, moving from fine chemicals to pharmaceuticals synthesis. Two different strategies can be employed for this transformation: direct hydrogenation with a pressure of H_2 gas and transfer hydrogenation (TH).

Being the most atom- and cost-efficient reagent used for green reduction reactions, inexpensive and, therefore, so suitable at big scale; industrial reduction processes are conducted using molecular hydrogen (H_2). However, the handling of this gaseous molecule has some shortcomings:

a) Hydrogen is typically stored and transported in pressurized cylinders compromising the desired simplicity.

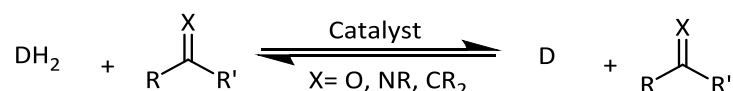
b) Due to the low solubility of this gas in common laboratory solvents, it will always result in two-phase systems.

Therefore, the use of hydrogen gas for industrial application is undesirable and large price tag equipment are required. For this reason, during the last years, the desire of facing this problem has awoken a great interest in developing attractive and “greener” alternatives for this method.

1.2.1 Hydrogen transfer (HT)

Aiming to overcome the problems listed above when working with H₂ gas, transfer hydrogenation reactions has been embraced as a great alternative. These reactions have gained much attention during the last decades due to the ideal conditions achieved in terms of catalytic activity, selectivity and high atom economy.

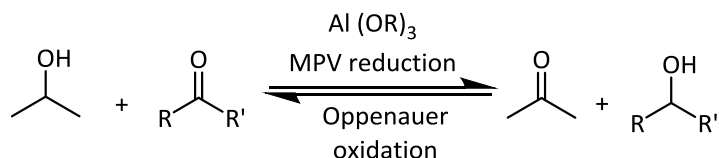
The concept of hydrogen transfer refers to a process where a hydrogen molecule is added onto a multiple bond, using a different hydrogen source than gaseous H₂, in the presence of a catalyst.⁸ The catalyst transfers a hydride and a proton from an organic substrate behaving as a hydrogen donor (DH₂) to an unsaturated substrate that acts as hydrogen acceptor (Scheme 1). In this way, a convenient and powerful method to access various hydrogenated compounds is performed.



Scheme 1: Hydrogen transfer from a donor molecule (DH₂) to an unsaturated functional group (acceptor).

The increasing success of this technique arises from its operational simplicity: no hydrogen pressure is used, no special equipments are required, the major side products can be recycled and both the hydrogen donors and catalysts are usually readily available, inexpensive, and easy to handle. Thanks to their low toxicity and low cost, the most frequently used hydrogen donors are 2-propanol, formic acid and formate salts. Acetone is formed as by-product when 2-propanol is used, while gaseous CO₂ leaves the reaction mixture when formic acid or its salts are employed. Suitable hydrogen acceptors (H-acceptors) are ketones, α,β-unsaturated carbonyl compounds, α,β-unsaturated acids and esters, imines and nitro-compounds.

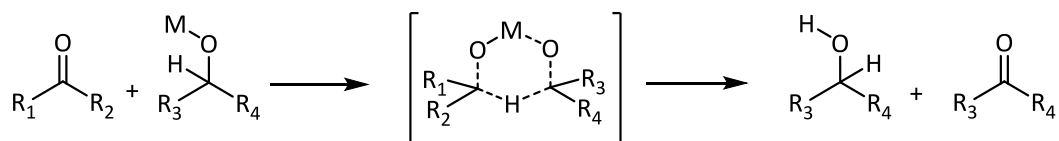
The first transfer hydrogenation reaction comes from Knoevenagel (1903) and from Wieland (1912), who saw dihydroarene disproportionation to give arene and tetrahydroarene with a heterogeneous Pd catalyst at elevated temperature. Two decades later, in the mid-1920s, Meerwein and Schmidt, Ponndorf and Verley (VPM)⁹ (Scheme 2) reported the earliest examples of transfer hydrogenation reactions with carbonyl compounds. In the original version of this reduction, stoichiometric amount of aluminium isopropoxide was used to promote hydrogen transfer from 2-propanol to aldehydes and ketones, giving the corresponding primary and secondary alcohols. Over a decade later, Oppenauer reported the reverse reaction, where alcohols were oxidised to aldehydes and ketones by aluminium *tert*-butoxide, using acetone as the hydrogen acceptor.



Scheme 2: MPV reduction and Oppenauer oxidation

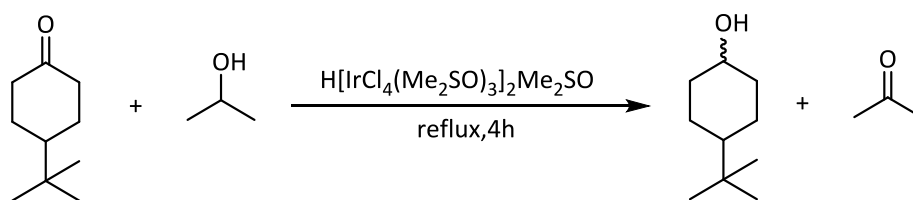
In this homogeneous VPM reduction, a direct TH through the formation of a cyclic six-membered transition state in which both the reducing alcohol and the carbonyl are coordinated to the same metal centre was proposed to take place, and the reversibility of the catalytic cycle of the MPV reduction was exploited (Scheme 3). In this way, transfer hydrogenation–dehydrogenation reaction, in which hydrogen is transferred from an alcohol

to an unsaturated bond, is an environmentally benign method for reducing unsaturated compounds or oxidizing alcohols.



Scheme 3: TH in the MPV reduction via cyclic transition state.

This one-pot oxidation-reaction-reduction synthesis has been further developed during the last past decades, traditionally employing precious transition metal catalysts (such as Ru, Rh, Ir or Os) in homogeneous catalysis. In the 1960s, Henbest¹⁰ reported the first example of a transition metal-catalysed hydrogen transfer using an iridium hydride DMSO complex as a catalyst (Scheme 4). In 1975, Sasson¹¹ reported the first ruthenium-catalysed hydrogen transfer reaction using $\text{RuCl}_2(\text{PPh}_3)_3$.



Scheme 4: First example of a transition metal-catalysed hydrogen transfer

Some years later, in 1991, Bäckvall *et al.*¹² described the effect of NaOH on the $[\text{RuCl}_2(\text{PPh}_3)_3]$ -catalysed transfer hydrogenation. While in the presence of 2.4 mol% of base, the Ru complex (0.1 mol%) catalyses efficient transfer hydrogenation from *iso*-propanol to both aliphatic and aromatic ketones with rates up to 900 turnovers per hour (T: 82 °C); in the absence of NaOH no hydrogenation occurs. Later Bäckvall *et al.*¹² showed that the increased reactivity is due to the formation of a highly active dihydride species, $[\text{RuH}_2(\text{PPh}_3)_3]$.

Significant breakthroughs and developments of TH have been achieved in the past few years. This great progress was witnessed in several aspects of the published studies, such as exploration of catalyst diversity, design of more efficient ligands or stabilizers to improve precious metal catalysts, use of abundant biometal catalysts involving Fe, Co, and Ni, development of recyclable catalysts and exploration of “green” hydrogen donors. Notably, in 2015, Sadler’s group¹³ disclosed TH catalysis in cell in the presence of Noyori-type ruthenium complexes using nontoxic concentrations of formate as a hydride donor, a new anticancer strategy.

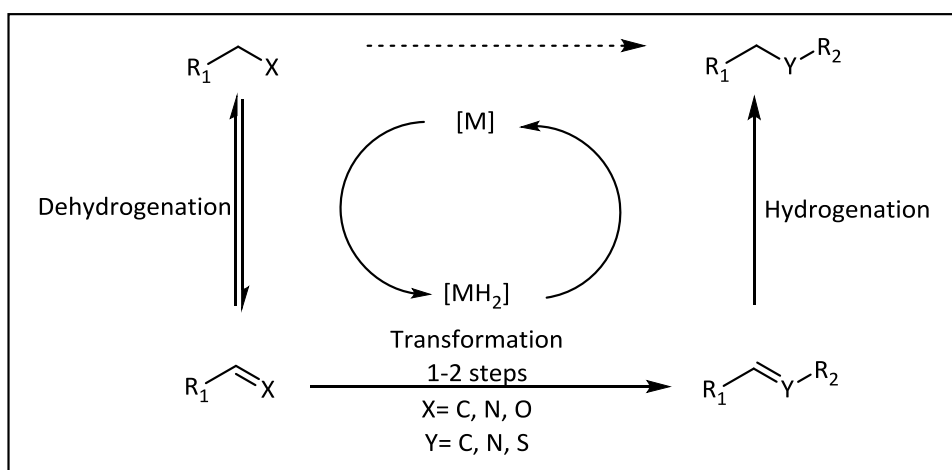
Although remarkable progress in TH reductions has been made, many unsolved problems and challenges remain in many reported results. For instance, most of the known catalytic reactions with abundant metal catalysts are either limited in scope or do not qualify for practical applications. Further work is also required to seek artificial enzymes for the extremely efficient catalytic TH, to use the TH process in convenient cascade reaction by combination with other transformations, and to push these catalysts, especially supported heterogeneous catalysts, to their use in multikilogram scale synthesis toward industrial production.

1.2.2 Hydrogen borrowing (HB). Glycerol as hydrogen source

Combining the advantages of transfer hydrogenation with additional *in situ* transformations, borrowing hydrogen (BH) methodology has received great attention in recent years as a greener alternative to conventional alkylation reactions.

The BH principle, also called hydrogen auto-transfer, is a powerful strategy which combines TH (avoiding the direct use of molecular hydrogen) with one or more intermediate reactions to form more complex molecules without the need for tedious separation or isolation processes.¹⁴

A basic scheme of this concept is depicted in Scheme 5. This strategy typically relies on three steps: (i) dehydrogenation, (ii) intermediate reaction, and (iii) hydrogenation. The borrowing hydrogen strategy begins with a metal-catalysed dehydrogenation, by virtue of which a usually less reactive donor molecule is temporarily converted into a more reactive substrate (e.g., an alkane transforms into an alkene, an alcohol into an aldehyde, or a ketone and an amine into an imine). The more activated intermediate can undergo further transformations to give an unsaturated compound that will be reduced with the intervention of the metal hydrides generated during the first dehydrogenation step.



Scheme 5: Basic scheme of the BH methodology

The key of this concept is that the hydrogen from a donor molecule will be stored by a catalytic metal fragment to afterwards, be released in a final hydrogenation step; hence the reaction name. Following the above Scheme 5, the development of catalytic systems in borrowing hydrogen catalysis involves metal complexes or stabilized metal particles in which H₂ dissociation and recombination is simple, preferably without requiring severe reaction conditions.

Borrowing hydrogen methodology is very attractive for its potential, operational simplicity and atom economy, offering several environmental benefits over traditional approaches.

Today BH is used in numerous applications that show a good tolerance of other functional groups in both C-C and C-N bond forming processes (Witting reactions, N-heterocycles synthesis, N-Alkylation of amines/amides, etc).

The increasing global challenge to develop more sustainable catalytic methodologies and the effort to switch precious metals to earth-abundant first row transition metals in catalysis, has developed a branch based on Mn, Fe, Co, Ni and Cu. In this context, Morrill et al.¹⁵

published in 2019 a review describing the recent advances in homogeneous borrowing hydrogen catalysis using those metals.

N-alkylation of amines using alcohols via the borrowing hydrogen approach has been reported using different homogeneous catalysts. In 2015, Kempe and co-workers employed Co(II) PNP pincer precatalyst (2 mol%) and KOt-Bu (1.2 equiv.) as base and obtained a wide range of secondary amine products in high yields, working at 80°C. Fe(II) phthalocyanine¹⁶ and a (cyclopentadienone)iron carbonyl precatalyst¹⁷ were also reported as successful catalysts in the N-alkylation by borrowing hydrogen approach.

In the same way homogeneous Co¹⁸, Fe¹⁹, Mn²⁰-catalysed C-alkylation processes *via* HB method has also been widely developed during the last decade.

However, the objective to develop new processes to achieve green and sustainable synthesis of chemicals, place one-pot procedures with heterogeneous catalysis as an encouraging alternative to homogeneous processes. Separation and recycling of the catalyst and easiest purification of products allows a decrease in energy consuming operations. In 2015 Shimizu²¹ reviewed the use of heterogeneous catalysts for C–C, C–N and C–S bond formation reactions by borrowing hydrogen methodology. As reported, N-alkylation of amines employing alcohols has been effectively described by using noble metal catalysts such as Pd, Ru, Ag, Au, Pt,... and also non-noble metal catalysts like Fe²², Cu²³, Ni and Mn. Shi et al.²⁴ reported in 2013 that NiCuFeO_x/Al₂O₃ acted as an effective catalyst under additive-free conditions showing a wide substrate scope. Beller²⁵ described also the catalysed N-alkylation of sulfonamides with benzylalcohols by Ru/Fe₃O₄ producing sulfonamide derivatives as intermediates in drug synthesis.

N-alkylation of NH₃ or urea²⁶ with alcohols, alkylation at acidic CH₂ and CH₃ groups^{27,28} with alcohols, self and cross-alkylation²⁹ of alcohols, synthesis of quinolones³⁰ from nitroarenes and alcohols, alkylation of amines³¹ with amines or asymmetric transfer hydrogenation catalysts³²; are all well described procedures that employ borrowing hydrogen methodologies.

Despite the range of innovative strategies that have been developed in this area, mechanistic details based on theoretical studies as well as novel preparation methods of structurally well-defined multifunctional catalysts for the development of new and more efficient strategies are always welcome.

Being the main by-product in the manufacture of biodiesel fuel (~10% w/w glycerol is typically formed in the process), glycerol constitutes a non-toxic, biodegradable and recyclable compound with excellent features to be used as building block (Figure 5), green solvent and hydrogen source in TH reactions.

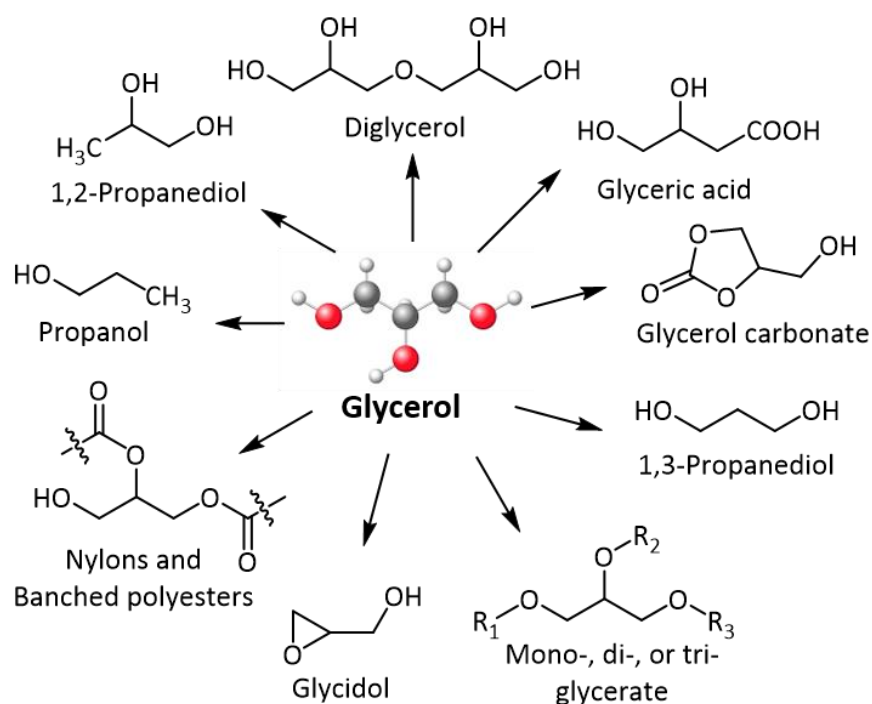
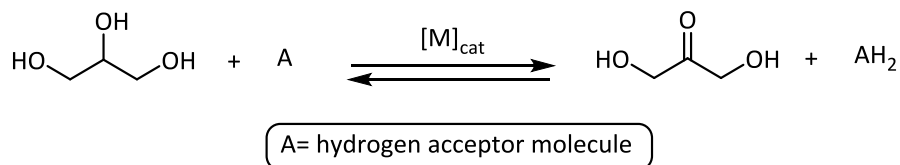


Figure 5: Glycerol as building block

Because of its unique combination of physical and chemical properties, the possibility of using glycerol as an environmentally friendly ‘donor solvent’ in transfer hydrogenation-dehydrogenation reactions has gained increasing attention during the last years. Replacing the most commonly employed hydrogen sources in transfer hydrogen (TH) reactions, such as 2-propanol, tetralin or formic acid/triethylamine mixtures; by the use of glycerol, reactions are not only economically appealing but also more environmentally friendly. In contrast to transfer hydrogenation with EtOH, where acetaldehyde is formed, the corresponding dehydrogenation product from glycerol is dihydroxyacetone (Scheme 6), which, as a ketone, is expected to have a much lower tendency for potentially deleterious CO transfer to the metal catalyst. The oxidized form of glycerol is also considered as an industrial relevant molecule^{33,34} and so, constitute another interest in TH processes from glycerol. As already reviewed in 2013 by Cadierno et al.,³⁵ glycerol constitutes a promising reducing agent for metal-catalysed transfer hydrogenation reactions of organic compounds, such as aldehydes, ketones^{36–38}, olefins³⁹ and nitroarenes^{36,37}.



Scheme 6: Generation of dihydroxyacetone from glycerol by transfer hydrogenation (TH).

Glycerol as hydrogen donor was first used by Crotti and co-workers⁴⁰ in 2009 for the reduction of acetophenone catalysed by Ir(diene)(N-N)X. They observed that glycerol dehydrogenation⁴¹ does selectively occur at the secondary hydroxyl group giving dihydroxyacetone, whereas acetophenone was reduced to phenylethanol.

The same year, the first example of the reduction of carbon-carbon double bonds in glycerol was described by Wolfson and co-workers.⁴² As they reported, by employing Pd/C in

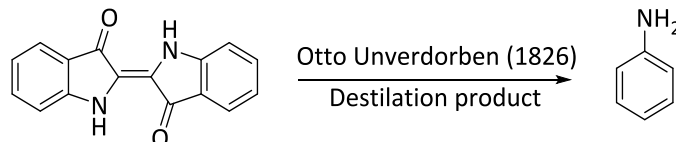
the presence of glycerol, styrene and cyclohexane were fully hydrogenated, while bulky alkenes and linear aliphatic were only partially reduced.

Reduction of aromatic nitrocompounds was also studied using glycerol as solvent and reducing agent in presence of Ni Raney as catalyst by Wolfson and co-workers⁴¹. In 2011, D. Tavor et al.³⁶ successfully produced aniline using Ni Raney and employing glycerol as solvent and hydrogen source. Milder conditions were described by Gawande et al.³⁷ in 2012 using magnetic nanoparticles of Fe₃O₄-Ni, obtaining a wide range of anilines with different substituents.

Although glycerol shows encouraging features as sustainable and green solvent, some drawbacks can be pointed, such as its high viscosity at room temperature and the low solubility with high hydrophobic compounds and gases, reducing in this way the mass transport competences. To overcome these limitations, microwaves and ultrasound irradiation⁴³ has already been employed, improving heat and mass transfer capabilities and therefore, accelerating the reactions.

1.2.3 Nitroarenes

Aminocompounds, and specifically aniline and its derivatives, represent a huge market portion in the organic chemical industry. Aniline was firstly isolated almost 200 years ago (1826) as product of the dry distillation of indigo by the German chemist Otto Unverdorben (Scheme 7). Some years later, aniline was prepared for the first time by reduction of nitrobenzene in the presence of sodium sulfides as stoichiometric reductants, reaction that maintains the name of its discoverer, Nikilay N. Zinin.⁴⁴



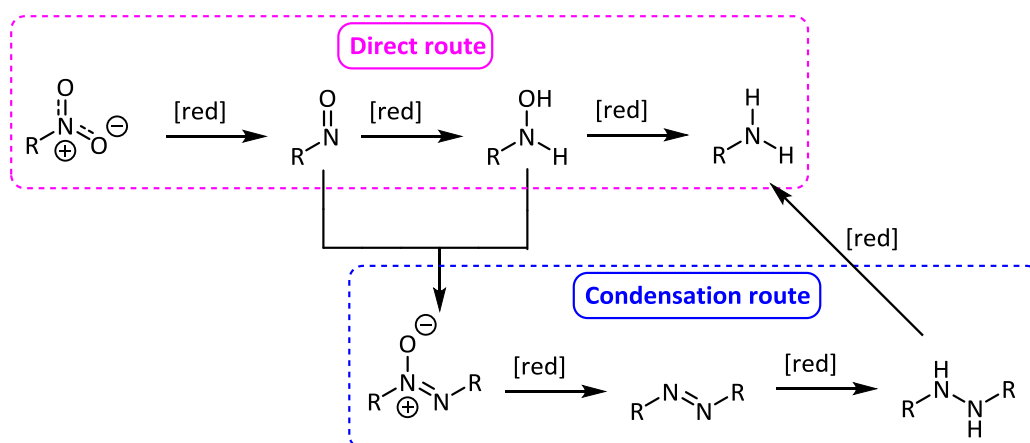
Scheme 7: In 1826, aniline was first isolated as dry distillation product of indigo.

In 1851, Piria reported a two-step procedure for the synthesis of anilines from nitroarenes: in the first step the nitro group is converted into an aminosulfonic acid which is then transformed into the final product by hydrolysis with mineral acids. Pierre J.A Bechamp demonstrated the use of metallic iron in acidic media as reducing agent in the nitrobenzene reduction in 1854 and for a long time, and even nowadays, the main manufacturing process for anilines was based on this method. However, this classic stoichiometric process is becoming much less attractive due to the environmental concern, and much effort has been spent on the development of efficient methodologies for reduction of nitroarenes. In this respect, catalysis represent the cornerstone for efficient production of such molecules and during the last years, many catalytic systems have been developed by different chemical industries (Table 2).

Table 2: Industrially applied processes for the reduction of nitrobenzene to aniline. Reproduces from Beller *et al.*⁴⁵

Catalyst	Company	Reaction conditions
Ni sulfides	Bayer, Allied	300-475 °C
Cu, Mn, Fe	ICI	300-475 °C
Pd/Al ₂ O ₃	Bayer	250-350 °C 7 bar
Cu/SiO ₂ (Cr, Ba and Zn as promoters)	BASF, Cynamide, Lonza	270-290 °C 5 bar
Pd-Pt/C (Fe as modifier)	DuPont (Dow Chemicals)	90-200 °C 6 bar

The classical scheme of the nitrobenzene reduction to aniline follows the mechanism of hydrogenation described by Haber-Lukashevich (Scheme 8) in 1898 (based on electrochemical experiments), and updated by V.P. Shmonina. As shown in Scheme 8, two different pathways can be proposed: a) the direct route, in which the nitro compound is reduced to the corresponding nitroso, aryl/alkyl hydroxylamine, and finally aniline; and b) the condensation route, which involves the condensation of nitroso with N-aryl/alkyl hydroxylamine species giving rise to the corresponding azoxy-intermediate. Further on, the latest is converted into azo-, hydrazo-, and finally aniline. This hydrogenation scheme has been recognized by most authors, who confirmed the reaction mechanism by experimental methods in lot of different works. However, as recently reviewed by Sassykova *et al.*⁴⁶, there are alternative judgments for the nitrobenzene reduction that have been reported in literature.



Scheme 8: Proposed Mechanism by Haber and co-workers

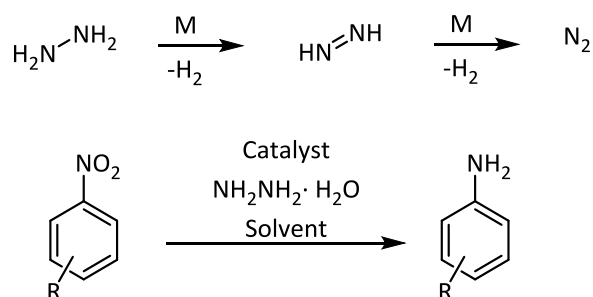
The hydrogenation of nitrobenzene is a very well-established reaction that does not imply important selectivity problems. However, the situation is different when working in presence of functionalized nitro compounds containing C-C, C-heteroatoms multiple bonds, halogen atoms, carboxylic acid derivatives, or heterocycles. Unfortunately, under operative conditions, these substrates do not show sufficient selectivity and therefore, modifications of existing catalysts or their tailor-made versions are required.

Starting with Bechamp reduction⁴⁷, a century-old process where a lot of metallic waste is generated, recent advances provide methods using catalytic metals and clean reaction conditions.

Molecular hydrogen in the presence of metal/metal oxide can cause clean reduction of a nitro group into an amine, and therefore, it has been commonly employed for this transformation. The use of this gas in combination with Fe-based metal/metal oxide NPs and nitrogen-doped carbonaceous supports for nitrobenzene hydrogenation was first reported in 2013 by Beller et al.⁴⁸ and has been shown to be promising for other various reductive transformations. The group of Q. H. Yang reported a similar material using CNTs as support instead of carbon, what was further demonstrated by Z. Hou and co-workers⁴⁸ in 2016. Catalytic activity of Ag and Co using H₂ as reductant was first published in 1921⁴⁹ by O. W. Brown and later on, in 1975, Bayer A.D patent the use of Co for this transformation.

However, as previously discussed, despite of being the first option when performing industrial scaling up, the use of hydrogen gas comes with several disadvantages. Thence, in situ generation of gaseous H₂ during a reduction process can avoid the use of sophisticated equipment and wastage due to excess use of gas under pressure. Therefore, typically, in laboratory scale, different non-gaseous reducing agents have been employed for this transformation.

Hydrazine is often an alternative, which formally decomposes into di-hydrogen and di-nitrogen under catalytic conditions and allow the reduction transformation (Scheme 9).



Scheme 9: Reduction of nitroarenes in presence of hydrazine hydrate

Reduction of aromatic nitro compounds to anilines with N₂H₄ as reducing agent take place at low temperature and has been successfully performed in the presence of different catalysts. In 2012 polymeric PEG-35k-Pd NPs were used by Yadav et al.⁵⁰ giving anilines in quantitative yield. One year later, Yu et al.⁵¹ claim the selective reduction of nitro group in the presence of other reducible vinyl and aldehyde groups, employing Pd NPs (1.36%) immobilized on carbon nanospheres. Similarly Pd/C was also studied for selective reduction of halogenated nitrobenzenes using hydrazine hydrate under reflux or microwave (MW) conditions by Li and coworkers⁵². Iron in different forms (Fe(Acac)₃,⁵³ Graphene-Fe₃O₄,^{54,55} FeSO₄-Fe phthalocyanine⁵⁶) have also exhibited excellent activities for the selective reduction of nitroarenes in the presence of hydrazine. Compared with Fe, only few reports using heterogeneous Co-based catalysts for the reduction of nitro compounds were published with N₂H₄. In 2017, Rawat and co-workers⁵⁷, prepared a catalyst composed of Co₃O₄ supported onto SiO₂/Al₂O₃-mixed oxide by an impregnation method that showed good activity even in presence of reducible functional groups. In a related work, X.Wang et al.⁵⁸ reported the preparation of a mesoporous γ-Al₂O₃-supported Co catalyst by coprecipitation/impregnation

followed by treatment at 700 °C in N₂ atmosphere that were applied for a variety of functional nitroarenes to the corresponding arylamines with hydrazine.

However, the toxicity of hydrazine and its well-known use as rocket fuel may have to be taken into account during large-scale reduction processes.

In the same way, sodium borohydride under aqueous or protic conditions (Scheme 10) is hydrolysed giving H₂, and therefore is widely used as reducing agent. In fact, a multitude of catalysts based on coinage (Au, Ag, Cu)^{59–63}, noble (mostly Pd and Pt)⁶⁴, and non-noble (Ni, Co, Fe)^{65–67} metals can catalyse this reaction.



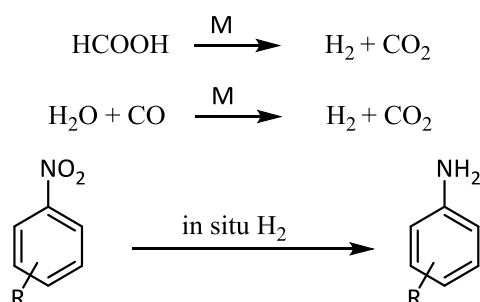
Scheme 10: Reduction of nitroarenes in presence of sodium borohydride

Metallic Fe NPs were proposed by the groups of K. Hanna⁶⁷ and Y. Cai.⁶⁵ In the first case, they demonstrated that the NaBH₄ enhanced significantly the reactivity of nanoscale zero-valent iron in oxygen environments. Y. Cai and coworkers developed an operationally simple protocol for the one-pot preparation of citrate-coated Fe(0) NPs, which allow for nitro reductions. A complex of Fe(II) and citrate was in situ prepared and reduced with NaBH₄ in the same vessel containing the nitro compounds.

Pd(II) phthalocynine was used with low catalyst loading (1 mol%) along with NaBH₄ in ethanol by Verma et al.⁶⁸ in 2014. Numerous Co-based catalysts using NaBH₄ as reductant were explored for the reduction of nitroarenes to anilines, especially in the reduction of 4-NP to 4-AP as model system. Both bulk catalysts, supported and unsupported Co-based⁶⁹ NPs were found to be active, leading to a large amount of reports on this topic.

Nevertheless, the price of this reductant as well as the formation of salts as byproducts prevent, in most cases, larger scale applications.

CO₂ gas along with H₂ can be both obtained by decomposition of formic acid or its salts and by the CO–H₂O mixture (commonly known as water gas) in the presence of a metal support (Scheme 11). This molecular H₂ evolved can be used for reduction reactions, leaving no residual wastes.



Scheme 11: Reduction of nitroarenes in presence of formic acid and by the CO–H₂O mixture.

Continuous hydrogenation of nitrobenzene to aniline was developed by Poliakoff and coworkers in high-temperature pressurized water (HTPW) using H₂ generated by thermal decomposition of HCOOH.⁷⁰ This reaction was carried out in the absence of any added catalyst and can be conveniently performed on a laboratory scale. Ru and Ir catalysts⁷¹, which are not particularly selective under the conditions of conventional hydrogenation carried out with molecular hydrogen, when used in the aqueous-phase reforming/hydrogenation (APR/Hyd)

process, become >99.9% selective for hydrogenation of o-chloronitrobenzene to o-chloroaniline.

Also hypophosphites have been used as reducing agents, since they get oxidized to phosphonates as shown in Scheme 12.⁷²



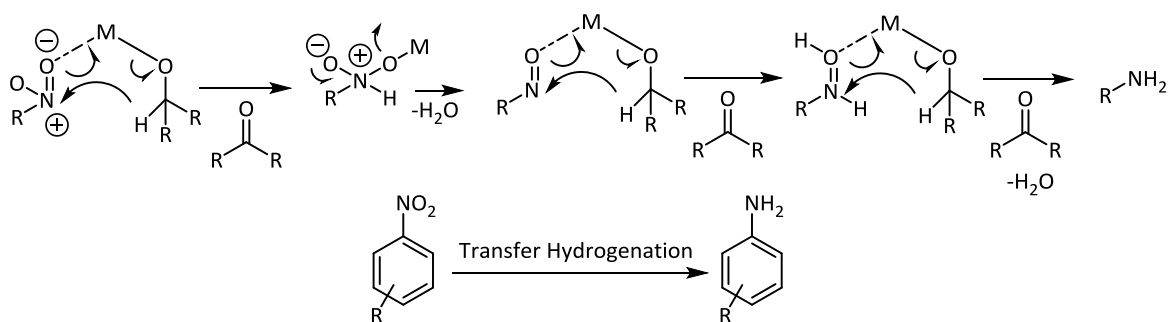
Scheme 12: Oxidation of hypophosphites to phosphonates

In 2013, Oba et al.⁷³ reported the used of sodium hypophosphite as hydrogen source in water (containing 1% w/w Tween 20) for reduction of nitro compounds catalysed by Pd/C (10 mol%). Aromatic as well as aliphatic nitro compounds were reduced to amines at 50 °C in more than 99% yields. Also in 2013, a similar procedure was described by Popowycz and coworkers,⁷⁴ where nitroarenes were reduced to corresponding anilines in the presence of CN, ester, keto and halogen groups.

However, even if formic acid is cheap and shows low toxicity in diluted solutions, it is corrosive with metals, and especially in heterogeneous catalysis, what constitutes a challenging task since many nanostructured catalysts are degraded by HCOOH.

Metal reductions as such are very selective in reducing the nitro functionality^{75–77}, but stoichiometric requirement of metals makes these processes unattractive. Active metal can react with water to liberate hydrogen and this liberated hydrogen in the presence of metal can bring about reduction of a nitro group.

Aiming to overcome these problems, transfer hydrogenation reactions has also been embraced as a great alternative in this field. In this way, transfer hydrogenation–dehydrogenation reaction, in which hydrogen is transferred from an alcohol to an unsaturated bond, has become an environmentally benign method for reducing unsaturated compounds or oxidizing alcohols (Scheme 13).



Scheme 13: Transfer hydrogenation nitroarenes reduction.

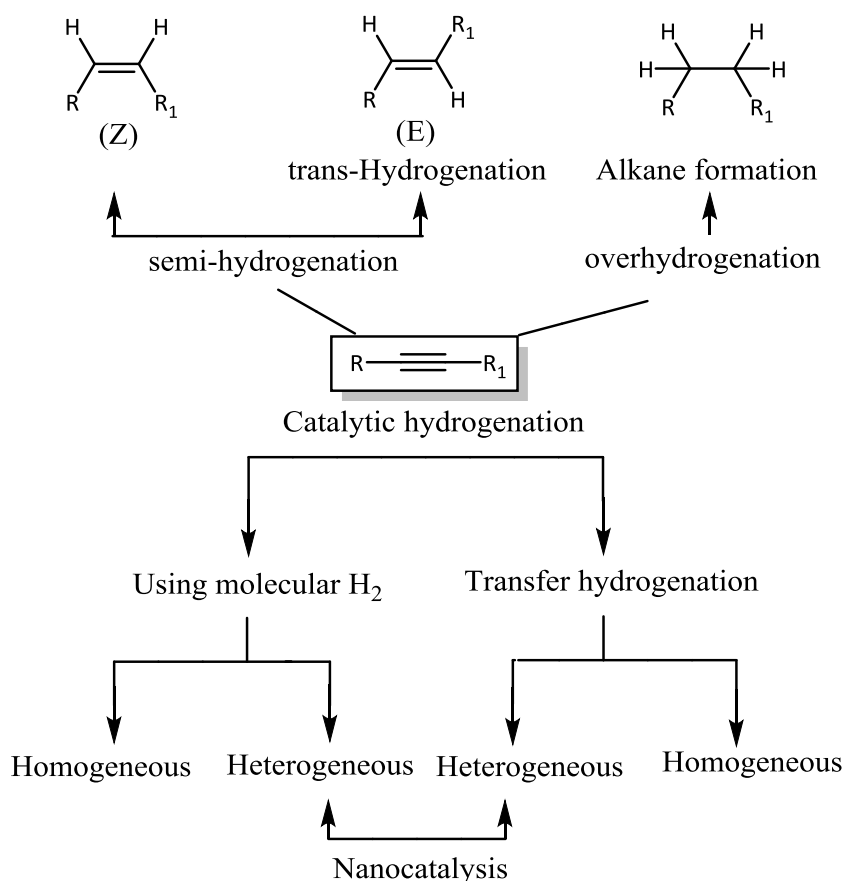
In 2012, Ru(0) NPs⁷⁸ were generated by incipient impregnation of RuCl₃ into the nanopores of an acid activated montmorillonite clay followed by polyol reduction. This system showed efficient catalytic activity in the chemoselective transfer hydrogenation reduction of substituted nitrobenzenes to corresponding anilines with high yield of conversion and selectivity. Ag-mesoporous polytriallylamine catalyst was reported under similar conditions by Salam et al.⁷⁹ In 2014, S. Velmathi et al.⁸⁰ studied the catalytic activity of Fe-SBA-15 for the catalytic hydride transfer reaction of aromatic nitro compounds using 2-propanol as hydrogen source. Pinacol as a chemoselective and environmentally benign reducing agent for sulfoxides and nitroaromatics assisted by readily available dichlorodioxomolybdenum(VI) complexes as

catalysts was employed by R. Sanz et al.⁸¹, showing good yields under MW conditions and acetone and water are the only by-products in this reduction. D-Glucose, an abundantly available carbohydrate, was reported by Kumar et al.⁸² as a source of hydrogen in a catalyst-free aqueous system. Pd-based catalyst in presence of cyclohexadiene or MeOH⁸³ have also shown effective properties as hydrogen transfer source in this reaction. A heterogeneous Fe₃O₄-Ni magnetic NP catalyst was demonstrated for hydrogen-transfer reactions by using the environmentally friendly solvent glycerol as a hydrogen donor by Gawande et al.⁸⁴

Despite the high number of publications on this topic, this area of research involving methods for the reduction of nitroarenes continues to attract synthetic chemists due to problems associated with selectivity and cost of process. This indicates that the topic remained of high interest to academic and industrial chemists alike and there is every sign to expect similarly active developments in the future.

1.2.4 Alkynes

Chemo- and stereo-selective semi-hydrogenation of alkynes leading to the preferential formation of cis- or trans-alkenes, and avoiding over-hydrogenation or reduction of other functional groups, is an important reaction that can be achieved by using either a homogeneous or a heterogeneous catalyst (Scheme 14).



Scheme 14: Major facets of alkyne hydrogenation⁸⁵

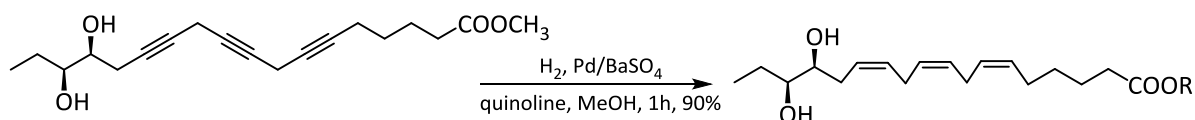
Many biologically active molecules incorporate carbon-carbon double bond(s) with well-defined configurations (E or Z), such as β -carotene, polyene antifungal drugs, crocacin, but also polyunsaturated fatty acids (PUFAs), pheromones, and cruentaren. In the last few decades, several methods have been developed to stereochemically control the desired

configurations: (i) creation of carbon-carbon double bonds (e.g., Wittig,⁸⁶ Horner-Emmons-Wadsworth,⁸⁶ Julia-Kocienski,⁸⁷ Peterson,⁸⁸ Takai olefination,⁸⁹ olefin metathesis⁹⁰); (ii) cross-coupling reactions⁹¹; (iii) reduction of alkynes^{92–94}; and (iv) elimination of halides.

However, most of the above-mentioned reactions led to (E)-isomers or isomerization of (Z)- to (E)-alkenes, side reactions, poor stereoselectivity and function tolerance, etc. Among the reactions providing (Z)-alkenes, the selective semihydrogenation of internal alkynes constitute an important step in the synthesis of vitamins, natural products, polymerization; and it can be accomplished by two different ways: using H₂ gas or by transfer hydrogenation reactions.

Catalytic hydrogenation employing Lindlar catalyst⁹⁵ constitute the most popular method for preparing cis-alkenes from alkynes. This heterogeneous catalyst consists of palladium (5%) deposited on calcium carbonate, treated with lead acetate. However, despite its widespread use, it has several disadvantages including possible over-reduction to alkanes, isomerization, double bond migration, poor reproducibility, small tolerance with other reducible functional groups and safe handling requirements due to the use of H₂. Actually, very few chemists reported that they preferred this procedure in comparison with other methods.

Some of those drawbacks have been partially overcome when performing the hydrogenation reactions over Pd/BaSO₄ catalyst (Scheme 15), known as well as the “modified” Lindlar catalyst. This reaction is generally run at room temperature at atmospheric pressure, and in methanol or ethanol^{96,97}. Many natural products have been prepared *via* this system. For instance, Karrer et al.⁹⁸ reported already in 1950 the synthesis of β-carotene and lycopins, one of the commonest natural pigments, with a good yield. However, besides these good to excellent yields, many reactions proceeded with moderate yields only, meaning therefore poor selectivity.



Scheme 15: Alkyne hydrogenation over Pd/BaSO₄ catalyst⁹⁷

Since Brown's publication⁹⁹ in 1973 showing the potential in the semihydrogenation of alkynes, chemists emphasized the effectiveness of P2–Ni catalyst for the hydrogenation of some very complex molecules and several authors concluded that this catalyst is far superior than other reduction methods. For instance, starting from a diyne containing both CH₂OH and CH₂OTBS groups, Feutrill et al.¹⁰⁰ preferred the P2–Ni catalyst rather than the Lindlar catalyst, which gave erratic results. Nowadays the Brown catalyst is widely used for achieving high stereo-, chemo-, and regioselectivity. Thus, as for the Lindlar catalyst, the Brown system has shown its appealing potential for the partial reduction of skipped dienes,^{101,102} trienes,^{103–105} and tetraenes.^{106,107}

The Ti-mediated process and hydroboration reaction together with the Zn-activated system^{108,109} seem appealing, since they are much easier to set up than the hydrogenation reaction involving hydrogen gas. In addition, interestingly, no overreduction is observed. However, those processes did not catch too much the chemists' attention, mostly because of the disappointing yields (rather weak in comparison with the ones obtained in Lindlar or

Brown procedures; the limitation of some functional groups' resistance; and significant risk of isomerization).

Despite the impressive number of contributions and results obtained, it seems that it is always a challenge to succeed with alkyne reduction in the presence of other alkynes and/or alkenes. Thus, new and better chemo- and stereo-selective procedure are required.

As already mentioned, transfer hydrogenation reactions has become popular during the last few years thanks to better chemo- and stereo-selective transformation, as well as more sustainable nature. As mentioned above, most often the transfer agent is an alcohol (such as 2-propanol) or formic acid, giving respectively acetone and CO₂ as by-products after the hydrogenation reaction. As depicted in Table 3, a number of TH reactions in presence of different metal catalysts has been reported for this transformation. Sato et al.¹¹⁰(Table 3, entry 1) showed transfer hydrogenation of alkynes using HCO₂H-NEt₃ as hydrogen donor in the presence of Pd⁰-catalys affording cis-alkenes with excellent yields. In 2008 Hauwert and co-workers¹¹¹ (Table 3, entry 2) described the transfer semihydrogenation of alkynes catalysed by a zero-valent palladium N-heterocyclic carbene complex using also HCO₂H-NEt₃ as the hydrogen donor. The same hydrogen source was used by Belger et al.¹¹² and Monfredini and coworkers¹¹³ using a Ru-catalyst and a tri-palladium complex, respectively (Table 3, entries 3 and 4). In 2010, Hua and co-workers¹¹⁴ found that DMF/KOH acted as an efficient hydrogen source for the palladium-catalysed chemo- and stereo-selective transfer semihydrogenation of alkynes to afford the corresponding (Z)-alkenes in good yields (Table 3, entry 5). Polymethylhydrosiloxane (PMHS) has also been widely used as hydrogen source^{115–118} in this kind of reaction. The catalytic system comprising Cu(OAc)₂ with PMHS as the hydrogen source was shown by Wang et al.¹¹⁹ to be efficient in the catalytic semihydrogenation of internal and terminal alkynes (Table 3, entry 7). Another convenient method for the (Z)-selective semihydrogenation of alkynes under copper catalysis by using silane and alcohol as hydrogenating agents was reported by Tsuji co-workers¹¹⁶ (Table 3, entry 8). 2-propanol was used by Kominami et al.¹²⁰ as solvent and hydrogen source for the photocatalytic hydrogenation of alkynes over Cu-TiO₂ (Table 3, entry 9).

Table 3: Transfer hydrogenation of alkynes.

Enter	Catalytic conditions	H ₂ transfer agent	Reference
1	[Pd ₂ (dba) ₃]-PBU ₃ (Pd 5 mol%, phosphine 10 mol%), HCO ₂ H/NEt ₃ (6 equiv), THF, 40 °C, 1–2.5 h		110
2	[Pd] Catalyst (1 mol%), HCO ₂ H/NEt ₃ (5 equiv), CH ₃ CN or THF, reflux	HCO ₂ H/Et ₃ N	111
3	Ru(PPh ₃) ₂ H ₂ (1.25 mol%), DMF/HCO ₂ H (1:2, 4–5 equiv), rt, 1–7.5 h		112
4	[Pd ₃] ⁺ (0.03 mol%, P(4-Me-C ₆ H ₄) ₃ (0.09 mol%), N ₂ , 80 °C		113
5	Pd(OAc) ₂ (2 mol%), DMF 920 equiv)/KOH (15 equiv), 145 °C, 6–9 h	DMF/KOH	114
6	[IPrCuO-t-Bu] (0.5 mol% or 2 mol%), PMHS (1.2 / 2 equiv), i-BuOH (terminal alkyne, 1.2 equiv,) or t-BuOH (internal alkyne, 2.5 equiv); toluene 25–45 °C, 1–8 h	PMHS	115

7	Cu(OAc) ₂ ·H ₂ O (0.05 equiv), IPr.HCl (0.05 equiv), t-BuOK (0.1 equiv), t-BuOH (2.0 equiv), toluene		119
8	Cu(OAc) ₂ ·H ₂ O (2 mol%), CF ₃ Ar-Xan (4 mol %), hexane:THF (1:1), 25–65 °C, 20 h		116
9	Cu/TiO ₂ (0.5 wt% of substrate), 2-propanol (5 mL), hm, rt, 2–8 h	2-propanol	120

In the past decades, remarkable achievements have been made and many efficient reactions catalysed by Pd- Rh- Ru- Ni- Va-Bi and Au- have been reported for the hydrogenation of alkynes to give selectively alkenes. However, replacement of these metals, the use of safer hydrogen sources and over-hydrogenation are still the key issues for this hydrogenation reaction.

1.3 Copper catalysis

As it is already well known, one of the most direct ways of pursuing sustainable chemistry is the development of more selective catalytic approaches toward the synthesis of chemical products. In this way, the creation of more economical and environmentally friendly new synthetic technologies constitute a key target in both industry and academic laboratories. The design of chemical products and processes that reduce or eliminate the use and generation of hazardous substances constitute one of the fundamental pillars of green chemistry.¹²¹ Catalysis^{122,123} plays a central role in the achievement of high atom-economy for reactions and offers numerous green chemistry benefits including lower energy requirements, catalytic versus stoichiometric amounts of materials, higher selectivity, and a minor use of processing and separation agents.

The application of catalysts is ubiquitous in the chemical industry,^{124–127} in areas ranging from pharmaceuticals¹²⁸ to polymers to petroleum processing. More than 90% of all industrial processes are based on this topic. The widespread utilization by industry of catalytic processes reflects the economic and environmental benefits achieved by this field.

Two different ways of performing catalysis can be defined, homogeneous and heterogeneous^{129–131}. This distinction is linked to the fact that the catalyst operates respectively in the same phase where the reaction occurs (homogeneous catalysis) or in a different phase (heterogeneous catalysis). A great variety of homogeneous catalysts are well known and have been widely used in organic synthesis such as Bronsted and Lewis acids¹³², metal complexes,^{133,134} metal ions or biocatalysts (enzymes).^{135,136} However, recovery and reuse of expensive catalysts after catalytic reactions is an important factor for sustainable process management. Therefore, heterogeneous catalysis^{126,137,138} addresses the goals of green chemistry by providing the ease of separation of product and catalyst, thereby eliminating the need of performing distillation or extraction.

As already anticipated, attractive alternatives to noble metal catalysts are requested. Due to this, during the most recent decade, an explosive development of copper catalysed reactions has been observed.^{139,140}

This growth may be driven by a couple of factors:

- a) Copper chemistry is highly diverse. The variety of copper oxidation states (Cu^0 , Cu^I , Cu^{II}) allow the possibility of developing a wide number of reactions, and so, a number of applications. Copper coordinates easily to heteroatoms and to π -bonds and is well-known to activate terminal alkynes. The Ullman¹⁴¹ and Goldberg C–C and C–N cross-coupling¹⁴² reactions were discovered over a century ago and their development has really blossomed over the past twenty years. The simplicity and efficiency of this metal has also opened a door for an extensive number of research procedures such as click reactions¹⁴³, oxidations¹⁴⁴, reductions¹⁴⁵ and C–H activations.¹⁴²
- b) Compared with other metal transition catalysts, copper is an earth-abundant metal, making its use more cost effective and more sustainable.

However, compared to other catalytic methodologies, Cu-catalysed couplings are still affected by some drawbacks: despite all the efforts put into the research so far, these Cu-mediated processes have not yet reached the high levels which characterise Pd chemistry, either in rate, efficiency or scope. Moreover, Cu-based coupling reactions are still in some sense unpredictable the mechanism not being yet completely understood. On the other hand, however, Cu catalysis shows some interesting advantages over Pd or other metals. First of all, Cu is cheaper than many of the other metals used in catalysis, and has attracted recently high interest from the industry. The range of nucleophiles suitable for Ullmann arylations has become wider with time, and nowadays N-, O-, S-, P- and C-aryl bonds formation are easily accessible through these processes. Such bonds can be found in many bioactive organic compounds, as well as in material chemistry. Also, the scope of Cu-catalysed cross coupling reactions is increasing, and it seems to be somewhat complementary to that of Pd-based methodologies. Finally, in many cases, Cu-catalysed reactions work well without any ligand, and when required, the ligands are usually structurally quite simple and inexpensive (ligands for Pd chemistry are often complex, expensive and air-sensitive).

1.3.1 Nanoparticles

Nanosynthesis deserves special concern and over the past decades, nanoparticle synthesis has received enormous attention thanks to the extensive applications in catalysis, sensing, electronics, photonics and medicine. Back in 1993, Bawendi and co-workers¹⁴⁶ pioneered the controlled synthesis of nanoscale CdE (E = S, Se, Te) with narrow size distribution using a very simple pyrolysis method.

From that moment, and especially during the last years, metallic nanoparticles¹⁴⁷ have been broadly used as catalysts due to their high active surface area and high reactivity. Compared with other conventional heterogeneous catalysts, these particles are great valuable in terms of low catalyst loading, high atom economy and, therefore, more sustainable nature. An understanding of the mechanisms by which NPs form and grow is important for the development of their synthetic methods. NP growth, the size and shape of the products are mainly controlled by the properties of the precursor and the reaction conditions. In this regard, capping agent, reducing agent and solvent used for their synthesis should be considered from a green chemistry perspective, involving the utilization of nontoxic capping agents, less hazardous reducing agents, and selection of environmentally benign solvents. Unfortunately, despite many experiments and computational studies, the exact mechanisms involved in these processes are still not entirely clear.

Synthesis of CuNPs¹⁴⁸ is commonly performed by applying the same procedures that has been described for the preparation of other metal nanoparticles. Two principal methods can be named: “bottom-up”, in which atomic level precursors are used to synthesize the nanosize material; and “top-down”, in which a bulk solid is broken down into smaller components in order to obtain the desired species. Generally, the bottom-up approach has become more widely held thanks to the advantages in offering the possibility of controlling and modulating stability, properties and morphology of the final nanoparticles. This synthesis is mainly divided in seven methods, including thermal reduction, sonochemical reduction, metal vapour synthesis, chemical reduction, vacuum vapour deposition, radiation methods and micro emulsion techniques. Among all these methods, the greatest feasibility and so, the most extended thanks to its simplicity and low cost is the chemical reduction. The growth of CuNPs is assumed to occur in accordance with the Ostwald ripening process (i.e., “the smaller NPs sacrifice themselves to make the larger NPs in order to decrease surface-to-bulk ratios”). Cu atoms or clusters that dissociate from the surfaces of smaller particles can be entrapped in the polyimide matrix, after which they can diffuse into the bulk phase of the matrix to enable further NP growth. This process has been described as “diffusion-controlled aggregative growth of CuNPs”¹⁴⁹.

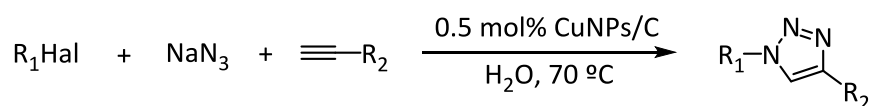
Cu-based nano-catalysts have found many applications in nanotechnology, including catalytic organic transformations¹⁴³, electro-catalysis¹⁵⁰, and photo-catalysis¹⁵¹. As when using homogeneous catalysis, these particles have been used in heterogeneous catalysis with various oxidation states.

When working with Cu⁰ based NPs, one of the main issues is their susceptibility to be oxidised under ambient air or some other oxidant conditions giving Cu^I and/or Cu^{II} species, and so hindering their applications. For overcoming this problem, some antioxidants as citric acid, or stabilizing and capping agents such as PVP¹⁵², some surfactants like cetyltrimethyl ammonium bromide (CTAB)^{153,154} or some ligands as polyols¹⁵⁵ have been widely used.

Unsupported CuNPs have been barely studied compared with the supported one due to their inherent tendency toward particle agglomeration, what makes the presence of stabilizing agents or solid supports mandatory in most cases. Pioneering work by the groups of Rothenberg¹⁵⁶ and Orgueira with Cu(0) nanoclusters was followed by the use of mixed Cu/Cu oxide nanoparticles¹⁵⁷ and poly-(vinylpyrrolidone)-stabilized CuNPs¹⁵⁸, all of which catalysed the reaction of preformed azides and terminal alkynes.

Aiming to increase the catalyst recyclability as well as decrease the metal loading, catalysts composed of CuNPs over different supports : activated carbon (CuNPs/C)^{159,160} (

Scheme 16), silica^{161,162} (CuNPs/Silica) and diverse metal oxides¹⁶³ have shown salient features that made the reactions much more efficient and sustainable than with the unsupported counterpart.

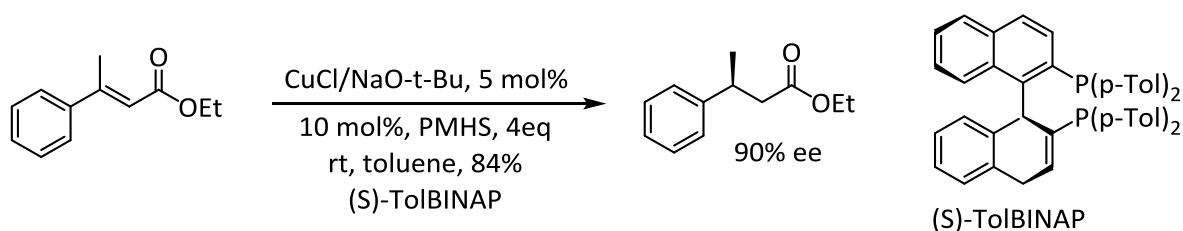


*Scheme 16: click chemistry catalysed by CuNPs over activated carbon*¹⁶⁰

1.3.2 Copper catalysis in reduction reactions.

Due to copper abundance, low cost and high chemo-, regio-, and stereoselectivities associated, much attention has been paid during the last years to develop copper-catalysed reduction of unsaturated compounds^{94,117,164,165,166,167,143,168–170}. As already mentioned, due to the increasing concern about the environmental issues, alternative hydrogen sources such as formic acid, alcohols, PMHS... have been also widely studied. However, generally, bulky and expensive ligands are still necessary.

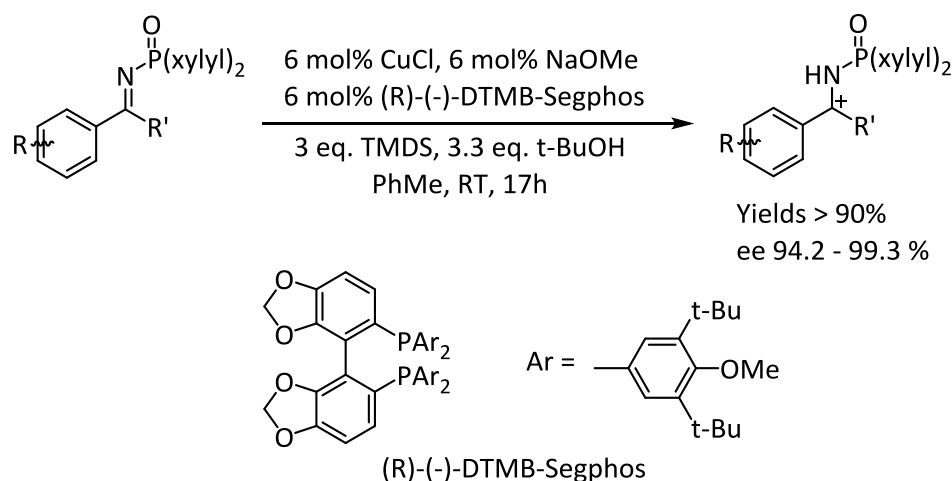
Given the rich history of copper chemistry in conjugate addition reactions is not surprising that remarkable advances in the asymmetric, catalytic hydrosilylation of α,β -unsaturated systems have occurred over the last few years^{171,172}, largely due to the development of new copper-based catalysts. The first enantioselective catalytic, asymmetric hydrosilylation of α,β -unsaturated esters was published by Buchwald's group¹⁷³ in 1999 (Scheme 17). The catalyst was generated in situ (from CuCl and NaO-t-Bu with (S)-Tol-BINAP as the chiral ligand) and the use of poly(methylhydrosiloxane) (PMHS), {TMSO-[Si(H)Me]_n-OTMS}, was also introduced in this paper. Consistently, good to excellent ee values (80-92%) were obtained over a range of substrates. This process has since been applied by Buchwald's group to the reduction of a variety of other systems including α,β -unsaturated lactones and lactams¹⁷⁴ and cycloalkenones¹⁷⁵.



Scheme 17: Buchwald asymmetric hydrosilylation of α,β -unsaturated esters¹⁷³

In 2006 Lipshutz's group¹⁷² disclosed the first heterogeneous copper-catalysed asymmetric hydrosilylation of enones and enoates by using their new catalyst based on Cu-H in charcoal. Ultrasonication was employed in order to improve the distribution of Cu(II) into the solid.

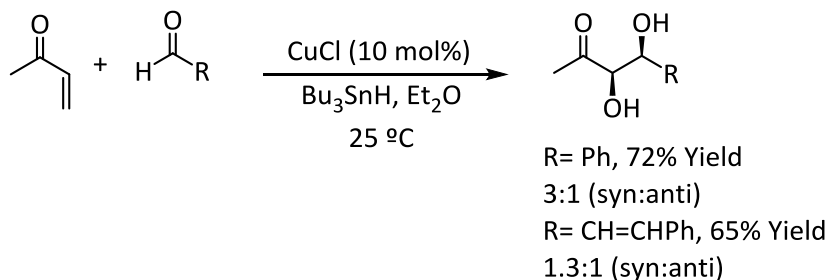
Reduction of carbonyl or imino group by using silane as reducing agent has been reported in presence of different metal transition catalysts; especially Rh, Ir and Ru based catalysts have shown to be very efficient in this kind of transformations. However, the discovery of new catalytic systems which allowed the use of cheaper silanes brought a rebirth in this field and during the last 20 years some new catalyst based on Zn, Cu and Rh have been discovered and developed, what indicates the fast development in this area. There is only one example in the use of a chiral copper hydride in the enantioselective hydrosilylation of prochiral imines that was reported by Lipschutz *et al.*¹⁷⁶ in 2004 (Scheme 18). Using a catalytic amount of copper (I)/ chiral diphosphine system, highly efficiency with regard to both chemical yields and enantioselectivities were obtained.



TMDS = tetramethyldisiloxane

Scheme 18: Cu(I)-catalysed hydrosilylation of imine

The issues of selectivity posed by the aldol reaction continue to inspire the development of increasingly effective protocols for stereocontrolled aldol addition. Following to the pioneering work of Revis in 1987¹⁷⁷, research in the area of catalytic reductive aldol coupling has flourished and in this regard, catalytic systems that employ cost-effective reductants that minimize or entirely avoid generation of stoichiometric by-products has been identified. The first catalytic reductive aldol coupling to employ a copper catalyst was reported in 1998 by K. Maruoka et al.¹⁷⁸ (Scheme 19). Copper (I) chloride in combination with tributyltin hydride showed unique character as an initiator of certain radical reactions, not only by promoting the formation of the enolate but also catalyzing the sequent aldehyde addition by acting as a Lewis acid. Obtaining good products with high isolating yields, this method has been applied to the coupling of vinyl ketones to aliphatic, aromatic and unsaturated aldehydes.



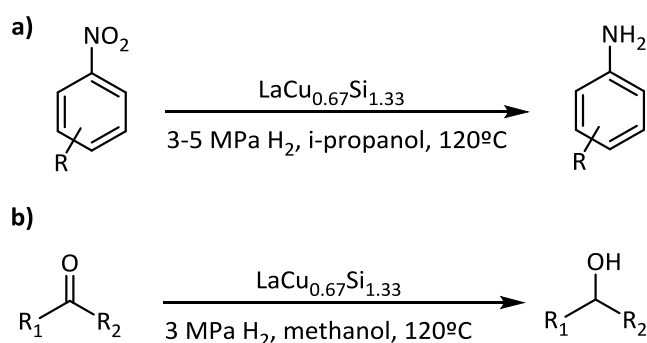
Scheme 19: Copper-initiated radical addition of Bu_3SnH to enones resulting in reductive aldol coupling

In 2005, H.W. Lam et al.¹⁷⁹ reported the intramolecular reductive aldol reaction of α,β -unsaturated esters with ketones catalysed by copper bisphosphine complexes, affording five- and six-membered β -hydroxylactones in high stereoselectivities. This methodology was extended to the synthesis of 4-hydroxypiperidin-2-ones, which are formed through the cycloreduction of corresponding α, β -unsaturated keto-amides. Afterwards, in the same way, some other copper-catalysed reductive aldol coupling have been reported.

Conventionally, the so-called "Stryker's reagent", phosphine-coordinated hexameric copper hydride $[CuH(PPh_3)]_6$, copper hydride species generated in situ from hydrosilanes and copper catalysts¹¹⁷ have been used for this transformation. The use of hydrosilanes¹¹⁷ as a stoichiometric reducing reagent was introduced in 1984 by Brunner¹⁸⁰ and established by

Lipshutz.¹⁸¹ Since then this pattern has been exploited in a wide range of organic transformations. Huanyang Cao et al.⁹⁴, using hypophosphorous acid as hydrogen source, described in 2013 a novel copper catalysed semihydrogenation of alkynes at 130 °C for 4h using hexamethylenetetramine (HMTA) as ligand. In 2015¹¹⁷, a copper catalyst generated in situ from widely available $\text{Cu}(\text{OAc})_2 \cdot \text{H}_2\text{O}$ and imidazolium salt in the presence of *t*-BuOK showed high efficiency for the semihydrogenation of triple bonds. The use of molecular hydrogen (H_2) as reducing agent for this type of reactions was reported by Semba et al¹⁶⁴. In 2016, a readily available copper complex $[(\text{PPh}_3)\text{CuCl}]$, was efficiently employed for the semihydrogenation of internal alkynes to give *Z*-alkenes in a highly stereoselective manner under an atmosphere of H_2 . In 2016 Teichert and co-workers¹⁸² employed an *N*-hydroxyalkyl NHC (*N*-heterocyclic carbene) ligand under a high hydrogenation pressure (100 atm) to selectively obtain *Z*-alkenes from alkynes. Also in 2016 Wakamatsu T. et al¹⁸³, developed a copper-catalysed semihydrogenation system using a commercially available simple *N*-heterocyclic carbene ligand under atmospheric pressure of H_2 , without the requirement of an exogenous proton source.

Also for the reduction of nitroarenes a series of Cu-catalysts were reported, and only few of them in presence of molecular hydrogen as reductant^{184–186}. As example, in 2017, Hosono and co-workers¹⁸⁴ reported a copper based intermetallic electride for the hydrogenation of both nitroarenes to anilines and ketones and aldehydes to alcohols (Scheme 20).



Scheme 20: Copper catalysed reduction of nitroarenes (a) and carbonylic (b) compounds

The Cu-based intermetallic electride $\text{LaCu}_{0.67}\text{Si}_{1.33}$ was found to exhibit excellent catalytic activity for various selective hydrogenation reactions; possessing both a high carrier density and much higher activity than conventional transition metal nanoparticles on oxide or carbon supports.

However, most of copper-based heterogeneous systems for nitro reductions published since 2000 make use of NaBH_4 as reductant. In 2012, H. K. Kadam and S. G. Tilve¹⁸⁷ used CuBr_2 as precatalyst, which was in situ reduced to copper NPs, showing full conversion and high yield of aniline at room temperature after 5 h. Two years later, another in situ approach was reported by P. Bharali and co-workers¹⁸⁸. The effect of different stabilizers (PEG, CMC and PVP) in the CuNPs catalysed reduction of nitroarenes was studied by J. Santhanalakshmi et al.¹⁸⁹ in 2012, showing the lowest activity of PVP, while PEG and CMC presented a similar one. Biomass-derived catalysts have been reported by C. Tamuly and co-workers¹⁹⁰ (2014) and A. R. Fajardo and co-workers¹⁹¹ in 2017. In the first case, CuO nanoparticles using the peel of *Musabalbisiana* with flower like hierarchical architectures was reported, while in the second one CuNPs were synthesized and stabilized into a chitosan/poly(vinylalcohol)(CP) based film

using a simple protocol under mild conditions. A number of composites in which iron is used as the magnetic core in order to obtain an easily separable material have been reported. In 2014, R. K. Sharma and co-workers¹⁹² demonstrated Cu(II) on silica-coated Fe₃O₄ as magnetically separable core-shell composite (Figure 6) for the reduction of nitroarenes in water. Freshly prepared iron NPs were activated with 0.1 M HCl in ethanol and water, followed by the addition of 25% NH₄OH and TEOS. Once the material was isolated, it was grafted covalently with Cu(Acac)₂ in chloroform and in the presence of NaBH₄ it catalytically active for the reduction of nitroarenes within up to 1 h.

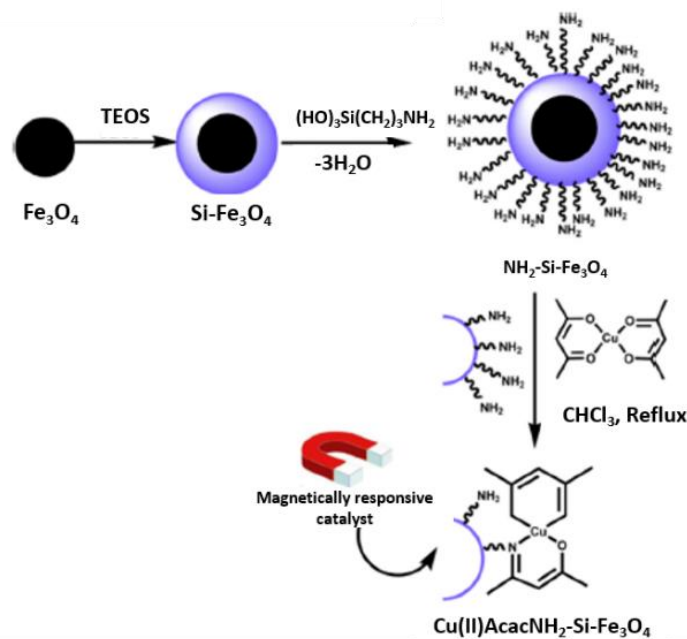


Figure 6: Synthesis of a magnetically separable copper-based catalyst for nitroreduction, as reported by R.K. Sharma and co-workers.¹⁹²

Same as the previous system, other several approaches for a magnetically separable Cu-catalyst has been described in literature^{193–196}.

Copper on coordination polymers as reusable catalysts has also been demonstrated to be efficient in this kind of reaction. Recently, in 2017, S.P. Anthony and co-workers¹⁹⁷ synthesized seven different materials by complexation of Cu²⁺ with and amino acid-based reduced Schiff base ligand, showing high efficiency in presence of NaBH₄ in the nitro reduction.

Highly chemoselective heterogeneous systems for the reduction of nitroarenes, using a hydrogen transfer methodology, has also been developed in the presence of different reducing agents such as ammonium formate¹⁹⁸, isopropanol¹⁹⁹, hydrazine hydrate^{200,201},...

However, despite the high diversity of applications in which copper has been involved, further research should be devoted to the design of durable heterogeneous catalysts that enables organic chemistry to be exploited competently on a large scale with negligible copper contamination of the products. In view of the economic and green surrounding issues, avoiding the huge and costly ligands would be an attractive alternative for this type of transformations.

1.4 Enabling technologies in heterogeneous catalysis

Due to the great worry about the environmental situation, industrial safety and sustainable development, attractive alternative processes are urgently required and always welcome. As described by Kumar et al. in 2012²⁰², different techniques have been developed and reported for process intensification (PI) in green synthesis. PI technologies comprise a wide number of advantages such as shorter reaction time, energy sufficient, waste reduction, improvement process flexibility and so, the interest and the number of publications in this field has vastly increased during the last decades.

Enabling technologies²⁰³ can be defined as equipment's or/and methodologies that alone or in combination are able to replace conventional methods and develop more efficient alternative environmental procedures.

In recent years these so-called non-conventional energy sources, such as microwaves (MW), ultrasound (US), ball mill (BM) and microreactors have made access to much simpler chemical procedures by using heterogeneous catalysts, greener solvents and promoting faster and more selective transformations. Scientists are recently devoting a great deal of research to design lower impact protocols to operate, and lot of different fields have already been extremely promoted by these alternative technologies. Recently, a review took stock of alternative technologies currently available in laboratories that facilitate the synthesis of organometallic complexes²⁰⁴ and allow the access to compounds that cannot be obtained in any other way. Moreover, access to cyclodextrines derivatives²⁰⁵ in much simple ways, extractions of a number of compounds²⁰⁶⁻²⁰⁸ and a wide amount of synthetic processes²⁰³ are all key developments in the design of greener protocols.

Besides batch reactors, in the last decade these techniques have been adapted to flow systems²⁰⁹⁻²¹³, which provide greater efficiency, flexibility, lower energy consumption and easy scale up. In 2012, Morschhäuser et al.²¹⁰ introduced the microwave-assisted continuous flow synthesis in industrial scale as a safe and highly energy efficient process for organic reaction mixtures (with or without solvent) under high-temperature/high-pressure conditions. In the same way, the effect of ultrasound^{209,213} has also been demonstrated to have a great effect while performing continuous flow.

As science moves forward, so does our need to properly harness all the new technologies and better integrate all disciplines and contributing knowledge generators. The current search for energy-saving and more selective protocols has turned ultrasound and microwave into useful alternatives to prolonged heating in metal-catalysed reactions.

1.4.1 Microwave irradiation.

1.4.1.1 Technique

In 1940s, Percy Spencer observed accidentally the heating phenomenon with microwaves when he realized that the candy bar in his pocket melted while working on radar technology. Further investigation showed that microwaves could increase the internal temperature of food much faster than a conventional oven, so this led to the production of the first commercial domestic microwave oven in 1954. From 1986, when Gedgy et al.²¹⁴ and Giguere et al.²¹⁵ published the first application of commercial microwave oven for organic synthesis, this technology has been widely developed^{216,217}. Thanks to its environmentally friendly and

efficient nature, nowadays microwaves signify a versatile tool that attracts worldwide researchers' attention.

Organic transformations were firstly performed by domestic microwave ovens^{218,219}, however, the literature results were therefore accompanied by uncertainties relating to both reproducibility and safety. The introduction of purpose-built microwave units for synthetic organic chemistry has enlarged the range of applications over the years, especially with the development of the monomode reactor designed for synthesis. Recently, de la Hoz et al.²²⁰ published a critical review about the effect of microwave irradiation in organic synthesis. It is surprising that even now when microwave irradiation is a well-established methodology, the number of publications is still increasing (Figure 7). This indicates that the topic remained of high interest to academic and industrial chemists alike and there is every sign to expect similarly active developments in the future.

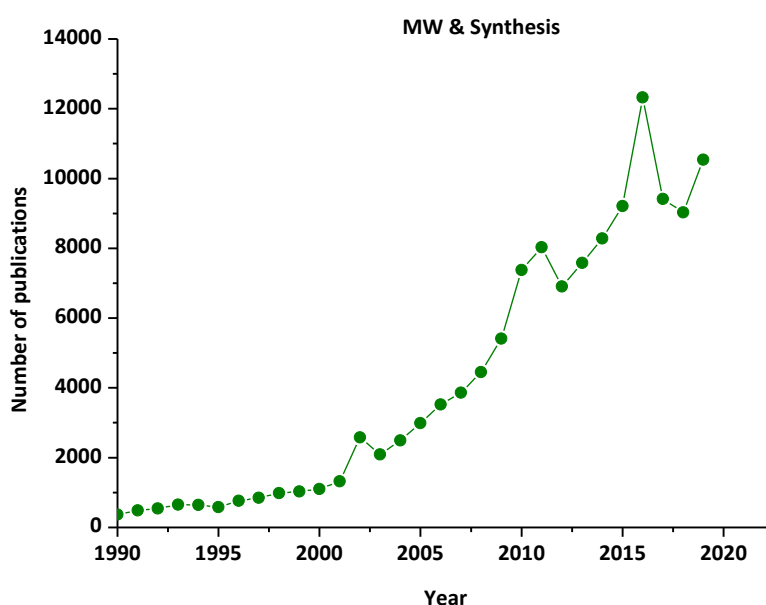


Figure 7: Number of publications in Microwave Assisted Organic Synthesis (MAOS).

The range of microwaves irradiation (Figure 8) is defined from 0,3 and 300 GHz, but every domestic system and laboratory oven operates at 2.45 GHz of frequency, what correspond to 12.24 cm of wave length and $1.6 \cdot 10^{-3}$ eV of energy. This frequency was set because it is in the centre of the unlicensed ISM (Industrial, Scientific and Medical) band and therefore, its use avoids any kind of interference with the telecommunications applications. The energy coming from microwave irradiation is not enough to induce chemical reactions, so the influence of microwave energy on chemical transformations is strictly thermal.

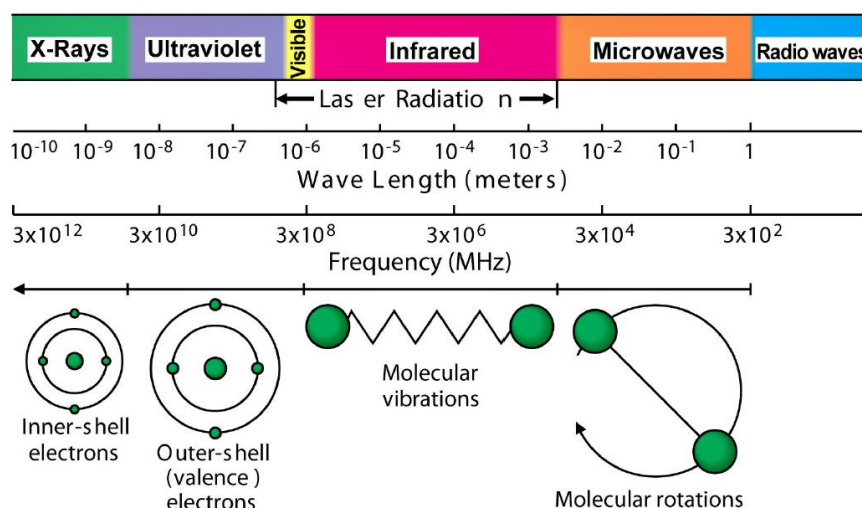


Figure 8: Microwave range in the electromagnetic spectrum.

The reaction rate (k) increases proportionally with the increase of absolute temperature (T) and frequency factor (A) and decreases proportionally with the increase of transition state energy (ΔG^\ddagger , i.e. energy activation). Thus, the increase in the pre-exponential factor A , which is representative of the probability of molecular impacts, could enhance reaction rates. This collision efficiency can be effectively influenced by mutual orientation of polar molecules involved in the reaction. As this factor depends on the atoms vibration frequency at the reaction interface, it could be postulated that microwave field might affect it²²¹.

$$k = A \exp(-\Delta G^\ddagger/RT)$$

Electromagnetic radiation combine both electric and magnetic field, propagating through the space and carrying out the energy. The electric component is the responsible of microwave heating effect by two different mechanisms (Figure 9): dipolar polarization and ionic conduction. Dipolar polarization refers to an interaction in which polar molecules try to align themselves with the fast changing electric field of the microwave. The second method of transferring energy is ionic conduction, which appears if there are ionic species or free ions present in the substance being irradiated.

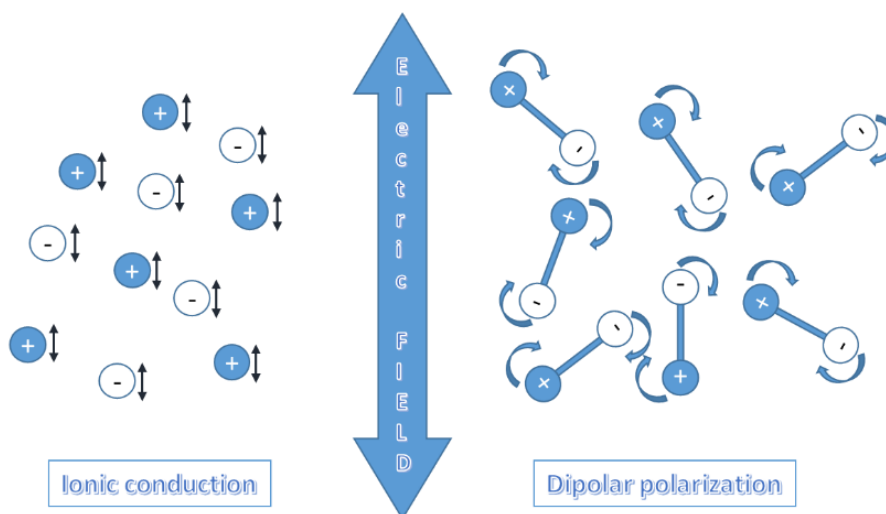


Figure 9: Microwave heating effect: ionic conduction and dipolar polarization.

Solvents constitute one of the crucial components and play an important role in organic synthesis, having a big influence in the reaction outcome. Since microwave directly couple with the molecules present in the reaction mixture, the characteristic of the solvents (and concretely its polarity) become a significant component. The more polar a reaction mixture is, the higher is the ability to absorb microwave irradiation and the rapid its temperature rises.

Many factors characterize the polarity of a solvent. The main individual solvents absorbing characteristics are dielectric constant, dipole moment, tangent delta and dielectric loss. The dielectric constant can be defined as the ratio of the electric permeability of the material to the electric permeability of free space, and so, the ability of the solvent to store electric charges. The dipole moment is the product of the distance between the centres of charge in the solvent molecule multiplied by the magnitude of the charge. The molecules having a large dipole moment have also a large dielectric constant. The tangent delta, also known as the loss tangent, describes how efficiently microwave energy is converted into thermal one. The parameter that best provides the coupling efficiency of a particular solvent is the dielectric loss, what define the amount of input microwave that is lost to the sample and is dissipated as heat.

Solvent (bp °C)	Dielectric Constant (ϵ')	Solvent	Tan δ	Solvent	Dielectric Loss (ϵ'')
Water (100)	80.4	Ethylene Glycol	1.350	Ethylene Glycol	49.950
Formic Acid (100)	58.5	Ethanol	.941	Formic Acid	42.237
DMSO (189)	45.0	DMSO	.825	DMSO	37.125
DMF (153)	37.7	2-Propanol	.799	Ethanol	22.866
Acetonitrile (82)	37.5	1-Propanol	.757	Methanol	21.483
Ethylene Glycol (197)	37.0	Formic Acid	.722	Nitrobenzene	20.497
Nitromethane (101)	36.0	Methanol	.659	1-Propanol	15.216
Nitrobenzene (202)	34.8	Nitrobenzene	.589	2-Propanol	14.622
Methanol (65)	32.6	1-Butanol	.571	Water	9.889
NMP (215)	32.2	Isobutanol	.522	1-Butanol	9.764
Ethanol (78)	24.3	2-Butanol	.447	NMP	8.855
Acetone (56)	20.7	2-Methoxyethanol	.410	Isobutanol	8.248
1-Propanol (97)	20.1	<i>o</i> -Dichlorobenzene	.280	2-Butanol	7.063
MEK (80)	18.5	NMP	.275	2-Methoxyethanol	6.929
2-Propanol (82)	18.3	Acetic Acid	.174	DMF	6.070
1-Butanol (118)	17.1	DMF	.161	<i>o</i> -Dichlorobenzene	2.772
2-Methoxyethanol (124)	16.9	1,2-Dichloroethane	.127	Acetonitrile	2.325
2-Butanol (100)	15.8	Water	.123	Nitromethane	2.304
Isobutanol (108)	15.8	Chlorobenzene	.101	MEK	1.462
1,2-Dichloroethane (83)	10.4	Chloroform	.091	1,2-Dichloroethane	1.321
<i>o</i> -Dichlorobenzene (180)	9.9	MEK	.079	Acetone	1.118
Dichloromethane (40)	9.1	Nitromethane	.064	Acetic Acid	1.079
THF (66)	7.4	Acetonitrile	.062	Chloroform	0.437
Acetic Acid (113)	6.2	Ethyl Acetate	.059	Dichloromethane	0.382
Ethyl Acetate (77)	6.0	Acetone	.054	Ethyl Acetate	0.354
Chloroform (61)	4.8	THF	.047	THF	0.348
Chlorobenzene (132)	2.6	Dichloromethane	.042	Chlorobenzene	0.263
<i>o</i> -Xylene (144)	2.6	Toluene	.040	Toluene	0.096
Toluene (111)	2.4	Hexane	.020	<i>o</i> -Xylene	0.047
Hexane (69)	1.9	<i>o</i> -Xylene	.018	Hexane	0.038

Table 4: Dielectric constant (ϵ'), tan δ and dielectric loss (ϵ'') for 30 common solvents (measured at room temperature and 2450 MHz)

Table 4 gather a list of solvents that can be divided in three different groups: low, medium and high absorbing solvents. The low absorbing molecules are those that have dielectric losses smaller than 1.00. Medium absorbers would generally have values between 1.00 and 13.99 and high absorbers upper than 14.00.

Sometime, the use of a very low absorbing solvent as hexane when performing a reaction under microwave electric field can help to selectively heat the other absorbing molecules in the media, allowing a selective and more efficient process.

Another important parameter when talking about microwave irradiation is the penetration depth (D_p)²²². According to the definition, the penetration depth is the point where only 37% of the initially irradiated microwave power is still present. These values are only tabulated for a few materials and only for one temperature or for a small range of temperatures. Because the penetration depth and the dissipation factor are both strongly dependent on temperature, this fact has to receive special attention for the scaling-up of chemical reactors for industrial applications.

Some of the penetration depths of the microwaves in common solvents at room temperature are listed in Figure 10. Particularly significant is that the penetration depth of the 2.45 GHz microwaves into almost all non-polar solvents tends to be rather extensive compared to the one in polar solvents.

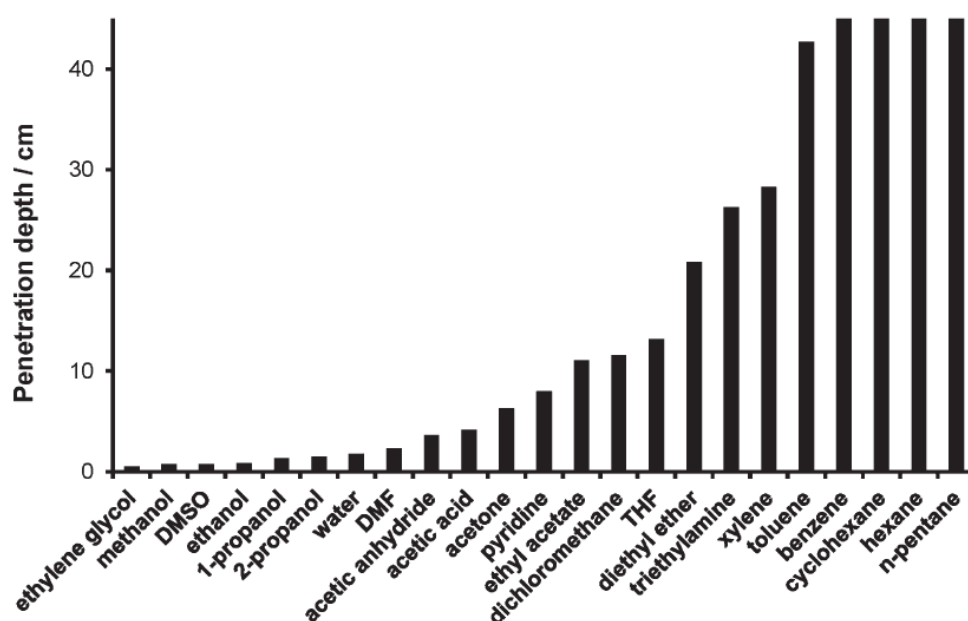


Figure 10. Penetration depths of the 2.45 GHz microwaves for some common solvents. Reproduces from Horikoshi et al. Copyright 2008 by the American Chemical Society.

Since it is directly proportional to the value of λ ($D_p \propto \lambda$), when increasing the frequency of the microwave irradiation, the penetration depth of the electric wave decreases (Figure 11).

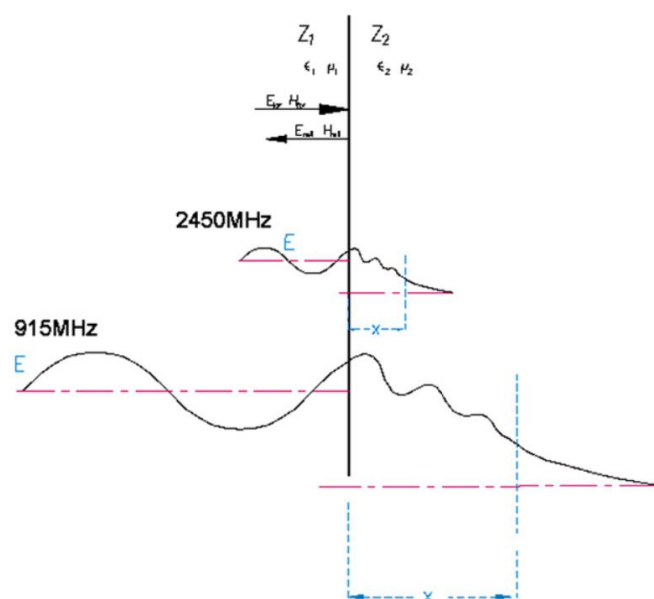


Figure 11: Penetration depth (denoted with blue x) of the electric wave decreases with increasing frequency. The left side represents air, the right side a material.

1.4.1.2 Microwave in heterogeneous catalysis

Shortly after the discovery of the beneficial effects of microwave irradiation on organic synthesis, the field underwent a rapid and broad expansion. Several books and reviews were published providing regular updates on the ever-increasing growth of this research field, with a recent example that focuses on the application of microwaves in catalysis. In 2009, Varma²²³ introduced the application of solid catalysts to microwave-assisted organic synthesis (MAOS). More recently, in 2017, Kokel et al. published a review focusing on the application of microwaves in heterogeneous catalysis²²⁴ and since then a broad array of new heterogeneous catalytic applications have been reported and reviewed periodically.

Despite of the risk that using metal particles inside the microwave cavity can cause, it is possible to perform organic catalytic reactions by using well-dispersed metal particles in a high boiling point polar solvent. Whittaker and Mingos²²⁵ described this process in 1995 and defined all the main safety features to reduce the risk of arcing. After that, several reactions have been carried out in the presence of solid catalysts for a potential application of microwave radiation in materials synthesis. Tsukahara and co-workers²²⁶ reported the occurrence of non-equilibrium local heating of DMSO molecules in the proximity of Co and Fe particles. Such non-equilibrium local heating led to enhanced dechlorination of 2-chloroethylbenzene and 4-phenylbutyl chloride since the reaction field temperature for the microwave system was approximately 55 K greater than the bulk solution temperature (473 K) under microwave irradiation. In 2011, Gutmann and co-workers²²⁷ showed that formation of an organomagnesium Grignard reagent could be both activated and deactivated by the microwaves' electric field strength. They attributed the activation as resulting either from a "cleansing effect" on the Mg surface or from the formation of more reactive spherical Mg particles due to mild electrostatic discharges (arcing) between individual Mg turnings. Also, in 2011, Horikoshi and Serpone²²⁸ described the generation of hot-spots and their impact in the heterogeneous Suzuki-Miyaura coupling reaction for the synthesis of 4-methylbiphenyl in toluene solvent in the presence of Pd/AC. In this case, the generation of hot-spots in the

heterogeneous catalysed reaction system occurring in a nonpolar solvent had a negative impact on the reaction product (Figure 12).

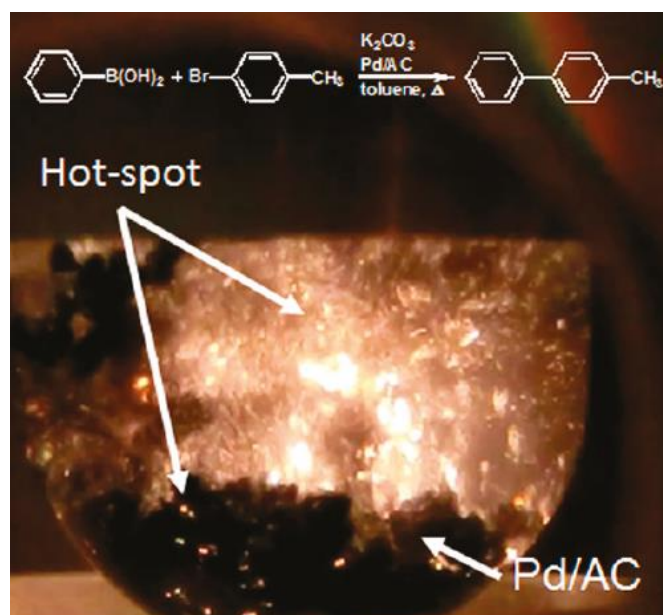


Figure 12: High-speed camera photographs of the electric discharges occurring on the Pd/AC catalyst surface during the Suzuki-Miyaura coupling reaction under E-field conditions (120 s irradiation). Reproduces from Horikoshi et al. Copyright 2011 by the American Chemical Society²²⁸

Given the usually excellent microwave absorption capability of most solid catalysts, it is beyond doubt that the combination of microwave activation with heterogeneous catalysis carries almost unlimited opportunities in synthesis design for environmentally benign processes.

1.4.2 Ultrasound irradiation

1.4.2.1 Technique

Ultrasound can be defined as the sound of a frequency beyond that to which the human ear can respond. The usual range of human hearing is between 16 Hz and 18 kHz, so the ultrasound range can be considered from 20 kHz to 500 MHz (Figure 13).

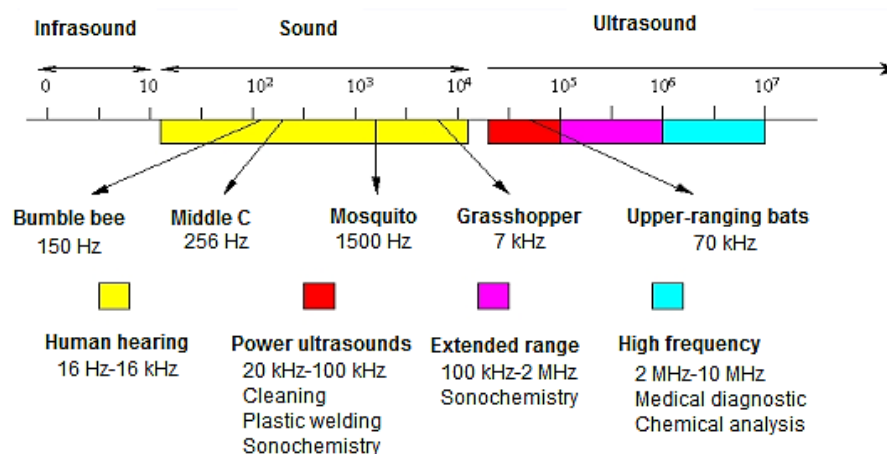


Figure 13: The frequency ranges of the sound

The use of low ultrasonic power and very high frequencies (MHz) do not affect the physical or chemical character of the medium that is probed, so they are widely used in a whole range of sophisticated techniques for non-destructive testing and medical²²⁹ imaging; all essentially based on the pulse-echo technique. On the other hand, the use of lower frequencies (mostly from 20-40 kHz) and higher power can produce significant physical and chemical variations in the medium through the generation and subsequent collapse of cavitation bubbles. This constitute the basis of sonochemistry.^{230,231} Therefore sonochemistry can be defined as a branch of chemical research based on the effect that acoustic cavitation produce by ultrasonic power on chemical reactions.

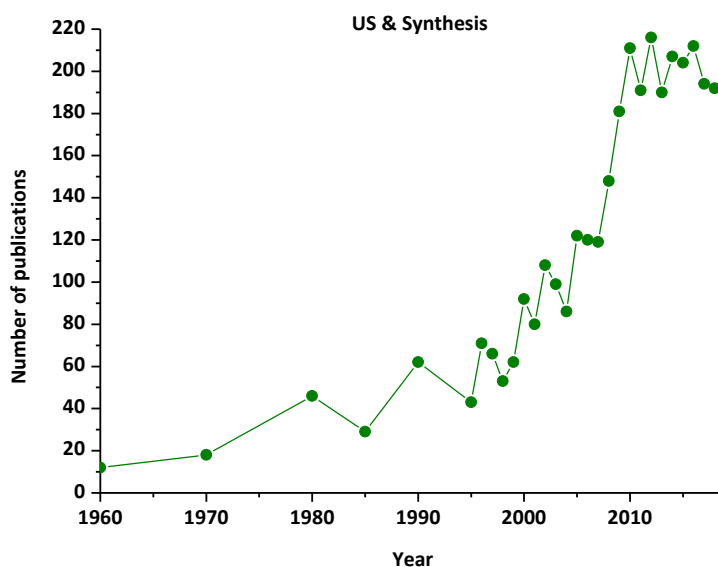


Figure 14: Number of publications in Ultrasound Assisted Organic Synthesis.

If we imagine a bubble suspended in a liquid and then we send sound through that liquid, the bubble will expand and contract with the expansion and compression waves of the sound. This oscillation, growth, and potential rapid collapse of the bubble occurs in all liquids irradiated with sufficient intensity of sound or ultrasound and is called “acoustic cavitation”. Immediately before the commencement of collapse, the bubble has some total energy that will converse into heat inside the bubble and define the origin of both sonochemistry and sonoluminescence.

The chemical effect observed by ultrasonic irradiation can be explained by the formation, expansion and following collapse of cavitation bubbles²³¹ (Figure 15, Figure 16). It is the fact of these bubbles collapse that generates the necessary energy for chemical and mechanical transformations. The production of very high local temperatures (≈ 5000 °C) and pressures (more than 1000 atm) are the responsible of these unique effects.

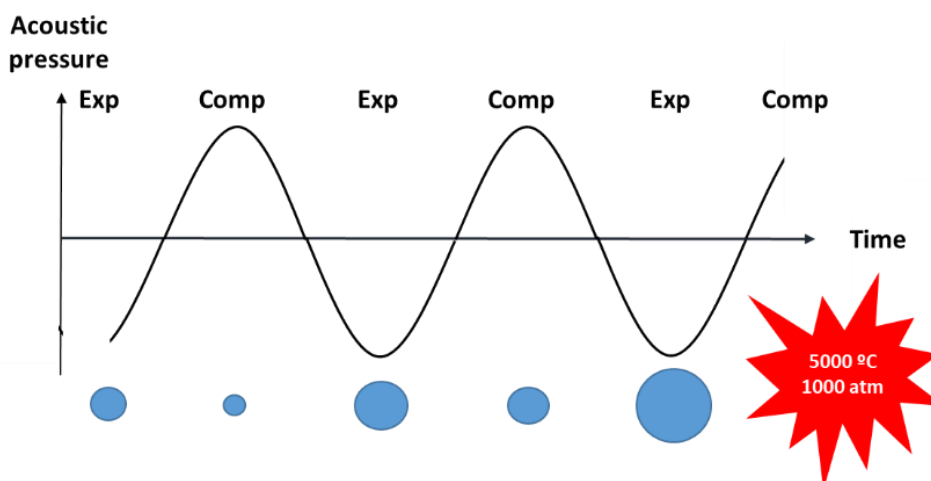


Figure 15: Chemical effect of ultrasonic irradiation.

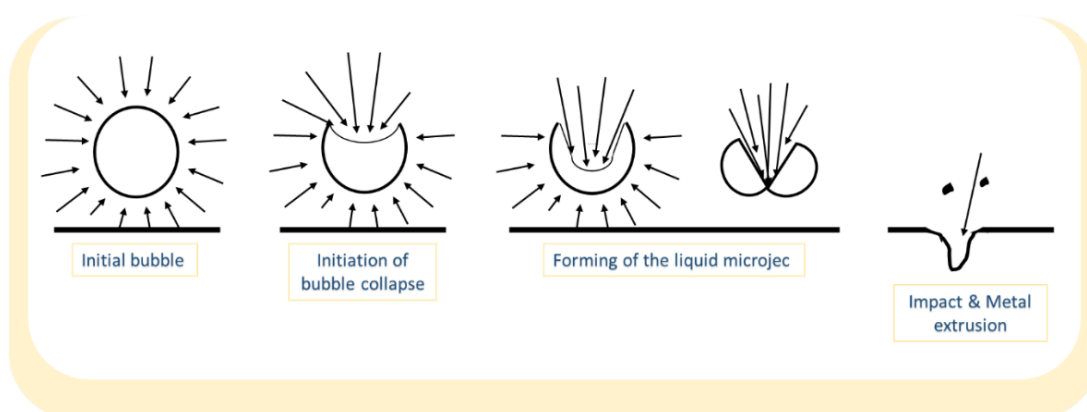


Figure 16: Formation, expansion and collapse of cavitation bubbles.

Two different methods for the introduction of ultrasound into a system can be principally describe, the ultrasonic cleaning bath and the ultrasonic prob. Both systems rely upon the piezoelectric transducer as an ultrasound source. One of the main disadvantages is the fact of having an optimum performance when a fixed frequency (that depends on the particular transducer) is applied. In most cases, the optimum frequency for commercial baths is around 40 kHz and for commercial probes is around 20 kHz.

Although the ultrasonic bath is the cheapest and widely used source of ultrasounds, some disadvantages can be named if comparing with the probes. Like any other sound wave, ultrasound is propagated via a series of compression and rarefaction waves induced in the molecules of the medium through which it passes. This fact suppose that the amount of energy that reaches the reaction while working with the sonic-bath is very low (normally between 1 and 5 Wcm^{-2}).

The nature of sonochemical reactions has been widely studied and a set of empirical rules²³² has been established in order to provide some clues and better understand the effects of this irradiation.

- a) In homogeneous reaction, the chemical effects can be explained by assuming that sequential electron transfers are favoured by ultrasonic irradiation.

- b) In heterogeneous liquid-liquid or solid-liquid reactions, bubbles cavitation near the interface will cause disruption and mixing, resulting in the formation of fine emulsions, and therefore being particularly beneficial in the enhancement of phase-transfer catalysis.
- c) In heterogeneous reactions, the biphasic system will also be subjected to the mechanical component of shock waves, in addition to the chemical activation.

Same as when working with microwave irradiation, controlling external parameters such as amplitude, frequency, temperature and type of ultrasonic generator is crucial when describing sonochemical protocols.

1.4.2.2 Ultrasound in heterogeneous catalysis

The generation of high kinetic energy from mechanical energy obtained from cavitation phenomena is also considered as a green process intensification. Ultrasound is known for its capacity in enhancing particles dispersion and favoring mechanical depassivation. In this way, a liquid in which discrete particles are homogeneously distributed is created and due to this, reactions involving metals represent one the favourite domain of sonochemistry. Homogenization of heterogeneous phases and catalyst dispersion entails a higher catalyst surface and so, a more efficient process. Among the three different methods of introducing ultrasound into a reaction media (cleaning bath, ultrasonic probe and the ultrasonic continuous reactor), the sonic probe can be considered the most efficient one since the energy heads straight into the reaction solution. This system has proved to be particularly effective when referring to an efficient mixing and higher mass transport. The well-known cleaning effect of ultrasonic waves not only provides a depassivated layer, but also facilitates the diffusion of the reagent from the solution to the metal, the electron transfer from the active surface to the reducible point of the organic substrate, and finally the extraction of an ion from the surface to generate a soluble product.

The first commercial application of ultrasound dates back to 1917 with the echo sounding technique developed by Langevin for estimation of the depth of water. By the 1960s,^{233,234} the industrial uses of power ultrasound were well accepted and from this moment it has been developed a whole range of techniques based on this irradiation^{235,236}. Already in 1986, Suslick et al.²³⁷ discovered that ultrasonic irradiation of nickel powder increases its activity as a hydrogenation catalyst by $>10^5$. They found that ultrasonic irradiation of the powder causes remarkable changes in particle aggregation, surface morphology, and thickness of the surface oxide coating. Another typical example is the acid-catalysed acetalisation of sugars published in 1986 by Luche et al. With mechanical stirring, the reaction is slow and side products resulting from acid catalysis accompany the process. These ionic side reactions remain unaffected by sonication but the heterogeneous ketalisation is accelerated due to an efficient agitation process, resulting in being a cleaner and high-yielding reaction. In 2010, Cravotto et al.²³⁸ described a copper catalysed azide-alkyne cycloaddition promoted by ultrasound irradiation claiming that US favors mechanical depassivation and enhances both mass transfer and electron transfer from the metal to the organic acceptor.

US has also been widely used in organic synthesis on heterogeneous system involving immiscible liquids, since sonication can produce very fine emulsion and allows any reaction between these species in the interfacial region. Thus, in many heterogeneous reactions, the application of US can have the same effect as a different high-speed agitator in which fluids

do not cavitate. In some cases, sonochemistry can completely remove the need for phase transfer agents, as is the case in the generation of dichlorocarbene by the direct reaction between powdered sodium hydroxide and chloroform at 40 °C using an ultrasonic bath.²³⁹

1.4.3 Combined microwave and ultrasound irradiation. Synergic effects.

1.4.3.1 Technique

Synthetic chemists are more and more paying attention to combinations of enabling technologies in order to achieve the double goal of having highly efficient transformations while getting energy and time saving.

As already described, more efficient and more selective transformations have been observed thanks to the use of non-conventional techniques such as microwave and ultrasound. Aiming to obtain more effective, cleaner and safer processes, during the last years, several research groups have been focused on developing a hybrid combination of these two irradiation sources, what represents a valuable tool in process intensification. However, the combination if these two techniques should involve safety and technical considerations. Because of their different nature and the incompatibility to different conditions and materials, the combination of MW and US reactors may be potentially hazardous and so, knowing the restrictions of the system and the reaction is fundamental before applying the combined irradiation (Table 5).

Table 5: US versus MW: a matter of striking differences. Reproduces from G. Cravotto et al.²⁴⁰

Application	Ultrasound	Microwaves
Reaction media	Aqueous and organic solvents	MW-absorbing liquids, solvent-free protocols
Use of bulk metals	Favourite domain	Forbidden practice
Acceleration	Variable (from min to h)	Large (min, even seconds!)
Activation	Cavitation	Thermal effects (specific non-thermals)
Scaling-up	Possible but still a challenge	Possible
Chemical effects	Selectivity changes, mechanistic switching, waste reductions	Selectivity changes, waste reductions
Other effects	Light emission, cleaning, micro streaming	Heating above boiling points, change in solvent properties

For example, the sonic horn it is usually made of titanium, but if we want to insert it inside the microwave chamber, evidently, a piece of metal can be dangerous. Hence, to overcome this problem, in our group it has been developed a combined system by inserting an ultrasonic horn made of pyrex inside the modified cavity of a multimode microwave oven (Figure 17). Both sources can be coupled in sequential or simultaneous modes^{240–244}.



Figure 17: Combined MW/US reactor.

This combination of both sources in a single process can enhance the heat and mass transfer as well as the catalytic effects on selected reactions, providing a reliable and cost-effective strategy for improving synthetic transformations efficiency. Prevention of agglomeration and dispersion achieved by ultrasonic cavitation and selective heating acquire thanks to the microwave irradiation, allow a tremendous combination that represents an emerging technological innovation that deserves widespread attention in fine-chemical and pharmaceutical research.

This combination represents an emerging technological innovation that during the last ten years has undergone a great increase (Figure 18).

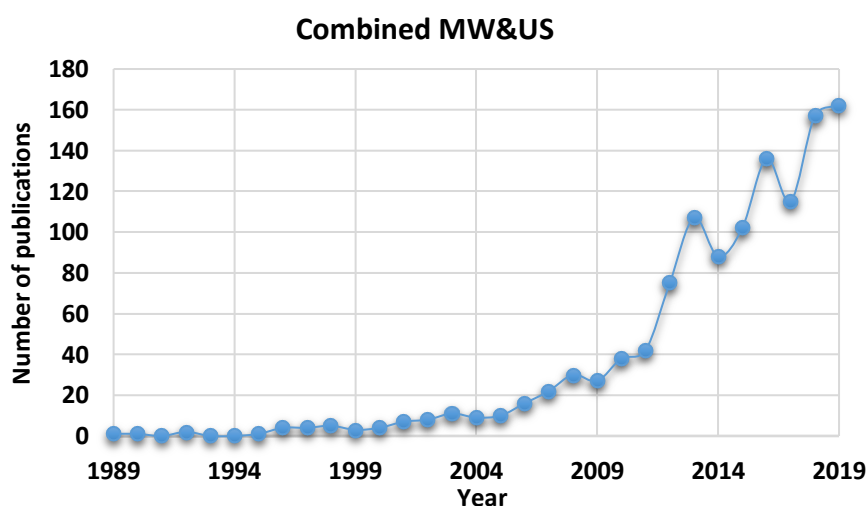


Figure 18: Number of publications for MW/US combined irradiation since 1989.

1.4.3.2 Combined MW and US in heterogeneous catalysis

The first paper on this subject was published in 1995 by M.Maeda et al. who reported the chemical effects achieved under this combined irradiation. One year later, J.Berlan and coworkers²⁴⁵ described the application of the system in organic reactions, and in particular, for pyrolysis and esterification.

Combined MW/US irradiation can either be performed in simultaneous mode or otherwise sequentially by circulating the reacting mixture through the two compartments.²⁴⁶

In our group, this combined irradiation has been studied already for several years. In 2007, Cravotto and Cintas²⁴⁰ described a number of examples showing that combined US/MW irradiation represents an emerging technological innovation that deserves widespread attention in fine-chemical and pharmaceutical research. The same year, in collaboration with Palmisano²⁴³, Heck coupling reactions were performed ligandless and with very low catalyst load under MW and US irradiation. In 2011²⁴⁴, leveraging the increased of glycerol production, this compound was used as solvent in three different organic transformations: the catalytic transfer hydrogenation of benzaldehyde to benzyl alcohol in which glycerol plays the dual role of the solvent and hydrogen donor, the palladium-catalysed Suzuki cross-coupling; and the Barbier reaction. Glycerol allowed excellent acoustic cavitation and combined with microwave the efficacy of the process was increased.

1.4.4 Mechanochemistry

1.4.4.1 Technique

Mechanochemistry is frequently used in a broad sense, covering any chemical reaction induced mechanically. During the last years, this technique is becoming more intensely studied and several reactions between solids have been promoted quickly and quantitatively, with either no solvent addition or only nominal amounts.

IUPAC defines a mechano-chemical reaction as a “chemical reaction that is induced by the direct absorption of mechanical energy” with a note “shearing, stretching, and grinding are typical methods for the mechano-chemical generation of reactive sites, usually macroradicals, in polymer chains that undergo mechano-chemical reactions”.

In May 2014, around 100 experts gathered to discuss about the rising importance of mechanochemistry in making, understanding and manipulating molecules. The entitled Mechanochemistry: “From Functional Solids to Single Molecules,²⁴⁷ the 256th Faraday Discussion” brought together a diversity of academic and industrial researchers, experimentalists and theoreticians, students, as well as experienced researchers, to discuss the changing face of mechanochemistry.

Two main reasons make mechanochemistry an appealing technique. Firstly, our current dependence on solvents appears increasingly unsustainable since it is wasteful of fossil-derived, environmentally problematic, hazardous and energy-demanding with regard to solvent production, purification and recycling. Secondly, it is increasingly clear that is effective, and even advantageous, in ever-widening types of synthesis.²⁴⁸ The hallmark of mechanochemistry is achieving chemical transformations by milling or grinding, without the need of bulk dissolution of reactants.

The easiest way of performing mechano-chemical reactions is by manual methods, using the mortar and the pestle. The rubbing of the pestle on the sides of the mortar and the friction of reagents the one against the other, provide the energy required to proceed the reaction and to obtain the final products, which can be recovered directly without adding any additional solvent. Grinding is the general term used for describing the mechanical action by hard surfaces on a material, normally to break up the material and reduce its particle size.

Very small amounts of added liquid can dramatically accelerate, and even enable, mechanochemical reactions between solids.

To realize more intense and effective homogenization compared to that obtained using the hand mortar, specific mills instruments, known as ball-mill, are commercially available. There are a number of different types of mills on the market differing in their capacity, speed of operation and their ability to control the operation; however, on a laboratory scale, the planetary ball mill is most common one. All reagents are introduced into a grinding jar in the presence of one or more balls (or beads) and the jar rotates around a central axis, while spinning around its own axis. All grinding jars in turn undergo a rotational movement in the opposite direction compared to that induced by a wheel (or disk) on which they are fixed. The dynamic energy necessary to convert reactants to products derived from the impact forces and friction generated by the difference in speeds between the balls and the jars (Figure 19).

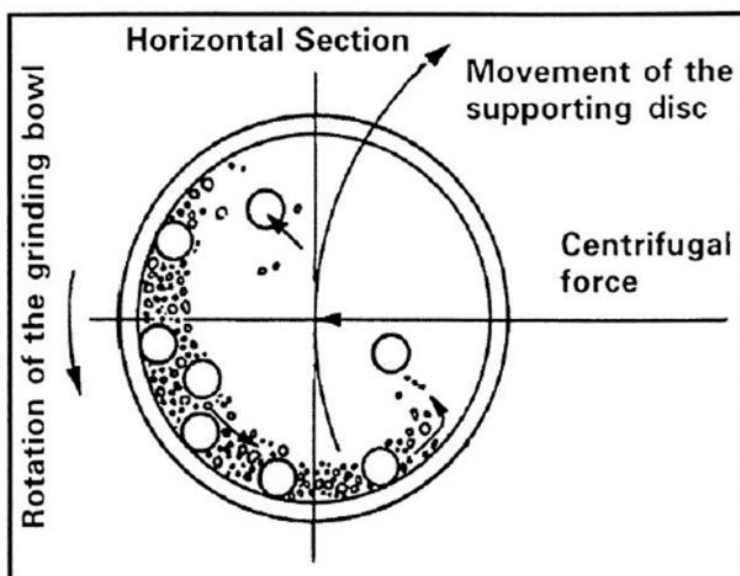


Figure 19: Schematic depicting the ball motion inside the ball mill.

Such planetary motion creates centrifugal forces which emulate the effect of gravity in industrial-scale roller mills, offering a direct connection to scale-up on an industrial scale.

In contrast to manual grinding, which is open and susceptible to a range of environmental factors, ball milling offers an enclosed solvent-free reaction environment with well-defined parameters for optimizing reactivity. Some of the parameters that have an important effect are: type of mill, milling container, milling speed, milling time, type, size and size distribution of the grinding medium, ball-to-powder weight ratio and milling atmosphere. The most modern versions of these instruments allow also the control of the reaction temperature thanks to a heating or cooling system inside.

Modern mechanochemistry²⁴⁹ is rapidly expanding into almost every area of chemistry and materials science, changing its focus from alloying and inorganic materials²⁵⁰ to catalysis, selfassembly,²⁵¹ and synthesis of molecular structures.²⁵² Recent progress in this area has been done by the Boldyreva group,²⁵³ who demonstrated that different types of mechanical motion can lead to different products and reaction kinetics in the same milling vessel.

1.4.4.2 Mechanochemistry in heterogeneous catalysis

The past decade has witnessed an explosive growth of interest in mechanochemical reactions by milling or grinding, and rapid expansion of mechanochemical methodologies into different areas of chemistry, from supramolecular chemistry and organic synthesis to metal-organic frameworks and nanoparticle synthesis. Metal-promoted and metal-catalysed reactions have been widely employed in contemporary organic synthesis, and their mechanochemical reactions have been reviewed²⁵⁴. This vibrant progress claims that most chemical transformations established in solution can be conducted and improved by mechanochemical techniques, such as neat grinding or liquid-assisted grinding (LAG). Whereas most pioneering work in organic mechanochemistry has focused on stoichiometric reactions, it is now clear that mechanochemistry offers access to a rich variety of metal-catalysed or organocatalytic transformations. Palladium-catalysed reactions are one of the most important and most extensively investigated transition metal-catalysed transformations. In 2000, Nielsen and co-workers²⁵⁵ explored the solvent-free coupling of aryl halides and phenylboronic acid in a planetary mill catalysed by Pd(PPh₃)₄, obtaining the Suzuki product in very good yields. Few years later, another report of a mechanochemical Suzuki coupling conducted by manual grinding was provided by Braga et al.²⁵⁶, who performed the synthesis of 1,10-disubstituted ferrocene derivatives by grinding together 1,10-ferrocenediboronic acid with either 4-bromopyridine or 5-bromopyrimidine in the presence of a palladium catalyst dispersed on solid support (Al₂O₃-KF or Al₂O₃-KOH). More recently, Klingensmith and Leadbeater²⁵⁷ reported the ligand-free Suzuki reaction using Pd(OAc)₂ in a mixer mill operating at 30 Hz. The Heck reaction is another powerful palladium-catalysed coupling reaction for the formation of C-C bonds, involving aryl or vinyl halides and activated alkenes. The first report of a mechanochemical Heck coupling was in 2004, when Tullberg and co-workers²⁵⁸ conducted the reaction of aryl halides and protected amino acrylates in a planetary ball mill and from that study a number of publications have been reported for this transformation.²⁵⁹⁻²⁶¹

Copper-catalysed reactions have also been widely implemented in ball mill. The mechanochemical protocol for azide-alkyne cycloaddition was firstly reported by Stolle group²⁶² affording triazole derivatives in high yields after 10 min of milling. Based on the good results, polymerization was also investigated in the ball mill. Copper catalysed C-N coupling as well as Cu(II)-catalysed multicomponent reactions²⁶³ between aldehydes, amines, and alkynes has also been studied under mechanochemical strategy.

Fe-, Rh-, Ag-, Zn- catalysed reactions have also been explored to show the suitability of dehydrogenative couplings, olefin metathesis, Diels-Alder cycloadditions, etc applying the mechanical milling protocol.

Interestingly, mechanochemical asymmetric synthesis showed great potential for desymmetrization, aldol, Michael and alkylation reactions.²⁶⁴⁻²⁶⁷

Ball milling in production scale was reported by Ferdi Schüth et al.²⁶⁸ in 2013, proving its suitability for industrial applications of the Solid-Catalysed CO oxidation.

Considering it, metal-catalysed mechanochemical organic synthesis is up for an excellent start, with huge potential to expand beyond laboratory work toward industrial processes.

1.4.5 Ultrasonic and microwave-assisted synthesis of metal nanoparticles

Ultrasonic frequencies between 20 kHz and 15 MHz have also been used to synthesize various nanostructures. Sonication promotes chemical reactions via acoustic cavitation, in which bubbles are formed and then implode in a way that generates very high localized temperatures and pressures. Sonochemical techniques give the possibility to prepare nanomaterials under ambient conditions without the need for high temperatures, high pressures, or extended reaction times.

In 2018, Lenardao et al.²⁶⁹ published a review describing reaction examples that have been reported to be positively affected by the US-promoted cavitation. One year later, several examples of Heck reaction, Suzuki-Miyaura, Knoevenagel condensation, Mannich reaction,... and many other organic transformations has been described by Banerjee²⁷⁰, who published another review exploring the wide range of advantages that ultrasound-assisted strategy offers when combined with nanocatalysis. The effectiveness of a catalyst increases in nano size due to the enhancement of active surface area. Thus, an effective collaboration between nano-catalyst and ultrasound is one of the facile tools to develop environmentally sustainable protocol. In 2015, Ying et al.²⁷¹ synthesized an amine functionalized silica coated Fe₃O₄ nanoparticles that successfully employed for the Knoevenagel condensation under ultrasound irradiation. Mannich reaction between cyclohexanone, primary amines and different aldehydes was demonstrated by Saadatjoo *et al.*²⁷² to be highly enhanced by ultrasound, obtaining the corresponding β -amino carbonyl compounds in the presence of a catalytic amount of magnetically separable γ -Fe₃O₄ nanoparticles in ethanol at room temperature. Several reports are also available in the literature on silver nanoparticles using sonochemistry^{273–275}.

Sabbaghzadeh and co-workers²⁷⁶ reported a sonication-based protocol for preparing monodisperse metallic CuNPs of different sizes using ethylene glycol as a capping agent and hydrazine monohydrate as the reducing agent. Sonication made it possible avoiding the formation of polydispersed Cu materials. A similar protocol has been used to prepare amorphous CuNPs, nanocrystalline Cu₂O embedded in a polyaniline matrix, and NPs based on CuO and Cu₂O without any surfactants and templates.²⁷⁷ Gedanken and co-workers²⁷⁸ prepared CuNPs by a sonochemical method using a reduction process involving radical species originating from water molecules under the influence of ultrasound. The resulting H \cdot radicals efficiently reduced Cu²⁺ to metallic CuNPs. As described by Cerchier in 2017,²⁷⁹ the use of ultrasound proved to be critical for increasing the production of the copper nanoparticles. The use of L-ascorbic acid as a reducing agent with ultrasound irradiation allowed the production of Cu nanoparticles with a size that can be comparable to nanoparticles produced with sodium borohydride. Recently, Sukri et al.²⁸⁰ described the synthesis of highly pure Cu-NPs without and with honey using ultrasonic assistance. The protein and carbohydrate of honey might contribute as the stabilizing and reducing agent for the CuNPs.

The influence of microwave irradiation has also been widely studied in nanosynthesis since it can address the problem of heating inhomogeneity, while providing a scalable platform for industrial applications. By judicious choice of the solvents, passivating ligands, and reactants, the nanomaterial precursors can be selectively heated preferentially with regards to the solvent or passivating ligand. As it is already well known, microwaves' wavelength has a strong

impact on the penetration depths, and so highly affects the heating rates of the reaction mixture.

From 1990, lot of publications has been reported about the synthesis of inorganic nanoparticles in presence of microwave dielectric heating and several authors have rationalized this phenomena observed during the formation of NC formation under MW conditions by thermal/kinetic effects^{281–284}.

In 2011 Kappe et al.²⁸⁵ described the nucleation as well as the subsequent growth in the formation of nanocrystals (NCs) controlled by MW. Chang et al.²⁸⁴ claim that NCs obtained by MW irradiation are comparatively smaller in size than those prepared by conventional heating and it can be explained based on the timing of nucleation and growth periods. In general, the higher the nucleation velocity is, the smaller the ultimate nanocrystals will be. The describe how crystal sizes of silicalite-1 and VSB-5 increase in the order of the materials synthesized by MW–MW<MW–CE<CE–MW<CE–CE (CE=Conventional electric heating).

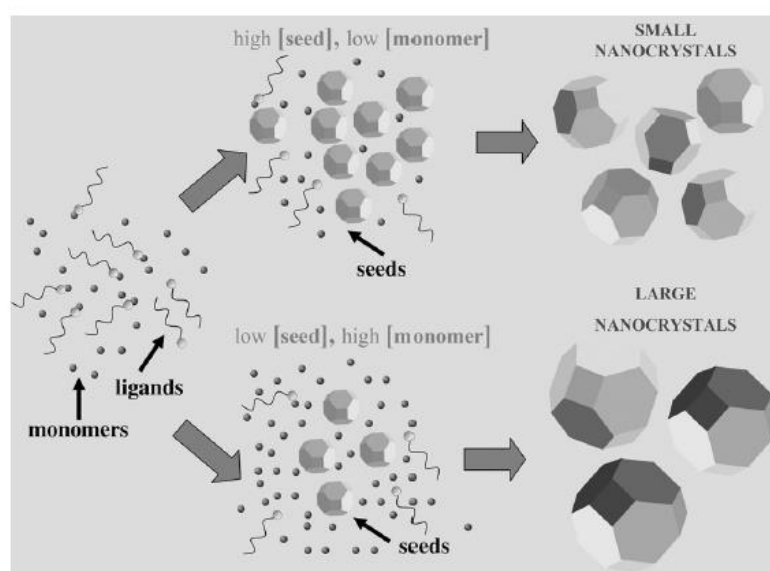


Figure 20: Schematic representation of the most common mechanism of size control realized in MW-assisted colloidal nanocrystal synthesis by one-pot, single-step reaction schemes²⁸⁵.

In 2005, Strouse and co-workers²⁸⁶, described a microwave synthetic methodology and the influence of additives for a range of organically passivated binary and ternary III-V (InGaP, InP) and II-VI (CdSe) materials. Exploration of the power, temperature, time, and additive dependent growth was performed. Microwave chemistry appears to enhance reaction rates either by overcoming local intermediates which act as traps along the reaction trajectory or by increasing the microscopic temperature of the reaction.

Strategies	Evolution pathways	Prerequisites	Morphologies
Growth confined in micelles	Precursors dissolution in micelles	Reactions occur inside the micelles	Resembling templates
	Nucleation and growth in confined environment		
Crystal-oriented attachment	Formation of primary nanoparticles as the seeds	Weakly capped primary nanoparticles	One dimensional structures
	Aggregation epitaxially along specific directions		
Seed-catalysed growth	Seeds generation	Heterogeneous nucleation is energetically easier	Nanorods, nanowires, platelets and branched nanostructures
	Nucleation and growth on the specific sites provided by the seeds		
Evolution by facet-preferential ligand/surfactant adhesion	The growing nanoparticles are capped by surfactants	Capping agents with preferential affinity towards specific facets	Nanorods and nanoplates
	Anisotropic growth of nanoparticles		

Figure 21: Summary of strategies for different mechanisms of microwave synthesis²⁸⁷

***Chapter 2: Non-conventional energy
sources for nitro compounds and
alkynes reduction.***

2.1 Introduction

As previously described, aromatic amines are useful intermediates in the preparation of dyes, pharmaceuticals and agricultural chemicals and a variety of procedures involving reduction of aromatic nitrobenzenes using different metal catalysts and reducing agents are available for their synthesis. However, most procedures involve strong and hazardous reductants, harsh reaction conditions and low selectivities and yields. Thus, a simple- and inexpensive alternative synthetic process that combines heterogeneous catalysis in a green sustainable medium and non-conventional selective energy sources to promote fast chemical transformations is an appealing approach to the development of environmentally benign organic transformations.

Herein, new synthetic procedures for aromatic nitro compounds reduction have been studied and the influence of different enabling technologies (microwave, ultrasound and ball mill) have been assessed. Mechanical activation in the absence of catalyst in a planetary ball mill and in the presence of formate salts for the reduction of aryl nitro derivatives and alkyl/aryl azide have been successfully studied. Moreover, glycerol as an efficient capping agent in the production of CuNPs, and as a solvent and hydrogen donor in the Cu-catalysed reduction of nitroarene derivatives to anilines has been evaluated. Non-conventional and non-contact energy sources were used to create new transfer hydrogenation processes that benefit from additional actuation via intensified mass and heat transfer. The ability of dielectric heating and US irradiation to maximise catalyst dispersion have been explored with the aim of enhancing reaction rate. Efficient and hydride free method for the chemo selective reduction of aromatic nitro compounds to amino compounds and to azo compounds a single reaction step has been achieved. All of the activities that are presented herein have the final aim of developing a knowledge-based strategy and selecting appropriate technologies for the scale up of the optimised reaction to an industrial MW instrument and continuous flow.

2.2 Mechanochemical reduction of nitroarenes and alkyl/aryl azides without catalyst addition

Mechanochemical activation (grinding and ball milling) has not only been the object of this study because it grinds and crumbles inorganic materials, but also because it generates mechanical energy for the synthesis of organic molecules^{288,289}. The planetary ball mill has become a valid mean of producing green energy as seen in the growth of mechanochemical activation observed in various areas of organic chemistry, including C–C bond formation,^{290–292} organocatalysis,²⁹³ heterocyclic synthesis,²⁹⁴ cycloaddition,²⁹⁴ oxidative/reductive reactions,^{295,296} polymerisation,²⁹⁷ and supramolecular chemistry.²⁹⁸

Solid–gas reactions are facilitated by mechanical milling in reactive gases (nitrogen, oxygen and hydrogen),²⁹⁹ and this approach was initially used for preparation of hydrides in a hydrogen atmosphere. Mechanochemistry has also been extensively used in the hydrogen storage process, while other examples of mechanically promoted reactions performed in the presence of gaseous hydrogen have been described.³⁰⁰ Nevertheless, several mechanochemically activated alternatives to the use of gaseous hydrogen have been investigated: graphene oxide has been efficiently reduced in a magnesium-assisted mechanochemical reaction, a variety of aldehydes and ketones have been reduced to tetraalkoxyborates using unmodified sodium borohydride³⁰¹ and alkenes have been reduced

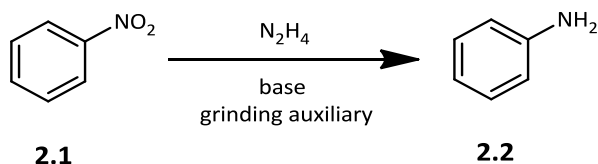
using hydrogen that was generated *in situ* from alkanes.³⁰² To the best of our knowledge, only a few studies have reported the reduction of aryl nitro and aryl azide compounds in a ball mill,³⁰³ and none of these reactions were performed under catalyst free conditions with hydrogen generated *in situ*.

The conversion of aromatic nitro compounds and azides to amines is a fundamental procedure in organic chemistry and, as previously described, a number of catalysts have been employed in this field with good to excellent results. Several investigations into the metal-free hydrogenation of nitroarenes have been published since 1995, and the most noteworthy have involved reduced graphene oxide/hydrazine hydrate, mesoporous carbon/hydrazine hydrate,^{304–306} thiourea and glucose.⁸² Concerns about safety and environmental burden therefore make metal free hydrogenation under mechanochemical activation extremely attractive. Thus, we report the reduction of nitrobenzenes, and aryl and benzyl azides in a planetary ball mill, without the addition of a catalyst, in the presence of reducing agents ammonium and sodium formate, and hydrazine.

Metallic Ni, Pd and Pt have all catalysed hydrazine decomposition over various supports at low temperatures,³⁰⁷ while hydrazine oxidation requires high temperatures without a catalyst. Although several attempts at using hydrazine in a ball mill have been described, they are limited to the synthesis of hydrazone and the cyclization of pyrazoles.^{308–310} Hydrazine is widely used despite being toxic, therefore in the present study its reactivity has been compared with formate salts as the hydrogen source for transfer hydrogenation.^{311–313} Ammonium formate thermally decomposes to hydrogen, carbon dioxide and ammonia³¹⁴ and by contrast, the thermal decomposition of alkali metal formates, such as sodium formate, leads to carbonate, oxalate and hydrogen. To the best of our knowledge, no previous works have described the use of formate salts in the reduction of aryl nitro derivatives under mechanochemical activation.

The reduction of nitrobenzene (**2.1**) with hydrazine was chosen as a representative model reaction for the optimisation of reaction conditions. The decomposition of hydrazine can be performed using two methods: catalytic decomposition (on metal surfaces and supported metal particles) and thermal decomposition.^{315–317}

As described in Table 6, the complete conversion of nitrobenzene was observed in the presence of 30 eq of hydrazine, while the reaction moved to completion and the intermediates were fully converted to aniline (**2.2**) in the presence of grinding agent and KOH (Table 6, entries 4-7). Even if the reaction showed good conversion in absence of grinding auxiliary, it helps homogeneity and mixing. As described in the Table 6, in presence of polar acidic basic or neutral auxiliary the reaction showed good conversion and yield, because of its chemical inertness we decided to prefer neutral alumina.²⁴⁹ From the comparison of different bases, KOH was found to be the suitable one, as already observed in a previously performed mechanochemically promoted Ullmann copper-catalysed reaction.¹⁴¹ The reaction rate decreased in the presence of only 20 or 10 eq of hydrazine. When performed in zirconia jar only starting material was recovered (Table 6, entry 11).

Table 6: Reduction of nitrobenzene with various bases and milling auxiliaries. ^{a)}

Entry	Auxiliary	Hydrazine (Eq)	Base	Ar-NH ₂ (%) ^{b)}	Intermediate distribution ^{b)}
1	no	30	no	89	Ar-NH-NH-Ar (4%)
2	Al ₂ O ₃ basic	30	K ₂ CO ₃	40	Ar-NH-NH-Ar (33%), Ar-N=N-Ar (15%)
3	Al ₂ O ₃ basic	30	NaOH	53	Ar-NH-NH-Ar (29%) Ar-N=N-Ar (18%)
4	Al ₂ O ₃ basic	30	KOH	99	-
5	Al ₂ O ₃ neutral	30	KOH	98	-
6	SiO ₂	30	KOH	99	-
7	Montmorillonite	30	KOH	99	-
8	Fuller Earth	30	KOH	25	Ar-NH-NH-Ar (48%), Ar-N=N-Ar (20%)
9	Al ₂ O ₃ basic	20	KOH	72	Ar-NO=N-Ar (27%)
10	Al ₂ O ₃ basic	10	KOH	77	Ar-NO ₂ (16%)
11 ^{c)}	Al ₂ O ₃ basic	30	KOH	0	

^{a)} Reaction conditions: nitrobenzene (4 mmol), bases (8 mmol), grinding auxiliary (1 g); 30 min, 650 rpm, stainless steel jar, 1500 balls ($\varnothing = 2$ mm) and 48 balls ($\varnothing = 5$ mm). ^{b)} Determined by GC-MS. ^{c)} The reaction was performed in zirconia jar

The reaction time and PM (planetary ball mill) rotation frequency (rpm, min⁻¹) were varied in order to better understand the reaction parameters (Figure 22). The model reaction was tested at 650, 500, 400 and 200 rpm for 10 min with complete conversion being obtained at 650 rpm, which confirms that an increase in kinetic energy promoted the reduction and that higher rotational speed enhanced conversion. Milling times of 10, 20, 30 min were tested, and the complete conversion of nitro benzene to aniline was attained after 30 min.

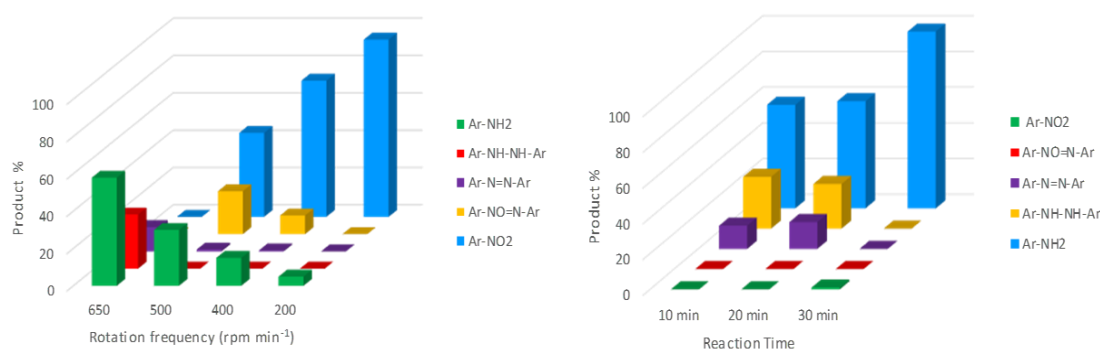


Figure 22. Influence of rotation frequency (top) and milling time (bottom) on conversion to aniline. Reaction conditions: nitrobenzene (0.5 mmol), hydrate hydrazine (30 eq) KOH (1 mmol), alumina (1 g), stainless steel jar, 1500 balls ($\varnothing = 2$ mm) and 48 balls ($\varnothing = 5$ mm); rpm and reaction time were varied as described in the graphs.

It is known that the reaction outcome is correlated to the number of stress events and the stress frequency, therefore ball diameter and the number of balls has high impact on the reaction yields. As previously described, by mixing 5 mm and 2 mm balls we could obtain a full conversion in 30 min. In order to understand the role of 2 and 5 mm balls when used alone, the reaction was repeated as described in the Table 7 (entry 2-3). The reaction gave 65 % yield with 2mm balls and it was decreased to 3% when only 5 mm ball were employed. Aiming to understand the influence of the active surface on the reaction conversion, we repeated the experiment keeping constant the balls weight in the entry 1, using 2mm balls (Table 7, entry 4) and 5 mm balls (Table 7, entry 5) alone. We could observe that, despite the larger surface area, the reaction with 2250 small balls showed a decrease in the reaction yield due to the reduction of dead volume in the jar. When 144 bigger balls were used, the reaction yield was slightly reduced to 90% maybe because of the reduction of sample homogeneity in energy transferring.

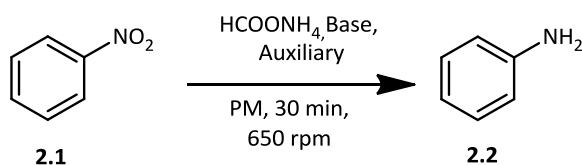
Table 7. Influence of ball size and number on reaction yield ^{a)}

Entry	Ball Number		Active surface	Yield (%) ^{b)}
	Small	Medium	Area ^{c)} (mm ²)	
	($\varnothing = 2$ mm)	($\varnothing = 5$ mm)		
1	1500	48	22608	>99
2	1500	-	18440	65
3	-	48	3768	3
4	2250	-	27660	33
5	-	144	11304	95

^{a)} Reaction conditions: nitrobenzene (0.5 mmol), hydrate hydrazine (30 eq) KOH (1 mmol), alumina (1 g), stainless steel jar, 650 rpm, 30 min; ^{b)} Isolated yield. ^{c)} Active surface area = surfaceballs

Ammonium formate, a safer and less toxic hydrogen source, was tested in order to improve the protocol's sustainability.³¹⁸ As shown in Table 8, the influence of alumina and the base on reaction yield was tested in the PM at 650 rpm for 30 min for optimisation purposes. A 97% yield was reached (Table 8, entry 3) when the reaction was performed in the presence of the grinding agent and KOH base.

Table 8. Reduction of nitrobenzene with ammonium formate under various conditions

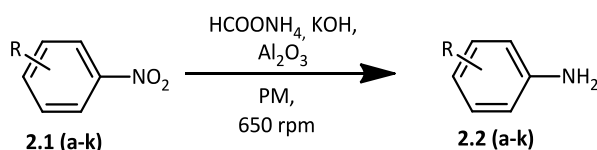


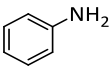
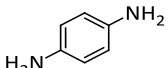
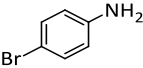
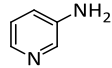
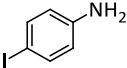
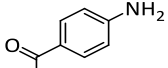
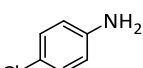
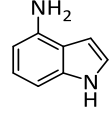
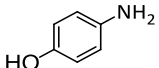
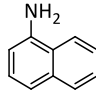
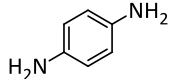
Entry ^{a)}	Base	Al ₂ O ₃	Ar-NH ₂ (%) ^{b)}	Ar-NO ₂ (%) ^{b)}
1	-	-	0	100
2	-	1 g	23	77
3	KOH (8eq)	1 g	97	0

^{a)} Reaction conditions: nitrobenzene (0.5 mmol), ammonium formate (30 eq) 30 min, 650 rpm, stainless steel jar, 1500 balls ($\varnothing = 2$ mm) and 48 balls ($\varnothing = 5$ mm). ^{b)} Determined by GC-MS.

The optimised procedure was then repeated with a selection of nitrobenzene derivatives to broaden the scope of the study. The reaction protocol was performed in the presence of nitrobenzene derivatives (0.5 mmol), KOH (1 mmol), HCOONH₄ (8 eq), alumina (1 g), in the planetary ball mill at 650 rpm for 30 min. High selectivities and yields were achieved with a number of both electron poor and electron rich substrates (Table 9). Nitro halide derivatives proved to be stable under these reaction conditions (Table 9, entry 2-4,) and reductive dehalogenation was not observed. Ammonium formate led to the full conversion of 1,4-dinitrobenzene without the addition of a catalyst (Table 9, entry 7), while 50% *p*-nitroaniline and 30% 1,4-diaminebenzene were produced. 30% conversion was observed when *p*-nitroaniline was reacted in the ball mill for 1h (Table 9, entry 6). It is worth noting that the ketone, nitro acetophenone, (Table 9, entry 9) was not reduced under these reaction conditions, but was quantitatively converted to the amino derivative.³¹⁹ In order to confirm that this procedure of aromatic nitro reduction may be performed in presence of other reducible groups like ketones, the hydrogenation of acetophenone was carried out in a separate experiment with HCOONH₄ in the planetary ball mill. The test confirmed that the proposed procedure is not able to reduce carbonyl species.

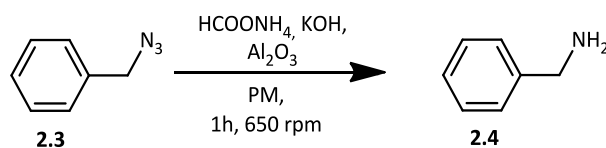
Table 9. Screening of the mechanochemical reduction of various nitrobenzene derivatives with ammonium formate. ^{a)}



Entry	Nitrobenzene	Time (h)	Yield ^{b)} % (Conv) ^{c)}	Entry	Nitrobenzene	Time (h)	Yield ^{b)} % (Conv) ^{c)}
1		0.5	97 (100)	7 ^{b)}		2	30 (100)
	2.2a				2.2g		
2		1	98 (100)	8		2	95 (100)
	2.2b				2.2h		
3		1	92 (100)	9		1	97 (100)
	2.2c				2.2i		
4		1.5	93 (100)	10		1.5	91 (100)
	2.2d				2.2j		
5		1.5	98 (100)	11		1	95 (100)
	2.2e				2.2k		
6 ^{f)}		2	30 (30)				
	2.2f						

^{a)} Reaction conditions: nitrobenzene derivatives (0.5 mmol), ammonium formate (30 eq), KOH (1 mmol), basic Al₂O₃ (1 g), 650 rpm, 30 min, stainless steel jar (50 mL), 1500 balls ($\phi = 2$ mm) and 48 balls ($\phi = 5$ mm); ^{b)} Isolated yield, compound purity proved by ¹H-NMR and ¹³C-NMR (see Chapter 5: Experimental details); ^{c)} Determined by GC-MS; ^{d)} The reaction was carried out with 16 mmol KOH; ^{e)} The reaction was carried out with 160 mmol ammonium formate and 16 mmol KOH, milling was maintained for 1h; ^{f)} p-nitroaniline; ^{g)} 1,4-dinitrobenzene

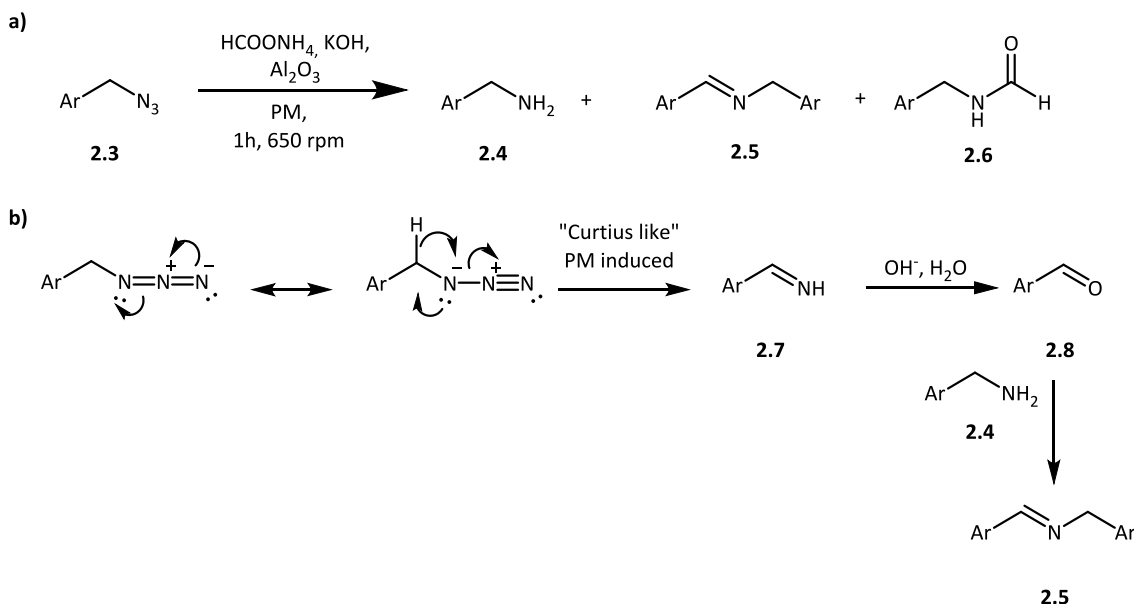
The reduction of azido derivatives was also attempted in order to broaden the scope of the study. The reduction of benzyl azide (**2.3**) with ammonium formate was selected as the model reaction (Scheme 21).



Scheme 21. Synthetic scheme for the reduction of benzyl azide with ammonium formate.

This approach to benzylamine (**2.4**) synthesis involves secondary competitive reactions, as the thermal decomposition of organic azides to imines gives benzaldehyde (**2.8**),³²⁰ and the

consequent formation of N-benzylidenebenzylamine (**2.5**).^{321–323} In fact it is known that Curtius-like rearrangement of benzylazide afforded to the imine (**2.7**) that we presumed to be precursor of benzaldehydes (**2.8**) and Schiff base as well [Scheme 22 a)b)]. In the presence of ammonium formate the formylation of the benzylamine with formic acid salts is a secondary reaction and was observed³²¹ (**2.6**).



Scheme 22: a) Schematic representation of the reduction of benzyl azide in the PM with ammonium formate and production of side products. b) Schematic representation of Curtius-like mechanism to obtain product 6 from benzylazide

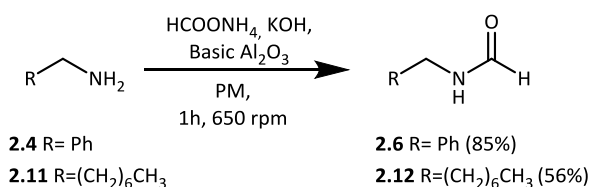
Ammonium formate and sodium formate were tested in order to further our knowledge of how reaction condition influence product distribution. Both silica and alumina were used as auxiliaries and the reaction was tested in presence and in absence of base. Results can be seen in Table 10. In a preliminary experiment, the stability of benzylazide was studied by subjecting it to milling in the stainless steel jar with alumina. As described in Table 10 (Entry 1), complete benzylazide conversion was observed after 1 hour at 650 rpm and the treatment resulted in the production of a number of side products, including benzaldehyde (**2.8**), benzylidenebenzylamine (**2.5**), benzamide (**2.6**) and benzylalcohol (**2.10**), which were identified. As previously discussed by Y. Sawama et al.,³²⁴ the components (Fe, Cr, Ni etc.) of the stainless steel balls and the planetary ball mill vessel act as the hydrogenation catalyst as they facilitate the generation of hydrogen from water and/or organic materials. When benzyl azide (**2.3**) was milled with ammonium formate, KOH and alumina, it selectively gave N-benzylformamide (**2.6**) in a 70% yield (Table 10, entry 3). However, without the base, about 50% of the starting material was recovered unconverted (Table 10, entry 5). To avoid the formylation of benzylamine, the protic ammonium salt was replaced with the sodium analogue. These conditions led to formamide production being reduced to 4%, while the major product was formed from the condensation of benzaldehyde and benzylamine (product **2.5**; Table 10, entry 6). The N-benzylformamide yield increased because of the acidity of the grinding powder when silica was used as the grinding auxiliary with sodium formate (Table 10, entry 8).

Table 10. Study of benzyl azide reduction with ammonium formate.

Entry	Reaction conditions ^{a)}	Ar-CH ₂ -N ₃ (%) ^{b)} 2.9	Ar-CH ₂ -NH ₂ (%) ^{b)} 2.4	Ar-CHO (%) ^{b)} 2.8	Ar-CH=N-CH ₂ -Ar (%) ^{b)} 2.5	Ar-CH ₂ -N(H)-CHO (%) ^{b)} 2.6	Ar-CH ₂ -OH (%) ^{b)} 2.10
1	-, Al ₂ O ₃ , PM, ^{a)} 1h, 650 rpm		3		35		16
2	-, Al ₂ O ₃ , 80°C, o.n ^{c)}	90		9 ^{e)}			
3	HCOONH ₄ , Al ₂ O ₃ /KOH, PM ^{a)} , 650 rpm, 1h	3	7	5	8	70	
4	HCOONH ₄ , Al ₂ O ₃ /KOH, 80 °C, o.n	37				4	58
5	HCOONH ₄ , Al ₂ O ₃ , PM, ^{a)} 650 rpm, 1h	49	14	3	10	27	
6	HCOONa, Al ₂ O ₃ , ^{d)} PM, ^{a)} 650 rpm, 1h			6	84	4	2
7	HCOONa, Al ₂ O ₃ , 80°C, o.n	84					16
8	HCOONa, SiO ₂ , PM, ^{a)} 650 rpm, 1h	1	9	4	42	30	

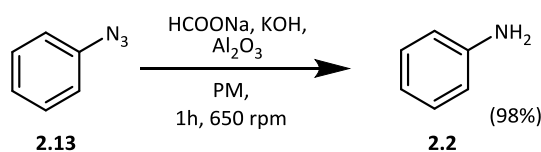
^{a)} Reaction conditions: benzyl azide (0.5 mmol), ammonium formate (15 mmol when added), sodium formate (10 mmol when added), KOH (1 mmol when added), grinding auxiliary (1 g), 1 h, 650 rpm, stainless steel jar (50 mL), 1500 balls ($\varnothing = 2$ mm) and 48 balls ($\varnothing = 5$ mm); ^{b)} Determined by GC-MS; ^{c)} MeOH was added to facilitate powder mixing; ^{d)} Basic Al₂O₃ was dried in an oven before use; ^{e)} the aldehyde was converted to dimethyl acetale and emiacetale.

The most selective reactions were performed under conventional conditions for the sake of comparison; benzylazide (**2.3**) (1 mmol), and either ammonium formate (30 mmol) or sodium formate (20 mmol), and MeOH (1mL) were heated at 80°C (Table 10, entries 2,4,7). Methanol was necessary to ensure the efficient mixing of powders. Benzylazide (**2.3**) was found to be quite stable at 80 °C with Al₂O₃ and only 10% was converted to benzaldehyde, in the form of dimethyl acetal and hemiacetal, after one night. Only 4% *N*-formyl benzylamine was observed when the reduction was repeated under conventional conditions in the presence of ammonium formate, while only the benzylalcohol (**2.10**) was produced from the reduction of benzaldehyde using sodium formate (Table 10, entry 7). Mechanochemistry's efficacy in producing *N*-formyl derivatives is proven by the direct formylation of benzyl- and octylamine in the ball mill, as described in Scheme 23. The desired products were obtained in 85% and 56% yields, respectively and interestingly we observed that under mechanochemical activation the formamide derivative resulted stable to hydrolysis of the amido moiety.



Scheme 23. Schematic representation of the formylation of octyl- and benzyl amine with ammonium formate in the PM.

Since the degradation of benzylazide involved the benzylic position, and the formylation side reaction was mainly facilitated by the nucleophilicity of the alkyl amine, we decided to test reduction with sodium formate, starting from aryl azides, which are more stable and less nucleophilic (Scheme 24). The reaction was performed in the presence of KOH because the base accelerates the reaction without affecting the purity of the desired product.



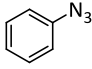
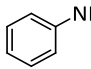
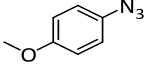
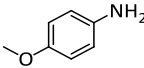
Scheme 24. Synthetic scheme for the reduction of an aryl azide using sodium formate. Reaction conditions: Phenyl azide (0.5 mmol), sodium formate (10 mmol), KOH (1 mmol), grinding auxiliary (1 g), 1 h, 650 rpm; stainless steel jar (50 mL), 1500 balls ($\varnothing = 2$ mm) and 48 balls ($\varnothing = 5$ mm)

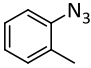
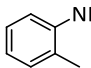
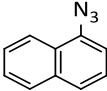
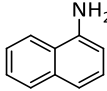
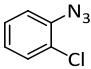
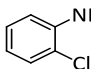
Gratifyingly, the reaction afforded the desired aniline in a 98% yield and its versatility was evaluated over a small series of differently substituted aryl azides. The azides were prepared according to a previously reported procedure,³²⁵ using CuSO₄ as the catalyst for the cross coupling of aryl boronic acid with sodium azide under mild reaction conditions. As described in Table 11, high yields were achieved in all cases, chlorobenzene was not affected by the dehalogenation reaction and ortho substituted derivatives were demonstrated to be reactive.

Table 11. Screening of the mechanochemical reduction of aryl azide derivatives with sodium formate^{a)}

$$\text{R-C}_6\text{H}_4\text{-N}_3 \xrightarrow[\text{PM, 1h, 650 rpm}]{\text{HCOONa, KOH, Al}_2\text{O}_3} \text{R-C}_6\text{H}_4\text{-NH}_2$$

2.13 (a,k,l-n) **2.2 (a,k,l-n)**

Entry	Aryl azides	Anilines	Time (h)	Yield ^{b)} % (Conv) ^{c)}
1	 2.13a	 2.2a	1.5	98 (100)
2	 2.13l	 2.2l	1.5	85 (98)

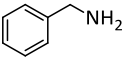
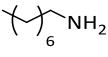
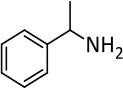

3			1	100 (100)
	2.13m	2.2m		
4			1	87 (92)
	2.13k	2.2k		
5			1.5	95 (98)
	2.13n	2.2n		

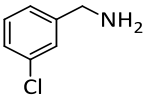
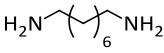
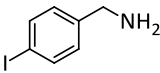
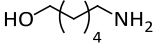
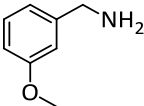
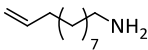
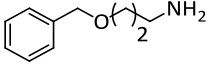
^{a)} Reaction conditions: aryl azide (0.5 mmol), sodium formate (10 mmol), KOH (1 mmol), basic Al₂O₃ (1 g), 650 rpm, stainless steel jar (50 mL), 1500 balls ($\varnothing = 2$ mm) and 48 balls ($\varnothing = 5$ mm); ^{b)} Isolated yield, compound purity proven by ¹H-NMR and ¹³C-NMR (see Chapter 5: Experimental details); ^{c)} Determined by GC-MS.

In order to prove the efficacy of the PM in the reduction of benzyl and alkyl azides, hydrazine was used as the reducing agent instead of formate salts. For organic azides to be manipulable or nonexplosive, the rule is that the number of nitrogen atoms must not exceed that of carbon, therefore the experiments were performed with benzyl azides or long chain alkyl derivatives.¹⁶⁸ As described in Table 12, the reaction quantitatively provided the desired set of 11 amines. Table 12 shows that various benzylic and linear azides with different functional groups can be reduced in 1h under the optimised reaction conditions. The -OMe and -Cl groups were unaffected, while *p*-iodobenzyl azide was reduced to benzylamine (Table 12, entry 4). Alkyl azides, and not just their benzylic counterparts, were efficiently reduced. In the presence of azido derivatives with a double bond, less than 10% amino alkane was detected (Table 12, entry 11).

Finally, an ICP analysis was performed to detect the metals released during the reduction. The model reaction of reduction of nitrobenzene with ammonium formate and alumina was performed in 0.5 mmol scale. Cr was detected in 1.32±0.3 g/kg, Fe 9.15±1.6 g/kg and Ni in 9.15±1.6 mg /kg.

Table 12. Screening of the mechanochemical reduction of alkyl/benzyl azide derivatives with hydrazine ^{a)}

Entry	Alkyl amines	Time (h)	Yield ^{b)} % (Conv) ^{c)}	Entry	Alkyl amines	Time (h)	Yield ^{b)} % (Conv) ^{c)}
1		1	98 (100)	7		1	96 (98)
	2.15a				2.15g		
2		1	100 (100)	8		1	90 (100)
	2.15b				2.15h		

3		1	100 (100)	9		1	94 (100)
	2.15c				2.15i		
4 ^{d)}		1	- (100)	10		1	60 (100)
	2.15d				2.15j		
5		1	99 (100)	11		1	81 (90)
	2.15e				2.15k		
6		1	80 (100)				
	2.15f						

^{a)} Reaction conditions: aryl/benzyl azide (0.5 mmol), hydrazine (15 mmol), KOH (10mmol), Alumina (1 g), 650 rpm, stainless steel jar (50 mL), 1500 balls ($\varnothing = 2$ mm) and 48 balls ($\varnothing = 5$ mm); ^{b)} Isolated yield, compound purity proven by ¹H-NMR and ¹³C-NMR (see Chapter 5: Experimental details); ^{c)} Determined by GC-MS; ^{d)} Benzylamine was formed as the product.

2.3 Copper catalysed reduction of aromatic nitrocompounds. Glycerol: an optimal hydrogen source

One way to pursue green synthesis is to improve the sustainable nature of the solvents, as they are directly responsible for the major environmental drawback generated by chemical processes. The use of bio-based and eco-friendly alternative solvents³²⁶ has been developed and evaluated over recent decades. As already discussed above, glycerol (1,2,3-propanetriol) is a common natural solvent that is rich in functionalities and is obtained in very large amounts as a co-product in biodiesel production.^{34,327} The rapid development of the biodiesel industry has resulted in an increase in glycerol production yields and a supply of low cost technical grade glycerol with a final purity of around 80–95%.³²⁷ More than 90% of the glycerol used today is refined to give purities of higher than 97%, and the process can take purity up to from 99.5% to 99.7%. Intensive research is conducted to find ways to valorise glycerol and many fields of interest focus on its transformation into chemicals and hydrocarbon fuels.³²⁸ Furthermore, its use as a convenient green reaction medium has been widely documented.^{35,42,329}

Selective and exhaustive reductions of nitrobenzenes in the presence of glycerol, used as a “sacrificial” hydrogen source, have been performed with Ni Raney⁴² and in the presence of a recyclable catalyst made of magnetic ferrite-Nickel NPs.⁸⁴ Furthermore, bio-based glycerol has been exploited in the Ru-catalysed, one-pot synthesis of imine and amine using nitrobenzene and alcohol as the starting materials.^{24,330} Glycerol has been utilised to prepare 1,2,3-trimethoxypropane, a green alternative for petroleum-based solvents, such as THF, toluene and dichloromethane. 1,2,3-trimethoxypropane has given good results in the Fe(acac)₃-catalysed transfer hydrogenation of carboxylic acids, nitriles, esters and nitrobenzene.³³¹

Despite its main disadvantage, i.e. its high viscosity at room temperature, glycerol is an optimal solvent for catalysis purposes because of its high polarity and capacity to remain in the liquid phase over a large temperature range (from 17.8 to 290 °C). Moreover, it has low vapour pressure, a long relaxation time and high acoustic impedance, meaning that it can be used under MW and US irradiation conditions. In fact, glycerol has a high loss factor, or loss tangent ($\tan \delta = 0.651$), at the standard MW frequency (2.45 GHz), which is indicative of high MW absorption and rapid heating. Several successful examples of MW-promoted organic syntheses in glycerol have therefore been described in the literature.^{34,244} Glycerol can be used under sonochemical conditions, although greater amounts of energy must be supplied to overcome the cohesive forces in the liquid, as it is a viscous solvent. Similarly to other polyols (e.g., ethylene glycol and polyethylene glycol), glycerol can act as both a solvent and reducing agent of metal precursors, and several applications have been developed in the field of metal-nanoparticle synthesis. Furthermore, glycerol can act as a stabiliser of nanometric species, leading to the straightforward recycling of the catalytic phase.³³² The conventional and MW-assisted preparation of NPs in glycerol has already been described in the literature and this field of interest is continuously growing.^{333–335} Cu(0)NPs have been efficiently prepared in glycerol,³³⁶ and some polyol-stabilised CuNPs have been used in the reduction of nitrobenzene.^{198,337,338} Although several applications for copper catalysis in transfer hydrogenation have already been reported in the literature,^{339–341} the use of CuNPs for nitrobenzene reduction via transfer hydrogenation has not received much attention, to the best of our knowledge.

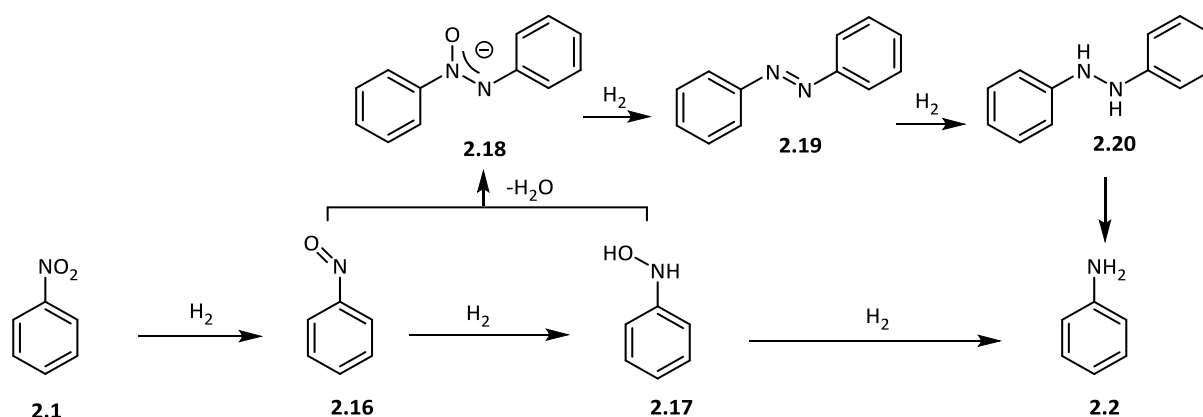


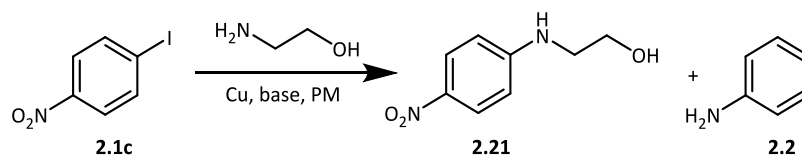
Figure 23: Reaction pathways for the hydrogenation of nitrocompounds to anilines

As despite in Figure 23 and already described in the introduction (1.2.3 Nitroarenes) the reduction mechanism of nitrobenzene passes through several intermediates (nitrosobenzene (**2.16**), azobenzene (**2.19**), diphenylhydrazine (**2.20**) and aniline (**2.2**)).

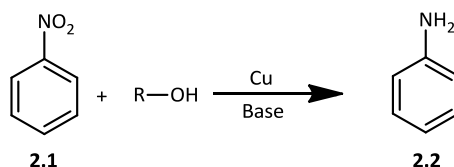
Herein, glycerol has been exploited as an efficient capping agent in the production of CuNPs, and as a solvent and hydrogen donor in the Cu-catalysed reduction of nitrobenzene derivatives to anilines.

From previous studies, while carrying out the N-arylation (**2.21**) of amino alcohols and diamines with Cu powder¹⁴¹, we observed an interesting reduction of the nitro group to an amino group (product **2.2**, Scheme 25) in trace amount (5%) in the coupling of 4-nitroiodobenzene (**2.1c**) with ethanolamine (Scheme 25). We proposed that copper hydride (CuH), generated in situ during the reaction was responsible for the reduction of NO₂ group.

Going deeply into this phenomenon, a preliminary model for the transfer hydrogenation (TH) of nitroaromatic derivatives with nitrobenzene and copper powder was set up (Scheme 26).



Scheme 25. N-arylation of Amino Alcohols and Diamines with Cu powder.



Scheme 26. Synthesis scheme of reduction of Nitrobenzene.

The standard reaction between nitrobenzene and the hydrogen source was carried out at 130 °C in oil bath for 5 hours with Cu powder and KOH as base.

Table 13 Influence of different reducing agents in the reduction of nitrobenzene^{a) b)}

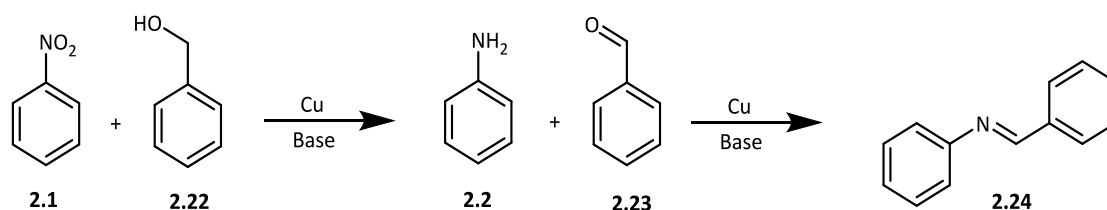
Entry	Reducing agent	Nitro (%)	Azo (%)	Azoxy (%)	Amine (%)
1	Ethanolamine	48	28	8	16
2	Ethylendiamine	41	43	0	16
3	3-Amino-1-propanol	18	67	8	7
4	2-Propanol	2	17	52	29
5	Butanol	9	33	36	22
6	1,4-butanodiol	52	0	35	12
7	Ethylen glycol	0	2	0	98
8	Glycerol	0	0	0	99

^{a)} Reaction conditions: nitrobenzene (1 mmol), KOH (2 mmol), Glycerol (40 mmol), Cu powder (2 mmol), 130°C, t: 5h, oil bath. ^{b)} Determinated by GC-MS

As depicted in Table 13, the model reaction (Scheme 26) was performed in the presence of different solvents, acting at the same time as transfer hydrogen donors. From the comparison of amino-alcohols, alcohols and amino compounds, we could observe that using aminoalcohols like the ethanolamine (Table 13, Entry 1) the reaction gives a mixture of products without showing any selectivity. However, using only the amino group with the ethylenediamine or a little aminoalcohol like 3-amino-1-propanol (Table 13, entry 2 and 3, respectively), the reaction was faster and more selective to the formation of azobenzene. After testing different alcohols, we could perceive that the use of a diol is selective to aniline only when it forms a chelate of small size, so while employing ethylen glycol or glycerol (Table 13, Entry 7 and 8, respectively). In this way, the use of a simple alcohol, such as 2-propanol or butanol (Table 13, Entry 4 and 5, respectively), does not give a selective conversion. This fact

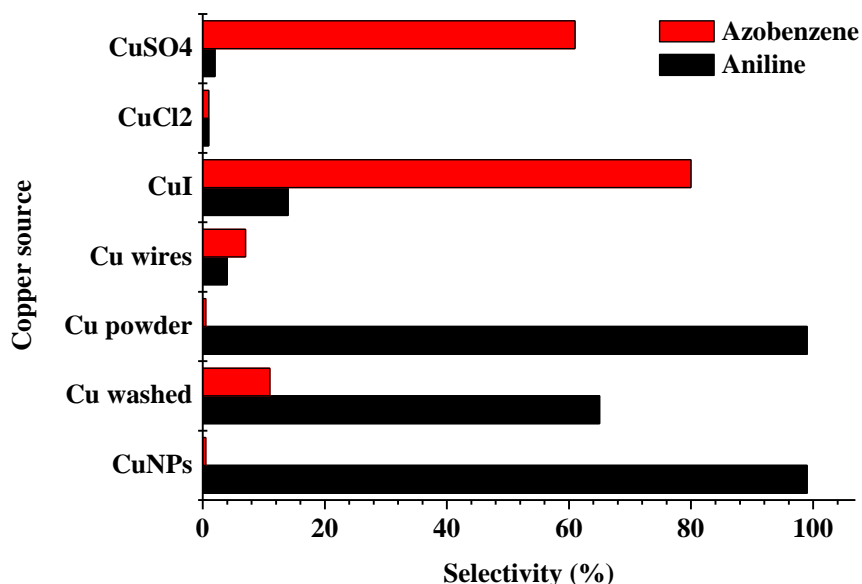
was also confirmed in presence of a longer carbon chain with 1,4-butanediol (Table 13, Entry 6), showing 62% of starting material after 5h of reaction.

In order to establish the desired hydrogen borrowing cycle that involves alcohol dehydrogenation, as well as nitro hydrogenation, we selected benzyl alcohol (Scheme 27, product **2.22**) and nitrobenzene (Scheme 27, product **2.1**) as model substrates. The alcohol, oxidizing itself in the presence of copper, makes this process possible. The presence of benzylidenaniline (**2.24**) can only be explained by the reaction between aniline and benzaldehyde (Scheme 27; products **2.2** and **2.23**, respectively), both of them end-reaction products.

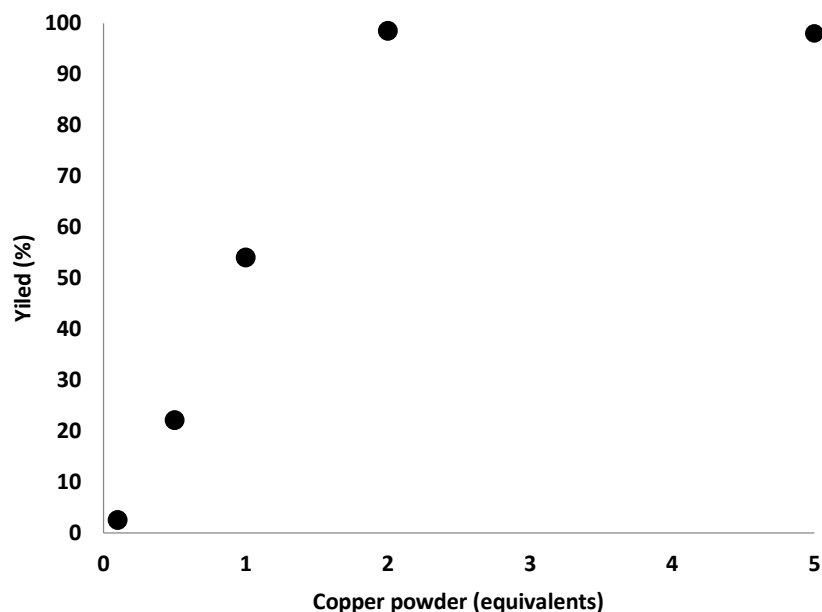


Scheme 27 Reduction of nitrobenzene with benzyl alcohol

Several copper sources were then tested and, as presented in Graph 1, the standard reaction was studied in the absence of catalyst, with copper powder, with washed copper (in order to clean the oxidized surrounded part), with copper wires and with copper in several oxidation states (CuI , CuCl_2 or CuSO_4). As despite, copper powder showed the best results, being the only copper source able to fully reduce the nitrobenzene to aniline.



Graph 1. Influence of different copper sources in the nitrobenzene reaction over glycerol at 130°C , t:5h, oil bath. Reaction conditions: nitrobenzene (1 mmol), KOH (2 mmol), solvent (40 mmol), Copper source (2 mmol). Determined by GC-MS.



Graph 2: Influence of copper catalyst loading in the nitrobenzene reaction over glycerol at 130°C for 5h. Reaction conditions: nitrobenzene (1 mmol), KOH (2 mmol), solvent (40 mmol), Cu powder. Determinated by GC-MS.

The quantity of catalyst was then studied and, as showed in Graph 2, an increase in the amount of copper equivalents leads to an increase in the product yield, reaching the maximum conversion with 2 equivalents. Any additional increase in copper quantity does not bring any benefit.

In order to reduce the high amount of copper needed to carry out this TH reaction, and at the same time, allow the use of enabling technologies such as microwaves and ultrasound²⁰¹, our attention has been attracted to the copper nanoparticles (CuNPs) catalysts^{279,342}. As already described, metal nanoparticles catalysts have gain lot of attention due to their high catalytic activities. Thanks to their extremely small dimensions and huge special surface, their activities far exceed those of conventional homogeneous catalysts. Although CuNPs are an efficient source of Cu, their potential applicability is restricted by copper's inherent instability under atmospheric conditions.

NPs were prepared using a slight modification of a published procedure. Different copper sources, bases and reducing agents were tested (Table 14). Moreover, we decided to avoid the use of poly *N*-vinyl pyrrolidone (PVP) and investigate the efficacy of glycerol alone as a means to cap and stabilise the NPs.

Then, the reactivity of CuNPs was tested in the model reaction of nitrobenzene reduction. As depicted in Table 14, the CuNPs obtained when using glycerol, NaOH as base and NaBH₄ as reducing agent (Table 14, entry 3) resulted in the higher conversion of nitrobenzene, obtaining 88% of aniline. We decided to continue performing the reaction optimization with those particles.

Table 14: Synthesis of CuNPs

Entry	Copper source	Solvent	Base ^{a)}	Reducing agent	Amine (%) ^{c)}
1	Cu(NO ₃) ₂ · 3H ₂ O (0.5M)	H ₂ O	NH ₄ OH (2M)	NaBH ₄ (2M)	56
2	Cu(NO ₃) ₂ · 3H ₂ O (0.5M)	H ₂ O	NaOH (2M)	NaBH ₄ (2M)	75
3	CuSO ₄ · 5H ₂ O (0.5M)	H ₂ O:Glycerol (5:1)	NaOH (2M)	NaBH ₄ (2M)	88
4	CuSO ₄ · 5H ₂ O (0.5M)	H ₂ O	NaOH (2M)	Pirocatechol (2M)	58

^{a)} The base solution is added until reaching pH: 11. ^{b)} The reducing agent is added until observing the formation of the CuNPs. ^{c)} Reaction conditions: nitrobenzene (1 mmol), KOH (2 mmol), solvent (40 mmol), CuNPs (10 mol%), t:1h, T:130°C, oil bath. Determinated by GC-MS.

Cu(0) NPs were prepared according to the “bottom-up” approach; by dispersing the copper salt in a basic solution (pH 11) of water and glycerol (5:1), using the polyol as the stabiliser and solvent. NaBH₄ was immediately added and the deep blue solution became a colourless one in which the dark NPs could be identified. Transmission electron microscopy (TEM) and particle-size distribution analyses were performed to characterise the prepared catalyst.

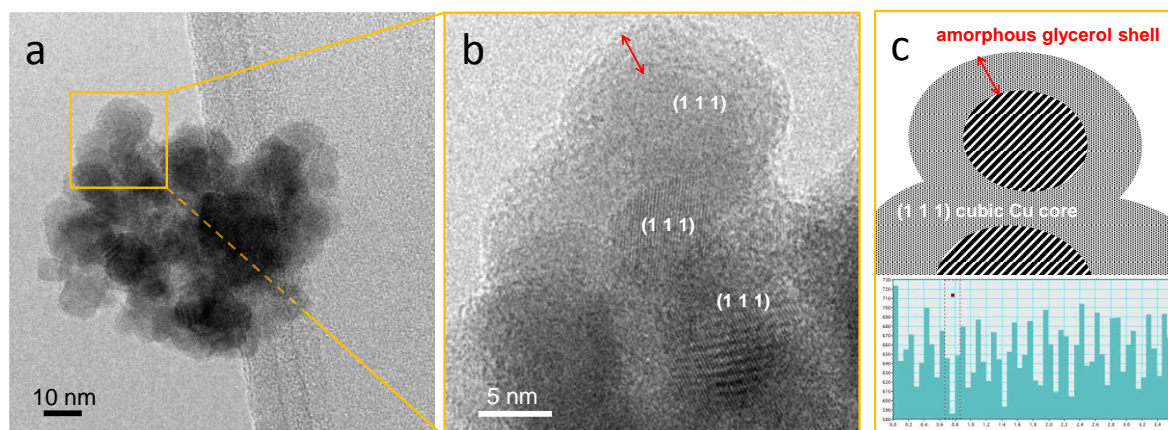


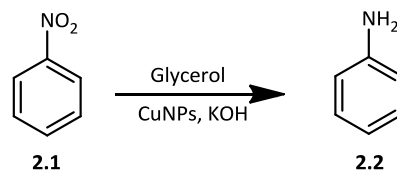
Figure 24. (a) HRTEM image of CuNPs, (b) zoom-in of the region shown in a, and (c) schematic representation of nanoparticle morphology and graph reporting the measurements of the spacings between the observed diffraction fringes. Instrumental magnification 300000 ×.

CuNPs with a roundish shape and an average size of 10.2 ± 3.0 nm were obtained. Moreover, the NPs tended to form aggregates (Figure 24a). HRTEM analyses showed that metallic crystalline Cu is formed, as demonstrated by the presence of diffraction fringes with spacing associated to the (1 1 1) plane of metallic Cu in the cubic phase (JCPDS file number 00-001-1242), as reported in Figure 24b and Figure 24c. Moreover, an amorphous layer was observed around the NPs (Figure 24b, red arrow). The characteristics of the synthetic procedure and the contrast phase make it reasonable to propose that the CuNPs are coated with a glycerol layer that acts both as a protecting agent and stabiliser. Indeed, the NPs did not coalesce under the electronic beam of the instrument, and presumably do not do so under the reaction conditions, proving that they are quite stable. The synthesised NPs can be described as having a core-shell morphology, in which the core is made up of crystalline Cu⁰ and the shell by glycerol molecules, as depicted in Figure 24c.

The existence of this morphology suggests that the glycerol layer mediates interactions between the metal active sites and the reagents. Moreover, besides having a stabilising

function, the glycerol layer can moderately promote NP dispersion in the glycerol solvent, therefore enhancing the active metallic surface area of the catalyst.

The reduction of nitrobenzene (**2.1**) to aniline (**2.2**) was performed in the presence of CuNPs and glycerol was used as the solvent and “sacrificial” hydrogen source (Scheme 28).



Scheme 28. CuNPs-catalysed reduction of nitrobenzene (**2.1**) using glycerol as reducing agent to obtain aniline (**2.2**).

As already done with the metallic copper, the standard reaction between nitrobenzene and the different hydrogen sources was carried out at 130 °C in oil bath for 1h with the CuNPs and KOH as base.

Table 15 Influence of different reducing agents in the reduction of nitrobenzene ^{a)}

Entry	Reducing agent	Catalyst	Nitrobenzene (%) ^{b)}	Azo (%) ^{b)}	Azoxybenzene (%) ^{b)}	Amine (%) ^{b)}
1	Ethanolamine	Metallic copper ^{c)}	48	28	8	16
		CuNPs ^{d)}	0	53	18	29
2	Ethylendiamine	Metallic copper ^{c)}	41	43	0	16
		CuNPs ^{d)}	0	47	0	53
3	3-Amino-1-propanol	Metallic copper ^{c)}	18	67	8	7
		CuNPs ^{d)}	0	8	63	8
4	2-Propanol	Metallic copper ^{c)}	2	17	52	29
		CuNPs ^{d)}	0	10	66	10
5	1,4-butanodiol	Metallic copper ^{c)}	52	0	35	12
		CuNPs ^{d)}	21	21	48	21
6	Ethylene glycol	Metallic copper ^{c)}	0	2	0	98
		CuNPs ^{d)}	0	1	1	98
7	Glycerol	Metallic copper ^{c)}	0	0	0	99
		CuNPs ^{d)}	0	0	0	99

^{a)} Reaction conditions: nitrobenzene (1 mmol), KOH (2 mmol), Solvent (40 mmol), oil bath, T: 130°C ^{b)} Determined by GC-MS ^{c)} Catalyst: Cu metallic powder (2 mmol), t: 5 hours. ^{d)} Catalyst: CuNPs (10 mol%), t: 2 hours.

Once again, as previously observed in Table 13, glycerol showed the highest selectivity to aniline. All solvents reflected the same behaviour and selectivity as when using the metallic copper, but CuNPs notably increased the reaction rate. While 5 hours were needed in the case of the bulky catalyst to present a considerable difference among the different solvents, 1 hour

was enough in the case of the NPs. Moreover, the catalyst quantity could be reduced from 200 mol% to only 5 mol% thanks to the high catalytic surface of the small particles. Thus, as shown in Table 16, the reaction was performed in glycerol and the parameters were optimised by varying the nature of the base, the reaction temperature and catalyst amounts. Several bases were tested: KOH, NaOH, K_2CO_3 , $CsCO_3$ and the best results (Table 16, entry 5) were obtained in the presence of 2 eq of KOH and 5 mol% of CuNPs.

Table 16. Optimisation of the Cu-Catalysed nitrobenzene reduction in glycerol

Entry	Reaction conditions	Temperature and time	Yields ^{a)}
1	K_2CO_3 (2 eq), CuNPs (5 mol%)	130 °C, 5 h	80
2	$CsCO_3$ (2 eq), CuNPs (5 mol%)	130 °C, 5 h	2
3	-, CuNPs (5 mol%)	130 °C, 5 h	1
4	NaOH (2 eq), CuNPs (5 mol%)	130 °C, 5 h	87
5	KOH (2 eq), CuNPs (5 mol%)	130 °C, 5 h	99
6	KOH (1 eq), CuNPs (5 mol%)	130 °C, 5 h	62
7	KOH (2 eq), CuNPs (2 mol%)	130 °C, 5 h	67
8	KOH (2 eq), CuNPs (10 mol%)	130 °C, 5 h	98
9	KOH (2 eq), CuNPs (5 mol%)	80 °C, 15 h	20
10	KOH (2 eq), CuNPs (5 mol%)	50 °C, 15 h	2
11	KOH (2 eq), CuNPs (5 mol%)	130 °C, 2 h	99
12 ^{b)}	KOH (2 eq), CuNPs (5 mol%)	US, 1 h	99
13 ^{c)}	KOH (2 eq), CuNPs (5 mol%)	MW 130 °C, 30 min	99

Reaction conditions: nitrobenzene (1 mmol), base (2 mmol), glycerol (40 mmol), CuNPs(5 mol%), oil bath, 5h. ^{a)} Determined by GC-MS. ^{b)} UP50Hz, F(kHz):30, P(W):50. ^{c)} CEM Mars 5, 130°C Pmax=400W.

The influence of US irradiation, given that the CuNPs usually aggregate, was investigated in order to improve reaction rate. US is known for its capacity to enhance particle dispersion and favour mechanical depassivation. Particle-size distribution was therefore measured before and after US treatment.

Freshly prepared CuNPs were sonicated for 10 min (UP50H, F(kHz):30, P(W):50) until a perfectly dispersed black solution was obtained. Offline particle-size distribution measurements (based on volume) were acquired and compared with those of freshly prepared NPs (Figure 25, red and blue curves). A laser diffractometer (Malvern, MasterSizer 3000 hydro SV) was employed and particle sizes were determined by measuring the intensity of scattered light when laser beam passed through a dispersed particulate sample. 0.5 mL of the sample ($C_{NP}=1g/L$) was injected into 6.5 mL of deionised water in the measurement cell (so that the resulting concentration in the cell was 0.07 g/L) and mixed for 5 min using a built-in magnetic stirrer. The obtained scattering curves were averages of three subsequent measurements. Unlike the TEM observations, the Cu particles here had larger sizes due to the

formation of aggregates, with an average size of 100 μm when suspended. US irradiation significantly influenced particle magnitude, with the size decreasing to 20 nm.

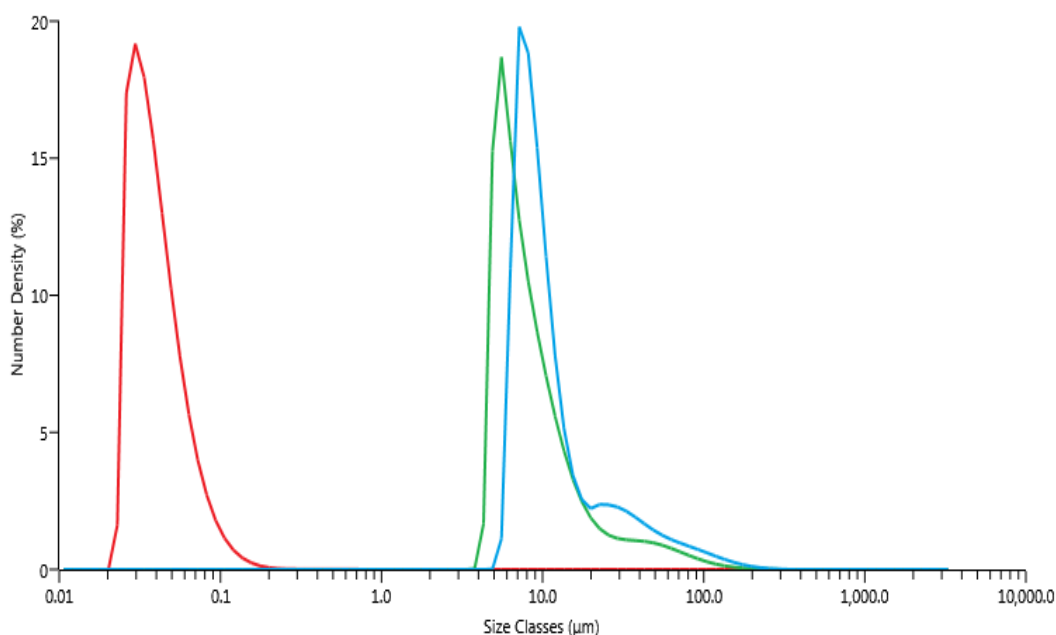


Figure 25. Particle-size distributions, PSD. Blue curve) freshly prepared CuNPs. Green curve) freshly prepared CuNPs after heating by MW irradiation for 10 min (Anton Paar Monowave 300, $T=130^{\circ}\text{C}$, $P_{\text{Max}}=400\text{W}$). Red curve) CuNPs after sonication for 10 min (Hielscher UP50H, $F(\text{kHz}):30$, $P(\text{W}):50$).

A kinetic study was performed to assess the influence of US sonication on the reaction rate; the nitrobenzene reduction was carried out under optimal reaction conditions in the presence of freshly prepared CuNPs and pre-sonicated CuNPs. As shown in Figure 26, sigmoidal behaviour was observed when the reaction was performed under conventional conditions and full conversion was obtained in 2 h. US pretreatment clearly had a significant effect on the reaction rate, and the complete conversion of nitrobenzene to aniline was achieved in 1 h. Excellent results were also obtained when the transfer hydrogenation of nitrobenzene was performed under MW irradiation, with the reaction time falling to 30 min (Table 16, entry 13). A slight effect on reaction rate was also observed when the reaction was performed under US irradiation, and full conversion was observed after 1 h (Table 16, entry 12).

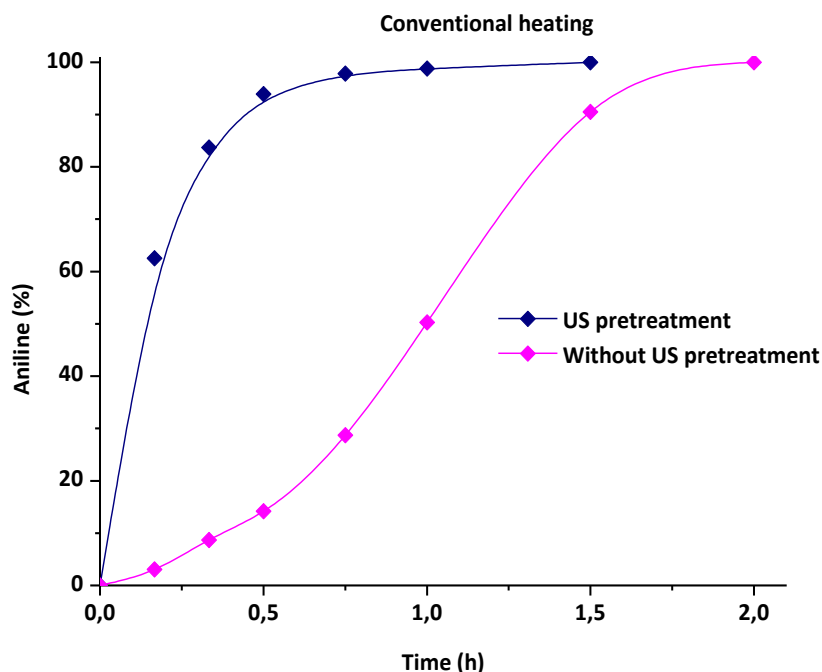


Figure 26. Nitrobenzene reduction profile with and without previous CuNP US-sonication. Pretreatment: CuNPs and glycerol, US irradiation 10 min (Hielscher UP50H, $F(\text{kHz}):30$, $P(\text{W}):50$). Reaction conditions: nitrobenzene (1 mmol), KOH (2 mmol), glycerol (40 mmol), CuNPs (5 mol%). 130 °C. The % of aniline was determined by GC-MS.

In order to dismiss any kind of metal leaching from the ultrasonic horn, and so, discharge the possibility of obtaining a better conversion due to a catalytic reason; another experiment was set up. The reaction was performed with conventional heating in an oil bath and the sonic horn was immersed inside the reaction solution, without applying any power. If there were the influence of any metal coming from the horn, the reaction outcome would increase. However, the kinetic obtained by conventional heating with and without the immersion of the sonic horn did not vary, so we could assume that the real effect was the better catalyst dispersion and not the leaching. After the previous find, we decided to accomplish the reaction under microwave and under ultrasound irradiation, once again with and without initial catalyst dispersion. The catalyst was previously dispersed in the glycerol for 10 min and after adding the nitrobenzene and the base, the reaction was performed under ultrasound irradiation and under microwave. The obtained results, showed in Figure 27 and Figure 28, strengthen the conclusion previously got. As depicted, the ultrasound allows a better catalyst dispersion and so, a faster nitrobenzene reduction.

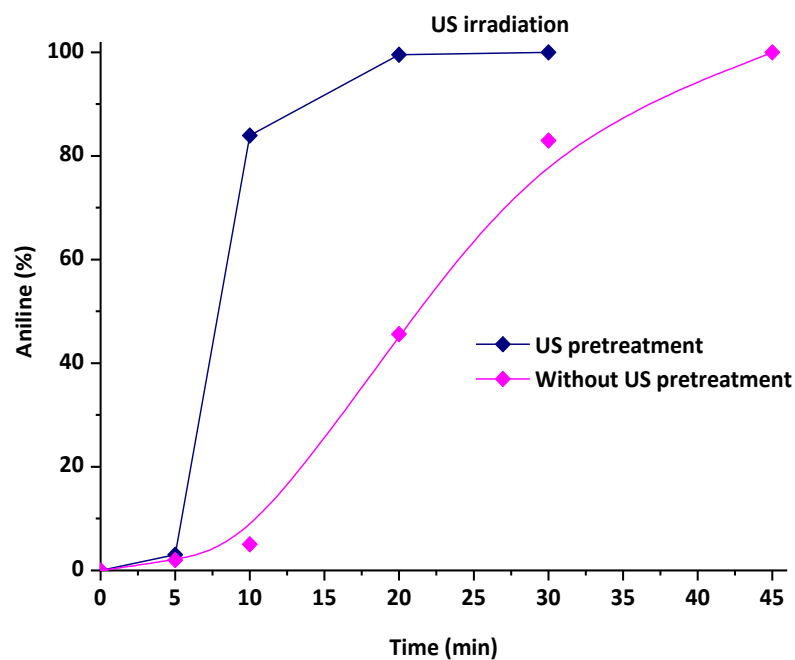


Figure 27. Nitrobenzene reduction profile with and without previous CuNP US-sonication. Pretreatment: CuNPs and glycerol, US irradiation 10 min (Hielscher UP50H, F(kHz):30, P(W):50). Reaction conditions: nitrobenzene (1 mmol), KOH (2 mmol), glycerol (40 mmol), CuNPs (5 mol%). US irradiation: t:1h (Hielscher UP50H, F(kHz):30, P(W):50). The % of aniline was determined by GC-MS.

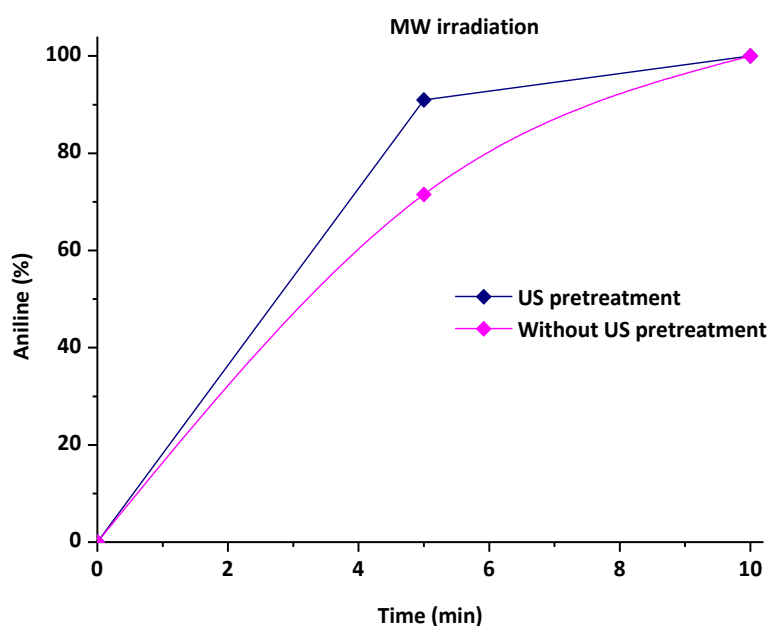


Figure 28. Nitrobenzene reduction profile with and without previous CuNP US-sonication. Pretreatment: CuNPs and glycerol, US irradiation 10 min (Hielscher UP50H, F(kHz):30, P(W):50). Reaction conditions: nitrobenzene (1 mmol), KOH (2 mmol), glycerol (40 mmol), CuNPs (5 mol%). MW irradiation: t: 10 min (CEM Mars 5, 130°C Pmax=400W). The % of aniline was determined by GC-MS.

2.4 MW-assisted copper-catalysed transfer hydrogenation reduction of nitrobenzene. Industrial MW-assisted scale-up.

Glycerol's high boiling point combined with its low environmental impact, cost, vapour pressure and high dielectric constant make it an optimal candidate for MW-promoted organic syntheses. Furthermore, as described in Hulsfold *et al.*, the interactions between MW and the heterogeneous metal-catalyst particles generates electrostatic discharges that can lead to the formation of active particles in the reaction media.^{343,344} It is for both of these reasons that MW irradiation was chosen for the optimisation of the CuNPs-catalysed transfer hydrogenation of nitrobenzene in glycerol.

A preliminary evaluation of the influence of MW irradiation on the nitrobenzene reduction was performed in a multimode MW oven (*CEM Mars 5*, max. power 400W). The reaction was carried out at 130 °C, and nitrobenzene was completely converted to aniline after 30 min (Table 16, entry 13).

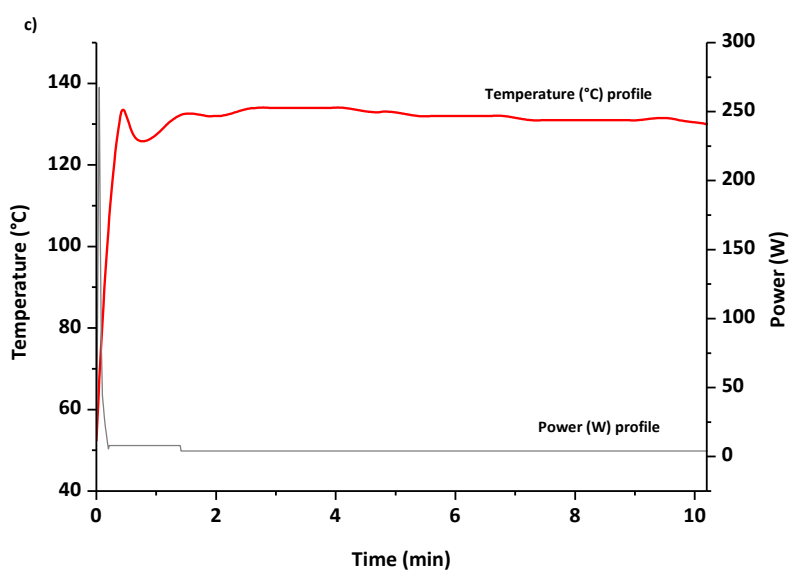
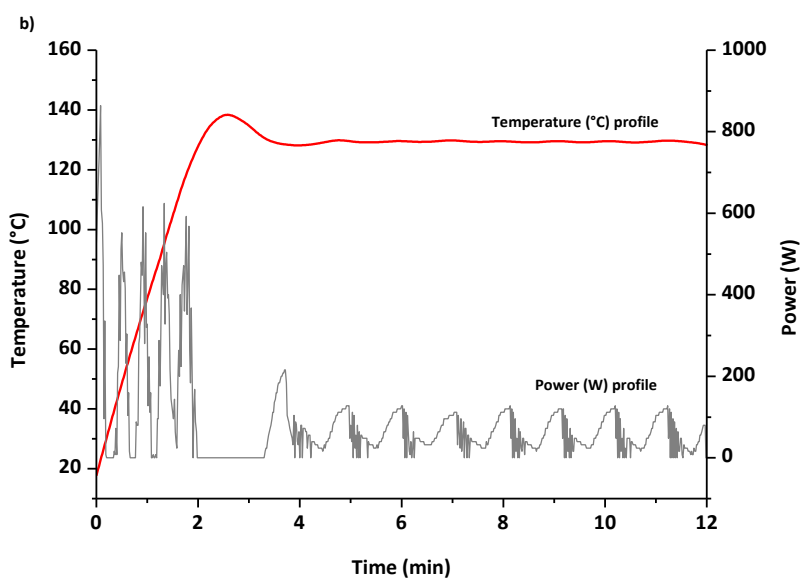
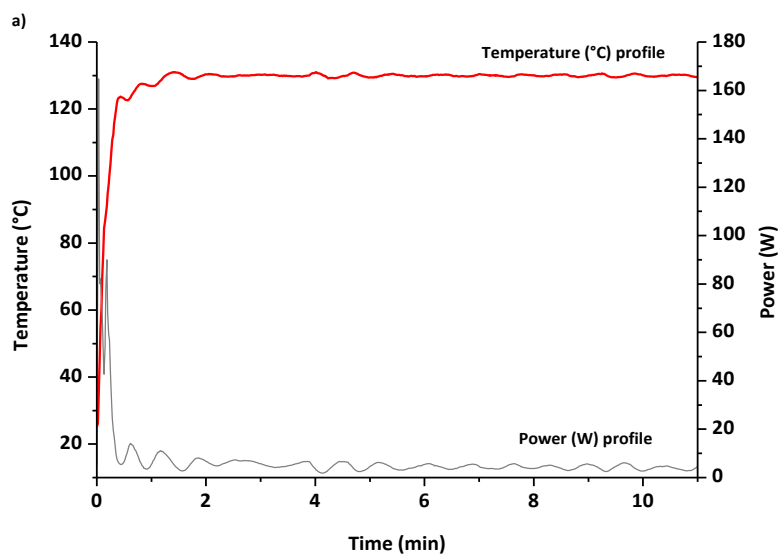
In order to identify the best technology for reaction scale-up, a number of MW devices were used for MW-assisted batch synthesis of aniline. Reactions were performed in constant temperature mode and, separately, in constant power mode in two monomode MW instruments (Anton Paar Monowave 300 and CEM Discover SP) and two multimode MW systems (CEM Mars 5 and Milestone MicroSynth). When constant temperature mode was used, the power was automatically adjusted to reach the set temperature as quickly as possible and then maintain it using a dynamic feedback power loop. In constant power mode, the instrument adjusted the power to reach the reaction temperature as quickly as possible and then set the chosen constant power (Figure 29 grey profiles). In order to maintain the desired temperature, the selected power was carefully evaluated in advance using trial-error methodology. As demonstrated in Figure 29, the constant power set for monomode MW instruments was 4 W, while 80 W was needed in the multimode MW. As depicted in Table 17 while the reactions were complete after 30 min in all the experiments, substantial differences after 15 min of reaction time depending on the type of MW cavity (monomode vs. multimode MW cavity) and on the temporal heating profile (constant power vs. constant temperature) were observed. Better results were always obtained after 15 min when the power was maintained constant (Table 17, entries 2,4,6,8). However, only in multimode-assisted reactors was full conversion obtained. The temperature and power profiles in all the MW instruments were registered when working with both methods: fixed temperature (Figure 29a, 23b) and fixed power (Figure 29c, 23d). Multimode systems have lower power density than monomode devices because of their large chambers, and higher power (80 W) is therefore required to bring the reaction mixture to the desired temperature. Higher MW power produces higher conversions, as MW electron-field effects are very important, meaning that electrostatic discharges can be generated via the interaction between MWs and the heterogeneous CuNPs, leading to the formation of active species in the reaction media. The differences observed when the reaction time was shortened to 15 min may be due to the amount of energy provided to the sample, as demonstrated by the fluctuation in the power provided when the system is set to work at constant temperature (see profiles Figure 29a and 23b), resulting in worse conversions than those obtained with constant power. As depicted in Table 17, the results of the reactions in the two monomode instruments (CEM Discover and Anton Paar Monowave 300) were similar to each other, as were those of the reactions in the two

multimode instruments (CEM Mars and Milestone Microsynth). In fact, reaction outcome did not depend on the instrument used, but differences between the monomode and multimode reactors were observed.

Table 17: MW-assisted nitrobenzene reduction optimisation.

Entry	Method	System	Apparatus	Reaction time (min)	Yield (%) ^{a)}
1	MW-T constant ^{b)}	Anton Paar Monowave 300	Monomode	15	21
				30	>99
2	MW-P constant ^{c)}	Anton Paar Monowave 300	Monomode	15	49
				30	>99
3	MW- T constant ^{b)}	CEM, Discover	Monomode	15	22
				30	>99
4	MW- P constant ^{c)}	CEM, Discover	Monomode	15	53
				30	>99
5	MW- T constant ^{b)}	CEM, MARS	Multimode	15	52
				30	>99
6	MW- P constant ^{d)}	CEM, MARS	Multimode	15	>99
				30	>99
7	MW- T constant ^{b)}	Milestone, MicroSynth	Multimode	15	58
				30	>99
8	MW- P constant ^{d)}	Milestone, MicroSynth	Multimode	15	>99
				30	>99

Reaction conditions: CuNPs (5 mol%) and glycerol were sonicated for 10 min, creating a perfectly dispersed black solution. Nitrobenzene (1 eq) and KOH (2 eq) were then added. a) Determined by GC-MS. b) Program: 2 min Pmax=400W heated as quickly as possible to reach 130 °C, then T= 130 °C c) Program: 2 min Pmax=100% heated as quickly as possible to reach 130 °C, then P: 4 W. d) Program: 2 min Pmax=400 W heated as quickly as possible, then constant P:80W.



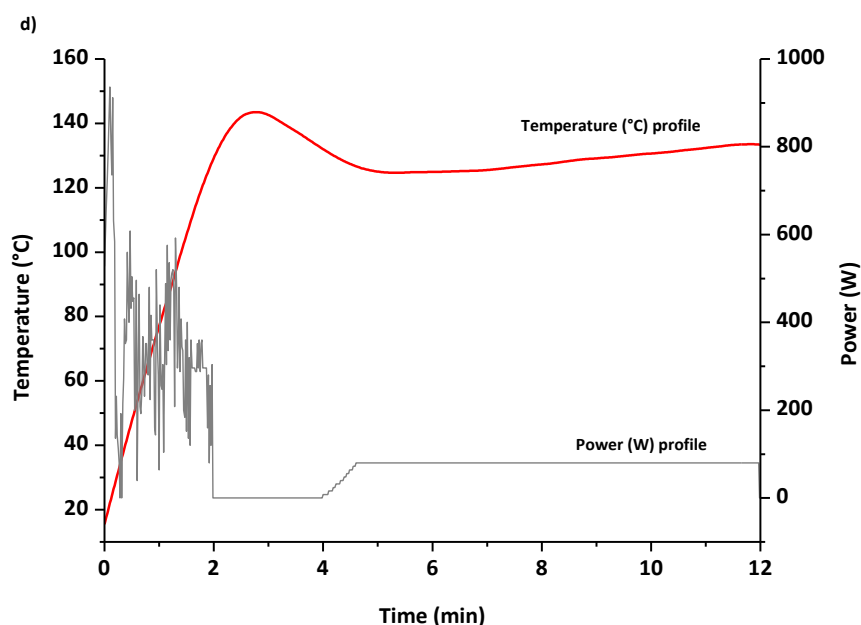
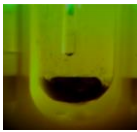

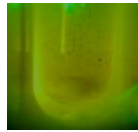
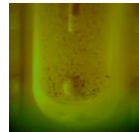
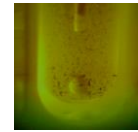
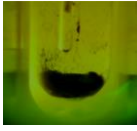
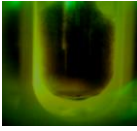
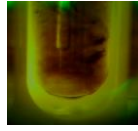
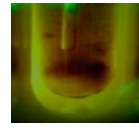



Figure 29. Temperature and power profile curves registered by MW instruments: a) Anton Paar Monowave 300, Program: 2 min $P_{max}=100\%$ heated as quickly as possible to reach 130 °C, then $T=130$ °C; b) Milestone MicroSynth, Program: 2 min $P_{max}=400$ W heated as quickly as possible to reach 130 °C, then $T=130$ °C; c) Anton Paar Monowave 300, Program: 2 min $P_{max}=100\%$ heated as quickly as possible to reach 130 °C, then $P: 4$ W; d) Milestone MicroSynth, Program: 2 min $P_{max}=400$ W heated as quickly as possible to reach 130 °C, then $P: 80$ W.

One of the main issues when working with Cu^0 -based NPs is their susceptibility to oxidation. Agglomeration is another effect that is usually observed when working with these small particles. Although the influence of MW irradiation on NP agglomeration has not been thoroughly studied yet, a few publications by Serpone *et al.*, have attempted to evaluate the formation of aggregates of activated-carbon-supported Pd as caused by an excessive number of hot spots. In this work, some experiments were carried out in a MW-reactor, Anton Paar Monowave 300, that was equipped with a USB Digital Microscope Supereyes B003+ in order to better understand CuNP behaviour inside the MW cavities. This multi-function microscope allowed us to follow the reaction when MW irradiation was applied. Firstly, glycerol was added to the test tube together with sequentially increasing quantities of CuNPs (2.5 mg, 10 mg, 20 mg and 40 mg). As depicted in Table 18 (Entries 1-2), the concentration of CuNPs highly influenced aggregation, and the precipitation of large particles can be observed after a few minutes when working with 10 mg/3 mL or higher concentrations. The particle-size distribution of CuNPs was therefore measured after the MW-promoted reduction of nitrobenzene in glycerol was performed in the same instrument (Anton Paar Monowave 300), and a similar size-distribution profile to that of freshly prepared NPs was detected (Figure 25, green profile).

Table 18: CuNPs behaviour when applying MW-irradiation

Entry	Method	1 min	3 min	5 min	8 min	10 min
1	2.5mg CuNPs + 3mL Glycerol					
2	10mg CuNPs + 3mL Glycerol					

(Anton Paar Monowave 300, Program: 2 min Pmax=100% heated as quickly as possible to reach 130 °C, then T= 130 °C). Recorded using USB Digital Microscope Supereyes B003+.

When referring to a green process, it is crucial to think about the need of being easily scalable from laboratory to industrial scale and so, essential to be safe and cost effective. There are two main paths for this task: batchwise and continuous flow.

The good results obtained for the reduction of aromatic nitro compounds under MW irradiation encourage us to explore the reaction scale-up in a MW batch reactor.

The scale-up of MW heating constitutes a growing demand for industry thanks to the successes achieved on the lab scale. At 2.45 GHz, the most commonly used MW frequency, the MW-penetration depth in common polar solvents is around a few centimetres. Because of this, the heating of bulk samples using MW irradiation has several limitations. Controlling the stirring rate to ensure and maintain the homogeneity of a solution and avoid thermal gradients must therefore be considered. As observed in the literature, most of the reactions that are accomplished under MW irradiation are performed at high temperatures in sealed vessels. Several approaches with different processing techniques can be used to scale-up a wide range of MW-promoted reactions,³⁴⁵ and the use of open reaction vessels in batch mode offers operational advantages that can address scale-up needs. The small cavity of monomode MW apparatus has to be replaced with a larger multimode unit when high volumes are processed. The reduction of nitrobenzene to aniline, which has already been optimised for a 15 mL volume (1 mmol of substrate) in our study, was scaled up to 500 mL to perform the scale-up experiments.

All scale-up experiments were performed in a MW instrument MEAM Explorer VP (<http://www.meam.be/>, Figure 30), which is a MW multimode oven designed as a multipurpose test device for various applications. This unique design provides access on four sides of the cavity, allowing multiple connections to be used for sensors and entrances/exits for gases or liquid products. In this case, the opening on the right side was used to measure the IR temperature of the sample, while the opening on the top was used to insert the glass stirring rod. Emissivity can be defined as the effectiveness of emitting energy in form of thermal irradiation and varies from 0 to 1. It is of high significance when the temperature is measured with an IR camera. Transmissivity refers to the proportion of the radiation that hits a body and ends up being transmitted through it without being absorbed or reflected, and describes the level of infrared radiation that permeates the object. While the emissivity value is intrinsic and only depends on sample nature, the transmissivity value also depends on the

shape of the vessel and its material. Both transmissivity and emissivity have to be measured to ensure the optimal calibration of the IR camera, allowing the temperature measured by the system to be as accurate as possible. The emissivity and transmissivity of the reaction mixture were determined by comparing the solution temperature measured by a thermocouple and an IR camera; the factors were 0.95 and 0.48, respectively. It is important to always place the IR camera in the same location in order to maintain constant parameter values. Once those parameters were obtained, a number of experiments were performed.

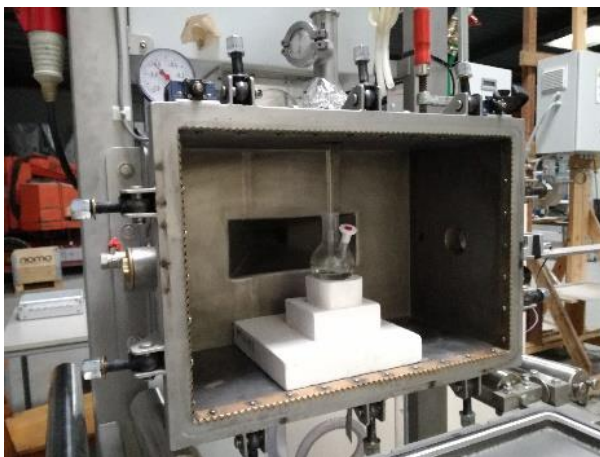


Figure 30. First generation multimode MW reactor. Internal cavity: 72L Power: 1.2 kW. MEAM Explorer VP.

Preliminarily, the reaction was carried out at 130 °C in a 250 mL round-bottom flask and a glass stick was used to stir the 90 mL solution (6 mmol). Two reactions were performed: one experiment was carried out at constant power (25-30 W), while power was varied in the second (from 40 W to 0 W). The temperature was maintained constant at 130 °C in both experiments. The histogram density of temperature in the cavity was registered using an IR camera (Optris PI Connect, Figure 31). The input power and reflective power were measured in order to identify the power value that was actually absorbed by the reaction solution. As depicted in Figure 32, a higher percentage of the delivered power was absorbed when power was maintained constant (Figure 32a compared to Figure 32b).

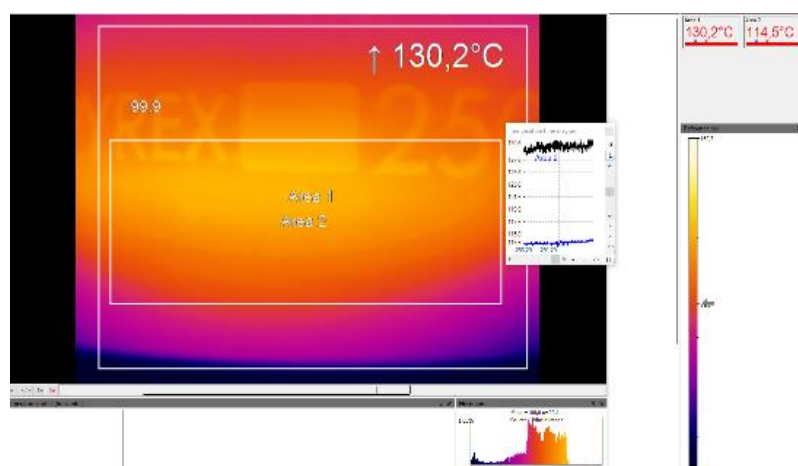


Figure 31. Histogram density of temperature recorded by IR camera Optris IP Connect. Reaction time: 10 min.

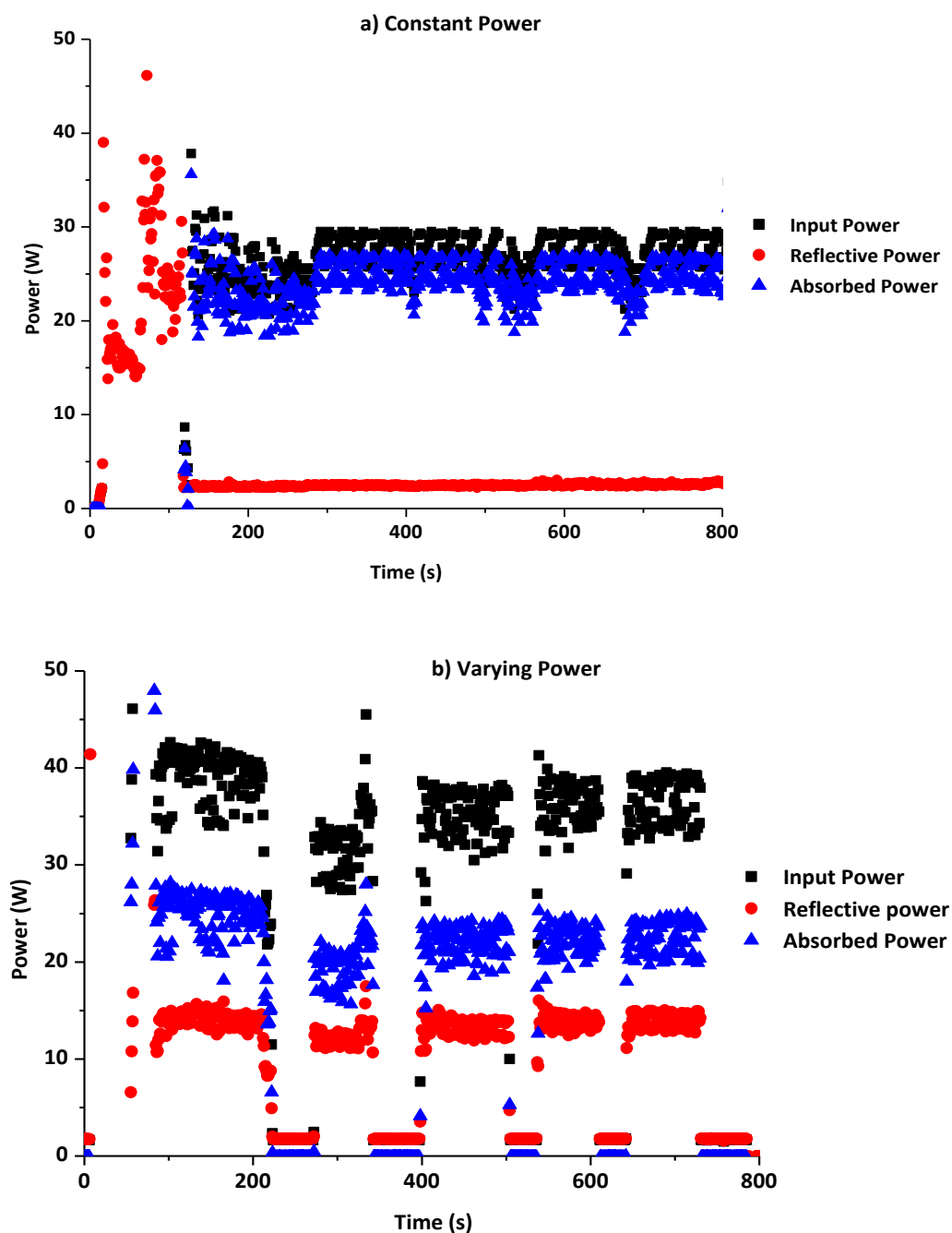


Figure 32 a) Power profile while working at constant power (25-30 W). b) Power profile while working at varying power (40 W-0 W) (The power meter displays 0-4W when the magnetron is completely off).

A number of reactions were performed to optimise the MW-heating protocol and scale-up the reaction. Results are summarised in Table 19. A 50 % yield of aniline was obtained after 20 min of MW irradiation when working with constant power when the reaction was performed on the 6 mmol scale (90 mL glycerol) in the presence of 10 mol% of CuNPs.

Table 19: Scale-up MW-assisted nitrobenzene reduction optimisation.

Entry	Method	Scale (mmol)/mL Glycerol	Catalyst (mol%)	T (°C)	t (min)	Yield (%) ^{a)}
1	MW (25-30W)	6 mmol/90 mL	10	130	20	50
2	MW-(40-0 W)	6 mmol/90 mL	10	130	20	35
3	Presonicated CuNPs, MW (25-30W) ^{b)}	6 mmol/90 mL	10	130	20	66
4	Presonicated CuNPs, MW (25-30W) ^{b)}	6 mmol/90 mL	5	130	20	60
5	Presonicated CuNPs, MW (25-30W) ^{b)}	6 mmol/90 mL	5	150	20	78
6	Presonicated CuNPs, MW (25-30W) ^{b)}	6 mmol/90 mL	5	150	45	>99
7	Presonicated CuNPs, MW (25-30W) ^{b)}	18 mmol/270 mL	5	150	45	93
8	Presonicated CuNPs, MW (25-30W) ^{b)}	18 mmol/270mL	5	150	60	>99
9	Presonicated CuNPs, MW (25-30W) ^{b)}	36 mmol/540mL	5	150	60	95

Reaction conditions: nitrobenzene(1eq), glycerol (200 eq), KOH (2 eq). ^{a)} Determinated by GC-MS. ^{b)} CuNPs were added into the glycerol and sonicated for 10 min, forming a perfectly dispersed black solution.

The conversion was reduced to 35 % with varying power, which demonstrates that the efficacy of MW promotion on the Cu-catalysed transfer hydrogenation of nitrobenzene is reduced when fluctuating power is used. In agreement with our previous results on the laboratory scale, the pretreatment of CuNPs with US significantly enhanced the reaction rate (Table 19, entry 3); 66% reduced product was achieved in this case.

When presonicated, the amount of catalyst could be reduced from 10 mol% to 5 mol% without a significant decrease in yield (Table 19, entry 4), while an increase in reaction temperature to 150 °C yielded 78% amino derivative in 20 min. As shown, full conversion of nitrobenzene to aniline was obtained when the reaction time was increased to 45 min (Table 19, entry 6). When the reaction was performed on a larger scale (18 mmol nitrobenzene/270 mL of glycerol), the reaction time was increased to 1 h in order to complete the reduction. Moreover, the reaction was also performed in a 1 L flask (36 mmol/540 mL of glycerol) with the initial solution being sonicated. A 95% yield was achieved once this reaction mixture was heated for a total time of 1 hour.

2.5 A simple set up for transfer hydrogenation in flow chemistry. Reduction of nitrobenzene over copper supported catalyst (Cu/Celite).

Compared to the batch alternative, continuous flow processing specifically address the scale-up needs and exhibit several benefits that make it particularly attractive for the industrial synthesis, in terms of efficacy, cost, equipment size, energy consumption, safety and waste generation, among other things. This technique has grown rapidly over the course of the last decade^{346–348} and, as shown in Figure 33, continuous flow and sustainable processing are stringently correlated.³⁴⁹

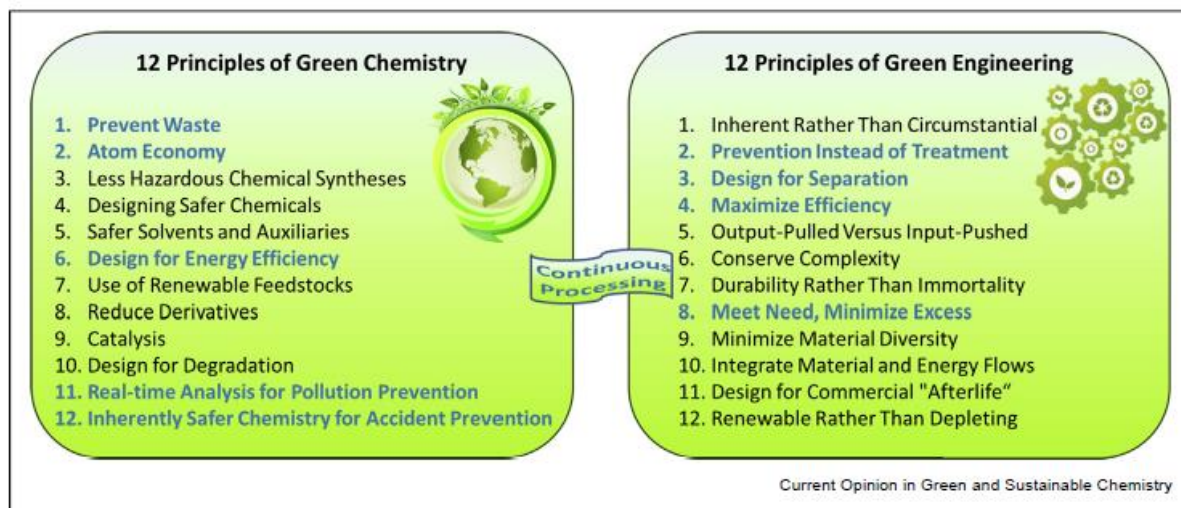


Figure 33: Twelve principles of green chemistry and green engineering and the impact of continuous processing highlighted in blue. (Why flow means green – Evaluating the merits of continuous processing in the context of sustainability Doris Dallinger and C. Oliver Kappe).³⁴⁹

The merits of continuous flow in the context of sustainability can be summarize as follows:

- Safety: Smaller reactor volumes are employed in flow continuous reactions, what minimize the harshness in case of accident.
- Yield and quality. The high efficiency in mass and heat transfer, precise control of the reaction temperature and the enhanced selectivities and yields, contributes toward greener and more sustainable processes.
- Speed increased. Since the lab-scale routes toward the desired product are suited to be scaled up linearly in flow with minimal re-optimization, the implementation of a new process to plant scale is less time consuming.



Figure 34: Merits of continuous flow in the context of sustainability.

For solid–liquid reactions, three different kind of reactor beds are mostly used (Figure 35). 1) Packed beds are characterized by the entire column or channel being filled with a solid material and so, particle movement is restricted. 2) In a fluidized bed reactor, the particles are free-flowing and suspended within the channel. 3) Mixed beds are a combination of a packed bed and a fluidized bed. The movement of the solid at the bottom of the reactor is restricted, while the top layers are suspended and mixed via the flowing liquid phase. Packed beds reactors offer the most convenience, owing to the limited experience required for their set up and use.

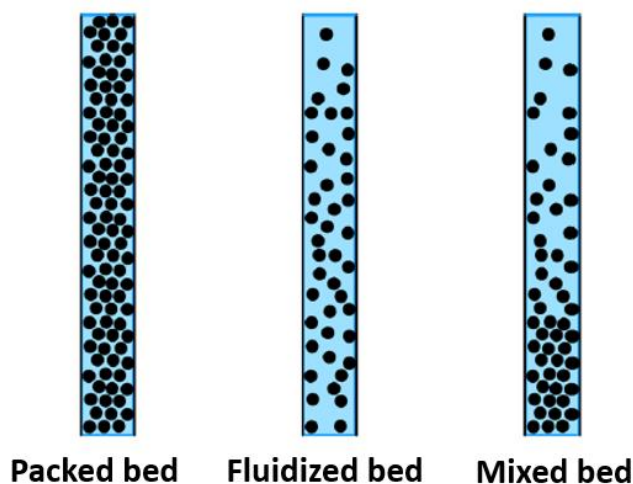


Figure 35. Different solid-liquid reactors, characterized by solid mass transfer. Within each bed, liquids typically exhibit slug flow or turbulent flow ³⁴⁸

The performance of hydrogenation reactions under flow chemistry^{350,351} has undergone a great increase during this recent period thanks to the important improvements in performance, safety and environmental impact. Flow approaches provide superior gas–liquid contact compared with traditional hydrogenation approaches, which are limited by the rate of hydrogen gas diffusion into the bulk solvent.

Due to this, reduction chemistry is well suited to flow chemistry given the inherent risks involved in such transformations. In most cases, hydrogen gas or hydride are used as reducing

agents, however, inline production of hydrogen could also be facilitated by smart systems such as the H-cube. Nevertheless, as already discussed in this work, the use of hydrogen gas for industrial application is undesirable and specialist and large price tag equipment are required. Hence, we decided to apply a transfer hydrogenation approach in continuous flow, as this would allow the hydrogen source to be part of the reaction mixture.

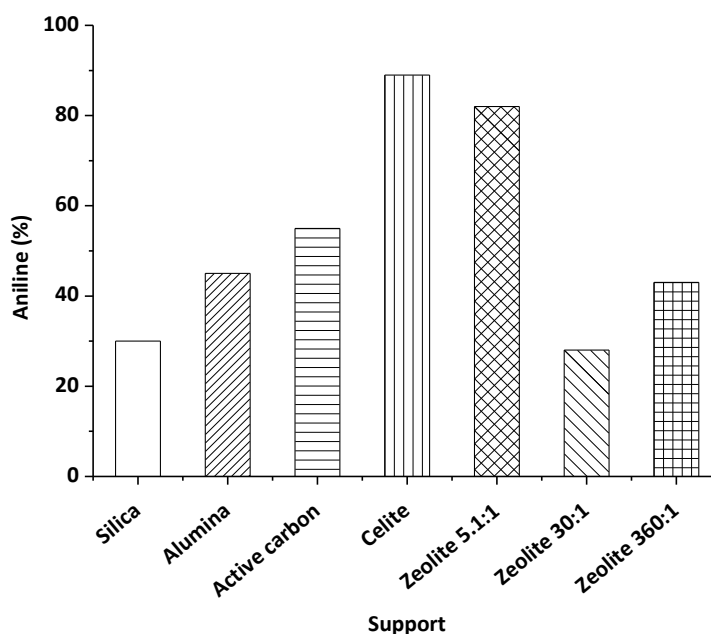
Transfer hydrogenation reactions have already been reported in flow chemistry. In 1998, Means et al. published a method in which palladium is used for the reduction of alkenes, using formic acid as hydrogen source and gravity to flow the solution through the column. More recently, in 2013, an efficient flow procedure was described by Ley et al. using hydrous zirconia for the transfer hydrogenation of ketones and aldehydes. Ammonium formate as reductant³⁵² was used with Pd/C or Raney-Ni proving to be optimal for the reduction of nitrocompounds in the presence of different functional groups. In 2017, Lindhardt et al.³⁵³ designed a transfer hydrogenation continuous flow using cyclohexene and a cosolvent (methanol or ethyl acetate) as the hydrogen donor in combination with palladium-on-charcoal. Reductions of standard functional groups, including double bonds, triple bonds, nitro group, ketones, and aldehydes were carried out.

In particular, given the importance of aromatic amino compounds, it is not surprising that a vast number of flow chemistry protocols have been reported for this process during the last decade. The reaction is usually performed under palladium^{352–354}, platinum and RANEY® nickel³⁵⁵ as catalysts, giving high yields. More recently, non-nobel metals like Ag³⁵⁶, Au^{357,358} and Fe^{359–361} have also been studied for this kind of transformations, but always using hydrogen gas or hydride as reducing agent.

As already mentioned, unsupported NPs tend toward particle agglomeration, and the presence of stabilizing agents or solid supports is mandatory in most cases. The recycling of metal catalysts is very important from economic and environmental points of view, and when working with unsupported metals it becomes a difficult task. Therefore, various novel methods have been proposed so far to immobilize/stabilize the active metal species and to separate/collect/reuse the dissolved metal species. In 2016, M. Hutchings and T. Wirth³⁵² reported a simple set up for the transfer hydrogenation in flow chemistry of nitrocompounds, azides and alkenes by using a packed-bed reactor with a palladium/charcoal catalyst and ammonium formate or triethylsilane as hydrogen/hydride source. However, avoiding noble metals like palladium is always desirable.

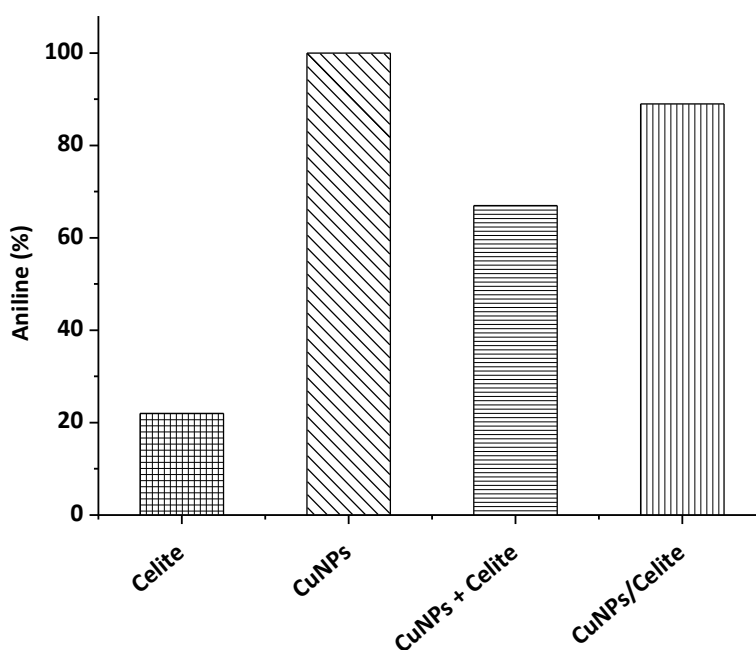
Here in, with the aim of preparing a non-nobel heterogeneous, robust as well as recyclable catalytic system for transfer hydrogenation reduction of nitrobenzene under continuous flow, different supports were tested.

A number of copper catalysts were prepared by impregnating the different supports with an aqueous solution of copper (II) sulfate followed by addition of NaOH and NaBH₄ in order to form the supported CuNPs over different materials. A preliminary study in the already optimized batch conditions was performed. In this case, ethylene glycol replaced the glycerol as solvent and hydrogen source in order to better allow the flow through the tubes and small bed packed reactor.



Graph 3. Reduction of nitrobenzene to aniline over different copper supported materials. Reaction conditions: nitrobenzene (1mmol), KOH (2 mmol), CuNPs/Support (5 mol%), ethylen glycol (15 mL). T: 130°C, t:1h. Determinated by GC-MS.

As despite in Graph 3, when using silica as support only 30% of aniline was obtained. Better results were obtained when alumina and active carbone were used, giving 45% and 55% respectively. Zeolites are aluminosilicate molecular sieves known to have great potential as basic catalysts and catalyst supports. Three different types of zeolites were also tested, but only the zeolite 5.1:1 gave high conversion, reaching 80% of aniline. The best result was observed when celite was used as support material and almost 90% of fully reduced product was formed.



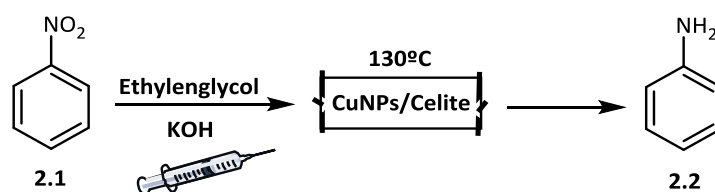
Graph 4. Reduction of nitrobenzene to aniline over: celite, CuNPs, CuNPs+Celite and CuNPs/Celite. Reaction conditions: nitrobenzene (1mmol), KOH (2 mmol), catalyst (5 mol%), ethylen glycol (15 mL). T: 130°C, t: 1h. Determinated by GC-MS.

In order to better understand the role of the support and for the sake of comparison, the inorganic support itself (celite), the fresh CuNPs, the physical mixture of CuNPs and celite and the CuNPs supported over celite (CuNPs/Celite) were tested in batch conditions.

As observed in Graph 4, the support itself gave a very low conversion, but when testing fresh CuNPs alone fully reduction to aniline was detected in one hour. These results were compared to the nitrobenzene reaction catalysed by a physical mixture of CuNPs and celite and a reaction performed when using the supported material (CuNPs/Celite). As despite, CuNPs/Celite showed higher efficiency, confirming the influence in supporting the metal catalyst on the reaction outcome. Despite the fact that the unsupported CuNPs gave the higher conversion and showed the higher activity, they cannot be recovered and reused, what means an importance drawback in terms of sustainability. Due to this, we decided to continue our study employing CuNPs/Celite as catalyst.

To investigate possible leaching of the copper catalyst, the standard reduction of nitrobenzene with ethylen glycol and KOH was selected and two sets of the reaction were carried out under the optimised conditions. One reaction set was quenched after thirty minutes and the product was determined by GC_MS analysis (42% yield). The catalyst was separated by filtration and the reaction was allowed to continue for one hour more, which resulted in almost no further conversion (43% yield). However, the set which contains the catalyst during the whole time showed 98% yield of aniline. The experimental results showed no significant change in the yield after catalyst separation, which clearly indicates very low copper leaching.

The catalytic activity of CuNPs/Celite was then investigated under continuous-flow conditions in a packed bed reactor, thereby allowing the reaction mixture to pass through the catalyst without the need of subsequent removal by filtration. An additional advantage to the application of the packed bed reactor approach is the presence of superstoichiometric amounts of catalyst, resulting in a significant reduction in the required residence time. Despite this superstoichiometric amount of Cu experienced by the limiting substrate, at any given time, in the reactor the overall flow system will become catalytic upon prolonged operation.



Scheme 29: Model reaction under continuous flow. Reaction conditions: nitrobenzene (1 mmol), base (2 mmol), ethylen glycol (40 mmol), CuNPs/Celite (5 mol%).

As all reactants are mixed prior to entering the packed bed reactor, a one-pump setup could be designed and the reaction mixture would be loaded by injection into a loop positioned between the pump and packed bed reactor (see Figure 36). An oil bath was employed as the heating source and the packed bed reactor was immersed, allowing the system to reach the desired reaction temperature in few minutes (130 °C). During the study two different packed bed reactor designs were tested, differing in the method of packaging and the amount of CuNPs/Celite catalyst loaded. Finally, the outcome of the reactor was collected into a flask and a small amount of the reaction mixture was analyzed by GC_MS to determine the conversion.

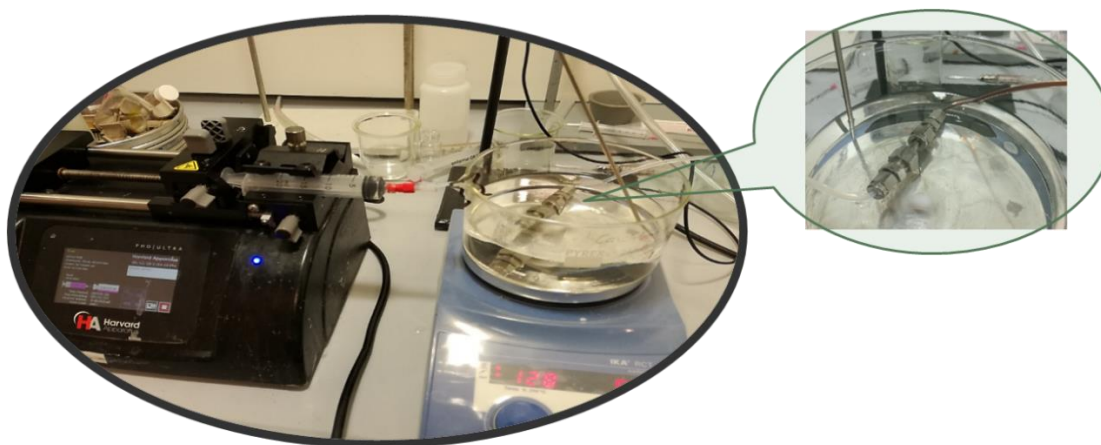
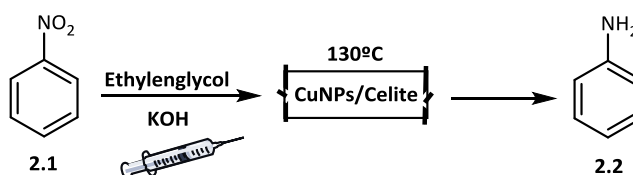


Figure 36: Schematic representation of the continuous flow system

The void volume of the packed bed reactor was determined by the weight difference of the dry and ethanol loaded column at room temperature correlated to the density of the liquid (4.1.4.2.2 Packed bed reactor unit).

The continuous flow reduction of nitrobenzene was chosen as model reaction (Scheme 29). Nitrobenzene and KOH dissolved in ethylen glycol was loaded onto the sample loop (2mL to a 1 mmol reaction scale) and then pumped through the packed bed reactor set at 130 °C.



Scheme 30: Model reaction under continuous flow. Reaction conditions: nitrobenzene (1 mmol), base (2 mmol), ethylen glycol (40 mmol), CuNPs/Celite (5 mol%).

Table 20. Optimisation of the Cu-Catalysed nitrobenzene reduction in ethylen glycol under continuous flow.

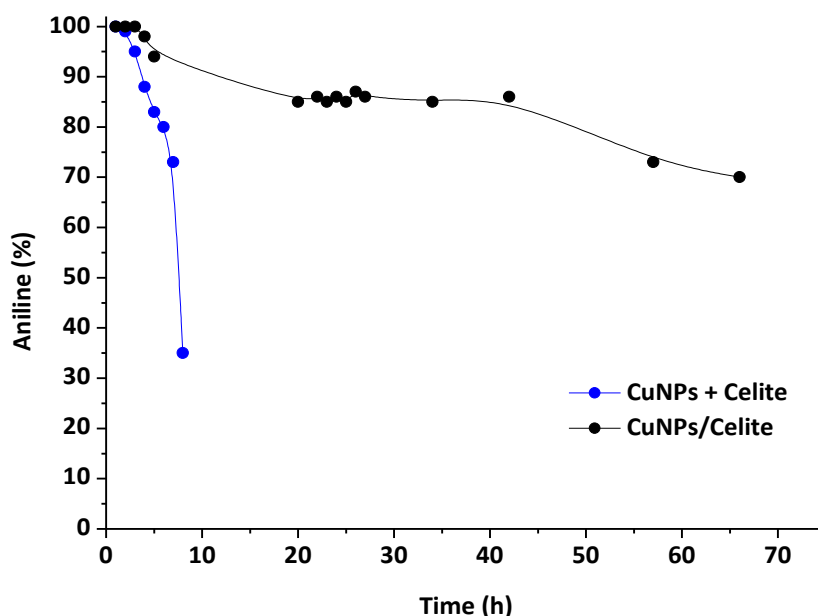
Entry	Catalyst	Conc. Nitrobenzene (mol/L)	Flow rate (mL/min)	Yields (%) ^{a)}
1	CuNPs/Celite (10 mol%)	0.5	0.05	58
2	CuNPs/Celite (10 mol%)	0.5	0.03	93
3	CuNPs/Celite (10 mol%)	0.5	0.02	96
4	CuNPs/Celite (5 mol%)	0.5	0.05	30
5	CuNPs/Celite (5 mol%)	0.5	0.03	56
6	CuNPs/Celite (5 mol%)	0.5	0.02	88
7	CuNPs/Celite (5 mol%)	0.3	0.02	92
8	CuNPs/Celite (5 mol%)	0.1	0.02	>99

Reaction conditions: nitrobenzene (1 mmol), base (2 mmol), ethylen glycol, CuNPs/Celite. ^{a)} Determined by GC-MS.

Using similar conditions to the previously optimised procedures in batch, screening of catalyst loading, initial substrate concentration and flow rates were then investigated (Table 20). Each experiment was performed with a fresh catalyst cartridge. Operating the system at a flow rate of 0.05 mL/min (Table 20, entry 1), corresponding to a residence time of 0.622 min,

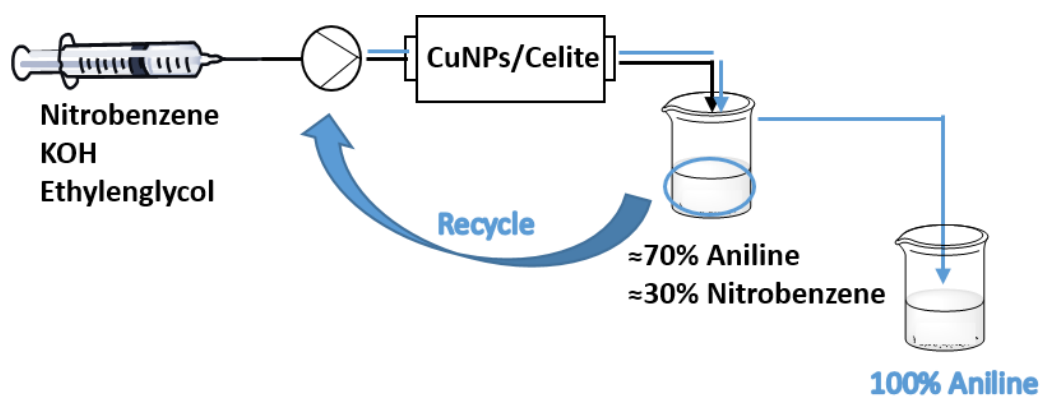
resulted in full selectivity to aniline with 58 % of yield. When variations in the flow rate were applied 0.03 mL/min and 0.02 mL/min (Table 20, entries 2-3), corresponding to 1.04 min and 1.55 min respectively, was observed that the nitrobenzene reduction increased when augmenting the residence time. A reduction of activity was observed when the catalyst amount was decreased to 5 mol% (Table 20; entries 4-6). For further comparison, the influence of the nitrobenzene initial concentration was also studied. As observed (Table 20, entries 7-8), the higher is the concentration the lower is the nitrobenzene conversion to aniline. When pumping a 0,1M solution through the 5 mol% bed packed reactor, it was showed that a conversion > 99% was achieved.

One of the most important features of immobilized catalysts in continuous applications is, apart from the activity of the catalyst, the ability to be used over several hours or even days. We therefore placed special emphasis on monitoring the CuNPs/Celite-catalysed reduction of nitrobenzene over a prolonged time period. From the data seen in Graph 5, when working with the physical mixture of CuNPs and celite, full conversion was retained for the first 2 hours of operation. Batch 3 begins to show traces of unconverted starting material, and in batch number 4 the average conversion had dropped 88%. After this point (batches 5 and 6) catalyst activity drops dramatically, and the experiment was stopped. However, when working with supported CuNPs over celite, the full conversion lasts for the first 4 hours and then it does not drop dramatically, but it remains around 85% conversion for around 50 hours. After 70 hours the conversion is 70%.

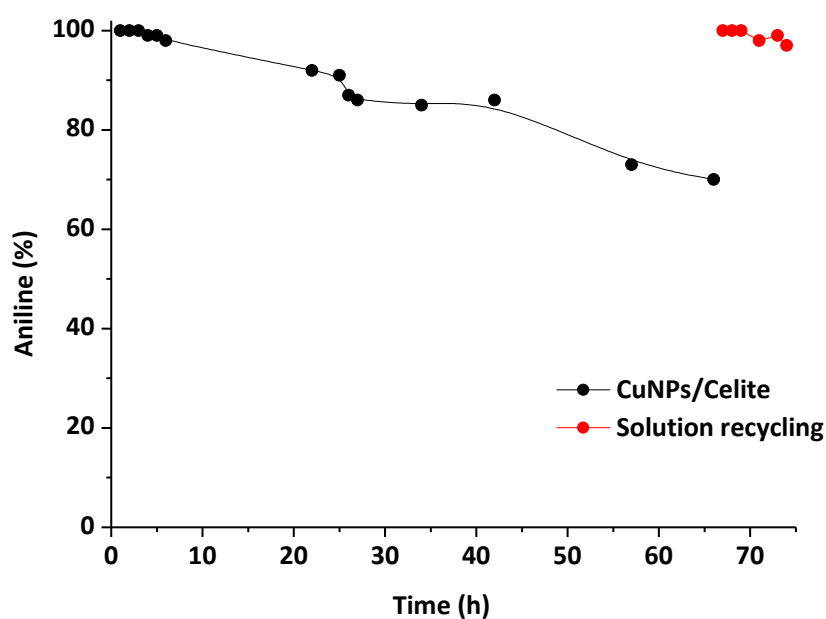


Graph 5: Long run studies for the continuous reduction of nitrobenzene in presence of two different conditions: CuNPs + Celite (blue curve) and CuNPs/Celite (black curve). Determined by GC-MS.

Oversaturation of the catalytically active species or a deactivating mechanism could be a possible explanation for the observed decrease in conversion. Therefore, two different ways were explored in order to obtain again the fully reduction product: solution recycling and catalyst reactivation. When the first method was applied, last fraction of the reaction was taken, with around 70% of conversion and recirculated (Scheme 31). As observed in Graph 6, the new batches showed full conversion to aniline.

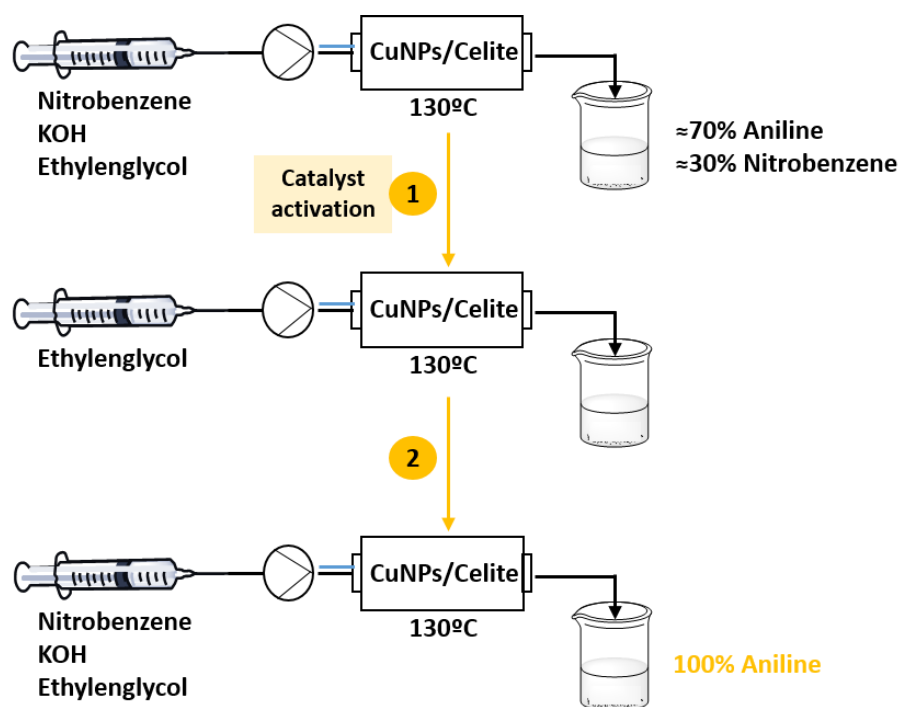


Scheme 31: Solution recycling

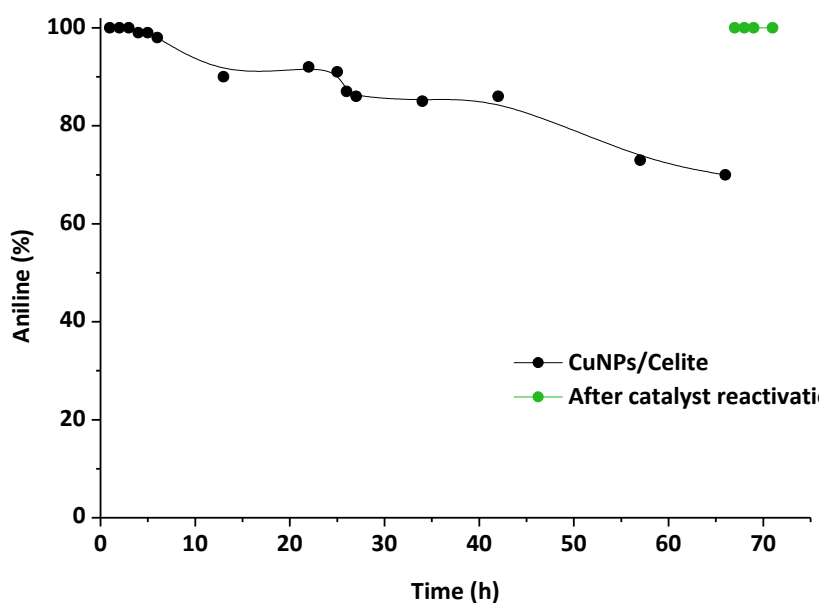


Graph 6: Solution recycling

When deciding to reactivate the catalyst (Scheme 32), some fresh ethylen glycol (3 batches) was flowed through the bed packed. In this way, being also the reaction solvent, ethylen glycol can play two different roles: a) cleaning the catalyst surface of some reaction reagents or products that could avoid the proper catalyst activity; b) reduce the catalyst active sites that have been oxidized during the reaction. After that, a new batch of nitrobenzene and base was flowed and, as perceived in Graph 7, full conversion to aniline was once again achieved.



Scheme 32: Catalyst reactivation



Graph 7: Catalyst reactivation

Figure 37 shows the appearance of different copper catalysts. As despite, the fresh CuNPs are black (Figure 37, (1)) and when supported over the celite the material shows a grey tint (Figure 37, (2)). When carrying out the model reaction (Scheme 30) in flow for 40 h and sequentially washing the catalyst with CHCl_3 and H_2O in order to remove the base and possible reagents and products on the catalyst surface, the material shows a light red color (probably due to the formation of Cu_2O) (Figure 37, (3)). However, when washing the catalyst only with CHCl_3 and so, when do not removing the KOH, the catalyst turns to green color (Figure 37, (4)), possibly due to the formation of $\text{Cu}(\text{OH})_2$.



Figure 37: Copper catalysts: (1) CuNPs, (2) CuNPs/Celite, (3) CuNPs/Celite (AR) washed with CHCl_3 and H_2O ; (4) CuNPs/Celite (AR) washed with CHCl_3 .

A new comparison was then set up. As depicted in Figure 38, after flowing ethylen glycol at 130°C (Figure 38, b) the catalyst recuperate the original color, disappearing the light red present in sample c, when the catalyst was recuperate without previously cleaning with the solvent.

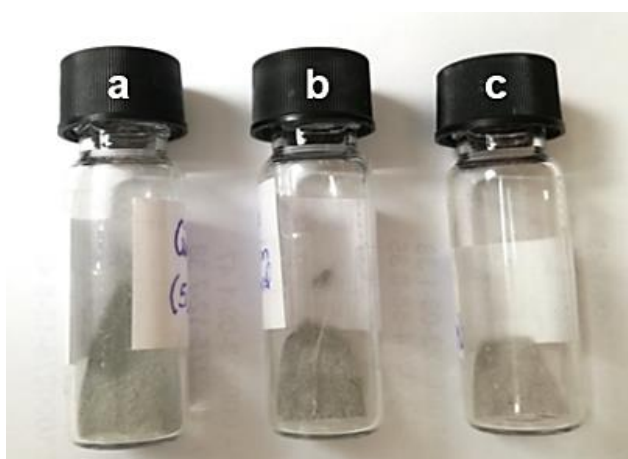


Figure 38: Copper catalysts: (a) fresh CuNPs/Celite, (b) CuNPs/Celite (AR) cleaned with ethylen glycol at 130°C and (c) CuNPs/Celite (AR) washed with CHCl_3 and H_2O .

In order to better understand the previous results, the materials were characterized by different techniques (UV, XRD, IR) to study their compositions.

IR spectroscopy of CuNPs/Celite and the physical mixture (CuNPs + Celite) was performed and compared with the spectral features of individual CuNPs and celite (Figure 39). The peak of the O-H stretching frequency belonging to the glycerol can be observed at 3433 cm^{-1} , either in CuNPs alone (blue curve) and when supported (black curve) or physically mixed (green curve).

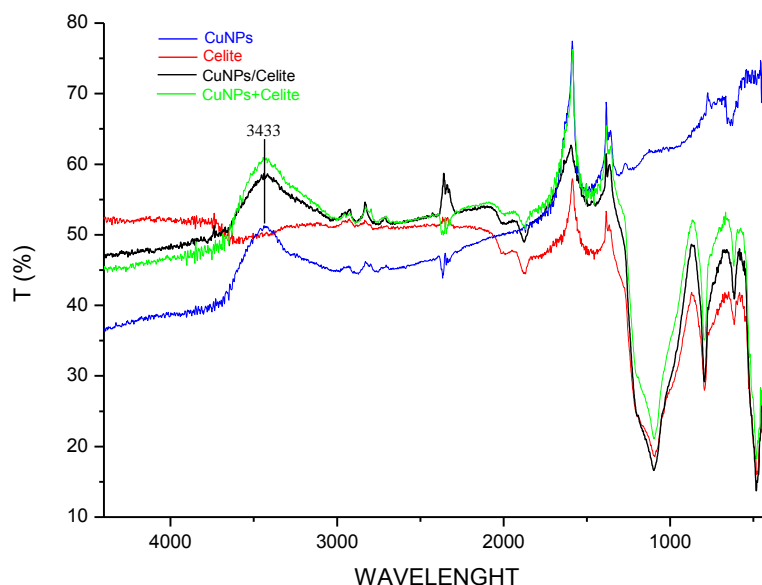


Figure 39: Characterization of CuNPs (blue curve), Celite (red curve), CuNPs/Celite (black curve) and CuNPs+Celite (green curve) by IR spectroscopy.

Characterization by UV-Vis spectroscopy was then performed. Copper can be present in different oxidation states: Cu^0 ($3d^{10} 4s^1$), Cu^+ ($3d^{10} 4s^0$) and Cu^{2+} ($3d^9 4s^0$). Unlike most transition metal ions in the zero-valent state, Cu^0 absorbs in the visible range ($3d$ - $4s$ transition) near 18200 cm^{-1} (550 nm). The spectrum of Cu^+ species comprises only metal-to-ligand charge transfer (MLCT) transitions in the UV region. Cu^{2+} entities show d - d transition appearing either in the visible (octahedral Cu(II)) or in the near-infrared reflectance (NIR) (tetrahedral Cu(II)) region).

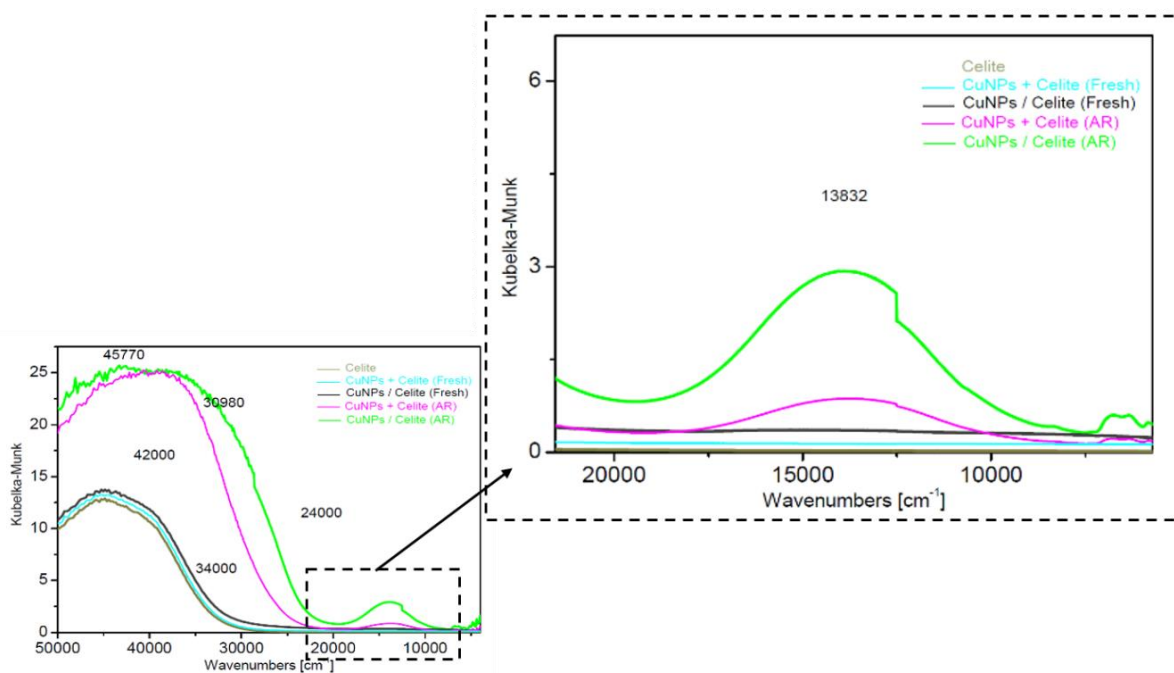


Figure 40: Characterization of Celite (brown curve), CuNPs+Celite (blue curve), CuNPs/Celite (black curve), CuNPs+Celite (AR) (pink curve) and CuNPs/Celite (AR) (green curve) by IR spectroscopy UV-Vis spectrum.

As we can observe in Figure 40, the inorganic support alone (celite) and the two fresh catalysts (before performing the reaction) have a similar UV-Vis spectrum. However, the two catalysts analyzed after carrying out the reaction (AR) (pink and green curves) show a UV-Vis spectrum consistent with Cu^{2+} d-d transitions, which shift from a wavelength of 800 nm to 730 nm (from 12500 cm^{-1} to 13700 cm^{-1}), meaning the oxidation of CuNPs (0) after reaction, what agree with the color change observed in Figure 37.

Characterization of the CuNPs alone and supported over celite was also investigated by X-ray diffraction (XRD). The diffraction pattern of the CuNPs shows peaks at 43.25° , 50.43° , 74.15° and 89.91° corresponding to the [111], [200], [220] and [311] planes of FCC copper. The patterns also display peaks at 36.82° and 62.80° which agree with [111] and [220] planes of FCC Cu_2O .

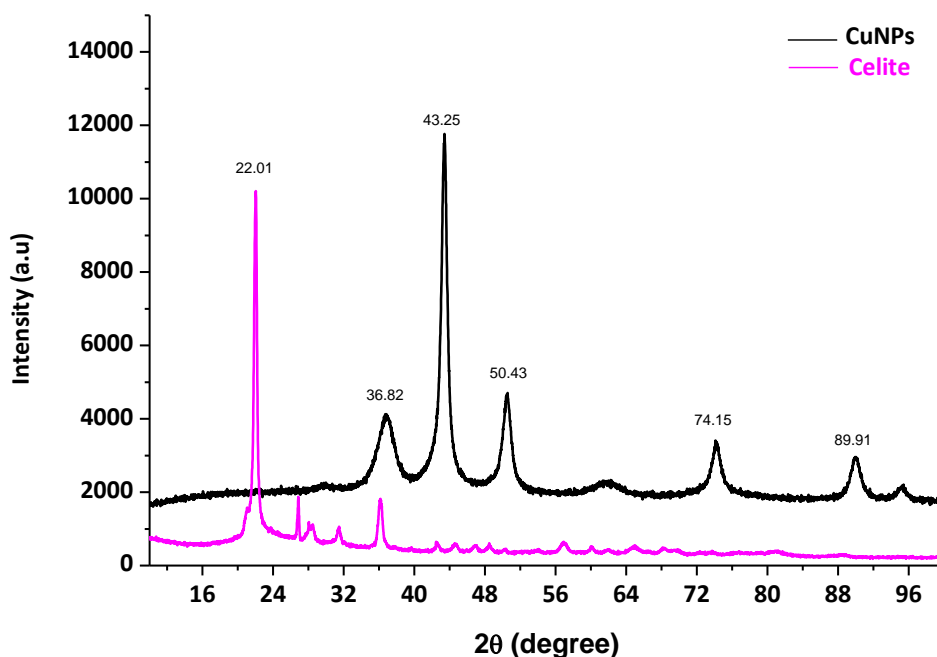


Figure 41: X-ray powder diffraction patterns of CuNPs (black curve) and Celite samples (pink curve).

Table 21. Data from JCPDS card 00-004-0836. Cu, cubic, Space group: $Fm\bar{3}m$

h k l	d [Å]	2Theta[deg]	I [%]
1 1 1	2.08800	43.298	100.0
2 0 0	1.80800	50.434	46.0
2 2 0	1.27800	74.133	20.0
3 1 1	1.09000	89.934	17.0
2 2 2	1.04360	95.143	5.0
4 0 0	0.90380	116.923	3.0
3 3 1	0.82930	136.514	9.0
4 2 0	0.80830	144.723	8.0

The synthesized copper nanoparticles supported over celite (CuNPs/Celite) and the mechanical mixture (CuNPs + Celite) were also characterized by XRD, showing peaks from both materials (Figure 42). As depicted, the intensity of the typical peak of copper (0) at 43.25° (corresponding to the [111] plane in FCC copper) is preferentially observed in the supported CuNPs (Figure 42, red curve).

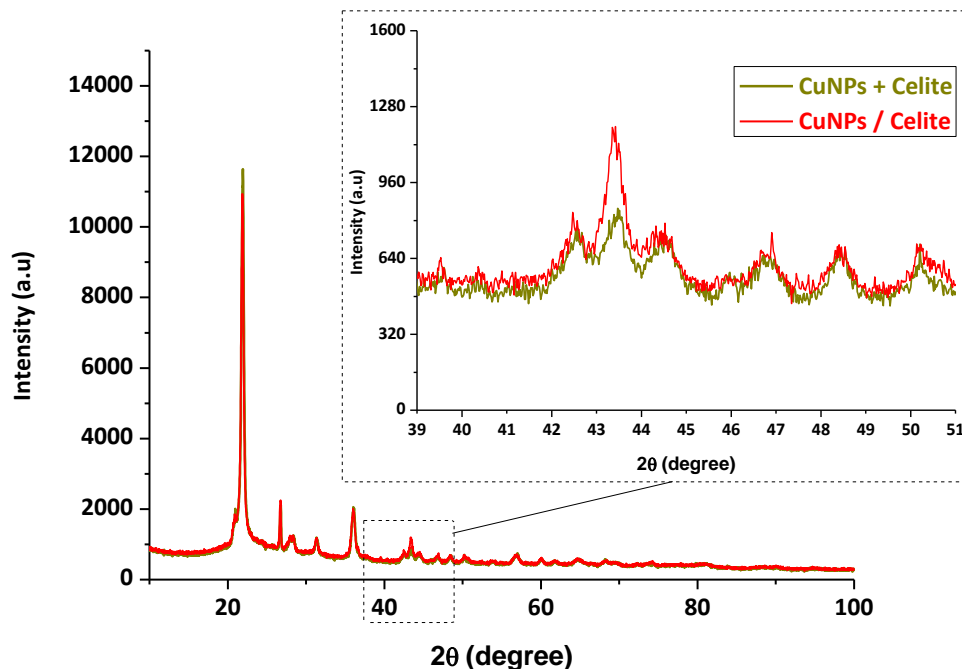


Figure 42. X-ray powder diffraction patterns of CuNPs/Celite (red curve) and CuNPs + Celite (green curve).

However, when analyzing the material after performing the reaction (Figure 43, green curve), the peak at 43.23° does not appear anymore, meaning the extinction of Cu (0) species in the catalyst after the reaction.

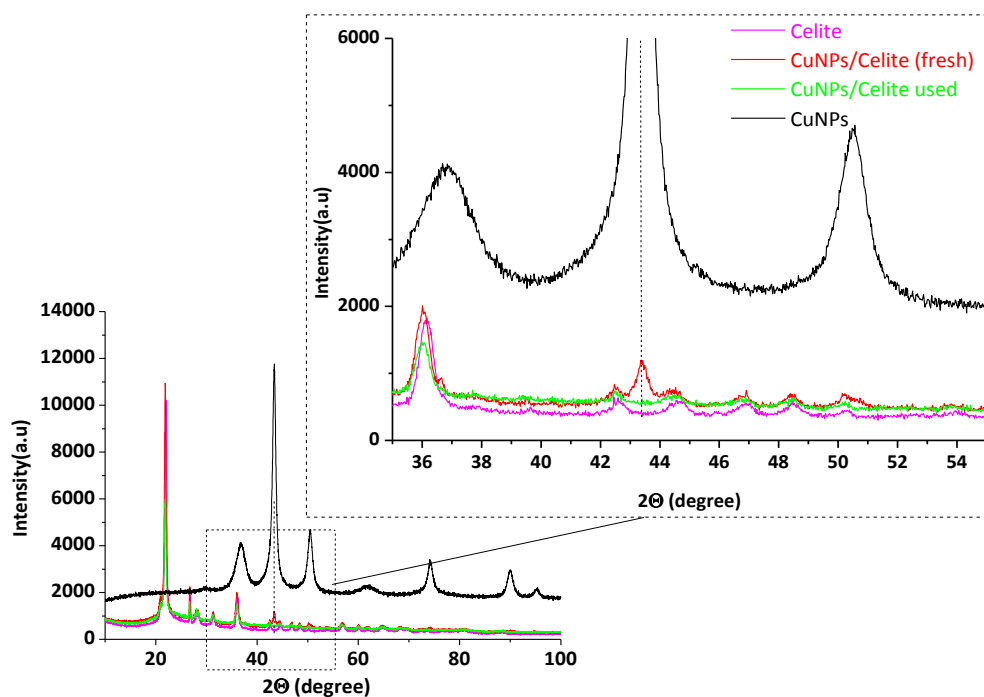


Figure 43: X-ray powder diffraction patterns of CuNPs (black curve), Celite (pink curve), CuNPs/Celite [before (red curve) and after reaction (green curve)] samples.

In order to better understand, the exhausted catalyst was then reactivated by flowing fresh ethylene glycol at 130 °C through the packed material, and the XRD analysis was then repeated (Figure 44).

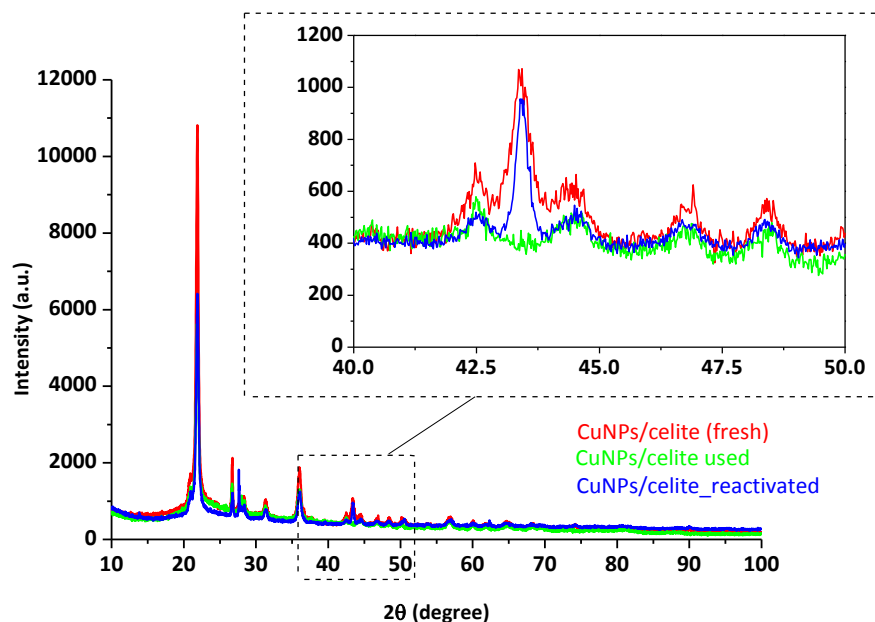


Figure 44: X-ray powder diffraction patterns of CuNPs/Celite_fresh (red curve), CuNPs/Celite_used (green curve) and CuNPs/Celite_reactivated (blue curve) samples.

As depicted, after using and reactivating the catalyst, the peak at 43.23° appears once again, confirming the presence of Cu (0) and, in this way, the reason why after flowing the ethylene glycol the nitrobenzene conversion is another time total.

2.5 Cu-catalysed TH of nitroarenes to amino or azo derivative *via* controllable transfer hydrogenation sources.

As depicted in Figure 23, one of the intermediates in the reduction mechanism of nitrobenzene are the aromatic azocompounds. These molecules are also considered high-value chemicals, since they are widely used as organic dyes, indicators, food preservatives, therapeutic agents, drugs, etc. While the synthesis of secondary aryl amines is a well known reaction and lot of synthetic routes have been reported, the synthesis of azocompounds is much more challenging, and it is usually obtained like a mixture of products.

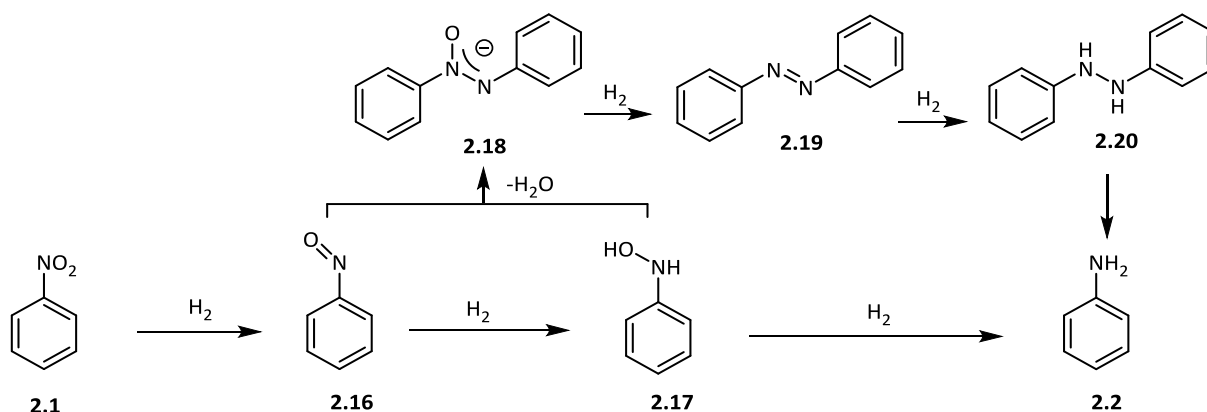


Figure 23: Reaction pathways for the hydrogenation of nitrocompounds to anilines

Three main pathways for their synthesis have already been described³⁶²: oxidation of anilines^{166,167,363,364} to nitrosocompounds, which react with aromatic amines (a) and reduction of aromatic nitro compounds^{362,365–367} to azoxycompounds and posterior rearrangement in presence of concentrated acids (b). The azocoupling reaction between a diazonium salt and an activated arene can be considered like the major industrial process in the synthesis of these compounds^{364,368} (c) (Figure 45).

In 1975 E. Bunce³⁶⁹ described the Wallach rearrangement of azoxybenzene to azobenzene in concentrated acidic media. N. Jiao et al.¹⁶⁷ developed in 2010 a novel copper-catalysed approach to symmetric and asymmetric aromatic substituted azobenzenes using dioxigen as the oxidant in the aerobic oxidative-dehydrogenative coupling of anilines. More recently, in 2016, Ag_{1-x}Ni_x alloy nanoparticles catalysed the synthesis of azo-derivatives from aromatics amines in mild conditions (60°C in open air).³⁶³

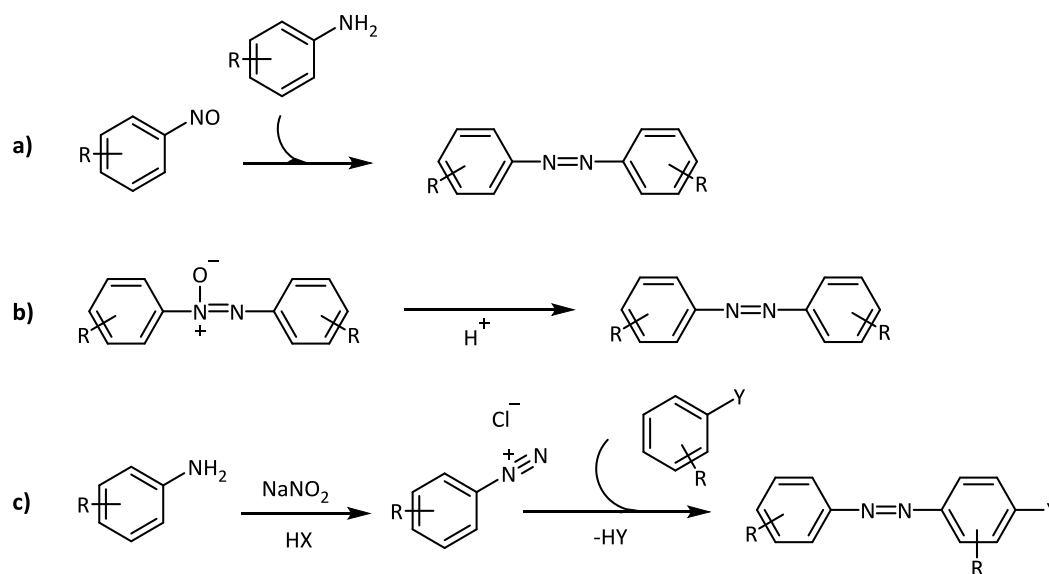


Figure 45: Azocompounds synthesis: a) Mills reaction; b) Wallach reaction and c) Azocoupling reaction

Even if all these processes are fairly effective, they involve several steps and generate a considerable number of by-products. An alternative for the synthesis of symmetric azocompounds is the reductive coupling of aromatic nitrocompounds using different types of reductive agents. However, this process also generates a large amount of non desirable products and implies intensive post-treatments. There is, therefore, a great interest to develop catalytic heterogeneous methods to directly produce azocompounds from aromatic nitrocompounds.

Catalysis by supported gold has been studied by X. Liu et al.³⁷⁰ without any external base or additives for the selective hydrogenative coupling of nitroarenes obtaining an efficient synthesis method using H₂ as reductant. In the same way, in 2014, Corma et al.³⁶² reported an efficient gold supported on nanocrystalline cerium oxide catalyst that allows the synthesis of symmetric azocompounds from nitrocompounds, using H₂ gas and under pressure. Iron-promoted reductive coupling of nitrobenzene was also described by G. Radivoy e co-workers³⁶⁶ in 2008 using iron(II) chloride tetrahydrate, lithium and a catalytic amount of 4,40-di-tert-butylbiphenyl (DTBB) as electron carrier.

Many other methods for the preparation of azo compounds have been described in the literature, most of them giving low yields and undesired side reactions products. In addition,

they require harsh conditions or can generate dangerous pollutants for the environment, limiting the easy scale up required when performing green synthesis. Consequently, new methodologies, milder reaction conditions and inexpensive reagents for this synthesis are welcome.

Here in we report an efficient and hydride free method for the chemo selective reduction of aromatic nitro compounds to amino compounds and to azo compounds in a single reaction step. While using high temperature, the full reduction to aniline is favoured, the use of softer conditions direct the process to a higher coupling rate, allowing a great selectivity in the synthesis of azocompounds.

When analysing deeply the Table 13, in which the reduction of nitrobenzene was performed in the presence of different solvents acting as transfer hydrogen donors, we could observed that using different reducing agents we could be selective to different reaction products. Due to the high value of azocompounds and known the difficulty in their selective synthesis from nitrobenzene reduction, we decided to optimise conditions (Table 22) in order to preferably obtain them.

Table 22. Optimisation of the Cu-catalysed nitrobenzene reduction to azobenzene ^{a)}

Entry	Reducing agent	T (°C)	Nitrobenzene (%) ^{b)}	Azoxybenzene (%) ^{b)}	Azobenzene (%) ^{b)}	Aniline (%) ^{b)}
1	Ethanalamine	130 ^{c)}	0	19	53	28
		80 ^{d)}	0	32	61	7
		55 ^{e)}	0	10	88	2
2	Ethylendiamine	130 ^{c)}	0	0	47	23
		80 ^{d)}	11	65	3	20
		55 ^{e)}	32	42	6	20
3	3-amine-1-propanol	130 ^{c)}	0	63	8	8
		80 ^{d)}	0	80	4	16
		55 ^{e)}	0	43	23	34
4	2-Propanol	130 ^{c)}	0	52	24	24
		80 ^{d)}	9	62	2	18
		55 ^{e)}	83	6	0	10
5	1,4-butanodiol	130 ^{c)}	21	48	21	20
		80 ^{d)}	89	4	0	7
		55 ^{e)}	97	1	0	2
6	Ethylene glycol	130 ^{c)}	0	0	2	98
		80 ^{d)}	>99	0	0	0
		55 ^{e)}	>99	0	0	0
7	Glycerol	130 ^{c)}	0	0	0	>99
		80 ^{d)}	80	0	0	20
		55 ^{e)}	>99	0	0	0

^{a)} Reaction conditions: nitrobenzene (1 mmol), KOH (2 mmol), reducing agent (40 mmol), CuNPs (5 mol%), oil bath. ^{b)} Determinated by GC-MS. ^{c)} Sample analysed after 1 hour reaction ^{d)} Sample analysed after 2 hours reaction. ^{e)} Sample analysed after 20 hours reaction.

The model reaction was then performed at different temperatures (130°C, 80°C and 55°C) in the presence of different solvents acting as TH reducing agents. From the results presented

in Table 22, we observed that the fact of changing the hydrogen donor molecule comes with the fact of obtaining different selectivities in the reaction product. As shown, in presence of ethanolamine (Table 22, entry 1), when performing the reaction at 80°C for 2h, higher selective to the formation of the azocompound was detected, giving 61% of azobenzene and 7% of the fully reduction product. However, when the synthesis was done at 55°C, the hydrogenation was preferentially directed to the formation of the azocompound, which was detected with 88% of selectivity after 20 hours. The formation of aniline stopped, been only observed with 2%. The fact that azobenzene is observed as a primary product and it is accumulated in the reaction media clearly demonstrates that a slow hydrogenation of the azoxybenzene intermediate favours the selectivity to the azocompound. So, the fact of employing a lower temperature benefits this process by not supplying enough energy to fully reduce the nitro to amino group. The ethylenediamine (Table 22, entry 2) did not show any selectivity, giving a mixture of products. In presence of 3-amine-1-propanol (Table 22, entry 3), the hydrogenation is faster but, once again, not selective, giving at 55°C a mixture of azoxybenzene/azobenzene/aniline (43/23/34). Afterwards, the reaction was performed using 2-propanol as solvent (Table 22, entries 4) and fully conversion was only observed at high temperature. When fixing 55°C for 20 hours, only 17% of conversion was detected, without showing selectivity to any product. As already observed, the formation of a small size chelates during the TH process favours the reduction mechanism, what supports and confirm the fact that the ethylen glycol and glycerol selectively form the aniline in 1h reaction time at 130°C (Table 22, entries 6-7) with fully conversion. This conversion is reduced when the reaction temperature is decreased to 80°C and 55°C, showing only 20% in the case of glycerol, but always maintaining the selectivity towards the aniline. The high viscosity of these two polyalcohols prevents the homogeneous magnetic stirring when decreasing the reaction temperature to 55 °C, thereby invalidating the nitrobenzene reduction. This reality was also reinforced in presence of a longer carbon chain with 1,4-butanodiol (Table 22, entries 5), which presented a low conversion at all three different temperatures.

Once the reaction conditions were optimised, the kinetic curve of the nitrobenzene reduction with copper catalyst and glycerol (Figure 46) or ethanolamine (Figure 47) acting both as solvents and hydrogen sources, were designed. As showed in Figure 46, the presence of glycerol and high temperatures leads exclusively to the fully reduction product. However, when using the ethanolamine and lower temperature conditions, the reaction stops at the intermediate stage of azobenzene. Both experiments were performed in presence of metallic Cu powder (Figure 46a and Figure 47a) and in presence of CuNPs (Figure 46b and Figure 47b). Analyzing the Figure 46, we can observe that the formation of the aminocompound occurs at high velocity, passing from the intermediate stages very fast and following the same trend in both graphs. However, when metallic copper is employed as catalyst, 5 hours of reaction time are necessary to fully reduce the nitrobenzene to aniline, and, in presence of CuNPs, besides decreasing a lot the catalyst quantity, the reaction time was decreased to only one hour.

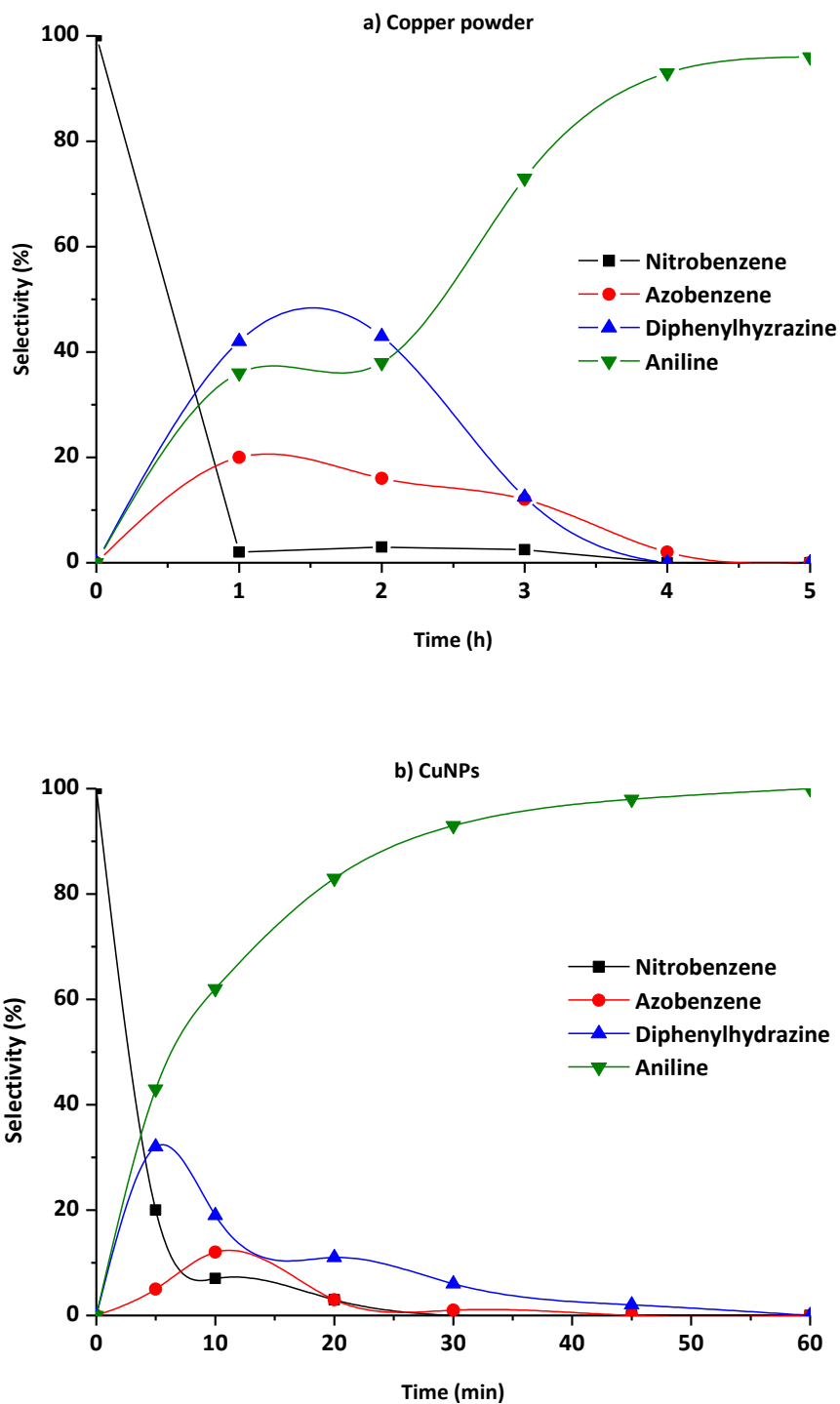


Figure 46: Nitrobenzene reaction profile over (a) Cu metallic powder (2 mmol) and (b) CuNPs (5mol%). Reaction conditions: nitrobenzene (1 mmol), KOH (2 mmol), glycerol (40 mmol), T:130°C. Determined by GC-MS.

In the same manner, the reaction kinetic was studied in presence of ethanolamine at 55°C (Figure 47). In this case, the hydrogenation is slower, showing during the first hours a progressive decrease of the starting material while appearing the azoxybenzene almost selectively. After that, the last mentioned intermediate begins to transform into the azobenzene, remaining selective to this product. Once more, the reaction kinetic was very

similar in presence of metallic copper and copper nanoparticles, but allowing a considerable decrease in catalyst amount, from 200 mol% to only 5 mol% in presence of NPs.

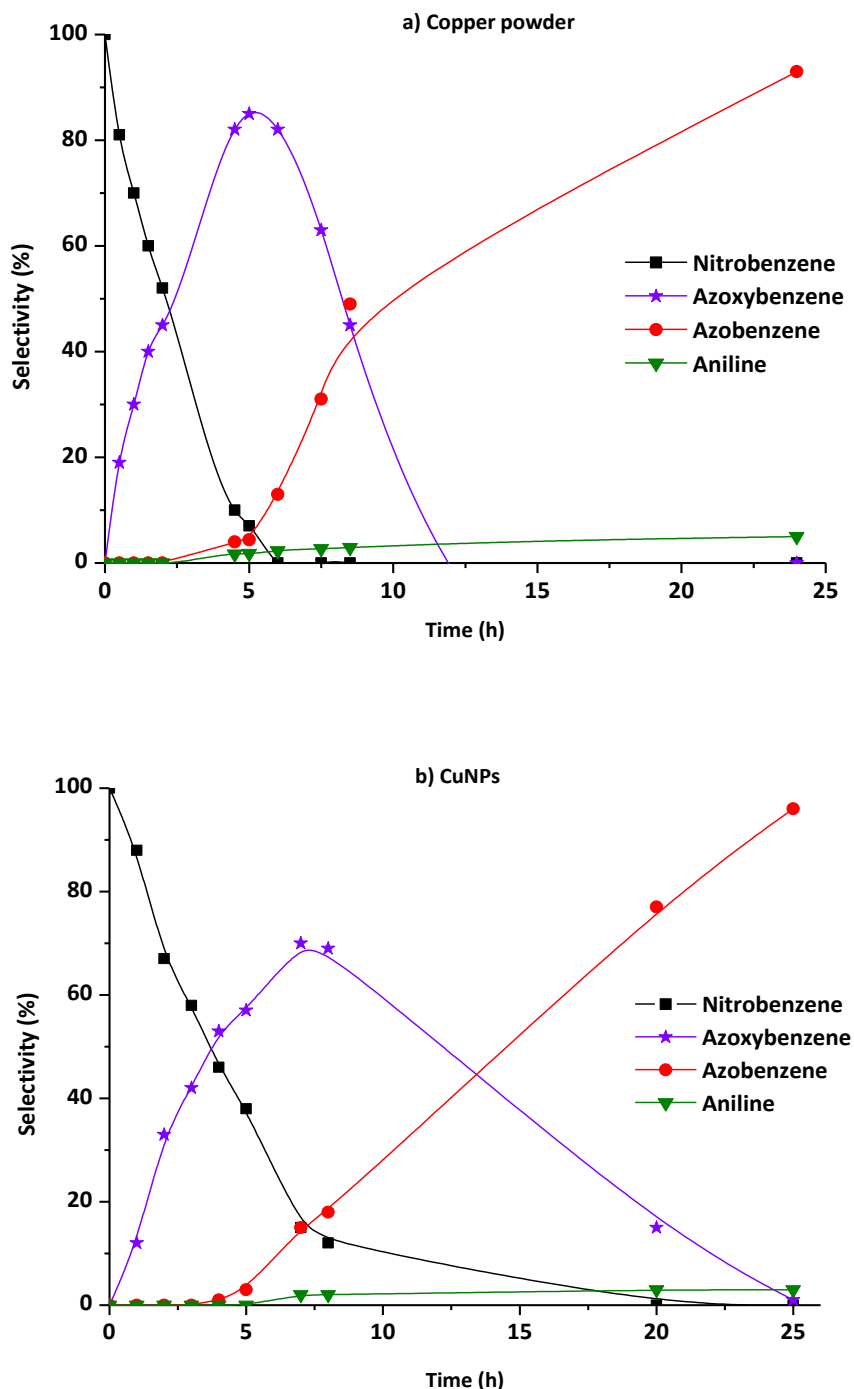


Figure 47: Nitrobenzene reaction profile over (a) Cu metallic powder (2 mmol) and (b) CuNPs (5mol%). Reaction conditions: nitrobenzene (1 mmol), KOH (2 mmol), ethanolamine (40 mmol), T:55°C. Determined by GC-MS.

To investigate the action of non conventional techniques, the selective reduction of nitrobenzene with glycerol was evaluated in the present of CuNPs under conventional stirring and under microwave and ultrasound irradiation, either alone and combined (Figure 48).

All reactions were carried out in parallel under the following conditions: 1) under stirring and conventional heating in an oil bath; 2) under MW alone (Milestone, MicroSynth); 3) under

US alone; 4) under combined MW/US irradiation. As shown in Figure 48, the reaction was greatly accelerated by combined MW/US irradiation as compared to either treatment used by itself or to conventional heating. Traditional stirring led to reaction completion in approximately 1 h, whereas a combination of both radiations decreased reaction time to 10 min. Ultrasonic cavitation helps to disperse and deagglomerate nanoparticles into the system, improving the material transfer at the catalytic particle surface. Glycerol physicochemical properties allow excellent acoustic cavitation under sonochemical condition⁴³ and fast dielectric heating.

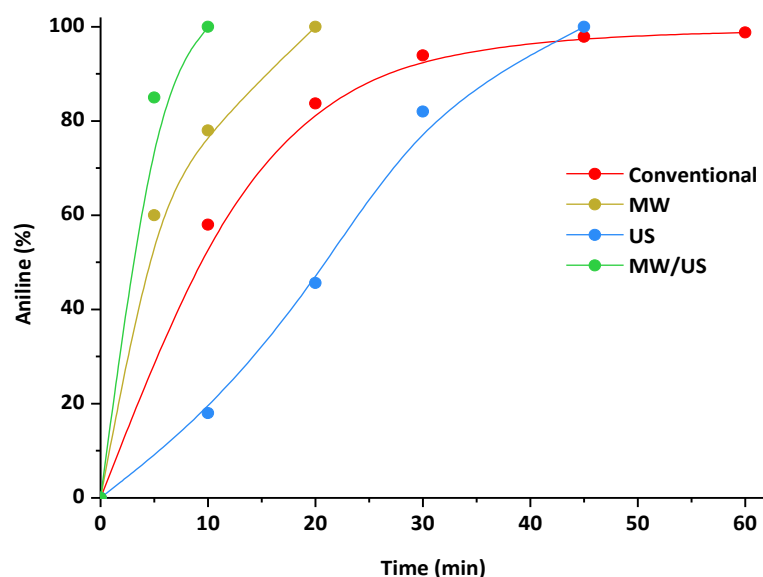
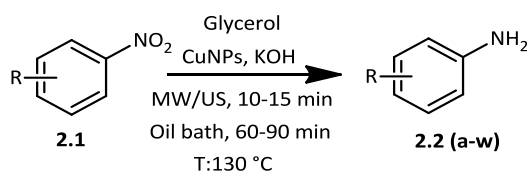


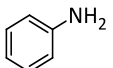
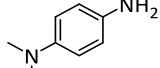
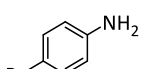
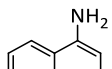
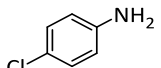
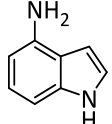
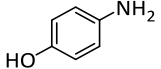
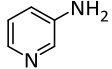
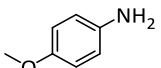
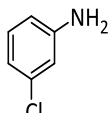
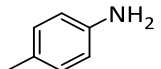
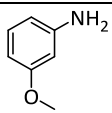
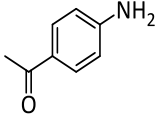
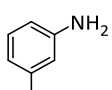
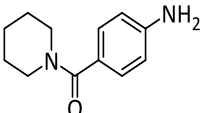
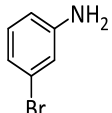
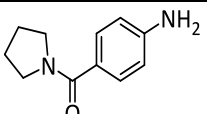
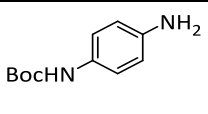
Figure 48. Reaction kinetic under different techniques: 1) Conventional: stirring, 2)US: Pyrex horn, P:30W, F:20,4kHz; 3)MW: Milestone, MicroSynth, Program: 2 min Pmax=400 W heated as quickly as possible to reach 130 °C, then P: 80 W; 4) MW/US: Combined reactor MW (P:80W) and Pyrex horn US(P:30W). Reaction conditions: nitrobenzene (1mmol), glycerol (40 mmol), KOH (2 mmol), CuNPs (5 mol%), T:130°C. Determinated by GC-MS.

The scope of the reaction was explored by reducing a number of nitroarenes with different functional groups (Table 23). Full conversion of the starting material was observed in all cases. Excellent yields and short reaction times were sufficient when both non-conventional techniques were employed simultaneously. It is worth mentioning that high selectivity and yields were observed in the presence of both electro and withdrawing substituents. Even in the presence of other reducible functional groups such as the ketone (Table 23, entries 7-9) was not reduced under these reaction conditions, but was quantitatively converted to the amino derivative.

Table 23. Scope of the hydride free reduction of aromatic nitrocompounds to aminocompounds catalysed by CuNPs.



Entry	Product	Yield [%] ^{b)} (%) ^{d)}	Entry	Product	Yield [%] ^{b)} (%) ^{d)}
-------	---------	--	-------	---------	--

1		93 (85)	10		94 (90)
	2.2a			2.2r	
2		87 (85)	11		92 (85)
	2.2b			2.2k	
3		92 (85)	12		88 (79)
	2.2d			2.2j	
4 ^{d)}		88 (80)	13		87 (82)
	2.2e			2.2h	
5		92 (90)	14		93 (87)
	2.2l			2.2s	
6		96 (91)	15		94 (90)
	2.2o			2.2t	
7		90 (82)	16		92 (88)
	2.2i			2.2u	
8		89 (85)	17		89 (86)
	2.2p			2.2v	
9		88 (86)	18		88 (>99)
	2.2q			2.2w	

Reaction conditions: nitroarene (3mmol), glycerol (20 mL), KOH (6 mmol), CuNPs (5 mol%), T:130°C. ^{b)} Isolated yield. Reaction performed under combined US (20.3 kHz, 30 Wcm⁻²) and MW (2.45 GHz, 80 W) irradiation

(MW/US). Compound purity proved by $^1\text{H-NMR}$ and $^{13}\text{C-NMR}$ (see Chapter 5: Experimental details), ^{c)} Isolated yield. Reaction performed under conventional stirring in oil bath at 130 °C. ^{d)} KOH (4 eq).

Table 23 shows that -Cl and -Br groups were unaffected in both, para- and meta-positions. In the same way, nitro-heterocycles (Table 23, entries 11-13) were also fully converted and isolated with high yields. Nitrophenol (Table 23, entries 4) was reduced in presence of a higher amount of base due to the slightly acidity of the starting material.

As reported, performing the same reaction in the present of ethanolamine at 55°C, selective reduction to the azocompound was achieved (Figure 49).

The same strategy followed in the fully reduction of nitrobenzene to aniline was successfully applied to the synthesis of azocompounds. As shown in Figure 49, using the ethanolamine in the present of CuNPs (5 mol%), the reaction was carried out in parallel under conventional conditions, microwave or ultrasound irradiation and combination of both sources (CMUI). Over again, the combination of both enabling technologies permit to obtain the desired product in a notable shorter reaction time. While using the conventional stirring the reduction reaction takes one full day, the enhancement of heat and mass transfer achieved when combining MW and US irradiations allows completing the reaction in 1 hour.

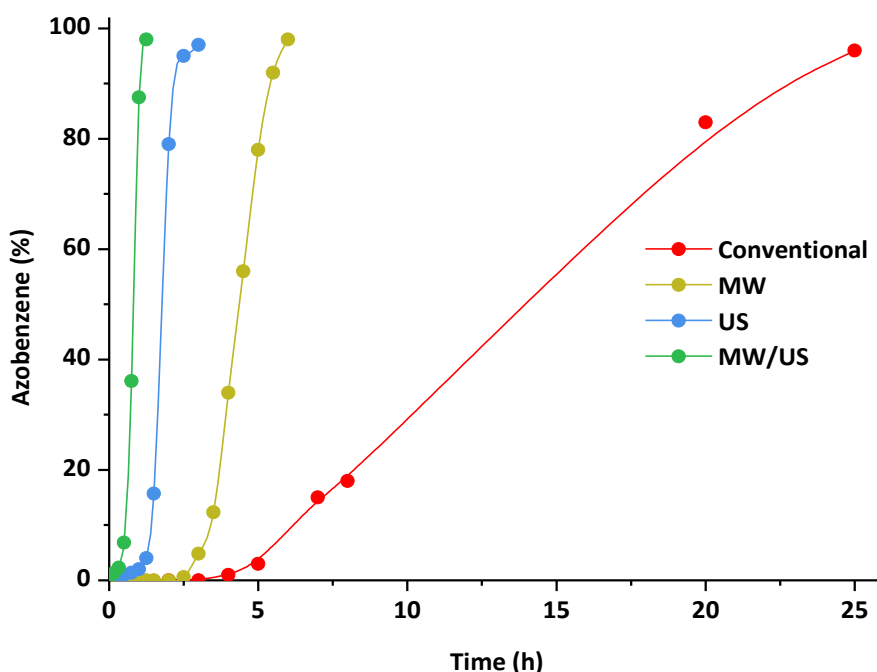


Figure 49. Reaction kinetic under different techniques: 1) Conventional: stirring, T:55°C, 2)US: Pyrex horn, P:15Wcm⁻², F:20,4kHz; 3)MW: Milestone, MicroSynth, Program: 2 min Pmax=200 W heated as quickly as possible to reach 55 °C, then P: 15 W; 4) MW/US: MW (P:15W) and Pyrex horn US(P:15W). Reaction conditions: nitroarene (1mmol), Ethanolamine (20 mL), KOH (2 mmol), CuNPs (5 mol%), T:55°C. Determined by GC-MS.

The scope of the reaction was explored by reducing a number of nitroarenes with different functional groups (Table 24).

Table 24. Scope of the hydride free reduction of aromatic nitrocompounds to azocompounds catalysed by CuNPs.

Reaction scheme: Nitroarene (2.1) with substituent R reacts with Ethanolamine, KOH, and CuNPs under MW/US (1h) and oil bath (20-24 h, 55°C) to form azo compound (2.19 a-j) with two R groups.

Entry	Product	Yield [%] ^{b)} (%) ^{c)}	Entry	Product	Yield [%] ^{b)} (%) ^{c)}
1		92 (86)	6		86 (80)
2		90 (84)	7		88 (85)
3		83 (72)	8		82 (79)
4		72 (68)	9		77 (70)
5		91 (87)	10		86 (82)

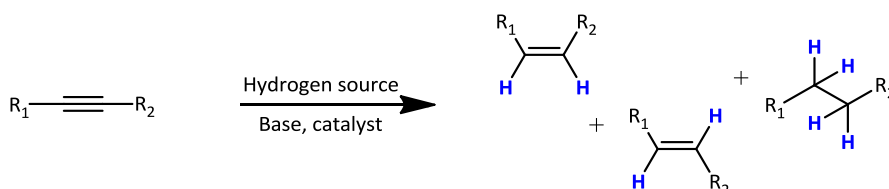
Reaction conditions: nitroarene (3mmol), Ethanolamine (20 mL), KOH (6 mmol), CuNPs (5 mol%), T:55°C. ^{b)} Isolated yield. Reaction performed under combined US (20.3 kHz, 15 Wcm⁻²) and MW (2.45 GHz, 15 W) irradiation (MW/US). Compound purity proved by ¹H-NMR and ¹³C-NMR (see Chapter 5: Experimental details), ^{c)} Isolated yield. Reaction performed under conventional stirring in oil bath at 55 °C.

Table 24 shows the conditions and results for a series of aromatic nitro compounds. It can be seen that the reduction of nitrobenzene gave azobenzene in excellent yield and the reducing system was also efficient in the case of aromatic nitro compounds bearing additional substituents, all of which were reduced to the corresponding symmetrical substituted azobenzenes in quantitative good yields. The -OMe, -N(CH₃)₂ and -Cl groups were unaffected, while both bromo-nitrobenzenes (Table 24, entries 4 and 9) were partially transformed to the N-arylated ethanolamine, giving the Ulman-type reaction product.

In summary, it has been demonstrated that CuNPs act as an efficient catalyst for the chemoselective reduction reaction of aromatic nitrocompounds to aminocompounds and azocompounds. The use of high temperatures allows the fast reduction to the fully reduced product, whereas the use of softer conditions facilitates the coupling reaction and the synthesis of the azocompound. The reaction proceeds through the transfer-hydrogenation mechanism, using glycerol and ethanolamine as green hydrogen sources. Enabling technologies such as microwave and ultrasound, either alone or combined, were successfully applied showing a notable increase in the reaction rate. Using this procedure, a wide range of amino and azocompounds have been isolated with high yields.

2.6 Copper catalysed selective semihydrogenation of alkynes to cis alkenes

The alkyne semihydrogenation poses challenges in stereoselectivity (E vs. Z) and chemoselectivity (overreduction of the formed alkene to the corresponding alkane) and thus serves as an ideal model reaction for catalyst development.



As previously described (1.2.4 Alkynes), the selective semihydrogenation of internal alkynes to (Z)-alkene constitute an important step in the synthesis of vitamins, natural products, polymerization, etc and a wide range of synthetically useful methods have been established for this goal. As such, the transition-metal-catalysed (especially palladium) semihydrogenation of alkynes with hydrogen dominates this field for decades and remarkable achievements have been made in presence of Pd- Rh- Ru- Ni- Va-Bi and Au.^{92,165,371–374} As already described, despite its widespread use, hydrogenation by Lindlar catalyst⁹⁵ has several disadvantages including possible over-reduction to alkanes, isomerization of (Z)- to (E)-alkenes, double bond migration, poor reproducibility, small tolerance with other reducible functional groups and safe handling requirements due to the use of flammable hydrogen gas. Therefore, replacement of these metals and new & better chemo- and stereo-selective procedures are required.

Cu catalysts are known to be highly selective but suffer from low activity. Therefore, they are frequently used in presence of other metals, improving in this way their activity. Palladium is one of those co-metals and the PdCu_y bimetallic systems^{375–377} has recently been widely used in catalytic reactions. In general, Pd catalysts are highly active but not selective unless they are poisoned with a second metal or a ligand. In this respect, the trade-off between activity and selectivity has successfully been achieved through bimetallic catalysts as well as improved stability. In 2016, the Pd–Cu₂O catalytic system was designed by Yang et al.³⁷⁸ showing high reactivity for the semihydrogenation of terminal alkynes; however, internal alkynes were not hydrogenated. In this context, F. P. da Silva et al.³⁷⁹ recently reported the synthesis of a PdCu₄ catalyst prepared by sol-immobilization on silica, which represented the best compromise between activity and selectivity for the semihydrogenation of internal and terminal alkynes, without any additive and under mild reaction conditions (30 °C and 1 bar of H₂). However, as already discussed, the inevitable use of flammable hydrogen gas in those

reactions prompts chemists to explore more safe and facile hydrogenation processes, transfer hydrogenation reactions.

In this regard, catalytic transfer hydrogenation (TH) emerges as a great alternative way to access Z-alkenes. As depicted in Table 3, a number of TH reactions in presence of various transfer hydrogenating reagents (such as $\text{HCO}_2\text{H}\cdot\text{NEt}_3$,¹¹⁰ DMF/KOH,¹¹⁴ PMHS¹¹⁵ or 2-propanol.¹²⁰) and different metal catalysts (mostly palladium and copper) has been reported for this transformation. Moreover, other well known hydrogen donors such as ammonia borane,³⁸⁰ formic acid–triethylamine³⁸¹ ethanol³⁸² and even water^{383,384} have been widely employed.

In general, for catalytic TH there is a need for easy-to-use and safe dihydrogen (H_2) sources, as these reactants are associated with the generation of one molecule of waste per turnover. Alcohols, such as the commonly employed isopropanol, fulfil the abovementioned criteria and, among them, the use of bio-based derived alcohols have lately received considerable attention as hydrogen donors due to their intrinsic advantages of easy availability and nontoxicity.

Copper, being a cost effective and a readily available metal, is highly attractive and has received lot of attention during the last decade. However, this metal poses formidable challenges with regard to catalytic transfer hydrogenations. Copper hydride catalysis³⁸⁵ is commonly performed in presence of hydrosilanes as reducing agents, generating silicon-based waste, and generally require elevated H_2 pressure. In a recent work published by T. Kaicharla et al.,³⁸⁶ a homogeneous copper hydride catalysis has been performed in presence of isopropanol for simple selective semihydrogenation of alkynes to (Z)-alkenes. They claim that the use of NHCs as key ligands leads to high chemoselectivity to alkene and stereoselectivity to the cis isomer, showing that both, high pressure equipment as well as waste-generating hydrosilanes can be circumvented. Another homogeneous copper-catalysed transfer semihydrogenation of various alkynes was also recently accomplished by H. Bao et al.³⁸⁷ in which a combined ethanol/ B_2Pin_2 system as the hydrogen source afforded Z-alkenes in high yields. However, it comes to a surprise that for pure heterogeneous nano-copper hydride catalysis, TH reduction for the selective semihydrogenation of alkynes has not been reported so far.

Thus, in view of the economic and green surrounding issues, avoiding the use of any kind of ligands in nanocopper-catalysed systems and performing TH strategy in presence of a biomass-derived hydrogen donor would be an attractive alternative for this type of transformations. To the best of our knowledge, the use of ethylene glycol as a hydrogenating agent in the catalytic reduction of alkynes has never been performed.

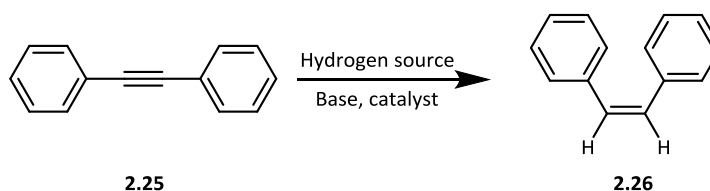
Here in, aiming to carry out reactions lowering the energy and time consumption, enabling technologies such as microwaves (MW) and ultrasounds (US) have been extensively applied. More selective and efficient processes have been described thanks to the use of these non conventional technologies. As far as we know, the selective reduction of alkynes to Z-alkenes have not been performed under microwave or ultrasound irradiation.

On the basis of our previous experience, MW heating and US irradiations, besides been among the most simple, inexpensive and valuable tools in applied chemistry, facilitate the reduction of the reaction time from several hours to just some minutes. Moreover, the

simultaneous irradiation of both techniques can enhance the heat and the mass transfer, dramatically reducing the reaction time.

Herein, we describe an efficient, hydride-free and ligand-free nanocopper-catalysed semihydrogenation of internal alkynes using the green and easily handled ethylen glycol as the hydrogen source for the selective production of (*Z*)-alkenes.

The reaction conditions were optimized employing diphenylacetylene (**2.25**) as a model substrate (Scheme 33). After screening a variety of reaction parameters, semihydrogenation of **2.25** gave (*Z*)-stilbene **2.26** selectively in high yield with only 5% formation of (*E*)-alkene and without overhydrogenation to the alkane.



Scheme 33. Copper-catalysed semihydrogenation of internal alkynes using an alcohol as hydrogen donor.

Various solvents including amino compounds, amino-alcohols and different alcohols were explored as hydrogen donor. As shown in Figure 50, while in presence of ethylenediamine and ethanolamine very small amount of product was detected; the use of serinol and isoserinol increased the conversion and the selectivity to the *Z*-stereoisomer, showing 28% and 44% respectively. When using only –OH groups as hydrogen source, the yields were higher. As depicted in Figure 50 the use of glycerol enlarged the reaction conversion to 58% and, when using ethylene glycol, the diphenylacetylene was fully converted to the stilbene with 70% of selectivity to the *Z*-alkene.

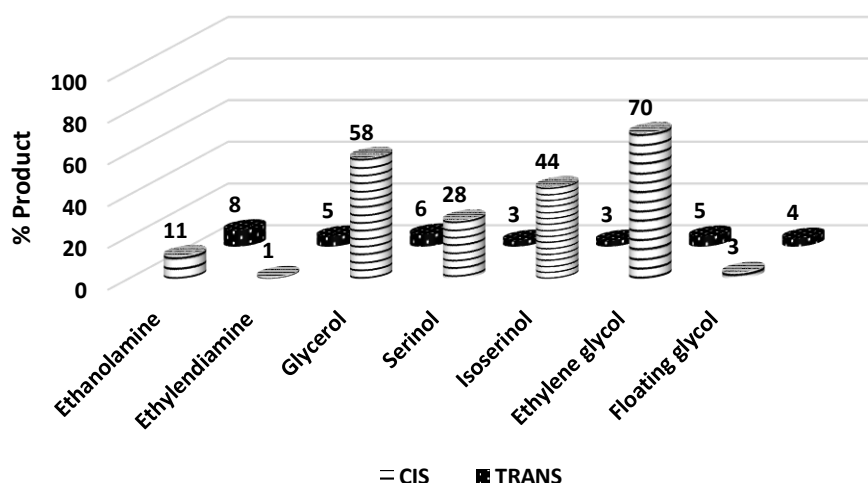


Figure 50. Screening of different reducing agents. Reaction conditions: Diphenylacetylene (1mmol), KOH (2 mmol), Cu metallic powder (2 mmol), solvent (40 mmol). T: 150°C, t:24h. Determined by GC-MS.

The preponderance of the *cis* isomer suggests that the reduction reaction takes place on the copper surface. The mechanism of the current copper-catalysed semihydrogenation of internal alkynes was proposed as shown in Figure 31.

The alcohol, oxidizing itself in the presence of copper, allows selective reduction to alkene. The presence of any trace of alkane was observed. Figure 31 shows how the presence of a solid catalyst leads to the formation of the (Z)- isomer. The interaction of the π cloud with catalyst allows the hydrogen atoms on the surface to bind on the same side of the molecule, leading to the formation of a specific isomer (Z). To confirm this, the reaction was tested using as solvent a solution made of copper, ethylene glycol and base. The solution was placed under the same conditions as the standard reaction and after one night, the floating liquid was used for the reaction. As can be observed from Figure 50, this procedure didn't lead to any good result, showing only 7% of conversion without any selectivity. Therefore, it can be excluded the fact of been a homogeneous catalysis.

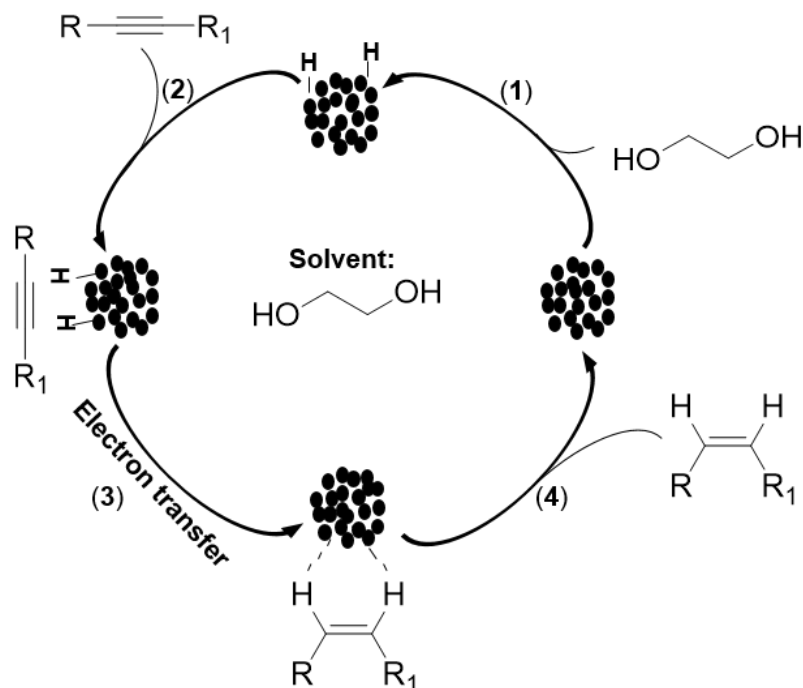


Figure 51. Proposed mechanism for the copper-catalysed semihydrogenation of internal alkynes forming the (Z)-isomer.

From our previous studies, it is known that, the role of the base is important in the presence of copper catalyst. For this reason, several bases were tested: KOH, NaOH, t-BuOH, K_2CO_3 , CsCO_3 , etc; obtaining the best results in presence of KOH.

Standard reaction (Scheme 33) was then studied in the presence of different copper sources using ethylene glycol as hydrogen donor and solvent. As we can observe in Figure 52, compound **2.26** was detected by gas chromatography in 35% yield in presence of Cu metallic powder after 10 h stirring in an oil bath at 150°C . Prolonging the reaction time to 24 hours the conversion increased to 75%, with 70% selectivity to the (Z)-isomer. In contrast, in the presence of copper salts such as CuI, CuCl and CuCl_2 as counterions, the (E)-isomer resulted as the main product, detected with 30%. This result can probably be explained with the higher solubility of the catalyst in the medium and at the same time a lower ability to coordinate the hydrogen for the reduction reaction. Other copper (II) salts like $\text{Cu}(\text{OAc})_2$ and CuSO_4 showed activity far less than the previously mentioned. Copper oxides were also tested and contrary to Cu(I)-oxide, in presence of Cu(II)-oxide a considerable amount of **3.2** was observed.

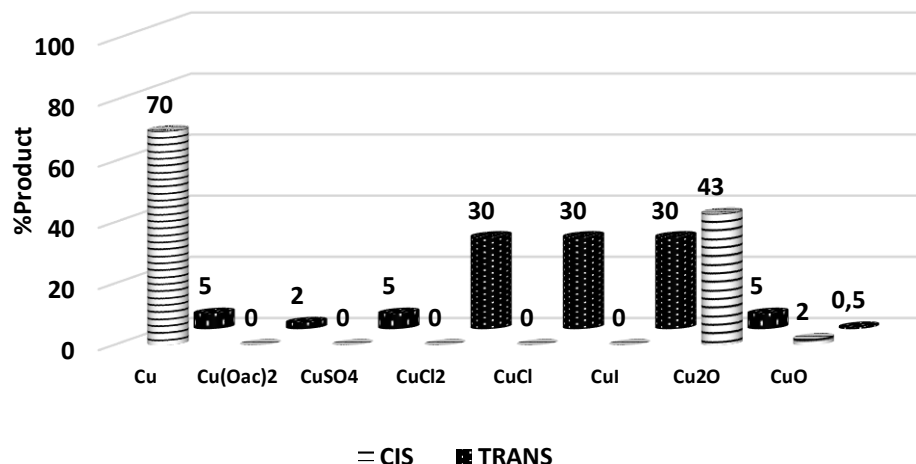


Figure 52. Copper source screening. Reaction conditions: Diphenylacetylene (1mmol), KOH (2 mmol), Cu metallic powder (2 mmol), ethylen glycol (40 mmol). T: 150°C, t: 24h. Determined by GC-MS.

Aiming to reduce the high amount of copper powder catalyst needed to carry out the reaction when using the bulky metal, CuNPs were tested. The standard reaction was performed in the presence of copper metal and metal NPs and both experiments were carried out in parallel under conventional stirring in an oil bath. As depicted in Figure 53, the use of CuNPs significantly reduce the quantity of catalyst required to complete the reaction. In this context, the use of bulk metal requires more than two days under conventional heating and it does not allow to obtain the fully conversion of nitrobenzene (70 % of conversion). However, the use of CuNPs showed a great reaction enhance, being able to get 100% of conversion in only two hours. The quantity of catalyst was also notably reduced, from 200 mol% Cu while using the bulky metal to 10 mol% in case of CuNPs. Moreover, the fastest the hydrogenation takes place, higher is the selectivity to the Z-product. As shown, in the present of small particles, the full conversion means also full selectivity to the cis-alkene, meanwhile 7% of trans-product is formed when the bulky catalyst is employed.

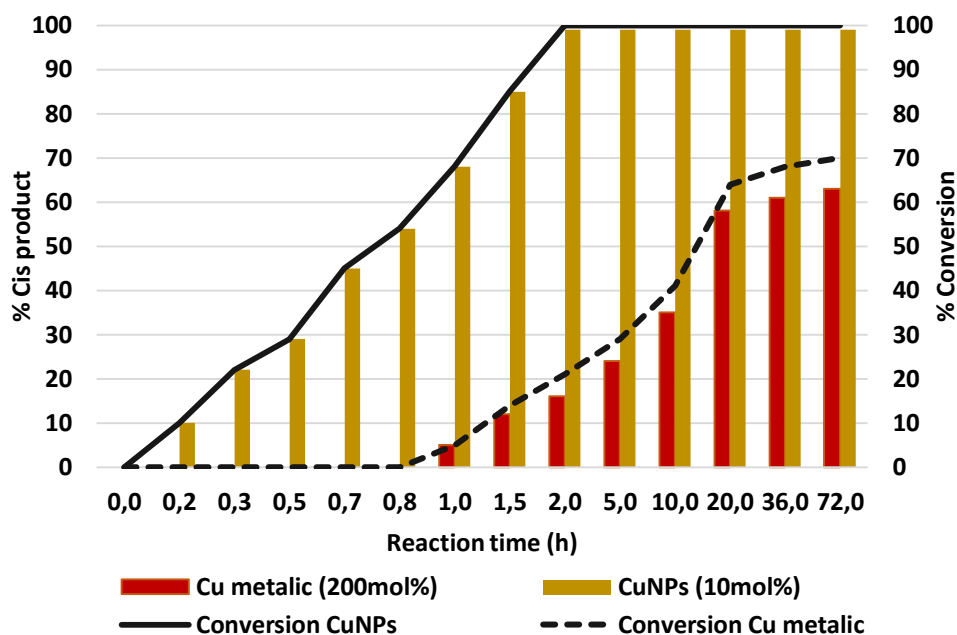


Figure 53. Reaction kinetic in presence of Cu metallic bulk and CuNPs. Reaction conditions: Diphenylacetylene (1mmol), KOH (2 mmol), copper, ethylen glycol (15 mL). T: 150°C. Determined by GC-MS.

In order to investigate the action of non conventional techniques, we evaluated the reduction of diphenylacetylene with ethyleneglycol (Scheme 33) in the present of CuNPs under conventional conditions, MW or US irradiation and combination of both of them (MW/US).

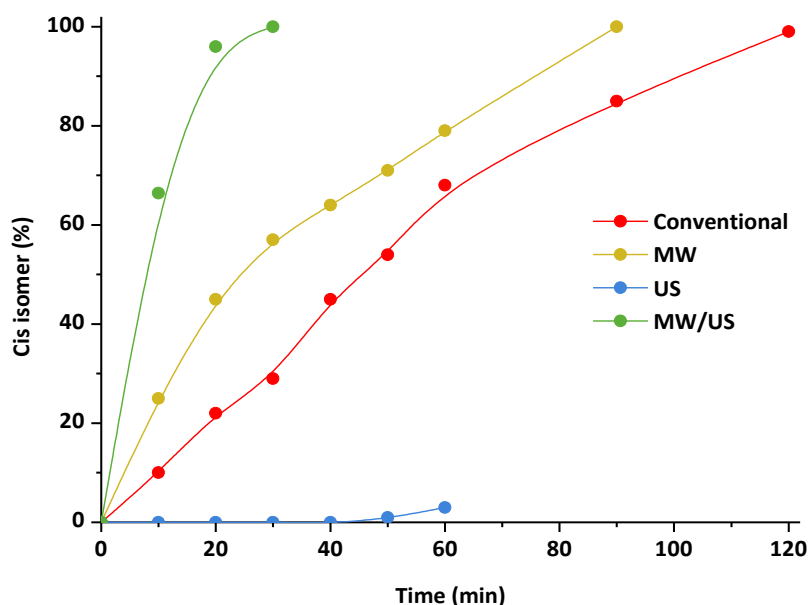


Figure 54. Reaction kinetic under different techniques. 1) Conventional: stirring, 2) US: Pyrex horn, P:30W, F:20,4kHz; 3) MW: Milestone, MicroSynth, Program: 2 min Pmax=400 W heated as quickly as possible to reach 150 °C, then P: 120 W; 4) MW/US: Combined reactor MW (P:110W) and Pyrex horn US(P:30W). Reaction conditions: Diphenylacetylene (1mmol), KOH (2 mmol), CuNPs (10 mol%), ethylen glycol (15 mL). T: 150°C. Determined by GC-MS.

As we can observe in Figure 54, fully conversion to Z-isomer was obtained after 2 hour stirring at 150°C under conventional conditions using 10% mol of Cu nanoparticles. As already

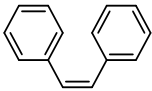
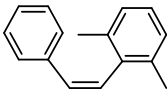
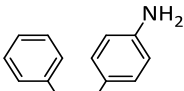
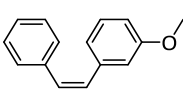
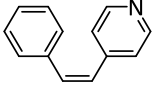
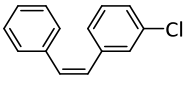
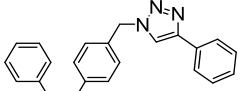
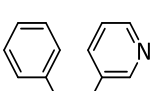
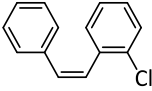
evidenced in the case of the nitro reduction, the use of non conventional techniques such as microwave and ultrasound have a big influence in the reaction by enhancing the heat and the mass transfer, and therefore, the reaction rate. Since working only with US irradiation the energy is not enough to heat the mixture up until the optimal temperature (150°C), the hydrogenation could not take place. However, the use of microwave irradiation greatly improved the reaction performance. Moreover, as already observed in previous studies, the simultaneous irradiation of MW and US (CMUI) allowed better reaction outcome in terms of the reaction rate and selectivity. As shown in Figure 54, when combining both enabling technologies (CMUI) for the selective hydrogenation of diphenylacetylene to Z-stilbene, only half an hour is enough to complete the reaction.

After the initial optimization, the reaction scope was explored by reducing a number of aromatic internal alkynes with different functional groups (Table 25).

Table 25. Scope of the hydride free reduction of aromatic alkynes to Z-alkenes catalysed by CuNPs^{d)}.

2.25 (a-s) $\xrightarrow[\text{KOH, CuNPs}]{\text{HO-CH}_2\text{-CH}_2\text{-OH}}$ 2.26 (a-s)

Entry	Product	Selectivity (%) [Isolated Yield(%)] ^{b)} (Conv) (%) ^{c)}	Entry	Product	Selectivity (%) [Isolated Yield(%)] ^{b)} (Conv) (%) ^{c)}
1		98 [92] (>99)	11		96 [75] (>99)
2 ^{d)}		98 [90] (>99)	12		97 [94] (>99)
3		97 [92] (>99)	13		91 [78] (>99)
4		98 [90] (>99)	14		97 [88] (>99)
5		96 [84] (>99)	15		74 [53] (>99)

6 ^{e)}		98 [80] (>99)	16		95 [82] (>99)
	2.26f			2.26p	
7		97 [86] (>99)	17		97 [85] (>99)
	2.26g			2.26q	
8		84 [62] (>99)	18		97 [86] (>99)
	2.26h			2.26r	
9		95 [78] (>99)	19		96 [87] (>99)
	2.26i			2.26s	
10		95 [82] (>99)			
	2.26j				

^{a)} Reaction conditions: Alkyne derivative (3mmol), Ethylen glycol (20 mL), KOH (6 mmol), CuNPs (5 mol%), T:150°C, method: MW/US combined reactor: MW (P:120W) and Pyrex horn US(P:30W), t:30 min. ^{b)} Isolated yield. Compound purity proved by ¹H-NMR and ¹³C-NMR (see Chapter 5: Experimental details), ^{c)} Determined by GC-MS, ^{d)} 1-nitro-4-(phenylethynyl)benzene as the substrate, ^{e)} 1-Bromo-4-(phenylethynyl)benzene as the substrate.

The hydrogenation of diphenylacetylene gave 99% conversion (by GC-MS) to the corresponding Z-alkene after 30 min using 5 mol% CuNPs catalyst at 150°C (Table 25, entry 1). Filtration, extraction and purification by chromatography on silica gel gave pure Z-stilbene in 92% yield. In order to broaden the scope of this reaction with regard to other functional groups, 1-nitro-4-(phenylethynyl)benzene (Table 25, entry 2) was used as the substrate, and complete conversion into an E/Z (2:98) mixture of 4-styrylbenzenamine (Table 25, entry 2) was obtained. As observed, under these reaction conditions also the nitro group was fully reduced to an amino group, confirming the study in our previous work (2.3 Copper catalysed reduction of aromatic nitrocompounds. Glycerol: an optimal hydrogen source) about the reduction of aromatic nitrocompounds using copper catalyst. The same phenomenon was observed when the -NO₂ group was present in the ortho position (Table 25, entry 13). However, notably, in the case of (Z)-1-(4-styrylphenyl)ethanone (Table 25, entry 5), the keto- group remained intact, showing a complete chemoselective hydrogenation towards the alkyne, with 99% conversion and 96% selectivity to the Z-alkene. Interestingly, no hydrogenolysis of the C-F and C-Cl bond took place during the hydrogenation of Chloro-(phenylethynyl)benzene and Fluoro-(phenylethynyl)benzene. After 30 min of reaction in the presence of 5 mol% of CuNPs, (Z)-1-fluoro-2-styrylbenzene (Table 25, entry 11) was achieved with E/Z (4/96) of selectivity. In the same manner, (Z)-1-chloro-2-styrylbenzene (Table 25, entry 10) and (Z)-1-chloro-3-styrylbenzene

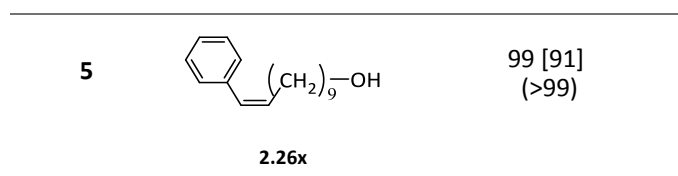
(Table 25, entry 18) were obtained with excellent selectivities E/Z (5/95) (3/97) and isolated yields, 82% and 86%, respectively. However, while using bromo as substituent, the hydrogenolysis gave as predominant reaction product the Z-stilbene instead of (Z)-1-bromo-4-styrylbenzene (Table 25, entry 6). The product of overhydrogenation, the 1-bromo-4-phenethylbenzene was observed in 5% yield. Worth noting was that alkynes bearing heterocycles such as pyridine were found to be good substrates and the corresponding alkenes were produced with high yields. The influence of the heteroatom was studied and the three different positions were compared. When the N was positioned in para-, full conversion was obtained in 30 minutes with a ratio of Z/E/alkane, 84:6:10 (determined by GC_MS) and the Z alkene was isolated with 62% yield. When reducing the ortho-N derivative, full conversion was as well detected in 30 minutes, but the Z/E/alkane ratio decline to 74:20:6. Interestingly, when the heteroatom was situated in meta-position, overhydrogenation to the alkane derivative was not observed. Instead, good selectivity with E/Z (4/96) was determined and 87% of Z-alkene was isolated. Another important aspect to notice is the fully alkyne conversion and the high selectivity to the (Z)-alkene independent of the substituents position in the aromatic ring. Even when reducing the 1,3-dimethyl-2-(phenylethynyl)benzene (Table 25, entry 16), which has two -Me in ortho position, fully conversion was achieved with Z/E/alkane ratio of 95/3/2.

Table 26. Scope of the hydride free reduction of alkynes to Z-alkenes catalysed by CuNPs^{a)}.

$$\text{R}-\text{C}\equiv\text{C}-\text{R}_1 \xrightarrow[\text{KOH, CuNPs}]{\text{HO}-\text{CH}_2\text{CH}_2-\text{OH}} \text{R}-\text{C}=\text{C}-\text{R}_1$$

2.25 (t-x) **2.26 (t-x)**

Entry	Product	Selectivity (%) [Isolated Yield](%) ^{b)} (Conv) (%) ^{c)}
1	 2.26t	10 [-] (>99)
2	 2.26u	98 [85] (>99)
3	 2.26v	99 [88] (>99)
4	 2.26w	97 [92] (>99)



^{a)} Reaction conditions: alkyne derivative (3mmol), ethylen glycol (20 mL), KOH (6 mmol), CuNPs (5 mol%), T:150°C, method: MW/US combined reactor: MW (P:120W) and Pyrex horn US(P:30W), t:30 min. ^{b)} Isolated yield. Compound purity proved by ¹H-NMR and ¹³C-NMR (see Chapter 5: Experimental details), ^{c)} Determined by GC-MS.

The reduction of a terminal alkyne under similar reaction conditions was also explored, however, a complicated mixture of degradation products was observed, without showing good selectivity to any derivative (Table 26, entry 1). In the same way, the scope of the reaction was investigated by reducing a number of aliphatic and aliphatic/aromatic internal alkynes with different functional groups. As observed, excellent selectivities to the Z-isomer were as well obtained for these molecules. When symmetric aliphatic alkynes such as 1,4-dietoxy (Table 26, entry 2) and 1,4-bis(benzyloxy) (Table 26, entry 3) were reduced fully conversion was observed and the (Z)-isomers were isolated with good yields, 85% and 88% respectively. By the same token, the semihydrogenation of aliphatic/aromatic internal alkynes (Table 26, entries 4 and 5) proceeded with high stereoselectivity, without further formation of alkane.

2.7 Conclusion

Despite its apparent simplicity, the reduction of nitro compounds constitutes a key and venerable transformation, which extends its importance to the chemical industry. Even though numerous papers and patents have been reported on the reduction of nitro derivatives with variable success, selective reduction of the nitro group is not easy to accomplish in the presence of other competing functionalities. Aiming to come up with sustainable and efficient approaches for this synthesis, we have developed different strategies:

A facile new protocol for selective reduction of nitro and azido derivatives that utilises the, mostly unexplored, mechanochemical approach was firstly explored. To the best of our knowledge, no report has described before the hydrogenation without catalyst addition being performed in a ball mill. This method benefits from the use of convenient, cost-effective and environmentally friendly formate salts as hydrogen donors. The ball milling reactions have proven themselves to be efficient, versatile and able to give products in short reaction times at high yields, which are also favoured by the easy workup. Challenging functional groups, such as -I, -Br, -Cl, -CO and -COMe, were well tolerated under the described reaction conditions. The advantages of our method include its metal-free nature, its use of eco-friendly and easily available formate salts as the hydrogen source and the ambient reaction conditions.

In the second part of this chapter, glycerol has been studied as a hydrogen donor for the exhaustive, fast and reproducible Cu-catalysed transfer hydrogenation of nitrobenzene to aniline. Small size, roundish-shape CuNPs were prepared in glycerol and, using HRTEM, it was possible to observe that the polyol layer mediates the interaction between the metal active sites and stabilises NP function. NP dispersion in glycerol was promoted by US irradiation and excellent results (complete conversion and >95% yield) were obtained after 2 h when CuNPs were employed for nitrobenzene reduction under conventional heating conditions at 130 °C.

The high polarity and low vapour pressure of glycerol allowed the effects of MW irradiation to be fully explored and, gratifyingly, the reaction was shortened to 15 min.

On the basis of this detailed study, in the third part of this section the reaction has been scaled-up using a MW-assisted batch reactor and a packed bed reactor for continuous flow. When working in batch, a constant power MW protocol was optimised and the reaction was scaled-up to 36 mmol/500 mL of glycerol in a multimode industrial MW reactor. Afterwards, aiming to prepare a heterogeneous as well as robust and recyclable catalytic system for nitrobenzene reduction, different inorganic supports were tested and the celite showed the best results in terms of nitrobenzene conversion. Knowing the several benefits of continuous flow if comparing with batch processing in terms of efficacy, cost, equipment size, energy consumption and safety; nitrobenzene reduction to aniline was optimised under continuous-flow conditions using a packed bed reactor. In this way, an inexpensive and easily prepared Cu/Celite catalyst provided chemoselective hydrogenation of nitroarenes to anilines using ethylen glycol as solvent and hydrogen source. Moreover, while batch recycle studies suffered from catalyst loss during the recovery procedure, preliminary studies using the packed-bed reactor under continuous flow operation were highly encouraging as good yields and a stable catalyst profile were achieved. The reduction reaction was then explored for a prolonged time period showing optimal results, with 70% of aniline production after 70 hours. Fully nitrobenzene conversion was obtained once again by two different ways: solution recycling and catalyst reactivation by flowing ethylen glycol (which a) cleans the catalyst surface of some reaction reagents or products and b) reduces the catalyst active sites that have been oxidized during the reaction).

Moreover, it has been demonstrated that copper nanoparticles act as an efficient catalyst for the chemoselective reduction reaction of aromatic nitrocompounds to aminocompounds and azocompounds, according to the hydrogen source employed. The use of high temperatures (130°C) in presence of glycerol allowed the fast reduction to the fully reduced product, whereas the use of softer conditions (55°C) with ethanolamine as hydrogen donor facilitates the coupling reaction and the synthesis of the azocompound. Enabling technologies such as microwave and ultrasound, either alone or combined, were successfully applied showing a notable increase in the reaction rate. Using this procedure, we have presented an efficient and convenient method for the chemoselective reduction of nitroarenes. It allowed us to isolate a wide range of amino and azocompounds bearing both electron-donating and electronwithdrawing substituents in excellent yields.

In the last section of this chapter, chemo- and stereo-selective semi-hydrogenation of alkynes to cis-alkenes, without further reduction to alkanes, has been explored. This reaction is of great significance in the polymer and fine chemical industries. The advantages of our method include its hydride-free nature, the use of eco-friendly and easily available ethylene glycol as the hydrogen source and the use of copper nanoparticles as low cost and stereoselective catalyst. The use of copper nanoparticles against the bulk metal permit the reduction of catalyst quantity from 200 mol% to only 10 mol%, showing at the same time a great increase in the reaction conversion, thanks to their extremely small dimensions and huge special surface. The use enabling technologies such as microwave and ultrasound, either alone and combined, allow a notable reduction in the reaction time and a high conversion thanks to the enhancement in the heat and mass transfer. As already despited in nitrobenzene reduction, ultrasound irradiation facilitates the catalyst dispersion increasing the catalyst active sites and

the microwave permit the selective and fast solution heating. These reactions have shown themselves to be efficient, selective, versatile and able to give products in short reaction times with high yields, isolating a wide range of internal aromatic and aliphatic alkynes.

***Chapter 3: Sonochemically-promoted
preparation of Cu- β -CD grafted silica***

3.1 Introduction

The design of novel organic-inorganic hybrid systems has achieved considerable success in several fields, including catalysis, photochemistry, biochemistry and optoelectronics.³⁸⁸ Numerous innovative studies have enriched the literature on this type of compound, and especially so in recent years.^{389–392} For example, a hybrid inorganic–organic, TiS₂ and ammonium-cation-based superlattice has recently been described as a promising flexible thermoelectric thin film.³⁹³ Moreover, an innovative system, consisting of a core of BaTiO₃, covered by PMMA, has been demonstrated to have tailorable dielectric properties.³⁹⁴ The key feature of this type of system is that its characteristics arise not only from the individual contributions of the phases, but also from the properties of the inner interface, which can also be predominant. The unique active behaviour of these hybrid systems is therefore not observed when the single components are used alone.³⁹⁵

Organic-inorganic hybrid systems have emerged as winning combinations in the general field of catalysis due to their enhanced heterogeneous properties. In fact, the immobilisation and stabilisation of organic active sites over inorganic solids has strongly improved recovery and recyclability characteristics.^{392–396} This type of material can be divided into two classes according to the nature of the organic-inorganic interface.³⁹⁷ Class I materials possess organic and inorganic components bonded together via weak interactions, such as van der Waals forces, hydrogen bonding and ionic bonds. Class II compounds are made up of stronger covalent or ionic-covalent interactions.³⁹⁸ This latter class has attracted much more interest from the field of catalysis due to the higher stability of its hybrid systems. Indeed, class II materials can be used under harsher reaction conditions, whereas class I systems are more sensitive and may be irreversibly damaged. For example, mesoporous silica, such as SBA-15 and MCM-41, has been functionalised with numerous organic ligands for several catalytic applications.^{399–402} The evolution of Class II hybrid components has led to the growth of materials in which catalytically active coordination-metal complexes are covalently anchored to inorganic substrates.^{403–406} Due to the impractical nature of infinitely recycling the metals, research is being directed to the utilisation of more abundant and inexpensive metals, such as iron, cobalt copper and nickel, in the place of precious metals.^{407–412} Specifically, copper catalysis has received a great deal of attention in recent years.^{413–417} In fact, copper has undergone thorough investigations in its role as a homogeneous catalyst and remarkable results have been achieved in many reactions, including oxidations, additions, C-C bond cleavage and Michael addition reactions.^{418–421} Therefore, the development of stable Cu catalysts that can be used in heterogeneous conditions has recently attracted considerable interest. For example, copper nanoparticles that are supported over silica have been studied as efficient catalysts for the hydrogenation of alkynes.⁴²² Furthermore, Cu that is supported over manganese oxide octahedral molecular sieves has been demonstrated to be an efficient catalyst for the synthesis of imidazoles.

The purpose of Cu organic-inorganic hybrid systems resides in the possibility of synthesising heterogeneous catalysts with the lowest possible metal dimensions in order to increase active surface area. The ambitious major objective in this field is therefore that of producing atomic-scale particles. This can be achieved via the selection of stable ligands for Cu that can be strongly anchored over the various solid supports. β -cyclodextrin (β -CD) has been demonstrated to be an attractive macromolecule for this purpose. β -CD is a cyclic

oligosaccharide composed of seven linked D-glucofuranose units and that can be represented as a toroid structure with narrow and wide openings corresponding to the primary and secondary hydroxyl groups, respectively.⁴²³ This peculiar structure means that β -CD can easily encapsulate copper and numerous other compounds.^{424–426} Several studies have proposed ingenious strategies for supporting Cu/ β -CD complexes. For example, Moradi *et al.*, have recently stabilised Cu(II)/ β -CD complexes over fibrous nanosilica and have successfully employed the material as a catalyst in the synthesis of oxazolidinones.⁴²⁷ Xia and co-workers have prepared a magnetically recoverable catalyst made of Cu(II)/ β -CD complexes anchored over ferric oxide and covered by silica.⁴²⁸ Shafiee *et al.*, have reported the preparation of functionalised PEGylated mesoporous silica nanoparticle-graphene oxide as a catalyst for the synthesis of imidazoles.⁴²⁹

Ultrasound (US) has seen widespread use in the promotion of organic syntheses^{246,430} and heterogeneous phase reactions.^{431,432} Significant effort has been devoted to organic synthesis with supported catalysts and reagents on the surfaces of cheap and recyclable mineral supports, such as clay, silica, alumina.⁴³³ However, only a limited number of publications have made reference to US-promoted silica derivatisation. The focus is mainly on Class I derivatives that possess organic and inorganic components. US irradiation has been efficiently employed to give silica-based nanocomposites. For example, guanidineacetic acid has been immobilised on the surface of modified Fe₃O₄@SiO₂,⁴³⁴ and carbon nanotubes have been derivatised with tetraethoxysilane using an ultrasonic sol-gel process.⁴³⁵ Only a few examples have studied the preparation of Class II derivatives, and an alkoxysilane derivate of thiacalix[4]arene has been efficiently covalently grafted onto silica.⁴³⁶

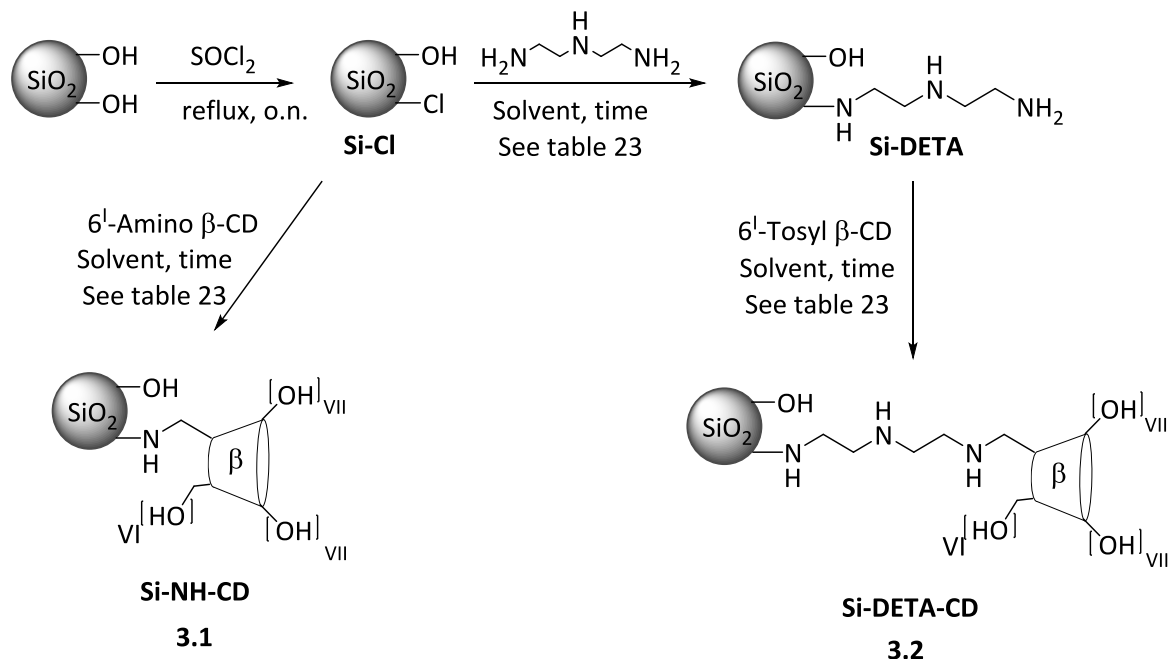
Herein, we describe a detailed investigation into the influence of US irradiation on the reaction rate of silica derivatisation to obtain CD-grafted silica. A number of routes have been explored and compared with the aim of obtaining this class of peculiar organic-inorganic hybrid material using a highly reproducible, efficient synthetic protocol. Commonly employed silica-grafting procedures entail long reaction times at high temperatures and the capability of US to shorten reaction times and operate at lower temperatures has been demonstrated. By supporting Cu(II) on the CD grafted silica, we were able to produce a green and sustainable copper catalyst for click azido-alkyne cycloadditions. The microwave (MW) promoted reaction was optimised without the addition of a reducing agent because of the presence of CD.

3.2 Organic-Inorganic hybrid material and its application in click chemistry

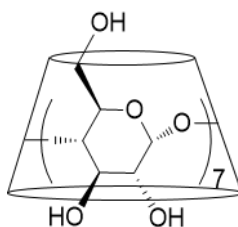
3.2.1 Synthesis of copper supported on Si-NH-CD and Si-DETA-CD

On the basis of our experience with covalently functionalised silica,^{437,438} the modification of silica surfaces *via* the grafting of organic compounds can lead to improve catalytic activity and may increase sorption capacity. With the aim of obtaining different silica-support-grafted β -CDs for Cu(II) species using a short and reliable synthetic protocol, two different routes were compared. Specifically, β -CD was anchored to silica via a diethylenetriamino spacer that can contribute to Cu binding strength, and amino CD was directly grafted onto the silica surface (Scheme 34). SIPERNAT 320 was used as amorphous silica, with a medium particle size and moderate absorption capacity. Preliminarily, silica was converted to silica chloride (Si-Cl) in presence of thionyl chloride, as has already been described in the literature,^{439,440} and the

resulting chloride ions were titrated with a silver nitrate solution in the presence of a potassium chromate solution, used as an indicator. 6^l amino-6^l-deoxy-β-CD was then reacted to obtain the Si-NH-CD derivatives. In the second route, which gives the Si-DETA-CD derivative, 6^l tosyl-β-CD was anchored to silica via a diethylenetriamino spacer. Chlorinate silica was then reacted with diethylenetriamine (DETA) and a nucleophilic substitution with 6^l-tosyl-β-CD was performed (Scheme 34).



Scheme 34. Synthetic schemes for the preparation of Si-NH-CD and Si-DETA-CD



Scheme 35. General structure of β-CD.

In order to optimise the reaction conditions, both schemes were performed under different reaction conditions, as depicted in Table 27. Thermogravimetric analyses (TGA) and IR spectra were carried out to measure the loading and to confirm the identity of the synthesised silica derivatives. TGA allows the grafting efficacy of every single step to be quantified by assuming that water is the only compound removed from the starting silica by surface dehydroxylation. The curves are all normalized to 150 °C to circumvent any possible solvent influence on yield calculations. When DETA was reacted with silica chloride, a number of solvents were compared under conventional conditions and a suspension of Si-Cl in toluene, chloroform and DMF was treated with the triamine derivative at 60 °C for 12 h. As represented in Figure 55, the TGA analyses of Si-DETA showed a higher degree of derivatisation when toluene was used as the solvent. The first derivative peak temperature (315 °C) indicates the point of greatest rate of change on the weight loss curve, and the profile was consistent in all three samples. The synthetic process was also performed under US irradiation in order to reduce the reaction time and improve functionalisation. US irradiation is considered to be a nonconventional

means to achieve efficient heating, dispersion, the deagglomeration of solids and improvements in mass transfer. It offers a facile, versatile synthetic tool for the preparation of nano/microstructured materials that are often unavailable via conventional methods. Several different frequencies (40 – 80 – 120 kHz) were used and compared when the reaction was repeated under US irradiation. For the sake of comparison, the reaction was irradiated for 2 and 4 h and the results obtained in toluene, were compared to reactions performed neat in diethylenetriamine as solvent. As depicted in Table 27, the same degree of substitution, that was measured by TGA after 2 h of US irradiation, was achieved after 12 h at 60 °C, while after 4 h of US irradiation the degree of substitution was maintained without improvement. Figure 56 shows the TGA profiles of Si-DETA batches obtained at a range of different frequencies, either in toluene or neat in 2 h. An increase in weight loss was observed when the reactions were subjected to 80 kHz irradiation. 40 kHz and 120 kHz fail to give the maximum degree of substitution under both sets of reaction conditions.

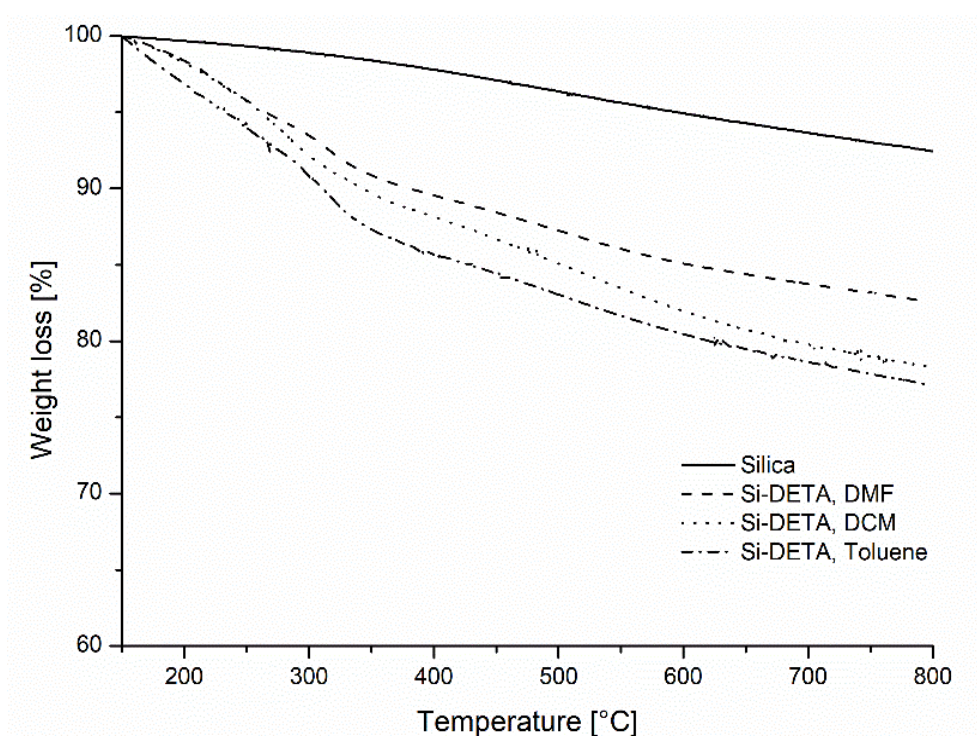


Figure 55. TGA profiles of starting silica and Si-DETA substrates (Table 27, entry 1-3). The reaction mixture was heated at 60 °C and conventionally stirred for 12 h. Three different solvents were tested. (solid line) starting silica; (dashed line) Si-DETA prepared in DMF, Table 27, entry 2; (dotted line) Si-DETA prepared in DCM, Table 27, entry 1; (dashed-dotted line) Si-DETA prepared in toluene, Table 27, entry 3.

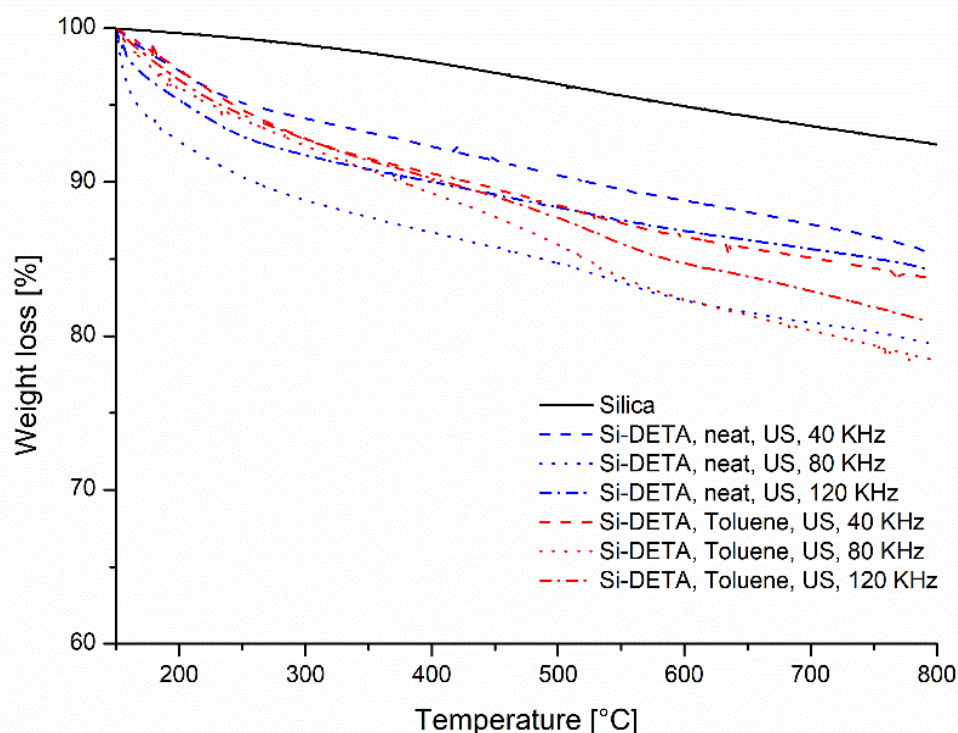


Figure 56. TGA profiles of silica and Si-DETA obtained using US irradiation at different frequencies (40 – 80 – 120 kHz), in neat conditions (Table 27, entries 7-9, blue lines) and in toluene (Table 27, entries 4-6, red lines). (solid line) starting silica; (blue, dashed line) Si-DETA, neat, US 40 kHz, Table 27, entry 7; (blue, dashed-dotted line) Si-DETA, neat conditions, 120 kHz, Table 27, entry 9; (red, dashed line) Si-DETA, toluene, 40 kHz, Table 27, entry 4; (red, dashed-dotted line) Si-DETA, toluene, 120 kHz, Table 27, entry 6; (blue, dotted line) Si-DETA, neat conditions, 80 kHz, Table 27, entry 8; (red, dotted line) Si-DETA, toluene, 80 kHz, Table 27, entry 5.

When β -CD was grafted onto Si-DETA via the nucleophilic replacement of 6^l-tosyl β -CD, the reaction was performed conventionally in DMF at 70 °C for 24 h (Table 27, entry 16). Looking at TGA (Figure 57), we can assume that DETA was acting as the leaving group, as the organic moiety on the silica surface was reduced in weight after the reaction if compared to the starting material. The interaction between β -CD and phenolphthalein (Php) was used to achieve the dual aims of measuring the amount of β -CD that maintains its inclusive properties when grafted onto the silica, and of investigating the inclusion capacity of the grafted β -CD. In combination with TGA, the amount of β -CD was measured via titration with Php in the buffer solution (pH = 10.5) 0.008 mM. The amount of grafted β -CD was measured on the basis of UV adsorbance, via interpolation from the standard curve. The change in Php absorbance was recorded on a UV spectrophotometer at 553 nm. When the grafting of CD was performed under conventional heating, by UV adsorbance of the Php solution we could detect the presence of solid supported β -CD and measure a w/w % of grafting of 1.3 mg/100 mg (Table 27, entry 16). The same sample analysed by TGA showed a decrease in total weight loss in the range 150 °C - 800 °C if compared to the starting Si-DETA derivative (see Figure 57). Based on this fact we assumed the instability of the precursor in the reaction condition, as furthermore confirmed by infrared analysis described below. Under US irradiation at 80 kHz, the grafting percentage increased to 3.3 % w/w, and PhP titration confirmed the derivatisation data (Table 27, entry 17). Unfortunately, we observed that the preparation of Si-DETA-CD was not reproducible, and so we proceeded with the direct grafting of 6^l amino β -CD to Si-Cl (Scheme 34).

Table 27. Synthesis of grafted silica

Entry	Product	Reaction condition	Time	Loading [w/w %]	Loading [μ mol/g]
1	Si-DETA	Si-Cl, DETA, DCM, reflux	12 h	14 ^(a)	1,37 · 10 ³ (c)
2	Si-DETA	Si-Cl, DETA, DMF, 60 °C	12 h	10 ^(a)	0,96 · 10 ³ (c)
3	Si-DETA	Si-Cl, DETA, toluene, 60 °C	12 h	15 ^(a)	1,49 · 10 ³ (c)
4	Si-DETA	Si-Cl, DETA, toluene,))) US, 40 kHz	2 h	9 ^(a)	0,87 · 10 ³ (c)
5	Si-DETA	Si-Cl, DETA, toluene,))) US, 80 kHz	2 h	14 ^(a)	1,35 · 10 ³ (c)
6	Si-DETA	Si-Cl, DETA, toluene,))) US, 120 kHz	2 h	11.5 ^(a)	1,12 · 10 ³ (c)
7	Si-DETA	Si-Cl, DETA, neat,))) US, 40 kHz	2 h	7,1 ^(a)	0,69 · 10 ³ (c)
8	Si-DETA	Si-Cl, DETA, neat,))) US, 80 kHz	2 h	13 ^(a)	1,26 · 10 ³ (c)
9	Si-DETA	Si-Cl, DETA, neat,))) US, 120 kHz	2 h	8,2 ^(a)	0,79 · 10 ³ (c)
10	Si-DETA	Si-Cl, DETA, toluene,))) US, 40 kHz	4 h	10 ^(a)	0,97 · 10 ³ (c)
11	Si-DETA	Si-Cl, DETA, toluene,))) US, 80 kHz	4 h	14.3 ^(a)	1,12 · 10 ³ (c)
12	Si-DETA	Si-Cl, DETA, toluene,))) US, 120 kHz	4 h	10.9 ^(a)	0,97 · 10 ³ (c)
13	Si-DETA	Si-Cl, DETA, neat,))) US, 40 kHz	4 h	8 ^(a)	0,77 · 10 ³ (c)
14	Si-DETA	Si-Cl, DETA, neat,))) US, 80 kHz	4 h	13.5 ^(a)	1,26 · 10 ³ (c)
15	Si-DETA	Si-Cl, DETA, neat,))) US, 120 kHz	4 h	9 ^(a)	0,88 · 10 ³ (c)
16	Si-DETA-CD	Si-DETA, 6-tosyl β -CD, DMF, 70 °C	24 h	1,3 ^(b)	11 ^(d)
17	Si-DETA-CD	Si-DETA, 6-tosyl β -CD, DMF,))) US, 80 kHz	4 h	3,3 ^(a) -3.4 ^(b)	30 ^(c,d)
18	Si-NHCD	Si-Cl, 6-amino β -CD, DMF, 60 °C	12 h	4.02 ^(a) -0.99 ^(b)	35 ^(c)
19	Si-NHCD	Si-Cl, 6-amino β -CD, H ₂ O, 60 °C	12 h	2.6 ^(a) -0.81 ^(b)	20 ^(c)
20	Si-NHCD	Si-Cl, 6-amino β -CD, DMF,))) US, 80 kHz,	2 h	3,81 ^(a) -0.68 ^(b)	30 ^(c)
21	Si-NHCD	Si-Cl, 6-amino β -CD, H ₂ O,))) US, 80 kHz,	2 h	7.12 ^(a) -0.60 ^(b)	60 ^(c)
22	Si-NHCD	Si-Cl, 6-amino β -CD, DMF,))) US, 80 kHz,	4 h	3,5 ^(a) -0.67 ^(b)	30 ^(c)
23	Si-NHCD	Si-Cl, 6-amino β -CD, H ₂ O,))) US, 80 kHz,	4 h	6.8 ^(a) -0.68 ^(b)	60 ^(d)

¹ Preparation of Si-DETA: Si-Cl (0,100 g), solvent (0,500 mL) and diethylenetriamine (0,500 mL). Preparation of Si-DETA-CD: Si-DETA (0,100 g), DMF (1,7 mL), 6'-tosyl- β -CD (0,100 g). Preparation of Si-NHCD: Si-Cl (0,100 g), solvent (2 mL), 6-amino β -CD (0,163 g). ^{a)} the w/w % grafting was measured on the basis of TGA; ^{b)} the w/w % grafting was based on PhP titration; ^{c)} mmol/g values were measured on the basis of TGA considering the organic moiety anchored to the silica surface; ^{d)} mmol/g of β -CD based on PhP titration.

As described in Table 27, when 6^l-amino-6^l-deoxy- β -CD was reacted with Si-Cl for 12 h at 60 °C in DMF, a w/w % degree of derivatisation of 4% was detected by TGA, while PhP titration detected only 0.99 % of β -CD, providing an inconclusive answer to the preservations of its properties (Table 27, entries 18-19). A higher percent of grafting was observed in water. When the reaction was repeated under US irradiation, the reaction reached the same degree of derivatisation in 2 h; after 4 h any improvement was observed. (Table 27, entries 20-23, Figure 57).

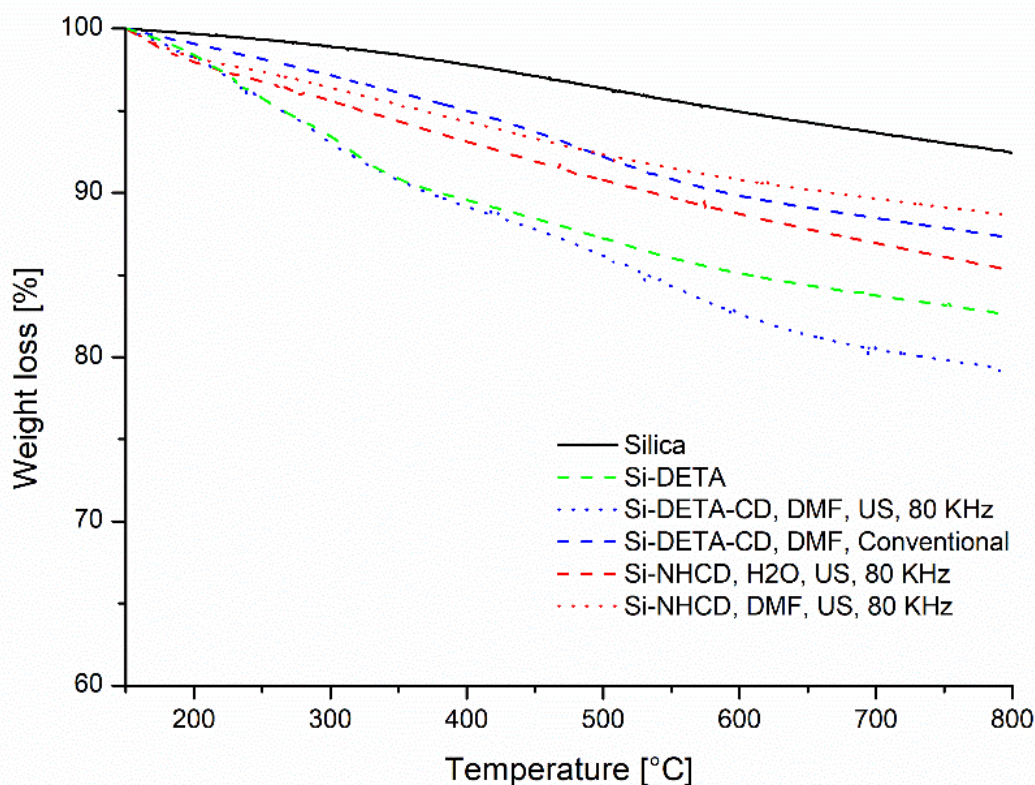


Figure 57: TGA profile of starting silica, Si-DETA (green line), Si-NHCD (red lines) and Si-DETA-CD (blue lines) prepared conventionally or under US irradiation. (solid line) starting silica; (red, dotted line) Si-NHCD US irradiation 80 kHz in DMF for 2 h, Table 27, entry 20; (blue, dashed line) Si-DETA-CD conventional heating in DMF at 70 °C for 24 h, Table 27, entry 16; (red, dashed line) Si-NHCD US irradiation 80 kHz in H₂O for 2 h, Table 27, entry 21; (green, dashed line) Si-DETA; (blue, dotted line) Si-DETA-CD US irradiation 80 kHz in DMF for 4 h, Table 27, entry 17.

Copper(II) forms a complex with CD in alkaline solution and the complexes with α - and β -CD have already been isolated and characterised.^{441,442} The efficacy of β -CD to direct and bind Cu when CD is bonded to silica has been already studied and its catalytic activity as a Lewis acid has been demonstrated.⁴⁴³ As the literature has focused mainly on the non-covalent bonding of β -CD onto the silica surface, we have aimed to explore the efficacy of β -CD that is covalently grafted onto silica to chelate Cu(II) and to exploit this system as catalyst for alkyne-azide cycloaddition (CuAAC) in absence of reducing agent.

Si-DETA-CD and Si-NHCD (Table 27, entries 17 and 22) were both loaded with Cu(II), the reaction was performed in a NaOH water solution to obtain a blue coloured catalyst.

3.2.2. Characterisation of copper supported on Si-NH-CD and Si-DETA-CD

Si-DETA, Si-DETA-CD and Si-NHCD (Table 27, entries 5, 17 and 21) were characterised by IR to prove the identity of the grafted silica. The same was done for Si-DETA-CD-Cu and Si-NHCD-Cu. As shown in Figure 58, the presence of the diethyltri-amino spacer on Si-DETA can be observed in spectrum c. This is characterised by a broad absorption band centred around 3000 cm^{-1} , which can be ascribed to hydrogen-bonded Si-OH and N-H groups. The expected νNH bands can be only seen as a modulation of the intense absorption, between 3400 and 3200 cm^{-1} . The corresponding weak δNH_2 mode is vibrating at similar frequency as physisorbed water (around 1600 cm^{-1}), while the band at 1510 cm^{-1} can be ascribed to the δNH vibrations of the secondary amines. Important changes can be observed in the spectrum (curve d) after the reaction with 6^l-tosyl- β -CD (and subsequent Cu inclusion). Namely, the high frequency region is dominated by an intense band centred at 3360 cm^{-1} (νOH), with clear $\nu\text{CH}/\nu\text{CH}_2$ bands at 2930 cm^{-1} (shoulder at 2860 cm^{-1}). The low frequency region shows the typical bending mode of physisorbed water $\delta\text{H}_2\text{O}$ centred at 1603 cm^{-1} (shoulder at 1662 cm^{-1}), and a complex group of bands with between 1500 and 1250 cm^{-1} (δCH and δOH). These features can be safely ascribed to the presence of β -CD, even if the assignment of the shoulder at 1662 cm^{-1} to physisorbed water alone is not straightforward. Similar results were obtained with the sample prepared with direct Si-NH-CD (curve e). The main difference is in the relative intensity of the bands assigned to $\delta\text{H}_2\text{O}$ modes. A comparison of the spectra of β -CD and Cu-CD (not reported) has led us to propose that this vibrational mode is sensitive to the presence of the Cu(II) ions included in the cavity and at the rim of the CD cavity. These results thus confirm the presence of β -CD on the silica in the various preparations. However, the changes in the high frequency region passing from Si-DETA to Si-DETA-CD (curves c and d), suggest a decrease in the amount of the diethyltri-amino spacer, confirming the instability of Si-DETA when submitted to reaction with 6^l-tosyl- β -CD. Hydroxyl group of CD may act as nucleophile, as well as DETA cannot be efficiently and reproducibly washed from the silica surface because of strong interactions with surface silanol/ silanolate groups.⁴⁴⁴

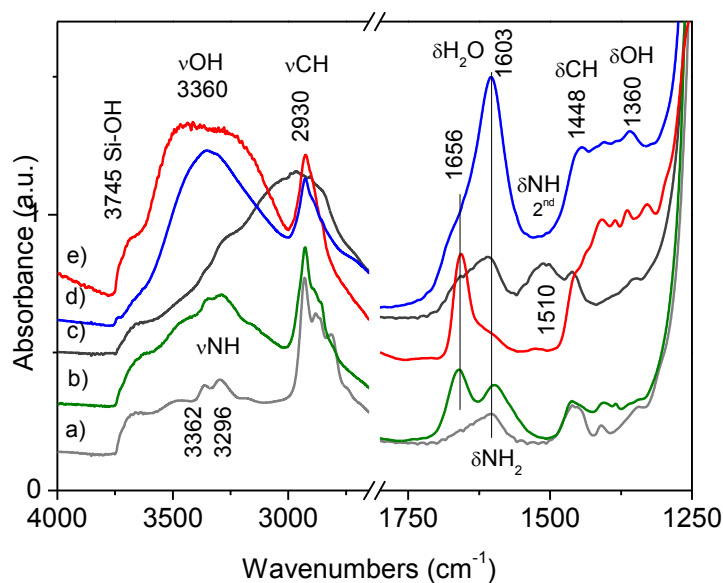


Figure 58. Infrared spectra of a) Si-diAm; b) Si-diAm-CD-Cu; c) Si-DETA; d) Si-DETA-CD-Cu, e) Si-NHCD. All samples were outgassed at 80 °C before measurements.

The presence of Cu on the catalysts was monitored by Diffuse Reflectance UV-Vis-NIR spectroscopy. For example (see Figure 59), we report the spectrum of Si-NHCD-Cu (blue curve) compared to the spectra of the reference materials (β -CD, SiO₂ and Si-NHCD). The spectra can be divided into three regions: i) UV (200-400 nm), corresponding to O²⁻ \rightarrow Cu(II) Charge Transfer (CT) transitions; ii) Visible (400-800 nm), corresponding to the ligand-field d-d transitions of Cu(II) ions; and iii) NIR (800-2500 nm), where the overtone and combination modes of infrared modes can be observed. The NIR region analysis allows us to further confirm the presence of the CDs that are linked to the silica support, and to confirm the involvement of OH groups in the coordination of the Cu ions. Indeed, all the hybrid-material spectra show signals, in this region, that are a mixture of the vibrational modes of SiO₂ (Si-OH overtone ν_{0-2} OH, $\nu+\delta_{H_2O}/\nu+\delta_{OH}$ combination modes of physisorbed water and of Si-OH groups) and those of CD (ν_{0-2} OH, $\nu+\delta_{H_2O}$, ν_{0-2} CH, $\nu_{OH}+\nu_{CO}$). On the other hand, the UV-Vis region of Si-NHCD-Cu clearly shows the typical fingerprint of hexacoordinated Cu(II) ions, with a CT component at 260 nm and an intense and broad d-d band at 700 nm. These results are in agreement with the structures proposed in Ref ⁴⁴⁵, which involve hexacoordinated Cu(II) ions in the cavity and at the rim of the CD cavity, coordinated by H₂O molecules, OH/O⁻ CD groups and/or extra ligands.

ICP Analyses of Si-NHCD-Cu and Si-DETA-CD-Cu quantified the Cu content on the Silica: at 10.1 mg/g and 7.2 mg/g of Cu, respectively.

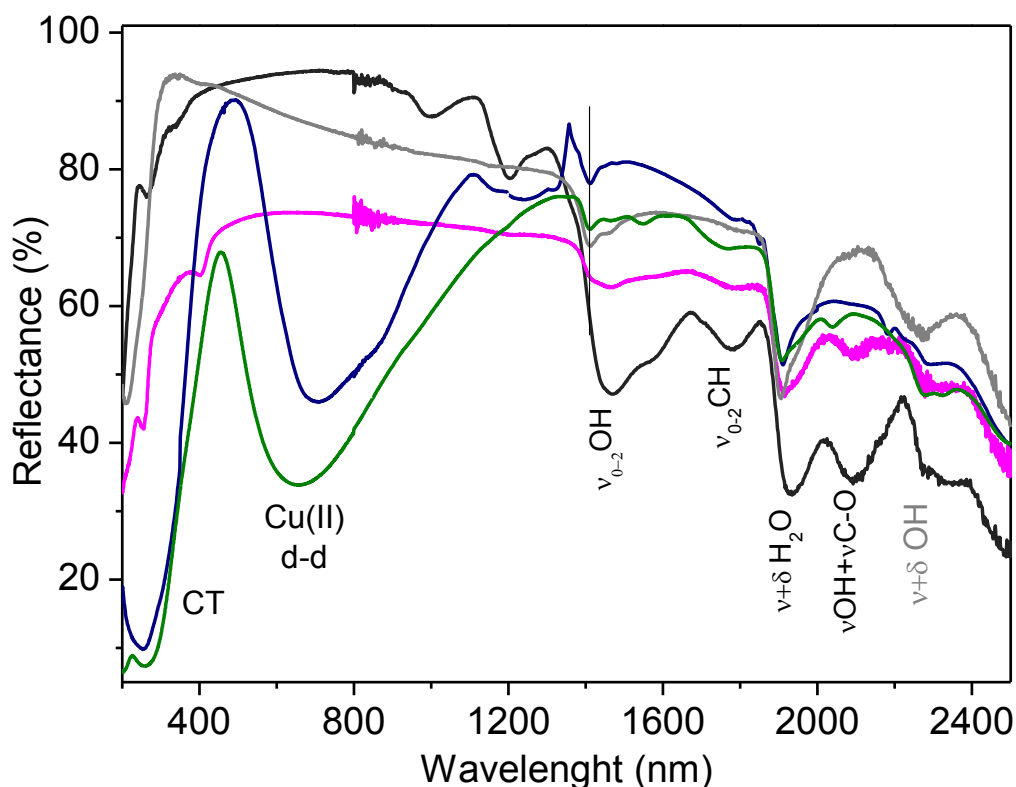
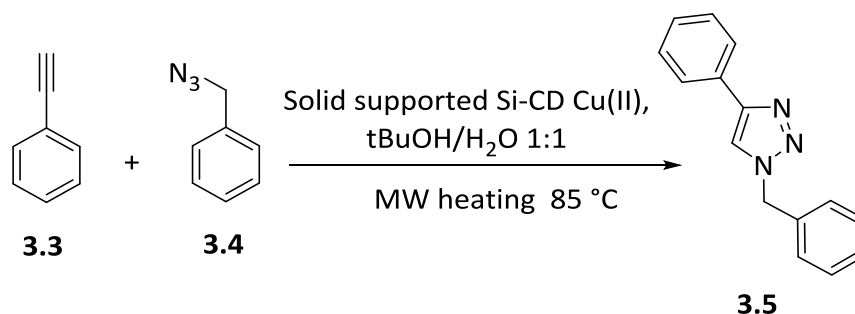


Figure 59. DR UV-Vis-NIR spectra of: SiO₂ (grey); β -CD (black); Si-NHCD (pink); Si-NHCD-Cu (blue) and Si-diAm-CD-Cu (green).

3.2.3. Test of catalytic activity of copper supported systems

Cu(II)- β -CD has been proven to be a reliable, water soluble green catalyst for 1,2,3-triazole synthesis without the addition of a reducing agent.⁴²⁶ Both the catalysts were tested in a model CuAAC reaction.



Scheme 36. Model reaction for CuAAC test of Si-NHCD-Cu and Si-DETA-CD-Cu.

Table 28. Panel test of CuAAC reaction.

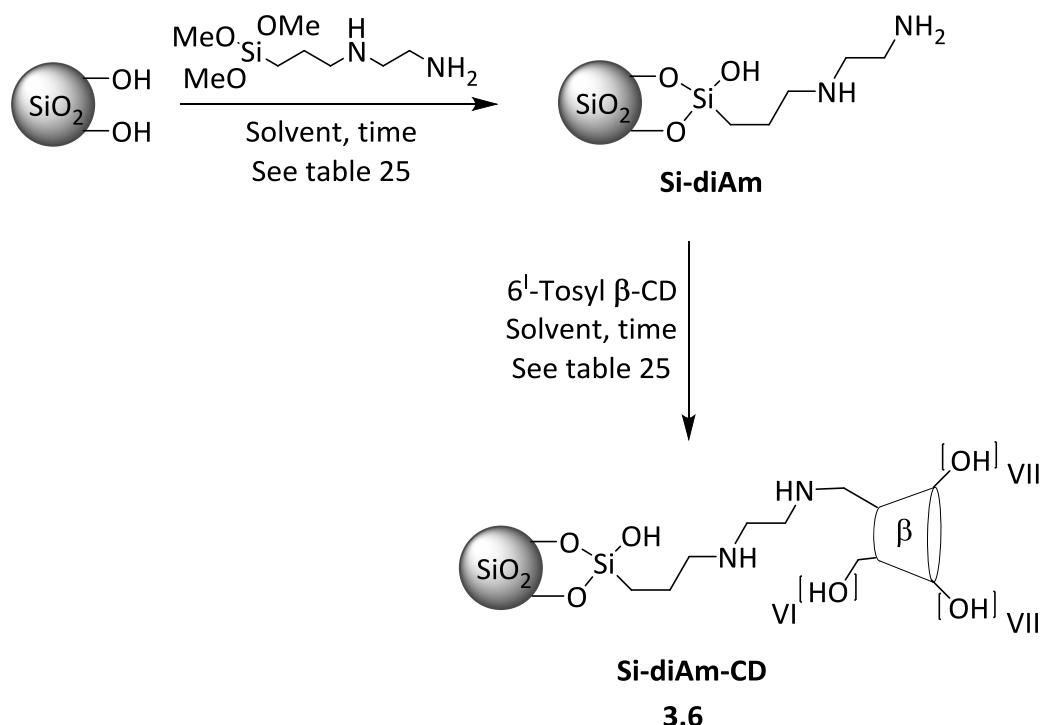
Entry	Catalyst, Cu mol%	Yield [%] ^(a)
1	Cu(OAc) ₂ , 5 mol%	14
2	CuSO ₄ , 5 mol%	0
3	β -CD- CuSO ₄ , 5 mol%(physical mixture)	0
4	β -CD-Cu, 5 mol%(complex)	55
5	Si-NHCD-Cu, 4 mol%, (17 mg)	5
6	Si-DETA-CD-Cu, 4 mol% (24 mg)	>99
7	Si-DETA-CD-Cu, 2 mol% (12 mg)	>99
8	Si-DETA-CD-Cu, 1 mol% (6 mg)	>99
9	Si-DETA-CD-Cu, 0.5 mol% (3 mg)	80
10	Si-DiAm-CD, 4 mol% (11 mg)	>99
11	Si-DiAm-CD, 2 mol% (5.5 mg)	65
12	Silica-Cu (12 mg)	4
13	Si-DETA-Cu (12 mg) ^a	0

Reaction conditions: benzyl azide (0,0676 mmol, 1 eq), phenylacetylene (1 eq), H₂O:tBuOH (1:1; 500 μ L), 85 °C, 1 h or MW 85 °C 20 min^(a) Determined by GC-MS.

As depicted in Table 28, the click Cu-catalysed cyclisation of benzyl azide and phenylacetylene was repeated under a number of reaction conditions and the different copper sources were compared. The reaction was performed at 85 °C for 1h. Silica supported Si-NHCD-Cu and Si-DETA-CD-Cu showed differing catalytic activities. In fact, only the second acted as an efficient catalyst for CuAAC .

Table 28, entries 5-6). As already observed in the Php titrations, it shows a higher inclusion capability when CD is bound to the silica with a spacer, furthermore, the triamino spacer can stabilise Cu(II) species. Si-DETA-CD-Cu shows high efficiency even when used in very small amounts. However, a reduction of activity was observed when the catalyst amount was decreased to 0.5 mol% (Table 28, entries 6-8). Cu(II) salts Cu(OAc)₂ and CuSO₄ were tested, for the sake of comparison, and the reaction was compared to a click reaction that was catalysed by a previously prepared Cu(II)-β-CD complex, and a reaction using a physical mixture of CuSO₄ and β-CD. Only the Cu(II)-β-CD complex gave satisfactory results and a 55% yield was recovered. In order to understand the influence of silica and the amino spacer on reaction outcome, Si-Cu and Si-DETA-Cu were tested to confirm that the complex between the copper ions and β-CD plays a key role in the performance of the reaction, in which β-CD acts as ligand for copper and the reducing agent.

In order to obtain a stable silica-supported β-CD derivative with a polyamino spacer, Si-diAm-CD was synthesised on the basis of our previous experience (See Scheme 37).



Scheme 37. Schematic representation of Si-diAm-CD (3.6) synthesis

Silica was derivatised with 3-(2-aminoethylamino)propyltrimethoxysilane (AEPS) to obtain Si-diAm. As described in Table 29, we can confirm that US irradiation reduced the reaction time to 2 h, whereas the same degree of substitution was achieved after 36 h at 80 °C under conventional heating and magnetic stirring. No differences in activation were observed between the use of 40 and 80 kHz and both were very efficient. In order to obtain the efficient grafting of β-CD, 6-O-tosyl β-CD was reacted at 60 °C for 60 h and 4.7 %w/w derivatisation was observed by TGA, while 2.8% was measured by Php titration. US irradiation at 80 kHz in a US bath was insufficient to obtain a satisfactory grafting percent, because of the low reaction temperature (45 - 50 °C) An increase in grafting percentage was observed when the reaction was prolonged to 6 days. The synergic effect of combined MW and US irradiation was also exploited. Enhancing the silica dispersion, increasing the active surface and allowing a

selective MW irradiation; the combined system permit to obtain high efficacy of grafting in short time, 4 h, and 6.1 ww% derivatization was afforded. As depicted in Figure 60, the first derivative TGA profile of Si-diAm indicates that the degradation peak is approximately at 314 °C when CD is grafted. Two degradation steps are visible, the peaks are at 298 °C and at 413 °C.

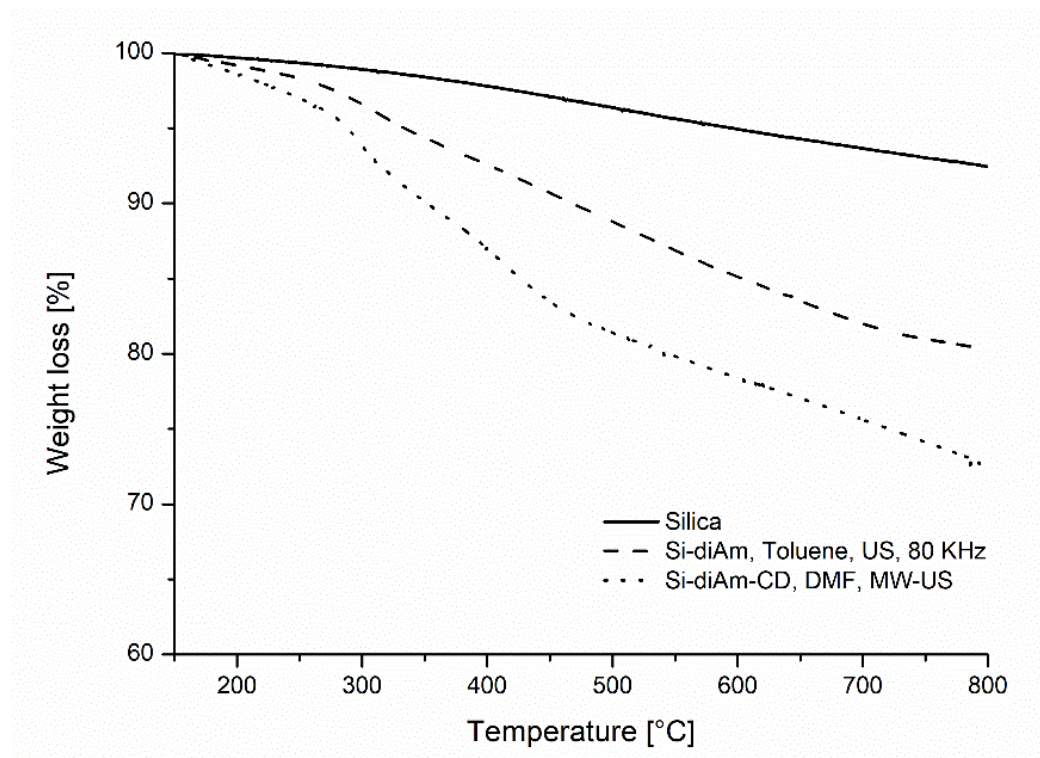


Figure 60. TGA profile of Si-DiAm-CD. (solid line) starting silica; (dashed line) Si-diAm, obtained in US at 80 kHz, 2 h, toluene, Table 25, entry 4; (dotted line) Si-diAm-CD, MW-US combined irradiation at 100 °C, 4 h, DMF, Table 25, entry 9.

Table 29. Synthesis of Si-diAm-CD

Entry	Product	Reaction condition	Time	Loading [w/w%]	Loading [μ mol/g]
1	Si-diAm	Silica, AEPS, toluene, 80 °C	6 h	6.5 ^(a)	290 ^(c)
2	Si-diAm	Silica, AEPS, toluene, 80 °C	36 h	13.6 ^(a)	610 ^(c)
3	Si-diAm	Silica, AEPS, toluene,))) US, 40 kHz	2 h	14 ^(a)	640 ^(c)
4	Si-diAm	Silica, AEPS, toluene,))) US, 80 kHz	2 h	12 ^(a)	540 ^(c)
5	Si-diAm	Silica, AEPS, toluene,))) US, 80 kHz	4 h	13 ^(a)	600 ^(c)
6	Si-diAm-CD	Si-diAm, 6'-tosyl- β -CD, DMF, 60 °C	60 h	4.7 ^(a) -2.15 ^(b)	42 ^(c)
7	Si-diAm-CD	Si-diAm, 6'-tosyl- β -CD, DMF, 60 °C	6 days	6.1 ^(a) -2.8 ^(b)	54 ^(c)

8	Si-diAm-CD	Si-diAm, 6 ^l -tosyl-β-CD, DMF,))) US, 80 kHz	4 h	1.7 ^(a) -1.18 ^(b)	15 ^(c)
9	Si-diAm-CD	Si-diAm, 6 ^l -tosyl-β-CD, DMF,))) MW/US, 100 °C	4 h	6.1 ^(a) -2.09 ^(b)	54 ^(c)

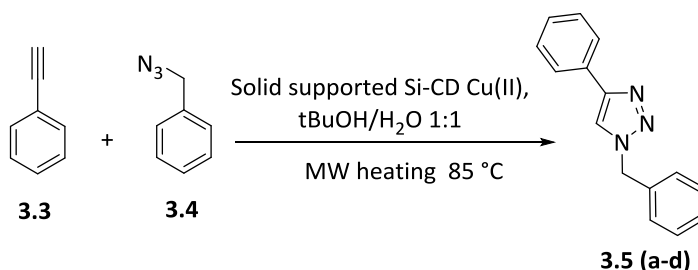
¹ Preparation of Si-diAm: silica powder (0,100 g), toluene (1 mL), AEPS (0,040 mL). Preparation of Si-diAm-CD: Si-diAm (0,100 g), DMF (1,5 mL), 6^l-tosyl-β-CD (0,100 g). a) measured by TGA, the weight loss was calculated on the basis of the starting material (see Figure 6); b) the w/w % grafting was based on PhP titration; c) mmol/g of organic moiety grafted on silica surface.

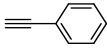
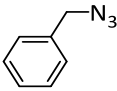
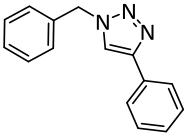
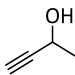
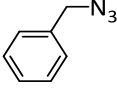
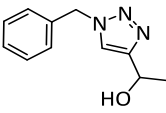
Si-diAm-CD was loaded with Cu(II) in basic conditions and the catalysts, Si-diAm, and Si-diAm-CD were characterised by IR and DR UV-Vis-NIR.

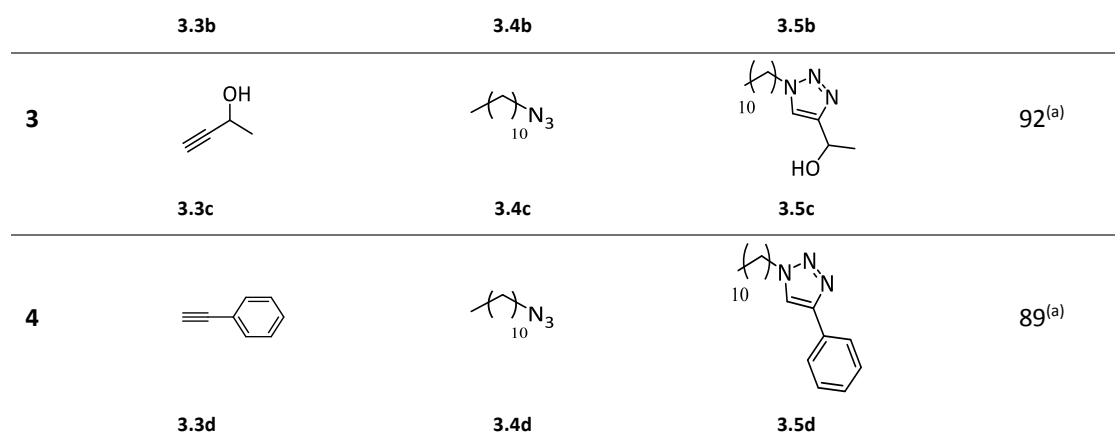
The IR spectra of Si-diAm and Si-diAm-CD are reported in Figure 58. Si-diAm (curve a) shows very clear νNH (3362 and 3296 cm⁻¹), νCH bands (2932, 2870 and 2806 cm⁻¹) and δNH₂ bands (ca 1600 cm⁻¹), which are preserved after reaction to graft CD (Si-diAm-CD, curve b). This proves Si-diAm's increased stability during the reaction with CD, as compared to Si-DETA derivatisation in which the bands were partially displaced (curves c and d). An analysis of the low frequency region of the spectra shows the fingerprints of β-CD (δH₂O, δCH and δOH). Diffuse Reflectance UV-Vis-NIR spectroscopy showed the presence of Cu after the reaction between CuSO₄ and Si-diAm-CD, and the typical fingerprint of hexacoordinated Cu(II) ions (d-d band at 650 nm and CT at 260nm), can be observed. ICP analysis showed a loading of 15.5 mg/g of copper.

When catalytic activity was tested in a model reaction (CuAAC of benzyl azide and phenyl acetylene), it was possible to evaluate the high catalytic activity of Si-DETA-CD-Cu. A slightly higher amount of catalyst was employed in order to obtain full conversion, and the reaction was successful in the presence of 4 mol % of catalyst. Alkyl and aryl azido derivatives, as well as alkynes, were tested to prove not only the efficacy, but also the versatility of the system. Full conversion was observed, and the product was isolated without purification (Table 30).

Table 30. Synthetic results of conventional Cu-supported catalyst.



Entry	Alkyne	Azide	Product	Yield [%]
1	 3.3a	 3.4a	 3.5a	99 ^(a)
2	 3.3b	 3.4a	 3.5b	95 ^(a)



Reaction conditions: azide (0,0676 mmol, 1 eq), terminal alkyne (1 eq), H₂O (250 μ L), tBuOH (250 μ L), 11 mg of catalyst (4 mol %), MW heating at 85 $^{\circ}$ C, 1 h. a) Yields determined by GC-MS.

3.3 Conclusion

In conclusion, the ability of US irradiation to speed up the synthetic procedures for silica grafting has been demonstrated. New β -CD grafted silicas have been synthesised and fully characterised. The influence that β -CD has on directing and activating Cu(II) on the silica surface for CuAAC reactions, in absence of a reducing agent, has been studied and confirmed. Low cost, green, fast and efficient procedures can be exploited to obtain Cu- β -CD-grafted silica with polyamino spacers under US irradiation. The catalyst shows excellent performance in CuAAC reactions.

Chapter 4: Experimental details

4.1 Non-conventional, non-contact energy sources for nitroarenes and alkynes reduction.

4.1.1 Mechanochemical reduction of nitroarenes and alkyl/aryl azides without catalyst addiction

4.1.1.1 Materials and methods

All chemicals were purchased from Sigma-Aldrich (Milan, Italy) and used without further purification. Reactions were monitored by TLC on Merck 60 F254 (0.25 mm) plates (Milan, Italy), which were visualized by UV inspection and/or by heating after a spraying with 0,5% ninhydrin in ethanol or phosphomolybdic acid. Mechanochemical reactions were carried out in a Planetary Ball Mill (PM100 Retsch GmbH, Haan, Germany) using either 50 mL grinding jars and milling balls (both made in stainless steel). NMR spectra (300 MHz and 75 MHz for ^1H and ^{13}C , respectively) were recorded on a Bruker 300 Avance instrument (Milan, Italy) at 25 °C. Chemical shifts were calibrated to the residual proton and carbon resonances of the solvent; DMSO- d_6 ($\delta\text{H} = 2.54$, $\delta\text{C} = 39.5$), CDCl_3 ($\delta\text{H} = 7.26$, $\delta\text{C} = 77.16$), D_2O ($\delta\text{H} = 4.79$). Chemical shifts (δ) are given in ppm, and coupling constants (J) in Hz. GC-MS analyses were performed in a GC Agilent 6890 (Agilent Technologies, Santa Clara, CA, USA) that was fitted with a mass detector Agilent Network 5973, using a 30 m capillary column, i.d. of 0.25 mm and film thickness 0.25 μm . GC conditions were: injection split 1:20, injector temperature 250 °C, detector temperature 280 °C. Gas carrier: helium (1.2 mL/min), temperature program: from 70 °C (2 min) to 300 °C at 5 °C/min.

4.1.1.2 General procedures

4.1.1.2.1 General Procedure for the nitrobenzene reduction reaction

The milling jar (50 mL; stainless steel) was equipped with 1500 milling balls ($\varnothing = 2$ mm, stainless steel) and 48 medium balls ($\varnothing = 5$ mm, stainless steel). Nitrobenzene (0.5 mmol), ammonium formate (15 mmol), KOH (1 mmol), and basic Al_2O_3 (1 g) were added in the given order. Milling was performed at 650 rpm for 30 min, 1, 1.5 and 2 hours. After the milling jar was cooled to room temperature, the crude products were transferred and the solid washed with CH_2Cl_2 (3×10 mL) and water (3×10 mL) to recover the desired product. After concentration to half volume under vacuum, the mixture was extracted with CH_2Cl_2 , washed with H_2O three times and finally dried (Na_2SO_4). The crude products were dried and analysed using GC-MS. Impure products were purified by flash chromatography on silica gel (hexane-EtOAc) to afford the desired product. Products were analysed using ^1H NMR and ^{13}C NMR spectroscopy after dissolution in an appropriate solvent.

4.1.1.2.2 General Procedure for the aryl azide reduction reaction

The milling jar (50 mL; stainless steel) was equipped with 1500 milling balls ($\varnothing = 2$ mm, stainless steel) and 48 medium balls ($\varnothing = 5$ mm, stainless steel). The aryl azides (0.5 mmol), sodium formate (10 mmol), KOH (1 mmol), and basic Al_2O_3 (1 g) were added in the given order. Milling was accomplished at 650 rpm for 1 and 1.5 hours. After the milling jar was cooled to room temperature, the crude products were transferred and the solid washed with CH_2Cl_2 (3×10 mL) and water (3×10 mL). After concentration to half volume under vacuum, the mixture was extracted with CH_2Cl_2 , washed with H_2O three times, and finally dried (Na_2SO_4). The crude products were dried and analysed using GC-MS. Impure products were purified by flash

chromatography on silica gel (hexane–EtOAc) to afford the desired product. Products were analysed using ^1H NMR and ^{13}C NMR spectroscopy after dissolution in an appropriate solvent.

4.1.1.2.3 General Procedure for the alkyl azide reduction reaction

The milling jar (50 mL; stainless steel) was equipped with 1500 milling balls ($\varnothing = 2$ mm, stainless steel) and 48 medium balls ($\varnothing = 5$ mm, stainless steel). The alkyl azides (0.5 mmol), hydrazine (15 mmol), KOH (1 mmol) and basic Al_2O_3 (1 g) were added in the given order. Milling was accomplished at 650 rpm for 1 hour. After the milling jar was cooled to room temperature, the crude products were transferred and the solid washed with filtered on paper using CH_2Cl_2 (3×10 mL) and water (3×10 mL). After concentration to half volume under vacuum, the mixture was extracted with CH_2Cl_2 , washed with H_2O three times, and finally dried (Na_2SO_4). The crude products were dried and analysed using GC–MS. Impure products were purified via flash chromatography on silica gel (hexane–EtOAc) to afford the desired product. Products were analysed using ^1H NMR and ^{13}C NMR spectroscopy after dissolution in an appropriate solvent.

4.1.2 Copper catalysed reduction of aromatic nitrocompounds. Glycerol: an optimal hydrogen source

4.1.2.1 Materials and methods

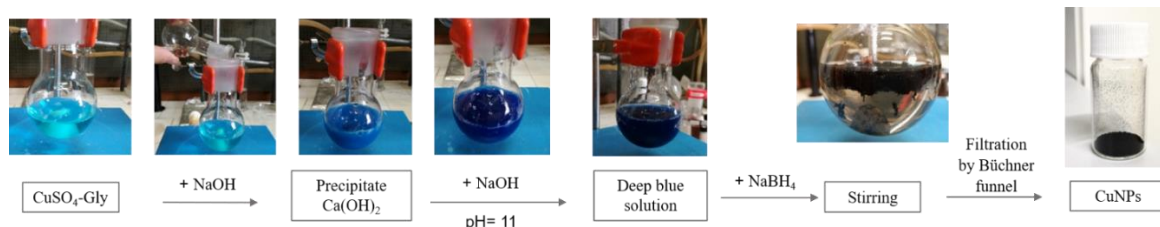
All commercially available reagents and solvents were used without further purification. Reactions were monitored by TLC on Merck 60 F254 (0.25 mm) plates (Milan, Italy), which were visualized by UV inspection and/or by heating after a spraying with 0.5% ninhydrin in ethanol. Reactions were carried out in conventional oil bath by magnetic stirring, under US irradiation (Hielscher *Ultrasonic horn UP50H*) and under different MW devices, both monomode (Anton Paar Monowave 300, CEM Discover SP) and multimode (CEM Mars 5 and Milestone MicroSynth). For MW-assisted reaction scale up a 1.2kW Multimode MW was used located in the MEAM Test and Training Center, based in Herk-de-Stad in Belgium. NMR spectra (300 MHz and 75 MHz for ^1H and ^{13}C , respectively) were recorded. Chemical shifts were calibrated to the residual proton and carbon resonances of the solvent, CDCl_3 ($\delta\text{H} = 7.26$, $\delta\text{C} = 77.16$). Chemical shifts (δ) are given in ppm, and coupling constants (J) in Hz. GC-MS analyses were performed in a GC Agilent 6890 (Agilent Technologies, Santa Clara, CA, USA) that was fitted with a mass detector Agilent Network 5973, using a 30 m capillary column, i.d. of 0.25 mm and film thickness 0.25 μm . GC conditions were: injection split 1:10, injector temperature 250 $^\circ\text{C}$, detector temperature 280 $^\circ\text{C}$. Gas carrier: helium (1.2 mL/min), temperature program: from 50 $^\circ\text{C}$ (5 min) to 100 $^\circ\text{C}$ (1 min) at 10 $^\circ\text{C}/\text{min}$, to 230 $^\circ\text{C}$ (1 min) at 20 $^\circ\text{C}/\text{min}$, to 300 $^\circ\text{C}$ (5 min) at 20 $^\circ\text{C}/\text{min}$. HRMS was determined using a MALDI-TOF mass spectra (Bruker Ultraflex TOF mass spectrometer, Milan, Italy).

4.1.2.2 General procedures

4.1.2.2.1 General Procedure for synthesis of copper nanoparticles

A Copper (II) sulfate solution (1.5 mL of a 0.01 M solution in water/glycerol 5:1) was stirred and was followed dropwise by addition of 2 M NaOH aqueous solution to adjust the solution pH up to 11. After stirring for 10 min, 0.5 M NaBH_4 in water was added into the flask. Firstly, the deep blue solution gradually became colourless, and then it turned burgundy, which shows the formation of copper colloid. The copper nanoparticles were filtered on a Büchner funnel with a sintered glass disc using water and methanol to wash the catalyst.

Copper nanoparticles were characterized by transmission electron microscopy (TEM) and high resolution TEM (HR-TEM). The measurements were carried out with a JEOL 3010-UHR instrument operating at 300 kV and equipped with a LaB₆ filament. Digital micrographs were acquired by a Gatan (2k x 2k)-pixel Ultrascan1000 CCD camera and processed by Gatan digital micrograph. To obtain a good dispersion of the sample and to avoid any modification induced by the use of a solvent, the powders were briefly contacted with the Cu grids coated with lacey carbon, resulting in the adhesion of some particles to the grid by electrostatic interactions.



4.1.2.2.2 Catalyst dispersion

When previous catalyst dispersion was required, the required quantity of CuNPs was weighted, added to a rounded-bottom flask with the needed amount of glycerol and sonicated for 10 min (*Hielscher Ultrasonic horn UP50H, frequency 30 kHz, power 50 W*). A perfectly dispersed black solution was then observed (Figure 61).

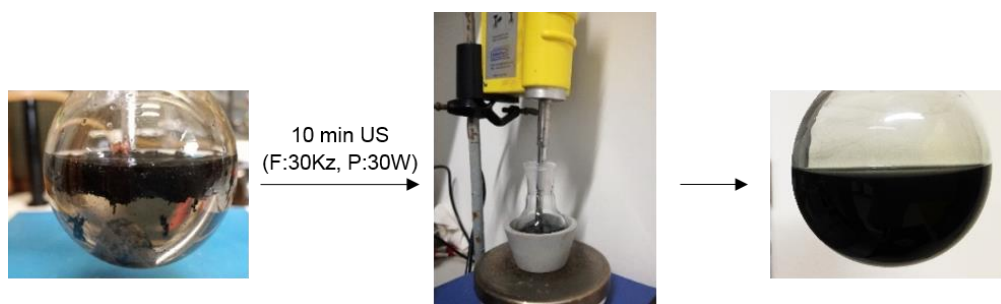


Figure 61: High catalyst dispersion promoted by US irradiation. Conditions: $t:10\text{min}$, $F:30\text{KHz}$, $P:30\text{W}$.

4.1.2.2.3 Particles size distribution

Freshly prepared CuNPs were sonicated for 10 min (UP50H, F(kHz):30, P(W):50) till a perfectly dispersed black solution was observed. Particle size distribution offline measurements (based on volume) were performed and compared with freshly prepared NPs (Figure 9, Curves red and blue). Particle size distribution was also measured on CuNPs after a MW promoted reaction of reduction of nitrobenzene in glycerol (Anton Paar Monowave 300) and we could observe that a similar profile of size distribution was detected if compared to freshly prepared NPs (Figure 9, Curve green). A Laser diffractometer (Malvern, MasterSizer 3000 hydro SV) was employed and the particles size was determined by measuring the intensity of light scattered as a laser beam passes through a dispersed particulate sample. 0.5 mL of the sample ($C_{\text{NP}}=1\text{g/L}$) was injected in 6.5 mL of deionized water in the measurement cell (so that the resulting concentration in the cell was 0.07 g/L) and mixed for 5 min using a built-in magnetic stirrer. The obtained scattering curves were averages of three subsequent measurements.

4.1.2.2.4 Optimised procedures for nitrobenzene reduction to aniline:

- Under conventional heating: CuNPs (3 mg, 5 mol%) in a rounded-bottom flask with 3 mL of glycerol were sonicated for 10 min (Hielscher *Ultrasonic horn UP50H*, $F(\text{kHz}):30$, $P(W):50$). A perfectly dispersed black solution was observed. The KOH (112 mg, 2 mmol) and the nitrobenzene (123 mg, 1 mmol) were then added and the reaction was heated at 130 °C under magnetic stirring for 2 h. The reaction mixture was cooled down to room temperature and filtered to remove CuNPs. 10 mL of water was added and extracted with ethyl acetate (2x10 mL). To the organic phase, aqueous HCl (0.01M) was added and after extraction the aqueous phase was basified with NaOH (0.01 M), extracted with ethyl acetate (3x20 mL) and dried (Na_2SO_4). Product was analyzed using ^1H NMR and ^{13}C NMR spectroscopy. Isolated yield 97%.

4.1.3 MW-assisted copper-catalysed transfer hydrogenation reduction of nitrobenzene. Industrial MW-assisted scale-up.

4.1.3.1 Materials and methods

All commercially available reagents and solvents were used without further purification. Reactions were monitored by TLC on Merck 60 F254 (0.25 mm) plates (Milan, Italy), which were visualized by UV inspection and/or by heating after a spraying with 0.5% ninhydrin in ethanol. Reactions were carried out in conventional oil bath by magnetic stirring, under US irradiation (Hielscher *Ultrasonic horn UP50*) and under different MW devices, both monomode (Anton Paar Monowave 300, CEM Discover SP) and multimode (CEM Mars 5 and Milestone MicroSynth). For MW-assisted reaction scale up a 1.2kW Multimode MW was used located in the MEAM Test and Training Center, based in Herk-de-Stad in Belgium (Figure 6). NMR spectra (300 MHz and 75 MHz for ^1H and ^{13}C , respectively) were recorded. Chemical shifts were calibrated to the residual proton and carbon resonances of the solvent, CDCl_3 ($\delta\text{H} = 7.26$, $\delta\text{C} = 77.16$). Chemical shifts (δ) are given in ppm, and coupling constants (J) in Hz. GC-MS analyses were performed in a GC Agilent 6890 (Agilent Technologies, Santa Clara, CA, USA) that was fitted with a mass detector Agilent Network 5973, using a 30 m capillary column, i.d. of 0.25 mm and film thickness 0.25 μm . GC conditions were: injection split 1:10, injector temperature 250 °C, detector temperature 280 °C. Gas carrier: helium (1.2 mL/min), temperature program: from 50 °C (5 min) to 100 °C (1 min) at 10 °C/min, to 230 °C (1 min) at 20 °C/min, to 300 °C (5 min) at 20 °C/min. HRMS was determined using a MALDI-TOF mass spectra (Bruker Ultraflex TOF mass spectrometer, Milan, Italy)

4.1.3.2 General procedures

4.1.3.2.1 General procedure for MW-assisted batch reactor.

- Microwave-assisted reaction: When previous catalyst dispersion was required, CuNPs (15 mg, 5 mol%) were weighted, added to a rounded-bottom flask with 15 mL of glycerol and sonicated for 10 min (Hielscher *Ultrasonic horn UP50H*, $F(\text{kHz}):30$, $P(W):50$). A perfectly dispersed black solution was observed. The KOH (560 mg, 10 mmol) and the nitrobenzene (625 mg, 5 mmol) were then added and the reaction was carried out. Homogeneous MW distribution was ensured by inserting a magnetic stirrer. Different MW devices were employed: both monomode systems (Anton Paar Monowave 300 and CEM Discover SP) and multimode systems (CEM Mars 5 and Milestone MicroSynth). Two different methods were used for applying MW irradiation: a) fixed temperature and b) fixed power.

- Monomode systems (Anton Paar Monowave 300, CEM Discover SP): 2 min were required to achieve the reaction temperature (130 °C) using the program “Heat as fast as possible” (Maximum power 400 W). When performing the reaction at fixed temperature, the program “hold” was selected in order to main the temperature constant (130 °C) during the reaction time. In this mode the MW-reactor automatically adjusts the power to reach the indicated temperature. Reaction time: 30 min. When performing the reaction at fixed power, the program “constant power” was selected (4 W). In this way, a constant set power maintains the reaction mixture at the desired temperature (130 °C). Reaction time: 15 min.
- Multimode systems (CEM Mars 5 and Milestone MicroSynth): 2 min were required to achieve the reaction temperature (130 °C) (Maximum power 400 W) (CEM Mars 5: Power 100%). When performing the reaction at fixed temperature, the power was left at 400 W and 130 °C were selected as constant temperature, so the MW-reactor could automatically adjusts the power. Reaction time: 30 min. When performing the reaction at fixed power, the reaction mixture was irradiated with constant power (80 W) for the whole reaction time. Reaction time: 15 min.

The reaction mixture was cooled down to room temperature and filtered to remove CuNPs. 30 mL of water were added and extracted with ethyl acetate (2x30 mL). To the organic phase, aqueous HCl (30 mL, 0.01M) was added and after extraction the aqueous phase was basified with NaOH (0.01 M), extracted with ethyl acetate (3x60 mL) and dried (Na₂SO₄). Product was analyzed using ¹H NMR and ¹³C NMR spectroscopy. Isolated yield 98%. When using the Anton Paar Monowave 300 reactor, the reaction temperature is controlled simultaneously by a ruby thermometer (a fiber optic sensor immersed into the reaction mixture that accurately delivers the internal temperature during the whole reaction process) and the IR sensor that provides an external temperature measurement of reaction vials. When employing the CEM Discover SP, the temperature measurements were determinate by an IR sensor and when using both multimode systems (CEM Mars 5 and MicroSynth) fiber optics where installed.

4.1.3.2.2 General methods for MW-assisted batch reactor. Industrial MW system.

Scale up experiments were performed with the MW multimode instrument MEAM Explorer VP (1.2 kW). Emissivity (0.95) and transmissivity (0.48) of the reaction solvent (glycerol) were firstly determined in order to ensure an optimal calibration of the IR camera and so, to ensure the measured reaction temperature. These values remain constant when measured with the reaction mixture. The IR camera was always set in the same position. CuNPs (18 mg, 5 mol%), in a rounded-bottom flask with glycerol (90 mL) were sonicated for 10 min (Hielscher *Ultrasonic horn UP50H, F(kHz):30, P(W):50*). A perfectly dispersed black solution was observed. The KOH (672 mg, 12 mmol) and the nitrobenzene (748 mg, 6 mmol) were then added and the reaction was carried out. When the reaction was scaled-up to 18 and 36 mmol of nitrobenzene, the pertinent reagents quantities were added: glycerol (200 eq), KOH (2 eq) and CuNPs (5 mol%). Homogeneous MW distribution was ensured by inserting a stir bar. When performing the reaction at fixed temperature, 2 min ($P_{\max}=100\%$) were required to achieve the reaction temperature (130 °C). In this mode the MW-reactor automatically adjusts the power (40 W – 0 W) to maintain constant the desired temperature (130 °C) during the whole reaction time. When performing the reaction at fixed power, 25-30 W was maintained. In this way, a constant set power maintains the reaction mixture at the desired temperature (130

°C). Reaction time: 45 min (6mmol Nitrobenzene), 60 min (18 mmol and 36 mmol). Reaction workup was performed as described in the previous MW promoted procedure.

4.1.4 A simple set up for transfer hydrogenation in flow chemistry. Reduction of nitrobenzene over copper supported catalyst (Cu/Celite).

4.1.4.1 Materials and methods

All commercially available reagents and solvents were used without further purification. The used Ethylen glycol contained no less than 99 wt.% of the main substance. Reactions were monitored by TLC on Merck 60 F254 (0.25 mm) plates (Milan, Italy), which were visualized by UV inspection and/or by heating after a spraying with 0,5% ninhydrin in ethanol. NMR spectra (300 or 600 MHz and 75 or 125 MHz for ^1H and ^{13}C , respectively) were recorded. Chemical shifts were calibrated to the residual proton and carbon resonances of the solvent, CDCl_3 ($\delta\text{H} = 7.26$, $\delta\text{C} = 77.16$). Chemical shifts (δ) are given in ppm, and coupling constants (J) in Hz. GC conditions were: injection split 1:10, injector temperature 250 °C, detector temperature 280 °C. Gas carrier: helium (1.2 mL/min), temperature program: from 50 °C (5 min) to 100 °C (1 min) at 10 °C/min, to 230 °C (1 min) at 20 °C/min, to 300 °C (5 min) at 20 °C/min. HRMS was determined using a MALDI-TOF mass spectra (Bruker Ultraflex TOF mass spectrometer, Milan, Italy).

4.1.4.2 General procedures

4.1.4.2.1 Set-up for the packed bed reactor unit

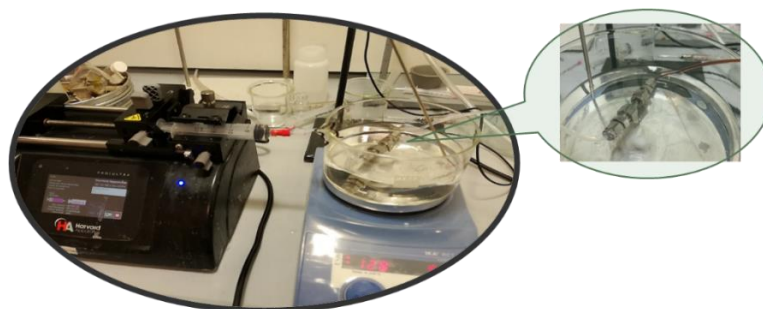


Figure 62: Schematic representation of the packed bed reactor (PBR)

The experimental setup consisted of a syringe pump (PHD ULTRA, Harvard Apparatus), a packed bed reactor (PBR) (Stainless steel tube with O.D. $\frac{1}{4}$ inch and I.D of 3.8 mm), a heating mantle and an oil bath (see Figure 62). All units were connected using PTFE tubing (o.d. $\frac{1}{8}$ in., i.d. $\frac{1}{16}$ inch) and standard HPLC fittings (all with an i.d. of 0.70, mm, $\frac{1}{8}$ inch tubing). Two frits were placed at both sides of the packed bed reactor unit (pore size $10\ \mu\text{m}$, and diameter 0.189"). The PBR was heated by immersing the reactor inside the oil bath (130°C).

4.1.4.2.2 Packed bed reactor unit

The packed bed reactor has a length of 2.6 cm and a i.d. of 0.38 cm. The total volume of the reactor was determined:



$$V_t: (\pi \cdot r^2) \cdot l = [3.14 \cdot (0.19 \text{ cm})^2 \cdot 2.6 \text{ cm}] = 0,295 \text{ cm}^3$$

Once the packed bed reactor was filled with the catalyst, the internal volume was determined by weighing the freshly PBR (Mass 1) and then pumping a solvent (ethanol) through the reactor to fill the void with it. The packed bed reactor was then weighed again (Mass 2). The reactor volume was determined by $R_v = (\text{Mass 2} - \text{Mass 1}) / \text{solvent density}$.

$$R_v = (\text{Mass 2} - \text{Mass 1}) / \text{ethanol density} = 0,0311 \text{ cm}^3$$

4.1.4.2.3 Set up volume

In order to determine the total volume, the whole system was emptied out and following completely refilled with ethanol, resulting 7,5 mL.

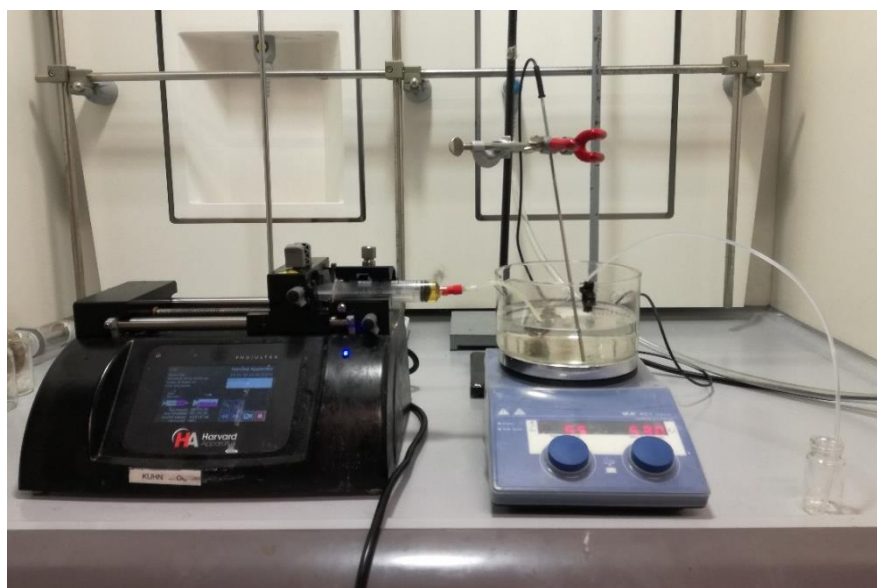


Figure 63: Entire set up

4.1.4.2.4 General procedure for the catalyst synthesis (CuNPs/Celite)

A Copper (II) sulfate solution (18 mL of a 0.25 mM solution in water:glycerol (5:1)) was stirred and was followed dropwise by addition of 2 M NaOH aqueous solution to adjust the solution pH up to 11. The supported material (Celite® 545, 500 mg) was then added. After stirring for 10 min, 0.5 M NaBH₄ in water was added into the flask while sonicating in the ultrasonic bath in order to have well dispersed particles. The deep blue solution gradually became colourless, and then it turned burgundy, which shows the formation of copper colloid. The copper nanoparticles supported on celite (CuNPs/Celite) were filtered on a Büchner funnel with a sintered glass disc using water and methanol to wash the catalyst.

4.1.4.2.5 General procedure for the continuous flow reaction

Experimental studies were performed in the laboratory-scale set-up described earlier (Figure 62, Figure 63), using a packed bed reactor (PBR) loaded with 150 g of celite supported CuNPs. Nitrobenzene (1 mmol) and KOH (2 mmol) were dissolved in 2 mL of ethylen glycol. The reaction mixture was pumped into the micro-reactor at the indicated flow rate (mL/min) at room temperature and when arriving to the heating device the solution was warmed up to 130 °C, and so the reduction reaction started to take place. The contact time (τ) was determined as the ratio between the catalyst volume in the reactor V_r (cm³) and the total inlet rate of the mixture (cm³/s). Reaction products were cooled at the reactor outlet, collected and

then analyzed after three reactor volumes. The mixture was extracted twice with water and CH_2Cl_2 . After that, the organic part was again extracted with acid water (HCl 0.01M) and then, the aqueous phase was basified with NaOH, extracted with CH_2Cl_2 and finally dried (Na_2SO_4). Products were analyzed using ^1H NMR and ^{13}C NMR spectroscopy and GC-MS chromatography.

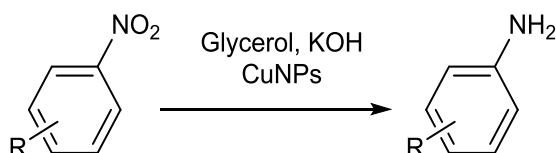
4.1.4 Cu-catalysed TH of nitroarenes to amino or azo derivative via controllable transfer hydrogenation sources.

4.1.4.1 Material and methods

All chemicals were purchased from Sigma-Aldrich (Milan, Italy) and used without further purification. Reactions were monitored by TLC on Merck 60 F254 (0.25 mm) plates (Milan, Italy), which were visualized by UV inspection and/or by heating after a spraying with 0,5% ninhydrin in ethanol or phosphomolybdic acid. Reactions were carried out in conventional oil bath and in a combined system MW/US. This device has been design in our laboratory by inserting a sonic horn made of pirex inside a RotoShynth (Milestone) microwave chamber (Figure 1). NMR spectra (300 or 600 MHz and 75 or 125 MHz for ^1H and ^{13}C , respectively) were recorded. Chemical shifts were calibrated to the residual proton and carbon resonances of the solvent; DMSO- d_6 ($\delta\text{H} = 2.54$, $\delta\text{C} = 39.5$), CDCl_3 ($\delta\text{H} = 7.26$, $\delta\text{C} = 77.16$), D_2O ($\delta\text{H} = 4.79$). Chemical shifts (δ) are given in ppm, and coupling constants (J) in Hz. GC-MS analyses were performed in a GC Agilent 6890 (Agilent Technologies, Santa Clara, CA, USA) that was fitted with a mass detector Agilent Network 5973, using a 30 m capillary column, i.d. of 0.25 mm and film thickness 0.25 μm . GC conditions were: injection split 1:20, injector temperature 250 $^\circ\text{C}$, detector temperature 280 $^\circ\text{C}$. Gas carrier: helium (1.2 mL/min), temperature program: from 70 $^\circ\text{C}$ (2 min) to 300 $^\circ\text{C}$ at 5 $^\circ\text{C}/\text{min}$.

4.1.4.2 General procedures

4.1.4.2.1 Optimised procedures for nitro-derivatives reduction to amino-derivatives:



- Conventional conditions: Nitrobenzene (3 mmol), KOH (6 mmol) and nano-copper catalyst (5mol%) were dissolved in 20 mL of glycerol. The reaction was carried out under magnetic stirring in an oil bath at 130 $^\circ\text{C}$ for 1 hour. The crude product was analyzed by GC-MS. Then the mixture was extracted twice with water and CH_2Cl_2 . After that, the organic part was again extracted with acid water (HCl 0.01M). Then, the aqueous phase was basified with NaOH, extracted with CH_2Cl_2 and finally dried (Na_2SO_4). Products were analysed using ^1H NMR and ^{13}C NMR spectroscopy, MS and GC-MS chromatography.

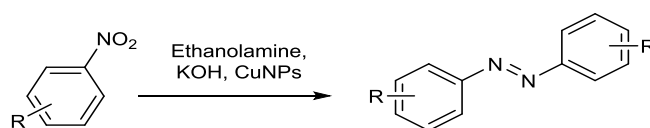
- Synthesis under microwave irradiation: Nitrobenzene (3 mmol), KOH (6 mmol) and nano-copper catalyst (5mol%) were dissolved in 20 mL of glycerol. The reaction was carried out under MW irradiation at 150 $^\circ\text{C}$ for 15 min. The reaction mixture was then cooled down to room temperature. The crude product was analyzed by GC-MS. Then the mixture was extracted twice with water and CH_2Cl_2 . After that, the organic part was again extracted with acid water (HCl 0.01M). Then, the aqueous phase was basified with NaOH, extracted with CH_2Cl_2

and finally dried (Na_2SO_4). Products were analysed using ^1H NMR and ^{13}C NMR spectroscopy, MS and GC-MS chromatography.

- Synthesis under ultrasound irradiation: Nitrobenzene (3 mmol), KOH (6 mmol) and nano-copper catalyst (5mol%) were dissolved in 20 mL of glycerol. The reaction mixture was sonicated by using a Pyrex horn (20.3 kHz, 30 W) for 45 min. The reaction mixture was then cooled down to room temperature. The crude product was analyzed by GC-MS. Then the mixture was extracted twice with water and CH_2Cl_2 . After that, the organic part was again extracted with acid water (HCl 0.01M). Then, the aqueous fase was basified with NaOH, extracted with CH_2Cl_2 and finally dried (Na_2SO_4). Products were analysed using ^1H NMR and ^{13}C NMR spectroscopy, MS and GC-MS chromatography.

-Synthesis under microwave and ultrasound combined irradiation: Combined US (20.3 kHz, 30 Wcm^{-2}) and MW (2.45 GHz, 80 W) irradiation was carried out in an oven (Microsynth-Milestone) equipped with a Pyrex horn inserted. The reaction mixture with nitrobenzene (3 mmol), KOH (6 mmol), nano-copper catalyst (2,5mol%) and 20 mL of glycerol was irradiated with combined MW/US for 10 min. The crude was then cooled down to room temperature. The crude product was analyzed by GC-MS. Then the mixture was extracted twice with water and CH_2Cl_2 . After that, the organic part was again extracted with acid water (HCl 0.01M). Then, the aqueous fase was basified with NaOH, extracted with CH_2Cl_2 and finally dried (Na_2SO_4). Products were analysed using ^1H NMR and ^{13}C NMR spectroscopy, MS and GC-MS chromatography.

4.1.4.2.2 Optimised procedures for nitro-derivatives reduction to azo-derivatives:



-Conventional conditions: Nitrobenzene (3 mmol), KOH (6 mmol) and nano-copper catalyst (5 mol%) were dissolved in 20 mL of ethanolamine. The reaction was carried out under magnetic stirring in an oil bath at 50-60 °C over night (20-25 hours). The mixture was extracted three times with water and CH_2Cl_2 and finally dried (Na_2SO_4). The crude product was analyzed by GC-MS and purified by chromatography on silica gel to afford the desired product. Products were analysed using ^1H NMR and ^{13}C NMR spectroscopy, MS and GC-MS chromatography.

-Synthesis under microwave irradiation: Nitrobenzene (3 mmol), KOH (6 mmol) and nano-copper catalyst (5 mol%) were dissolved in 20 mL of ethanolamine. The reaction was carried out under MW irradiation at 50-60 °C for 6 hours and a half, always with a constant power of 15 W. The reaction mixture was then cooled down to room temperature. The mixture was extracted three times with water and CH_2Cl_2 and finally dried (Na_2SO_4). The crude product was analyzed by GC-MS and purified by chromatography on silica gel to afford the desired product. Products were analysed using ^1H NMR and ^{13}C NMR spectroscopy, MS and GC-MS chromatography.

-Synthesis under ultrasound irradiation: Nitrobenzene (3 mmol), KOH (6 mmol) and nano-copper catalyst (5 mol%) were dissolved in 20 mL of ethanolamine. The reaction mixture was sonicated by using a Pyrex horn (20.3 kHz, 20 W cm^{-2}) for 3 h. The reaction mixture was then cooled down to room temperature. The mixture was extracted three times with water and CH_2Cl_2 and finally dried (Na_2SO_4). The crude product was analyzed by GC-MS and purified by

chromatography on silica gel to afford the desired product. Products were analysed using ^1H NMR and ^{13}C NMR spectroscopy, MS and GC-MS chromatography.

Synthesis under microwave and ultrasound combined irradiation: Combined US (20.3 kHz, 15 Wcm^{-2}) and MW (2.45 GHz, 15 W) irradiation was carried out in an oven (Microsynth-Milestone) equipped with a Pyrex horn inserted. The reaction mixture with nitrobenzene (3 mmol), KOH (6 mmol), nano-copper catalyst (5 mol%) and 20 mL of ethanolamine was irradiated with combined MW/US for 1 h. The crude was then cooled down to room temperature. The mixture was extracted three times with water and CH_2Cl_2 and finally dried (Na_2SO_4). The crude product was analyzed by GC-MS and purified by chromatography on silica gel to afford the desired product. Products were analysed using ^1H NMR and ^{13}C NMR spectroscopy, MS and GC-MS chromatography.

4.1.5 Copper catalysed selective semihydrogenation of alkynes to cis alkenes

4.1.5.1 Material and methods

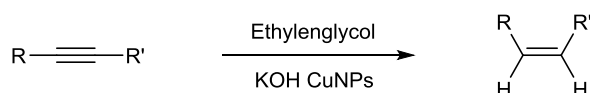
All chemicals were purchased from Sigma-Aldrich (Milan, Italy) and used without further purification. Reactions were monitored by TLC on Merck 60 F254 (0.25 mm) plates (Milan, Italy), which were visualized by UV inspection and/or by heating after a spraying with 0,5% ninhydrin in ethanol or phosphomolybdic acid. Reactions were carried out in conventional oil bath and in a combined system MW/US. This device has been design in our laboratory by inserting a sonic horn made of pirex inside a RotoShynth (Milestone) microwave chamber (Figure 1). NMR spectra (300 or 600 MHz and 75 or 125 MHz for ^1H and ^{13}C , respectively) were recorded. Chemical shifts were calibrated to the residual proton and carbon resonances of the solvent; DMSO- d_6 ($\delta\text{H} = 2.54$, $\delta\text{C} = 39.5$), CDCl_3 ($\delta\text{H} = 7.26$, $\delta\text{C} = 77.16$), D_2O ($\delta\text{H} = 4.79$). Chemical shifts (δ) are given in ppm, and coupling constants (J) in Hz. GC-MS analyses were performed in a GC Agilent 6890 (Agilent Technologies, Santa Clara, CA, USA) that was fitted with a mass detector Agilent Network 5973, using a 30 m capillary column, i.d. of 0.25 mm and film thickness 0.25 μm . GC conditions were: injection split 1:20, injector temperature 250 $^\circ\text{C}$, detector temperature 280 $^\circ\text{C}$. Gas carrier: helium (1.2 mL/min), temperature program: from 70 $^\circ\text{C}$ (2 min) to 300 $^\circ\text{C}$ at 5 $^\circ\text{C}/\text{min}$.

4.1.5.2 General procedures

4.1.5.2.1 Optimised procedure for alkynes synthesis

Conventional conditions: Aryl halide (1 mmol) and phenylacetylene (1,2 mmol) were added to a flask containing 0.02 mol % $\text{Pd}(\text{PPh}_3)_2\text{Cl}_2$ and 0.05 mol % CuI , in 10 mL of THF anhydrous. The mixture was stirred at room temperature overnight under nitrogen atmosphere. After completion of the reaction (monitored by GC), water was added to the reaction mixture and crude product extracted with dichlorometane. For further purification, the organic solvent was removed under vacuum and the resulting residue was purified by column chromatography on silica gel using petroleum ether and ethyl acetate as eluents. The pure product was analyzed by ^1H , ^{13}C NMR spectroscopy

4.1.5.2.2 Optimised procedure for alkynes semihydrogenation to Z-alkenes



Conventional conditions: Phenylacetylene (1 mmol), KOH (2 mmol) and copper nanoparticles catalyst (10 mol%) were dissolved in 20 mL of ethylene glycol. The reaction was carried out under magnetic stirring in an oil bath at 150 °C for 2 hour. The crude product was filtered on Büchner funnel with a sintered glass disc using CH₂Cl₂ and water to wash the catalyst. After concentration under vacuum to half volume, the mixture was extracted with water and CH₂Cl₂, washed with H₂O three times and finally dried (Na₂SO₄). The crude product was analyzed by GC-MS and purified by chromatography on silica gel. Products were analysed using ¹H NMR and ¹³C NMR spectroscopy, MS and GC-MS chromatography.

Synthesis under microwave irradiation: Phenylacetylene (1 mmol), KOH (2 mmol) and copper nanoparticles catalyst (10 mol%) were dissolved in 15 mL of ethylene glycol. The reaction was carried out under MW irradiation at 150 °C for 90 min, always with a constant power of 120W. The reaction mixture was then cooled down to room temperature. The crude product was extracted with water and CH₂Cl₂, washed with H₂O three times and finally dried (Na₂SO₄). The crude product was analyzed by GC-MS and purified by chromatography on silica gel. Products were analysed using ¹H NMR and ¹³C NMR spectroscopy, MS and GC-MS chromatography.

Synthesis under ultrasound irradiation: Phenylacetylene (1 mmol), KOH (2 mmol) and copper nanoparticles catalyst (10 mol%) were dissolved in 15 mL of ethylene glycol. The reaction mixture was sonicated by using a Pyrex horn (20.3 kHz, 40 W) for 60 min. Then, the reaction mixture was cooled down to room temperature. The crude product was extracted with water and CH₂Cl₂, washed with H₂O three times and finally dried (Na₂SO₄). The crude product was analyzed by GC-MS and purified by chromatography on silica gel. Products were analysed using ¹H NMR and ¹³C NMR spectroscopy, MS and GC-MS chromatography.

Synthesis under microwave and ultrasound combined irradiation: Combined US (20.3 kHz, 30 Wcm⁻²) and MW (2.45 GHz, 90 W) irradiation was carried out in an oven (Microsynth-Milestone) equipped with a Pyrex horn inserted. The reaction mixture with Phenylacetylene (1 mmol), KOH (2 mmol), copper nanoparticles catalyst (10 mol%) and 15 mL of ethylene glycol was irradiated with combined MW/US for 30 min. The crude was then cooled down to room temperature. The product was extracted using CH₂Cl₂, washed with H₂O three times and finally dried (Na₂SO₄). The crude product was analyzed by GC-MS and purified by chromatography on silica gel. Products were analysed using ¹H NMR and ¹³C NMR spectroscopy, MS and GC-MS chromatography.

4.2 Sonochemically-promoted preparation of Cu-β-CD grafted silica

4.2.1 Material and methods

All commercially available reagents and solvents were purchased from Sigma-Aldrich (Milan, Italy) and used without further purification. SIPERNAT 320 amorphous silica was supplied by Evonik Degussa. The synthesis of 6^l-amino-6^l-deoxy-β-CD and 6^l-O-*p*-Toluenesulfonyl-β-CD was performed following published synthetic procedure.⁴²⁶ β-CD was provided by Wacker Chemie (München, Germany). US irradiation at 40-80-120 kHz was performed in a ultrasound bath supplied by Weber ULTRASONICS GMBH. When reactions were carried out in a combined system MW/US the device has been designed in our laboratory by inserting a sonic horn made of pirex inside a RotoShynth (Milestone) microwave chamber.

Thermogravimetric analyses were performed using a thermogravimetric analyzer TGA 4000 (PerkinElmer) at $10\text{ }^{\circ}\text{C min}^{-1}$ operating with alumina crucibles that contained 10–20 mg of sample. The analyses were performed under an argon atmosphere at a starting temperature of $50\text{ }^{\circ}\text{C}$ and an end temperature of $800\text{ }^{\circ}\text{C}$. Total mass loss was attributed to the functional groups that were covalently attached to the sidewalls. UV–vis absorption spectra were measured on a dual-beam spectrophotometer (Agilent Technologies Cary 60, G6860AA) equipped with a 1 cm path length quartz cuvette. Elemental analyses were performed on an EA 1108 (Fison Instruments). Reactions were carried out in professional MW reactor (Monowave 400/200, Anton Paar GmbH) using reaction vial G10. Reactions were monitored by TLC on Merck 60 F254 (0.25 mm) plates (Milan, Italy), which were visualized by UV inspection. GC-MS analyses were performed in a GC Agilent 6890 (Agilent Technologies, Santa Clara, CA, USA) that was fitted with a mass detector Agilent Network 5973, using a 30 m capillary column, i.d. of 0.25 mm and film thickness 0.25 μm . GC conditions were: injection split 1:10, injector temperature $250\text{ }^{\circ}\text{C}$, detector temperature $280\text{ }^{\circ}\text{C}$. Gas carrier: helium (1.2 mL/min), temperature program: from $50\text{ }^{\circ}\text{C}$ (5 min) to $100\text{ }^{\circ}\text{C}$ (1 min) at $10\text{ }^{\circ}\text{C/min}$, to $230\text{ }^{\circ}\text{C}$ (1 min) at $20\text{ }^{\circ}\text{C/min}$, to $300\text{ }^{\circ}\text{C}$ (5 min) at $20\text{ }^{\circ}\text{C/min}$. HRMS was determined using a MALDI-TOF mass spectra (Bruker Ultraflex TOF mass spectrometer, Milan, Italy). The cations were determined with a Perkin Elmer Optima 7000 (Perkin Elmer, Norwalk, Connecticut, USA) inductively coupled plasma-optical emission spectrometer (ICP-OES).

4.2.2 General procedures

4.2.2.1 Preparation of chlorinate silica (Si-Cl)

10.5 mL of SOCl_2 were added dropwise to 1 g of silica SIPERNAT 320. The mixture was left stirring under reflux, o.n. The suspension was filtered and the powder was washed with chloroform and dried under vacuum.⁴⁴⁰

4.2.2.1.1 Si-Cl titration.

The amount of chloride present in the sample was determined via argentometric titration. The Mohr method was followed. The sample solution was titrated against a solution of silver nitrate of known concentration. Chloride ions react with silver(I) ions to give insoluble silver chloride (1):



1 g of Si-Cl was dispersed in 100 mL of a NaHCO_3 solution (0,005 M). The solution was stirred for 1 h at room temperature. Potassium chromate was used as an indicator, giving red silver chromate after all the chloride ions have reacted:



398 μL of K_2CrO_4 0.25 M were added and the solution was titrated with AgNO_3 0.1 M (2) to obtain the amount of chlorosilyl groups on silica surface ($\sim 0.9\text{ mmol g}^{-1}$).

4.2.2.2 Preparation of Si-DETA

Diethylenetriamine (0.500 mL) was dissolved in 0.500 mL of solvent (see Table 1, entries 1-3) and Si-Cl was added (0.100 g). The suspension was heated under stirring in an oil bath ($60\text{ }^{\circ}\text{C}$ for 12 h). When the reaction was performed in a US bath (40, 80 or 120 kHz, power 200 W),

the suspension was irradiated for 2-4 h in toluene or in diethylenetriamine (see Table 1, entries 4-15). The modified silica was then filtered, washed with water, methanol and chloroform and dried under vacuum at room temperature for 12 h.

4.2.2.3 Preparation of Si-DETA-CD

6^l-tosyl- β -CD (0.100 g, 0.077 mmol) was dissolved in DMF (1.7 mL) and Si-DETA (0.100 g) was added (Table 1, entries 16). The suspension was heated to 70 °C under magnetic stirring for 24 h. When the reaction was performed under US irradiation, the suspension reacted 4 h (power 200 W, frequency 80 kHz) (Table 1, entries 17). Silica was filtered, washed with water, methanol and chloroform, and dried under vacuum at room temperature for 12 h.

4.2.2.4 Preparation of Si-NHCD

6^l-amino-6^l-deoxy- β -CD (0.163 g, 0.14 mmol) was dissolved in DMF (2 mL) or water and then chlorinate silica (0.100 g) and pyridine (0.332 mL) were added (Table 1, entries 18-23). The suspension was either conventionally stirred at 60 °C for 12 h, or was irradiated in an US bath at 80 kHz for 2-4 h. Modified silica was filtered, washed with water, methanol and chloroform, and dried under vacuum at room temperature for 12 h.

4.2.2.5 Preparation of Si-DiAm

3-(2-Aminoethylamino)propyltrimethoxysilane (0.040 mL) was dissolved in toluene (1 mL) and silica SIPERNAT 320 (0.100 g) was added. The suspension was either heated under stirring in an oil bath (80 °C for 36 h) or the reaction was performed in a US bath (power 200 W, comparing 40 and 80 kHz as frequencies), as depicted in Table 2 (entries 1-5). Silica was filtered, washed with toluene and chloroform, and dried under vacuum at room temperature for 12 h.

4.2.2.6 Preparation of Si-DiAm-CD

6^l-O-*p*-Toluenesulfonyl- β -CD (0.100 g, 0.077 mmol) was dissolved in DMF (1.5 mL) and Si-DiAm (0.100 g) was added. The suspension was either heated to 60 °C and stirred for 60 h, or was irradiated by US (4 h, power 200 W, frequency 80 kHz) (entries 6-9 Table 3). The same procedure was repeated under MW and US combined irradiation: 1 g of Ts-CD was dissolved in 15 mL of DMF and 1 g of Si-DiAm was added. The suspension was heated at 100 °C for 4 h (average MW power 20 W, average US power 35 W). After cooling to room temperature, the modified silica was filtered, washed with water, methanol and chloroform, and dried under vacuum at room temperature for 12 h.

4.2.2.7 Cyclodextrin-supported silica and copper complexation

CD-supported silica (0.100 g) either Si-NH-CD; Si-DETA-CD, Si-diAm-CD were dispersed in 0.675 mL of NaOH 0.5 M. The suspension was stirred for 1 min by US irradiation and 0.719 mL of CuSO₄ 0.08 M were added dropwise. The mixture was irradiated for 10 seconds in an US bath and was then filtered and washed thoroughly with water and methanol, and, finally, dried under vacuum at room temperature for 12 h.

4.2.2.8 Click chemistry reaction

Azide (0,0676 mmol, 1 eq) and terminal alkyne (1 eq) were dissolved in 0,500 μ L of H₂O : tBuOH (1:1). Solid supported catalyst Si-NHCD-Cu or Si-DETA-CD-Cu or Si-diAm-CD-Cu was added as described in Table 2. The reaction was heated up at 85 °C, for 1 h or under MW

irradiation (85°C) for 20 min. The resulting mixture was filtered, washed with methanol and chloroform. The solvent was removed under vacuum to afford the triazole. All products were confirmed by ¹H NMR and GC-MS.

4.2.2.9 Physico-chemical characterization

Infrared spectra were recorded on a BRUKER FTIR-66 spectrophotometer with a resolution of 2 cm⁻¹, using a DTGS detector. Measurements were carried out using a home-made cell allowing in situ thermal treatment and room temperature measurement. Thin self-supporting pellets for transmission measurements (around 10 mg/cm²) were prepared with a hydraulic press. Before the measurements the samples were outgassed at 80 °C for 2 h in the same cell used for the measurements. β-CD and Cu-CD were measured after dilution in KBr, without thermal treatment (spectra not reported).

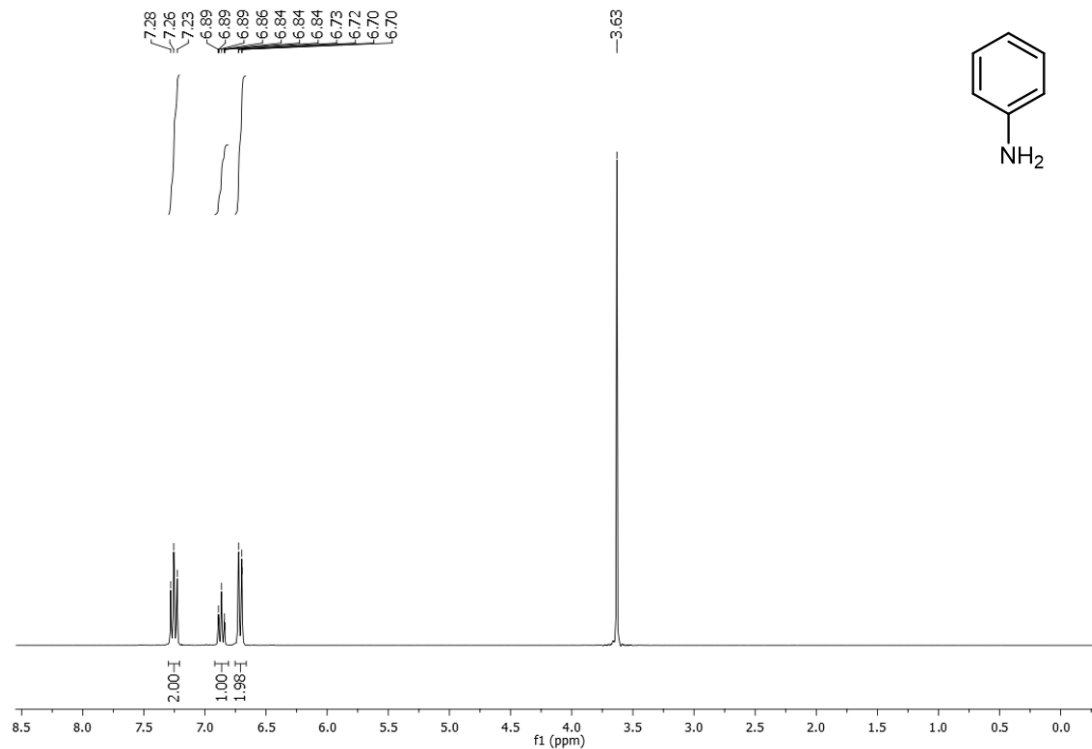
UV-Vis-NIR spectra were recorded in the 2500-200 nm range at 1 nm resolution on Cary 5000 UV-Vis-NIR spectrophotometer (Agilent) equipped with a Diffuse Reflectance attachment with integrating sphere coated by BaSO₄. Prior to each measurement, a baseline spectrum was collected by using Teflon as a reference. Spectra are reported as relative reflectance (R%), defined as:

$$R\% = R_{\text{sample}} / R_{\text{reference}} \cdot 100 \quad (3)$$

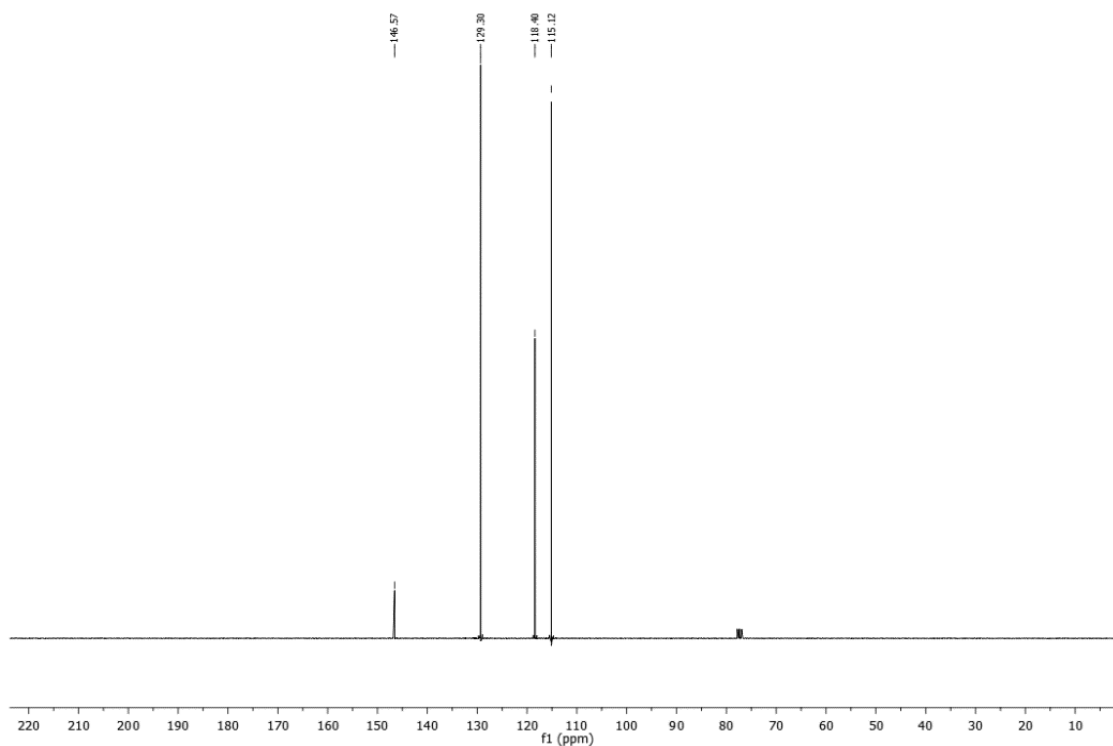
Supporting information

S-1. NMR Amino-derivatives

Aniline (2.2a)⁴⁴⁶: ¹H NMR (300 MHz, CDCl₃) δ 7.26 (2H, t, J = 6 Hz), 6.86 (1H, t, J = 9 Hz), 6.76 (2H, t, J = 6 Hz), 3.63 (2H, s) ppm; ¹³C NMR (75 MHz, CDCl₃) δ 146.57, 129.30, 118.40, 115.12 ppm.

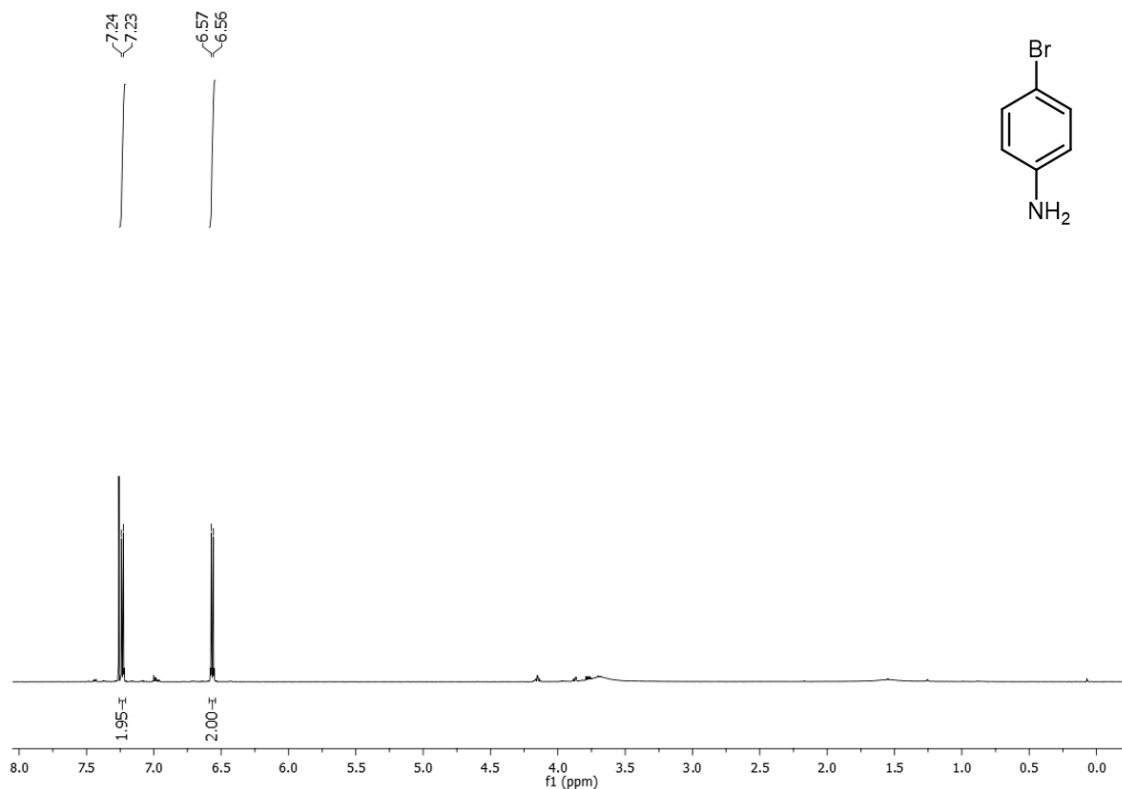


¹H NMR (300 MHz, CDCl₃) of Aniline (Table 9, Entry 1) (Table 11, Entry 1) (Table 23, Entry 1)

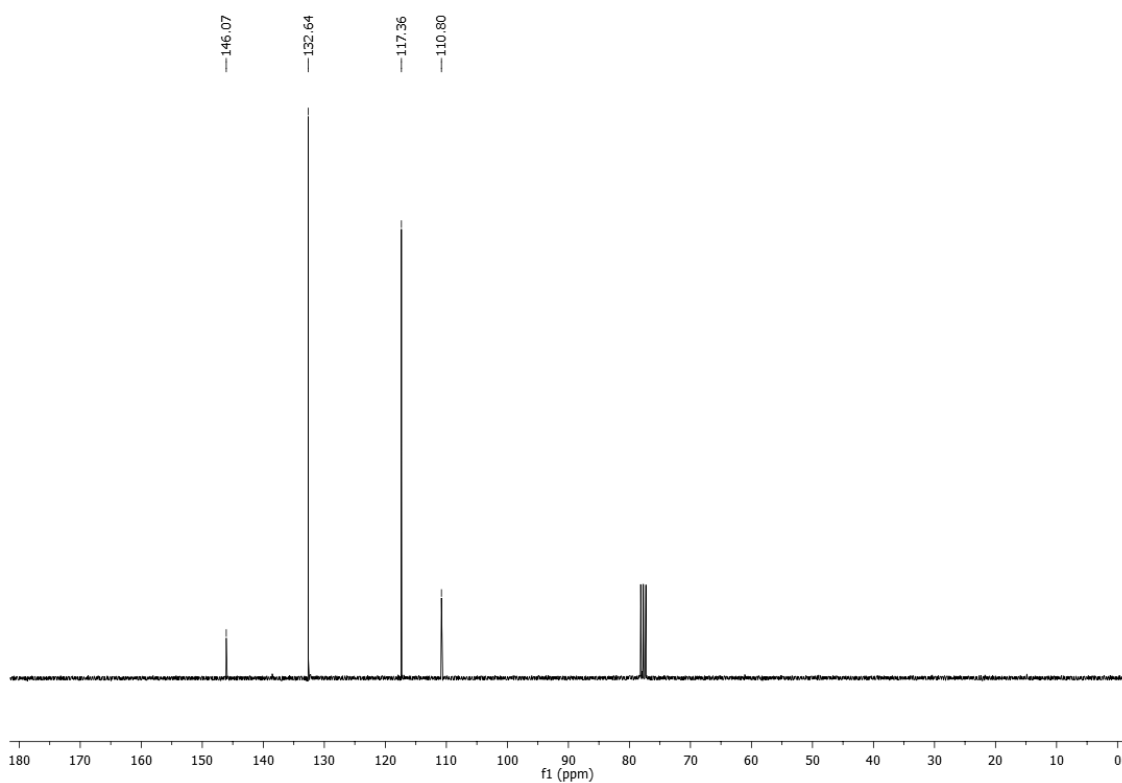


¹³C-NMR (75 MHz, CDCl₃) of Aniline (Table 9, Entry 1) (Table 11, Entry 1) (Table 23, Entry 1)

p-Bromoaniline (2.2b)⁴⁴⁷: ¹H NMR (300 MHz, CDCl₃) δ 7.24 – 7.23 (2H, d, J = 9 Hz), 6.57–6.56 (2H, d, J = 9 Hz) ppm; ¹³C NMR (75 MHz, CDCl₃) δ 145.07, 132.64, 117.36, 110.80 ppm.

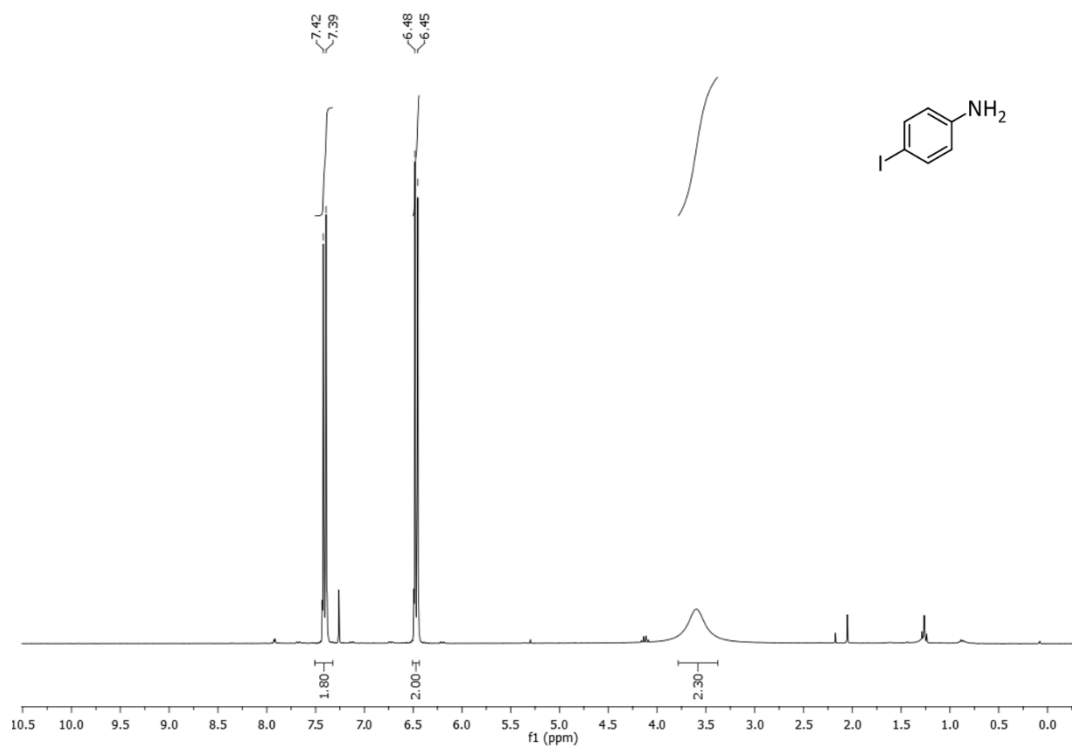


¹H NMR (300 MHz, CDCl₃) of p-Bromoaniline (Table 9, Entry 2) (Table 23, Entry 2)

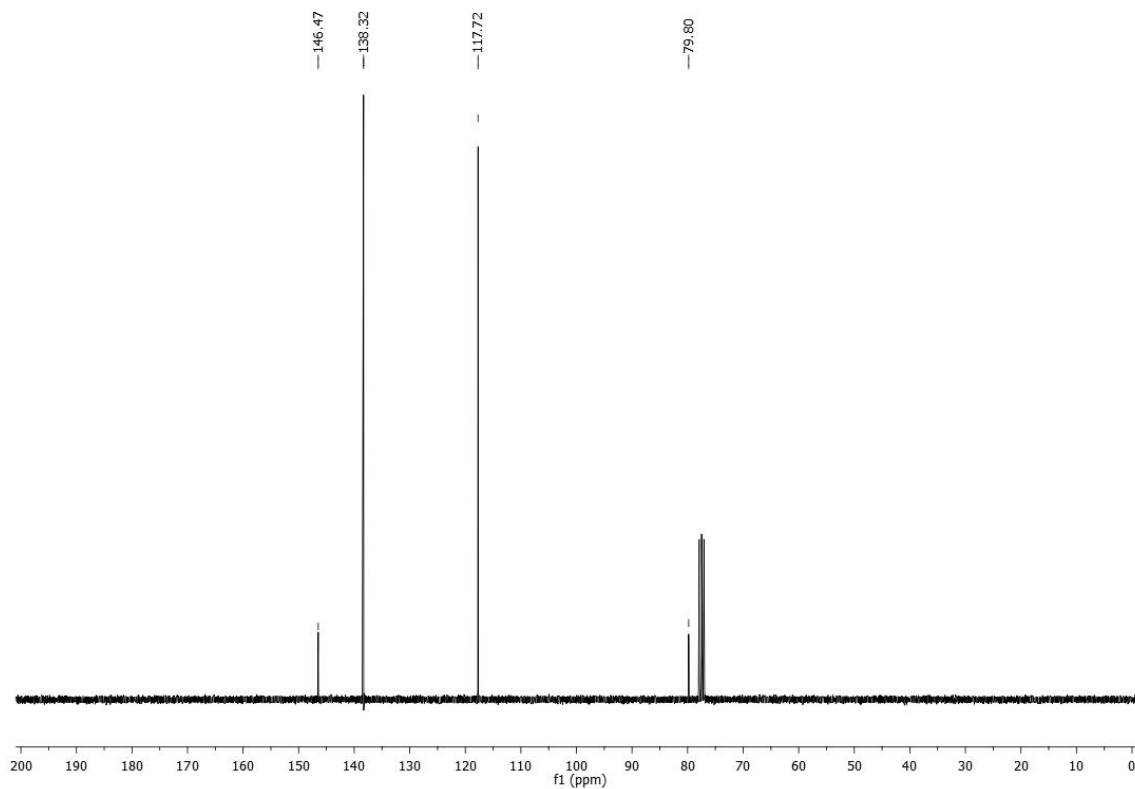


¹³C-NMR (75 MHz, CDCl₃) of p-Bromoaniline (Table 9, Entry 2) (Table 23, Entry 2).

p-Iodoaniline (2.2c)⁴⁴⁸: ¹H NMR (300 MHz, CDCl₃) δ 7.40 (2H, d, J = 9 Hz), 6.47(2H, d, J = 9 Hz) ppm; ¹³C NMR (75 MHz, CDCl₃) δ 146.47, 138.32, 117.72, 79.80. ppm.

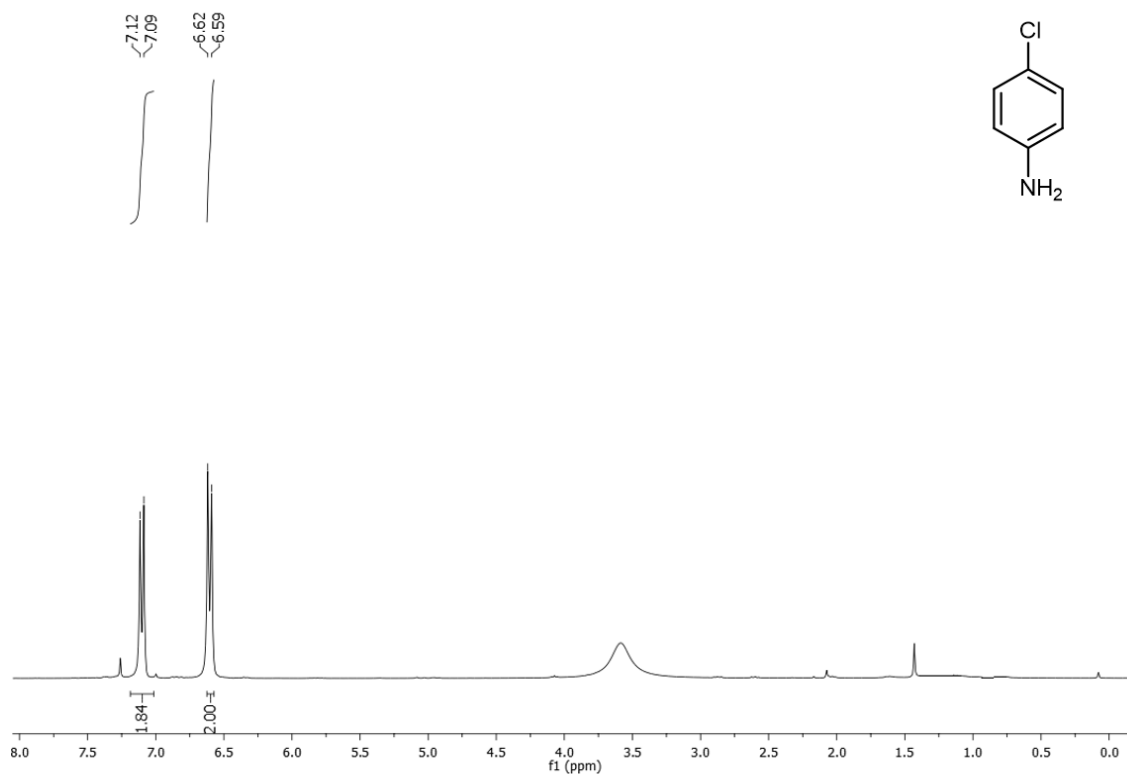


¹H NMR (300 MHz, CDCl₃) of p-Iodoaniline (Table 9, Entry 3).

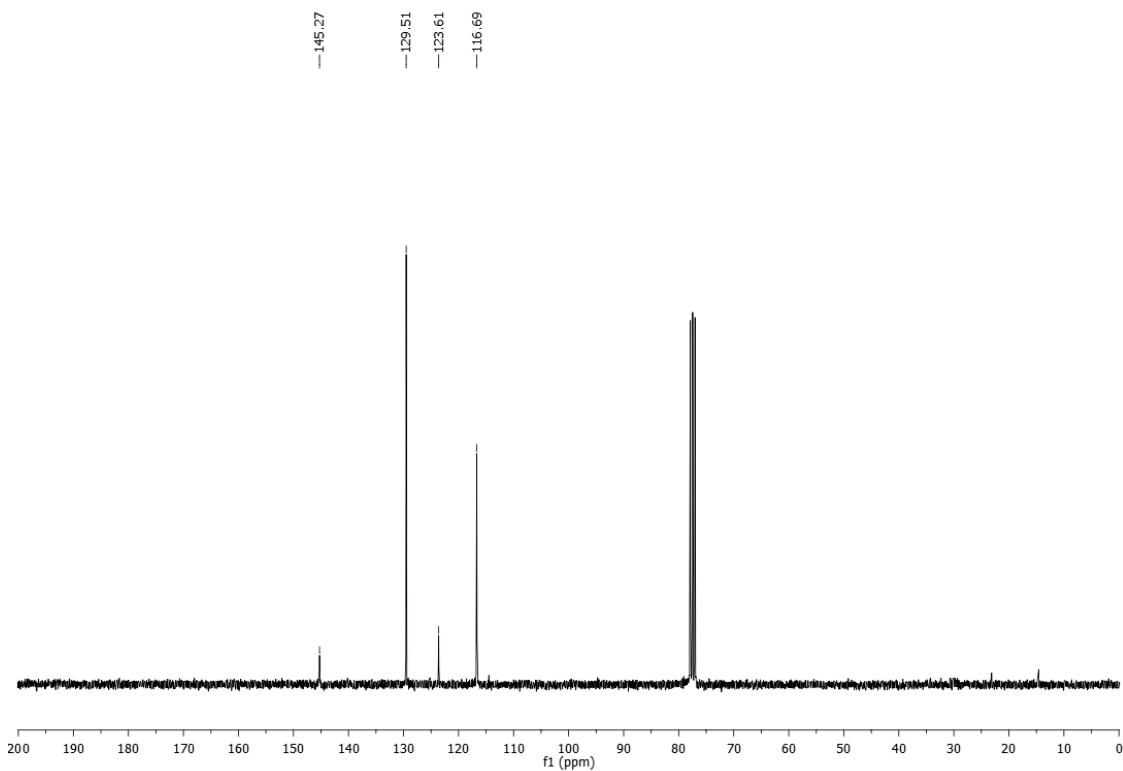


¹³C-NMR (75 MHz, CDCl₃) of p-Iodoaniline (Table 9, Entry 3)

***p*-Chloroaniline (2.2d)**⁴⁴⁶: ¹H NMR (300 MHz, CDCl₃) δ 7.10 (2H, d, J = 9 Hz), 6.61 (2H, d, J = 9 Hz) ppm; ¹³C NMR (75 MHz, CDCl₃) δ 145.27, 129.51, 123.61, 116.69 ppm.

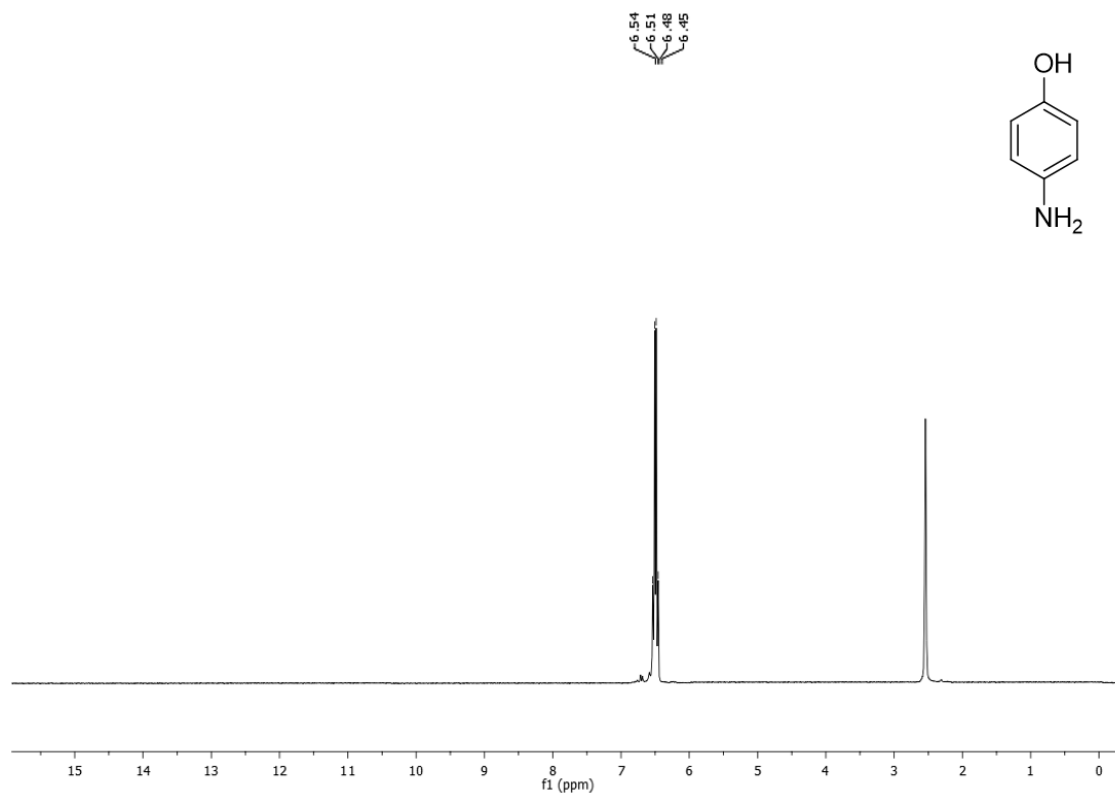


¹H NMR (300 MHz, CDCl₃) of *p*-Chloroaniline (Table 9, Entry 4) (Table 23, Entry 3).

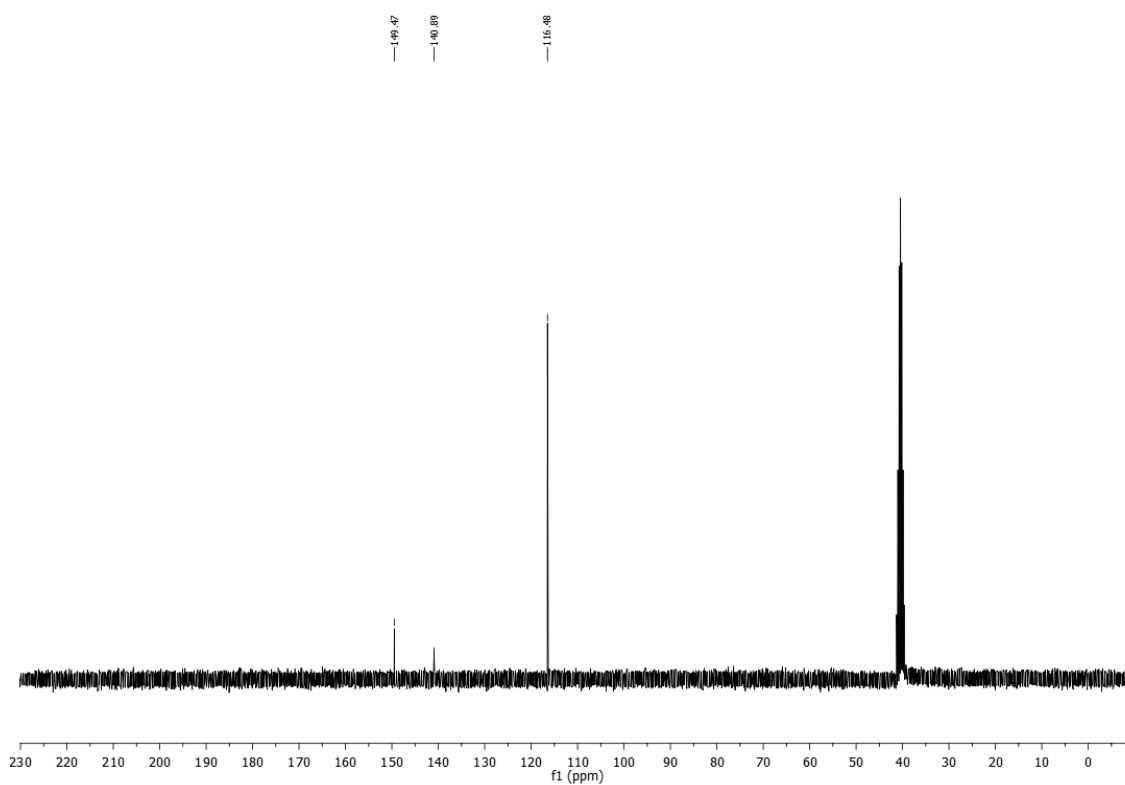


¹³C-NMR (75 MHz, CDCl₃) of *p*-Chloroaniline (Table 9, Entry 4) (Table 23, Entry 3).

***p*-Aminophenol (2.2e)**⁴⁴⁷: ¹H NMR (300 MHz, DMSO-d₆) δ 6.54- 6.45 (4H, m) ppm; ¹³C NMR (75 MHz, DMSO-d₆) δ 149.47, 140.89, 116.48 ppm.

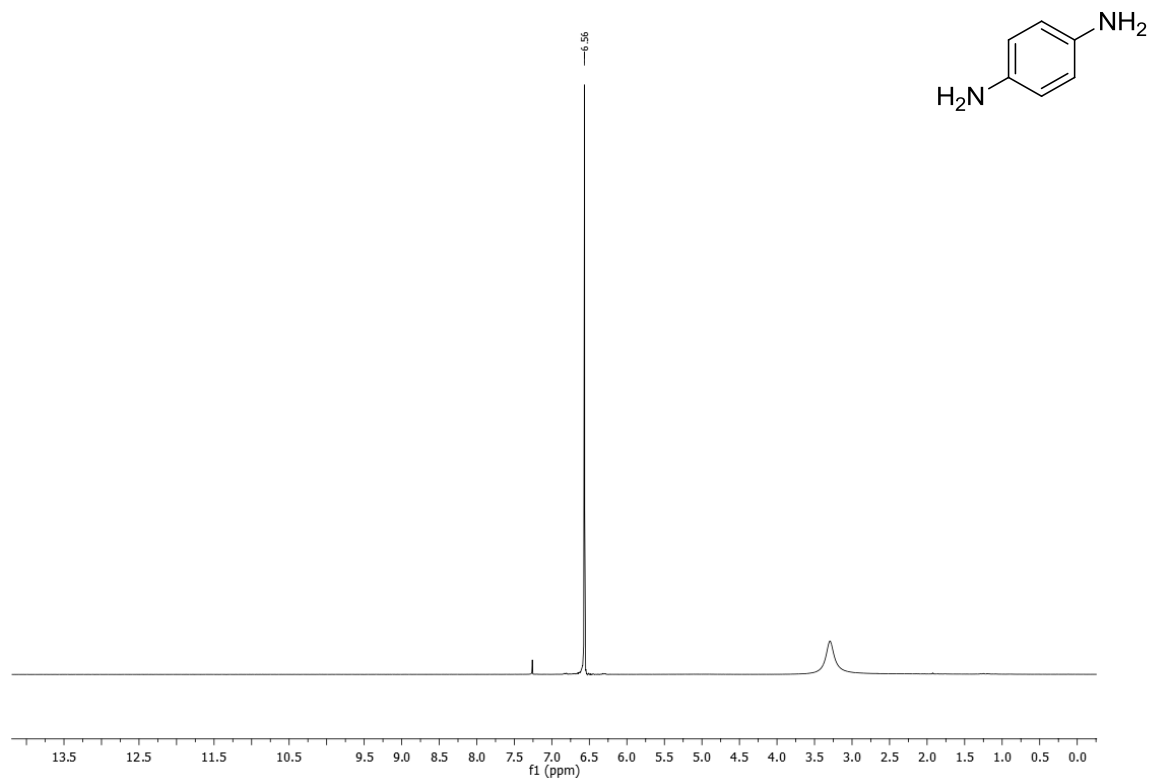


¹H NMR (300 MHz, DMSO-d₆) of *p*-Aminophenol (Table 9, Entry 5) (Table 23, Entry 4).

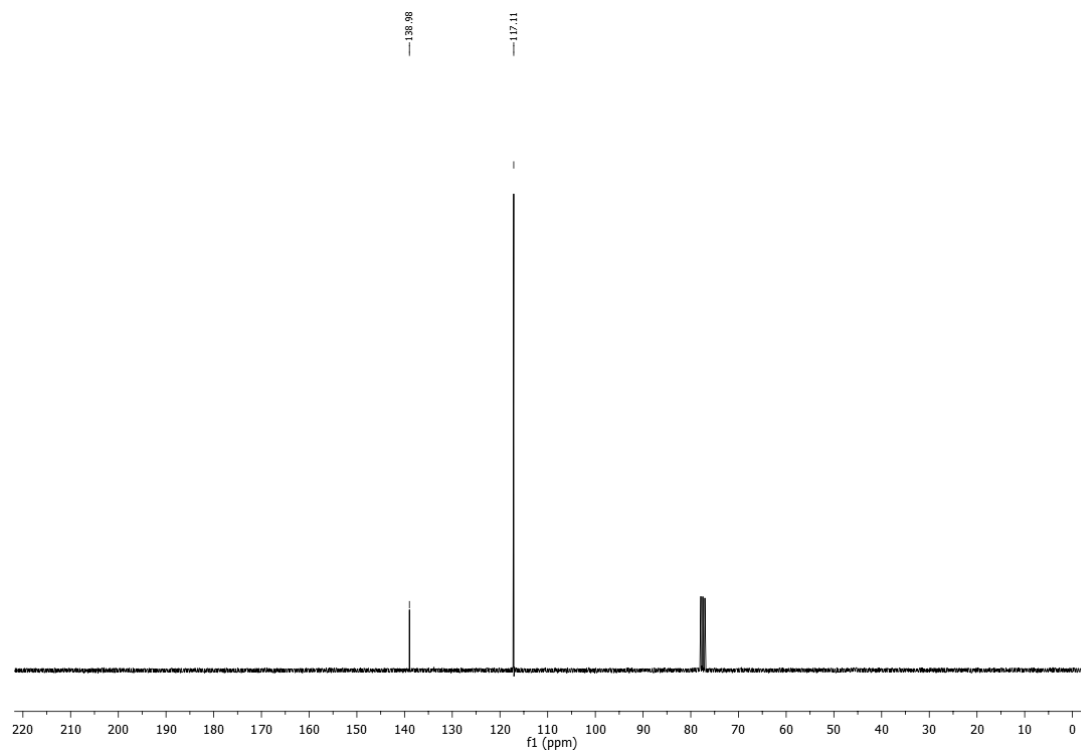


¹³C-NMR (75 MHz, DMSO-d₆) of *p*-Aminophenol (Table 9, Entry 5) (Table 23, Entry 4).

Benzene-1,4-diamine (2.2f)(2.2g)⁴⁴⁹: ¹H NMR (300 MHz, CDCl₃) δ (4H, s) 6.56 ppm; ¹³C NMR (75 MHz, CDCl₃) δ 138.98, 117.11 ppm.

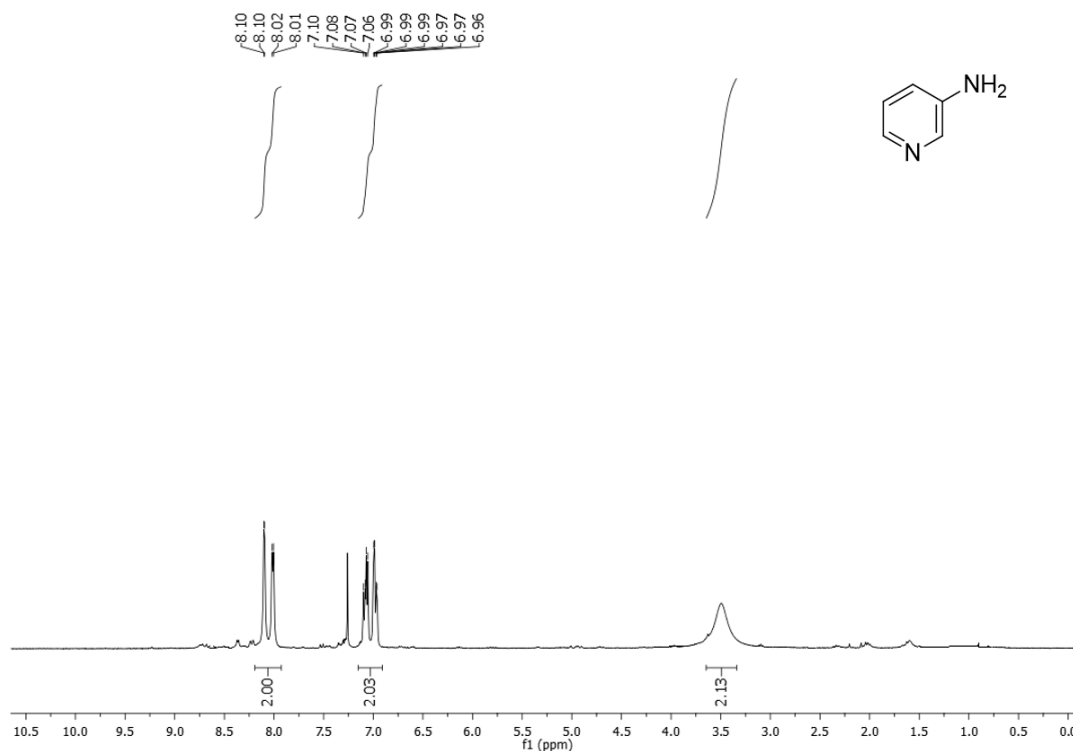


¹H NMR (300 MHz, CDCl₃) of benzene-1,4-diamine (Table 9, Entry 6).

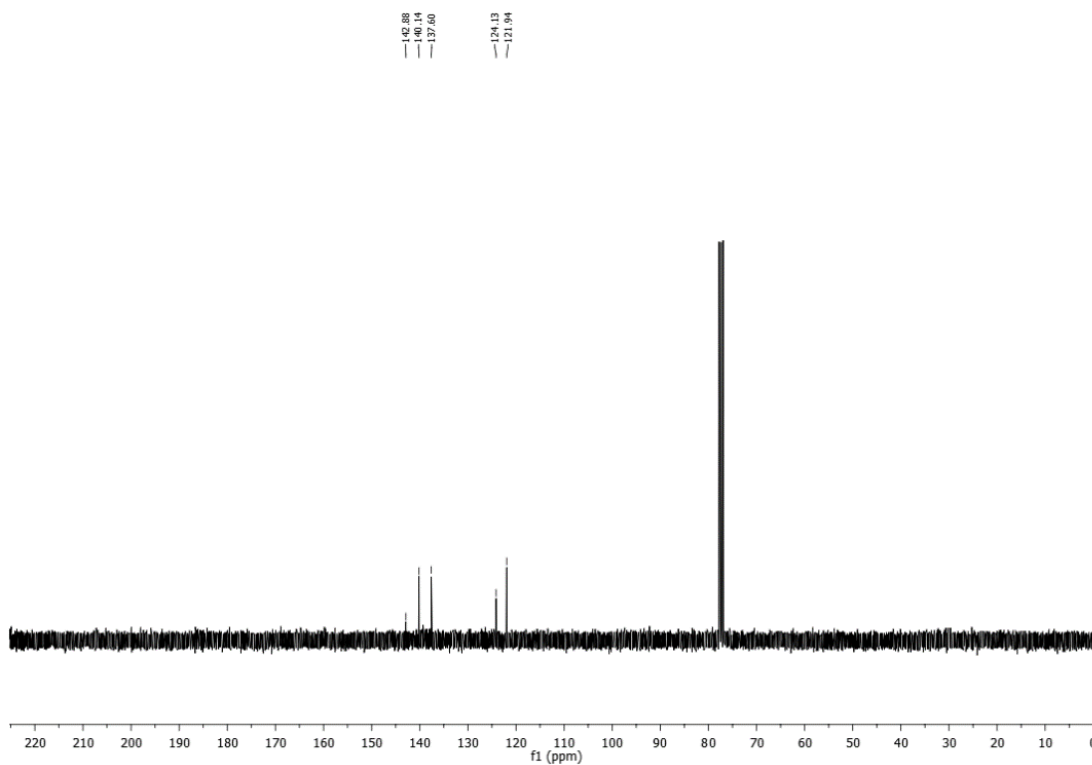


¹³C-NMR (75 MHz, CDCl₃) of benzene-1,4-diamine (Table 9, Entry 6).

3-Aminopyridine (2.2h)⁴⁵⁰: ¹H NMR (300 MHz, CDCl₃) δ 8.10- 8.01 (2H, m), 7.10- 7.06 (1H, m), 6.99-6.96 (1H,m), 3.51 (2H,s) ppm; ¹³C NMR (75 MHz, CDCl₃) δ 142.88, 140.14, 137.60, 124.13, 121.94 ppm

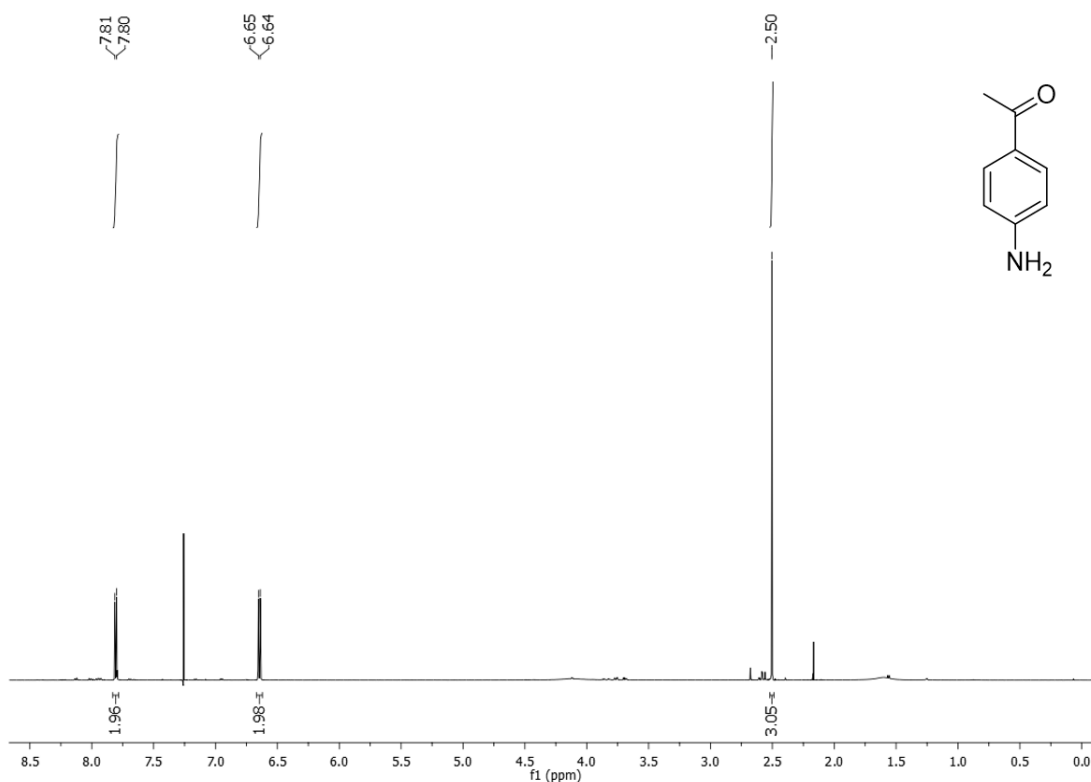


¹H NMR (300 MHz, CDCl₃) of 3-Aminopyridine (Table 9, Entry 8) (Table 23, Entry 13).

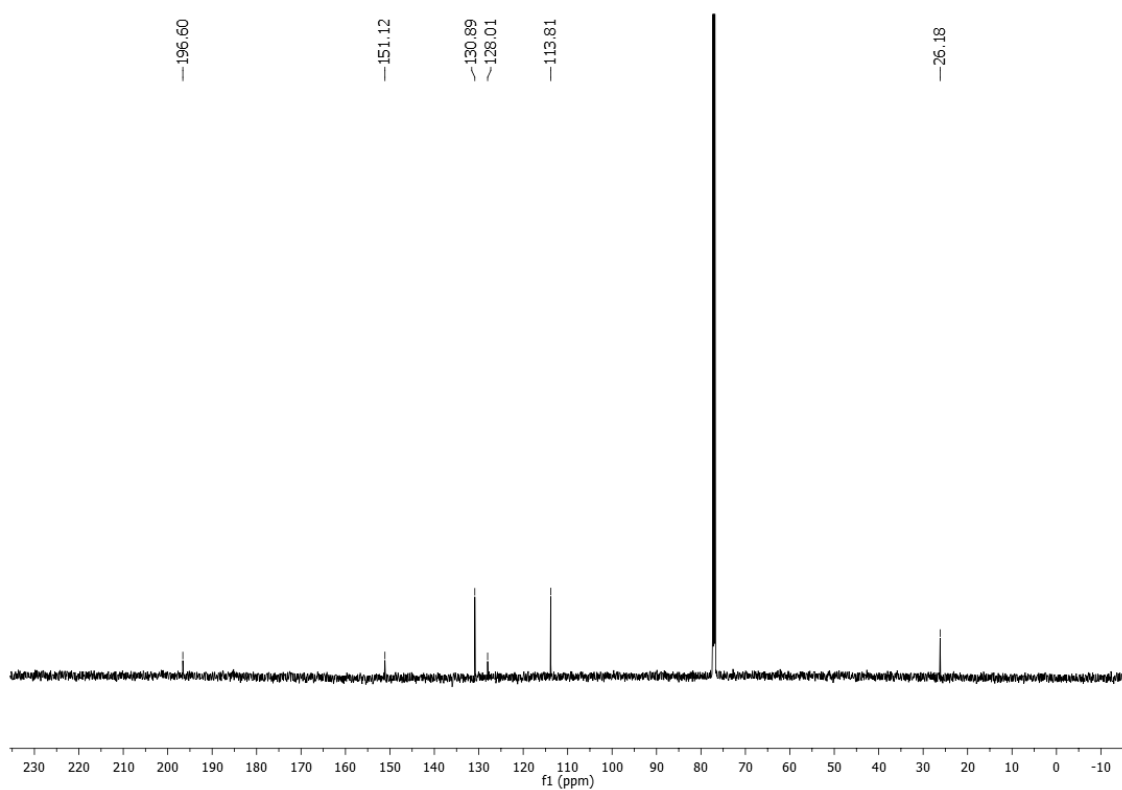


¹³C-NMR (75 MHz, CDCl₃) of 3-Aminopyridine (Table 9, Entry 8) (Table 23, Entry 13).

***p*-Aminoacetophenone (2.2i)**⁴⁴⁷: ¹H NMR (300 MHz, CDCl₃) δ 7.80 (2H, d, J = 9 Hz), 6.64 (2H, d, J = 9 Hz), 2.50 (3H, s) ppm; ¹³C NMR (75 MHz, CDCl₃) δ 196.85, 151.38, 131.13, 129.76, 114.07, 26.44 ppm.

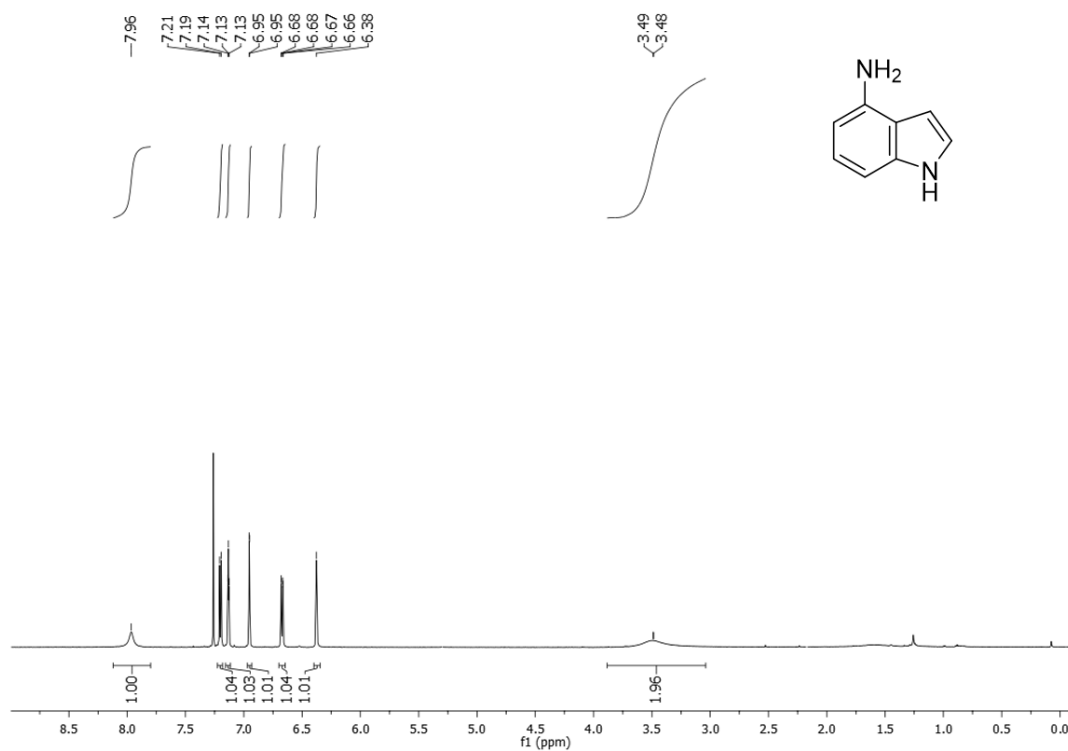


¹H NMR (300 MHz, CDCl₃) of *p*-Aminoacetophenone (Table 9, Entry 9) (Table 23, Entry 7).

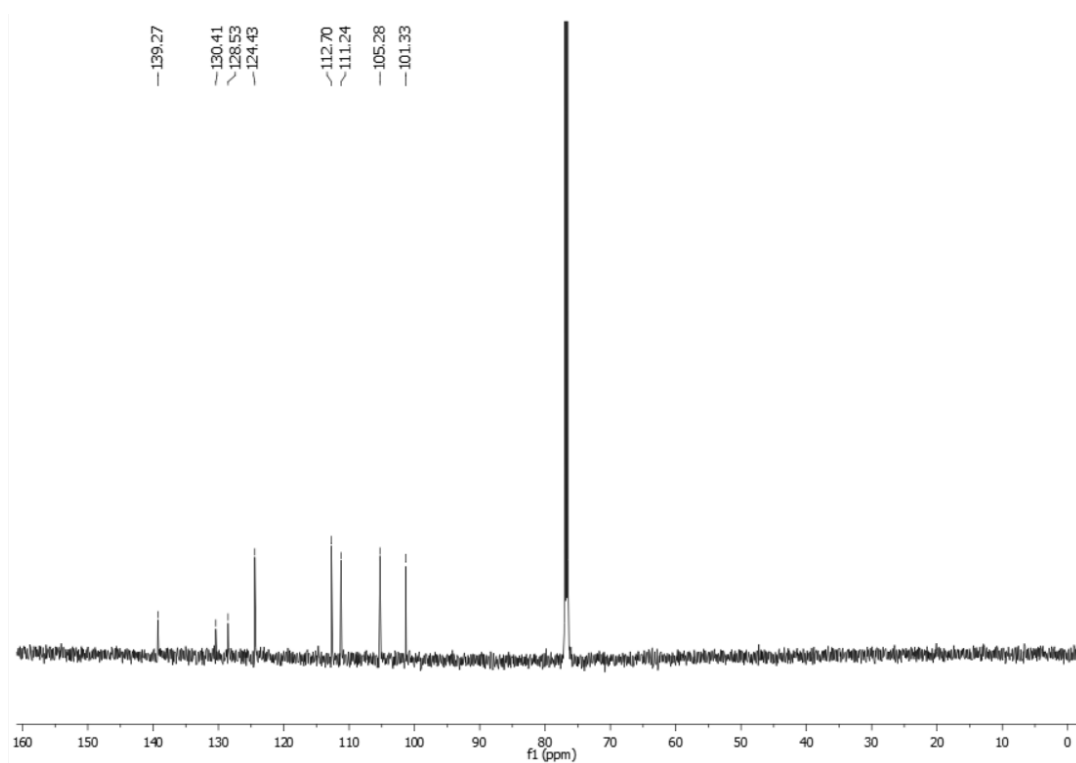


¹³C-NMR (75 MHz, CDCl₃) of *p*-Aminoacetophenone (Table 9, Entry 9) (Table 23, Entry 7).

5-Aminoindole (2.2j)⁴⁴⁷: ¹H NMR (600 MHz,) δ 7.96 (s, 1H), 7.20 (d, J = 8.5 Hz, 1H), 7.13 (t, J = 2.7 Hz, 1H), 6.95 (d, J = 1.9 Hz, 1H), 6.67 (dd, J = 8.5, 2.1 Hz, 1H), 6.38 (s, 1H), 3.49 (d, J = 2.6 Hz, 2H); ¹³C NMR (151 MHz, CDCl₃) δ 139.62, 130.74, 128.87, 124.77, 113.04, 111.58, 105.62, 101.66 ppm.

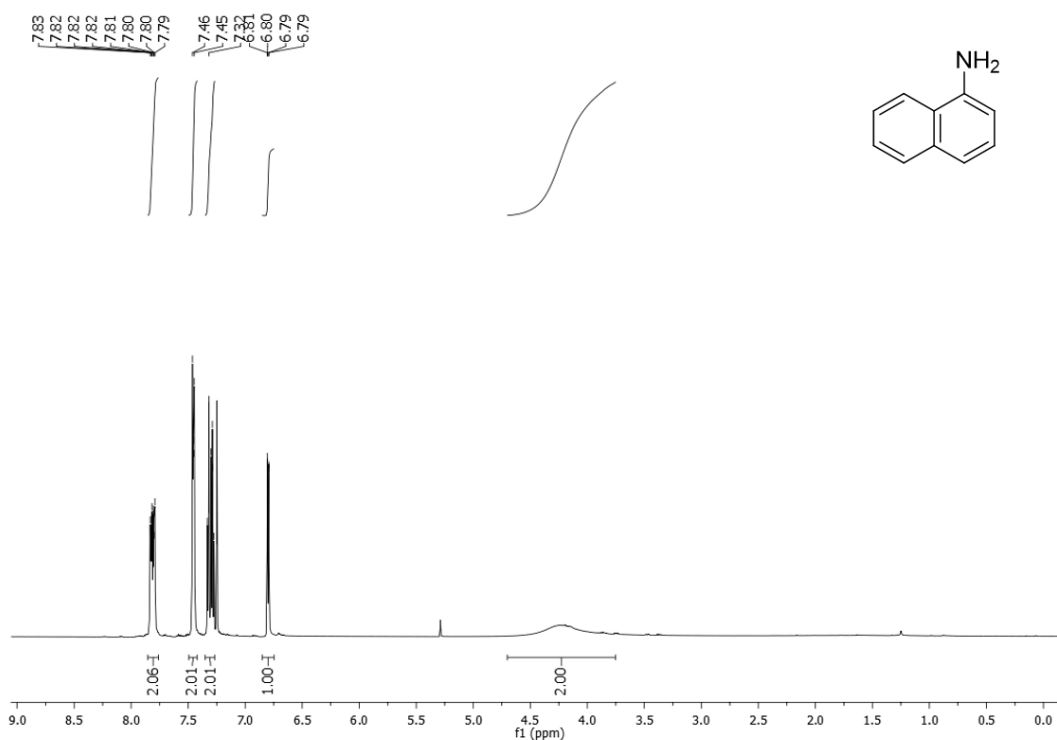


¹H NMR (600 MHz, CDCl₃) of 5-Aminoindole (Table 9, Entry 10) (Table 23, Entry 12).

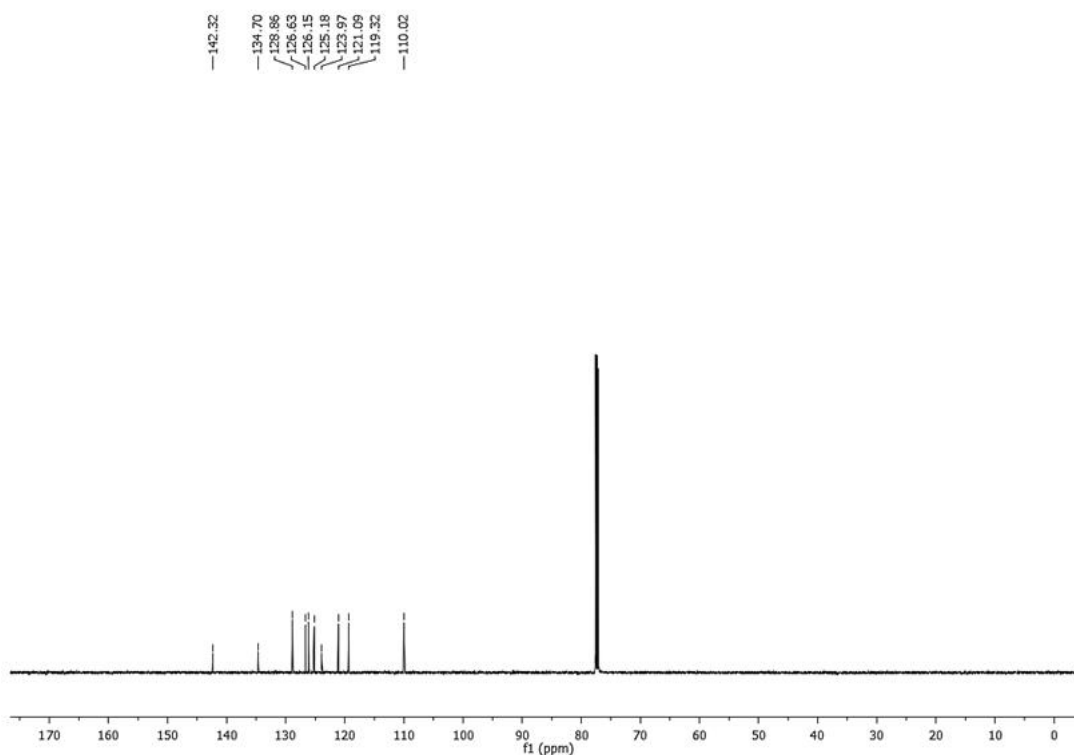


¹³C-NMR (151 MHz, CDCl₃) of 5-Aminoindole (Table 9, Entry 10) (Table 23, Entry 12).

1-Naphthylamine (2.2k)⁴⁴⁷: ¹H NMR (600 MHz, CDCl₃) δ 7.81 (ddd, *J* = 9.5, 6.3, 4.8 Hz, 2H), 7.49 – 7.42 (m, 2H), 7.30 (dt, *J* = 8.2, 7.7 Hz, 2H), 6.80 (dd, *J* = 7.2, 1.2 Hz, 1H), 4.70 – 3.75 (m, 2H).; ¹³C NMR (151 MHz, CDCl₃) δ 142.32, 134.70, 128.86, 126.63, 126.15, 125.18, 123.97, 121.09, 119.32, 110.02.

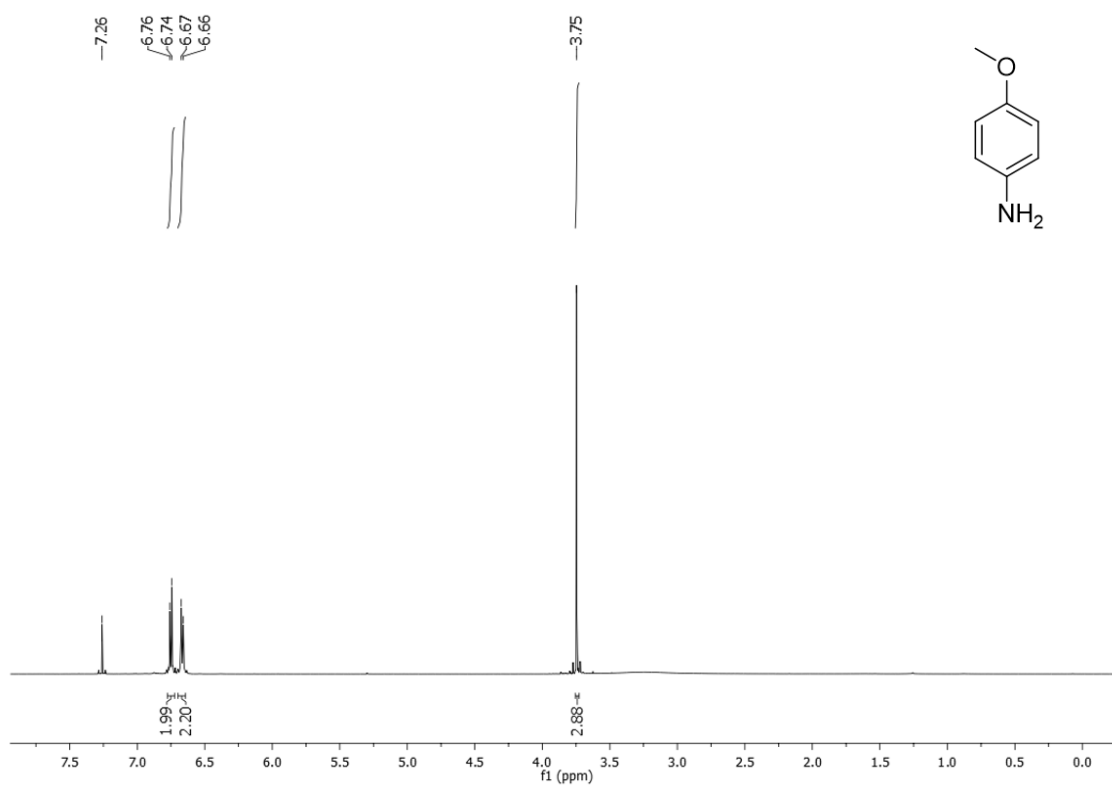


¹H NMR (300 MHz, CDCl₃) of 1-Naphthylamine (Table 9, Entry 11) (Table 11, Entry 4) (Table 23, Entry 11).

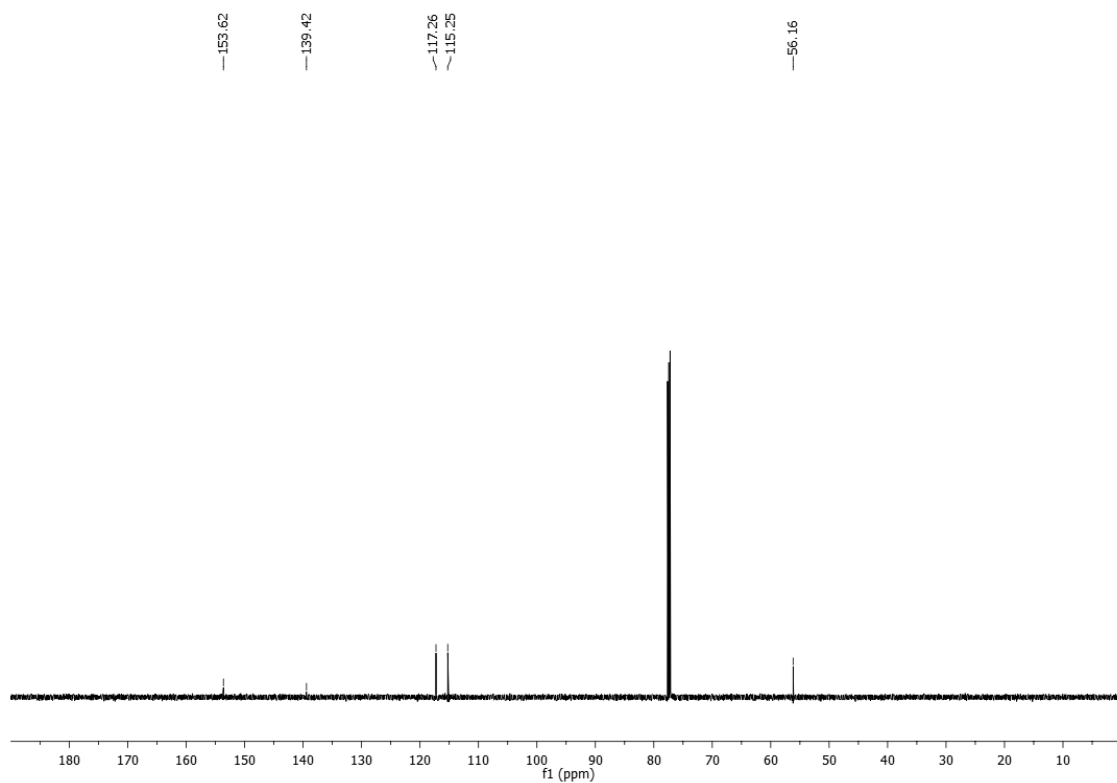


¹³C-NMR (151 MHz, CDCl₃) of 1-Naphthylamine (Table 9, Entry 11) (Table 11, Entry 4) (Table 23, Entry 11).

p-Aminoanisole (2.21)⁴⁴⁶: ¹H NMR (300 MHz, CDCl₃) δ 6.75 (2H, d, *J* = 9.4 Hz), 6.66 (2H, d, *J* = 9.3 Hz), 3.75 (s, 3H) ppm; ¹³C NMR (151 MHz, CDCl₃) δ 153.62, 139.42, 117.26, 115.25, 56.16 ppm.

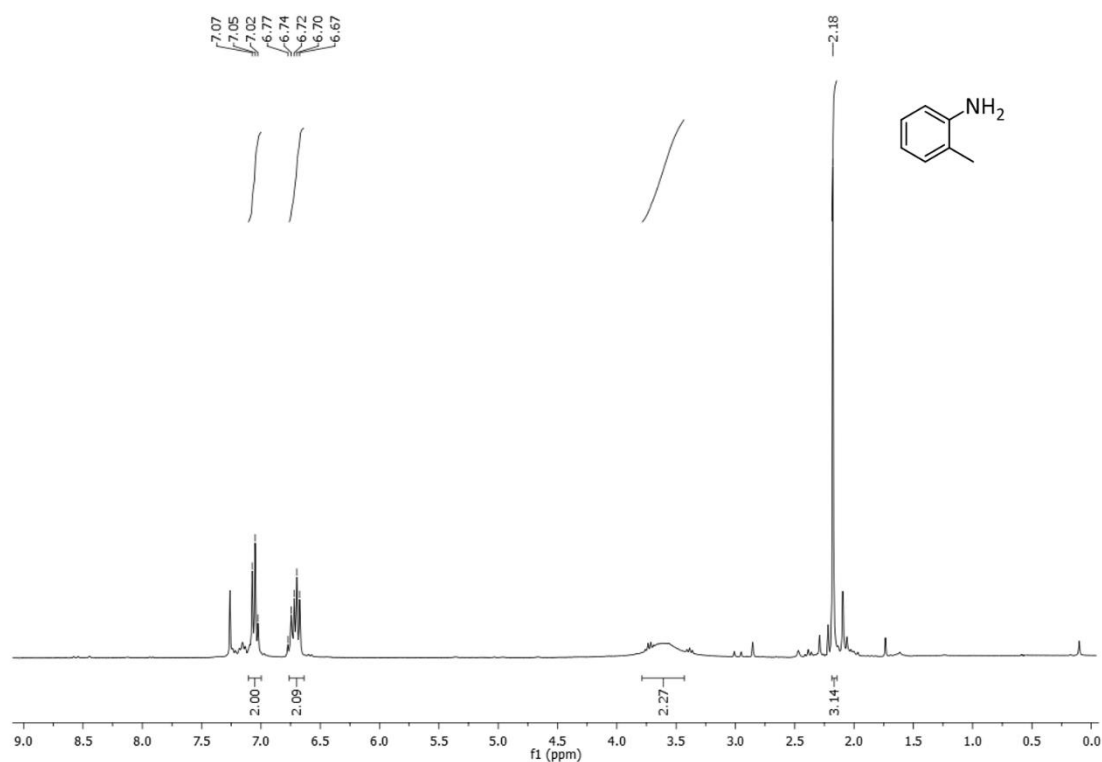


¹H NMR (600 MHz, CDCl₃) of p-aminoanisole (Table 11, Entry 2) (Table 23, Entry 5).

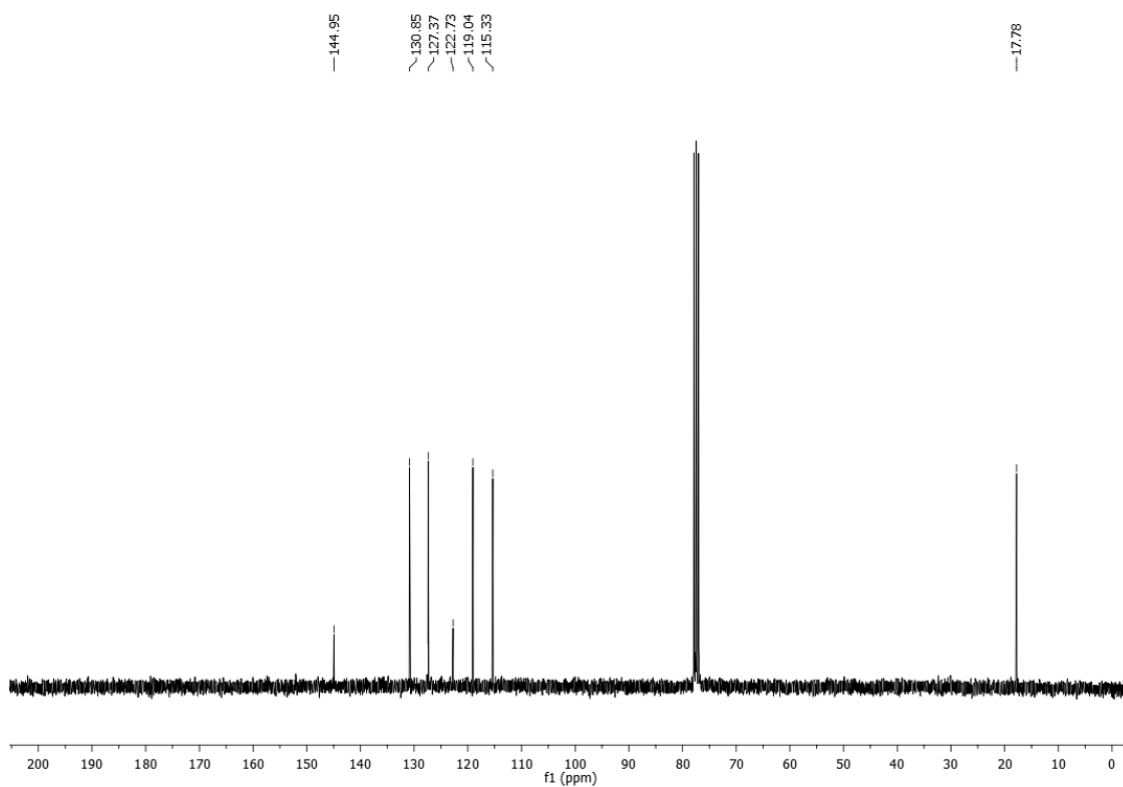


¹³C-NMR (151 MHz, CDCl₃) of p-Aminoanisole (Table 11, Entry 2) (Table 23, Entry 5).

***o*-Toluidine (2.2m)**⁴⁴⁷: ¹H NMR (300 MHz, CDCl₃) δ 7.07-7.02 (2H, m), 6.77- 6.67 (2H, m), 2.18 (3H, s) ppm; ¹³C NMR (75 MHz, CDCl₃) δ 144.85, 130.76, 127.28, 122.64, 118.94, 115.23, 17.68 ppm.

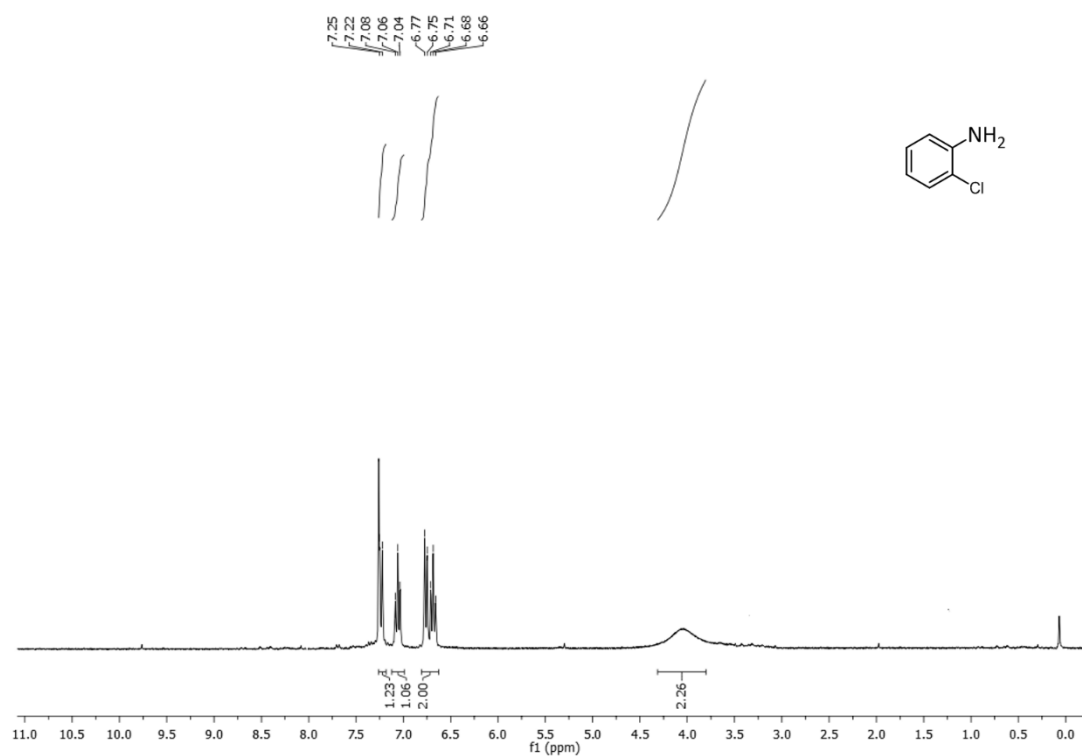


¹H NMR (600 MHz, CDCl₃) of *o*-Toluidine (Table 11, Entry 3).

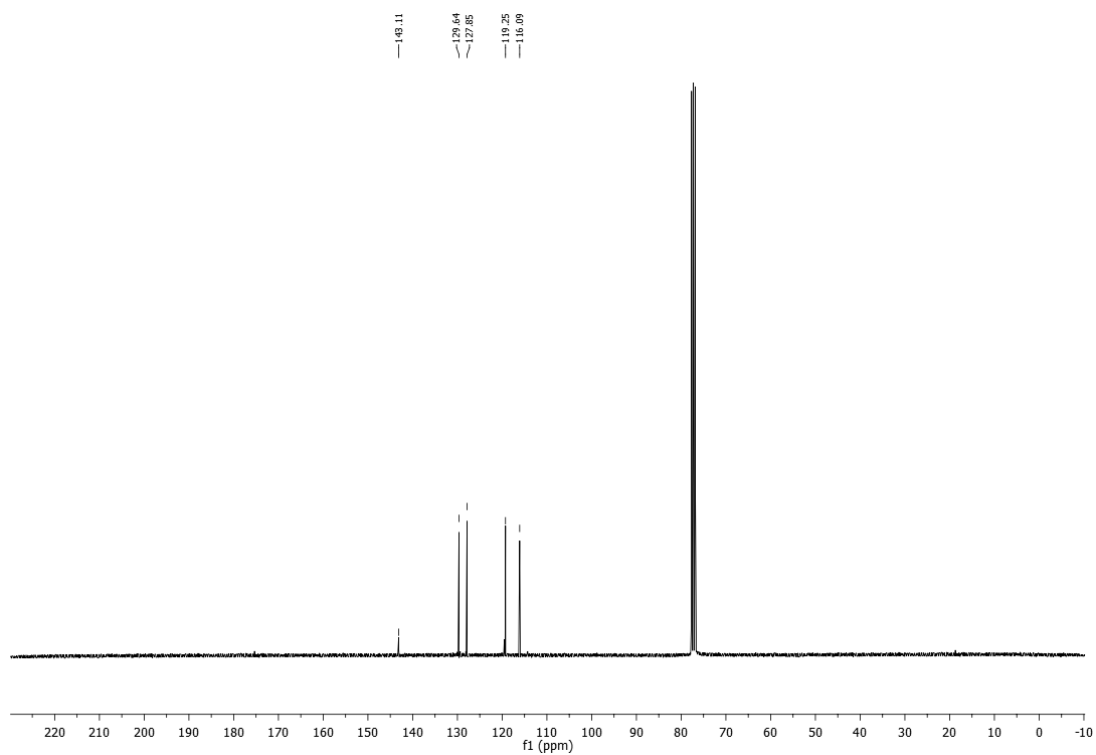


¹³C-NMR (75 MHz, CDCl₃) of *o*-Toluidine (Table 11, Entry 3).

2-Chloroaniline (2.2n)⁴⁵¹: ¹H NMR (300 MHz, CDCl₃) δ 7.25-7.22 (1H, m), 7.06 (1H, t, J = 6 Hz), 6.76 (1H, d, J = 6 Hz), 6.68 (1H, t, J = 6 Hz) ppm; ¹³C NMR (75 MHz, CDCl₃) δ 143.11, 129.64, 127.85, 119.25, 116.09 ppm.

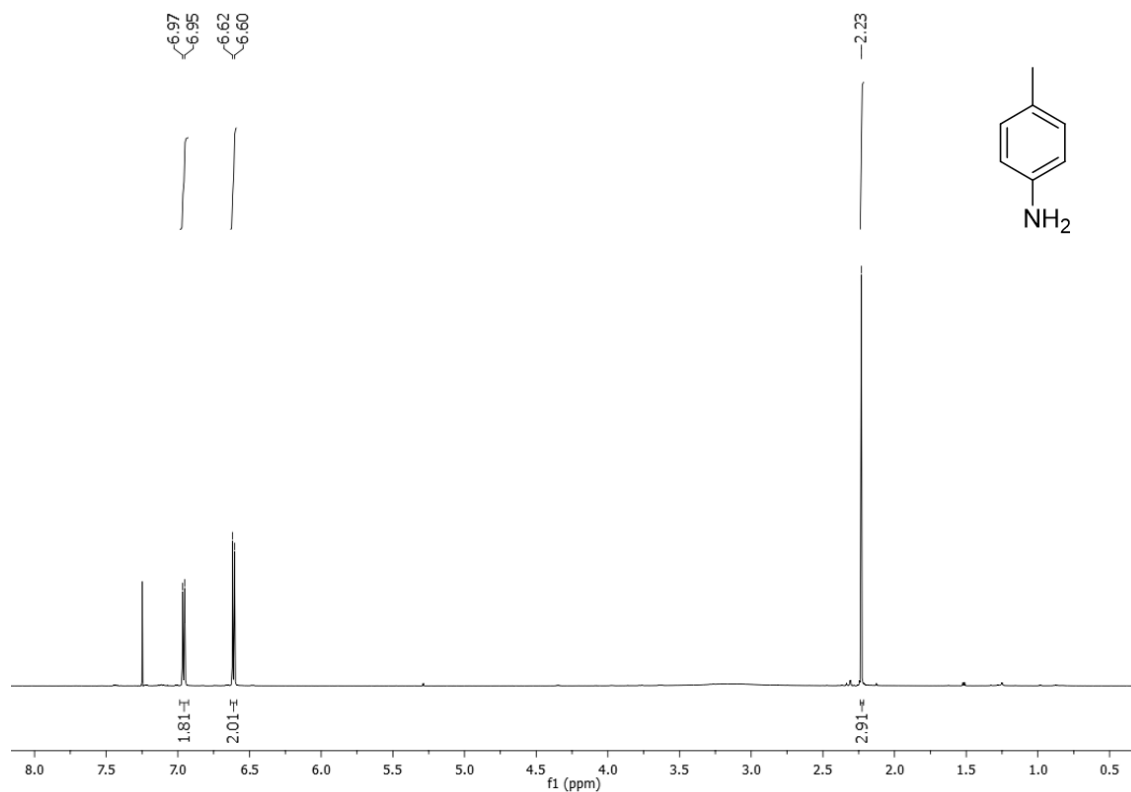


¹H NMR (600 MHz, CDCl₃) of 2-Chloroaniline (Table 11, Entry 5).

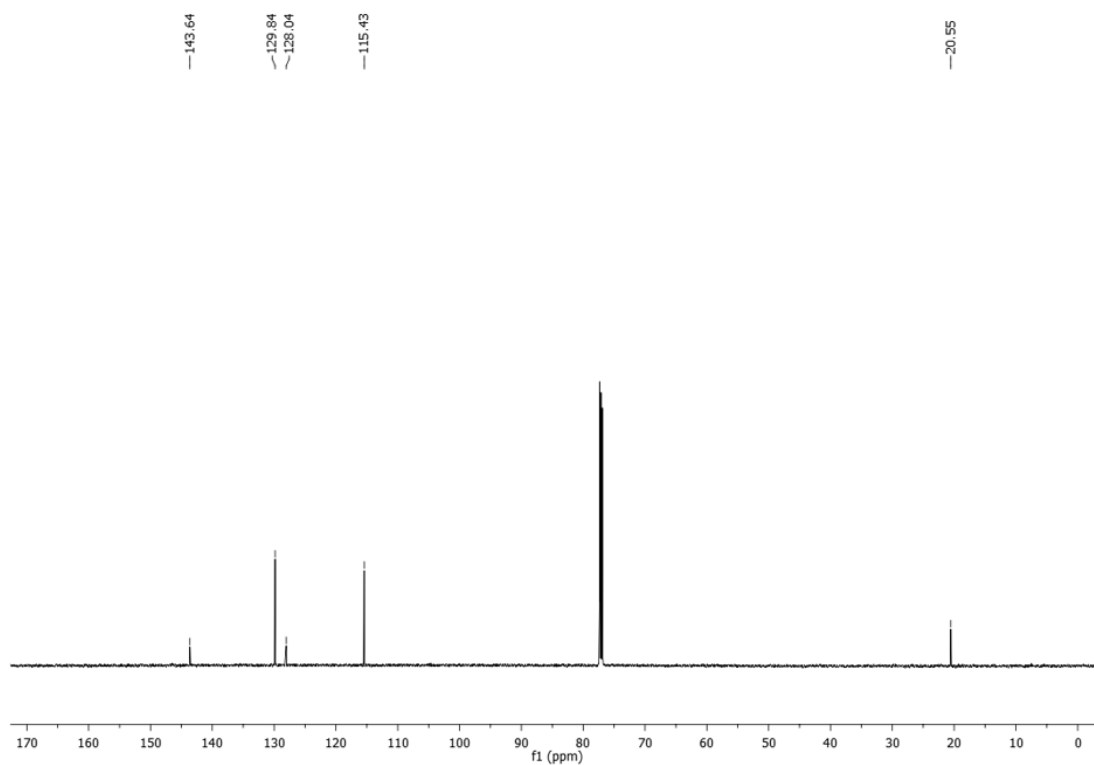


¹³C-NMR (75 MHz, CDCl₃) of 2-Chloroaniline (Table 11, Entry 5).

p-Aminotoluene (**2.20**)⁴⁴⁶: ¹H NMR (600 MHz, CDCl₃) δ 6.96 (2H, d, J = 18 Hz) 6.61 (2H, d, J = 12 Hz), 2.23 (3H, s) ppm; ¹³C NMR (151 MHz, CDCl₃) δ 143.64, 129.84, 128.04, 115.43, 20.55

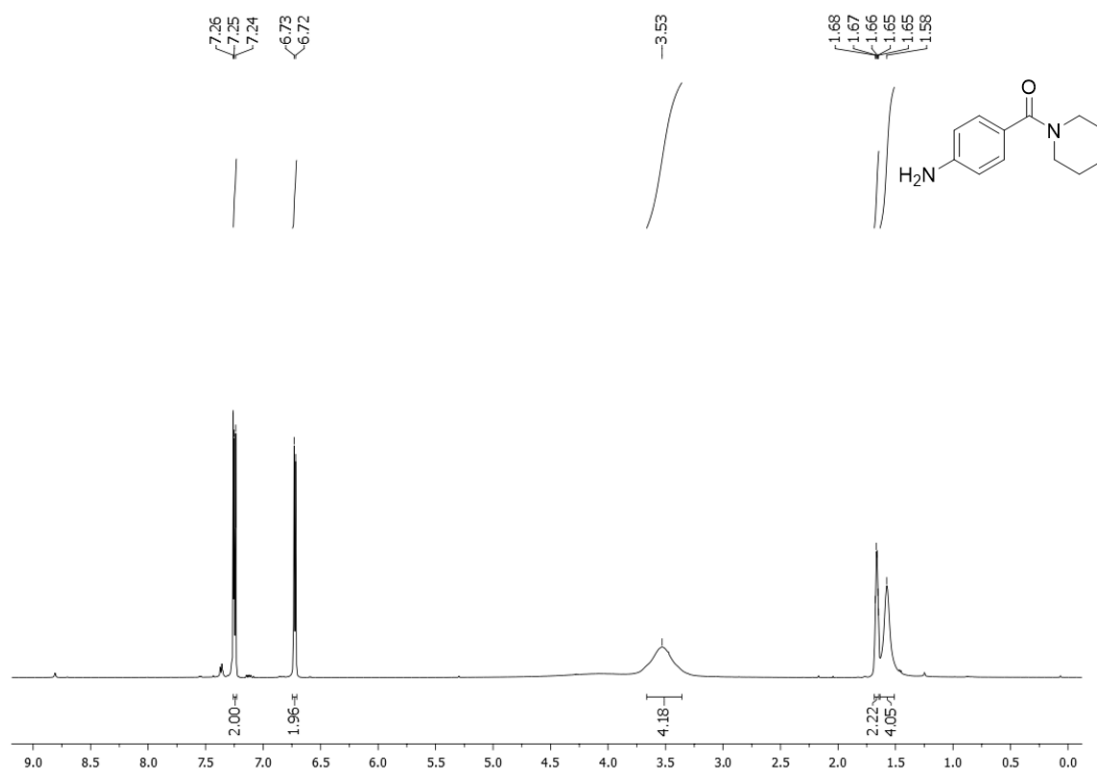


¹H NMR (300 MHz, CDCl₃) of p-Aminotoluene (Table 23, Entry 6).

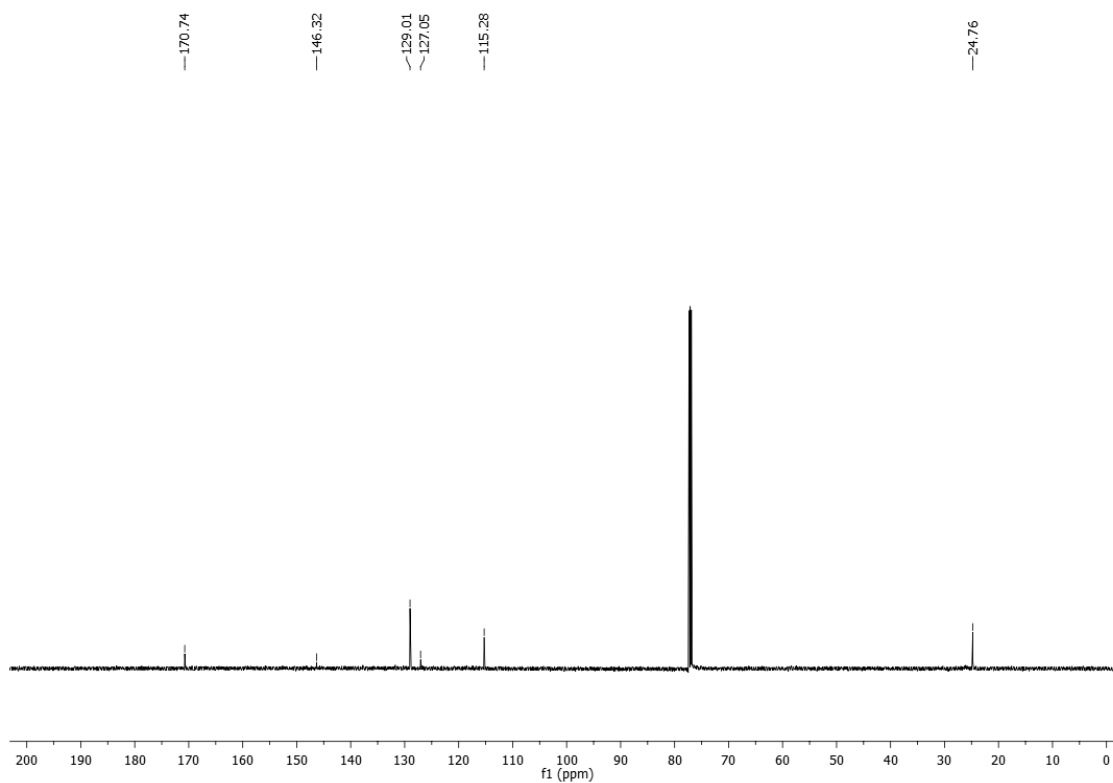


¹³C-NMR (151 MHz, CDCl₃) of p-Aminotoluene (Table 23, Entry 6).

4-(N-piperidinocarbonyl)aniline (2.2p)⁴⁵²: ¹H NMR (600 MHz, CDCl₃) δ 7.25 (d, *J* = 8.4 Hz, 2H), 6.72 (d, *J* = 8.5 Hz, 2H), 3.53 (s, 4H), 1.68 – 1.65 (m, 2H), 1.58 (s, 4H). ppm; ¹³C NMR (151 MHz,) δ 170.74, 146.32, 129.01, 127.05, 115.28, 24.76 ppm.

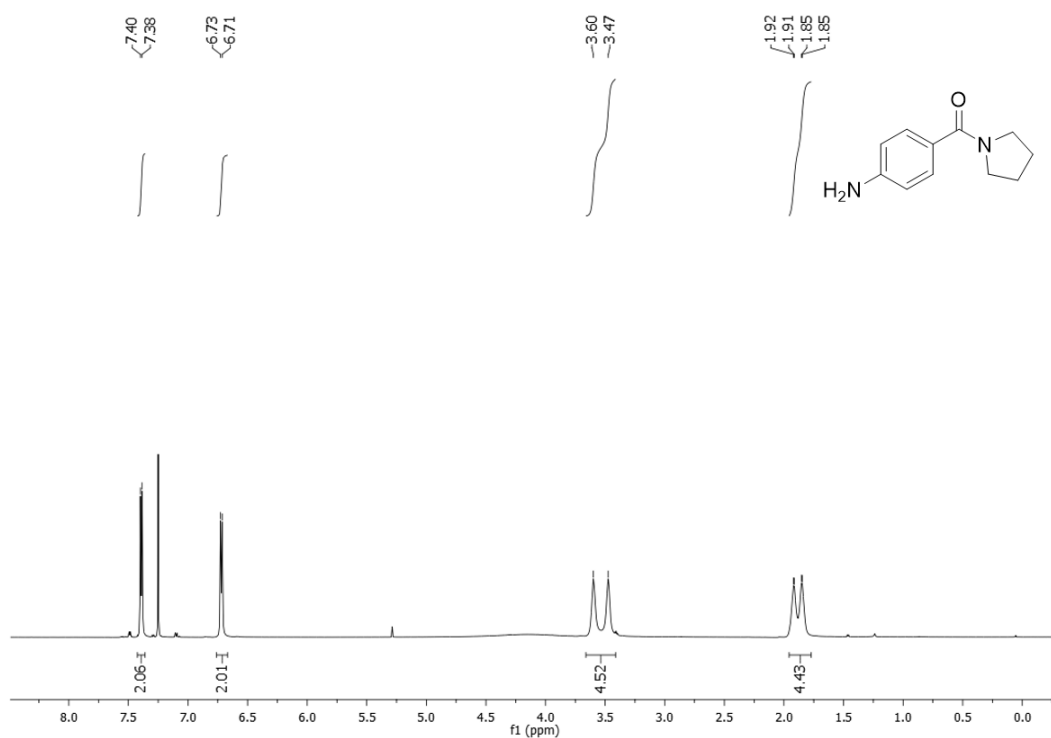


¹H NMR (600 MHz, CDCl₃) of 4-(N-piperidinocarbonyl)aniline (Table 23, Entry 8).

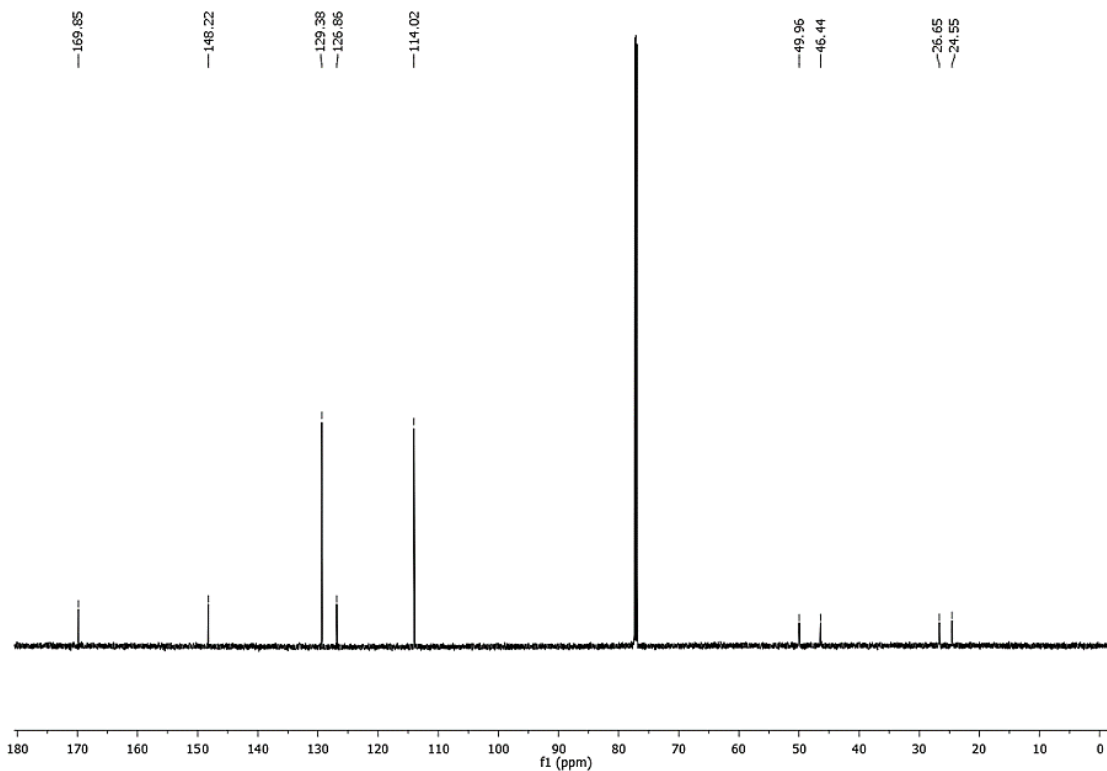


¹³C-NMR (151 MHz, CDCl₃) of 4-(N-piperidinocarbonyl)aniline (Table 23, Entry 8).

4-carboxamidopyrrolidinophenyl-aniline (2.2q)⁴⁵²: ¹H NMR (600 MHz, CDCl₃) δ 7.39 (d, J = 8.5 Hz, 2H), 6.72 (d, J = 8.4 Hz, 2H), 3.54 (d, J = 75 Hz, 4H), 1.88 (dd, J = 40.4, 4.6 Hz, 4H) ppm; ¹³C NMR (151 MHz, CDCl₃) δ 169.85, 148.22, 129.38, 126.86, 114.02, 49.96, 46.44, 26.65, 24.55 ppm.

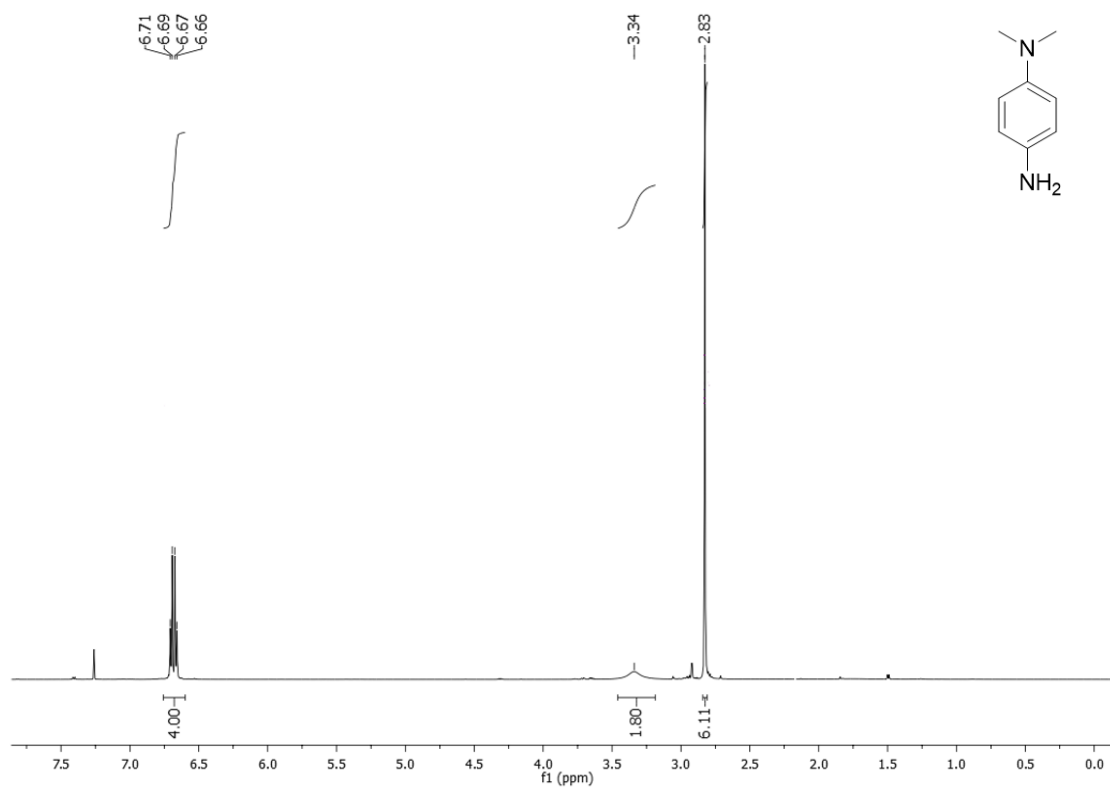


¹H NMR (600 MHz, CDCl₃) of 4-carboxamidopyrrolidinophenyl-aniline (Table 23, Entry 9).

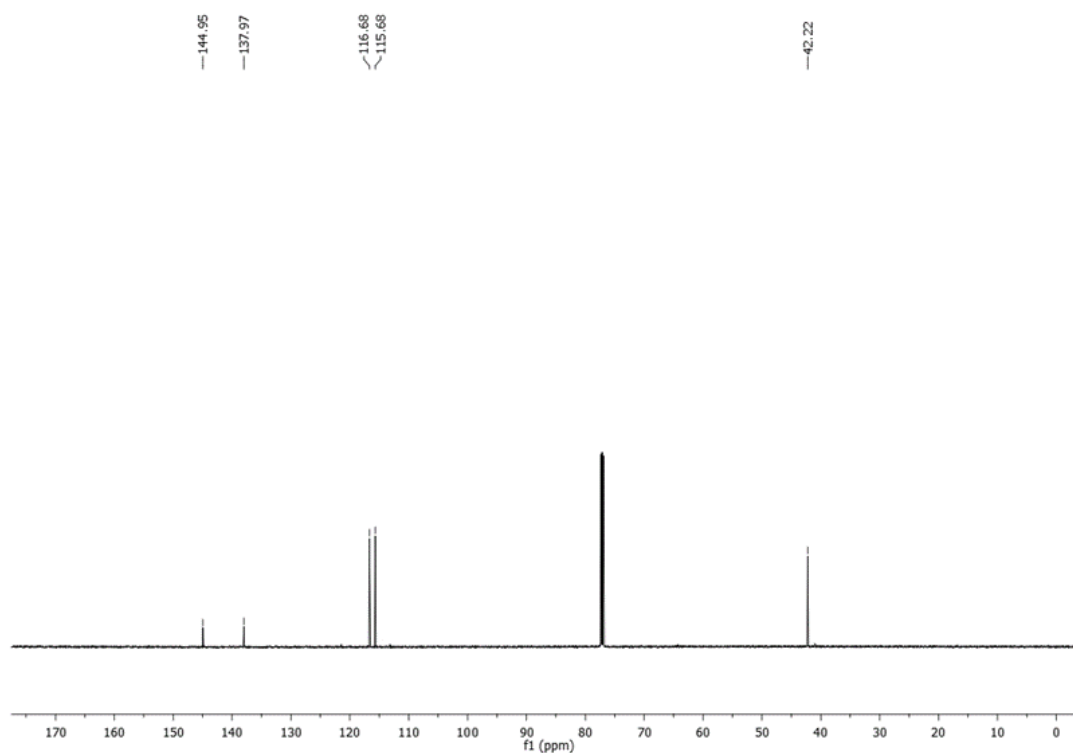


¹³C-NMR (151 MHz, CDCl₃) of 4-carboxamidopyrrolidinophenyl-aniline (Table 23, Entry 9).

***N,N*-dimethylbenzene-1,4-diamine (2.2r)**⁴⁵³: ¹H NMR (600 MHz, CDCl₃) δ 6.68 (4H, dd, *J* = 20.7, 8.9 Hz), 3.34 (s, 2H), 2.83 (6H, s) ppm; ¹³C NMR (151 MHz, CDCl₃) δ 144.95, 137.97, 116.68, 115.68, 42.22 ppm.

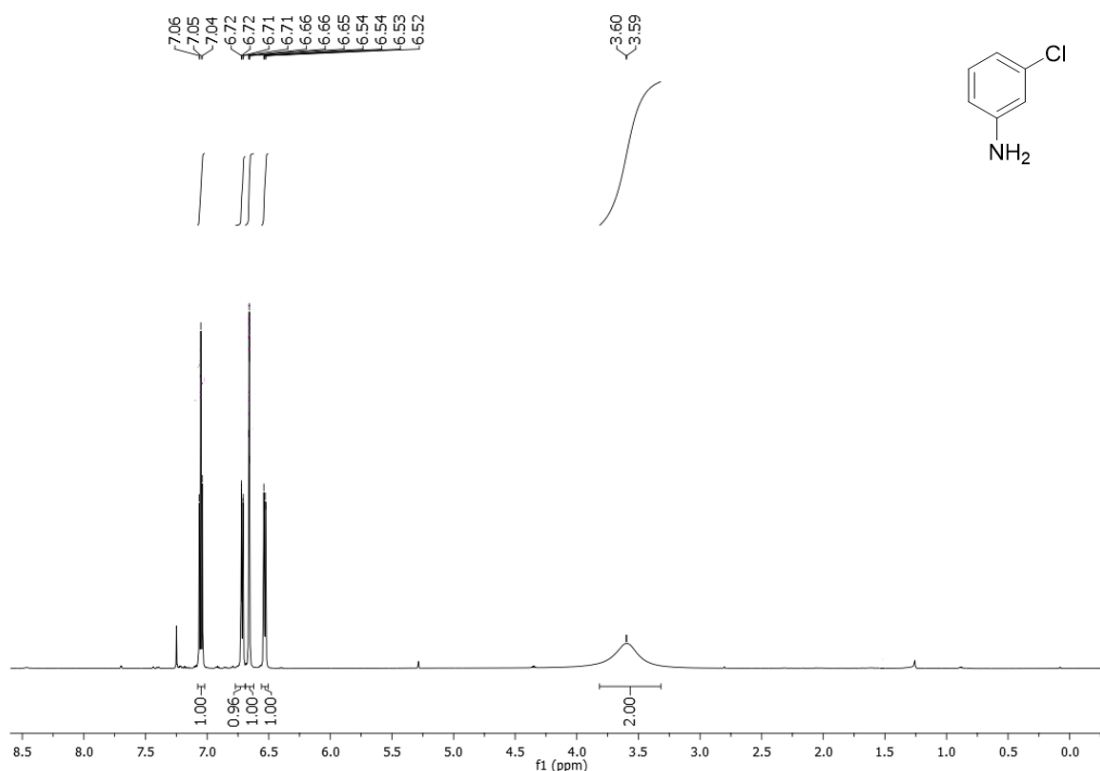


¹H NMR (600 MHz, CDCl₃) of *N,N*-dimethylbenzene-1,4-diamine (Table 23, Entry 10).

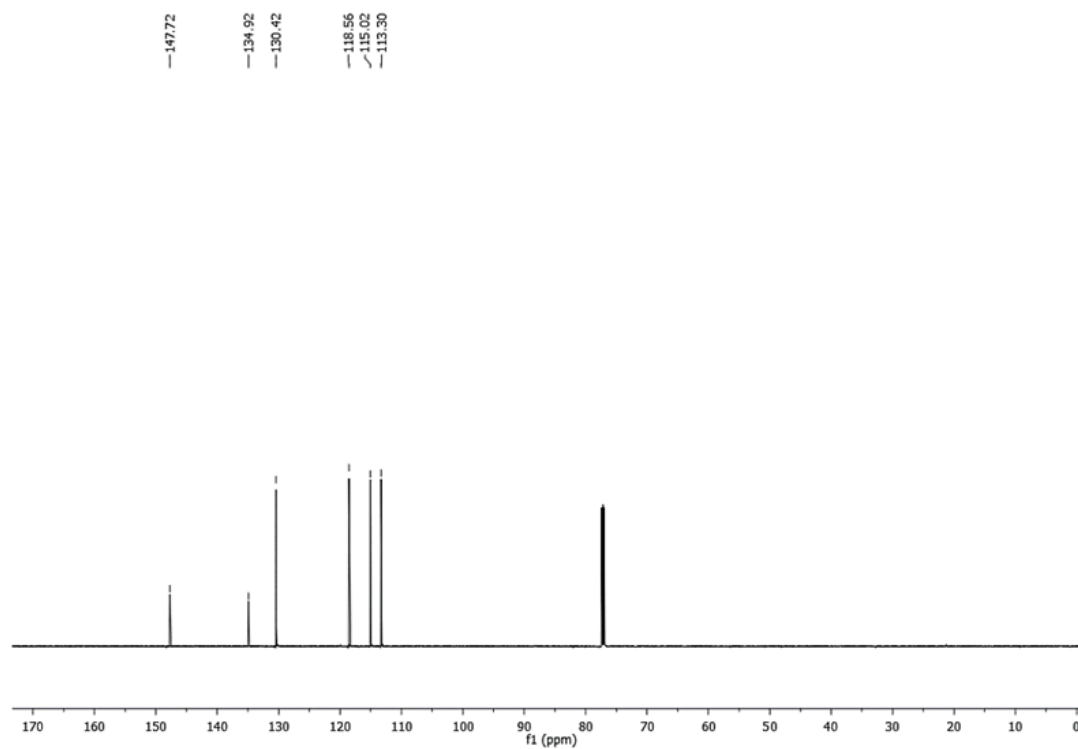


¹³C-NMR (151 MHz, CDCl₃) of *N,N*-dimethylbenzene-1,4-diamine (Table 23, Entry 10).

3-Chloroaniline (2.2s)⁴⁴⁹: ¹H NMR (600 MHz, CDCl₃) δ 7.05 (t, *J* = 8.0 Hz, 1H), 6.71 (dd, *J* = 7.9, 0.9 Hz, 1H), 6.66 (t, *J* = 1.9 Hz, 1H), 6.53 (dd, *J* = 8.1, 1.9 Hz, 1H), 3.60 (d, *J* = 3.4 Hz, 2H) ppm; ¹³C NMR (151 MHz, CDCl₃) δ 147.72, 134.92, 130.42, 118.56, 115.02, 113.30 ppm.

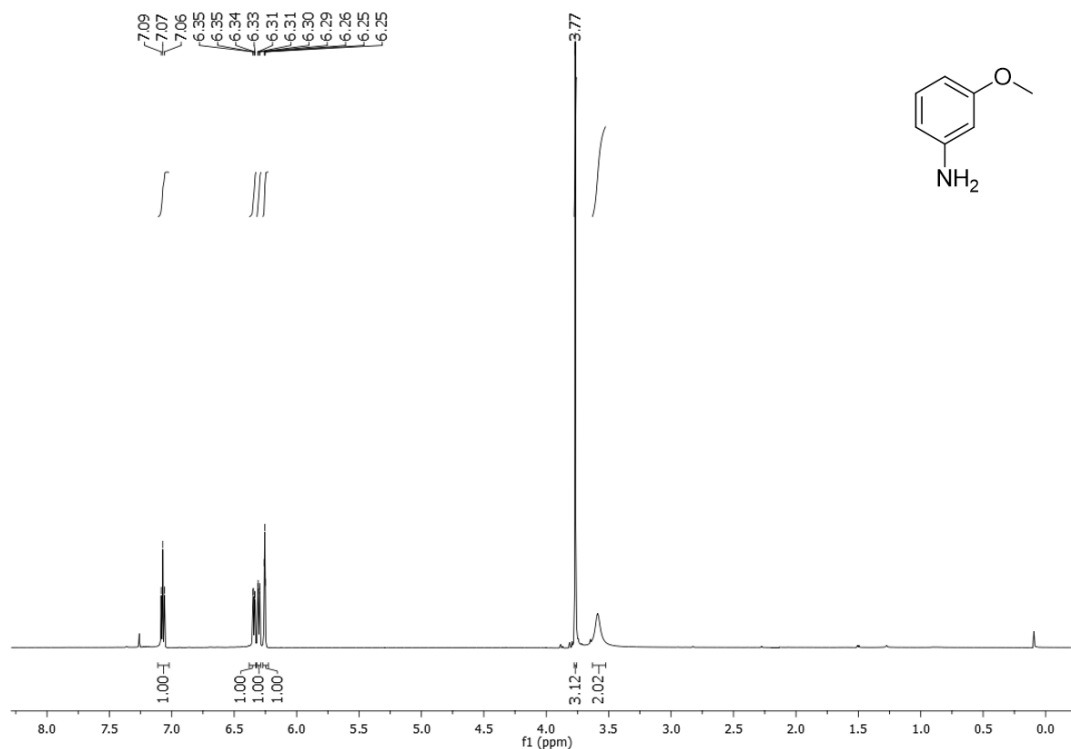


¹H NMR (600 MHz, CDCl₃) of 3-Chloroaniline (Table 23, Entry 14).

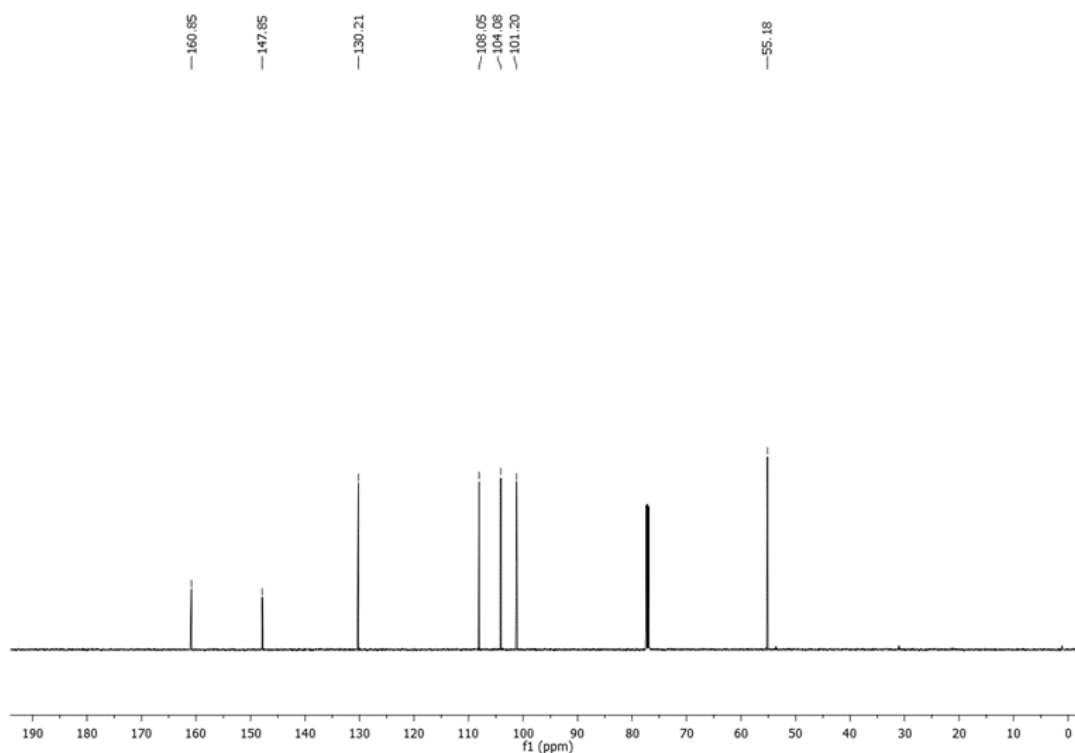


¹³C-NMR (151 MHz, CDCl₃) of 3-Chloroaniline (Table 23, Entry 14).

m-aminoanisole (2.2t)⁴⁵⁴: ¹H NMR (600 MHz, CDCl₃) δ 7.07 (t, *J* = 8.0 Hz, 1H), 6.34 (dd, *J* = 8.2, 2.0 Hz, 1H), 6.30 (dd, *J* = 7.9, 1.5 Hz, 1H), 6.25 (t, *J* = 2.2 Hz, 1H), 3.77 (s, 3H), 3.59 (s, 2H) ppm; ¹³C NMR (151 MHz, CDCl₃) δ 160.85, 147.85, 130.21, 108.05, 104.08, 101.20, 55.18 ppm.

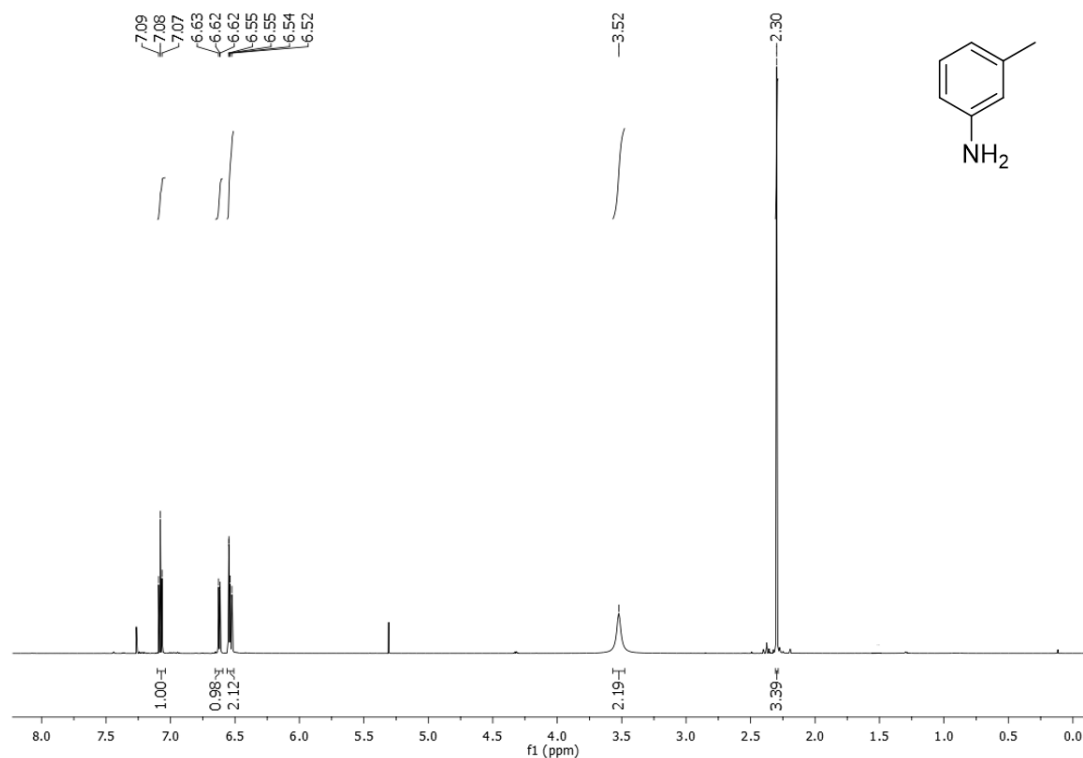


¹H NMR (600 MHz, CDCl₃) of *m*-aminoanisole (Table 23, Entry 15).

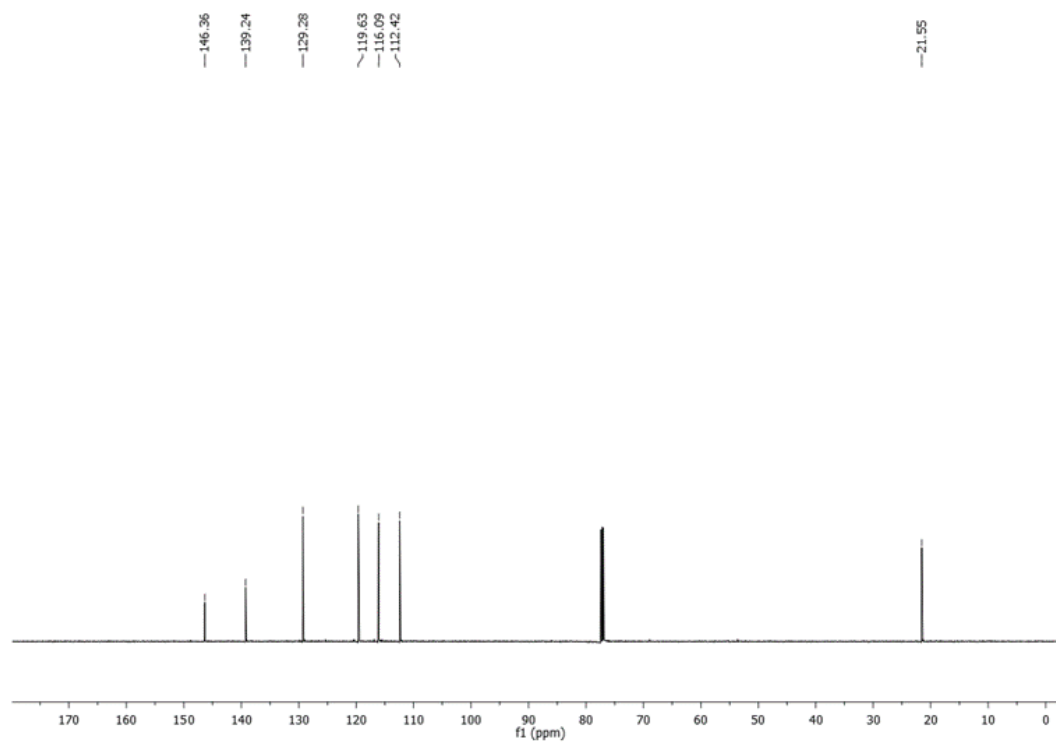


¹³C-NMR (151 MHz, CDCl₃) of *m*-aminoanisole (Table 23, Entry 15).

m-toluidine (2.2u)⁴⁵⁵: ¹H NMR (600 MHz, CDCl₃) δ 7.08 (t, *J* = 7.7 Hz, 1H), 6.65 – 6.59 (m, 1H), 6.54 (dd, *J* = 9.9, 4.2 Hz, 2H), 3.52 (s, 2H), 2.30 (s, 3H) ppm ; ¹³C NMR (151 MHz, CDCl₃) δ 146.36, 139.24, 129.28, 119.63, 116.09, 112.42, 21.55 ppm.

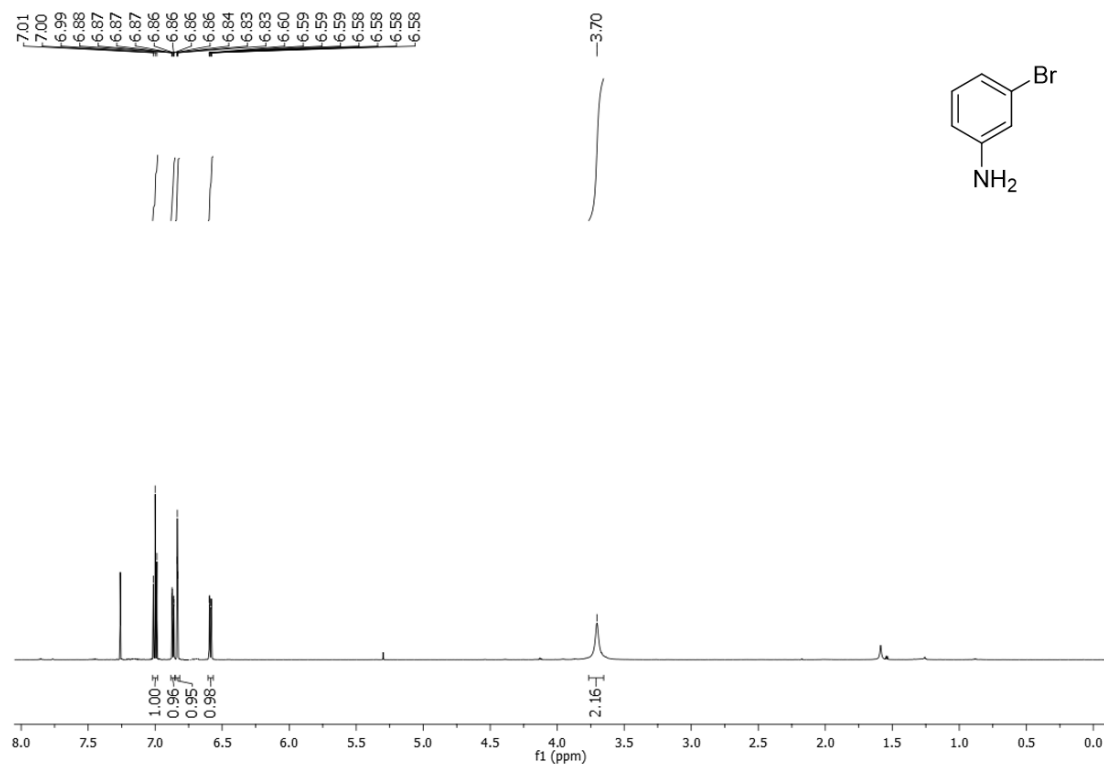


¹H NMR (600 MHz, CDCl₃) of m-toluidine (Table 23, Entry 16).

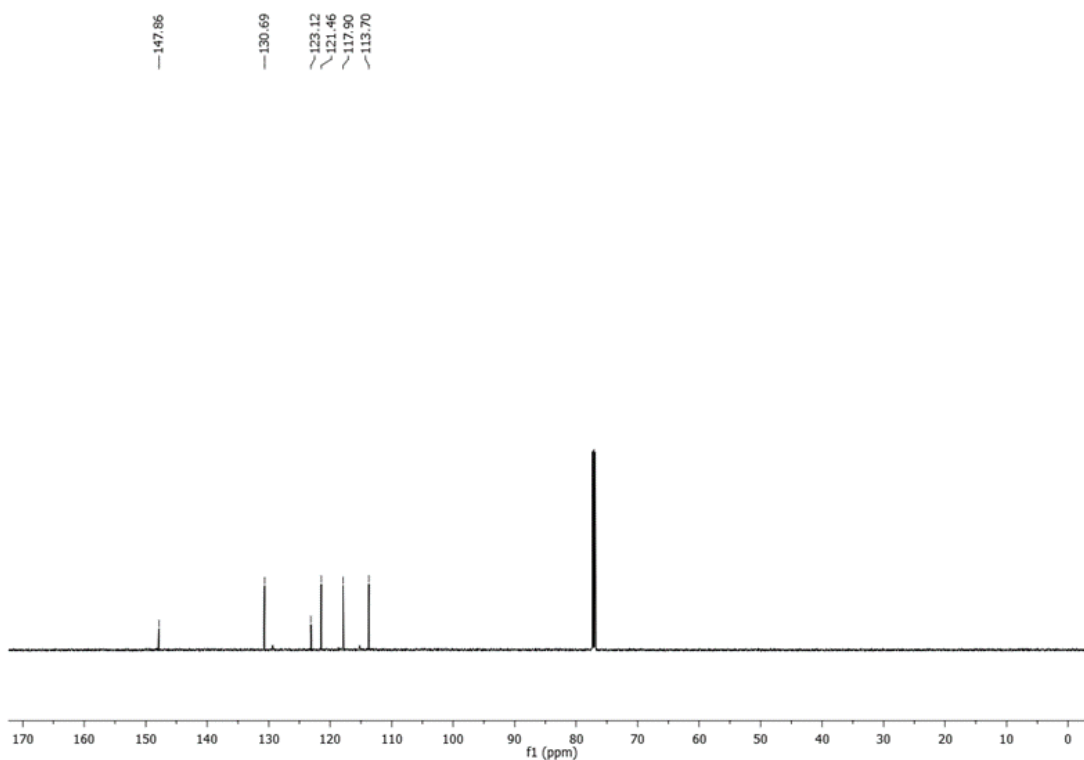


¹³C-NMR (151 MHz, CDCl₃) of m-toluidine (Table 23, Entry 16).

3-bromoaniline (2.2v)⁴⁴⁷: ¹H NMR (600 MHz, CDCl₃) δ 7.00 (t, *J* = 8.0 Hz, 1H), 6.87 (ddd, *J* = 7.9, 1.8, 0.9 Hz, 1H), 6.83 (t, *J* = 2.1 Hz, 1H), 6.59 (ddd, *J* = 8.1, 2.2, 0.9 Hz, 1H), 3.70 (s, 2H) ppm; ¹³C NMR (151 MHz, CDCl₃) δ 147.86, 130.69, 123.12, 121.46, 117.90, 113.70 ppm.

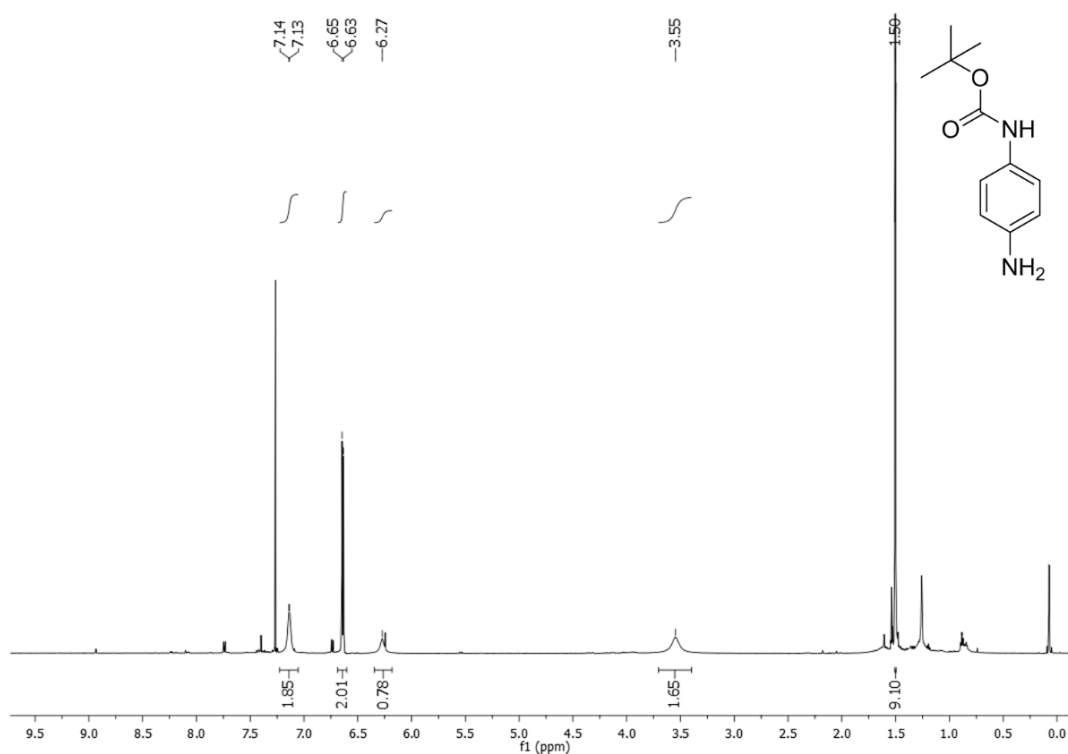


¹H NMR (600 MHz, CDCl₃) of 3-bromoaniline (Table 23, Entry 17).

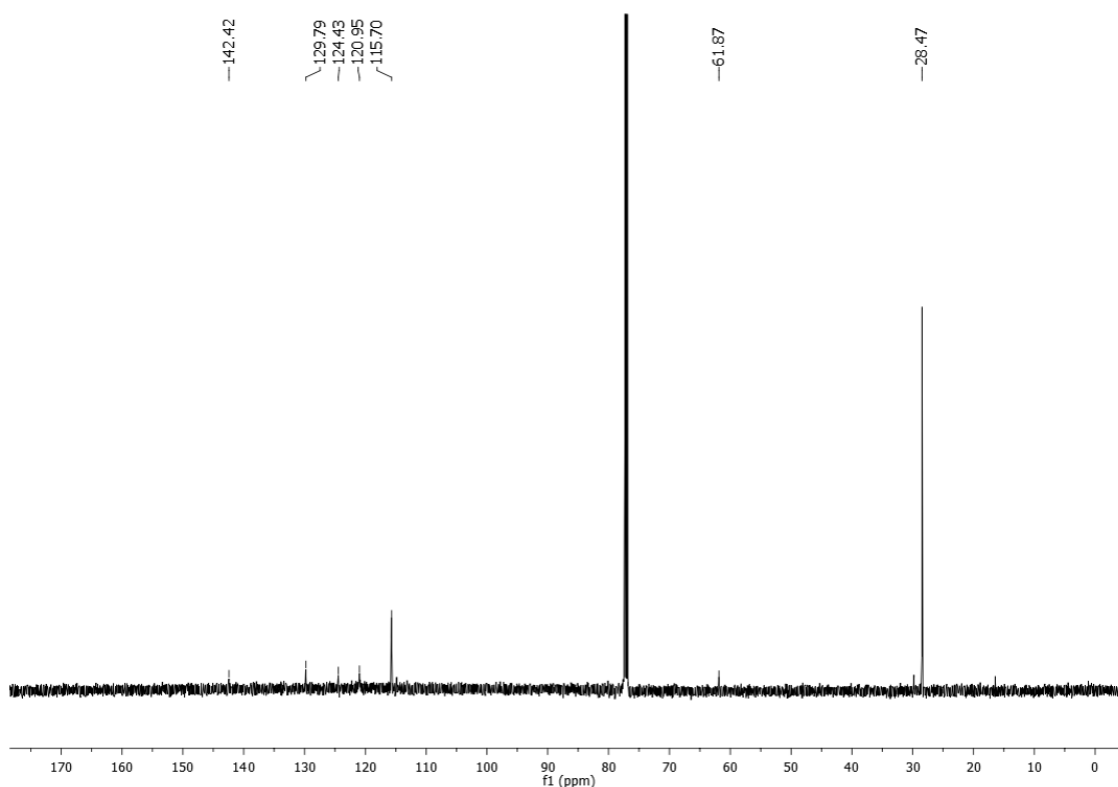


¹³C-NMR (151 MHz, CDCl₃) of 3-bromoaniline (Table 23, Entry 17).

Tert-butyl (4-hydroxyphenyl)carbamate (2.2w)⁴⁵⁶: ¹H NMR (600 MHz, CDCl₃) δ 7.14 (d, *J* = 3.9 Hz, 2H), 6.64 (d, *J* = 8.7 Hz, 2H), 6.27 (s, 1H), 3.55 (s, 2H), 1.50 (s, 9H).ppm; ¹³C NMR (151 MHz, CDCl₃) ppm.



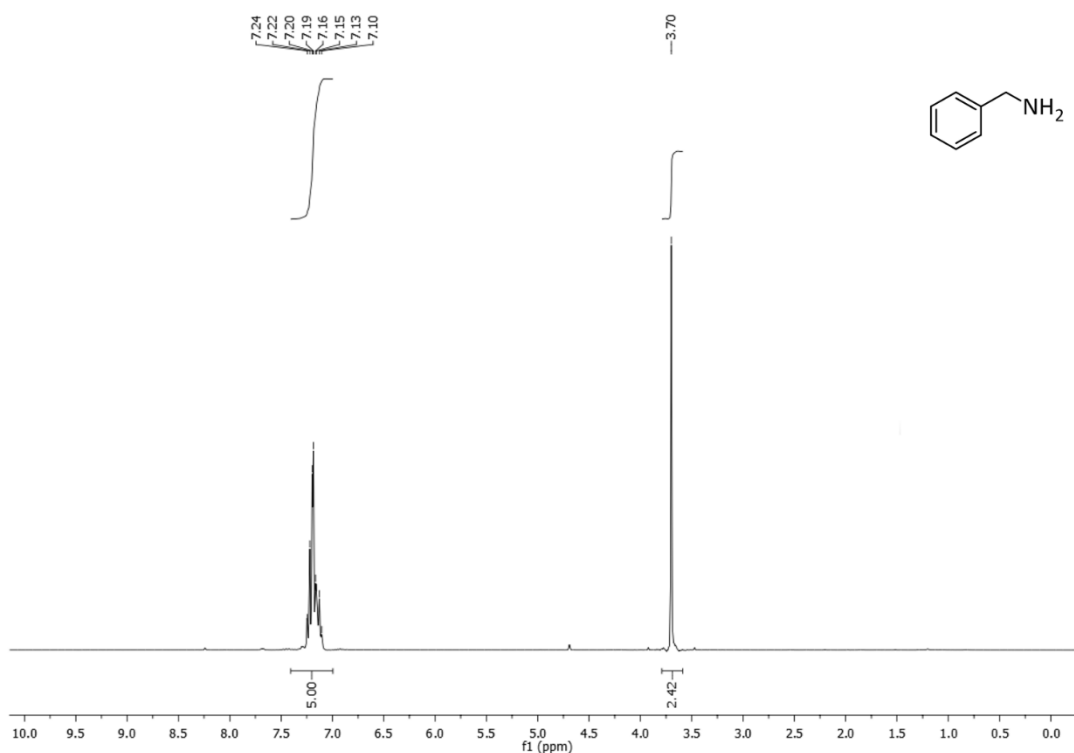
¹H NMR (600 MHz, CDCl₃) of Tert-butyl (4-hydroxyphenyl)carbamate (Table 23, Entry 18).



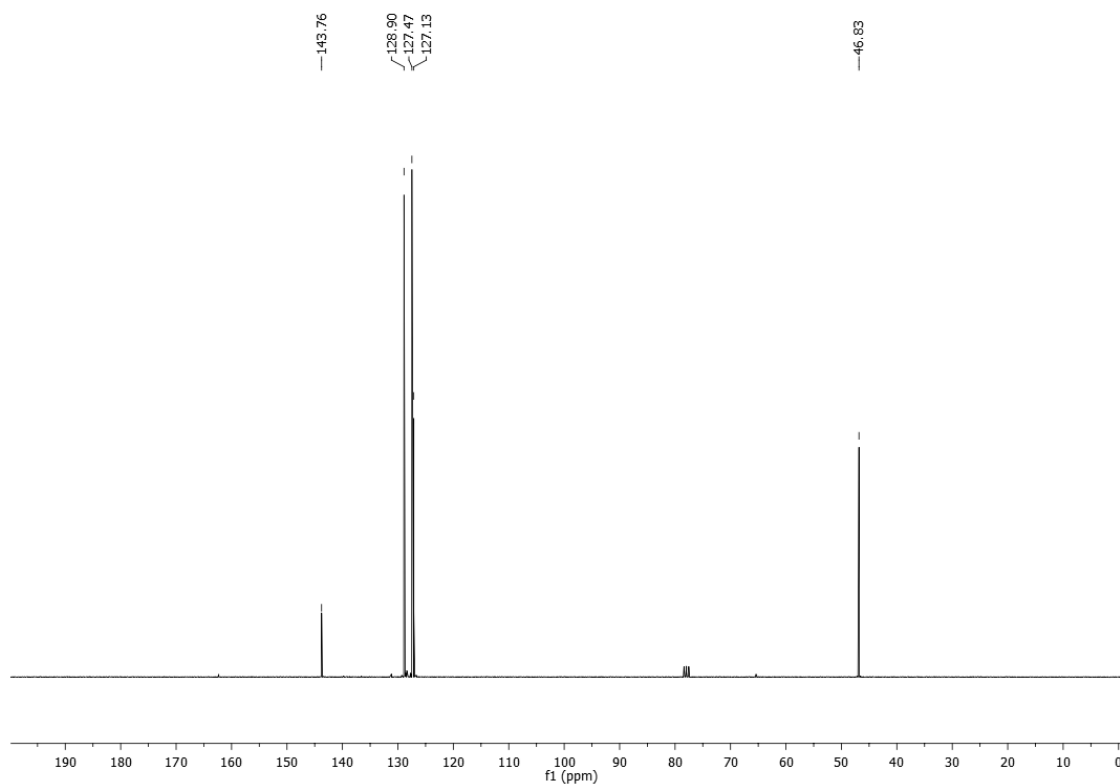
¹³C-NMR (151 MHz, CDCl₃) of Tert-butyl (4-hydroxyphenyl)carbamate (Table 23, Entry 18).

S-2. NMR Alkyl amines derivatives

Benzylamine (2.15a)⁴⁵⁷: ¹H NMR (300 MHz, CDCl₃) δ 7.24-7.10 (5H, m), 3.70 (2H, s) ppm;
¹³C NMR (75 MHz, CDCl₃) δ 143.16, 128.29, 126.87, 126.53, 46.23.

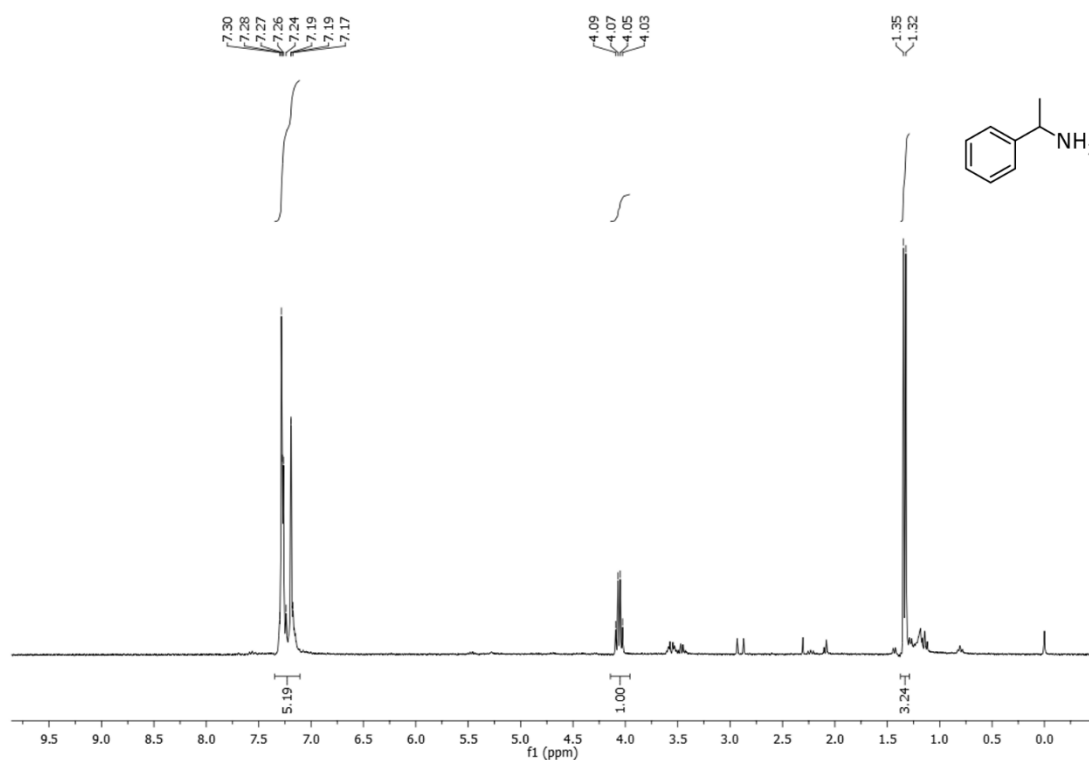


¹H NMR (300 MHz, CDCl₃) of Benzylamine (Table 12, Entry 1)

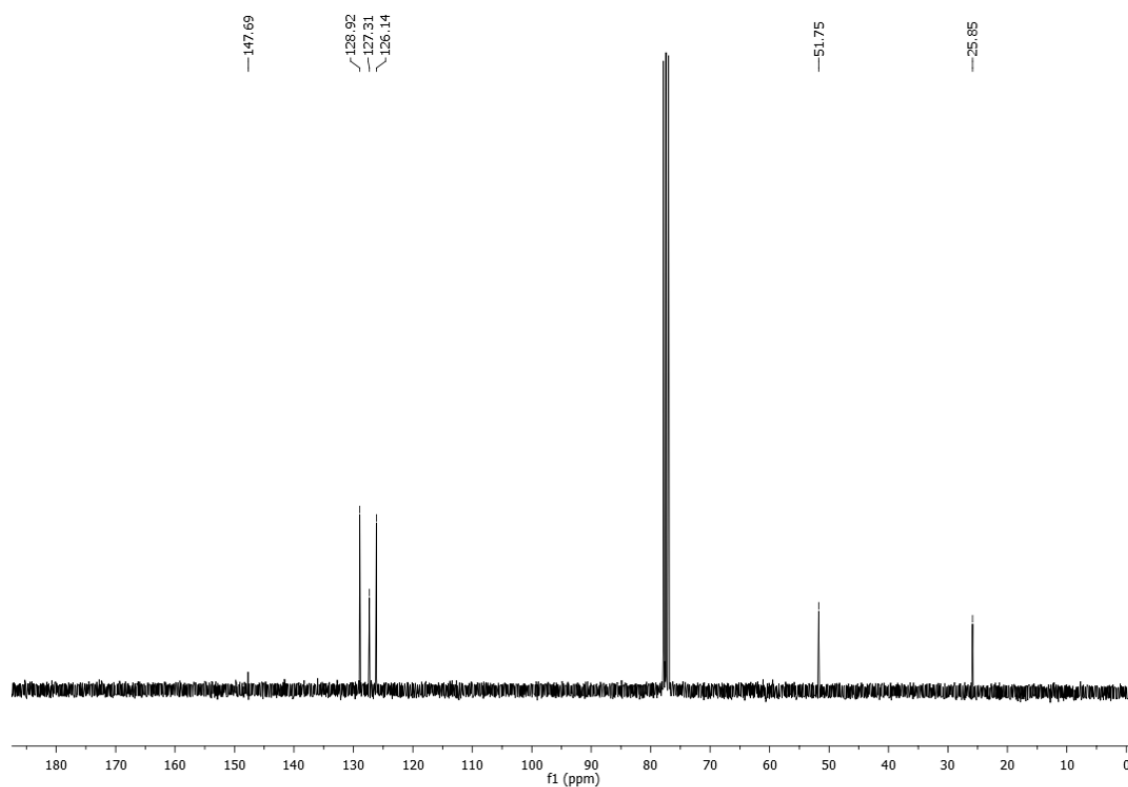


¹³C-NMR (75 MHz, CDCl₃) of Benzylamine (Table 12, Entry 1).

1-Phenylethylamine (2.15b)⁴⁵⁸: ¹H NMR (300 MHz, CDCl₃) δ 7.37-7.24 (5H, m), 4.13 (1H, q, J = 6 Hz), 1.40 (3H, d, J = 9 Hz) ppm; ¹³C NMR (75 MHz, CDCl₃) δ 147.69, 128.92, 127.31, 126.1, 51.75, 25.85 ppm.

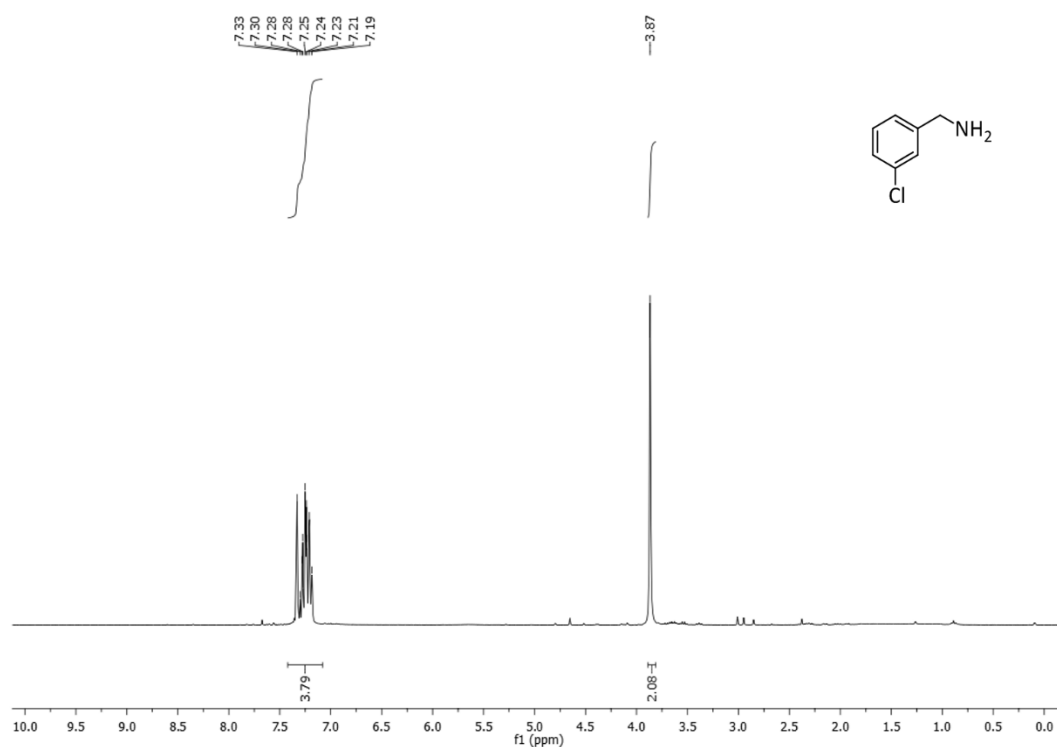


¹H NMR (300 MHz, CDCl₃) of 1-Phenylethylamine (Table 12, Entry 2).

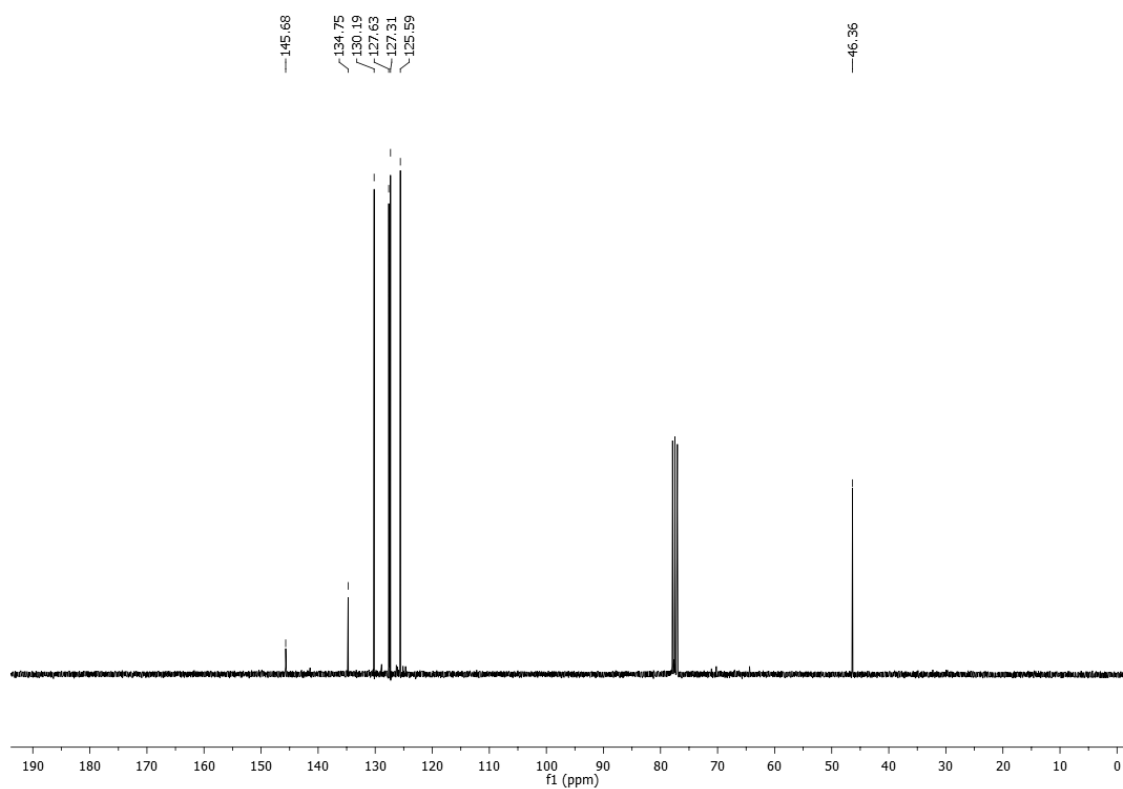


¹³C-NMR (75 MHz, CDCl₃) of 1-Phenylethylamine (Table 12, Entry 1).

3-Chlorobenzylamine (2.15c)⁴⁵⁹: ¹H NMR (300 MHz, CDCl₃) δ 7.33-7.30 (1H, m), 7.28- 7.19 (3H, m), 3.87 (2H, s) ppm; ¹³C NMR (75 MHz, CDCl₃) δ 145.57, 134.64, 130.08, 127.52, 127.20, 125.48, 77.36, 46.25 ppm.

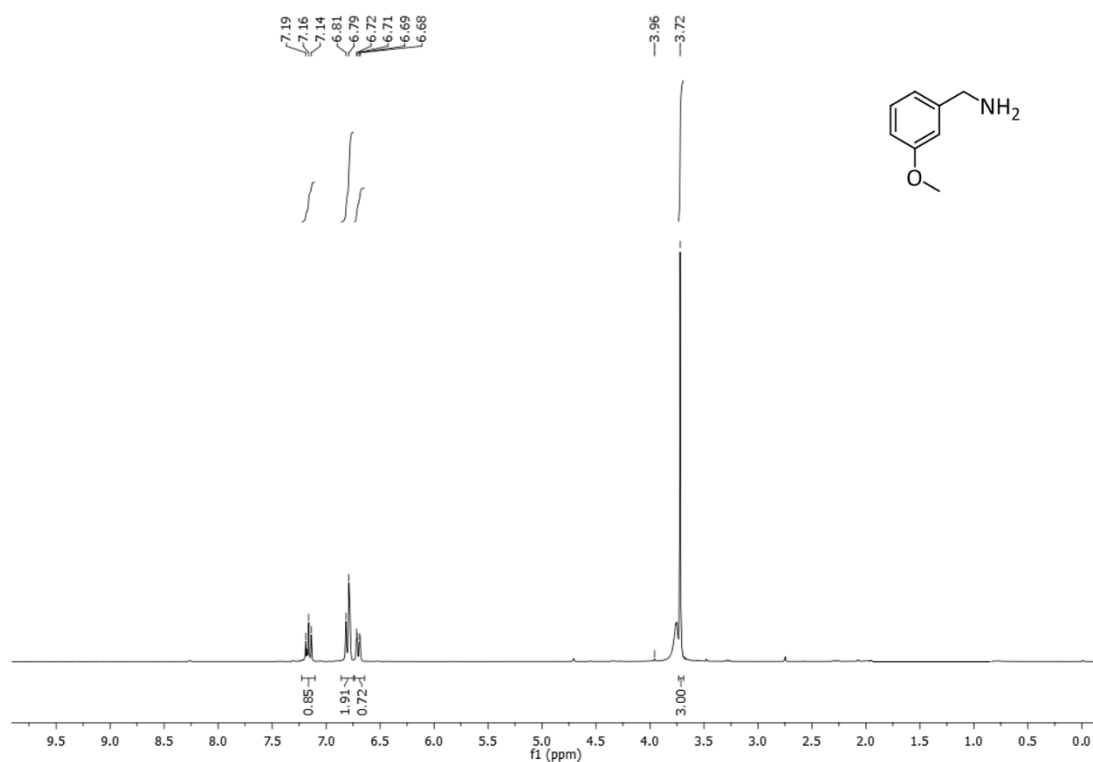


¹H NMR (300 MHz, CDCl₃) of 3-Chlorobenzylamine (Table 12, Entry 3).

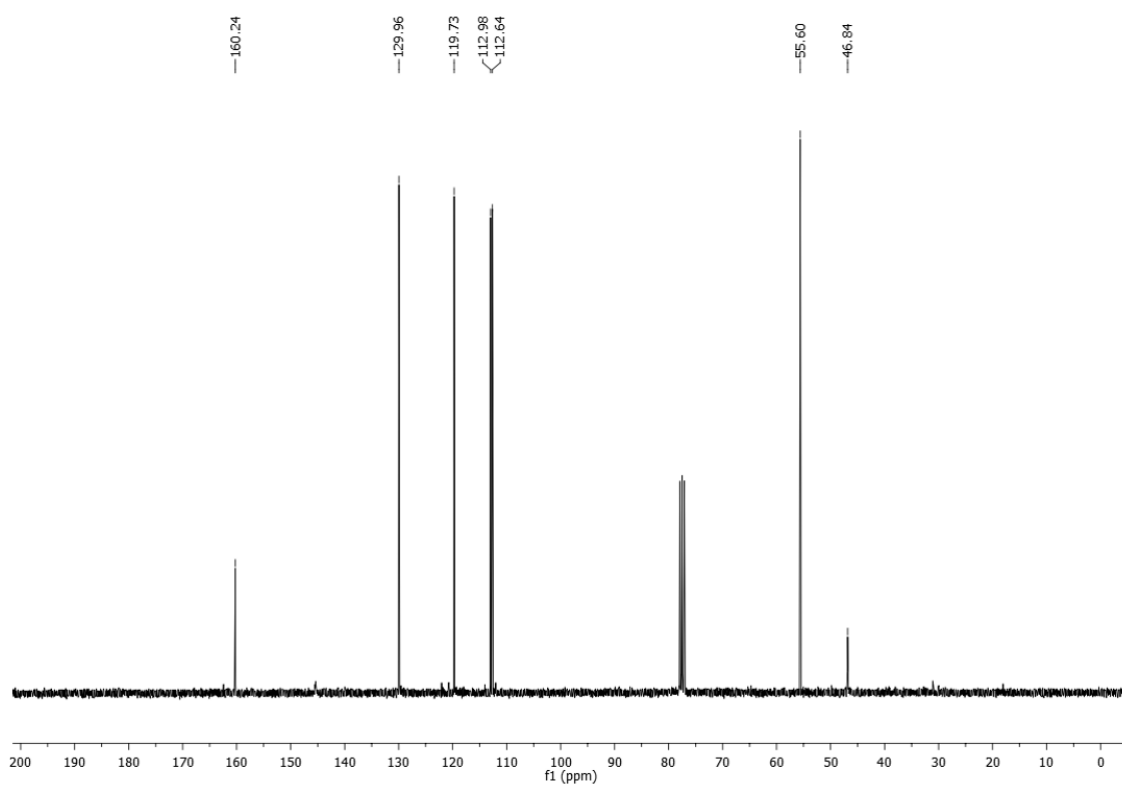


¹³C-NMR (75 MHz, CDCl₃) of 3-Chlorobenzylamine (Table 12, Entry 3).

3-Methoxybenzylamine (2.15e)⁴⁶⁰: ¹H NMR (300 MHz, CDCl₃) δ 7.16 (1H, t, J = 6 Hz), 6.81-6.79 (2H, m), 6.72- 6.68 (1H, m), 3.96 (2H, s), 3.72 (3H, s) ppm; ¹³C NMR (75 MHz, CDCl₃) δ 160.24, 129.96, 119.73, 112.98, 112.64, 55.60, 46.84 ppm.

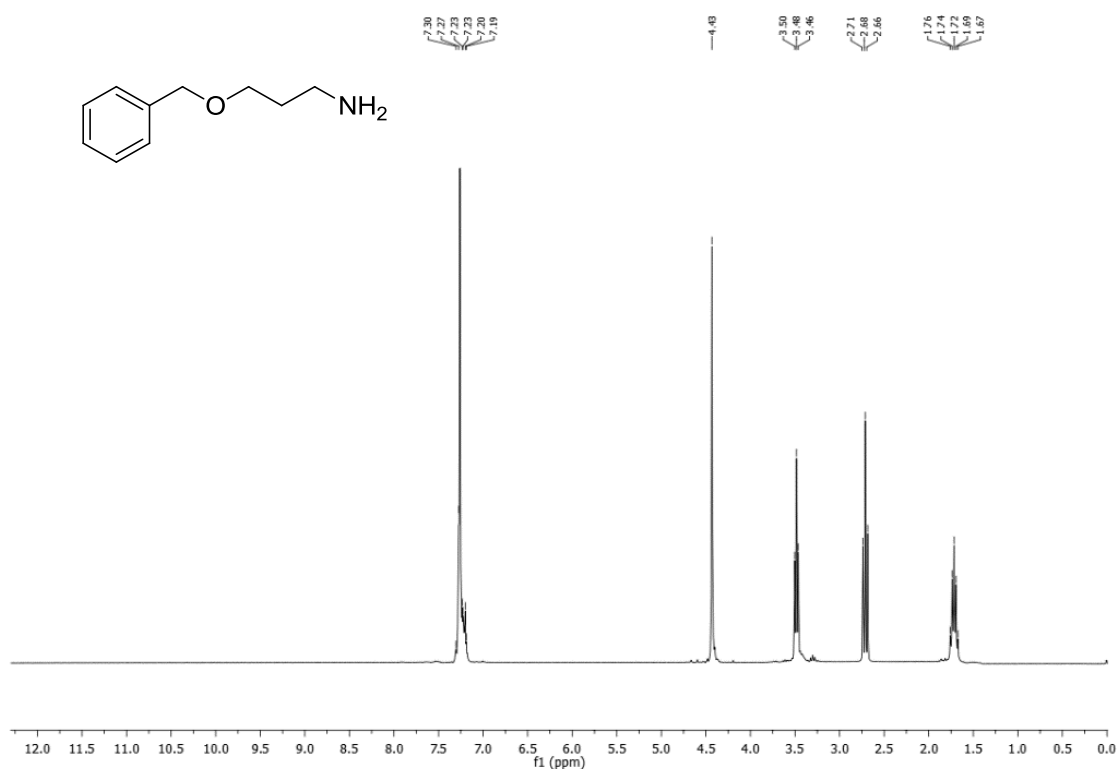


¹H NMR (300 MHz, CDCl₃) of 3-Methoxybenzylamine (Table 12, Entry 5)

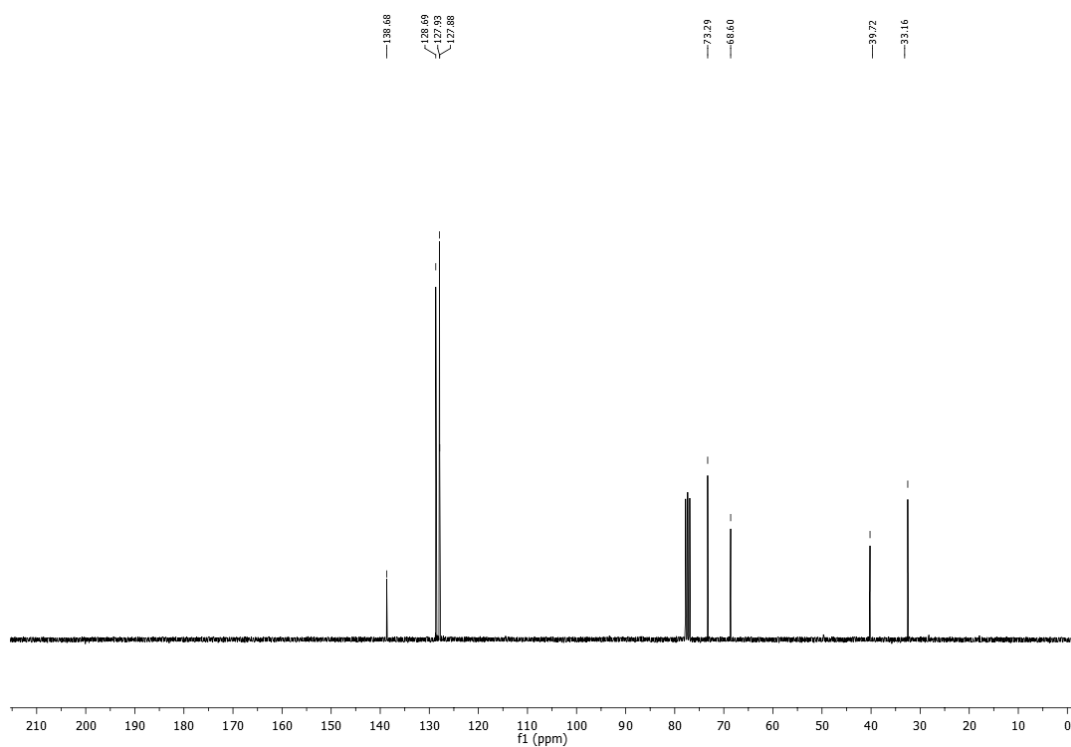


¹³C-NMR (75 MHz, CDCl₃) of 3-Methoxybenzylamine (Table 12, Entry 5).

3-Benzyloxypropylamine (2.15f)⁴⁶¹: ¹H NMR (300 MHz, CDCl₃) δ 7.30-7.19 (5H, m), 4.43 (2H, s), 3.48 (2H, t, J = 6 Hz), 2.68 (2H, t, J = 6 Hz), 1.70 (2H, q, J = 6 Hz) ppm; ¹³C NMR (75 MHz, CDCl₃) δ 138.68, 128.69, 127.93, 127.88, 73.29, 68.60, 39.72, 33.16.

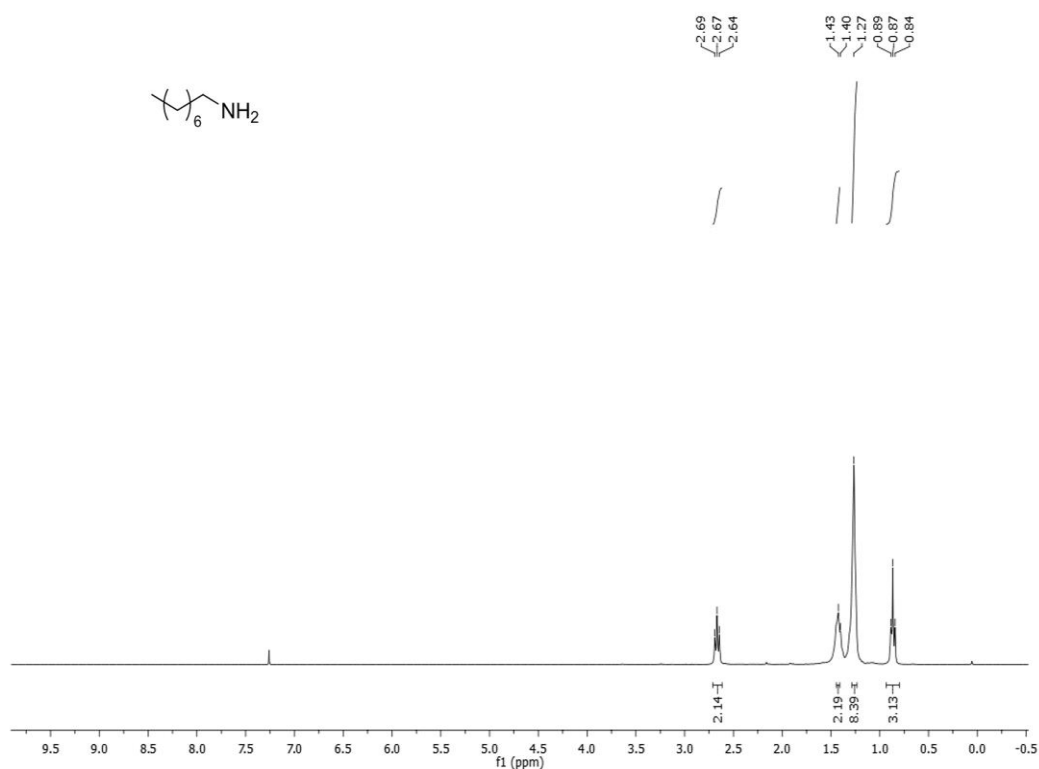


¹H NMR (300 MHz, CDCl₃) of 3-Benzyloxypropylamine (Table 12, Entry 6).

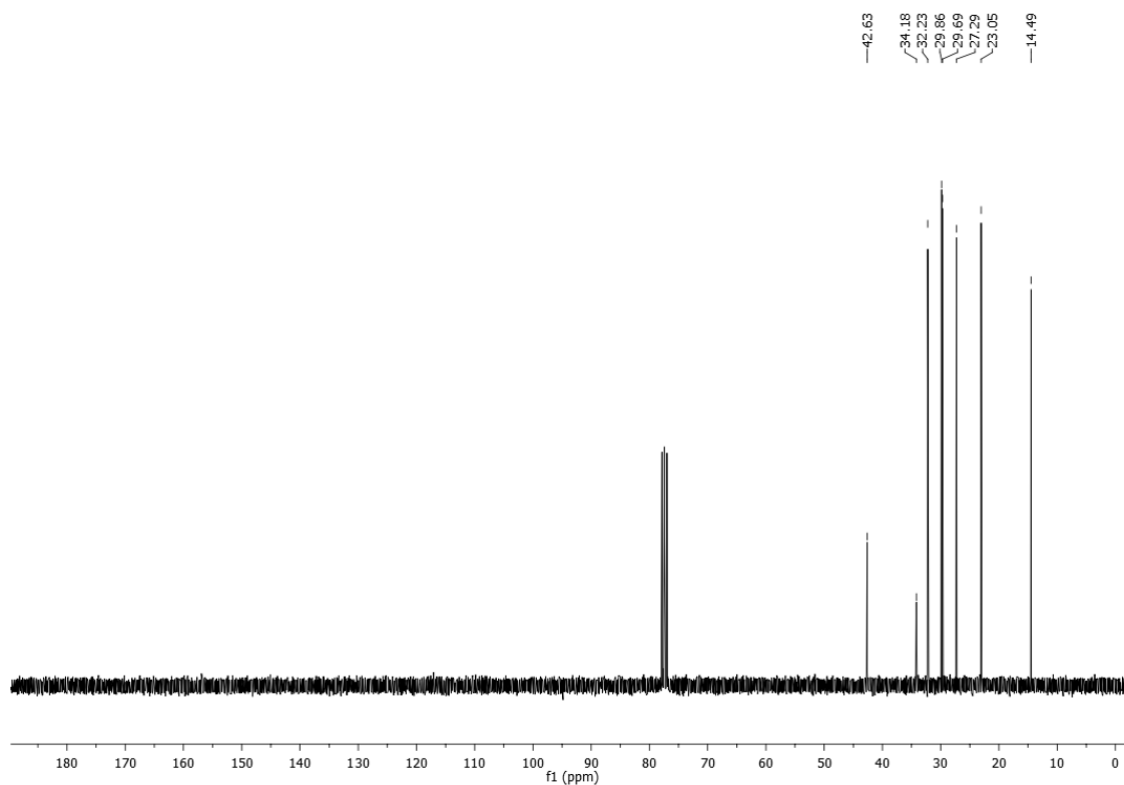


¹³C-NMR (75 MHz, CDCl₃) of 3-Benzyloxypropylamine (Table 12, Entry 6).

1-Octanamine (2.15g)⁴⁵⁹: ¹H NMR (300 MHz, CDCl₃) δ 2.67 (2H, t, J = 9Hz), 1.43-1.40 (2H, m), 1.27 (10H, m), 0.87 (3H, t, J = 6 Hz) ppm; ¹³C NMR (75 MHz, CDCl₃) δ 42.63, 34.18, 32.23, 29.86, 29.69, 27.29, 23.05, 14.49 ppm.

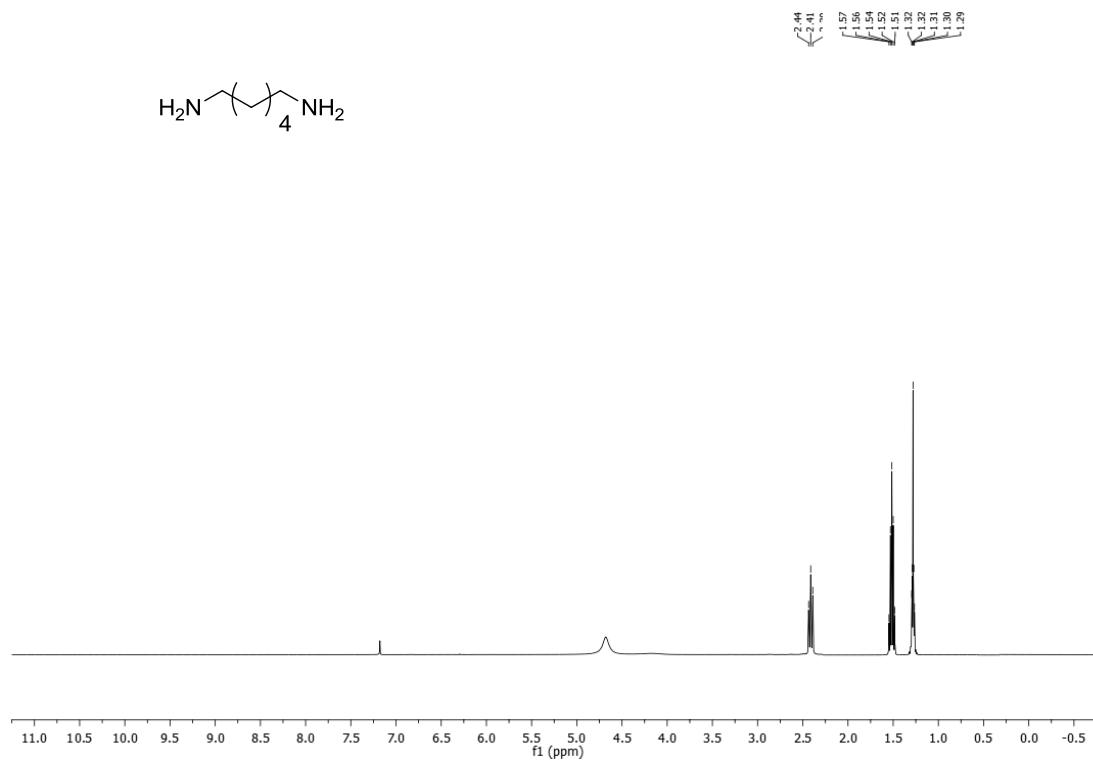


¹H NMR (300 MHz, CDCl₃) of 1-Octanamine (Table 12, Entry 7).

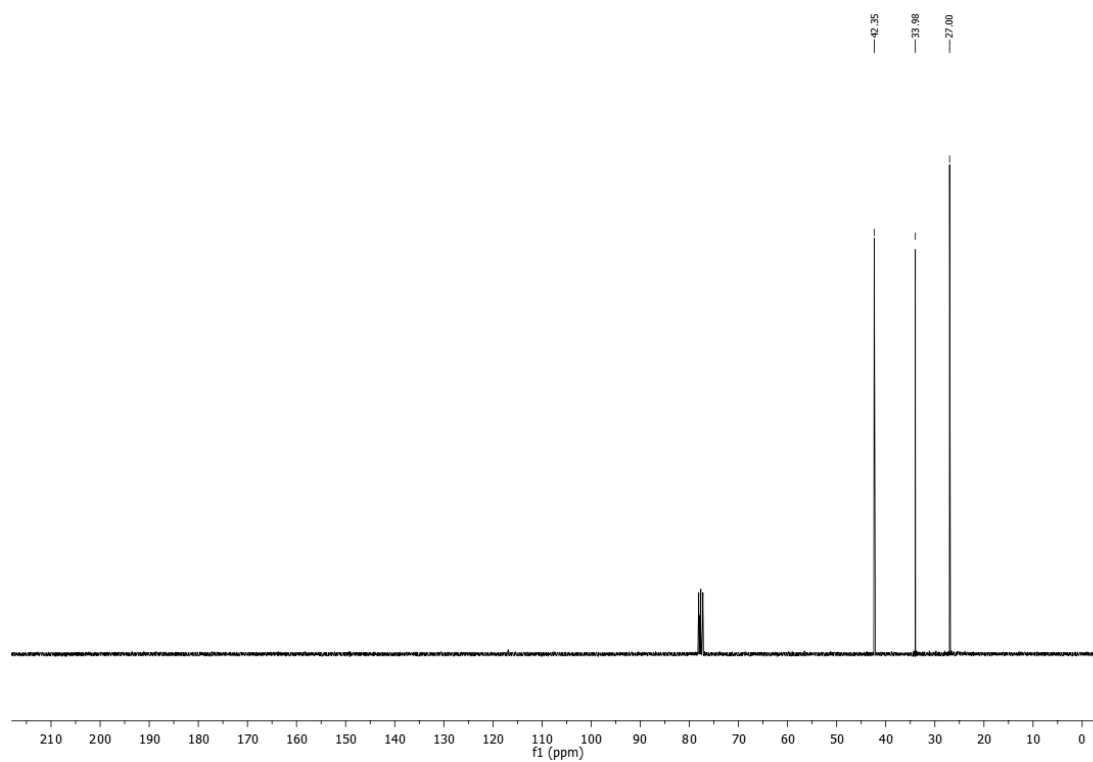


¹³C-NMR (75 MHz, CDCl₃) of 1-Octanamine (Table 12, Entry 7).

1,6-Diaminohexane (2.15h)⁴⁶²: ¹H NMR (300 MHz, CDCl₃) δ 2.41 (4H, t, J = 6 Hz), 1.54 (4H, q, J = 3 Hz), 1.31 (4H, q, J = 3 Hz) ppm; ¹³C NMR (75 MHz, CDCl₃) δ 42.35, 33.98, 27.00 ppm.

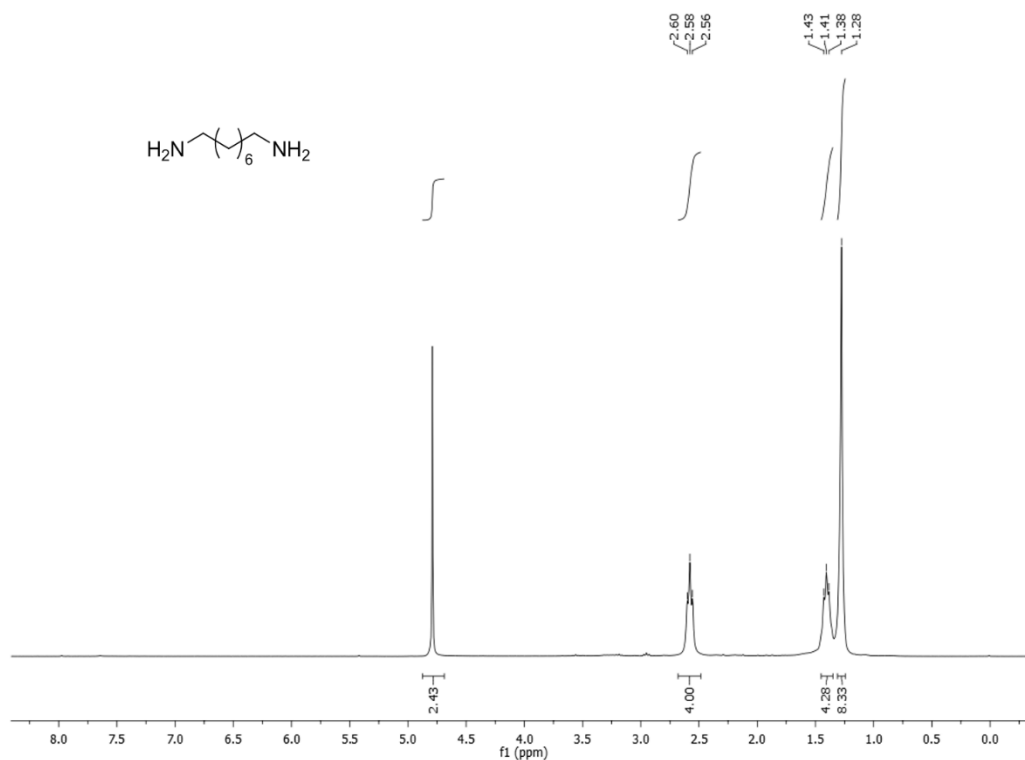


¹H NMR (300 MHz, CDCl₃) of 1,6-Diaminohexane (Table 12, Entry 8).

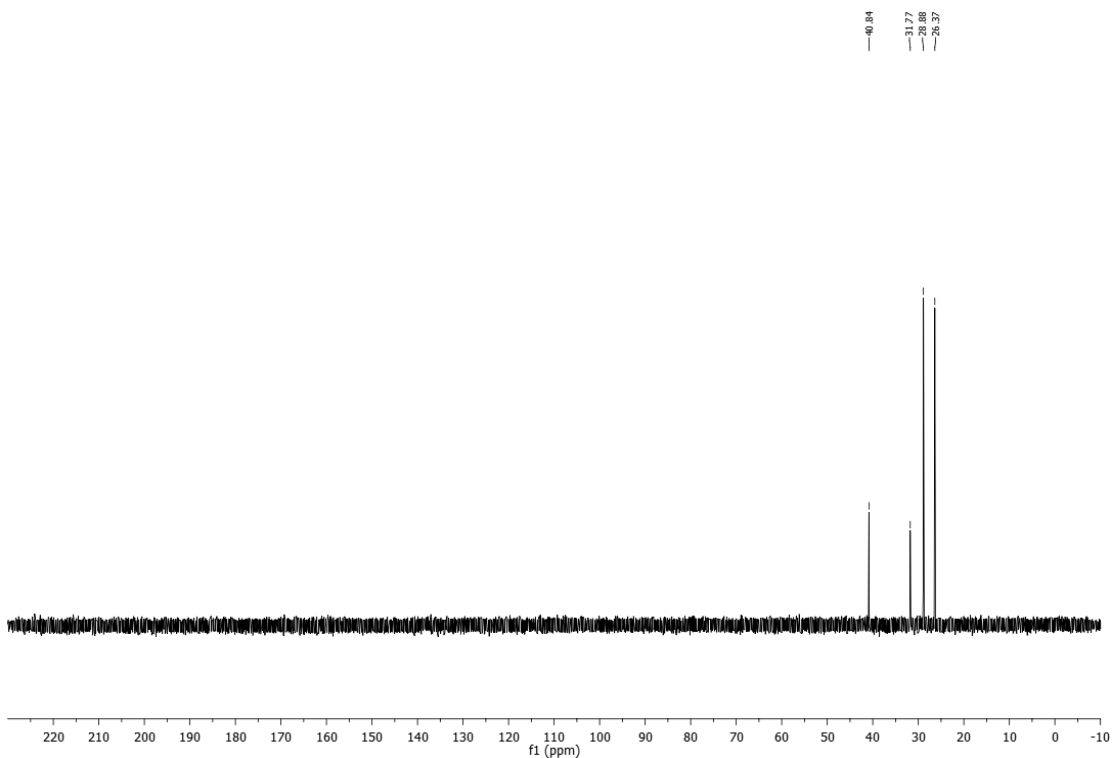


¹³C-NMR (75 MHz, CDCl₃) of 1,6-Diaminohexane (Table 12, Entry 8).

1,8-Diaminooctane (2.15i)⁴⁶³: ¹H NMR (300 MHz, D₂O) δ 2.58 (4H, t, J = 6 Hz), 1.43- 1.38 (4H, m), 1.28 (8H, m) ppm; ¹³C NMR (75 MHz, D₂O) δ 40.84, 31.77, 28.88, 26.37 ppm.

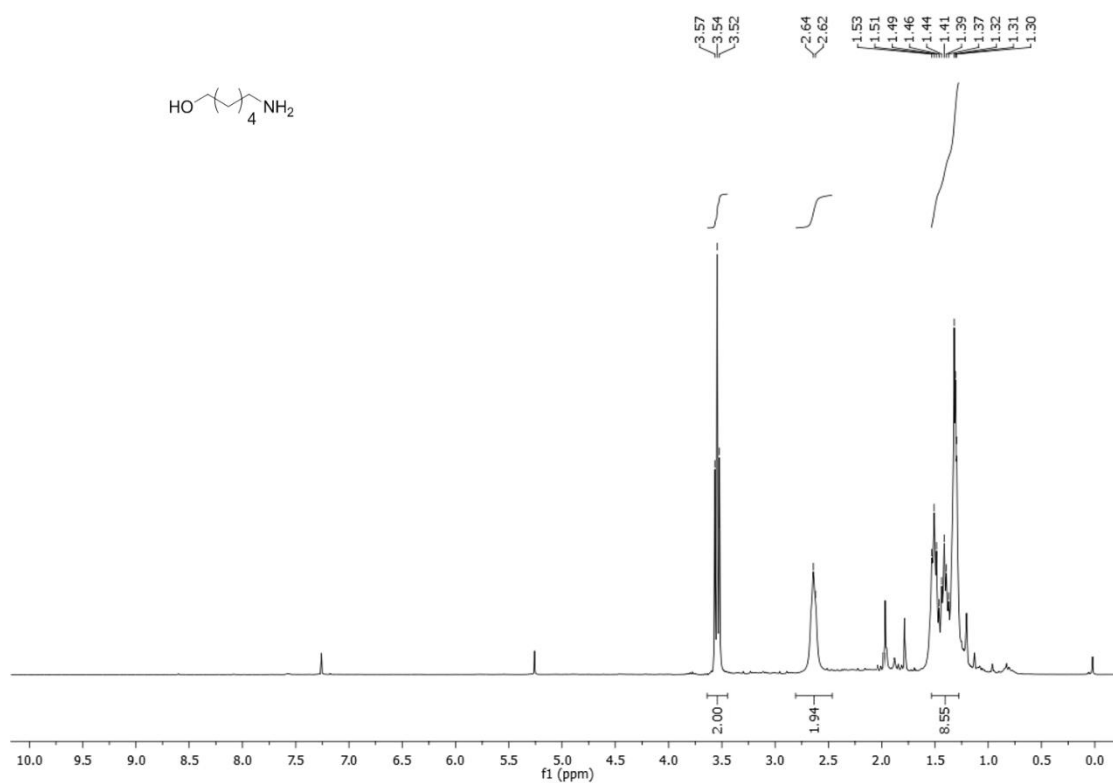


¹H NMR (300 MHz, D₂O) of 1,8-Diaminooctane (Table 12, Entry 9).

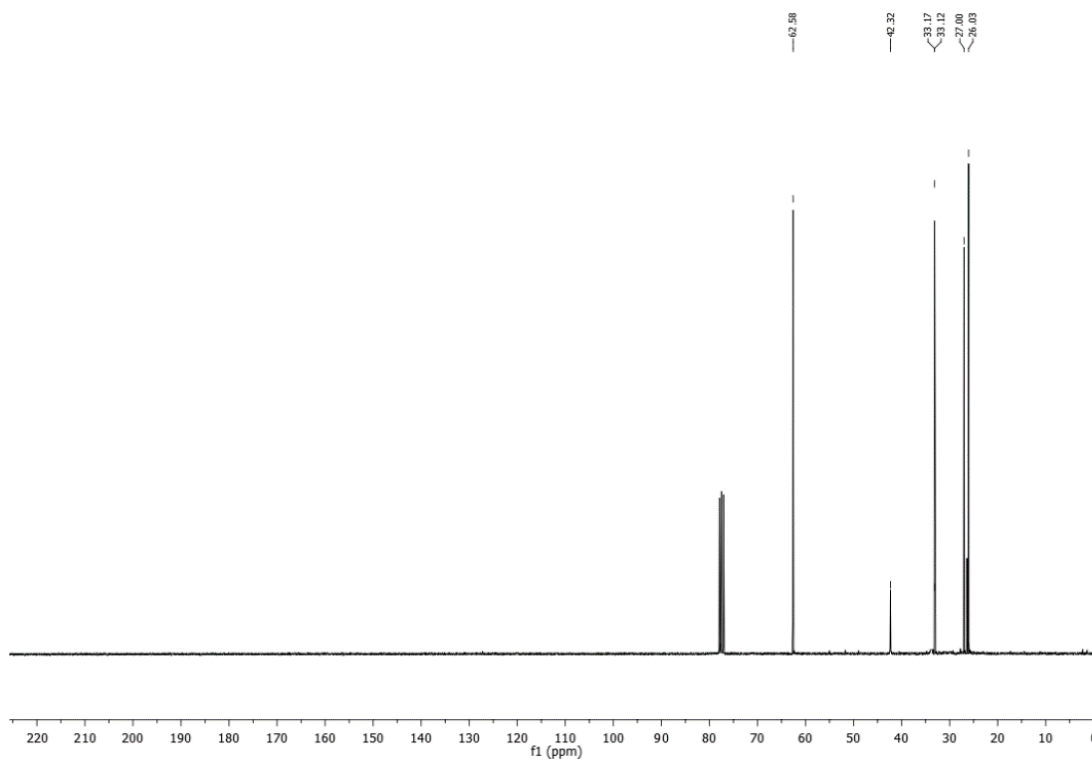


¹³C-NMR (75 MHz, D₂O) of 1,8-Diaminooctane (Table 12, Entry 9).

6-Amino-1-hexanol (2.15j)⁴⁶⁴: ¹H NMR (300 MHz, CDCl₃) δ 3.54 (2H, t, J = 6 Hz), 2.68 (2H, t, J = 6 Hz), 1.53-1.30 (8H, m) ppm; ¹³C NMR (75 MHz, CDCl₃) δ 62.58, 42.32, 33.17, 33.12, 27.00, 26.03 ppm.

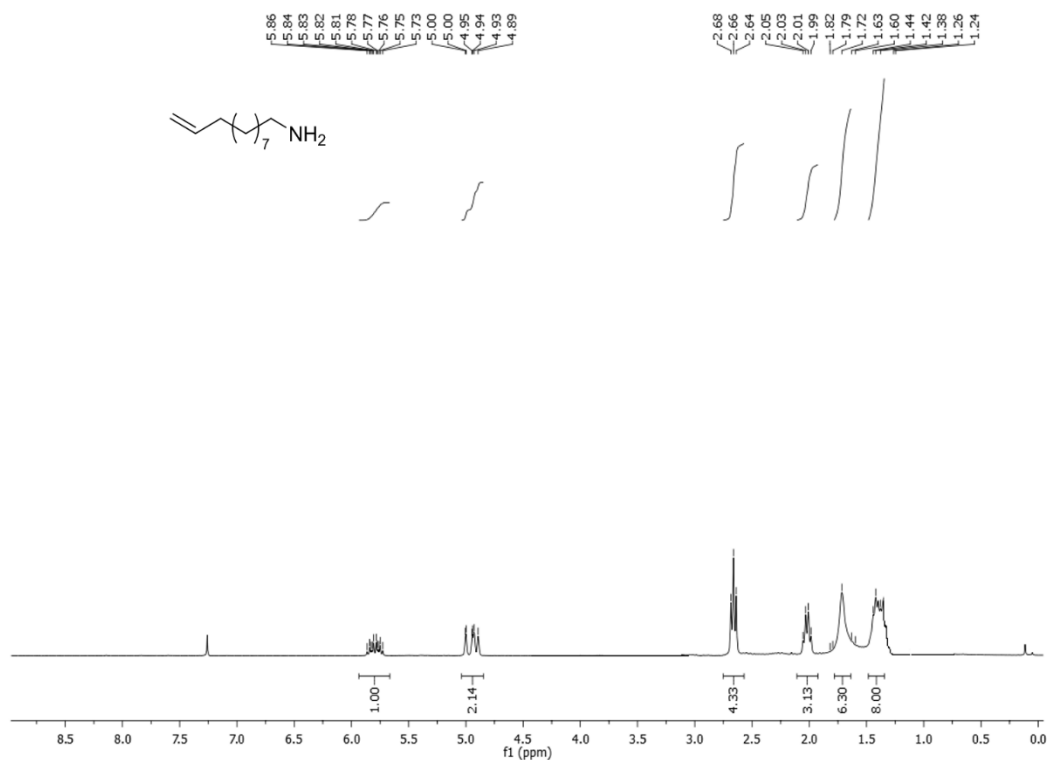


¹H NMR (300 MHz, CDCl₃) of 6-Amino-1-hexanol (Table 12, Entry 10).

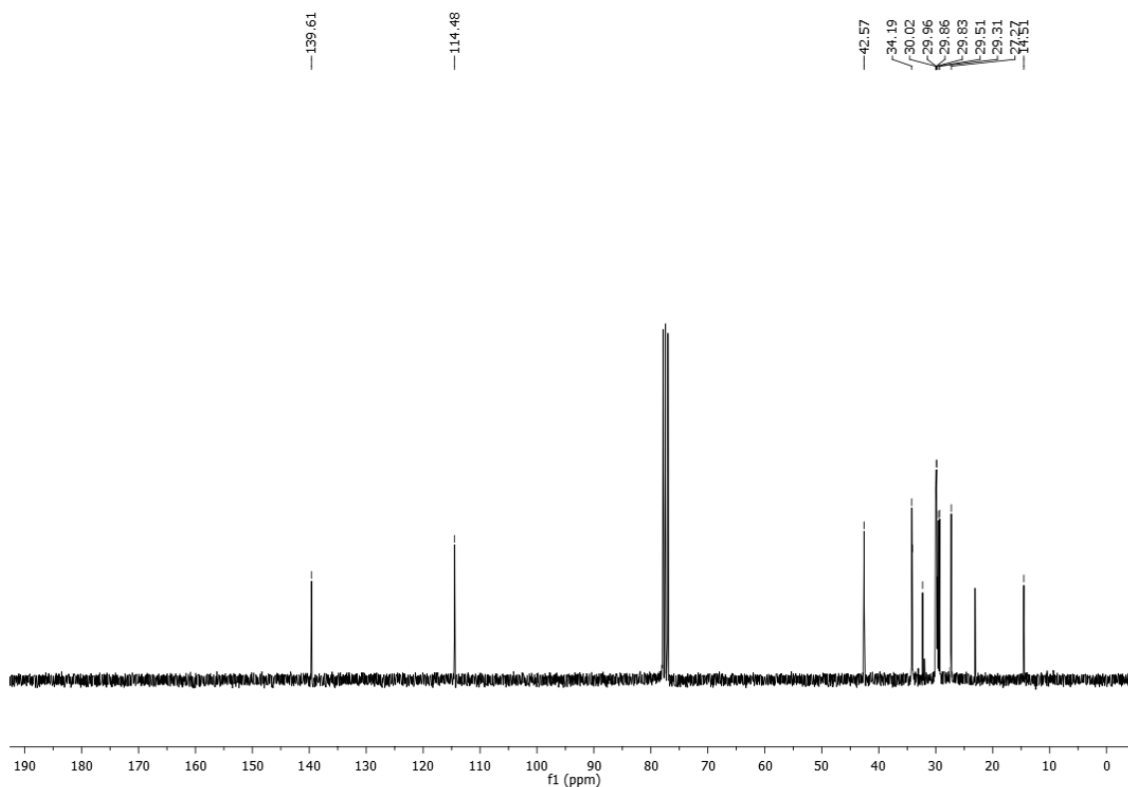


¹³C-NMR (75 MHz, CDCl₃) of 6-Amino-1-hexanol (Table 12, Entry 10).

10-Undecen-1-amine (2.15k)⁴⁶⁵: ¹H NMR (300 MHz, CDCl₃) δ 5.86- 5.73 (1H, m), 5.00-4.89 (2H, m), 2.66 (2H, t, J = 6Hz), 2.02 (2H, q, J = 6 Hz), 1.82- 1.60 (2H, m), 1.44-1.24 (12H, m) ppm; ¹³C NMR (75 MHz, CDCl₃) δ 139.54, 114.41, 42.50, 34.12, 32.23, 29.89, 29.44, 29.24, 27.20 ppm.



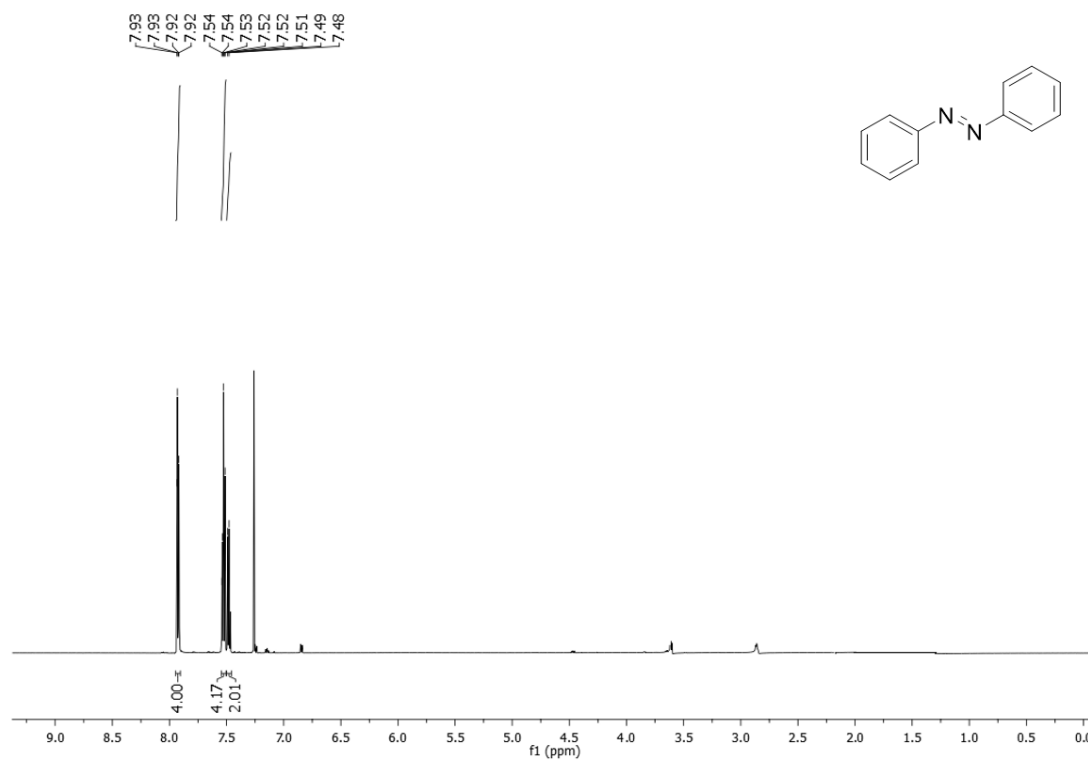
¹H NMR (300 MHz, CDCl₃) of 10-Undecen-1-amine (Table 12, Entry 11).



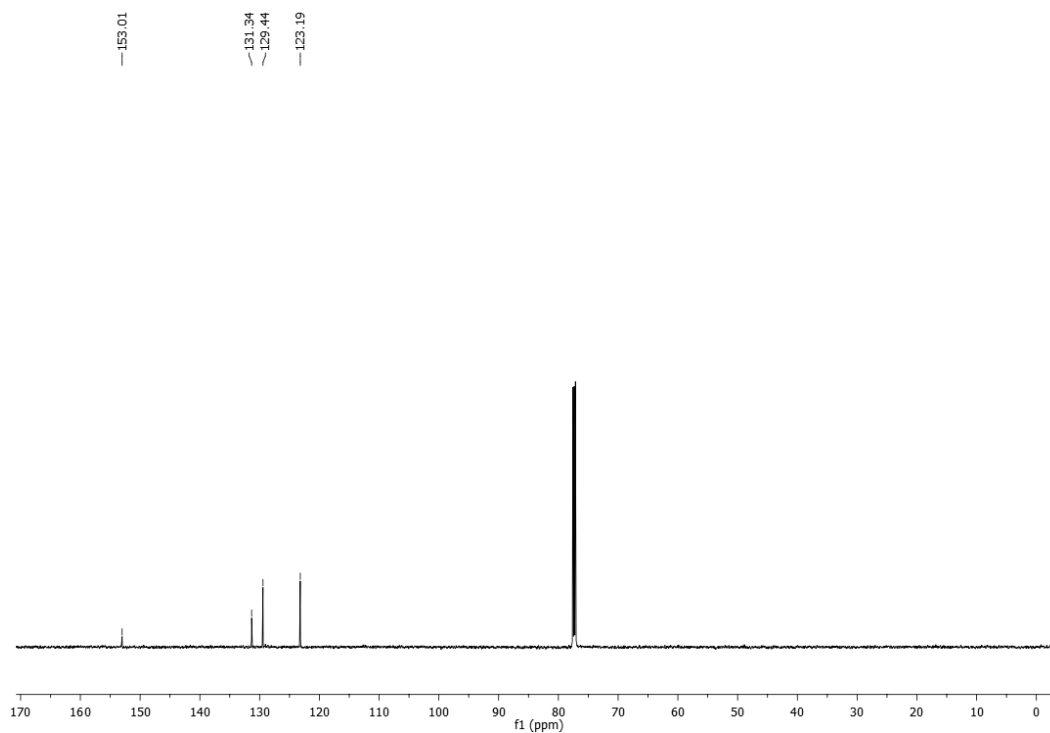
¹³C-NMR (75 MHz, CDCl₃) of 10-Undecen-1-amine (Table 12, Entry 11).

S-3. NMR Azo-derivatives

(E)-1,2-Diphenyldiazene (2.19a)¹⁶⁷: ¹H NMR (600 MHz, CDCl₃) δ 7.93 (dd, *J* = 8.4, 1.2 Hz, 4H), 7.55 – 7.50 (m, 4H), 7.48 (d, *J* = 7.2 Hz, 2H) ppm; ¹³C NMR (151 MHz, CDCl₃) δ 153.01, 131.34, 129.44, 123.19 ppm.

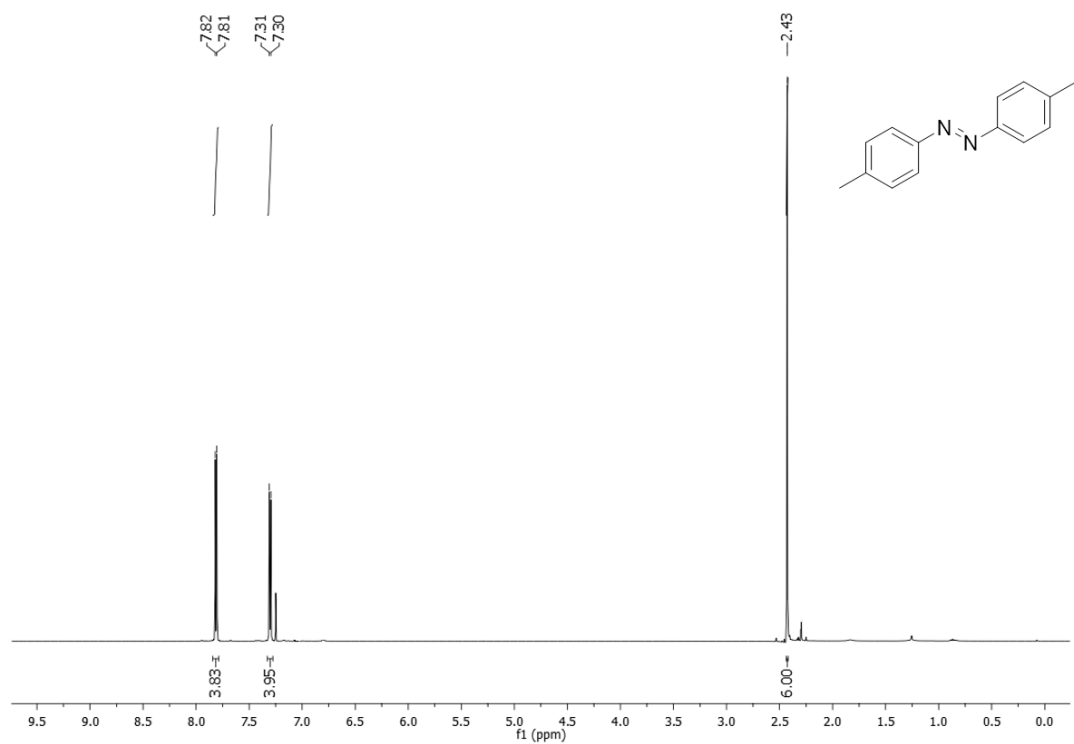


¹H NMR (600 MHz, CDCl₃) of (E)-1,2-diphenyldiazene (Table 24, Entry 1)

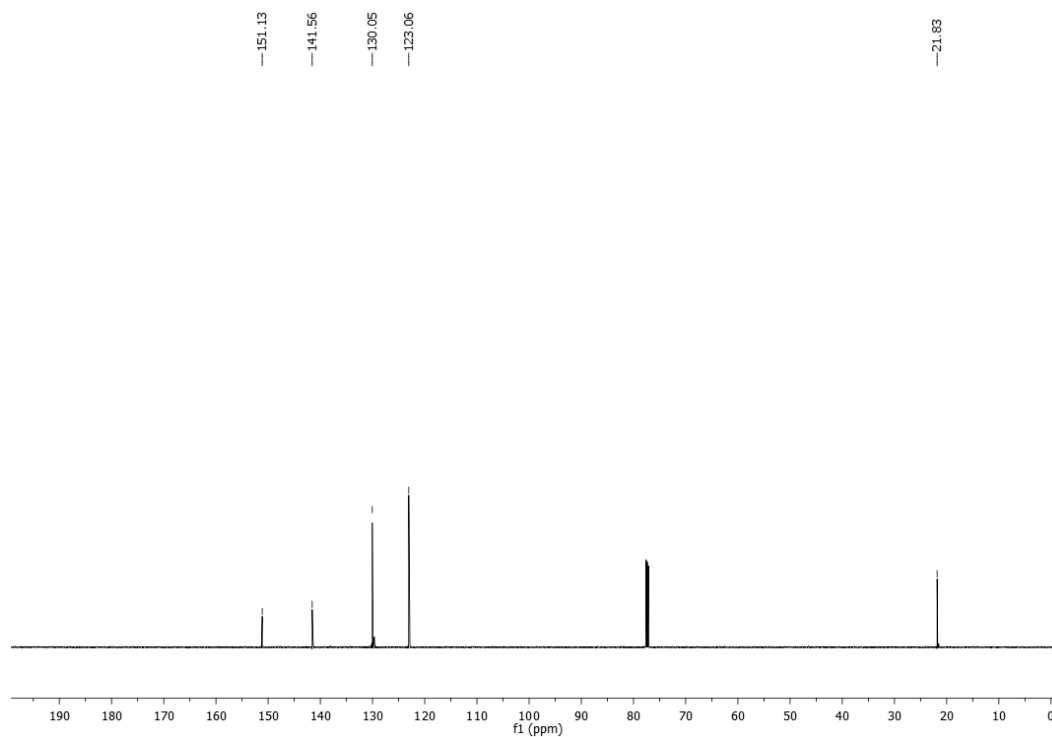


¹³C-NMR (151 MHz, CDCl₃) of (E)-1,2-diphenyldiazene (Table 24, Entry 1)

(E)-1,2-Di-*p*-tolylidiazene (2.19b)¹⁶⁷: ¹H NMR (600 MHz, CDCl₃) δ 7.81 (d, *J* = 8.3 Hz, 4H), 7.30 (d, *J* = 8.4 Hz, 4H), 2.43 (s, 6H) ppm; ¹³C NMR (151 MHz, CDCl₃) δ 151.13, 141.56, 130.05, 123.06, 21.83 ppm.

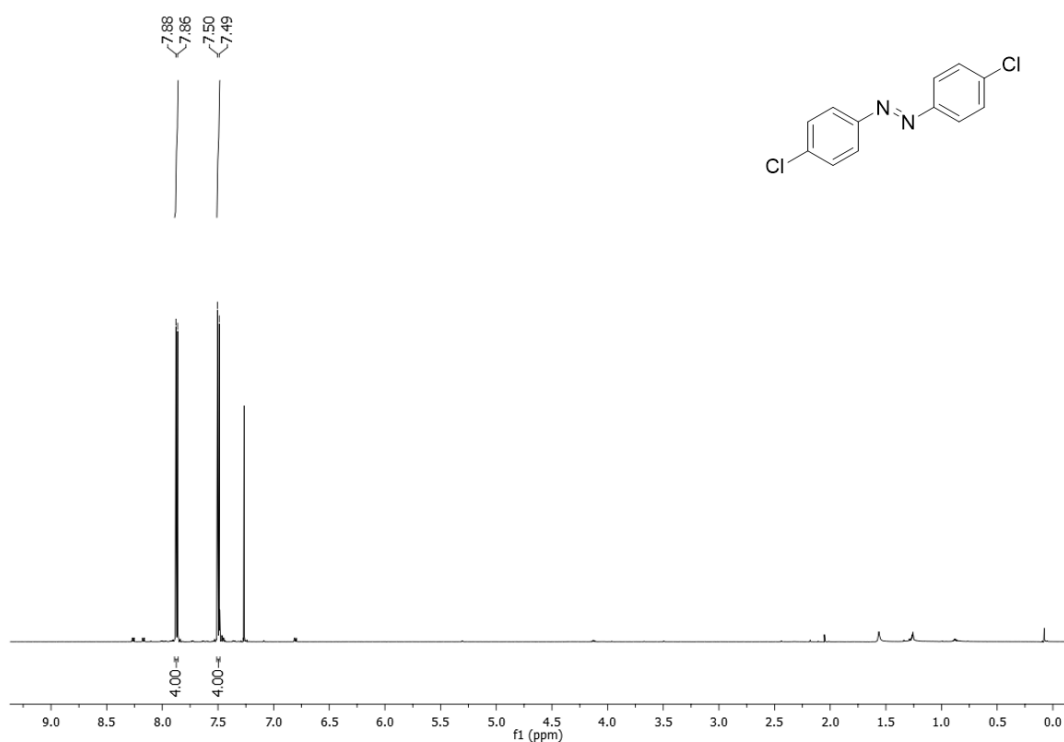


¹H NMR (600 MHz, CDCl₃) of (E)-1,2-di-*p*-tolylidiazene (Table 24, Entry 2)

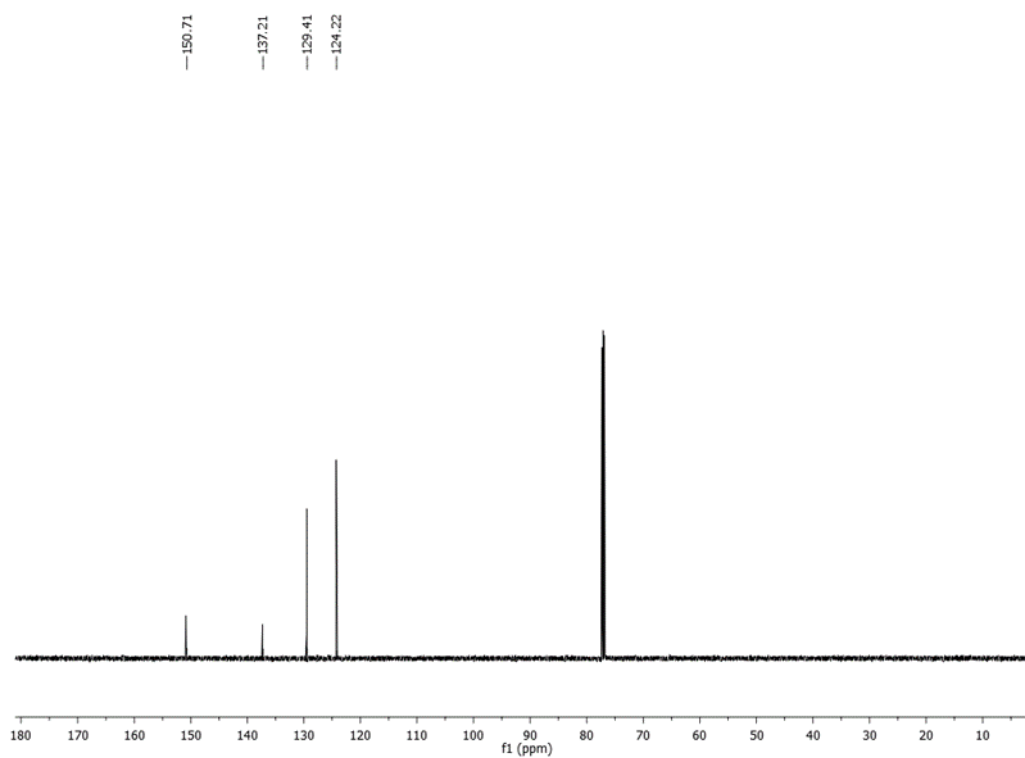


¹³C-NMR (151 MHz, CDCl₃) of (E)-1,2-di-*p*-tolylidiazene (Table 24, Entry 2)

(E)-1,2-bis(4-chlorophenyl)diazene (2.19c)¹⁶⁷: ¹H NMR (600 MHz, CDCl₃) δ 7.87 (d, *J* = 8.9 Hz, 4H), 7.50 (d, *J* = 8.9 Hz, 4H); ¹³C NMR (151 MHz, CDCl₃) δ 150.71, 137.21, 129.41, 124.22 ppm.

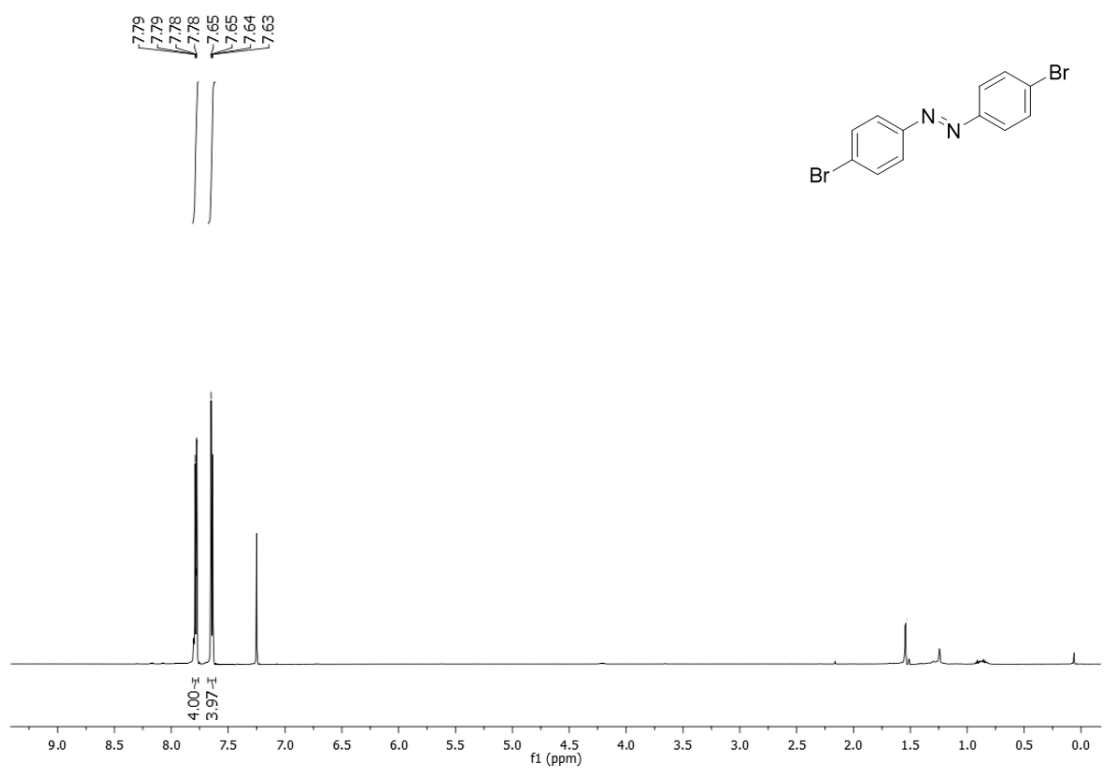


¹H NMR (600 MHz, CDCl₃) of (E)-1,2-bis(4-chlorophenyl)diazene (Table 24, Entry 4)

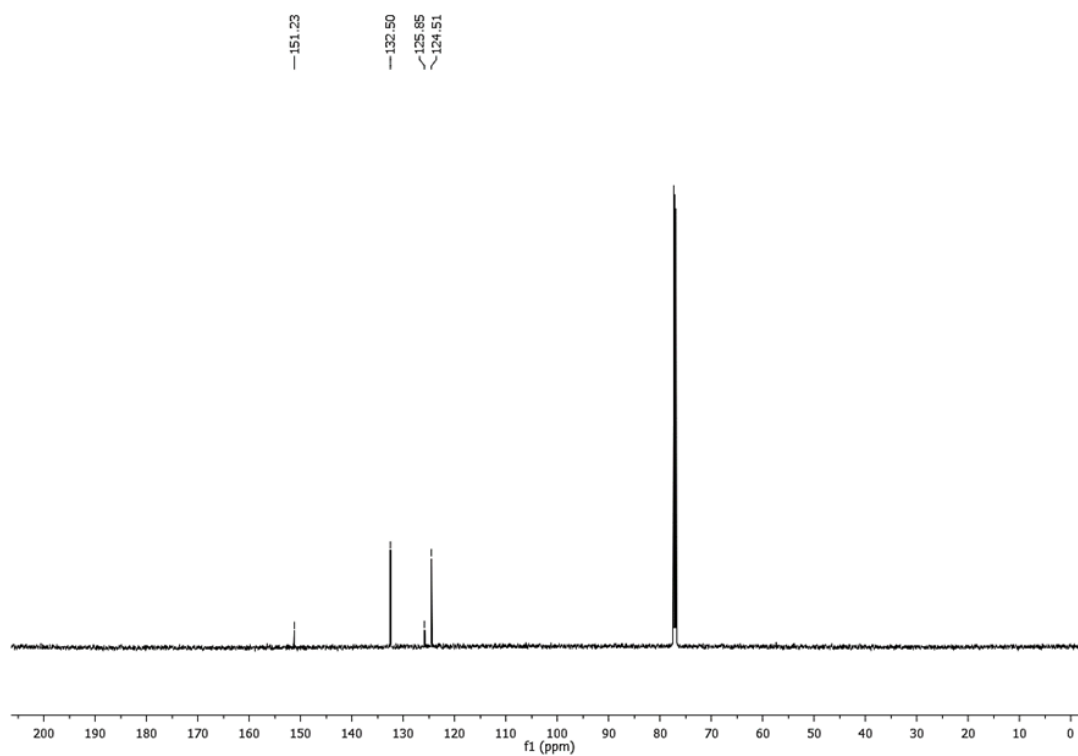


¹³C-NMR (151 MHz, CDCl₃) of (E)-1,2-bis(4-chlorophenyl)diazene (Table 24, Entry 3)

(E)-1,2-bis(4-bromophenyl)diazene (2.19d)¹⁶⁷: ¹H NMR (600 MHz, CDCl₃) δ 7.81 - 7.75 (m, 4H), 7.68 – 7.61 (m, 4H) ppm; ¹³C NMR (151 MHz, CDCl₃) δ 151.23, 132.50, 125.85, 124.51 ppm.

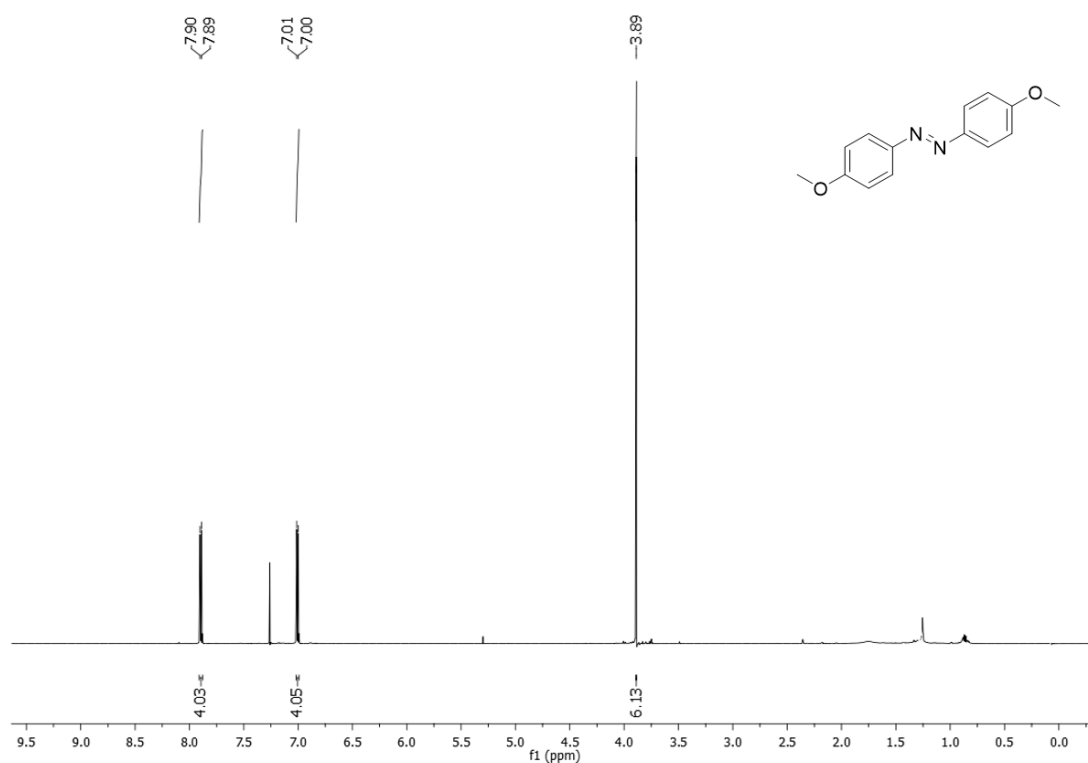


¹H NMR (600 MHz, CDCl₃) of (E)-1,2-bis(4-bromophenyl)diazene (Table 24, Entry 4)

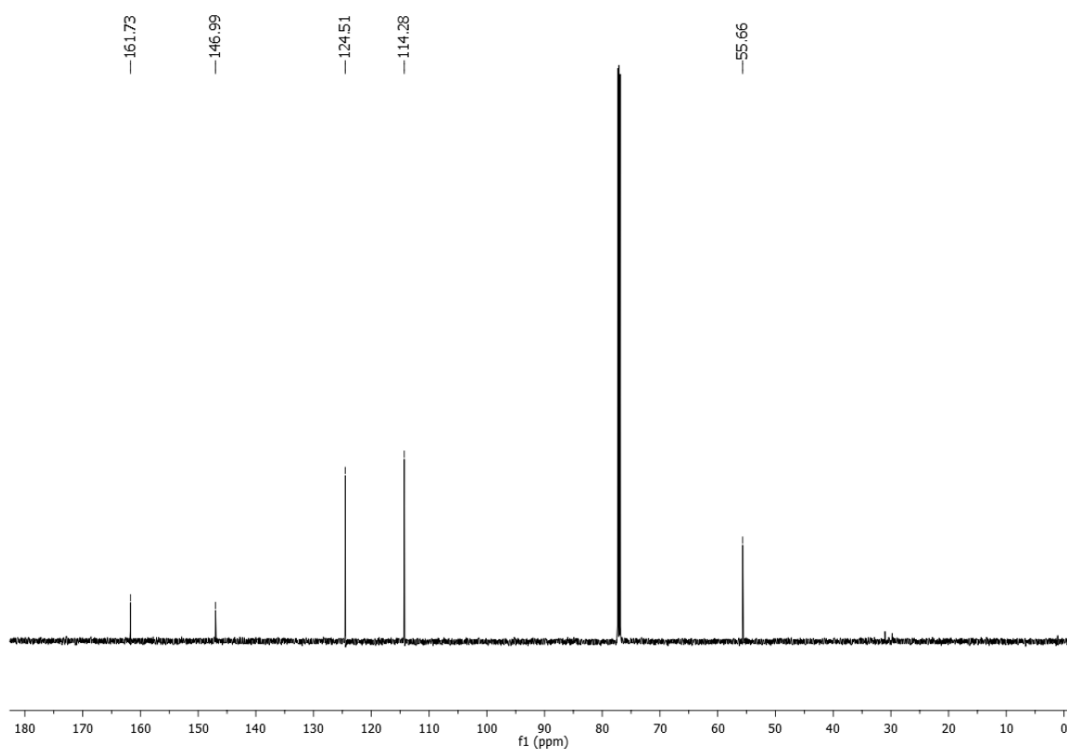


¹³C-NMR (151 MHz, CDCl₃) of (E)-1,2-bis(4-bromophenyl)diazene (Table 24, Entry 4)

(E)-1,2-Bis(4-methoxyphenyl)diazene (2.19e)¹⁶⁷: ¹H NMR (600 MHz, CDCl₃) δ 7.89 (d, *J* = 9.0 Hz, 4H), 7.01 (d, *J* = 9.0 Hz, 4H), 3.89 (s, 6H) ppm; ¹³C NMR (151 MHz, CDCl₃) δ 161.73, 146.99, 124.51, 114.27, 55.66 ppm.

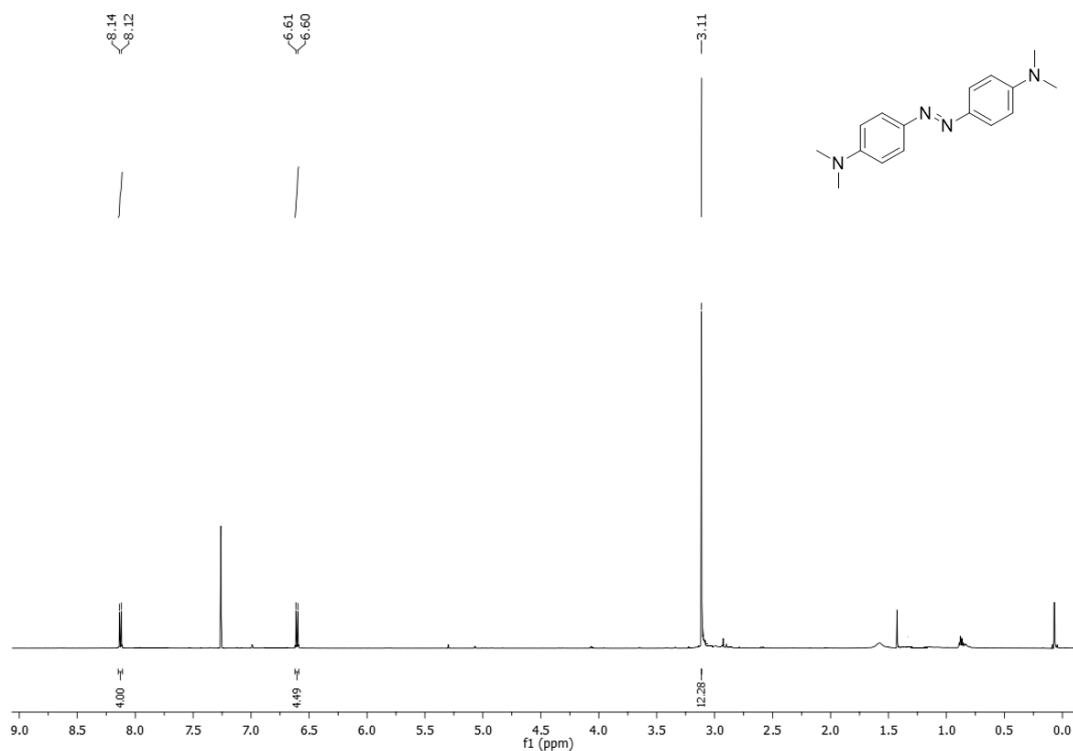


¹H NMR (600 MHz, CDCl₃) of (E)-1,2-Bis(4-methoxyphenyl)diazene (Table 24, Entry 5)

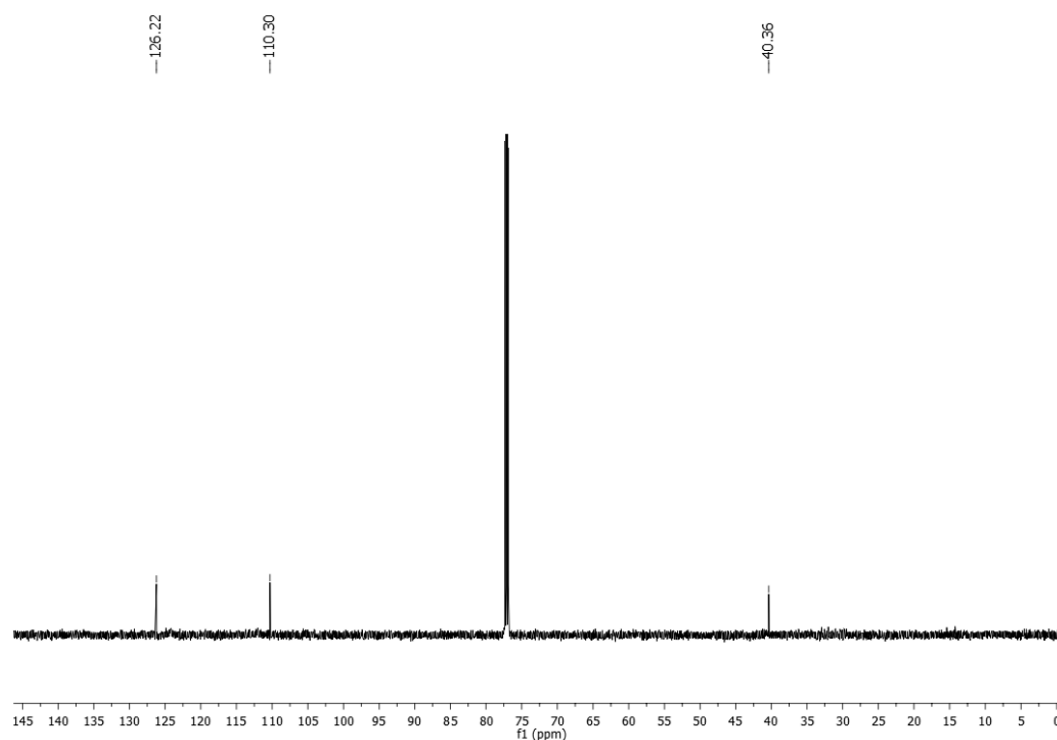


¹³C-NMR (151 MHz, CDCl₃) of (E)-1,2-Bis(4-methoxyphenyl)diazene (Table 24, Entry 5)

(E)-4,4'-(diazene-1,2-diyl)bis(N,N-dimethylaniline) (2.19f)⁴⁶⁶: ¹H NMR (600 MHz, CDCl₃) δ 8.13 (d, *J* = 9.4 Hz, 4H), 6.60 (d, *J* = 9.4 Hz, 4H), 3.11 (s, 12H) ppm; ¹³C NMR (151 MHz, CDCl₃) δ 126.21, 110.30, 40.36 ppm.

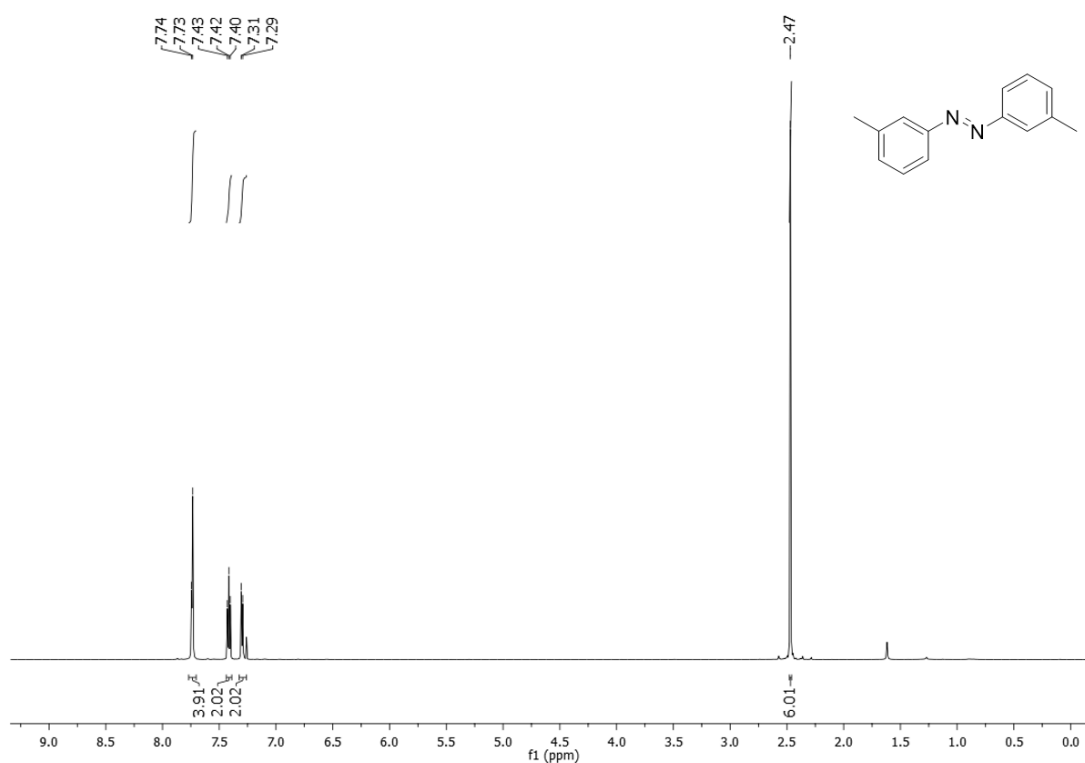


¹H NMR (600 MHz, CDCl₃) of 4,4'-(diazene-1,2-diyl)bis(N,N-dimethylaniline) (Table 24, Entry 6)

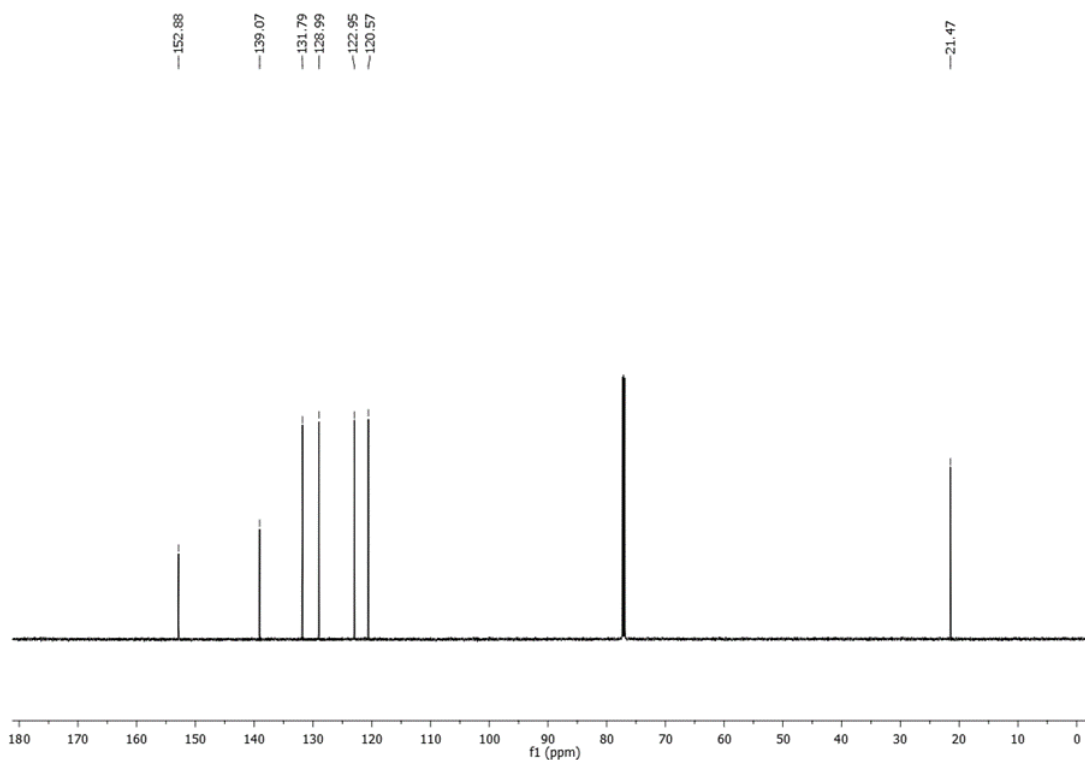


¹³C-NMR (151 MHz, CDCl₃) of 4,4'-(diazene-1,2-diyl)bis(N,N-dimethylaniline) (Table 24, Entry 6)

(E)-1,2-di-m-tolyldiazene (2.19g)¹⁶⁷: ¹H NMR (600 MHz, CDCl₃) δ 7.74 (d, *J* = 6.3 Hz, 4H), 7.42 (t, *J* = 8.0 Hz, 2H), 7.30 (d, *J* = 7.5 Hz, 2H), 2.47 (s, 6H) ppm; ¹³C NMR (151 MHz, CDCl₃) δ 152.88, 139.07, 131.79, 128.99, 122.95, 120.57, 21.47 ppm.

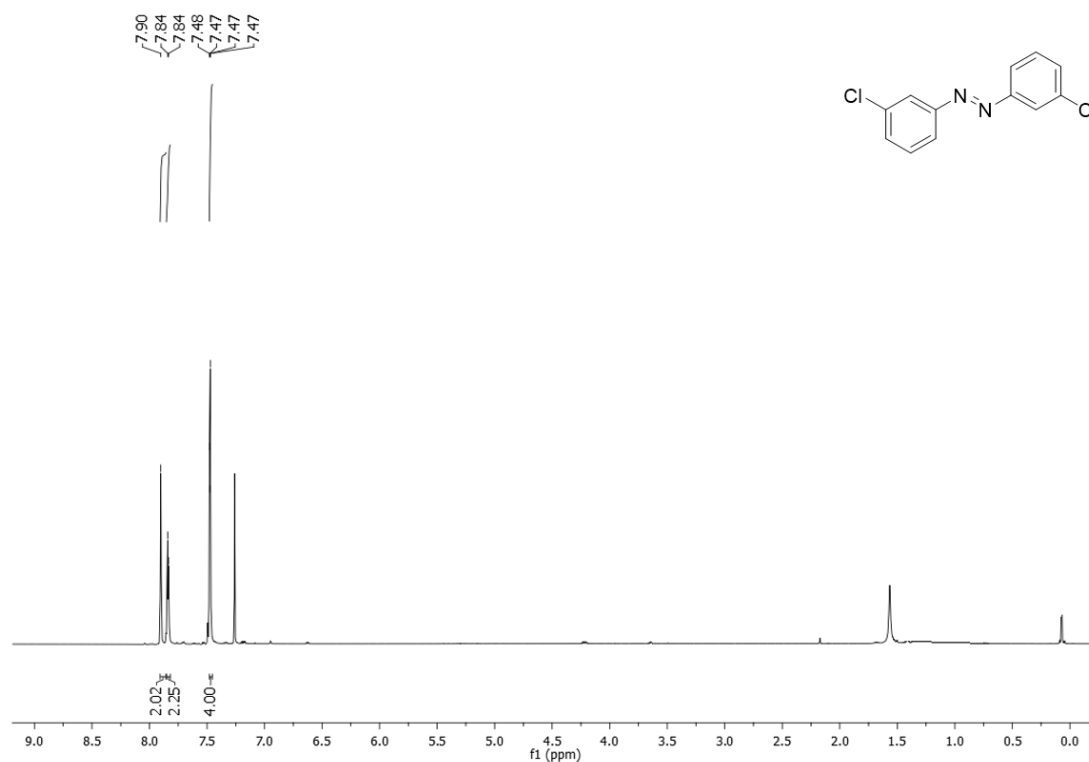


¹H NMR (600 MHz, CDCl₃) of (E)-1,2-di-m-tolyldiazene (Table 24, Entry 7)

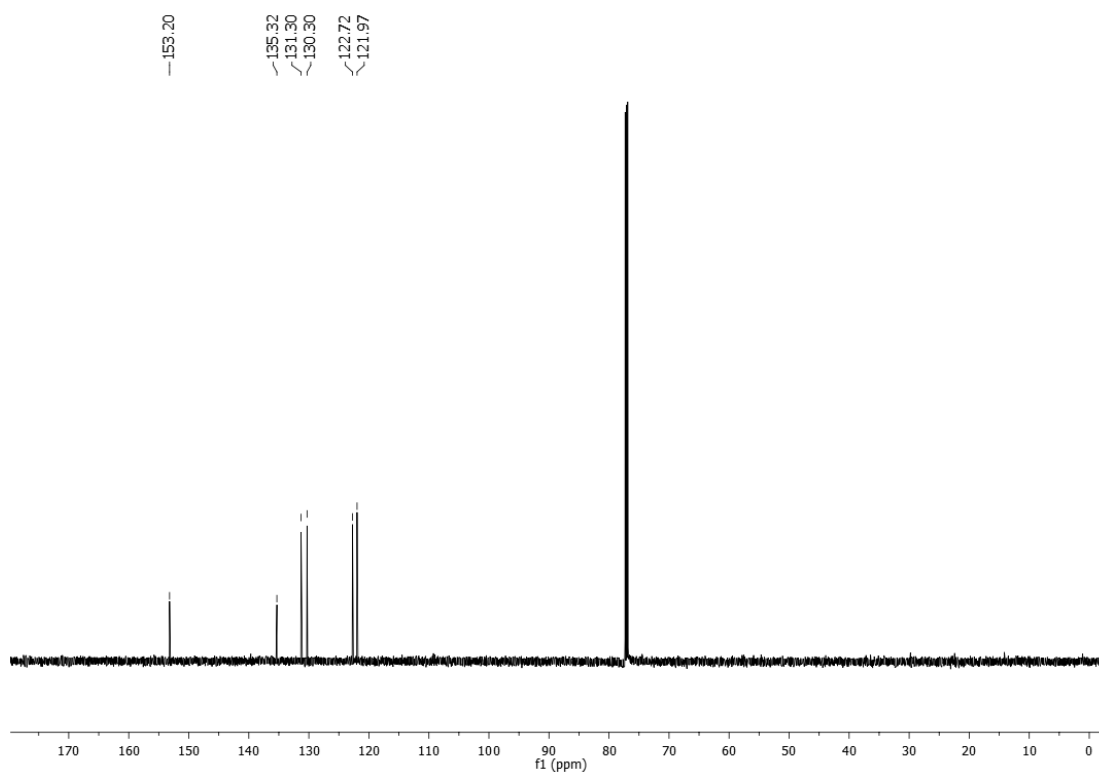


¹³C-NMR (151 MHz, CDCl₃) of (E)-1,2-di-m-tolyldiazene (Table 24, Entry 7)

(E)-1,2-bis(3-chlorophenyl)diazene (2.19h)³⁷⁰: ¹H NMR (600 MHz, CDCl₃) δ 7.90 (s, 2H), 7.84 (d, *J* = 3.9 Hz, 2H), 7.47 (dd, *J* = 3.8, 1.9 Hz, 4H) ppm; ¹³C NMR (151 MHz, CDCl₃) δ 153.20, 135.32, 131.30, 130.30, 122.73, 121.97 ppm.

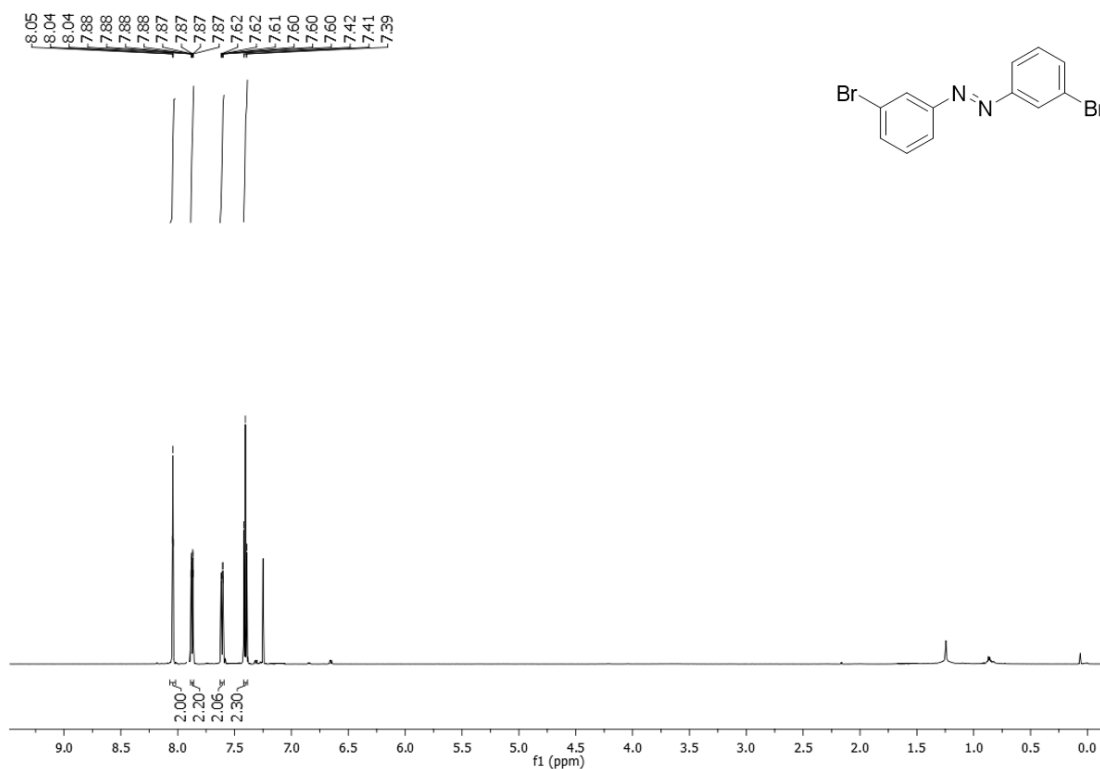


¹H NMR (600 MHz, CDCl₃) of (E)-1,2-bis(3-chlorophenyl)diazene (Table 24, Entry 8)

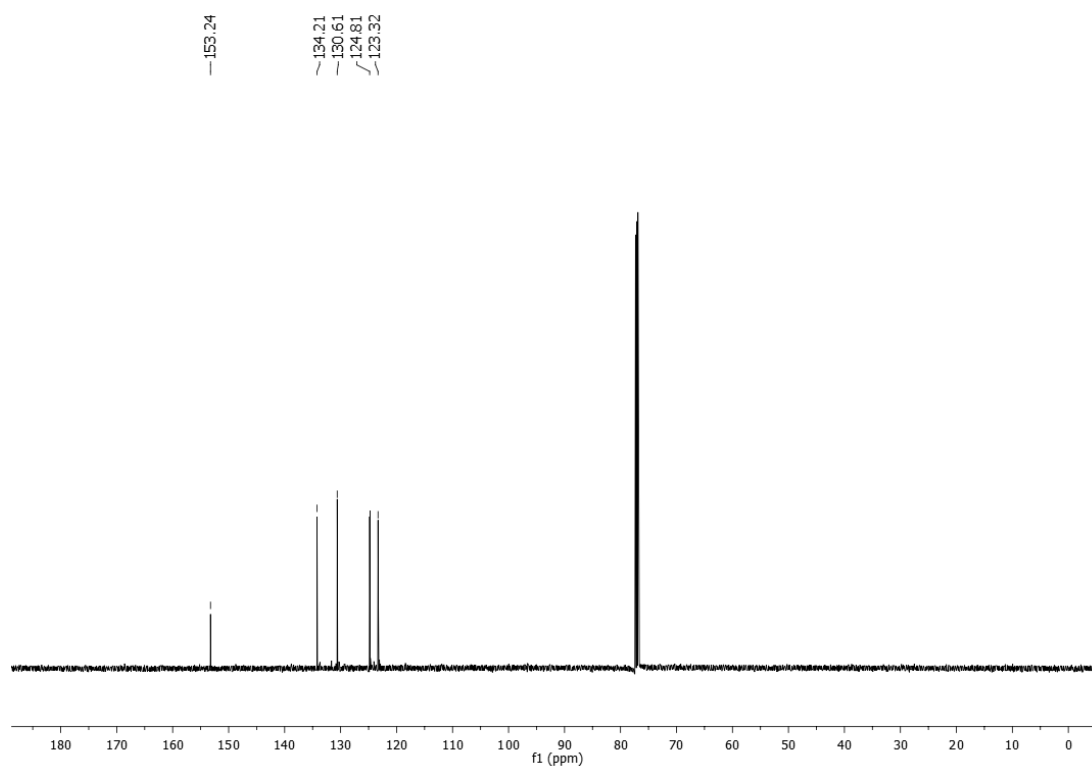


¹³C-NMR (151 MHz, CDCl₃) of (E)-1,2-bis(3-chlorophenyl)diazene (Table 24, Entry 8)

(E)-1,2-bis(3-bromophenyl)diazene (2.19i)³⁷⁰: ¹H NMR (600 MHz, CDCl₃) δ 8.07 – 8.02 (m, 2H), 7.87 (ddd, *J* = 7.9, 1.6, 1.0 Hz, 2H), 7.64 – 7.58 (m, 2H), 7.44 – 7.38 (m, 2H) ppm; ¹³C NMR (151 MHz, CDCl₃) δ 153.25, 134.21, 130.61, 124.81, 123.32 ppm

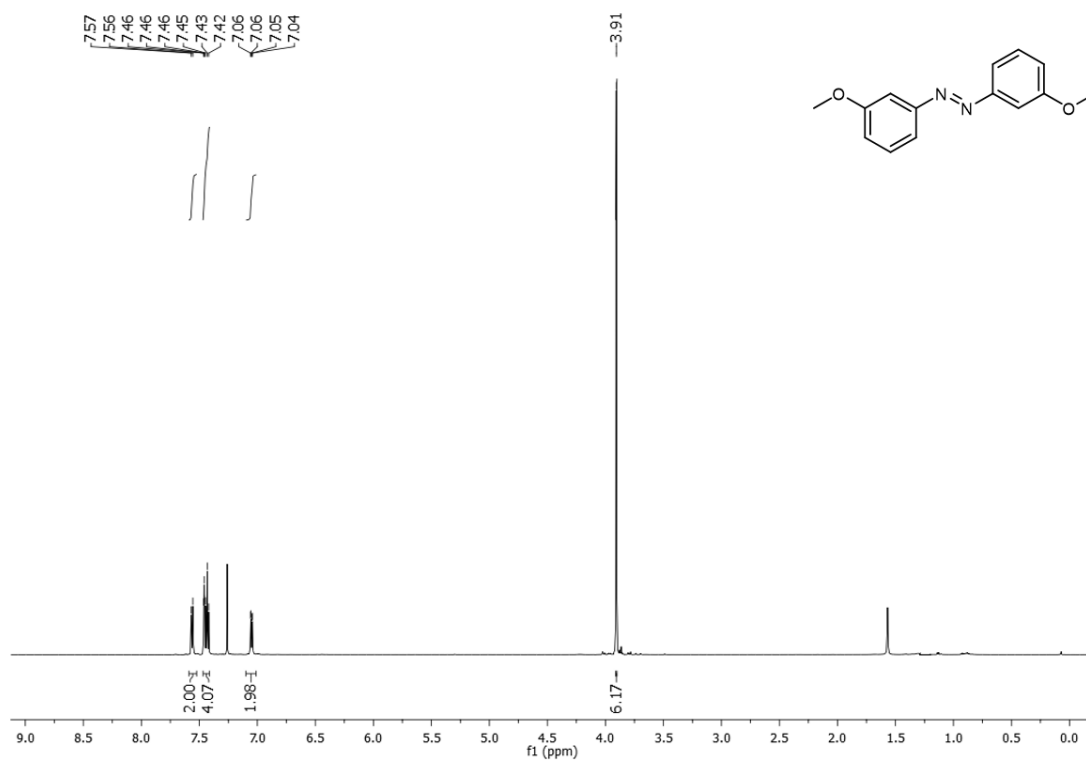


¹H NMR (600 MHz, CDCl₃) of (E)-1,2-bis(3-bromophenyl)diazene (Table 24, Entry 9)

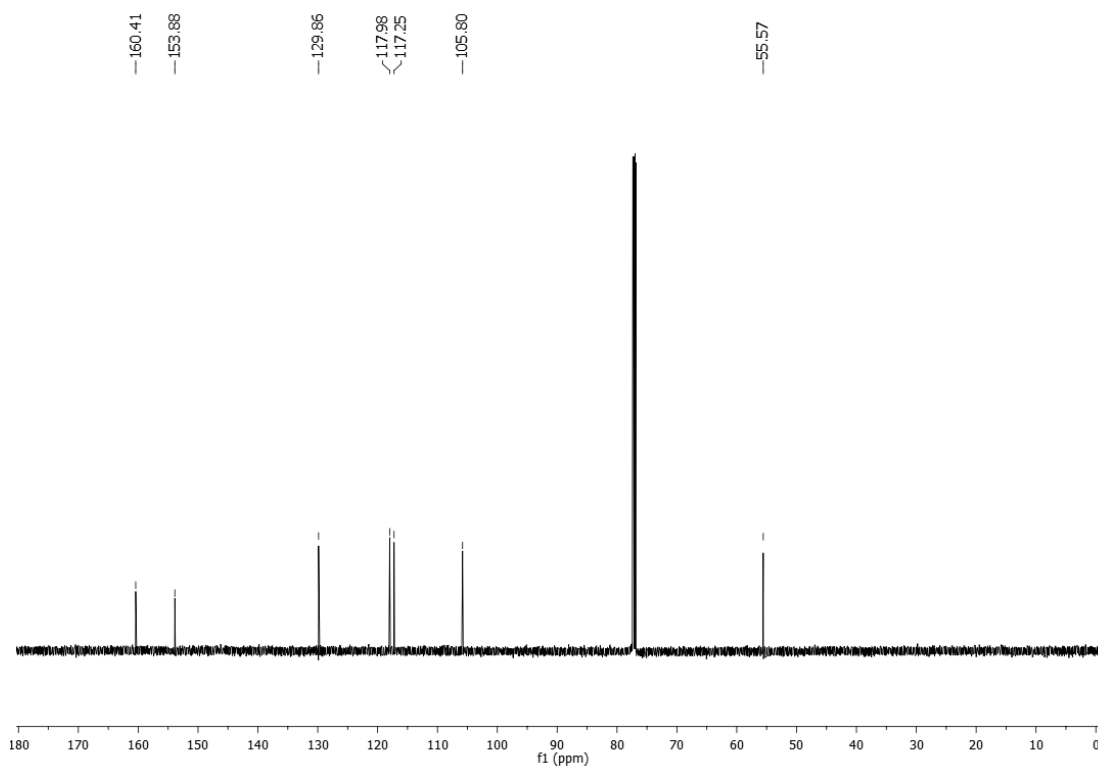


¹³C-NMR (151 MHz, CDCl₃) of (E)-1,2-bis(3-bromophenyl)diazene (Table 24, Entry 9)

(E)-1,2-bis(3-methoxyphenyl)diazene (2.19j)³⁷⁰: ¹H NMR (600 MHz, CDCl₃) δ 7.56 (d, *J* = 7.8 Hz, 2H), 7.45 (dt, *J* = 16.0, 5.0 Hz, 4H), 7.05 (dd, *J* = 8.2, 1.9 Hz, 2H), 3.91 (s, 6H) ppm; ¹³C NMR (151 MHz, CDCl₃) δ 160.42, 153.88, 129.87, 117.98, 117.25, 105.81, 55.57 ppm.



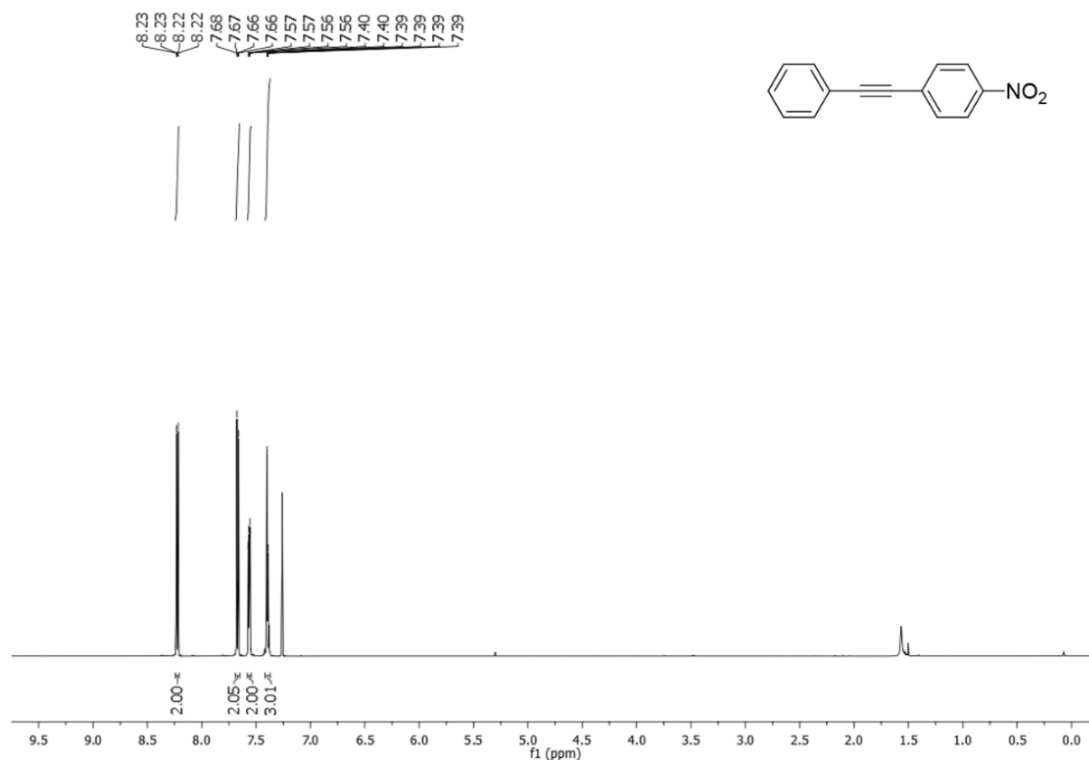
¹H NMR (600 MHz, CDCl₃) of (E)-1,2-bis(3-methoxyphenyl)diazene (Table 24, Entry 10)



¹³C-NMR (151 MHz, CDCl₃) of (E)-1,2-bis(3-methoxyphenyl)diazene (Table 24, Entry 10)

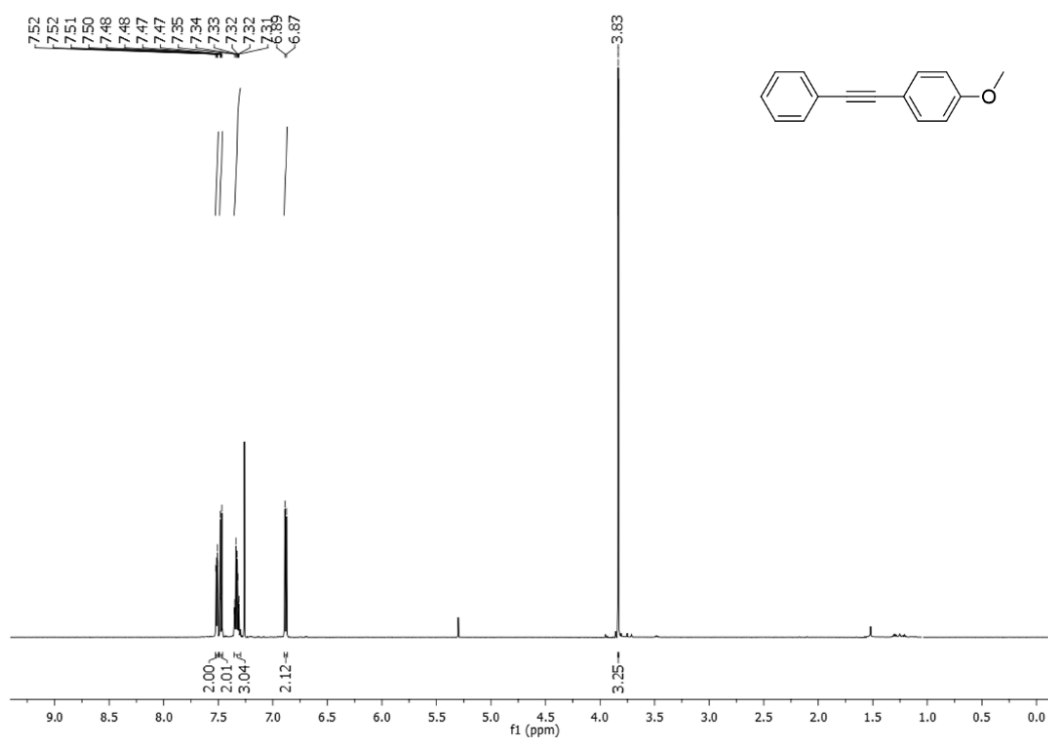
S-4. NMR alkynes-derivatives

1-nitro-4-(phenylethynyl)benzene⁴⁶⁷: ¹H NMR (600 MHz, CDCl₃) δ 8.24 – 8.21 (m, 2H), 7.69 – 7.65 (m, 2H), 7.56 (dd, *J* = 7.3, 2.4 Hz, 2H), 7.42 – 7.37 (m, 3H).



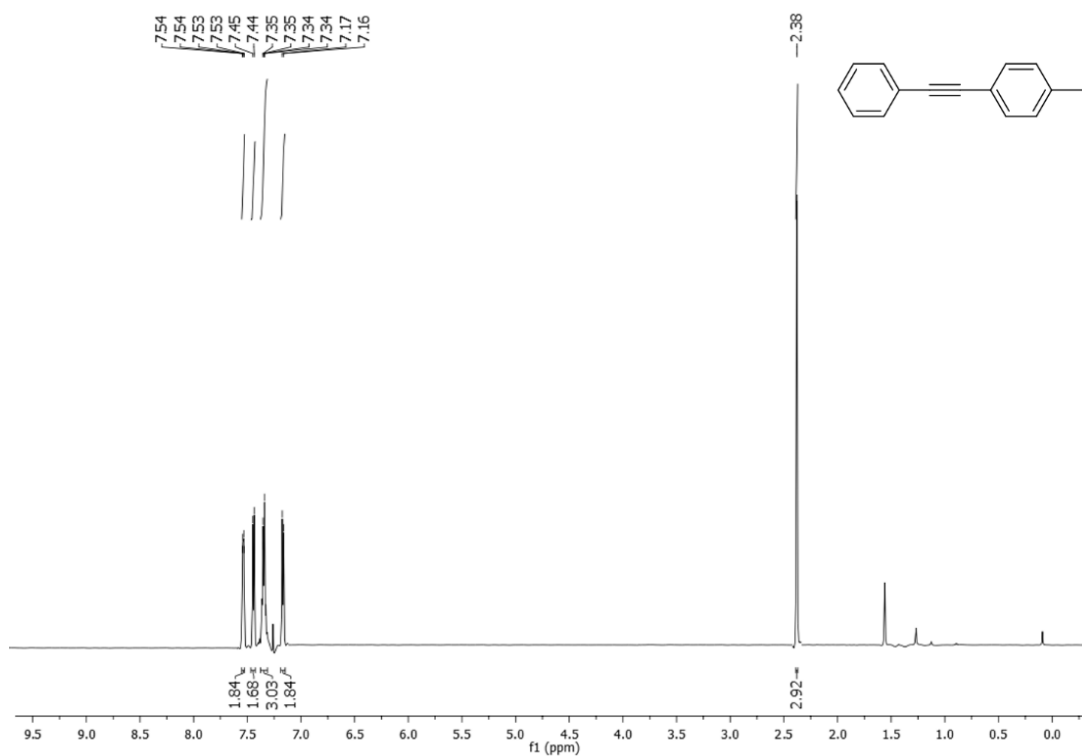
¹H NMR (600 MHz, CDCl₃) of 1-nitro-4-(phenylethynyl)benzene

1-methoxy-4-(phenylethynyl)benzene⁴⁶⁷: ¹H NMR (600 MHz, CDCl₃) δ 7.53 – 7.50 (m, 2H), 7.49 – 7.46 (m, 2H), 7.36 – 7.30 (m, 3H), 6.88 (d, *J* = 8.8 Hz, 2H), 3.83 (s, 3H).



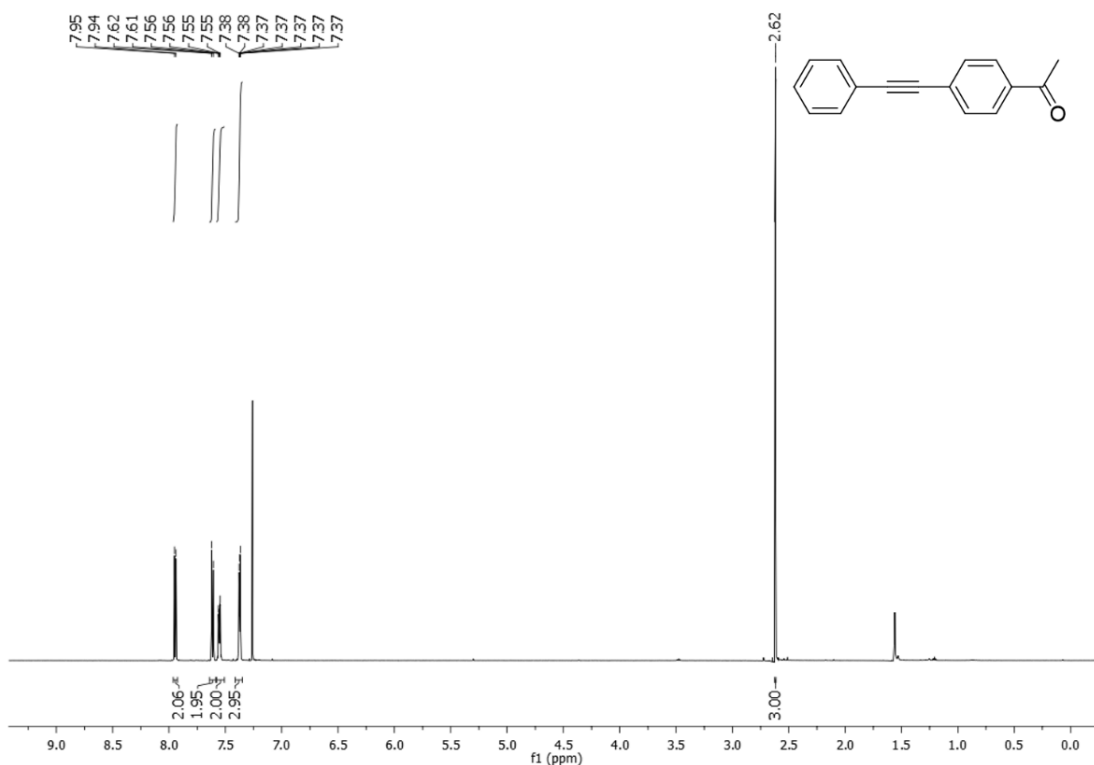
¹H NMR (600 MHz, CDCl₃) of 1-methoxy-4-(phenylethynyl)benzene

1-methyl-4-(phenylethynyl)benzene⁴⁶⁷: ¹H NMR (600 MHz, CDCl₃) δ 7.54 (dd, *J* = 7.9, 1.6 Hz, 3H), 7.44 (d, *J* = 8.1 Hz, 3H), 7.35 (dd, *J* = 7.3, 1.4 Hz, 5H), 7.17 (d, *J* = 7.8 Hz, 3H), 2.38 (s, 5H).



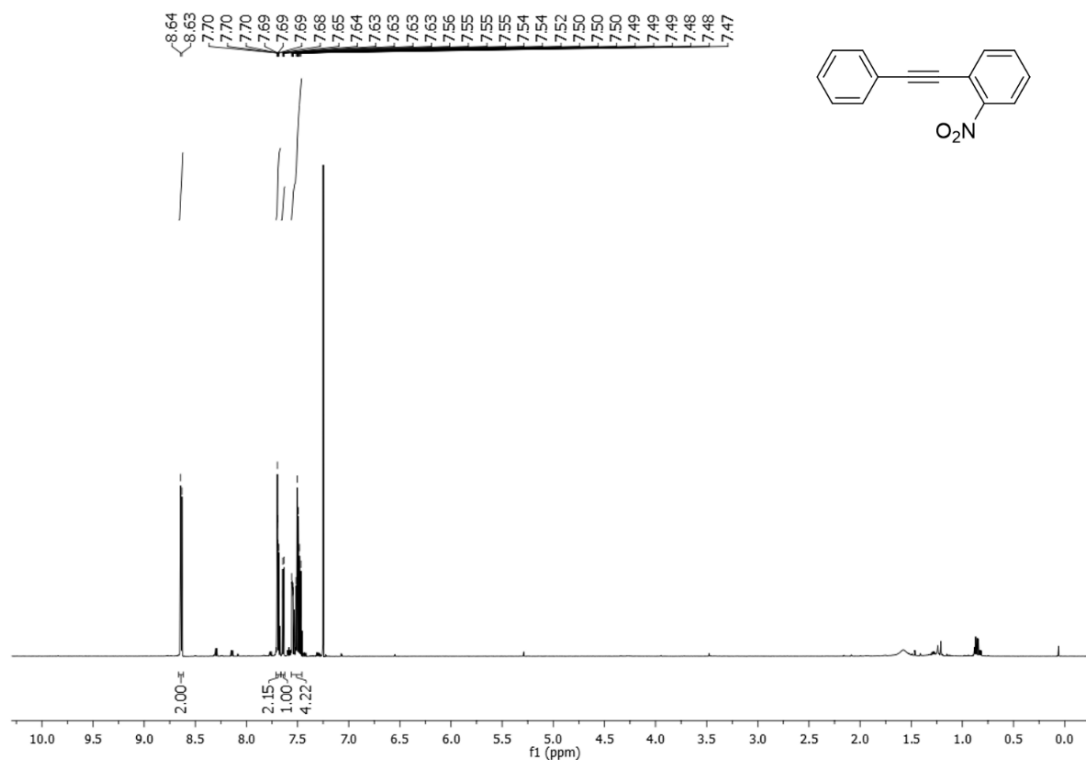
¹H NMR (600 MHz, CDCl₃) of 1-methyl-4-(phenylethynyl)benzene.

1-(4-(2-Phenylethynyl)phenyl)ethanone⁴⁶⁸: ¹H NMR (600 MHz, CDCl₃) δ 7.94 (d, *J* = 8.6 Hz, 2H), 7.61 (d, *J* = 8.6 Hz, 2H), 7.55 (dd, *J* = 6.6, 3.0 Hz, 2H), 7.41 – 7.35 (m, 3H), 2.62 (s, 3H).



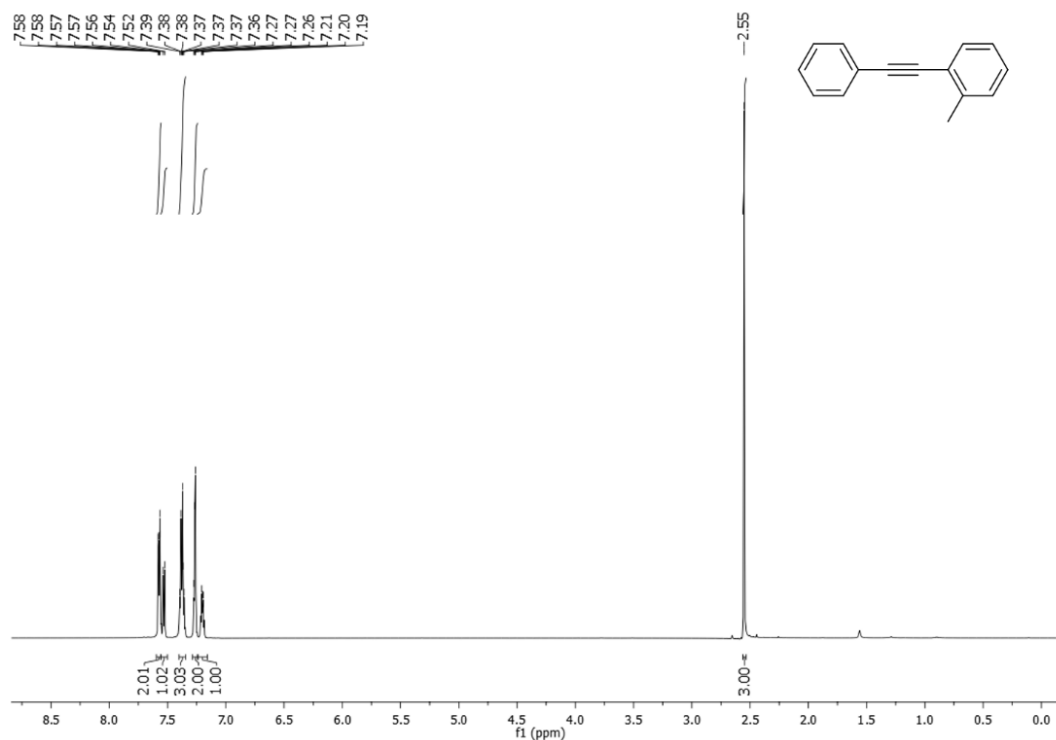
¹H NMR (600 MHz, CDCl₃) of 1-(4-(2-Phenylethynyl)phenyl)ethanone.

1-nitro-2-(phenylethynyl)benzene⁴⁶⁹: ¹H NMR (600 MHz,) δ 8.64 (d, $J = 7.1$ Hz, 2H), 7.71 – 7.66 (m, 2H), 7.66 – 7.63 (m, 1H), 7.51 (dddd, $J = 14.4, 13.6, 6.7, 3.9$ Hz, 4H).



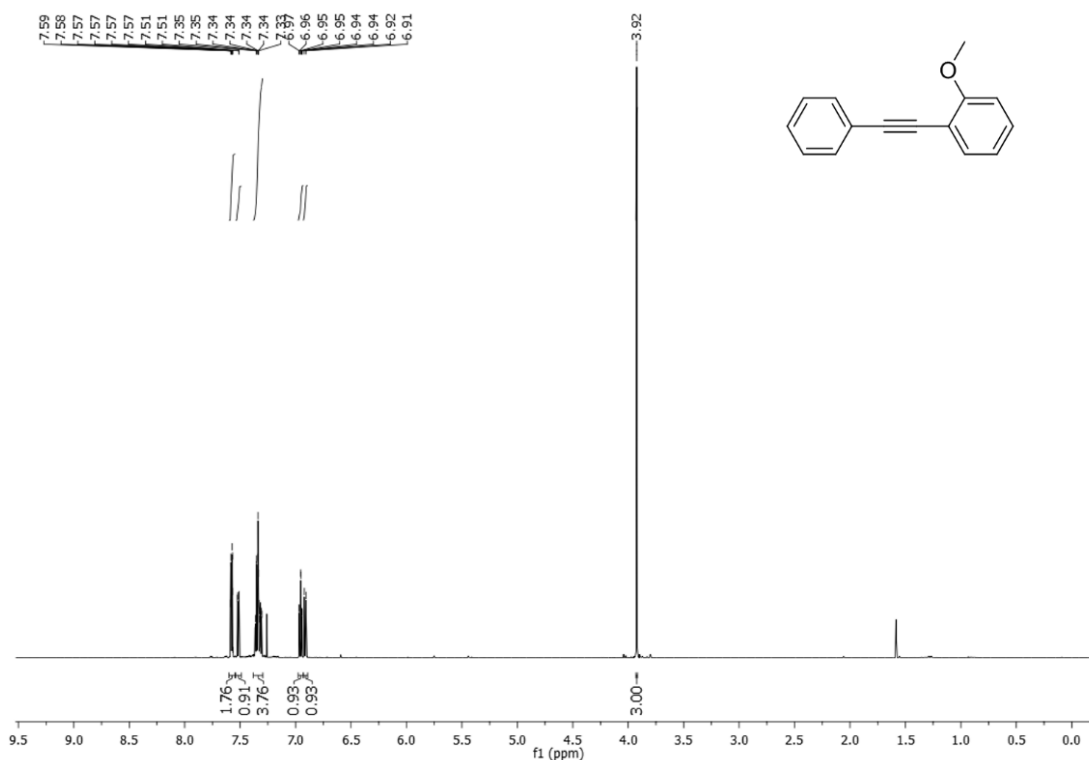
¹H NMR (600 MHz, CDCl₃) of 1-nitro-2-(phenylethynyl)benzene.

1-methyl-2-(phenylethynyl)benzene⁴⁶⁹: ¹H NMR (600 MHz, CDCl₃) δ 7.60 – 7.55 (m, 2H), 7.53 (d, $J = 7.5$ Hz, 1H), 7.40 – 7.34 (m, 3H), 7.29 – 7.24 (m, 2H), 7.24 – 7.16 (m, 1H), 2.55 (s, 3H).



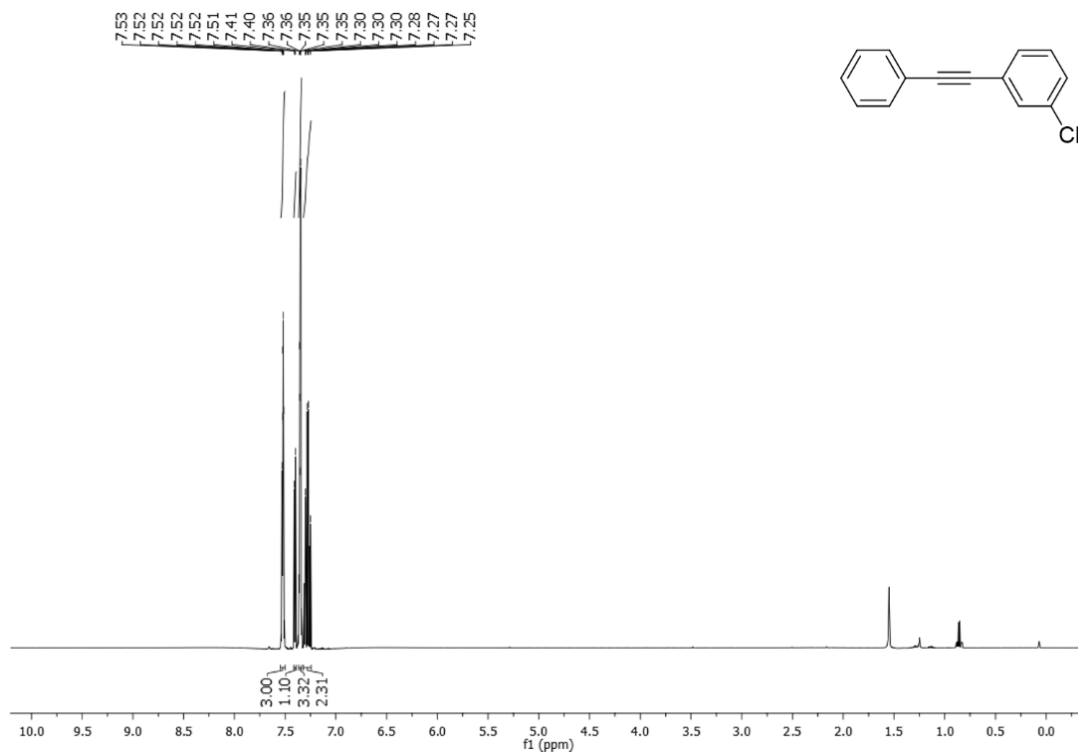
¹H NMR (600 MHz, CDCl₃) of 1-methyl-2-(phenylethynyl)benzene.

1-methoxy-2-(phenylethynyl)benzene⁴⁶⁹: ¹H NMR (600 MHz, CDCl₃) δ 7.60 – 7.55 (m, 2H), 7.54 – 7.49 (m, 1H), 7.38 – 7.30 (m, 4H), 6.95 (td, *J* = 7.5, 1.0 Hz, 1H), 6.91 (d, *J* = 8.4 Hz, 1H), 3.92 (s, 3H).



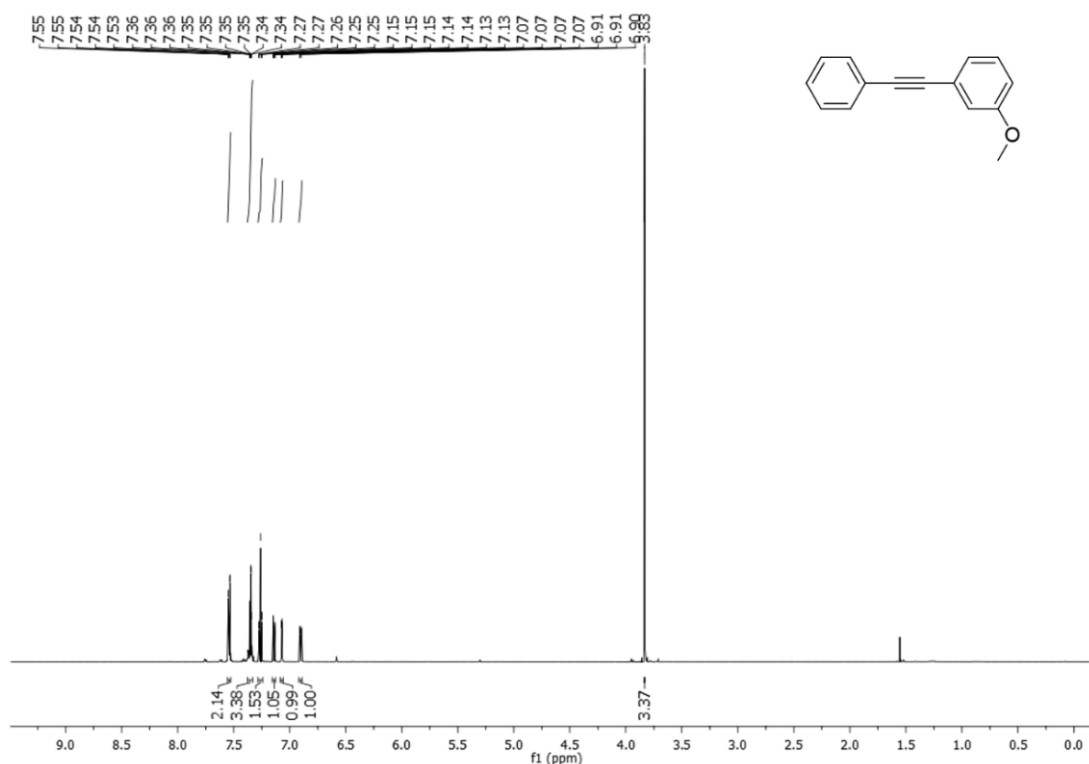
¹H NMR (600 MHz, CDCl₃) of 1-methoxy-2-(phenylethynyl)benzene.

1-Chloro-4-(2-phenylethynyl)benzene⁴⁷⁰: ¹H NMR (600 MHz, CDCl₃) δ 7.52 (dt, *J* = 3.6, 3.0 Hz, 3H), 7.40 (d, *J* = 7.4 Hz, 1H), 7.37 – 7.34 (m, 3H), 7.32 – 7.24 (m, 2H).



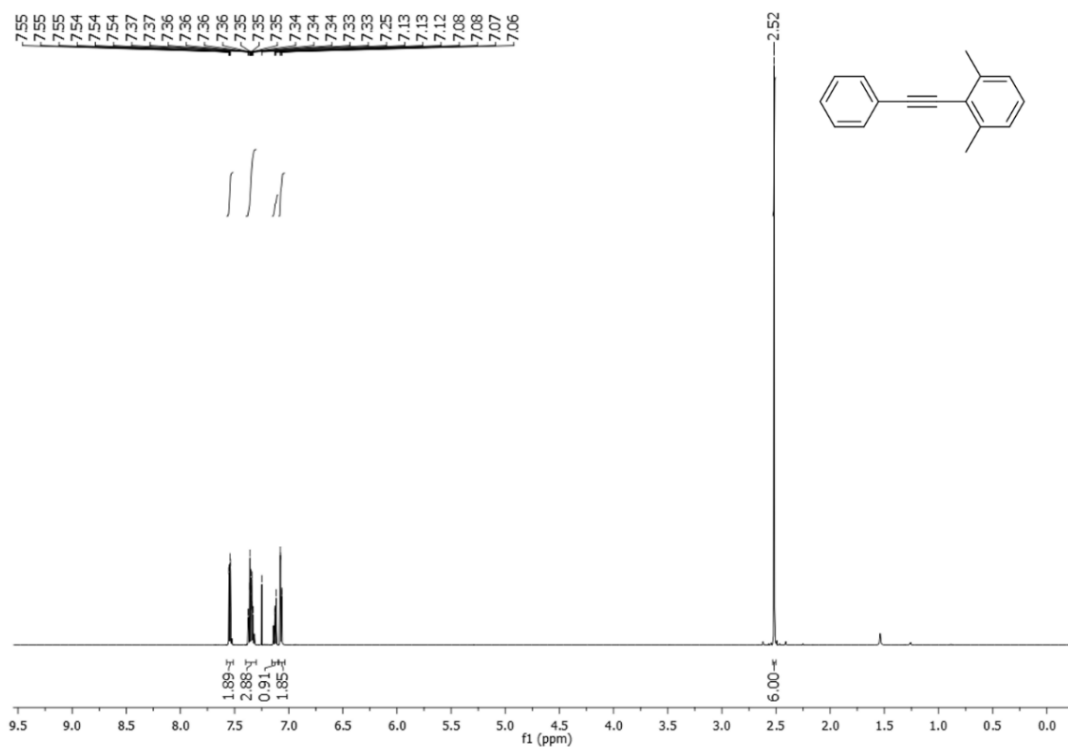
¹H NMR (600 MHz, CDCl₃) of 1-chloro-4-(2-phenylethynyl)benzene.

1-methoxy-3-(phenylethynyl)benzene⁴⁷¹: ¹H NMR (600 MHz, CDCl₃) δ 7.55 – 7.53 (m, 2H), 7.38 – 7.33 (m, 3H), 7.28 – 7.24 (m, 1H), 7.15 – 7.13 (m, 1H), 7.07 (dd, *J* = 2.6, 1.4 Hz, 1H), 6.90 (ddd, *J* = 8.3, 2.6, 1.0 Hz, 1H), 3.83 (s, 3H).



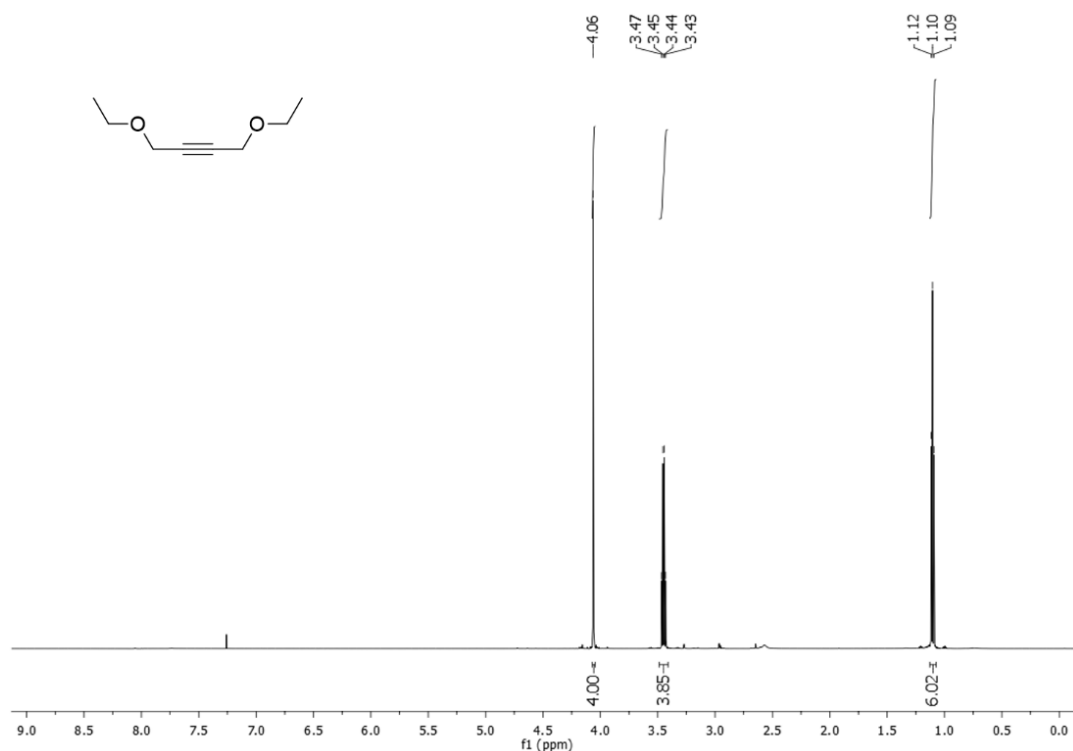
¹H NMR (600 MHz, CDCl₃) of 1-methoxy-3-(phenylethynyl)benzene.

1,3-dimethyl-2-(phenylethynyl)benzene⁴⁶⁹: ¹H NMR (600 MHz,) δ 7.57 – 7.51 (m, 2H), 7.40 – 7.30 (m, 3H), 7.15 – 7.10 (m, 1H), 7.07 (dd, *J* = 7.3, 0.5 Hz, 2H), 2.52 (s, 6H).



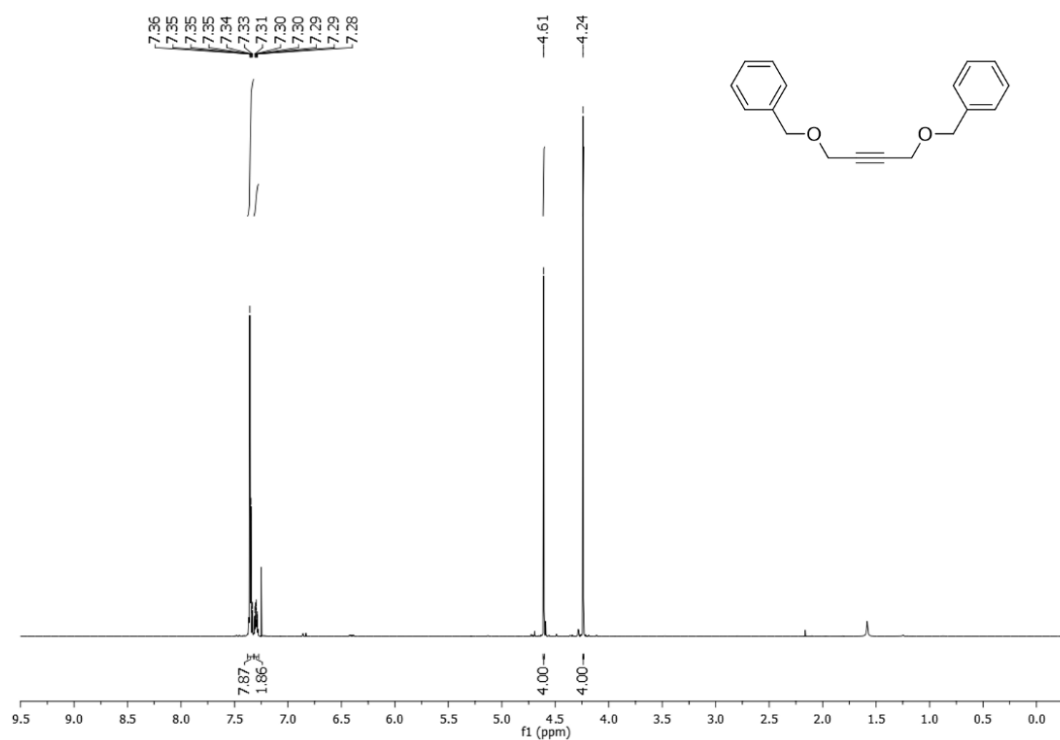
¹H NMR (600 MHz, CDCl₃) of 1,3-dimethyl-2-(phenylethynyl)benzene.

1,4-diethoxybut-2-yne: $^1\text{H NMR}$ (600 MHz, CDCl_3) δ 4.06 (s, 2H), 3.45 (q, $J = 7.0$ Hz, 2H), 1.10 (t, $J = 7.0$ Hz, 3H).



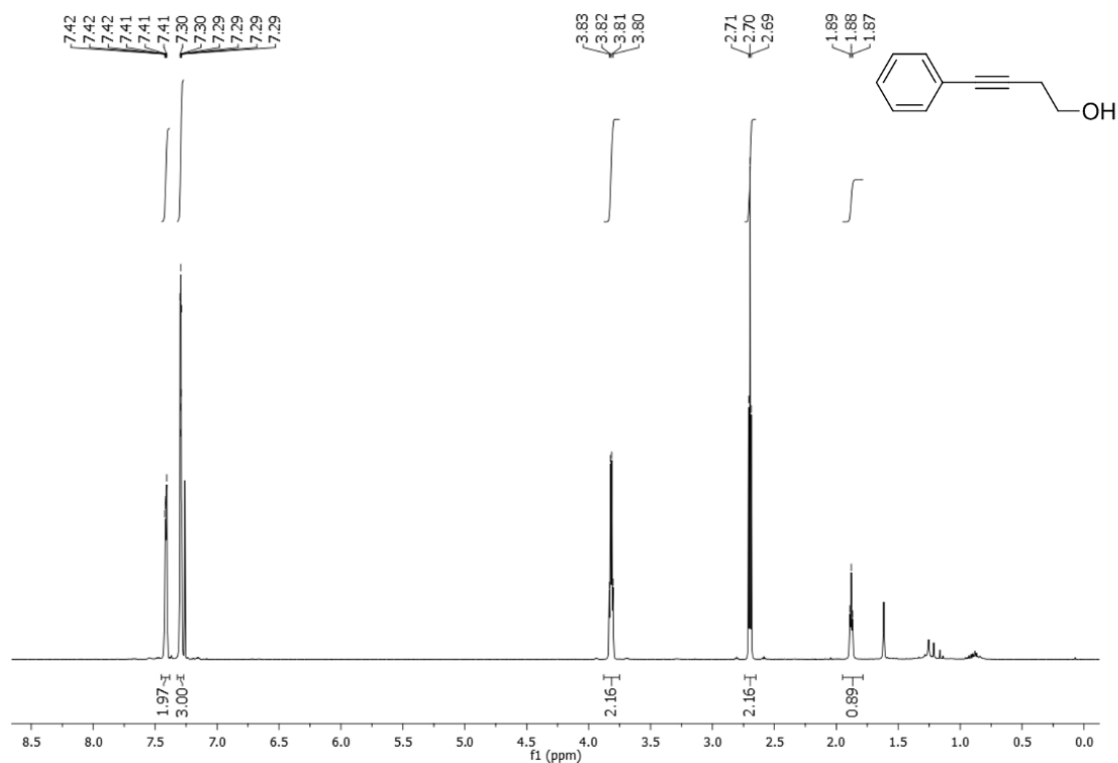
$^1\text{H NMR}$ (600 MHz, CDCl_3) of 1,4-diethoxybut-2-yne.

1,4-bis(benzyloxy)but-2-yne⁴⁷²: $^1\text{H NMR}$ (600 MHz, CDCl_3) δ 7.38 – 7.32 (m, 8H), 7.30 (td, $J = 5.6, 2.4$ Hz, 2H), 4.61 (s, 4H), 4.24 (s, 4H).



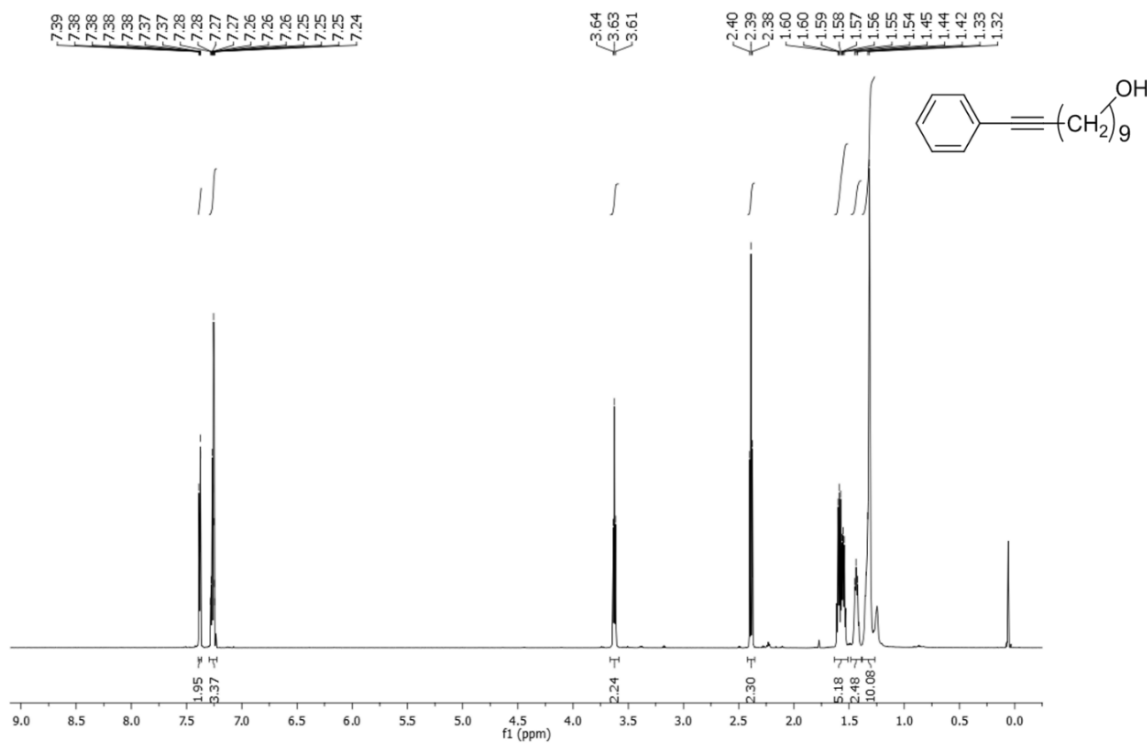
$^1\text{H NMR}$ (600 MHz, CDCl_3) of 1,4-bis(benzyloxy)but-2-yne.

4-phenylbut-3-yn-1-ol⁴⁷³: ¹H NMR (600 MHz, CDCl₃) δ 7.45 – 7.38 (m, 2H), 7.32 – 7.27 (m, 3H), 3.82 (q, *J* = 6.1 Hz, 2H), 2.70 (t, *J* = 6.3 Hz, 2H), 1.88 (t, *J* = 6.1 Hz, 1H).



¹H NMR (600 MHz, CDCl₃) of 4-phenylbut-3-yn-1-ol.

11-phenylundec-10-yn-1-ol⁴⁷⁴: ¹H NMR (600 MHz, CDCl₃) δ 7.39 – 7.28 (m, 2H), 7.27 – 7.24 (m, 3H), 3.63 (t, *J* = 6.7 Hz, 2H), 2.39 (t, *J* = 7.1 Hz, 2H), 1.57 (ddd, *J* = 14.4, 10.1, 4.9 Hz, 2H), 1.48 – 1.39 (m, 1H), 1.32 (d, *J* = 8.5 Hz, 4H).



¹H NMR (600 MHz, CDCl₃) of 11-phenylundec-10-yn-1-ol.

S-5. NMR (Z)-alkenes-derivatives

Cis stilben (2.26a)⁴⁷⁵: ¹H NMR (600 MHz, CDCl₃) δ 7.26 - 7.19 (m, 10H), 6.60 (s, 2H); ¹³C NMR (151 MHz, CDCl₃) δ 137.62, 130.63, 129.26, 128.60, 127.47 ppm.

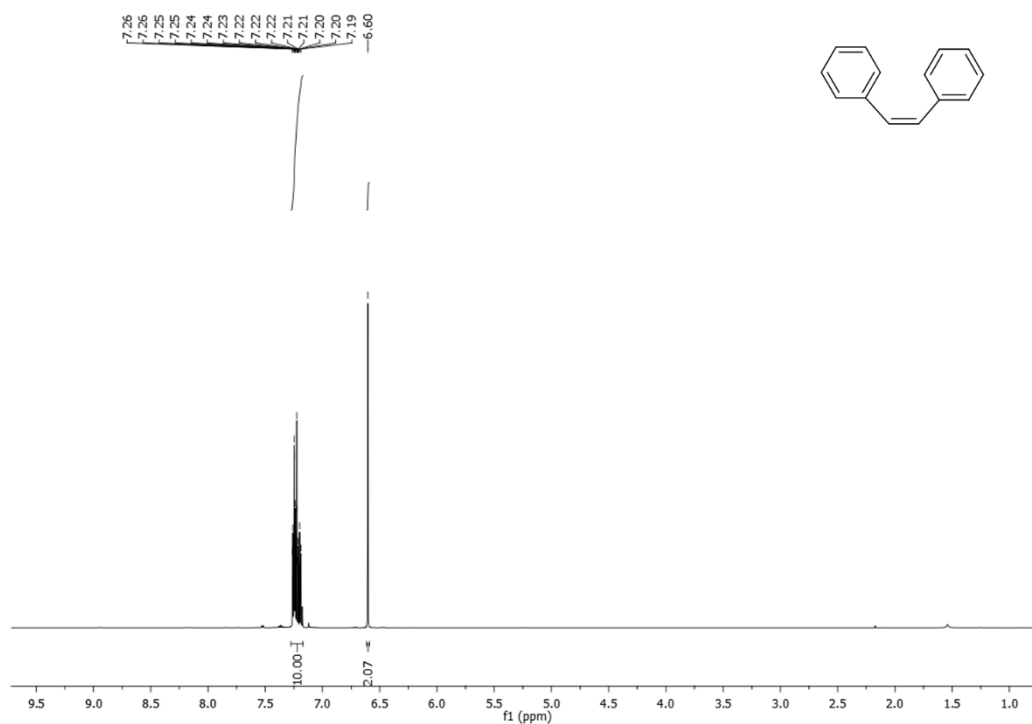


Figure 3. ¹H NMR (300 MHz, CDCl₃) of Aniline (Table 3, Entry 1)

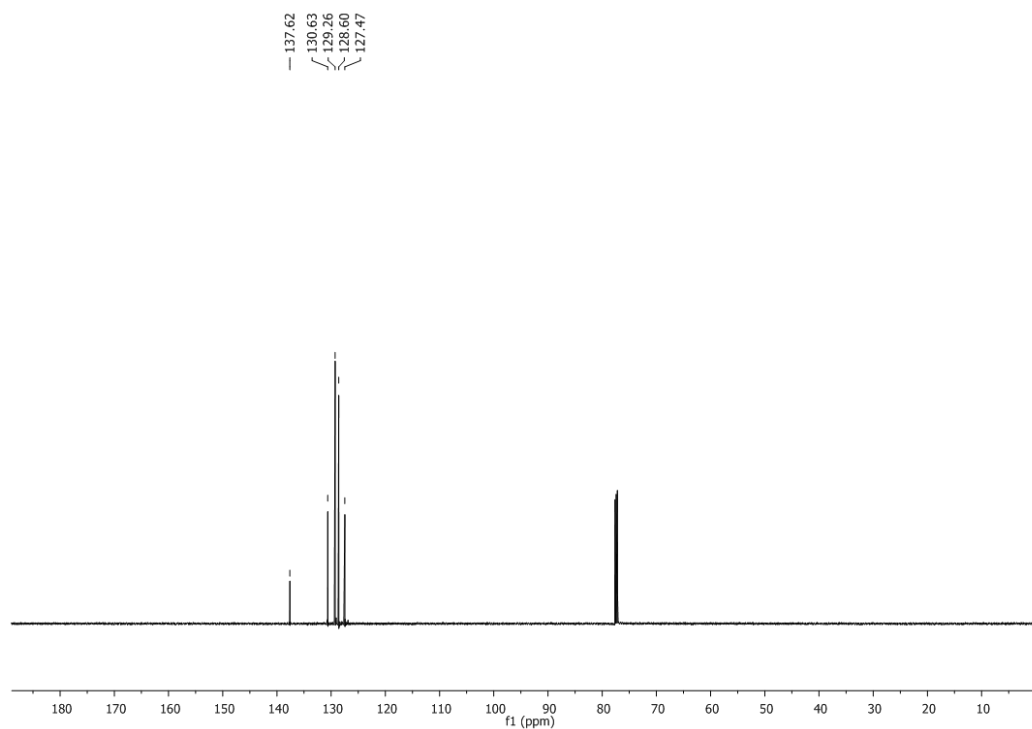
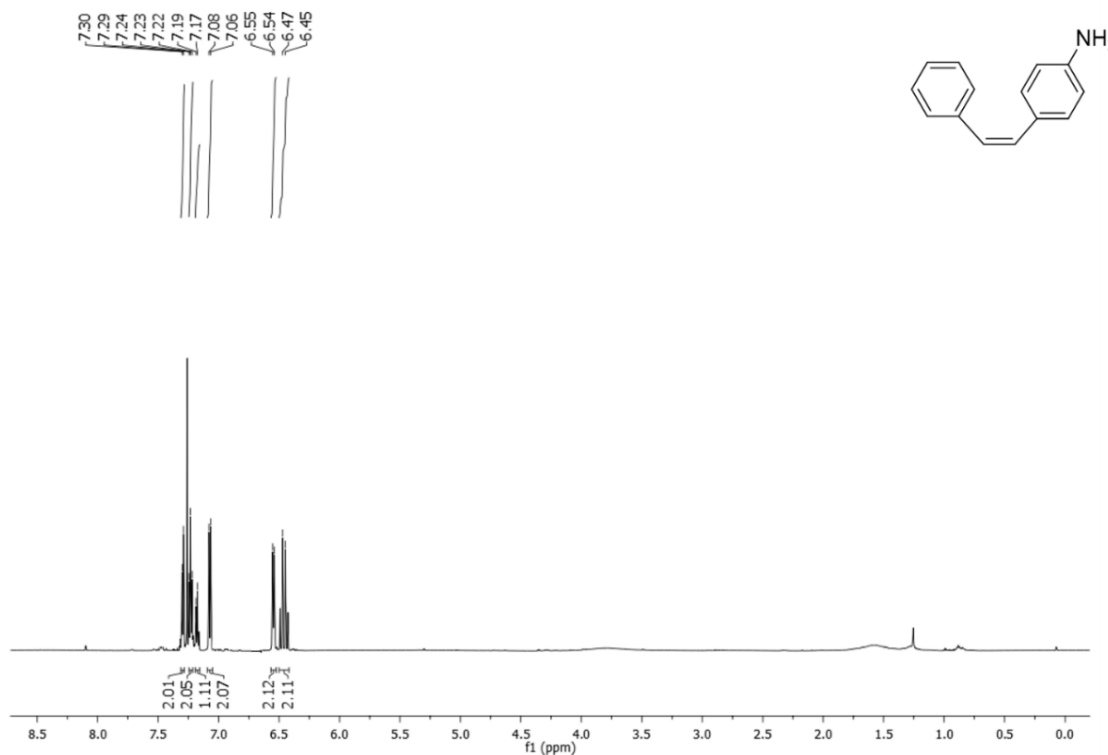
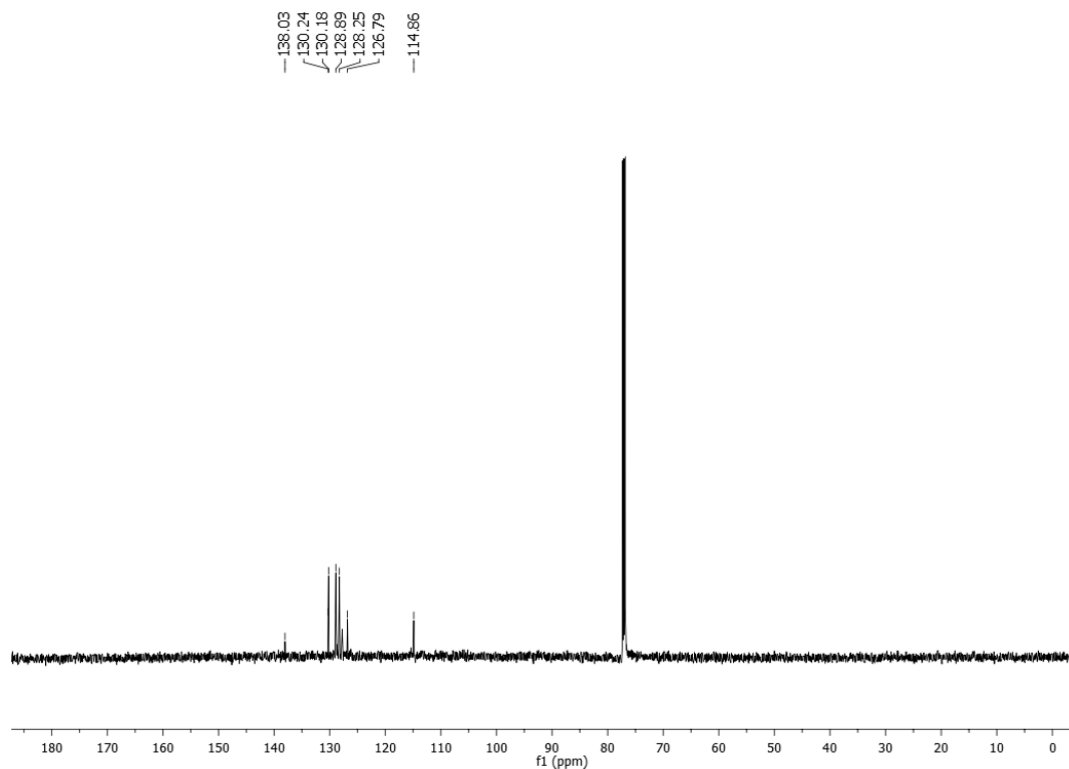


Figure 4. ¹³C-NMR (75 MHz, CDCl₃) of Aniline (Table 3, Entry 1)

(Z)- 4-styrylbenzenamine (2.26b) ⁴⁷⁶: ¹H NMR (600 MHz, CDCl₃) δ 7.30 (d, *J* = 7.5 Hz, 2H), 7.23 (t, *J* = 7.5 Hz, 2H), 7.18 (d, *J* = 7.3 Hz, 1H), 7.07 (d, *J* = 8.5 Hz, 2H), 6.55 (d, *J* = 8.4 Hz, 2H), 6.46 (d, *J* = 14.1 Hz, 2H) ppm; ¹³C NMR (151 MHz, CDCl₃) δ 138.03, 130.24, 130.18, 128.89, 128.25, 127.84, 127.74, 127.73, 126.78, 114.85 ppm.

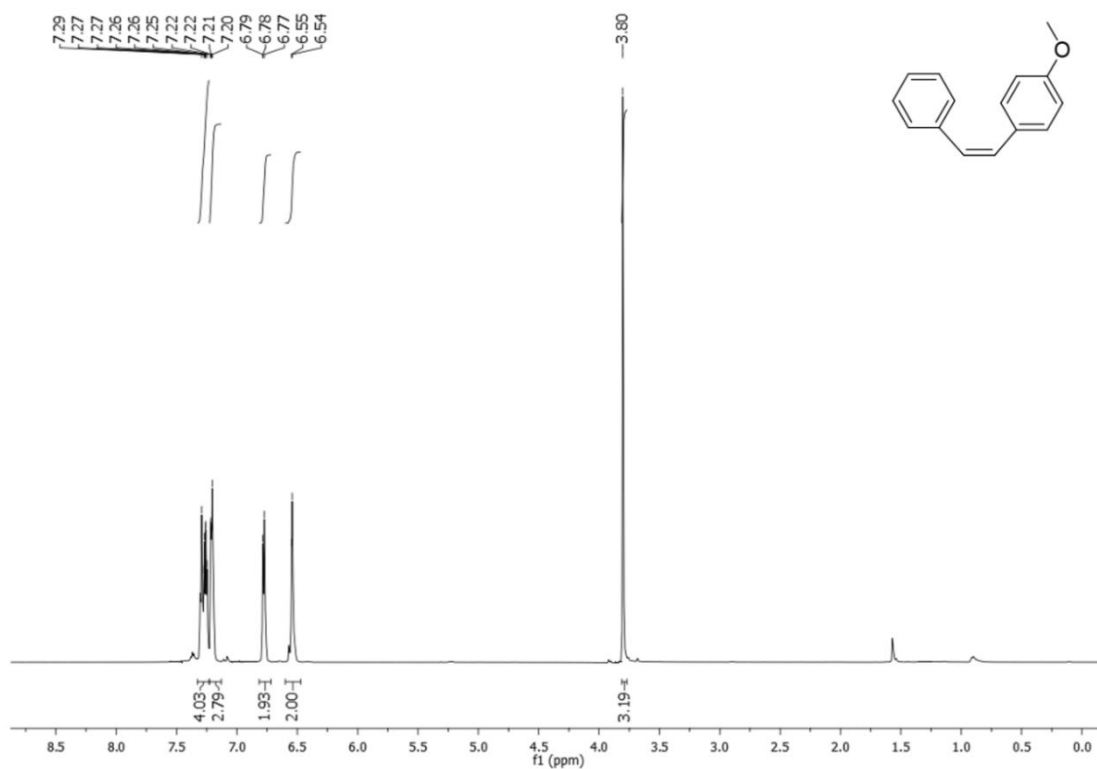


¹H NMR (600 MHz, CDCl₃) of (Z)- 4-styrylbenzenamine (Table 25, Entry 2)

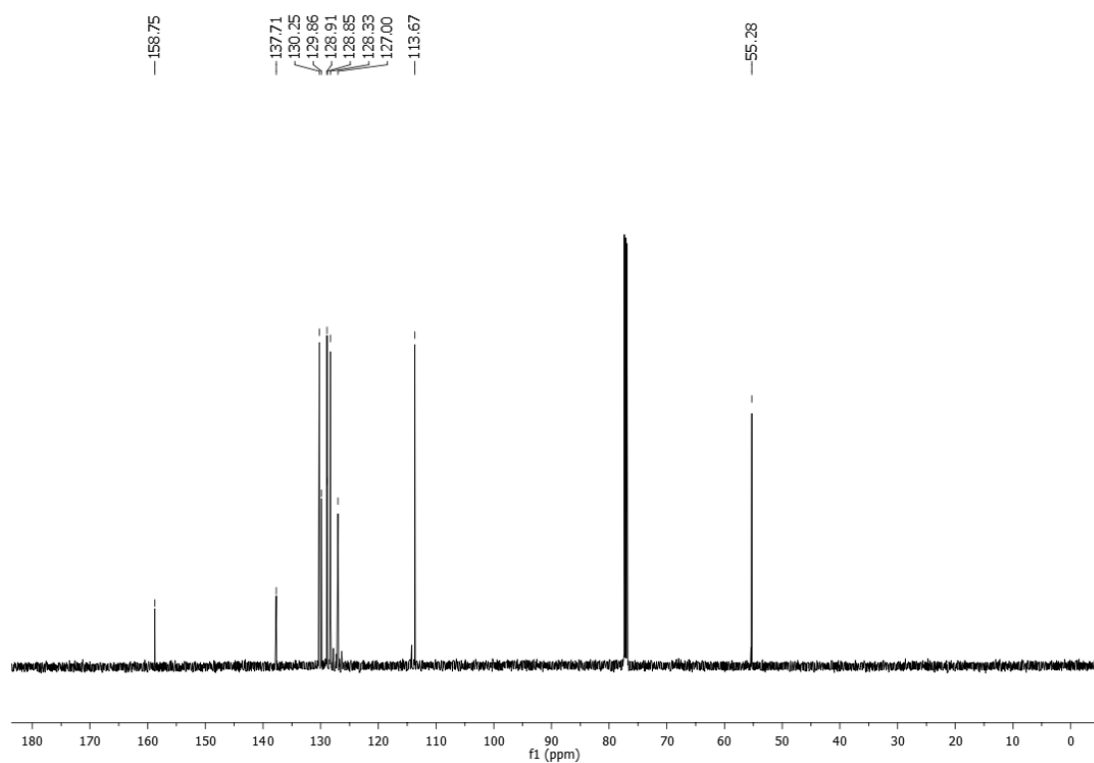


¹³C-NMR (151 MHz, CDCl₃) of (Z)-4-styrylaniline (Table 25, Entry 2).

(Z)-1-(4-methoxystyryl)benzene (2.26c)⁴⁷⁶: ¹H NMR (600 MHz, CDCl₃) δ 7.29 – 7.20 (m, 7H), 6.77 – 6.79 (m, 2H), 6.54 (d, 2H), 3.80 (s, 3H) ppm; ¹³C NMR (151 MHz, CDCl₃) δ 158.76, 137.71, 130.25, 129.86, 128.91, 128.85, 128.33, 127.00, 113.67, 55.28 ppm.

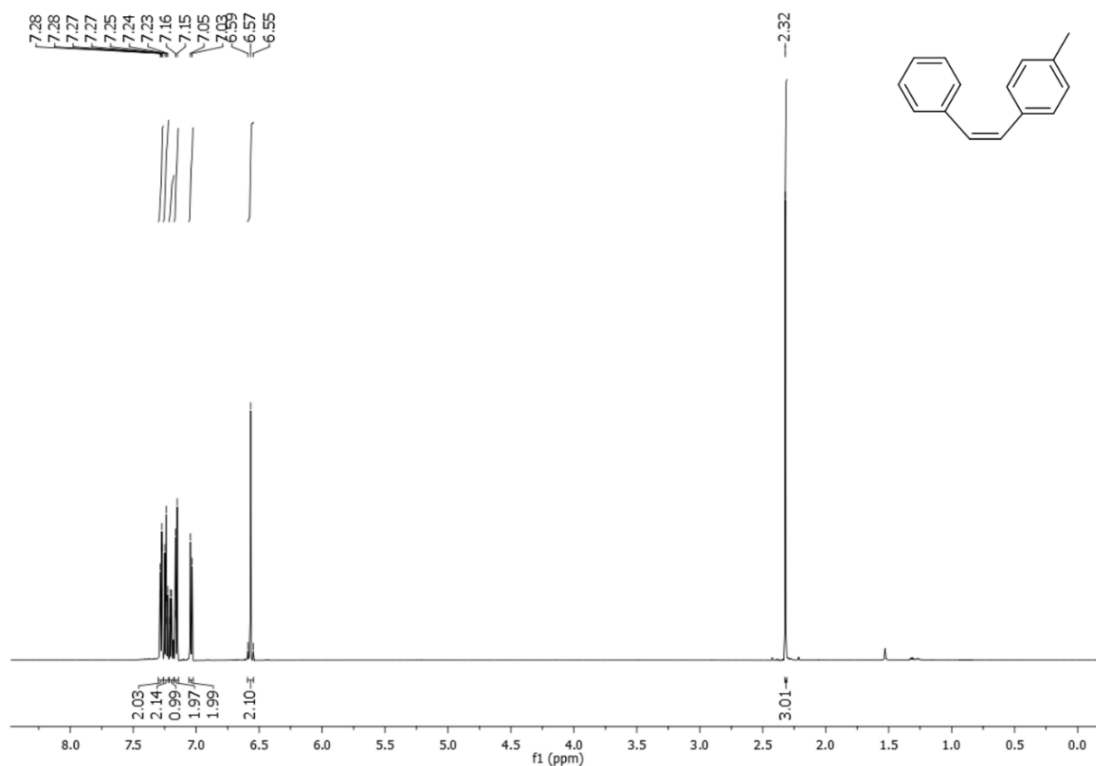


¹H NMR (600 MHz, CDCl₃) of (Z)-1-(4-methoxystyryl)benzene (Table 25, Entry 3).

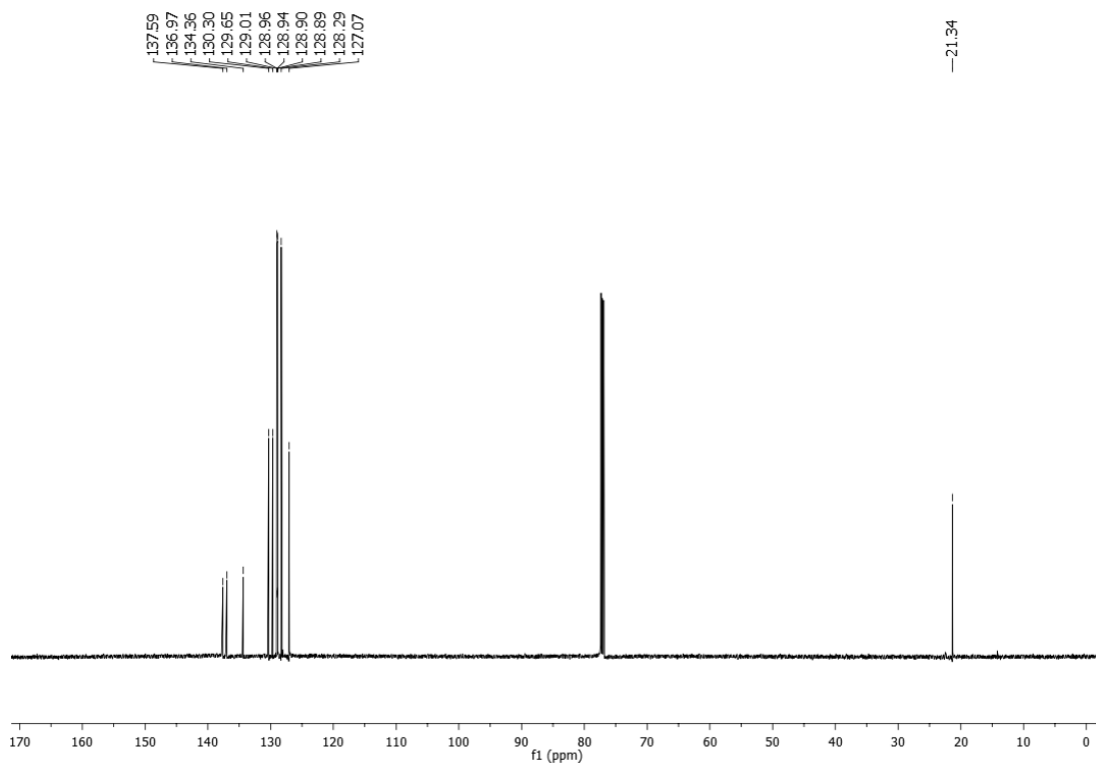


¹³C-NMR (151 MHz, CDCl₃) of (Z)-1-(4-methoxystyryl)benzene (Table 25, Entry 3).

(Z)-1-methyl-4-styrylbenzene (2.26d)³⁸⁰: ¹H NMR (600 MHz, CDCl₃) δ 7.30 – 7.26 (m, 2H), 7.24 (ddd, *J* = 7.4, 6.2, 1.4 Hz, 2H), 7.20 (dd, *J* = 5.1, 3.6 Hz, 1H), 7.19 – 7.15 (m, 2H), 7.04 (d, *J* = 7.9 Hz, 2H), 6.59 – 6.55 (dd, 2H), 2.32 (s, 3H) ppm; ¹³C NMR (151 MHz, CDCl₃) δ 137.59, 136.97, 134.36, 130.30, 129.65, 129.01, 128.95, 128.89, 128.29, 127.07, 21.35 ppm.

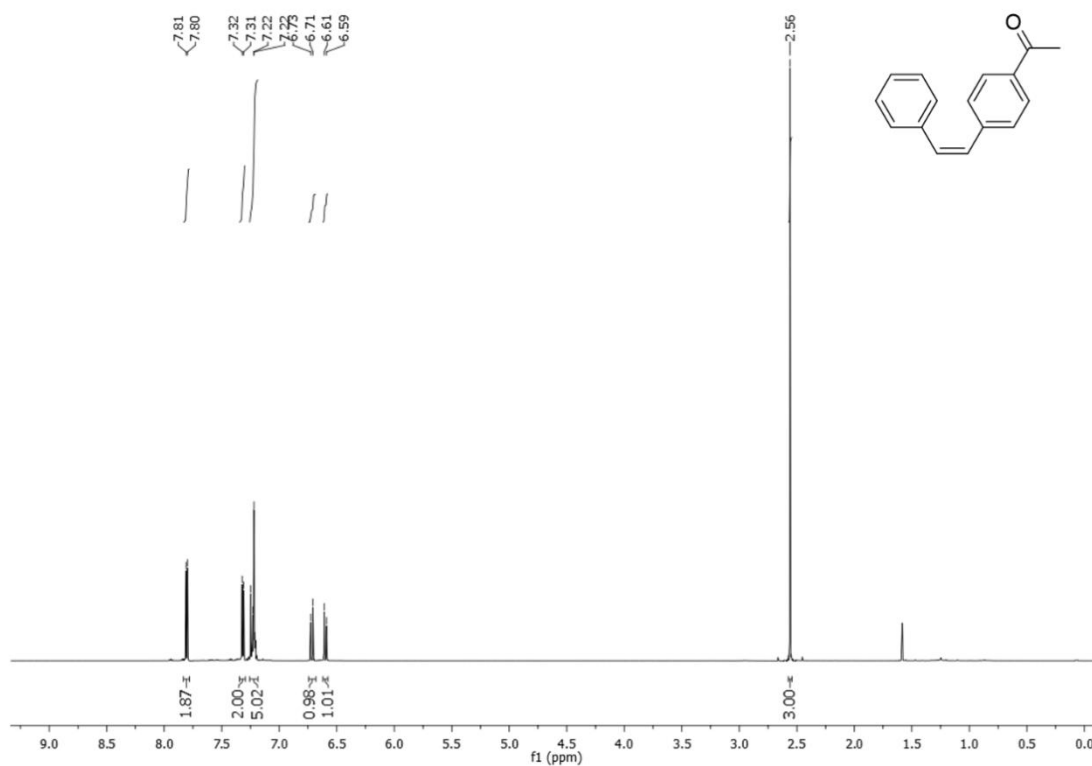


¹H NMR (600 MHz, CDCl₃) of (Z)-1-methyl-4-styrylbenzene (Table 25, Entry 4)

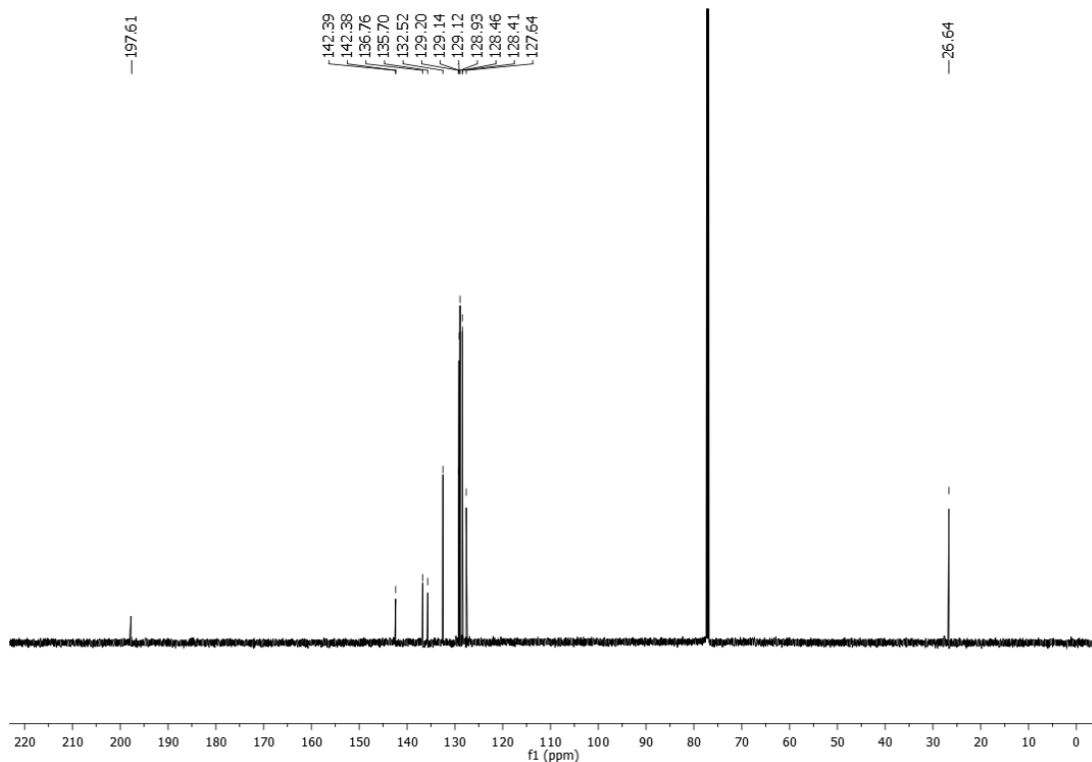


¹³C-NMR (151 MHz, CDCl₃) of (Z)-1-methyl-4-styrylbenzene (Table 25, Entry 4).

(Z)-1-(4-styrylphenyl)ethanone (2.26e)⁴⁷⁷: ¹H NMR (600 MHz, CDCl₃) δ 7.80 (d, *J* = 8.3 Hz, 2H), 7.32 (d, *J* = 8.1 Hz, 2H), 7.23 (dd, *J* = 11.8, 6.6 Hz, 5H), 6.72 (d, *J* = 12.2 Hz, 1H), 6.60 (d, *J* = 12.2 Hz, 1H), 2.56 (s, 3H) ppm; ¹³C NMR (151 MHz, CDCl₃) δ 197.61, 142.39, 136.76, 135.70, 132.52, 129.20, 129.14, 128.93, 128.46, 128.41, 127.64, 26.64 ppm.

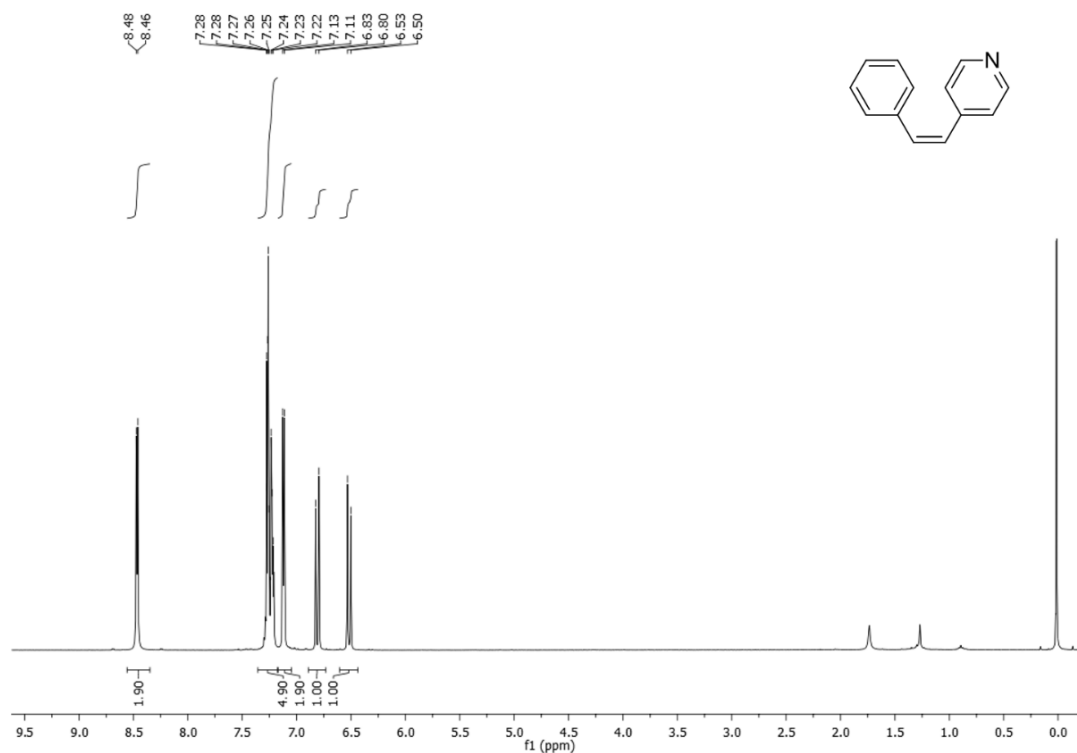


¹H NMR (600 MHz, CDCl₃) of (Z)-1-(4-styrylphenyl)ethanone (Table 25, Entry 5)

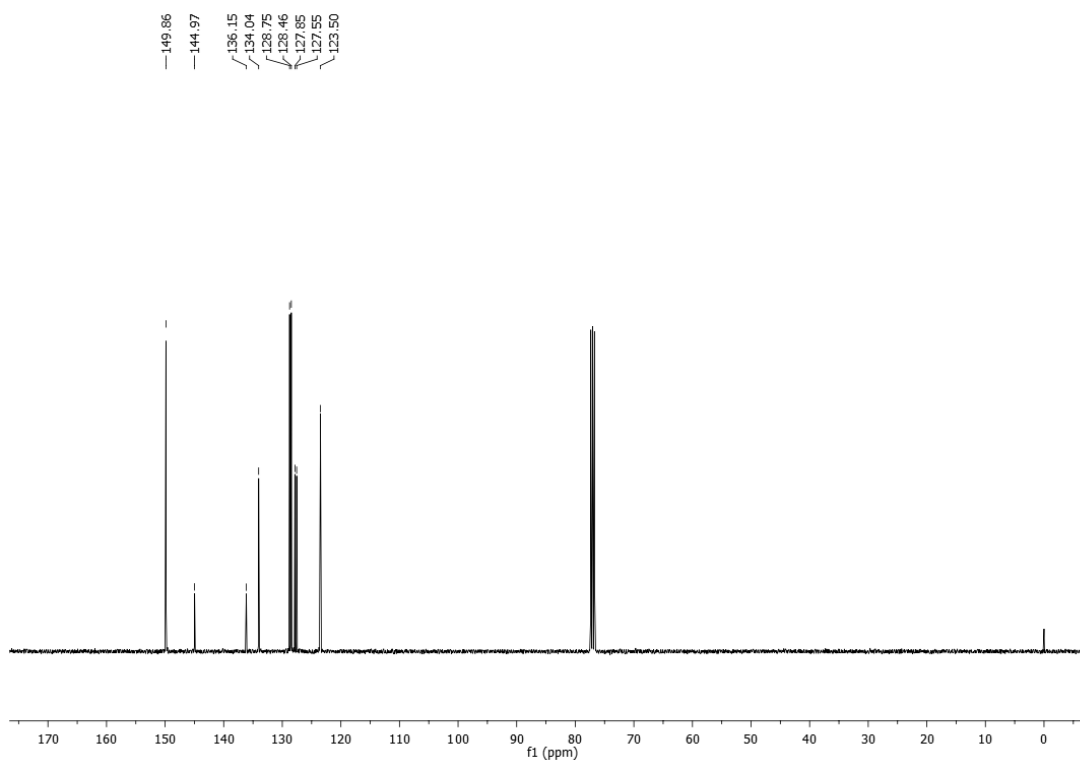


¹³C-NMR (151 MHz, CDCl₃) of (Z)-1-(4-styrylphenyl)ethanone (Table 25, Entry 5)

(Z)-2-styrylpyridine (2.26h)³⁸⁰: ¹H NMR (400 MHz, CDCl₃) δ 8.47 (d, *J* = 6.1 Hz, 2H), 7.25 (ddd, *J* = 14.9, 6.2, 2.6 Hz, 5H), 7.12 (d, *J* = 6.0 Hz, 2H), 6.81 (d, *J* = 12.3 Hz, 1H), 6.52 (d, *J* = 12.3 Hz, 1H). ppm; ¹³C NMR (101 MHz, CDCl₃) δ 149.86, 144.97, 136.15, 134.04, 128.75, 128.46, 127.85, 127.55, 123.50 ppm.

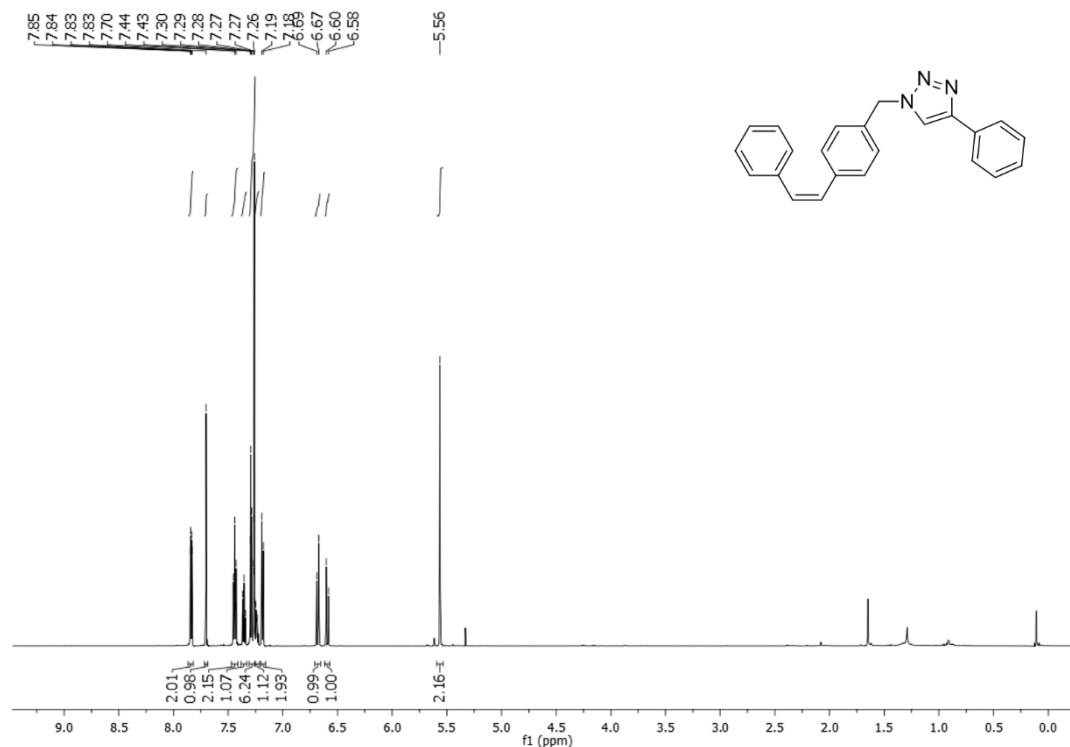


¹H NMR (600 MHz, CDCl₃) of (Z)-2-styrylpyridine (Table 25, Entry 8)

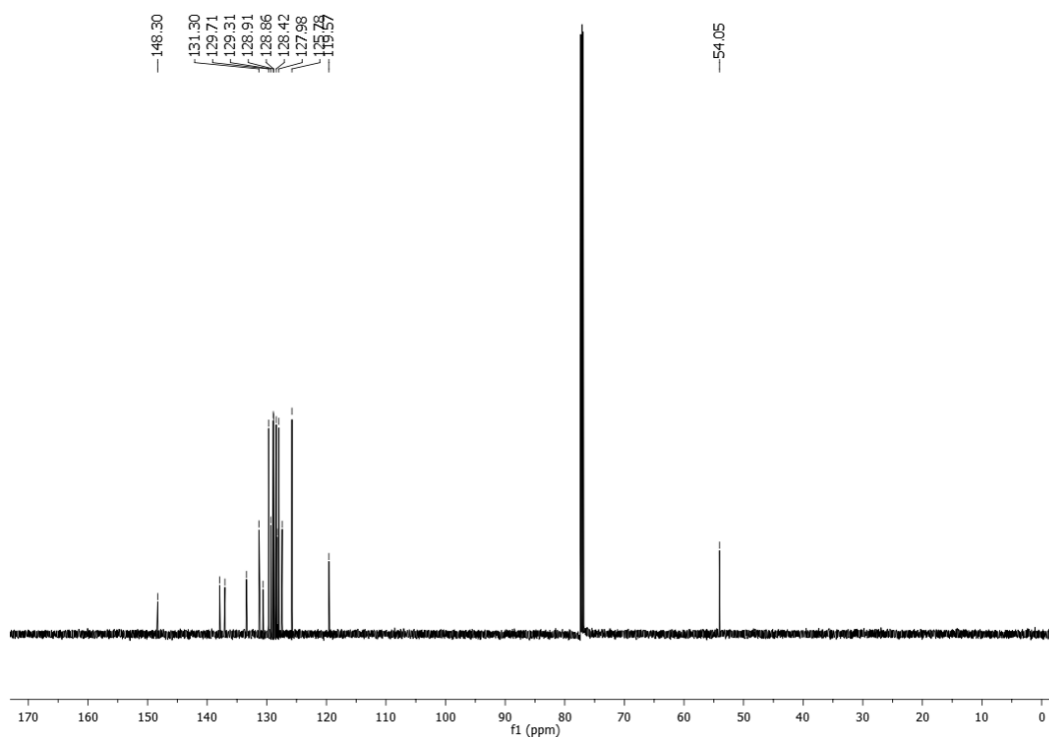


¹³C-NMR (151 MHz, CDCl₃) of (Z)-2-styrylpyridine (Table 25, Entry 8)

(Z)-4-phenyl-1-(4-styrylbenzyl)-1H-1,2,3-triazole (2.26i): ^1H NMR (600 MHz,) δ 7.84 (dd, J = 8.3, 1.2 Hz, 2H), 7.70 (s, 1H), 7.47 – 7.41 (m, 2H), 7.38 – 7.33 (m, 1H), 7.31 – 7.25 (m, 6H), 7.26 – 7.21 (m, 1H), 7.19 (d, J = 8.2 Hz, 2H), 6.68 (d, J = 12.2 Hz, 1H), 6.59 (d, J = 12.2 Hz, 1H), 5.56 (s, 2H); ^{13}C NMR (151 MHz, CDCl_3) δ 148.30, 131.30, 129.71, 129.31, 128.91, 128.86, 128.42, 127.98, 125.78, 119.57, 54.05 ppm.

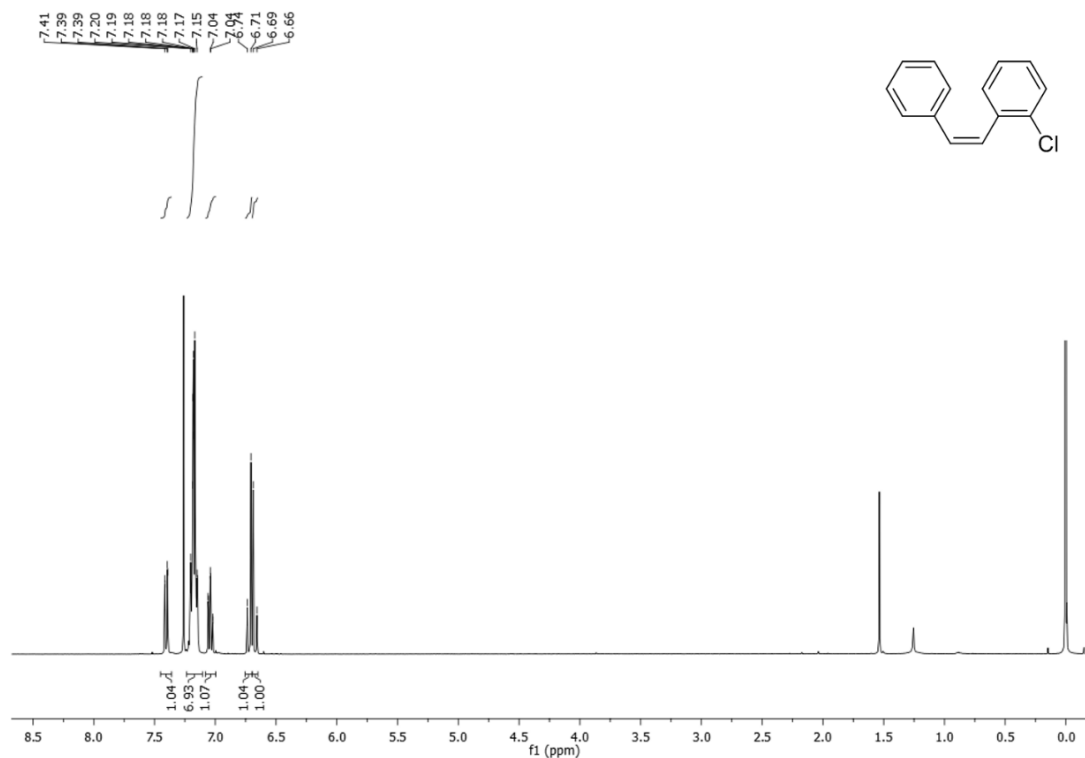


^1H NMR (600 MHz, CDCl_3) of (Z)-4-phenyl-1-(4-styrylbenzyl)-1H-1,2,3-triazole (Table 25, Entry 9)

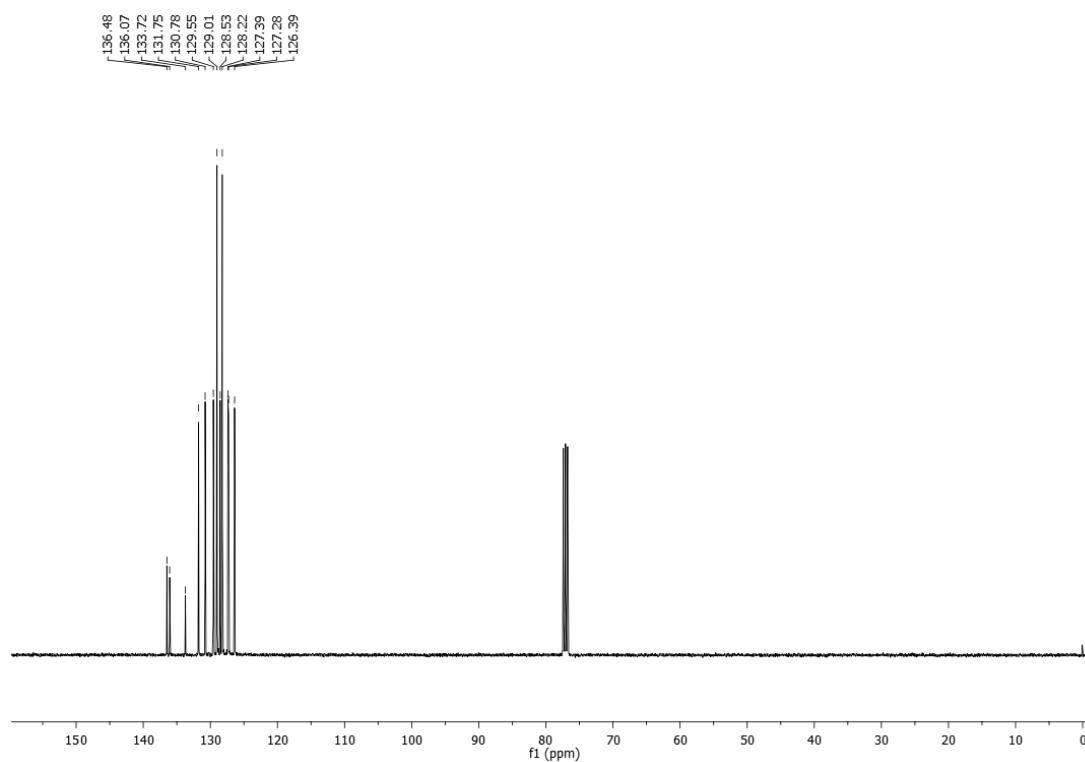


^{13}C -NMR (151 MHz, CDCl_3) of (Z)-4-phenyl-1-(4-styrylbenzyl)-1H-1,2,3-triazole (Table 25, Entry 9)

(Z)-1-chloro-2-styrylbenzene (2.26j)⁴⁷⁸: ¹H NMR (400 MHz, CDCl₃) δ 7.40 (dd, *J* = 8.0, 1.1 Hz, 1H), 7.24 – 7.11 (m, 7H), 7.04 (td, *J* = 7.5, 1.1 Hz, 1H), 6.72 (d, *J* = 12.2 Hz, 1H), 6.67 (d, *J* = 12.2 Hz, 1H).ppm ¹³C NMR (101 MHz, CDCl₃) δ 136.48, 136.07, 133.72, 131.75, 130.78, 129.55, 129.01, 128.53, 128.22, 127.39, 127.28, 126.39 ppm.

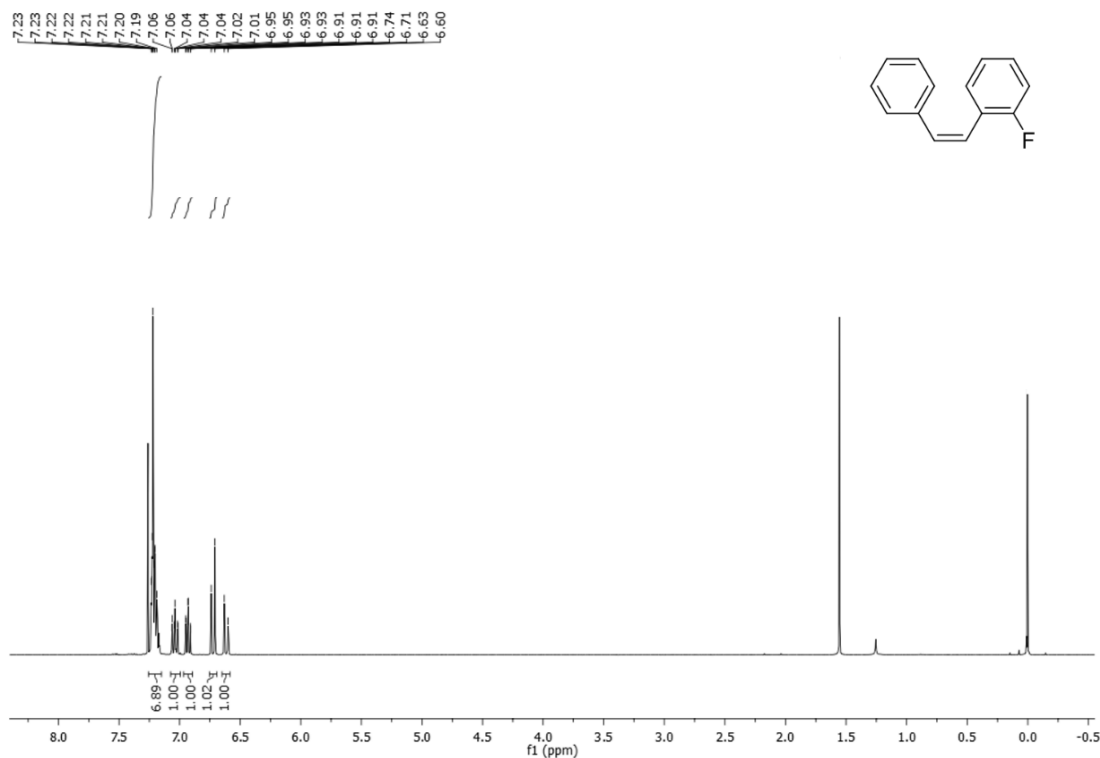


¹H NMR (600 MHz, CDCl₃) of (Z)-1-chloro-3-styrylbenzene (Table 25, Entry 10)



¹³C-NMR (151 MHz, CDCl₃) of (Z)-1-chloro-3-styrylbenzene (Table 25, Entry 10)

(Z)-1-fluoro-2-styrylbenzene (2.26k)⁴⁷⁶: ¹H NMR (400 MHz, CDCl₃) δ 7.26 – 7.15 (m, 7H), 7.04 (ddd, *J* = 10.0, 8.8, 1.2 Hz, 1H), 6.97 – 6.89 (m, 1H), 6.72 (d, *J* = 12.2 Hz, 1H), 6.62 (d, *J* = 12.2 Hz, 1H) ppm. ¹³C NMR (101 MHz, CDCl₃) δ 161.61, 132.24, 132.23, 130.53, 130.50, 128.98, 128.90, 128.75, 128.25, 127.39, 123.64, 123.60, 122.63, 122.60, 115.72 ppm.



¹H NMR (600 MHz, CDCl₃) of (Z)-1-fluoro-2-styrylbenzene (Table 25, Entry 11).

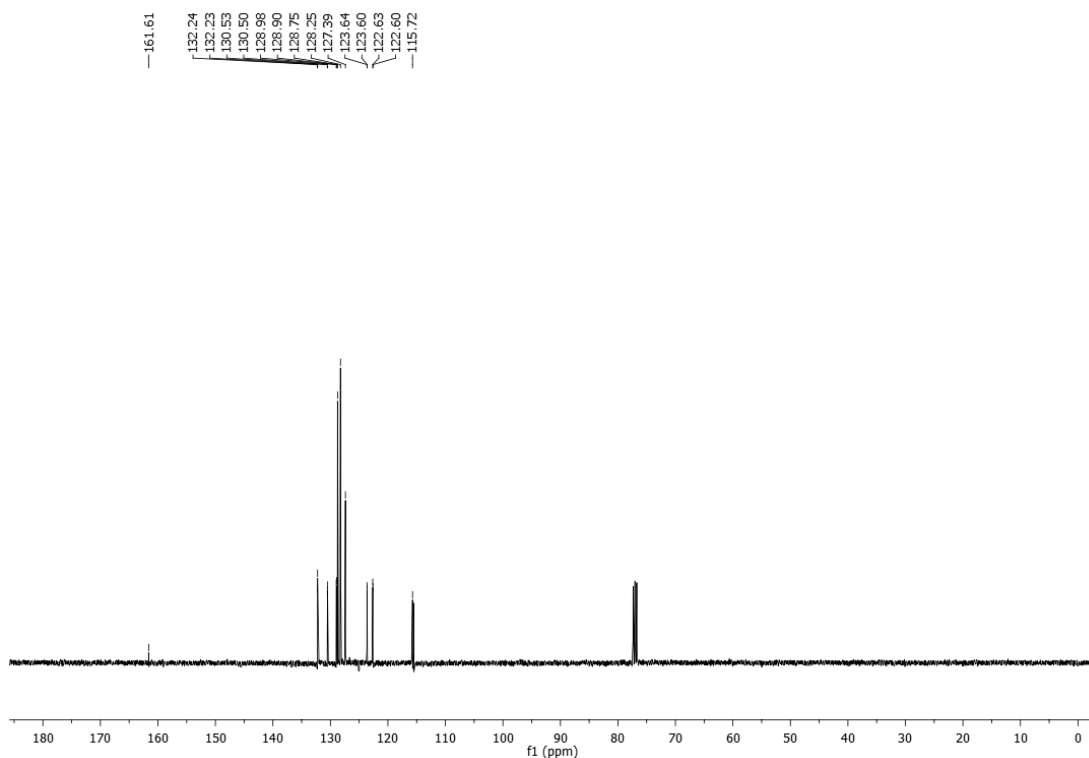
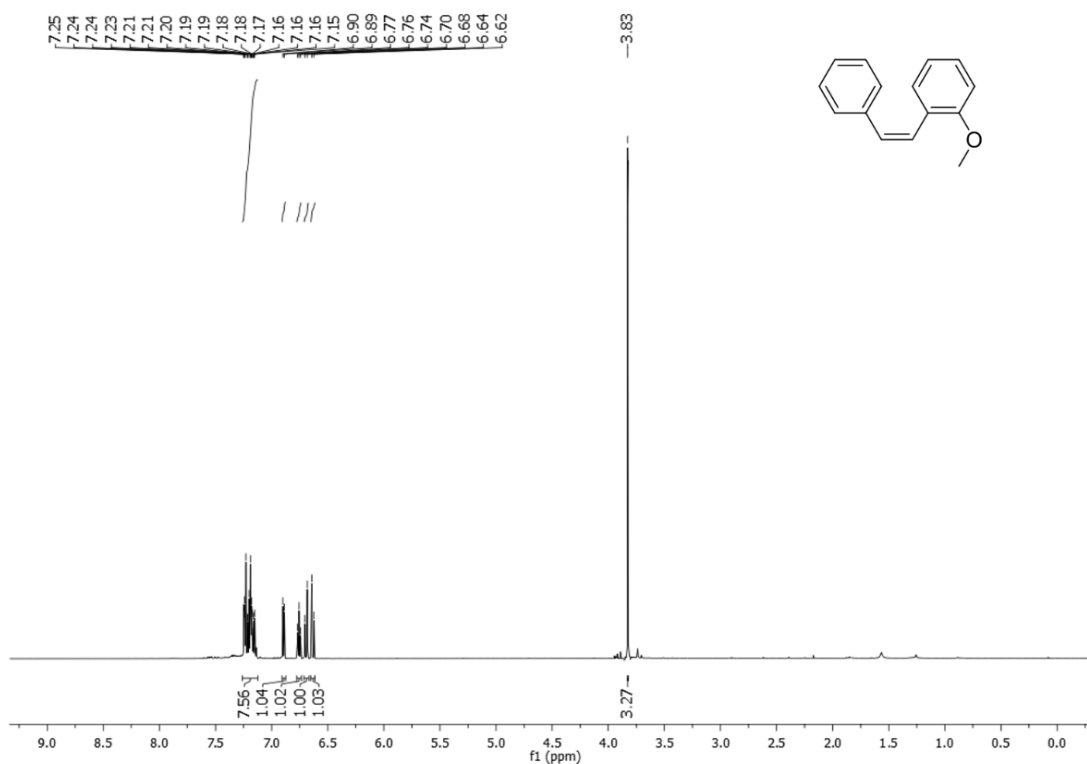
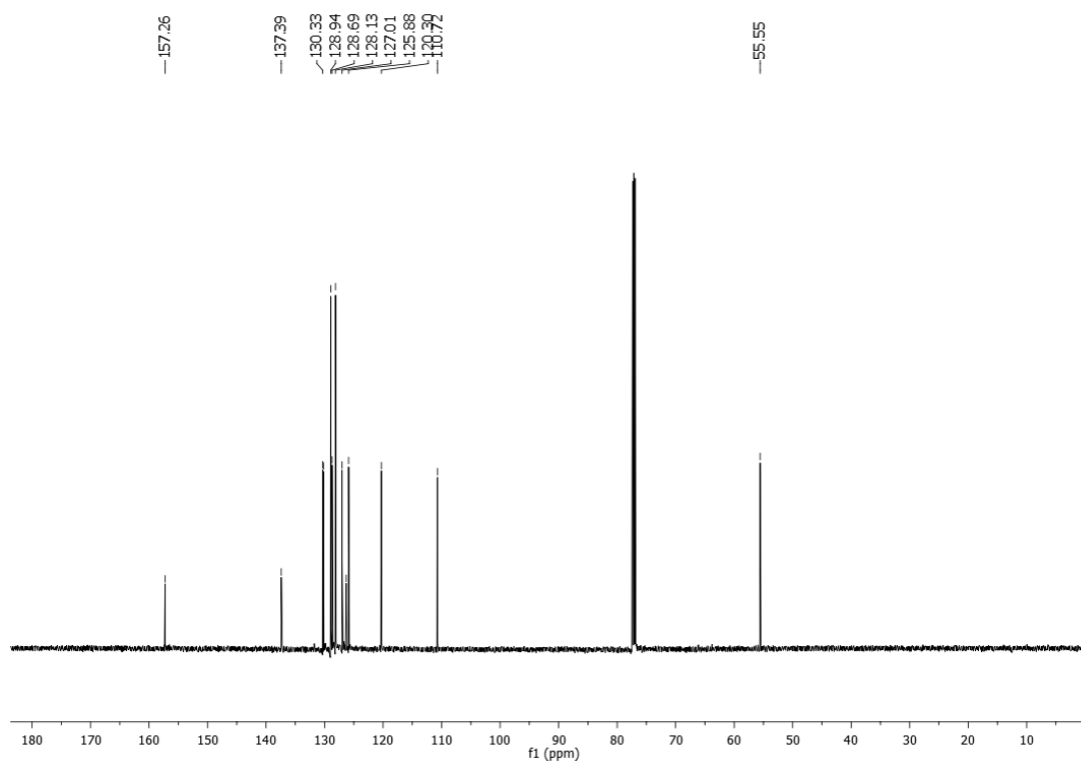


Figure 18. ¹³C-NMR (151 MHz, CDCl₃) of (Z)-1-fluoro-2-styrylbenzene (Table 25, Entry 11).

(Z)-1-(2-methoxystyryl)benzene (2.26I)⁴⁷⁹: ¹H NMR (600 MHz, CDCl₃) δ 7.20 (dddd, *J* = 13.7, 8.5, 6.0, 4.7 Hz, 7H), 6.89 (d, *J* = 8.2 Hz, 1H), 6.76 (t, *J* = 7.5 Hz, 1H), 6.69 (d, *J* = 12.3 Hz, 1H), 6.63 (d, *J* = 12.3 Hz, 1H), 3.83 (s, 3H).; ¹³C NMR (151 MHz, CDCl₃) δ 157.26, 137.39, 130.33, 130.19, 128.94, 128.69, 128.13, 127.01, 126.27, 125.88, 120.30, 110.72, 55.55 ppm.

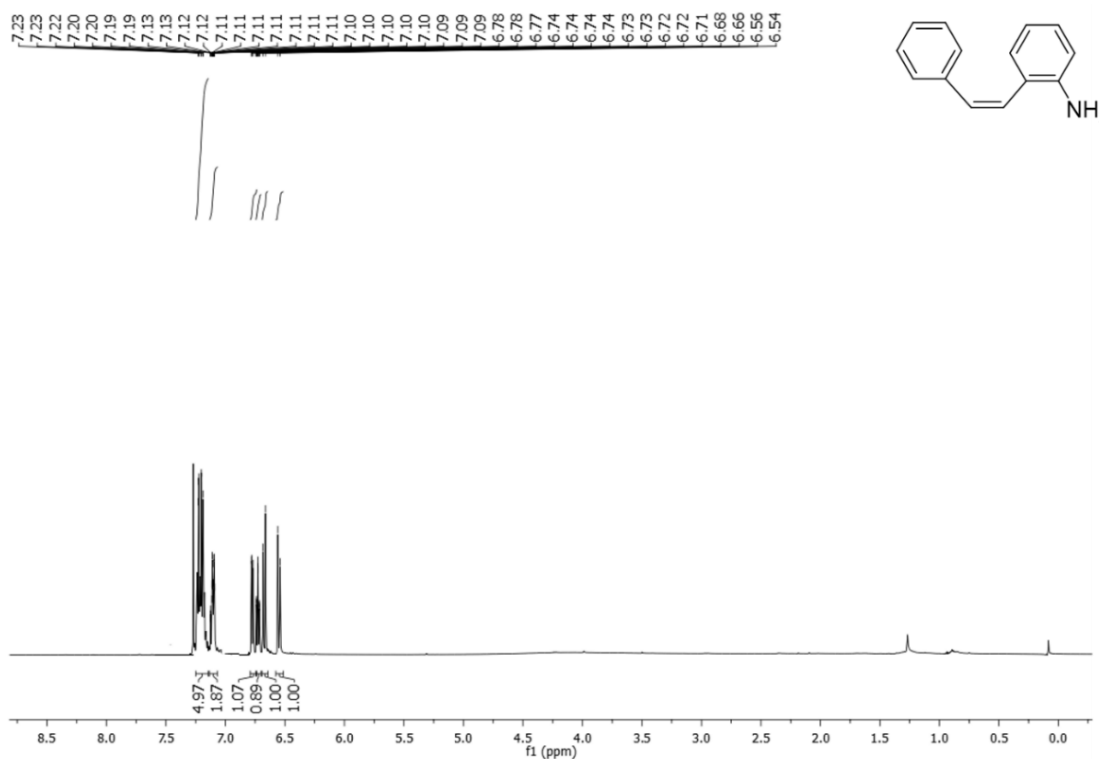


¹H NMR (600 MHz, CDCl₃) of (Z)-1-(2-methoxystyryl)benzene (Table 25, Entry 12).

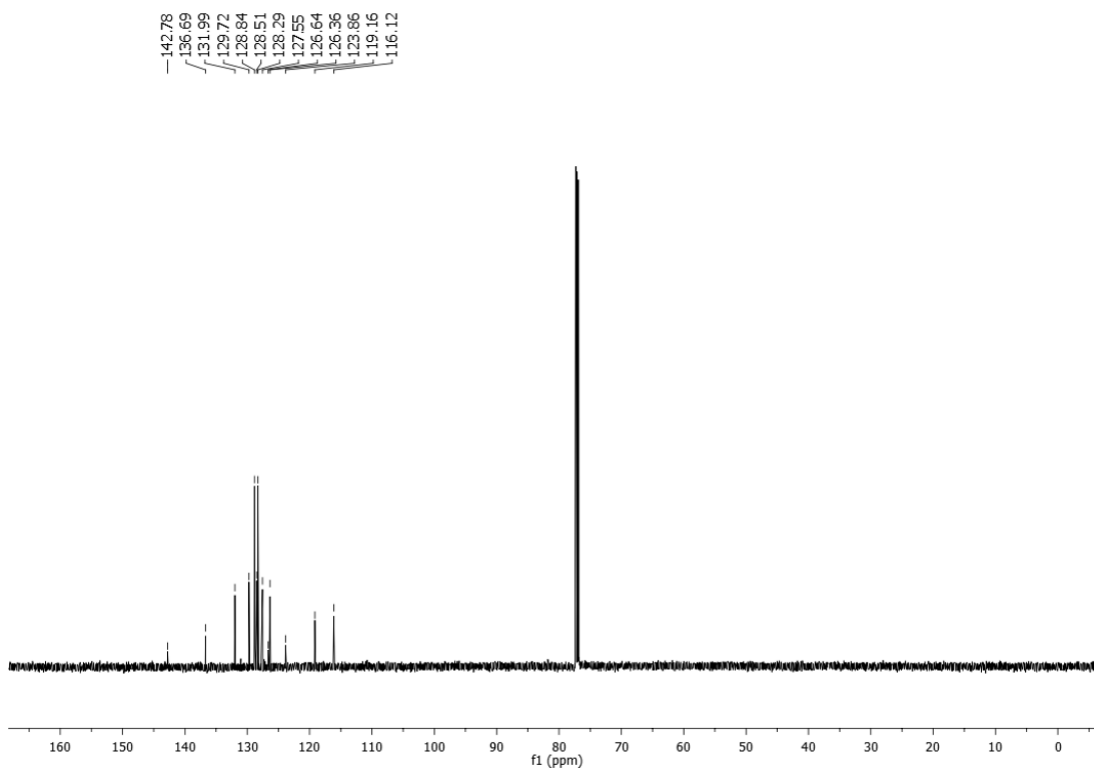


¹³C-NMR (151 MHz, CDCl₃) of (Z)-1-(2-methoxystyryl)benzene (Table 25, Entry 12)

(Z)-2-styrylaniline (2.26m)¹¹⁷: ¹H NMR (600 MHz, CDCl₃) δ 7.25 – 7.16 (m, 5H), 7.13 – 7.08 (m, 2H), 6.80 – 6.74 (m, 1H), 6.74 – 6.70 (m, 1H), 6.67 (d, *J* = 12.1 Hz, 1H), 6.55 (d, *J* = 12.1 Hz, 1H) ppm; ¹³C NMR (151 MHz, CDCl₃) δ 142.78, 136.70, 131.99, 129.72, 128.84, 128.77, 128.51, 128.29, 127.55, 126.64, 126.36, 123.86, 119.16, 116.12 ppm.



¹H NMR (600 MHz, CDCl₃) of (Z)-2-styrylaniline (Table 25, Entry 13)



¹³C-NMR (151 MHz, CDCl₃) of (Z)-2-styrylaniline (Table 25, Entry 13)

(Z)-1-methyl-2-styrylbenzene (2.26n)⁴⁸⁰: ¹H NMR (600 MHz, CDCl₃) δ 7.26 – 7.10 (m, 8H), 7.06 (t, *J* = 7.4 Hz, 1H), 6.65 (q, *J* = 12.2 Hz, 2H), 2.29 (s, 3H) ppm; ¹³C NMR (151 MHz, CDCl₃) δ 137.21, 137.12, 136.21, 130.60, 130.17, 129.64, 129.03, 129.01, 128.98, 128.96, 128.95, 128.19, 127.33, 127.14, 125.81, 20.00 ppm.

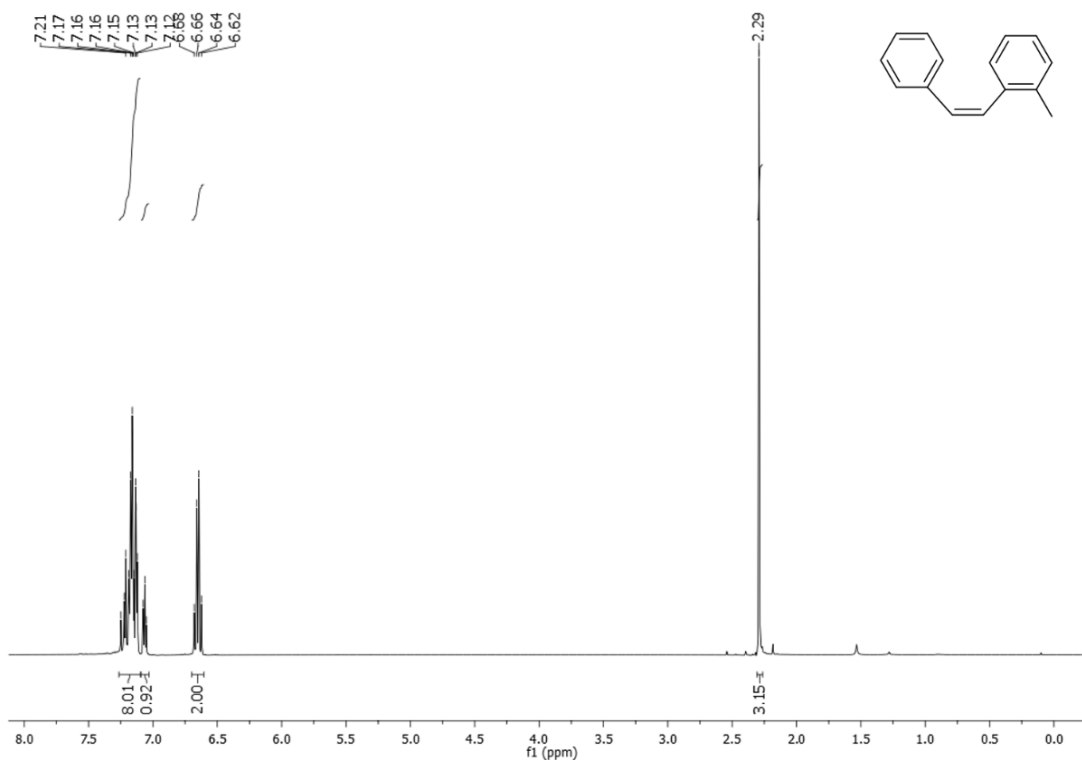


Figure 15. ¹H NMR (600 MHz, CDCl₃) of (Z)-1-methyl-2-styrylbenzene (Table 25, Entry 14)

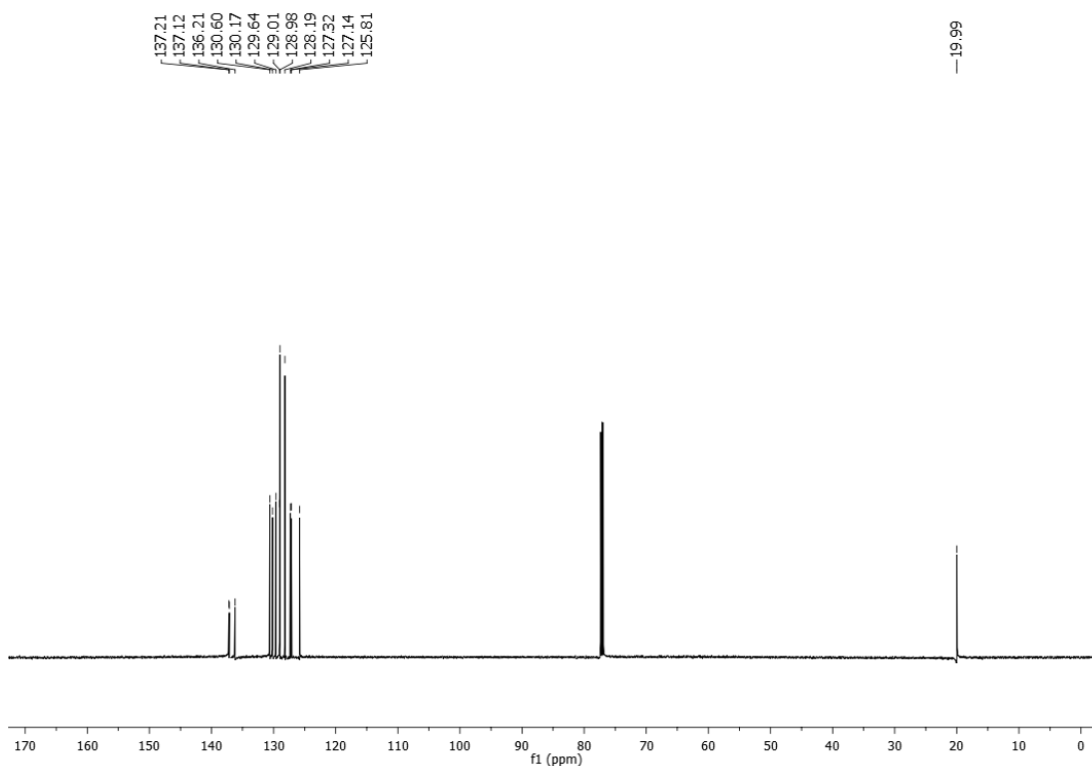
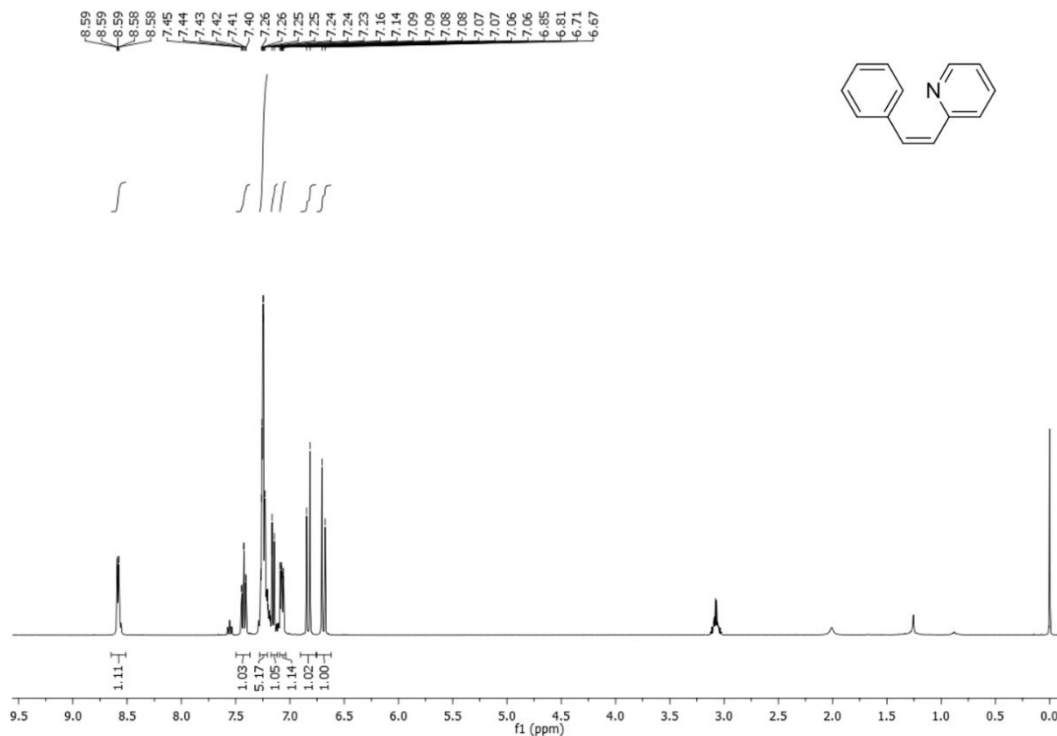


Figure 16. ¹³C-NMR (151 MHz, CDCl₃) of (Z)-1-methyl-2-styrylbenzene (Table 25, Entry 14)

(Z)-2-(2-phenylethenyl)pyridine (2.26o)³⁷³: ¹H NMR (400 MHz, CDCl₃) δ 8.65 – 8.51 (m, 1H), 7.42 (td, *J* = 7.7, 1.8 Hz, 1H), 7.28 – 7.21 (m, 5H), 7.15 (d, *J* = 7.9 Hz, 1H), 7.07 (ddd, *J* = 7.4, 4.8, 0.8 Hz, 1H), 6.83 (d, *J* = 12.5 Hz, 1H), 6.69 (d, *J* = 12.4 Hz, 1H). ppm; ¹³C NMR (101 MHz, CDCl₃) δ 156.35, 149.55, 136.65, 135.61, 133.24, 130.51, 128.87, 128.29, 127.58, 123.84, 121.74. ppm.



¹H NMR (600 MHz, CDCl₃) of (Z)-2-(2-phenylethenyl)pyridine (Table 25, Entry 15).

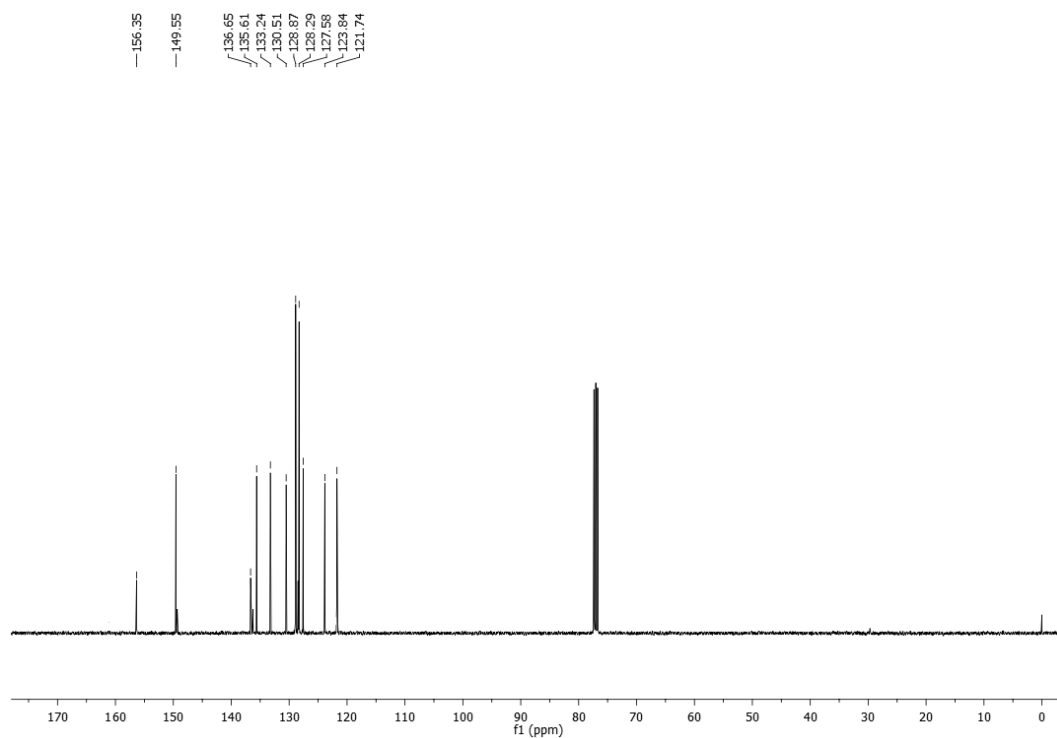
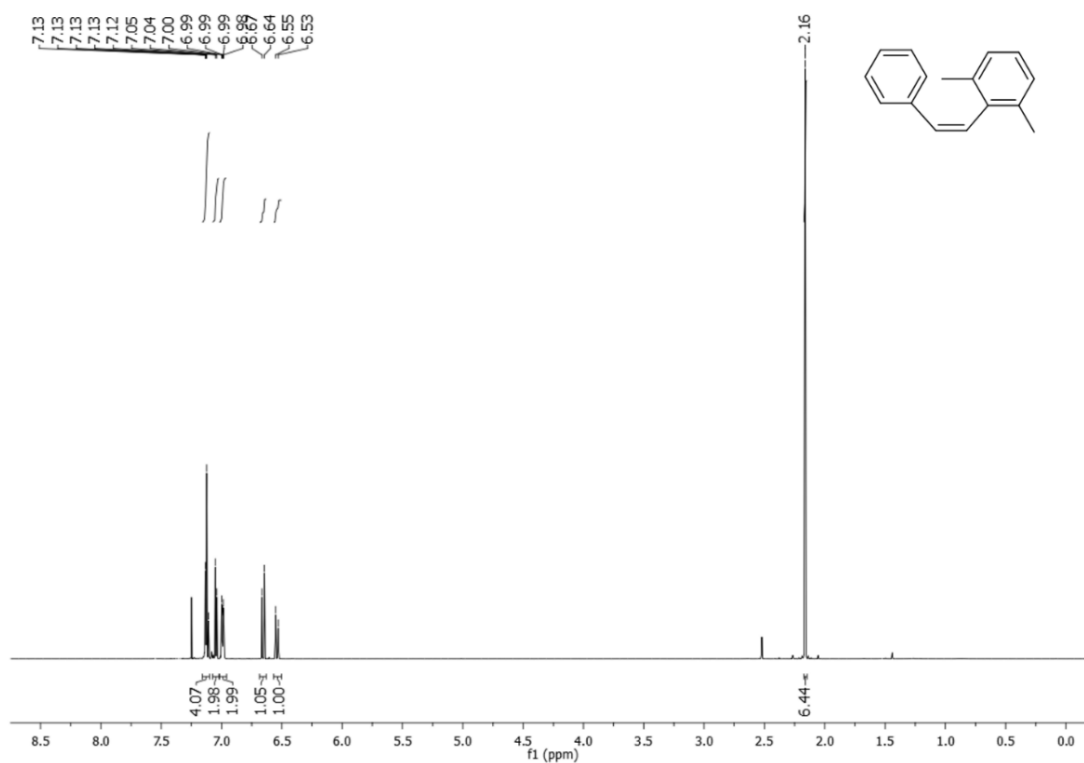
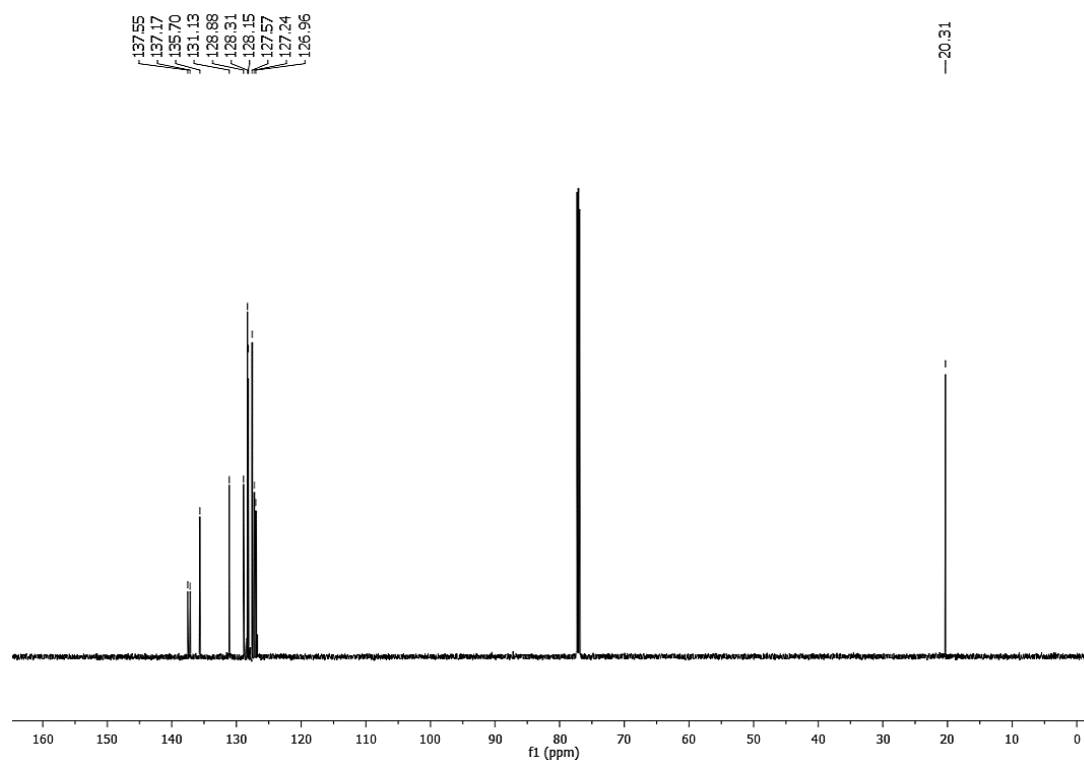


Figure 18. ¹³C-NMR (151 MHz, CDCl₃) of (Z)-2-(2-phenylethenyl)pyridine (Table 25, Entry 15).

(Z)-1,3-dimethyl-2-styrylbenzene (2.26p)⁴⁸¹: ¹H NMR (600 MHz, CDCl₃) δ 7.13 (dt, *J* = 10.1, 4.6 Hz, 4H), 7.04 (d, *J* = 7.5 Hz, 2H), 7.02 – 6.96 (m, 2H), 6.66 (d, *J* = 12.3 Hz, 1H), 6.54 (d, *J* = 12.3 Hz, 1H), 2.16 (s, 6H) ppm; ¹³C NMR (151 MHz, CDCl₃) δ 137.55, 137.17, 135.70, 131.13, 128.88, 128.31, 128.15, 127.57, 127.24, 126.96, 20.31 ppm.

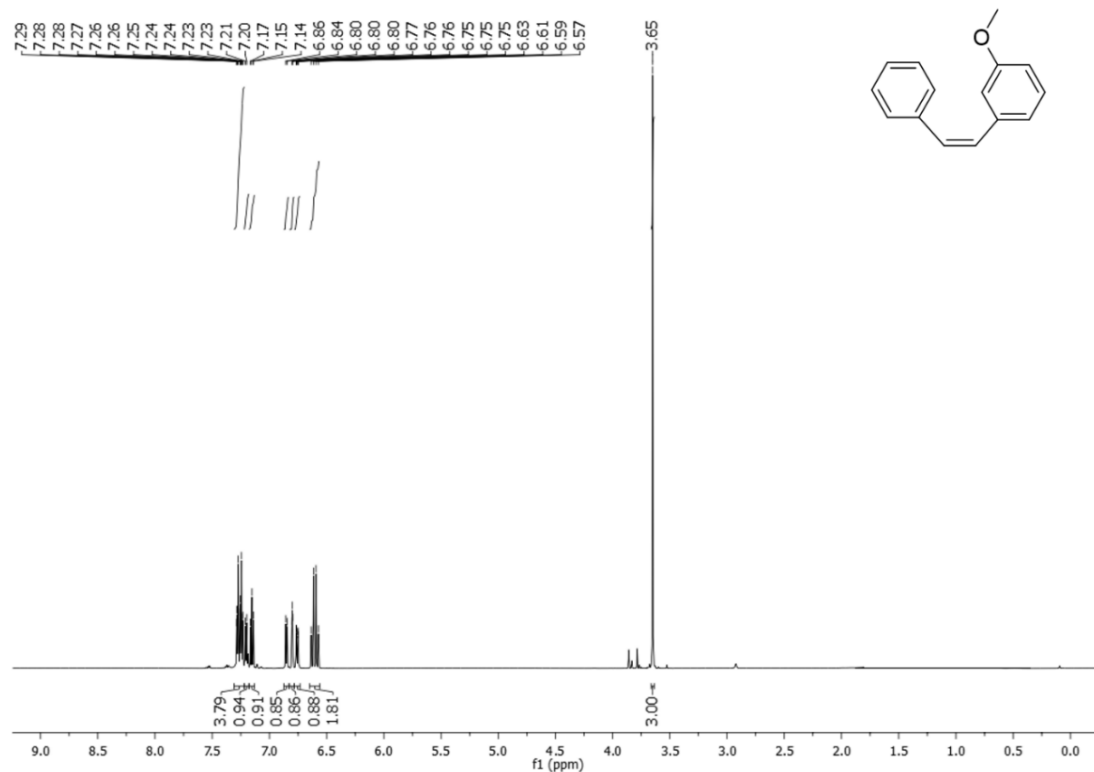


¹H NMR (600 MHz, CDCl₃) of (Z)-1,3-dimethyl-2-styrylbenzene (Table 25, Entry 16)



¹³C-NMR (151 MHz, CDCl₃) of (Z)-1,3-dimethyl-2-styrylbenzene (Table 25, Entry 16)

(Z)-1-(3-methoxystyryl)benzene (2.26q)⁴⁸²: ¹H NMR (600 MHz,) δ 7.31 – 7.22 (m, 4H), 7.20 (d, J = 7.1 Hz, 1H), 7.15 (t, J = 7.9 Hz, 1H), 6.85 (d, J = 7.6 Hz, 1H), 6.82 – 6.78 (m, 1H), 6.78 – 6.73 (m, 1H), 6.60 (q, J = 12.2 Hz, 2H), 3.65 (s, 3H). ppm; ¹³C NMR (151 MHz,) δ 159.44, 138.63, 137.36, 130.58, 130.24, 129.32, 129.01, 128.30, 127.24, 121.61, 113.81, 113.41, 55.09 ppm.



¹H NMR (600 MHz, CDCl₃) of (Z)-1-(3-methoxystyryl)benzene (Table 25, Entry 17)

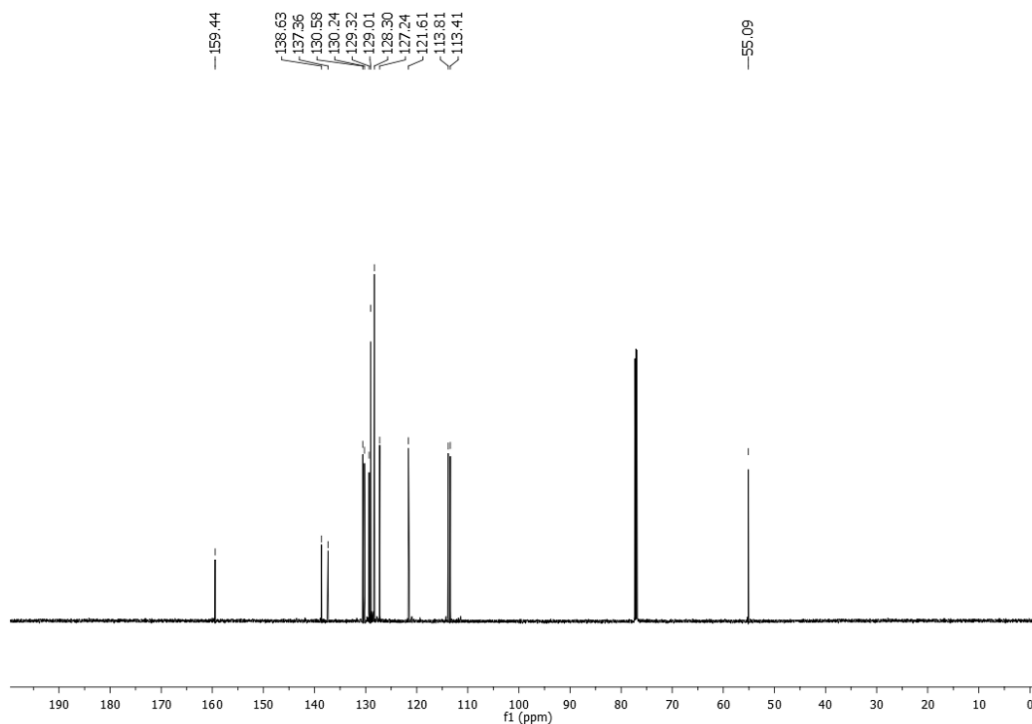
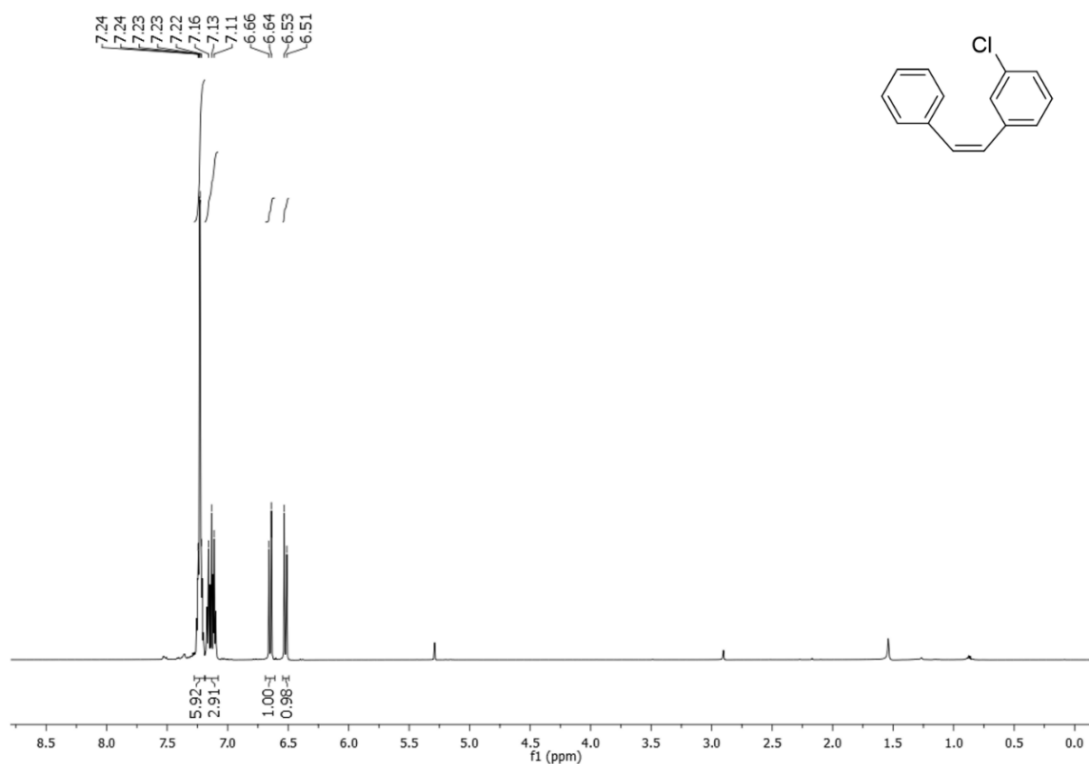
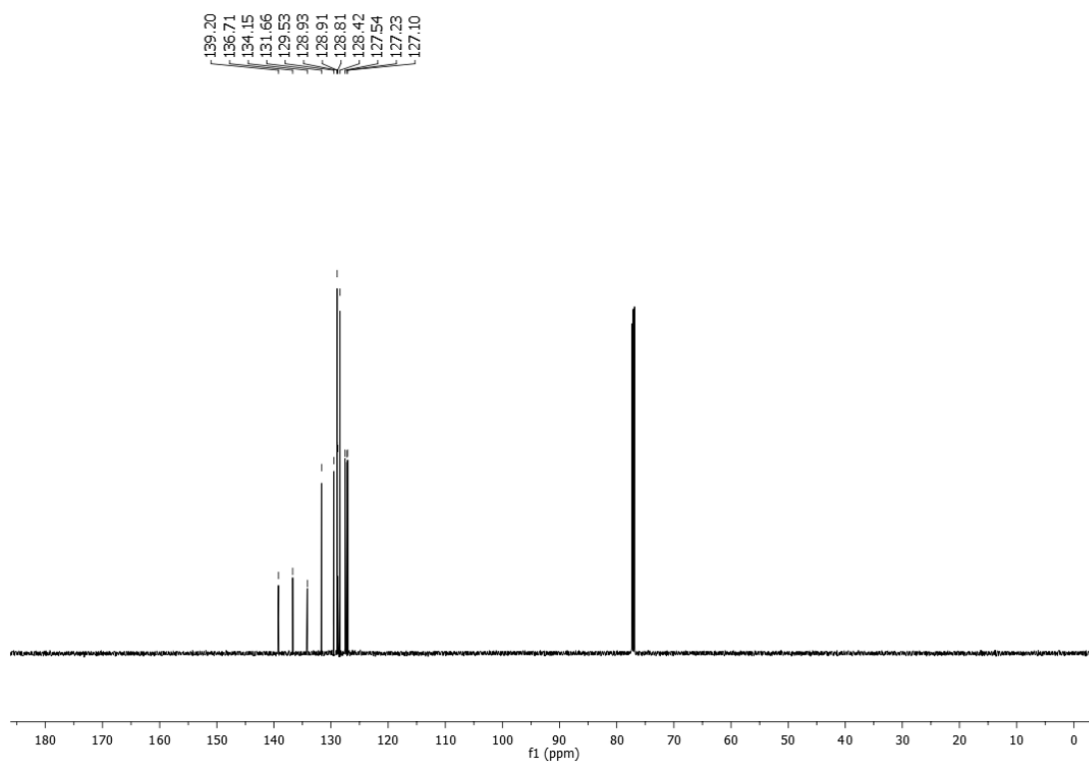


Figure 20. ¹³C-NMR (151 MHz, CDCl₃) of (Z)-1-(3-methoxystyryl)benzene (Table 25, Entry 17)

(Z)-1-chloro-3-styrylbenzene (2.26r)³⁸⁰: ¹H NMR (600 MHz, CDCl₃) δ 7.24 – 7.22 (m, 6H), 7.16 – 7.11 (m, 3H), 6.65 (d, *J* = 12.2 Hz, 1H), 6.52 (d, *J* = 12.2 Hz, 1H) ppm; ¹³C NMR (151 MHz, CDCl₃) δ 139.20, 136.71, 134.15, 131.66, 129.53, 128.93, 128.91, 128.81, 128.42, 127.54, 127.23, 127.10 ppm.

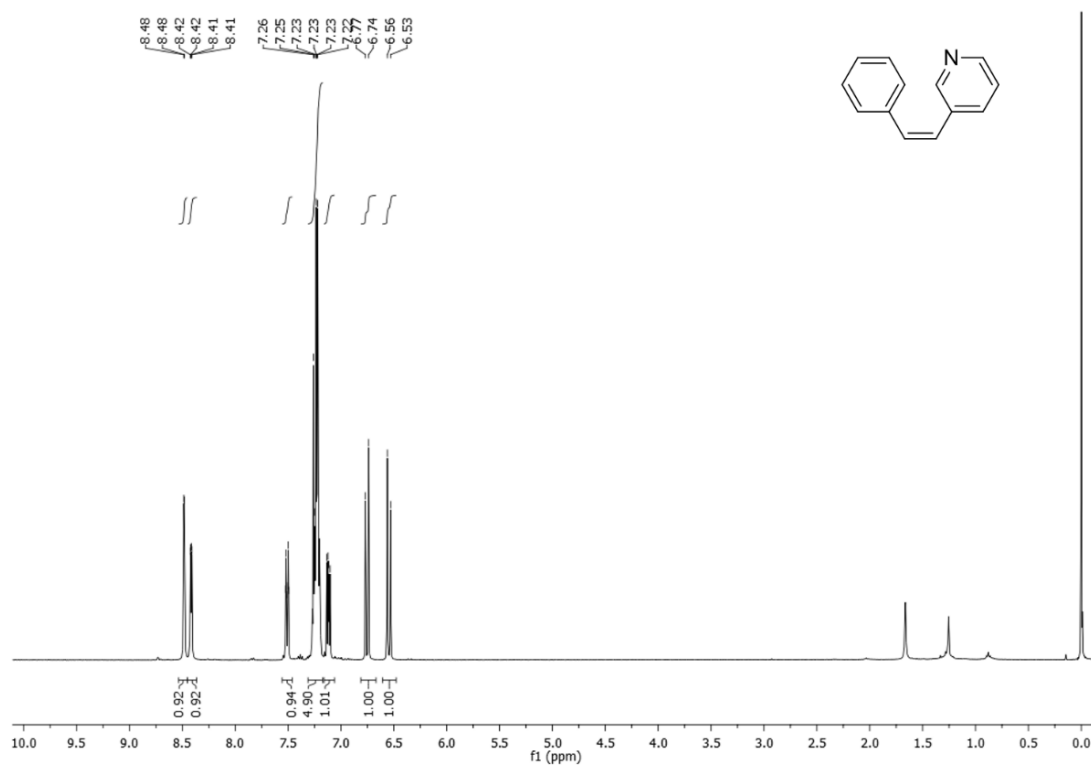


¹H NMR (600 MHz, CDCl₃) of (Z)-1-chloro-3-styrylbenzene (Table 25, Entry 18).

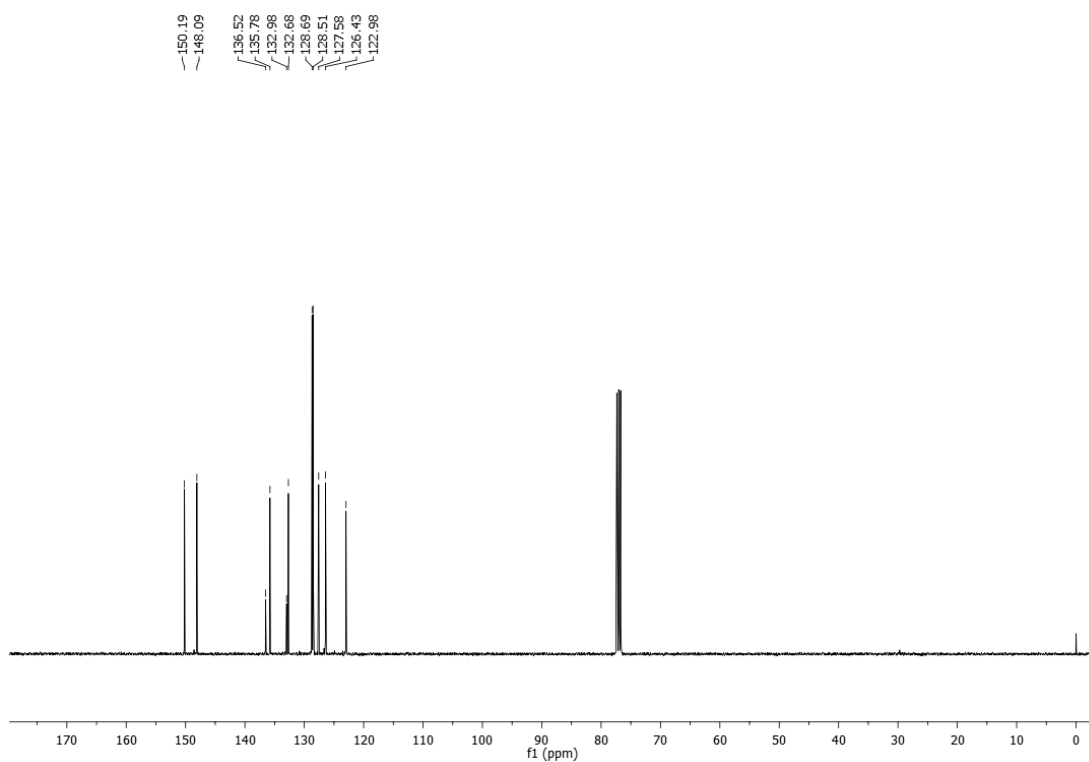


¹³C-NMR (151 MHz, CDCl₃) of (Z)-1-chloro-3-styrylbenzene (Table 25, Entry 18)

(Z)-3-styrylpyridine (2.26s)⁴⁸³: ¹H NMR (400 MHz, CDCl₃) δ 8.48 (d, *J* = 1.9 Hz, 1H), 8.42 (dd, *J* = 4.8, 1.4 Hz, 1H), 7.51 (dt, *J* = 7.9, 1.6 Hz, 1H), 7.31 – 7.17 (m, 5H), 7.12 (dd, *J* = 7.9, 4.8 Hz, 1H), 6.75 (d, *J* = 12.2 Hz, 1H), 6.55 (d, *J* = 12.2 Hz, 1H). ppm; ¹³C NMR (101 MHz, CDCl₃) δ 150.19, 148.09, 136.52, 135.78, 132.98, 132.68, 128.69, 128.51, 127.58, 126.43, 122.98 ppm.

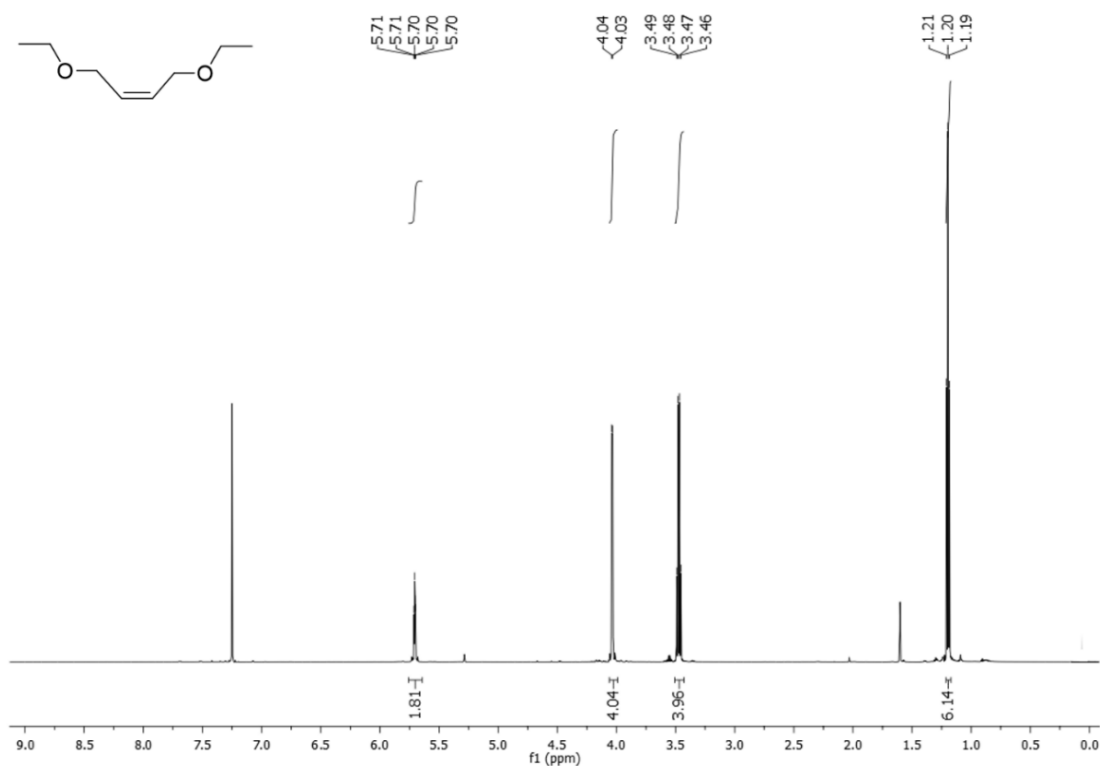


¹H NMR (600 MHz, CDCl₃) of (Z)-3-styrylpyridine (Table 25, Entry 19).

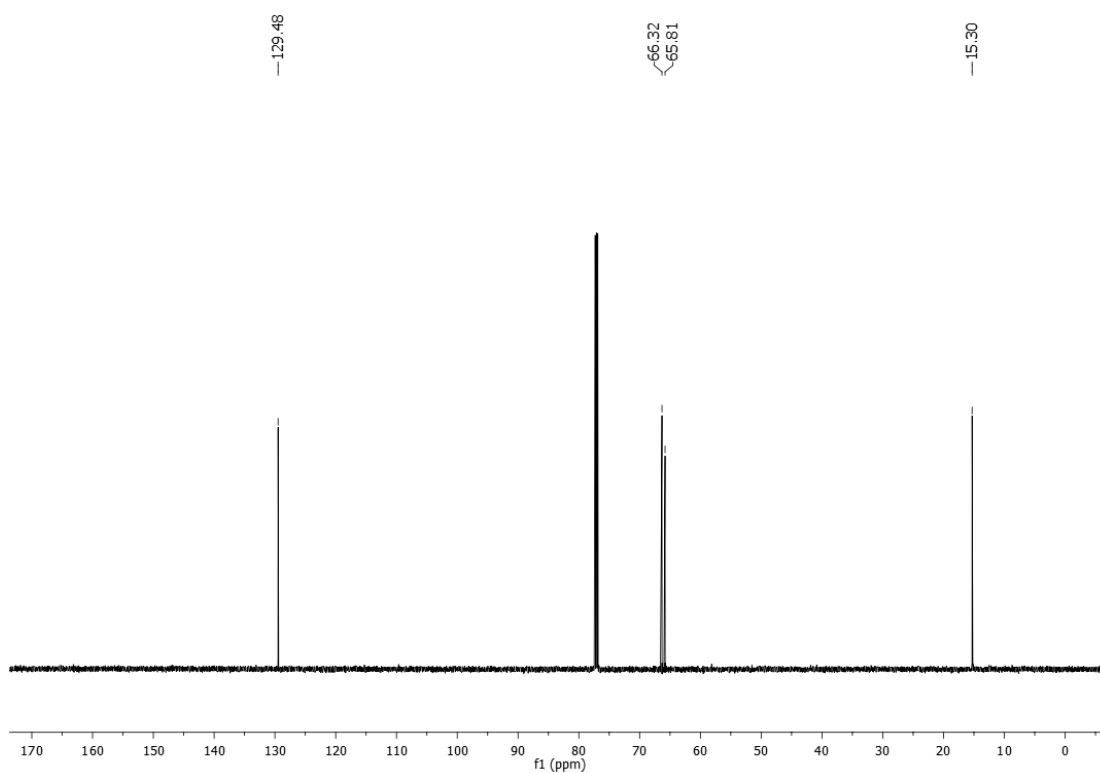


¹³C-NMR (151 MHz, CDCl₃) of (Z)-3-styrylpyridine (Table 25, Entry 19).

(Z)-1,4-diethoxybut-2-ene (2.26u): ^1H NMR (600 MHz, CDCl_3) δ 5.73 – 5.68 (m, 2H), 4.03 (d, $J = 4.8$ Hz, 4H), 3.47 (q, $J = 7.0$ Hz, 4H), 1.20 (t, $J = 7.0$ Hz, 6H) ppm; ^{13}C NMR (151 MHz, CDCl_3) δ 129.48, 66.32, 65.82, 15.30 ppm.

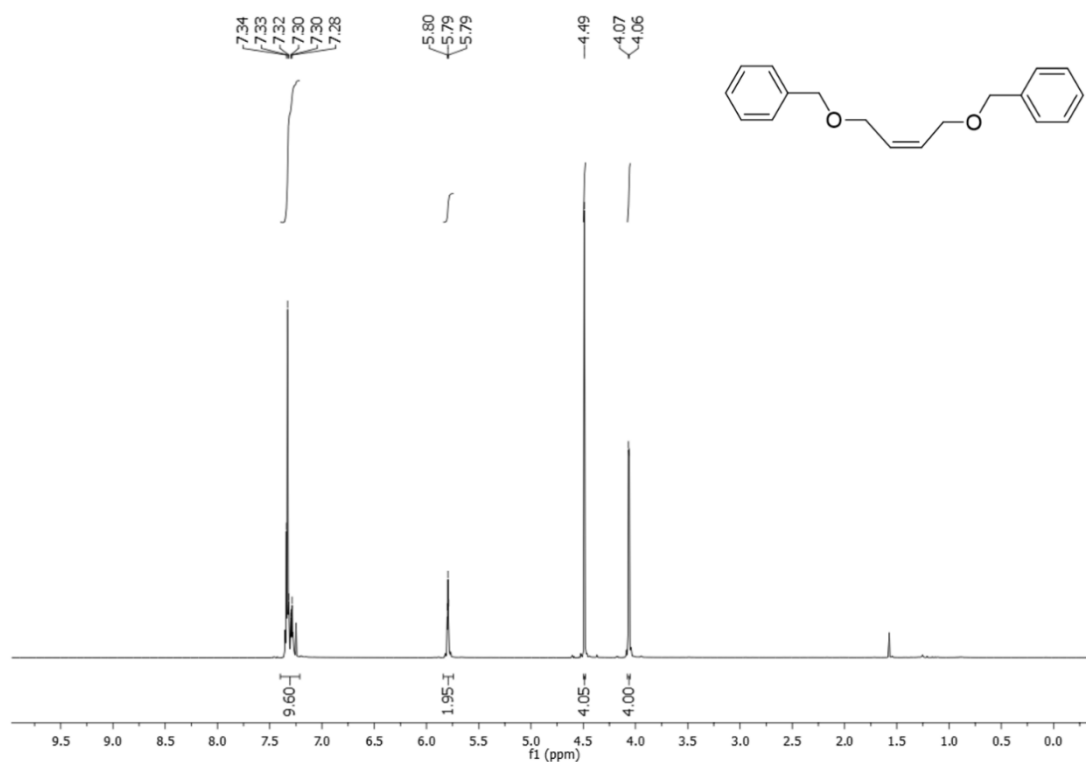


^1H NMR (600 MHz, CDCl_3) of (Z)-1,4-diethoxybut-2-ene (Table 26, entry 2).

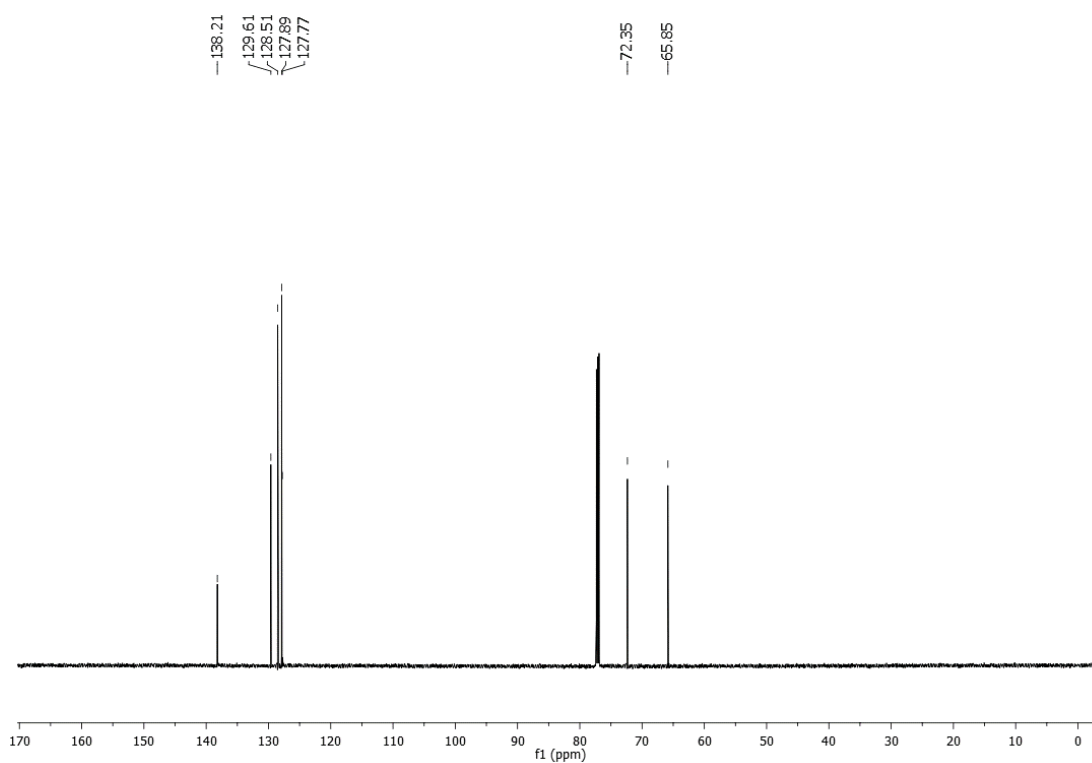


^{13}C -NMR (151 MHz, CDCl_3) of (Z)-1,4-diethoxybut-2-ene (Table 26, entry 2).

(Z)-1,4-bis(benzyloxy)but-2-ene (2.26v)⁴⁸⁴: ¹H NMR (600 MHz, CDCl₃) δ 7.31 (dt, *J* = 8.6, 6.6 Hz, 10H), 5.79 (t, *J* = 3.8 Hz, 2H), 4.49 (s, 4H), 4.06 (d, *J* = 4.7 Hz, 4H) ppm; ¹³C NMR (151 MHz, CDCl₃) δ 138.21, 129.61, 128.51, 127.89, 127.77, 72.35, 65.85 ppm.



¹H NMR (600 MHz, CDCl₃) of (Z)-1,4-bis(benzyloxy)but-2-ene (Table 26, entry 3)



¹³C-NMR (151 MHz, CDCl₃) of (Z)-1,4-bis(benzyloxy)but-2-ene (Table 26, entry 3)

(Z)-4-phenylbut-3-en-1-ol (2.26w)⁴⁸⁵: ¹H NMR (600 MHz, CDCl₃) δ 7.36 – 7.24 (m, 5H), 6.57 (d, *J* = 11.7 Hz, 1H), 5.68 (dt, *J* = 11.7 Hz, 1H), 3.73 (t, *J* = 6.5 Hz, 2H), 2.68 (t, *J* = 6.3 Hz, 2H), 2.60 (ddd, *J* = 13.9, 6.5, 1.8 Hz, 5H) ppm; ¹³C NMR (151 MHz, CDCl₃) δ 137.30, 131.62, 128.82, 128.39, 128.31, 126.91, 62.55, 32.07.

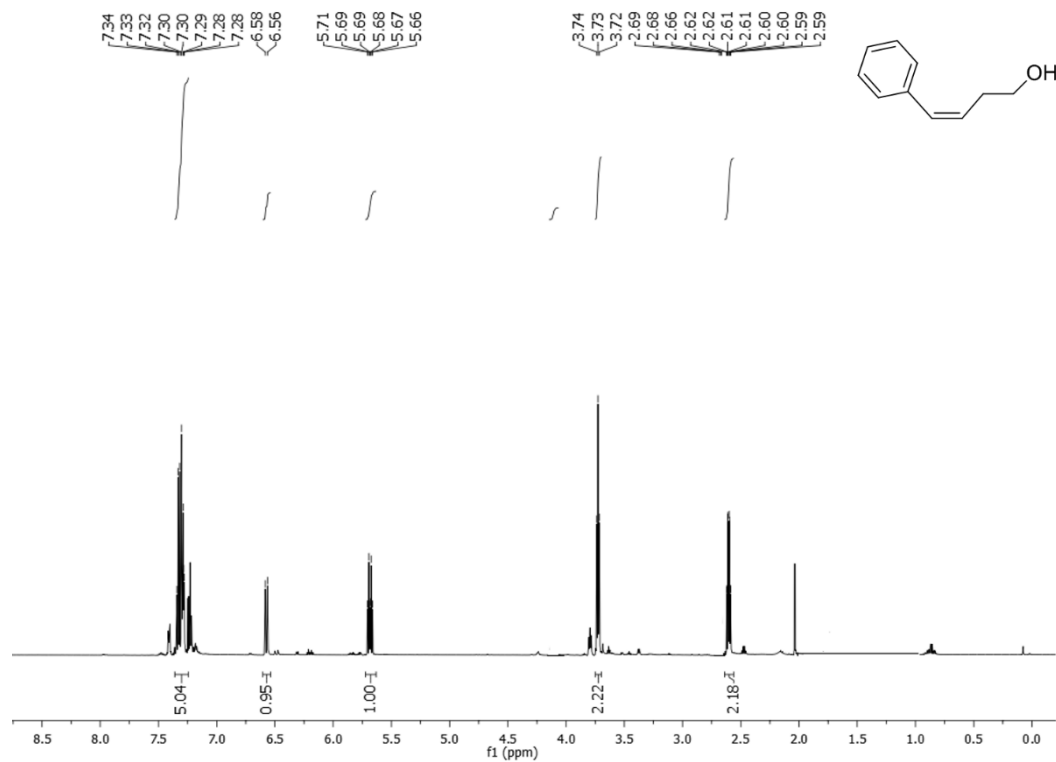
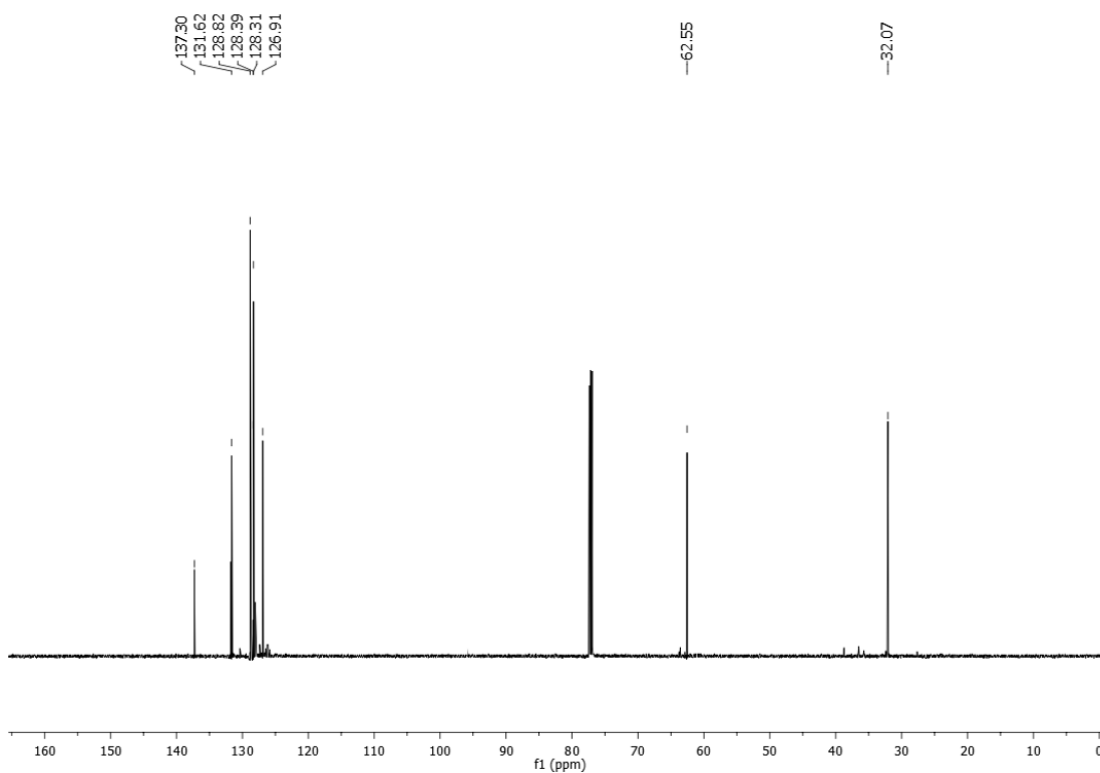
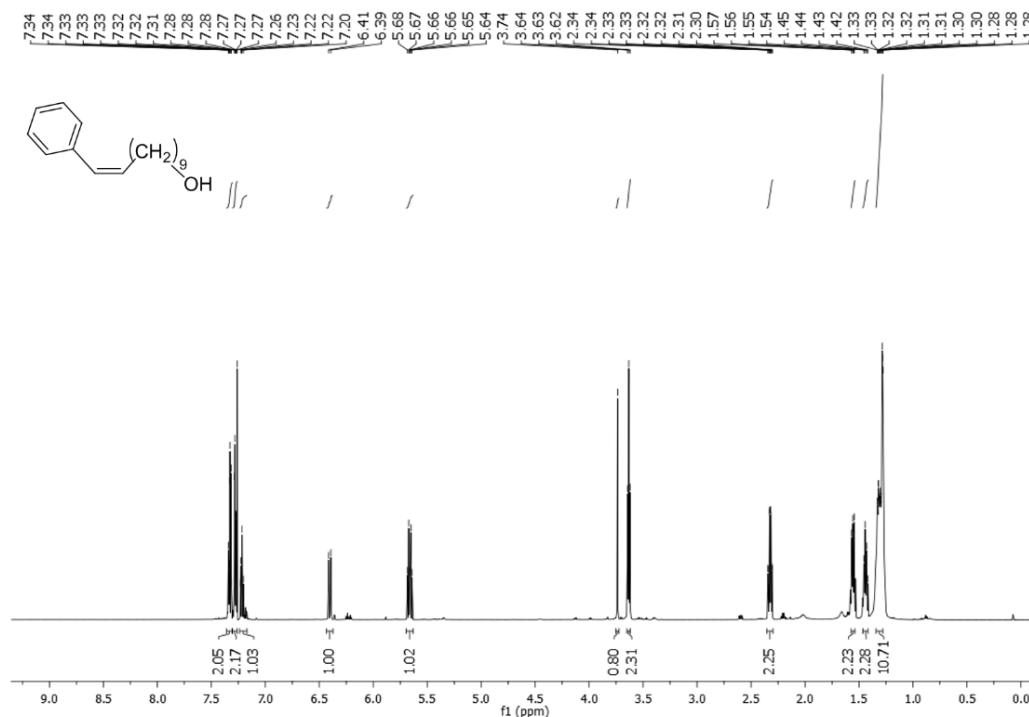


Figure 27. ¹H NMR (600 MHz, CDCl₃) of (Z)-4-phenylbut-3-en-1-ol (Table 26, entry 4).

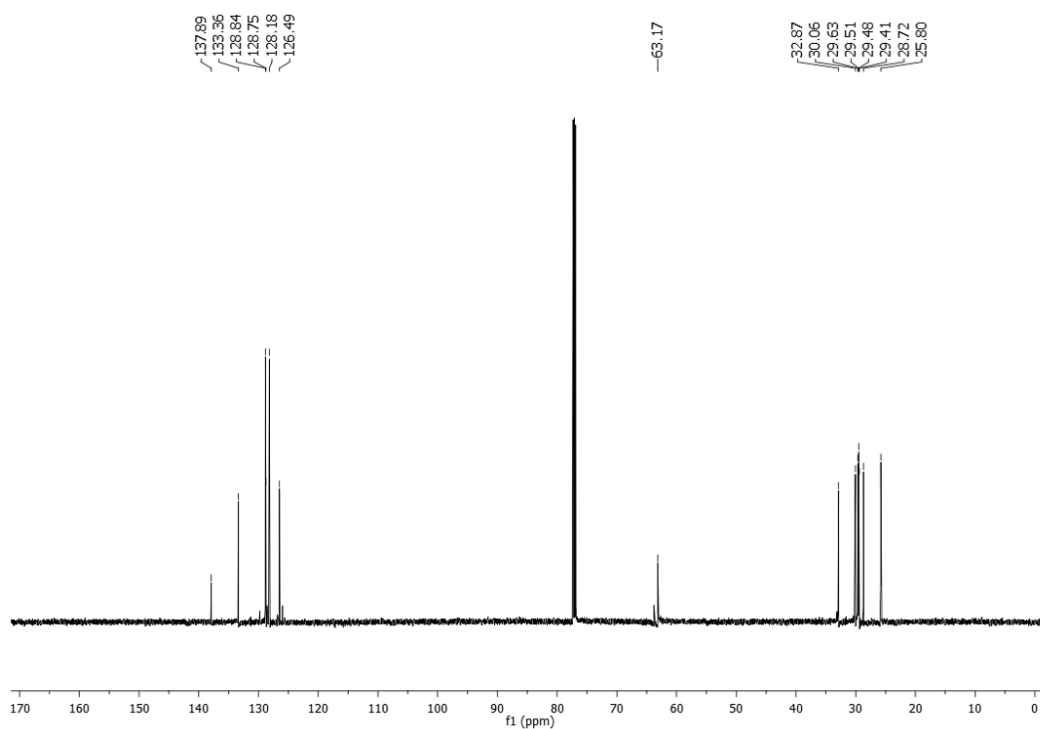


¹³C-NMR (151 MHz, CDCl₃) of (Z)-4-phenylbut-3-en-1-ol (Table 26, entry 4).

(Z)-11-phenylundec-10-en-1-ol (2.26x)⁴⁸⁶: ¹H NMR (600 MHz, CDCl₃) δ 7.36 – 7.31 (m, 2H), 7.31 – 7.26 (m, 2H), 7.24 – 7.17 (m, 1H), 6.40 (d, *J* = 11.7 Hz, 1H), 5.66 (dt, *J* = 11.7, 7.3 Hz, 1H), 3.74 (s, 1H), 3.63 (t, *J* = 6.7 Hz, 2H), 2.32 (ddd, *J* = 15.0, 7.4, 1.8 Hz, 2H), 1.56 (dd, *J* = 8.2, 6.7 Hz, 2H), 1.44 (dd, *J* = 15.2, 7.6 Hz, 2H), 1.34 – 1.28 (m, 10H) ppm; ¹³C NMR (151 MHz, CDCl₃) δ 137.89, 133.36, 128.84, 128.75, 128.18, 126.49, 63.17, 32.87, 30.06, 29.63, 29.51, 29.48, 29.41, 28.72, 25.80.



¹H NMR (600 MHz, CDCl₃) of (Z)-11-phenylundec-10-en-1-ol (Table 26, entry 5).



¹³C-NMR (151 MHz, CDCl₃) of (Z)-11-phenylundec-10-en-1-ol (Table 26, entry 5)

Appendix: Achievements

Papers

Published:

"Highly efficient nitrobenzene and alkyl/aryl azide reduction in stainless steel jars without catalyst addition" Katia Martina, Francesca Baricco, Silvia Tagliapietra, Maria Jesus Moran, Giancarlo Cravotto * and Pedro Cintas, *New J.Chem.*, **2018**, 42, 18881

"Sonochemically-Promoted Preparation of Silica-Anchored Cyclodextrin Derivatives for Efficient Copper Catalysis" K. Martina, F. Calsolaro, A. Zuliani, G. Berlier, F. Chavez-Rivas, M.J. Moran, R. Luque, G. Cravotto, *Molecules*, **2019**, 24, 2490

"Glycerol: an optimal hydrogen source for MW promoted Cu catalysed transfer hydrogenation of nitrobenzene to aniline" Maria Jesus Moran, Katia Martina, Georgios D. Stefanidis, Jeroen Jordens, Tom Van Gerven, Vincent Goovaerts, Maela Manzoli, Carlo Groffils, Giancarlo Cravotto, *Front. Chem*, **2019**, 8:34

Submitted:

"Tuneable copper catalysed transfer hydrogenation of nitrobenzenes to aniline or azo derivatives" Maria Jesus Moran, Katia Martina,* Francesca Baricco, Silvia Tagliapietra, Maela Manzoli, Giancarlo Cravotto,* *Adv. Synth. Catal.*, **2020**

In preparation:

"MW and US-assisted Cu-catalysed semihydrogenation of alkynes to Z-alkenes using ethylen glycol as solvent and hydrogen source"- Maria Jesus Moran Plata, Katia Martina and Giancarlo Cravotto.

"Efficient flow procedure for the transfer hydrogenation reduction of nitroderivatives using CuNPs/Celite as heterogeneous reusable catalyst"- Maria Jesus Moran Plata, Katia Martina and Giancarlo Cravotto.

Conferences Communications

Simposio Jovenes Investigadores (Badajoz, Spain) (7-10/11/2017) (Poster) "Copper-catalysed C-H activation REACTIONS under non-conventional techniques" Moran M.J., Martina. K., Cravotto G.

III Encuentro Jóvenes Investigadores SECAT (Valencia, Spain) (25-27/06/18) (Poster) "Selective hydride-free copper catalysed reduction of aromatic nitrocompounds", M.J. Moran, K. Martina, G. Cravotto.

Merck & Elsevier Young Chemist Symposium 2018 (Rimini, Italy) (19-21/11/2018) (Oral) "Copper (0) nanoparticles in glycerol: an efficient and versatile catalyst for hydride-free reduction of nitro derivatives", Maria Jesus Moran Plata, Katia Martina and Giancarlo Cravotto.

II International process intensification process (Leuven, Belgium) (27-29/05/2019) (Oral) "Green approach to copper catalysed reduction of nitro and alkyne under hydride free condition", Maria Jesus Moran Plata, Katia Marti and Giancarlo Cravotto.

A.CORBELLA” International Summer School on Organic Synthesis (Gargnano, Italy) (09-13/06/2019) (Oral) “Green approaches to nitrobenzene reduction”, M.J. Moran Plata, K. Martina, G. Cravotto.

VII Workshop of GC-CS (Padova, Italy) (05/07/2019) (Poster) “Combined Microwave and Ultrasound irradiation for efficient production and grafting of nanomaterials” Federica Calsolaro, Katia Martina, Maria Jesus Moran Plata, Gloria Berlier, Giancarlo Cravotto.

XXXIX Convegno Nazionale della Divisione di Chimica Organica (Turin, Italy) (08-12/09/2019) (Oral) “Non-conventional technologies for copper heterogeneous catalysts production and its applications in organic synthesis”, M.J Moran Plata, F. Calsolaro, K. Martina, G. Cravotto.

First International Conference on Unconventional Catalysis, Reactors and Applications (Zaragoza, Spain) (16-18/10/2019) (Oral) “Innovative approach to the synthesis and application of nanocatalysts” Katia Martina, Maria Jesus Moran Plata, Giancarlo Cravotto.

Secondments

1) KU Leuven, Leuven (Belgium)

Period: 10/01/2018 – 28/03/2018 & 28/10/2018 – 16/12/2018

Supervisors: T. Van Gerven, S. Kuhn and G. Stefanidis

Title: “Testing of model reactions under different reactors”

Activity: During the first period, Cu nanoparticles preparation and reactivity was explored under US irradiation. A laser diffractometer (Malvern, MasterSizer 3000 hydro SV) was employed and particle sizes were determined by measuring the intensity of scattered light. US irradiation significantly influenced particle magnitude, increasing the particles dispersion and so, the catalytic activity. Afterwards, Cu catalysed reduction of aromatic nitrocompounds was performed under different MW apparatus (monomode and multimode). Moreover, during the second period, a simple set-up for laboratory scale transfer hydrogenations reactions in continuous flow was designed for an efficient reduction of aromatic nitro compounds to anilines, catalysed by copper nanoparticles. The reaction was optimized varying solution concentration, reaction flow, residence time and catalyst loading.

2) Test Center, MEAM, (Belgium)

Period: 29/10/2018 – 30/11/2018

Supervisors: C. Groffils J.L.

Title: “Development of reactor design and reactions testing”

Activity: Microwave heating scaling-up of nitrobenzene reduction to aniline was successfully studied. When moving to high quantities, a little re-optimization was required if comparing with lab-scale. The optimization was focused on: solution concentration, catalyst loading, microwave input power and reaction temperature. Emissivity and transmissivity were firstly measured in order to set up all parameters. A number of reactions were performed to optimise the MW-heating protocol and scale-up the reaction to different volumes: 80 mL, 250 mL, 500 mL.

3) ARKEMA, Lyon, (France)

Period: 29/10/2018 – 30/11/2018

Supervisors: Dubois & J.L.Couturier

Title: "Cavitation for industrial processes. Oxidative cleavage of terminal alkenes"

Activity: Oxidative cleavage of different terminal alkenes was investigated and results were compared with the one obtained when working with internal double bonds, such as oleic acid. Oxidation of 1-Decene, methyl decanoate and 10-Undecenoic in presence of hydrogen peroxide catalysed by phosphotungstic acid was performed and nonanoic acid, mono-methyl azelate acid and sebacic acid were respectively synthesized. H₂O₂ concentration, different phase transfer agents and different catalysts loading were studied. In collaboration with Ana Luisa Soutello Maria, another PhD student from COSMIC project, further investigation will be performed.

Acknowledgement

And, in the blink of an eye, three years passed...

It seems it was yesterday when I firstly arrived to Turin, holding my father's hand without even imaging the wonderful experience that I was about to start.

If I had to describe this period in one word I would say: GROWTH. During these three years I had the opportunity to grow both, professionally and personally.

The begining was hard, being far away from family and friends, and finding yourself alone in another country is never easy. However, I have been very lucky to be sorrouded of amazing people in every city I was, who were able to make this trip much easier.

I also enjoyed this period improving languages, so I will try to do my best and thank each of you in the language that we were talking the most (even if you all know that nowadays I am not able to speak perfectly any language and I always mix all of them).

En primer lugar, quería dar las gracias a mis padres. Por mucho que me esfuerce no encuentro palabras para agradeceros vuestro esfuerzo y vuestro apoyo siempre y, en especial, durante estos tres años. La distancia no ha sido (y no es) fácil, pero vosotros habéis conseguido estar siempre cerca, aunque nos separaran miles de kilómetros. Gracias, por haber estado (y estar) siempre presente. Gracias por confiar siempre en mí, escucharme y apoyarme en cada una de mis decisiones. Todo lo que soy y dónde estoy lo debo a vosotros, a vuestro ejemplo y el amor con el que me habéis criado. Gracias a mi hermano, Javier. Gracias por haber estado siempre cuando te necesitaba, por haber confiado siempre en mí, por haber venido a visitarme a cada una de las ciudades y por haberme mostrado siempre tu apoyo. Os quiero.

Gracias a Bea y Silvia, gracias por vuestros mensajes diarios, sustento y por haberme demostrado día a día que la distancia no es más fuerte que nuestra amistad.

There is no better way of express my gratitude to Maryam, Hamid, Hammad, Ali, Eltjana, Brenda, Emma y Patri for being my "new family" in Olimpia; wonderful people coming from all around the world who make my first months in Italy much easier.

È bello poter dire un "Grazie" di cuore alle persone speciali che mi sono sempre state accanto nei momenti più duri, aiutandomi a superarli e, certamente, anche nei momenti più goiosi!

Grazie Katia. Grazie per essere stata non solo la mia tutor, ma anche per esserti presa cura di me in tutti i momenti. Grazie del tuo supporto, sostegno e per avermi insegnato tanto, non solo dal punto di vista professionale, ma anche personale. Ti ringrazio di cuore.

Grazie mille Giancarlo. Grazie per avermi dato la possibilità di fare il dottorato e per avermi accolta calorosamente nei tuoi laboratori.

Muchísimas gracias a Pedro. Gracias por tus buenos consejos (tanto personales como profesionales), por tu atención y disponibilidad permanentes. Gracias de corazón por haber estado siempre presente durante todos estos años.

Grazie infinite a Fede e Janet. Grazie per il supporto e la fiducia che mi avete sempre dato, grazie per l'immenso aiuto e, soprattutto, grazie per essere state la mia famiglia durante

questi anni. Non potrò mai ringraziarvi abbastanza per quanto mi avete aiutato. Mi sento davvero molto fortunata per aver trovato delle amiche come voi.

Veronika, dal profondo del mio cuore, ti ringrazio e apprezzo tutto ciò che hai fatto per me. Mi hai visto piangere, mi hai visto sorridere, mi hai visto crescere. Grazie per aver creduto in me ed avermi dato la forza per non arrendermi.

Grazie a tutti i dottorandi, borsisti e tesisti che sono passati dal laboratorio e senza i quali niente sarebbe stato uguale. Un grazie speciale a Marina e Francesca, per tutto il vostro aiuto in laboratorio e per avermi regalato la vostra amicizia. Grazie Ricky, Pietro, Theo, Clelia, Franci, Vale, Giulia, Marta, Andreea e Ale, per avere reso il laboratorio un posto più bello. Grazie di cuore ragazzi.

Grazie Francesco, Elisa, Fabio, Abby e tutti i tesisti che sono passati dal nostro gruppo. Un grazie speciale a Giorgio, che è sempre stato disponibile e mi ha aiutato tanto durante questi anni. Grazie della tua amicizia, è stato molto bello vivere questa esperienza con te, dal primo all'ultimo giorno nella discussione della tesi.

Grazie a Luisa, Stefano e Roby. Grazie della vostra disponibilità ed il vostro aiuto.

Thanks a lot COSMIC.

Thanks a lot to all of you, cosmicologist guys: Vidmantas, Ana Luisa, Prabhat, Ekim, Alessio, Roberta, Heidy, Luca, Mohamed, Dwayne, Fabio C, Claire, Gerardo and Fabio G.

Merci beaucoup, Ana. Tu as toujours cru en moi et je tenais à t'en remercier. Tu es toujours là pour moi, que cela soit dans les moments de joie ou de désespoir. Merci d'être mon amie e je suis impatient de partager encore beaucoup d'autres moments fantastiques avec toi. Un grand merci à tout le personnel d'Arkema. Merci à Gean-luc Dubois, Gean-luc Couturier et tous les techniciens a Lyon, pour toute votre aide et disponibilité.

Muchísimas gracias Heidy, gracias por tu apoyo, consejos, viajes, risas y por haberme regalado tu amistad. Gracias de corazón hermosa, espero volver a verte pronto.

Un grazie speciale a Fabio. Grazie per tutto il tuo aiuto in Belgio, sia in laboratorio che fuori, grazie del tuo supporto, per tutte le avventure vissute insieme e, soprattutto, grazie per avermi regalato la tua amicizia. Thanks a lot to all fantastic people that I met in KU Leuven, and specialy to Tom Van Gerven, Simon Kuhn and Georgios Stefanidis, who were always available and supported me a lot during my period there.

Grazie mille a Alessio e Camilla, grazie dalla vostra amicizia e dal vostro esempio, sia a livello professionale che personale.

Grazie mille Roby. Grazie per la tua disponibilità e il tuo aiuto. Sei stata un'ottima presi. Senza di te non sarebbe stato possibile.

Gracias a Dionis, Guille, Manu y Ferrán, por haber sido mi familia española en Turín.

Y por último, pero no por ello menos importante, gracias Riccardo, sei stato una bellissima sorpresa. Grazie per avermi sempre appoggiato e incoraggiato durante questi ultimi mesi, ed aver creduto in me. Tra di noi è nata la chimica. *Grazie di tutto amore!*

Bibliography

- (1) Clark, James H. Green chemistry: challenges and opportunities. *Green Chem.* **1999**, No. 1, 1–8.
- (2) Martina, K.; Baricco, F.; Tagliapietra, S.; Moran, M. J.; Cravotto, G.; Cintas, P. Highly efficient nitrobenzene and alkyl/aryl azide reduction in stainless steel jars without catalyst addition. *New J. Chem.* **2018**, *42* (23), 18881–18888.
- (3) Anastas, P.; Eghbali, N. Green chemistry: Principles and practice. *Chem. Soc. Rev.* **2010**, *39* (1), 301–312.
- (4) Centi G. Perathoner S. Selective Oxidation—Industrial. *Encycl. Catal.* **2003**, *77*, 287–297.
- (5) Anastas, P. T.; Williamson, T. C. Green Chemistry: An Overview. *Green Chem.* **2009**, 1–17.
- (6) Burns, N. Z.; Baran, P. S.; Hoffmann, R. W. Redox economy in organic synthesis. *Angew. Chemie - Int. Ed.* **2009**, *48* (16), 2854–2867.
- (7) Hendrickson, J. B. Systematic Synthesis Design. IV. Numerical Codification of Construction Reactions. *J. Am. Chem. Soc.* **1975**, *97* (20), 5784–5800.
- (8) Johnstone, R. A. W.; Wilby, A. H.; Entwistle, I. D. Heterogeneous Catalytic Transfer Hydrogenation and Its Relation to Other Methods for Reduction of Organic Compounds. *Chem. Rev.* **1985**, *85* (2), 129–170.
- (9) Akamanchi, K. G.; Noorani, V. R. Truly catalytic Meerwein-Ponndorf-Verley (MPV) reduction. *Tetrahedron Lett.* **1995**, *36* (28), 5085–5088.
- (10) Trocha-Grimshaw, J.; Henbest, H. B. Catalysis of the transfer of hydrogen from propan-2-ol to $\alpha\beta$ -unsaturated ketones by organoiridium compounds. a carbon-iridium compound containing a chelate keto-group. *Chem. Commun.* **1967**, No. 11, 544.
- (11) Sasson, Y.; Blum, J. Dichlorotris(triphenylphosphine)ruthenium-Catalysed Hydrogen Transfer from Alcohols to Saturated and α,β -Unsaturated Ketones. *J. Org. Chem.* **1975**, *40* (13), 1887–1896.
- (12) Chowdhury, R. L.; Bäckvall, J.-E. Efficient ruthenium-catalysed transfer hydrogenation of ketones by propan-2-ol. *J. Chem. Soc., Chem. Commun.* **1991**, *16* (16), 1063–1064.
- (13) Soldevila-Barreda, J. J.; Romero-Canelón, I.; Habtemariam, A.; Sadler, P. J. Transfer hydrogenation catalysis in cells as a new approach to anticancer drug design. *Nat. Commun.* **2015**, *6*.
- (14) Corma, A.; Navas, J.; Sabater, M. J. Advances in One-Pot Synthesis through Borrowing Hydrogen Catalysis. *Chem. Rev.* **2018**, *118* (4), 1410–1459.
- (15) Reed-Berendt, B. G.; Polidano, K.; Morrill, L. C. Recent advances in homogeneous borrowing hydrogen catalysis using earth-abundant first row transition metals. *Org. Biomol. Chem.* **2019**, *17* (7), 1595–1607.
- (16) Bala, M.; Verma, P. K.; Sharma, U.; Kumar, N.; Singh, B. Iron phthalocyanine as an efficient and versatile catalyst for N-alkylation of heterocyclic amines with alcohols: One-pot synthesis of 2-substituted benzimidazoles, benzothiazoles and benzoxazoles. *Green Chem.* **2013**, *15* (6), 1687–1693.
- (17) Yan, T.; Feringa, B. L.; Barta, K. Iron catalysed direct alkylation of amines with alcohols. *Nat. Commun.* **2014**, *5*, 1–7.
- (18) Deibl, N.; Kempe, R. General and Mild Cobalt-Catalysed C-Alkylation of Unactivated Amides and Esters with Alcohols. *J. Am. Chem. Soc.* **2016**, *138* (34), 10786–10789.
- (19) Quintard, A.; Constantieux, T.; Rodriguez, J. An iron/amine-catalysed cascade process for the enantioselective functionalization of allylic alcohols. *Angew. Chemie - Int. Ed.* **2013**, *52* (49), 12883–12887.
- (20) Peña-López, M.; Piehl, P.; Elangovan, S.; Neumann, H.; Beller, M. Manganese-Catalysed Hydrogen-Autotransfer C–C Bond Formation: α -Alkylation of Ketones with Primary Alcohols. *Angew. Chemie - Int. Ed.* **2016**, *55* (48), 14967–14971.
- (21) Shimizu, S. K.; Sci, C. As featured in : Catalysis Science & Technology. *Catal. Sci. Technol.* **2015**, *5*, 1412–1427.
- (22) Martínez, R.; Ramón, D. J.; Yus, M. Selective N-monoalkylation of aromatic amines with benzylic alcohols by a hydrogen autotransfer process catalysed by unmodified magnetite. *Org. Biomol. Chem.* **2009**, *7* (10), 2176–2181.
- (23) Likhar, P. R.; Arundhati, R.; Kantam, M. L.; Prathima, P. S. Amination of alcohols catalysed by copper-aluminium Hydrotalcite: A green synthesis of amines. *European J. Org. Chem.* **2009**, No. 31, 5383–5389.
- (24) Cui, X.; Dai, X.; Deng, Y.; Shi, F. Development of a general non-noble metal catalyst for the benign amination of alcohols with amines and ammonia. *Chem. - A Eur. J.* **2013**, *19* (11), 3665–3675.
- (25) Shi, F.; Tse, M. K.; Zhou, S.; Pohl, M.-M.; Radnik, J.; Huebner, S.; Jaehnisch, K.; Brueckner, A.; Beller, M. ChemInform Abstract: Green and Efficient Synthesis of Sulfonamides Catalysed by Nano-Ru/Fe 3 O 4 . . *ChemInform* **2009**, *40* (24), 1775–1779.
- (26) He, J.; Yamaguchi, K.; Mizuno, N. Selective synthesis of secondary amines via N-alkylation of primary amines and ammonia with alcohols by supported copper hydroxide catalysts. *Chem. Lett.* **2010**, *39* (11), 1182–1183.

- (27) Yamada, Y. M. A.; Uozumi, Y. A solid-phase self-organized catalyst of nanopalladium with main-chain viologen polymers: α -alkylation of ketones with primary alcohols. *Org. Lett.* **2006**, *8* (7), 1375–1378.
- (28) Motokura, K.; Nishimura, D.; Mori, K.; Mizugaki, T.; Ebitani, K.; Kaneda, K. A Ruthenium-Grafted Hydrotalcite as a Multifunctional Catalyst for Direct α -Alkylation of Nitriles with Primary Alcohols. *J. Am. Chem. Soc.* **2004**, *126* (18), 5662–5663.
- (29) Kose, O.; Saito, S. Cross-coupling reaction of alcohols for carbon-carbon bond formation using pincer-type NHC/palladium catalysts. *Org. Biomol. Chem.* **2010**, *8* (4), 896–900.
- (30) He, L.; Wang, J. Q.; Gong, Y.; Liu, Y. M.; Cao, Y.; He, H. Y.; Fan, K. N. Titania-supported iridium subnanoclusters as an efficient heterogeneous catalyst for direct synthesis of quinolines from nitroarenes and aliphatic alcohols. *Angew. Chemie - Int. Ed.* **2011**, *50* (43), 10216–10220.
- (31) Maiti, D.; Fors, B. P.; Henderson, J. L.; Nakamura, Y.; Buchwald, S. L. Palladium-catalysed coupling of functionalized primary and secondary amines with aryl and heteroaryl halides: Two ligands suffice in most cases. *Chem. Sci.* **2011**, *2* (1), 57–68.
- (32) Noyori, R. Asymmetric catalysis: Science and opportunities (nobel lecture). *Angew. Chemie - Int. Ed.* **2002**, *41* (12), 2008–2022.
- (33) Katryniok, B.; Kimura, H.; Skrzyńska, E.; Girardon, J. S.; Fongarland, P.; Capron, M.; Ducoulombier, R.; Mimura, N.; Paul, S.; Dumeignil, F. Selective catalytic oxidation of glycerol: Perspectives for high value chemicals. *Green Chem.* **2011**, *13* (8), 1960–1979.
- (34) Cintas, P.; Tagliapietra, S.; Calcio Gaudino, E.; Palmisano, G.; Cravotto, G. Glycerol: A solvent and a building block of choice for microwave and ultrasound irradiation procedures. *Green Chemistry*. 2014, pp 1056–1065.
- (35) Díaz-Álvarez, A.; Cadierno, V. Glycerol: A promising Green Solvent and Reducing Agent for Metal-Catalysed Transfer Hydrogenation Reactions and Nanoparticles Formation. *Appl. Sci.* **2013**, *3* (1), 55–69.
- (36) Tavor, D.; Gefen, I.; Dlugy, C.; Wolfson, A. Transfer hydrogenations of nitrobenzene using glycerol as solvent and hydrogen donor. *Synth. Commun.* **2011**, *41* (22), 3409–3416.
- (37) Branco, P. S.; Nogueira, I. Reduction of Nitroarenes and Carbonyl Compounds with Ni–Fe₃O₄ MNPs. *Synfacts* **2012**, *8* (12), 1388–1388.
- (38) Cadierno, V.; Francos, J.; Gimeno, J.; Nebra, N. Ruthenium-catalysed reduction of allylic alcohols: An efficient isomerization/transfer hydrogenation tandem process. *Chem. Commun.* **2007**, No. 24, 2536–2538.
- (39) Dobrovolná, Z.; Červený, L. Catalytic transfer hydrogenation of olefins. *Res. Chem. Intermed.* **1998**, *24* (6), 679–686.
- (40) Farnetti, E.; Kašpar, J.; Crotti, C. A novel glycerol valorization route: Chemoselective dehydrogenation catalysed by iridium derivatives. *Green Chem.* **2009**, *11* (5), 704–709.
- (41) Wolfson, A.; Dlugy, C.; Shotland, Y.; Tavor, D. Glycerol as solvent and hydrogen donor in transfer hydrogenation-dehydrogenation reactions. *Tetrahedron Lett.* **2009**.
- (42) Wolfson, A.; Dlugy, C.; Shotland, Y.; Tavor, D. Glycerol as solvent and hydrogen donor in transfer hydrogenation – dehydrogenation reactions. *Tetrahedron Lett.* **2009**, *50* (43), 5951–5953.
- (43) Cintas, P.; Tagliapietra, S.; Calcio Gaudino, E.; Palmisano, G.; Cravotto, G. Glycerol: A solvent and a building block of choice for microwave and ultrasound irradiation procedures. *Green Chemistry*. 2014, pp 1056–1065.
- (44) Hintermann, L. Comprehensive Organic Name Reactions and Reagents. By Zerong Wang. *Angew. Chemie Int. Ed.* **2010**, *49* (15), 2659–2660.
- (45) Formenti, D.; Ferretti, F.; Scharnagl, F. K.; Beller, M. Reduction of Nitro Compounds Using 3d-Non-Noble Metal Catalysts. *Chem. Rev.* **2019**, *119* (4), 2611–2680.
- (46) Sassykova, L. R.; Aubakirov, Y. A.; Sendilvelan, S.; Tashmukhambetova, Z. K.; Zhakirova, N. K.; Faizullaeva, M. F.; Batyrbayeva, A. A.; Ryskaliyeva, R. G.; Tyussyupova, B. B.; Abildin, T. S. Studying the Mechanisms of Nitro Compounds Reduction (A-Review). *Orient. J. Chem.* **2019**, *35* (1), 22–38.
- (47) Popat, V.; Padhiyar, N. Kinetic Study of Bechamp Process for P-Nitrotoluene Reduction to P-Toluidine. *Int. J. Chem. Eng. Appl.* **2013**, *4* (6), 401–405.
- (48) Jagadeesh, R. V.; Surkus, A.-E.; Junge, H.; Pohl, M.-M.; Radnik, J.; Rabeah, J.; Huan, H.; Schunemann, V.; Bruckner, A.; Beller, M. Nanoscale Fe₂O₃-Based Catalysts for Selective Hydrogenation of Nitroarenes to Anilines. *Science (80-)*. **2013**, *342* (6162), 1073–1076.
- (49) Brown, O. W.; Henke, C. O. Catalytic Preparation of Aniline. II. *J. Phys. Chem.* **1922**, *26* (3), 272–287.
- (50) Yadav, V.; Gupta, S.; Kumar, R.; Singh, G.; Lagarkha, R. Polymeric PEG35k-Pd nanoparticles: Efficient and recyclable catalyst for reduction of nitro compounds. *Synth. Commun.* **2012**, *42* (2), 213–222.
- (51) Lu, Y. M.; Zhu, H. Z.; Li, W. G.; Hu, B.; Yu, S. H. Size-controllable palladium nanoparticles immobilized on carbon

- nanospheres for nitroaromatic hydrogenation. *J. Mater. Chem. A* **2013**, *1* (11), 3783–3788.
- (52) Li, F.; Frett, B.; Li, H. Y. Selective reduction of halogenated nitroarenes with hydrazine hydrate in the presence of Pd/C. *Synlett* **2014**, *25* (10), 1403–1408.
- (53) Cantillo, D.; Moghaddam, M. M.; Kappe, C. O. Hydrazine-mediated reduction of nitro and azide functionalities catalysed by highly active and reusable magnetic iron oxide nanocrystals. *J. Org. Chem.* **2013**, *78* (9), 4530–4542.
- (54) Feng, C.; Zhang, H. Y.; Shang, N. Z.; Gao, S. T.; Wang, C. Magnetic graphene nanocomposite as an efficient catalyst for hydrogenation of nitroarenes. *Chinese Chem. Lett.* **2013**, *24* (6), 539–541.
- (55) Zhang, H.; Gao, S.; Shang, N.; Wang, C.; Wang, Z. Copper ferrite-graphene hybrid: A highly efficient magnetic catalyst for chemoselective reduction of nitroarenes. *RSC Adv.* **2014**, *4* (59), 31328–31332.
- (56) Sharma, U.; Verma, P. K.; Kumar, N.; Kumar, V.; Bala, M.; Singh, B. Phosphane-free green protocol for selective nitro reduction with an iron-based catalyst. *Chem. - A Eur. J.* **2011**, *17* (21), 5903–5907.
- (57) Reddy, P. L.; Tripathi, M.; Arundhati, R.; Rawat, D. S. Chemoselective Hydrazine-mediated Transfer Hydrogenation of Nitroarenes by Co₃O₄ Nanoparticles Immobilized on an Al/Si-mixed Oxide Support. *Chem. - An Asian J.* **2017**, *12* (7), 785–791.
- (58) Huang, H.; Tan, M.; Wang, X.; Zhang, M.; Guo, S.; Zou, X.; Lu, X. Synthesis of Mesoporous γ -Alumina-Supported Co-Based Catalysts and Their Catalytic Performance for Chemoselective Reduction of Nitroarenes. *ACS Appl. Mater. Interfaces* **2018**, *10* (6), 5413–5428.
- (59) Seo, E.; Kim, J.; Hong, Y.; Kim, Y. S.; Lee, D.; Kim, B. S. Double hydrophilic block copolymer templated Au nanoparticles with enhanced catalytic activity toward nitroarene reduction. *J. Phys. Chem. C* **2013**, *117* (22), 11686–11693.
- (60) Feng, Y. S.; Ma, J. J.; Kang, Y. M.; Xu, H. J. PdCu nanoparticles supported on graphene: An efficient and recyclable catalyst for reduction of nitroarenes. *Tetrahedron* **2014**, *70* (36), 6100–6105.
- (61) Layek, K.; Kantam, M. L.; Shirai, M.; Nishio-Hamane, D.; Sasaki, T.; Maheswaran, H. Gold nanoparticles stabilized on nanocrystalline magnesium oxide as an active catalyst for reduction of nitroarenes in aqueous medium at room temperature. *Green Chem.* **2012**, *14* (11), 3164–3174.
- (62) Andreou, D.; Iordanidou, D.; Tamiolakis, I.; Armatas, G. S.; Lykakis, I. N. Reduction of nitroarenes into aryl amines and N-aryl hydroxylamines via activation of NaBH₄ and ammonia-borane complexes by Ag/TiO₂ catalyst. *Nanomaterials* **2016**, *6* (3), 2–13.
- (63) Wu, H.; Huang, X.; Gao, M.; Liao, X.; Shi, B. Polyphenol-grafted collagen fiber as reductant and stabilizer for one-step synthesis of size-controlled gold nanoparticles and their catalytic application to 4-nitrophenol reduction. *Green Chem.* **2011**, *13* (3), 651–658.
- (64) Shil, A. K.; Sharma, D.; Guha, N. R.; Das, P. Solid supported Pd(0): An efficient recyclable heterogeneous catalyst for chemoselective reduction of nitroarenes. *Tetrahedron Lett.* **2012**, *53* (36), 4858–4861.
- (65) He, S.; Niu, H.; Zeng, T.; Wang, S.; Cai, Y. A Facile and Efficient Method for Continuous Reduction of Nitroaromatic Compounds Through the Cyclic Transformation Between Fe(II)-complexes and Nano Zero-valent Iron. *ChemistrySelect* **2016**, *1* (11), 2821–2825.
- (66) Vernekar, A. A.; Patil, S.; Bhat, C.; Tilve, S. G. Magnetically recoverable catalytic Co-Co₂B nanocomposites for the chemoselective reduction of aromatic nitro compounds. *RSC Adv.* **2013**, *3* (32), 13243–13250.
- (67) Bae, S.; Gim, S.; Kim, H.; Hanna, K. Effect of NaBH₄ on properties of nanoscale zero-valent iron and its catalytic activity for reduction of p-nitrophenol. *Appl. Catal. B Environ.* **2016**, *182*, 541–549.
- (68) Verma, P. K.; Bala, M.; Thakur, K.; Sharma, U.; Kumar, N.; Singh, B. Iron and palladium(II) phthalocyanines as recyclable catalysts for reduction of nitroarenes. *Catal. Letters* **2014**, *144* (7), 1258–1267.
- (69) Piña, S.; Cedillo, D. M.; Tamez, C.; Izquierdo, N.; Parsons, J. G.; Gutierrez, J. J. Reduction of nitrobenzene derivatives using sodium borohydride and transition metal sulfides. *Tetrahedron Lett.* **2014**, *55* (40), 5468–5470.
- (70) Garcia-Verdugo, E.; Liu, Z.; Ramirez, E.; Garcia-Serna, J.; Fraga-Dubreuil, J.; Hyde, J. R.; Hamley, P. A.; Poliakov, M. In situ generation of hydrogen for continuous hydrogenation reactions in high temperature water. *Green Chem.* **2006**, *8* (4), 359–364.
- (71) Pietrowski, M. Selective hydrogenation of ortho-chloronitrobenzene over Ru and Ir catalysts under the conditions of the Aqueous-Phase Reforming of bioethanol. *Green Chem.* **2011**, *13* (7), 1633–1635.
- (72) Hoffman, D. C. Chemistry of the Heaviest Elements. *Radiochim. Acta* **1996**, *72* (1), 1–6.
- (73) Oba, M.; Kojima, K.; Endo, M.; Sano, H.; Nishiyama, K. Palladium-catalysed transfer hydrogenation of organic substrates by hypophosphite in water containing a nonionic surfactant. *Green Chem. Lett. Rev.* **2013**, *6* (3), 233–236.
- (74) Baron, M.; Métaf, E.; Lemaire, M.; Popowycz, F. Reduction of aromatic and aliphatic nitro groups to anilines and amines with hypophosphites associated with Pd/C. *Green Chem.* **2013**, *15* (4), 1006–1015.

- (75) Schabel, T.; Belger, C.; Plietker, B. A mild chemoselective Ru-catalysed reduction of alkynes, ketones, and nitro compounds. *Org. Lett.* **2013**, *15* (11), 2858–2861.
- (76) Desai, D. G.; Swami, S. S.; Dabhade, S. K.; Ghagare, M. G. FeS-NH₄Cl-CH₃OH-H₂O: An efficient and inexpensive system for reduction of nitroarenes to anilines. *Synth. Commun.* **2001**, *31* (8), 1249–1251.
- (77) Kelly, S. M.; Lipshutz, B. H. Chemoselective reductions of nitroaromatics in water at room temperature. *Org. Lett.* **2014**, *16* (1), 98–101.
- (78) Sarmah, P. P.; Dutta, D. K. Chemoselective reduction of a nitro group through transfer hydrogenation catalysed by Ru 0-nanoparticles stabilized on modified Montmorillonite clay. *Green Chem.* **2012**, *14* (4), 1086–1093.
- (79) Salam, N.; Banerjee, B.; Roy, A. S.; Mondal, P.; Roy, S.; Bhaumik, A.; Islam, S. M. Silver nanoparticles embedded over mesoporous organic polymer as highly efficient and reusable nanocatalyst for the reduction of nitroarenes and aerobic oxidative esterification of alcohols. *Appl. Catal. A Gen.* **2014**, *477*, 184–194.
- (80) Sanjini, N. S.; Velmathi, S. Iron impregnated SBA-15, a mild and efficient catalyst for the catalytic hydride transfer reduction of aromatic nitro compounds. *RSC Adv.* **2014**, *4* (30), 15381–15388.
- (81) García, N.; García-García, P.; Fernández-Rodríguez, M. A.; Rubio, R.; Pedrosa, M. R.; Arnáiz, F. J.; Sanz, R. Pinacol as a new green reducing agent: Molybdenum-catalysed chemoselective reduction of sulfoxides and nitroaromatics. *Adv. Synth. Catal.* **2012**, *354* (2–3), 321–327.
- (82) Kumar, M.; Sharma, U.; Sharma, S.; Kumar, V.; Singh, B.; Kumar, N. Catalyst-free water mediated reduction of nitroarenes using glucose as a hydrogen source. *RSC Adv.* **2013**, *3* (15), 4894–4898.
- (83) Furukawa, S.; Yoshida, Y.; Komatsu, T. Chemoselective hydrogenation of nitrostyrene to aminostyrene over Pd- and Rh-based intermetallic compounds. *ACS Catal.* **2014**, *4* (5), 1441–1450.
- (84) Gawande, M. B.; Rathi, A. K.; Branco, P. S.; Nogueira, I. D.; Velhinho, A.; Shrikhande, J. J.; Indulkar, U. U.; Jayaram, R. V.; Ghumman, C. A. A.; Bundaleski, N.; et al. Regio- and chemoselective reduction of nitroarenes and carbonyl compounds over recyclable magnetic ferrite-nickel nanoparticles (Fe₃O₄-Ni) by using glycerol as a hydrogen source. *Chem. - A Eur. J.* **2012**, *18* (40), 12628–12632.
- (85) Swamy, K. C. K.; Reddy, A. S.; Sandeep, K.; Kalyani, A. Advances in chemoselective and/or stereoselective semihydrogenation of alkynes. *Tetrahedron Lett.* **2018**, *59* (5), 419–429.
- (86) Edmonds, M.; Abell, A. Modern Carbonyl Olefination - The Wittig Reaction. **2003**, 1–17.
- (87) Blakemore, P. R. The modified Julia olefination: Alkene synthesis via the condensation of metallated heteroarylalkylsulfones with carbonyl compounds. *J. Chem. Soc. Perkin 1* **2002**, *2* (23), 2563–2585.
- (88) Peterson, D. J. A Carbonyl Olefination Reaction Using Silyl-Substituted Organometallic Compounds. *J. Org. Chem.* **1968**, *33* (2), 780–784.
- (89) Takai, K.; Nitta, K.; Utimoto, K. Simple and Selective Method for RCHO → (E)-RCH=CHX Conversion by Means of a CHX₃-CrCl₂ System. *J. Am. Chem. Soc.* **1986**, *108* (23), 7408–7410.
- (90) Grubbs, R. H. Robert H. Grubbs (Ed.) Handbook of Metathesis Catalyst Development.
- (91) Trost, B. M.; Ball, Z. T.; Jöge, T. A chemoselective reduction of alkynes to (E)-alkenes. *J. Am. Chem. Soc.* **2002**, *124* (27), 7922–7923.
- (92) Alonso, F.; Osante, I.; Yus, M. Highly stereoselective semihydrogenation of alkynes promoted by nickel(0) nanoparticles. *Adv. Synth. Catal.* **2006**, *348* (3), 305–308.
- (93) Hauwert, P.; Maestri, G.; Sprengers, J. W.; Catellani, M.; Elsevier, C. J. Transfer semihydrogenation of alkynes catalysed by a zero-valent palladium N-heterocyclic carbene complex. *Angew. Chemie - Int. Ed.* **2008**, *47* (17), 3223–3226.
- (94) Cao, H.; Chen, T.; Zhou, Y.; Han, D.; Yin, S. F.; Han, L. B. Copper-catalysed selective semihydrogenation of terminal alkynes with hypophosphorous acid. *Adv. Synth. Catal.* **2014**, *356* (4), 765–769.
- (95) Lindlar, H.; Dubuis, R. Palladium Catalyst for Partial Reduction of Acetylenes. *Org. Synth.* **2003**, No. September, 89–89.
- (96) Miyaoka, H.; Yamada, Y. Total synthesis of marine oxylipins. *Yuki Gosei Kagaku Kyokaiishi/Journal Synth. Org. Chem.* **2001**, *59* (6), 599–606.
- (97) Spinella, A.; Caruso, T.; Coluccini, C. First total synthesis of natural aplyolides B and D, ichthyotoxic macrolides isolated from the skin of the marine mollusk *Aplysia depilans*. *Tetrahedron Lett.* **2002**, *43* (9), 1681–1683.
- (98) Karrer, P.; Eugster, C. H. Synthese von Carotinoiden II. Totalsynthese des β-Carotins I. *Helv. Chim. Acta* **1950**, *33* (5), 1172–1174.
- (99) Brown, C. A.; Ahuja, V. K. "P-2 nickel" catalyst with ethylenediamine, a novel system for highly stereospecific reduction of alkynes to cis-olefins. *J. Chem. Soc. Chem. Commun.* **1973**, No. 15, 553–554.

- (100) Feutrill, J. T.; Rizzacasa, M. A. Total Synthesis of (+)-Crocacin A. *Aust. J. Chem.* **2003**, *56* (8), 783–785.
- (101) Peng, S.; McGinley, C. M.; Van Der Donk, W. A. Synthesis of Site-Specifically Labeled Arachidonic Acids as Mechanistic Probes for Prostaglandin H Synthase. *Org. Lett.* **2004**, *6* (3), 349–352.
- (102) Hansen, T. V.; Stenstrøm, Y. science First total synthesis of (-)-aplyolide A.pdf. **2001**, *12*, 1407–1409.
- (103) Řezanka, T.; Nedbalová, L.; Sigler, K. Identification of very-long-chain polyunsaturated fatty acids from *Amphidinium carterae* by atmospheric pressure chemical ionization liquid chromatography-mass spectroscopy. *Phytochemistry* **2008**, *69* (12), 2391–2399.
- (104) Wei, H. X.; Truitt, C. L.; Paré, P. W. Synthesis of hydroxy-substituted unsaturated fatty acids and the amino-acid insect-derivative volicitin. *Tetrahedron Lett.* **2003**, *44* (4), 831–833.
- (105) Guiard, S.; Santelli, M.; Parrain, J. L. Gram scale-up synthesis of all-(Z)-cyclododecatetraene: A comparison between intramolecular Wittig and ring closing metathesis approaches. *Synlett* **2001**, No. 4, 553–556.
- (106) Qi, L.; Meijler, M. M.; Lee, S. H.; Sun, C.; Janda, K. D. Solid-phase synthesis of anandamide analogues. *Org. Lett.* **2004**, *6* (10), 1673–1675.
- (107) Balas, L.; Durand, T.; Saha, S.; Johnson, I.; Mukhopadhyay, S. Total synthesis of photoactivatable or fluorescent anandamide probes: Novel bioactive compounds with angiogenic activity. *J. Med. Chem.* **2009**, *52* (4), 1005–1017.
- (108) Hungerford, N. L.; Kitching, W. *YMGBr.* **1996**, 1697–1698.
- (109) Parenty, A.; Campagne, J. CP 2 TiCl₂ -catalysed hydroalumination of internal alkynes : an access to (Z) -olefins. **2002**, *43*, 1231–1233.
- (110) Tani, K.; Ono, N.; Okamoto, S.; Sato, F. o. **1993**, *2* (386), 386–387.
- (111) Hauwert, P.; Maestri, G.; Sprengers, J. W.; Catellani, M.; Elsevier, C. J. Transfer semihydrogenation of alkynes catalysed by a zero-valent palladium N-heterocyclic carbene complex. *Angew. Chemie - Int. Ed.* **2008**, *47* (17), 3223–3226.
- (112) Belger, C.; Neisius, N. M.; Plietker, B. A selective Ru-catalysed semireduction of alkynes to Z olefins under transfer-hydrogenation conditions. *Chem. - A Eur. J.* **2010**, *16* (40), 12214–12220.
- (113) Monfredini, A.; Santacroce, V.; Deyris, P. A.; Maggi, R.; Bigi, F.; Maestri, G.; Malacria, M. Boosting catalyst activity in cis -selective semi-reduction of internal alkynes by tailoring the assembly of all-metal aromatic tri-palladium complexes. *Dalt. Trans.* **2016**, *45* (40), 15786–15790.
- (114) Li, J.; Hua, R.; Liu, T. Highly chemo- and stereoselective palladium-catalysed transfer semihydrogenation of internal alkynes affording cis -alkenes. *J. Org. Chem.* **2010**, *75* (9), 2966–2970.
- (115) Cox, N.; Dang, H.; Whittaker, A. M.; Lalic, G. NHC-copper hydrides as chemoselective reducing agents: Catalytic reduction of alkynes, alkyl triflates, and alkyl halides. *Tetrahedron* **2014**, *70* (27–28), 4219–4231.
- (116) Semba, K.; Fujihara, T.; Xu, T.; Terao, J.; Tsuji, Y. Copper-catalysed highly selective semihydrogenation of non-polar carbon-carbon multiple bonds using a silane and an alcohol. *Adv. Synth. Catal.* **2012**, *354* (8), 1542–1550.
- (117) Wang, G.; Bin, H.; Sun, M.; Chen, S.; Liu, J.; Zhong, C. Copper-catalysed Z -selective semihydrogenation of alkynes with hydrosilane : a convenient approach to cis -alkenes. *Tetrahedron* **2014**, *70* (12), 2175–2179.
- (118) Suess, A. M.; Lalic, G. Copper-Catalysed Hydrofunctionalization of Alkynes. *Synlett* **2016**, *27* (8), 1165–1174.
- (119) Wang, G. H.; Bin, H. Y.; Sun, M.; Chen, S. W.; Liu, J. H.; Zhong, C. M. Copper-catalysed Z-selective semihydrogenation of alkynes with hydrosilane: A convenient approach to cis-alkenes. *Tetrahedron* **2014**, *70* (12), 2175–2179.
- (120) Kominami, H.; Higa, M.; Nojima, T.; Ito, T.; Nakanishi, K.; Hashimoto, K.; Imamura, K. Copper-Modified Titanium Dioxide: A Simple Photocatalyst for the Chemoselective and Diastereoselective Hydrogenation of Alkynes to Alkenes under Additive-Free Conditions. *ChemCatChem* **2016**, *8* (12), 2019–2022.
- (121) Anastas, P. T.; Kirchhoff, M. M.; Williamson, T. C. Catalysis as a foundational pillar of green chemistry. *Appl. Catal. A Gen.* **2001**, *221* (1–2), 3–13.
- (122) Anastas, P. T.; Bartlett, L. B.; Kirchhoff, M. M.; Williamson, T. C. The role of catalysis in the design, development, and implementation of green chemistry. *Catal. Today* **2000**, *55* (1–2), 11–22.
- (123) Sheldon, R. A. E factors, green chemistry and catalysis: An odyssey. *Chem. Commun.* **2008**, No. 29, 3352–3365.
- (124) Parshall, G. W.; Putscher, R. E. Organometallic chemistry and catalysis in industry. *J. Chem. Educ.* **2009**, *63* (3), 189.
- (125) Lindsay, M. J.; Walker, T. W.; Dumesic, J. A.; Rankin, S. A.; Huber, G. W. Production of monosaccharides and whey protein from acid whey waste streams in the dairy industry. *Green Chem.* **2018**, *20* (8), 1824–1834.
- (126) Enferadi-Kerenkan, A.; Do, T. O.; Kaliaguine, S. Heterogeneous catalysis by tungsten-based heteropoly compounds. *Catal. Sci. Technol.* **2018**, *8* (9), 2257–2284.

- (127) De Vries, J. G.; Jackson, S. D. Homogeneous and heterogeneous catalysis in industry. *Catal. Sci. Technol.* **2012**, *2* (10), 2009.
- (128) Hayler, J. D.; Leahy, D. K.; Simmons, E. M. A Pharmaceutical Industry Perspective on Sustainable Metal Catalysis. *Organometallics* **2019**, *38* (1), 36–46.
- (129) Astruc, D.; Lu, F.; Aranzaes, J. R. Nanoparticles as recyclable catalysts: The frontier between homogeneous and heterogeneous catalysis. *Angew. Chemie - Int. Ed.* **2005**, *44* (48), 7852–7872.
- (130) Farnetti, E.; Monte, R. Di; Kašpar, J. Homogenous and Heterogenous Catalysis. **1999**, *II*, 1–10.
- (131) Shylesh, S.; Schünemann, V.; Thiel, W. R. Magnetically separable nanocatalysts: Bridges between homogeneous and heterogeneous catalysis. *Angew. Chemie - Int. Ed.* **2010**, *49* (20), 3428–3459.
- (132) Hisashi, B.; Amamoto, Y. Review From designer Lewis acid to designer Br nsted acid towards more reactive and selective acid catalysis. *Proc. Jpn. Acad., Ser. B* **2008**, *84*, 134–146.
- (133) Gupta, K. C.; Sutar, A. K. Catalytic activities of Schiff base transition metal complexes. *Coord. Chem. Rev.* **2008**, *252* (12–14), 1420–1450.
- (134) Abu-Dief, A. M.; Mohamed, I. M. A. A review on versatile applications of transition metal complexes incorporating Schiff bases. *Beni-Suef Univ. J. Basic Appl. Sci.* **2015**, *4* (2), 119–133.
- (135) Lian, X.; Fang, Y.; Joseph, E.; Wang, Q.; Li, J.; Banerjee, S.; Lollar, C.; Wang, X.; Zhou, H. C. Enzyme-MOF (metal-organic framework) composites. *Chem. Soc. Rev.* **2017**, *46* (11), 3386–3401.
- (136) Zhang, Y.; Ge, J.; Liu, Z. Enhanced Activity of Immobilized or Chemically Modified Enzymes. *ACS Catal.* **2015**, *5* (8), 4503–4513.
- (137) Schlögl, R. Heterogeneous catalysis. *Angew. Chemie - Int. Ed.* **2015**, *54* (11), 3465–3520.
- (138) Liu, L.; Corma, A. Metal Catalysts for Heterogeneous Catalysis: From Single Atoms to Nanoclusters and Nanoparticles. *Chem. Rev.* **2018**, *118* (10), 4981–5079.
- (139) Surry, D. S.; Buchwald, S. L. Diamine ligands in copper-catalysed reactions. *Chem. Sci.* **2010**, *1* (1), 13–31.
- (140) Allen, S. E.; Walvoord, R. R.; Padilla-Salinas, R.; Kozlowski, M. C. Correction to Aerobic Copper-Catalysed Organic Reactions. *Chem. Rev.* **2014**, *114* (1), 899–899.
- (141) Martina, K.; Rinaldi, L.; Baricco, F.; Boffa, L.; Cravotto, G. Highly Efficient Mechanochemical N-Arylation of Amino Alcohols and Diamines with CuO Powder. *Synlett* **2015**, *26* (20), 2789–2794.
- (142) Ranjith, J.; Krishna, P. R. Copper-Catalysed Oxidative C–H Bond Functionalization of N-Allylbenzamide for Regioselective C–N and C–O Bond Formation. *Chem. - An Asian J.* **2019**, *14* (9), 1448–1451.
- (143) Alonso, F.; Moglie, Y.; Radivoy, G. Copper Nanoparticles in Click Chemistry. *Acc. Chem. Res.* **2015**, *48* (9), 2516–2528.
- (144) Wang, F.; Shi, R.; Liu, Z. Q.; Shang, P. J.; Pang, X.; Shen, S.; Feng, Z.; Li, C.; Shen, W. Highly efficient dehydrogenation of primary aliphatic alcohols catalysed by Cu nanoparticles dispersed on rod-shaped La₂O₂CO₃. *ACS Catal.* **2013**, *3* (5), 890–894.
- (145) Takeda, M.; Mitsui, A.; Nagao, K.; Ohmiya, H. Reductive coupling between aromatic aldehydes and ketones or imines by copper catalysis. *J. Am. Chem. Soc.* **2019**, *141* (8), 3664–3669.
- (146) Murray, C. B.; Norris, D. J.; Bawendi, M. G. Synthesis and Characterization of Nearly Monodisperse CdE (E = S, Se, Te) Semiconductor Nanocrystallites. *J. Am. Chem. Soc.* **1993**, *115* (19), 8706–8715.
- (147) Kant, N.; Zyryanov, G. V.; Majee, A.; Charushin, V. N.; Chupakhin, O. N.; Santra, S. Copper nanoparticles as inexpensive and efficient catalyst : A valuable contribution in organic synthesis. *Coord. Chem. Rev.* **2017**, *353*, 1–57.
- (148) Gawande, M. B.; Goswami, A.; Felpin, F. X.; Asefa, T.; Huang, X.; Silva, R.; Zou, X.; Zboril, R.; Varma, R. S. Cu and Cu-Based Nanoparticles: Synthesis and Applications in Catalysis. *Chemical Reviews*. 2016, pp 3722–3811.
- (149) Ikeda, S.; Akamatsu, K.; Nawafune, H.; Nishino, T.; Deki, S. Formation and growth of copper nanoparticles from ion-doped precursor polyimide layers. *J. Phys. Chem. B* **2004**, *108* (40), 15599–15607.
- (150) Raciti, D.; Wang, C. Recent Advances in CO₂ Reduction Electrocatalysis on Copper. *ACS Energy Lett.* **2018**, *3* (7), 1545–1556.
- (151) Christoforidis, K. C.; Fornasiero, P. Photocatalysis for Hydrogen Production and CO₂ Reduction: The Case of Copper-Catalysts. *ChemCatChem* **2019**, *11* (1), 368–382.
- (152) Zhu, H. T.; Zhang, C. Y.; Yin, Y. S. Rapid synthesis of copper nanoparticles by sodium hypophosphite reduction in ethylene glycol under microwave irradiation. *J. Cryst. Growth* **2004**, *270* (3–4), 722–728.
- (153) Ko, W. Y.; Chen, W. H.; Cheng, C. Y.; Lin, K. J. Architectural growth of Cu nanoparticles through electrodeposition. *Nanoscale Res. Lett.* **2009**, *4* (12), 1481–1485.

- (154) Tao, A. R.; Habas, S.; Yang, P. Shape control of colloidal metal nanocrystals. *Small* **2008**, *4* (3), 310–325.
- (155) Lin, Y. G.; Hsu, Y. K.; Chen, S. Y.; Lin, Y. K.; Chen, L. C.; Chen, K. H. Nanostructured zinc oxide nanorods with copper nanoparticles as a microreformation catalyst. *Angew. Chemie - Int. Ed.* **2009**, *48* (41), 7586–7590.
- (156) Pachón, L. D.; Van Maarseveen, J. H.; Rothenberg, G. Click chemistry: Copper clusters catalyse the cycloaddition of azides with terminal alkynes. *Adv. Synth. Catal.* **2005**, *347* (6), 811–815.
- (157) Molteni, G.; Bianchi, C. L.; Marinoni, G.; Santo, N.; Ponti, A. Cu/Cu-oxide nanoparticles as catalyst in the “click” azide-alkyne cycloaddition. *New J. Chem.* **2006**, *30* (8), 1137–1139.
- (158) Sarkar, A.; Mukherjee, T.; Kapoor, S. PVP-stabilized copper nanoparticles: A reusable catalyst for “click” reaction between terminal alkynes and azides in nonaqueous solvents. *J. Phys. Chem. C* **2008**, *112* (9), 3334–3340.
- (159) Alonso, F.; Moglie, Y.; Radivoy, G.; Yus, M. Multicomponent click synthesis of 1,2,3-triazoles from epoxides in water catalysed by copper nanoparticles on activated carbon. *J. Org. Chem.* **2011**, *76* (20), 8394–8405.
- (160) Alonso, F.; Moglie, Y.; Radivoy, G.; Yus, M. Click chemistry from organic halides, diazonium salts and anilines in water catalysed by copper nanoparticles on activated carbon. *Org. Biomol. Chem.* **2011**, *9* (18), 6385–6395.
- (161) White, B.; Yin, M.; Hall, A.; Le, D.; Stolbov, S.; Rahman, T.; Turro, N.; O’Brien, S. Complete CO oxidation over Cu₂O nanoparticles supported on silica gel. *Nano Lett.* **2006**, *6* (9), 2095–2098.
- (162) Nador, F.; Volpe, M. A.; Alonso, F.; Feldhoff, A.; Kirschning, A.; Radivoy, G. Copper nanoparticles supported on silica coated maghemite as versatile, magnetically recoverable and reusable catalyst for alkyne coupling and cycloaddition reactions. *Appl. Catal. A Gen.* **2013**, *455* (2010), 39–45.
- (163) Rodriguez, J. A.; Liu, P.; Wang, X.; Wen, W.; Hanson, J.; Hrbek, J.; Pérez, M.; Evans, J. Water-gas shift activity of Cu surfaces and Cu nanoparticles supported on metal oxides. *Catal. Today* **2009**, *143* (1–2), 45–50.
- (164) Semba, K.; Kameyama, R.; Nakao, Y. Copper-catalysed semihydrogenation of alkynes to Z-alkenes. *Synlett* **2015**, *26* (3), 318–322.
- (165) Yang, S.; Cao, C.; Peng, L.; Zhang, J. ChemComm synergistic catalyst for selective semi-. *Chem. Commun.* **2016**, *52*, 3627–3630.
- (166) Chemler, S. R. Copper catalysis in organic synthesis. *Beilstein Journal of Organic Chemistry*. November 19, 2015, pp 2252–2253.
- (167) Zhang, C.; Jiao, N. Copper-catalysed aerobic oxidative dehydrogenative coupling of anilines leading to aromatic azo compounds using dioxygen as an oxidant. *Angew. Chemie - Int. Ed.* **2010**, *49* (35), 6174–6177.
- (168) Rinaldi, L.; Martina, K.; Baricco, F.; Rotolo, L.; Cravotto, G. Solvent-free copper-catalysed azide-alkyne cycloaddition under mechanochemical activation. *Molecules* **2015**, *20* (2), 2837–2849.
- (169) Cintas, P.; Martina, K.; Robaldo, B.; Garella, D.; Boffa, L.; Cravotto, G. Improved Protocols for Microwave-Assisted Cu(I)-Catalysed Huisgen 1,3-Dipolar Cycloadditions. *Collect. Czechoslov. Chem. Commun.* **2007**, *72* (8), 1014–1024.
- (170) Sambiagio, C.; Marsden, S. P.; Blacker, A. J.; McGowan, P. C. Copper catalysed Ullmann type chemistry: From mechanistic aspects to modern development. *Chemical Society Reviews*. 2014, pp 3525–3550.
- (171) Czekelius, C.; Carreira, E. M. Catalytic Enantioselective Conjugate Reduction of β,β -Disubstituted Nitroalkenes. *Angew. Chemie - Int. Ed.* **2003**, *42* (39), 4793–4795.
- (172) Lipshutz, B. H.; Frieman, B. A.; Tomaso, A. E. Copper-in-charcoal (Cu/C): Heterogeneous, copper-catalysed asymmetric hydrosilylations. *Angew. Chemie - Int. Ed.* **2006**, *45* (8), 1259–1264.
- (173) Appella, D. H.; Moritani, Y.; Shintani, R.; Ferreira, E. M.; Buchwald, S. L. Asymmetric conjugate reduction of α,β -unsaturated esters using a chiral phosphine - Copper catalyst [14]. *J. Am. Chem. Soc.* **1999**, *121* (40), 9473–9474.
- (174) Hughes, G.; Kimura, M.; Buchwald, S. L. Catalytic enantioselective conjugate reduction of lactones and lactams. *J. Am. Chem. Soc.* **2003**, *125* (37), 11253–11258.
- (175) Chae, J.; Yun, J.; Buchwald, S. L. One-pot sequential Cu-catalysed reduction and Pd-catalysed arylation of silyl enol ethers. *Org. Lett.* **2004**, *6* (26), 4809–4812.
- (176) Lipshutz, B. H.; Shimizu, H. Copper(I)-catalysed asymmetric hydrosilylations of imines at ambient temperatures. *Angew. Chemie - Int. Ed.* **2004**, *43* (17), 2228–2230.
- (177) Revis, A.; Hilty, T. K. Novel synthesis of β -siloxy esters by condensation of carbonyls and trimethylsilane with α,β -unsaturated esters catalysed by RhCl₃. *Tetrahedron Lett.* **1987**, *28* (41), 4809–4812.
- (178) Ooi, T.; Doda, K.; Sakai, D.; Maruoka, K. Unique property of copper(I) chloride as a radical initiator as well as a Lewis acid: Application to CuCl-catalysed aldol reaction of α,β -unsaturated ketones with Bu₃SnH. *Tetrahedron Lett.* **1999**, *40* (11), 2133–2136.
- (179) Lam, H. W.; Joensuu, P. M. Cu(I)-catalysed reductive aldol cyclizations: Diastereo- and enantioselective synthesis of

β -hydroxylactones. *Org. Lett.* **2005**, *7* (19), 4225–4228.

- (180) Brunner, H.; Miehling, W. Asymmetrische katalysen. XXII. Enantioselektive hydrosilylierung von ketonen mit Cu-katalysatoren. *J. Organomet. Chem.* **1984**, *275* (2), c17–c21.
- (181) Lipshutz, B. H.; Keith, J.; Papa, P.; Vivian, R. A convenient, efficient method for conjugate reductions using catalytic quantities of Cu(I). *Tetrahedron Lett.* **1998**, *39* (26), 4627–4630.
- (182) Thiel, N. O.; Teichert, J. F. Stereoselective alkyne semihydrogenations with an air-stable copper(i) catalyst. *Org. Biomol. Chem.* **2016**, *14* (45), 10660–10666.
- (183) Wakamatsu, T.; Nagao, K.; Ohmiya, H.; Sawamura, M. Copper-catalysed semihydrogenation of internal alkynes with molecular hydrogen. *Organometallics* **2016**, *35* (10), 1354–1357.
- (184) Ye, T. N.; Lu, Y.; Li, J.; Nakao, T.; Yang, H.; Tada, T.; Kitano, M.; Hosono, H. Copper-Based Intermetallic Electride Catalyst for Chemoselective Hydrogenation Reactions. *J. Am. Chem. Soc.* **2017**, *139* (47), 17089–17097.
- (185) Kour, G.; Gupta, M.; Vishwanathan, B.; Thirunavukkarasu, K. (Cu/NCNTs): A new high temperature technique to prepare a recyclable nanocatalyst for four component pyridine derivative synthesis and nitroarenes reduction. *New J. Chem.* **2016**, *40* (10), 8535–8542.
- (186) Nuzhdin, A. L.; Artiukha, E. A.; Bukhtiyarova, G. A.; Derevyannikova, E. A.; Bukhtiyarov, V. I. Synthesis of secondary amines by reductive amination of aldehydes with nitroarenes over supported copper catalysts in a flow reactor. *Catal. Commun.* **2017**, *102* (June), 108–113.
- (187) Kadam, H. K.; Tilve, S. G. Copper(ii) bromide as a procatalyst for in situ preparation of active Cu nanoparticles for reduction of nitroarenes. *RSC Adv.* **2012**, *2* (14), 6057–6060.
- (188) Deka, P.; Deka, R. C.; Bharali, P. In situ generated copper nanoparticle catalysed reduction of 4-nitrophenol. *New J. Chem.* **2014**, *38* (4), 1789–1793.
- (189) Santhanalakshmi, J.; Parimala, L. The copper nanoparticles catalysed reduction of substituted nitrobenzenes: Effect of nanoparticle stabilizers. *J. Nanoparticle Res.* **2012**, *14* (9).
- (190) Tamuly, C.; Saikia, I.; Hazarika, M.; Das, M. R. Reduction of aromatic nitro compounds catalysed by biogenic CuO nanoparticles. *RSC Adv.* **2014**, *4* (95), 53229–53236.
- (191) de Souza, J. F.; da Silva, G. T.; Fajardo, A. R. Chitosan-based film supported copper nanoparticles: A potential and reusable catalyst for the reduction of aromatic nitro compounds. *Carbohydr. Polym.* **2017**, *161*.
- (192) Sharma, R.; Monga, Y.; Puri, A. Magnetically separable silica@Fe₃O₄ core-shell supported nano-structured copper(II) composites as a versatile catalyst for the reduction of nitroarenes in aqueous medium at room temperature. *J. Mol. Catal. A Chem.* **2014**, *393*, 84–95.
- (193) Ghonchepour, E.; Yazdani, E.; Saberi, D.; Arefi, M.; Heydari, A. Preparation and characterization of copper chloride supported on citric acid-modified magnetite nanoparticles (Cu²⁺-CA@Fe₃O₄) and evaluation of its catalytic activity in the reduction of nitroarene compounds. *Appl. Organomet. Chem.* **2017**, *31* (12), 1–8.
- (194) Parmekar, M. V.; Salker, A. V. Room temperature complete reduction of nitroarenes over a novel Cu/SiO₂@NiFe₂O₄ nano-catalyst in an aqueous medium—a kinetic and mechanistic study. *RSC Adv.* **2016**, *6* (110), 108458–108467.
- (195) Rajabzadeh, M.; Eshghi, H.; Khalifeh, R.; Bakavoli, M. Generation of Cu nanoparticles on novel designed Fe₃O₄@SiO₂/EP.EN.EG as reusable nanocatalyst for the reduction of nitro compounds. *RSC Adv.* **2016**, *6* (23), 19331–19340.
- (196) Yang, S.; Zhang, Z. H.; Chen, Q.; He, M. Y.; Wang, L. Magnetically Recyclable Metal–Organic Framework@Fe₃O₄ Composite-Catalysed Facile Reduction of Nitroarene Compounds in Aqueous Medium. *Appl. Organomet. Chem.* **2018**, *32* (3), 1–6.
- (197) Vinod Kumar, V.; Rajmohan, R.; Vairaprakash, P.; Mariappan, M.; Anthony, S. P. Copper-coordination polymer-controlled Cu@N-rGO and CuO@C nanoparticle formation: Reusable green catalyst for A³-coupling and nitroarene-reduction reactions. *Dalt. Trans.* **2017**, *46* (35), 11704–11714.
- (198) Saha, A.; Ranu, B. Highly chemoselective reduction of aromatic nitro compounds by copper nanoparticles/ammonium formate. *J. Org. Chem.* **2008**, *73* (17), 6867–6870.
- (199) Subramanian, T.; Pitchumani, K. Selective Reduction of Nitroarenes by using Zeolite-Supported Copper Nanoparticles with 2-Propanol as a Sustainable Reducing Agent. *ChemCatChem* **2012**, *4* (12), 1917–1921.
- (200) Singh, A.; Raj, T.; Singh, N. Highly selective and efficient reduction of nitroarenes by imidazolium salt stabilized copper nanoparticles in aqueous medium. *Catal. Letters* **2015**, *145* (8), 1606–1611.
- (201) Feng, H.; Li, Y.; Lin, S.; Van der Eycken, E. V.; Song, G. Nano Cu-catalysed efficient and selective reduction of nitroarenes under combined microwave and ultrasound irradiation. *Sustain. Chem. Process.* **2014**, *2* (1), 14.
- (202) Kumar, V.; Nigam, K. D. P. Process intensification in green synthesis. *Green Processing and Synthesis*. 2012, pp 79–

- (203) Fitzpatrick, D. E.; Battilocchio, C.; Ley, S. V. Enabling technologies for the future of chemical synthesis. *ACS Cent. Sci.* **2016**, *2* (3), 131–138.
- (204) Beillard, A.; Bantreil, X.; Métro, T. X.; Martinez, J.; Lamaty, F. Alternative technologies that facilitate access to discrete metal complexes. *Chem. Rev.* **2019**.
- (205) Cravotto, G.; Caporaso, M.; Jicsinszky, L.; Martina, K. Enabling technologies and green processes in cyclodextrin chemistry. *Beilstein J. Org. Chem.* **2016**, *12*, 278–294.
- (206) Manzoli, M.; Bonelli, B. Microwave, Ultrasound, and Mechanochemistry: Unconventional Tools that Are Used to Obtain “Smart” Catalysts for CO₂ Hydrogenation. *Catalysts* **2018**, *8* (7), 262.
- (207) Ascrizzi, R.; González-Rivera, J.; Pomelli, C. S.; Chiappe, C.; Margari, P.; Costagli, F.; Longo, I.; Tiné, M. R.; Flamini, G.; Duce, C. Ionic liquids, ultra-sounds and microwaves: An effective combination for a sustainable extraction with higher yields. the cumin essential oil case. *React. Chem. Eng.* **2017**, *2* (4), 577–589.
- (208) Calcio Gaudino, E.; Tabasso, S.; Grillo, G.; Cravotto, G.; Dreyer, T.; Schories, G.; Altenberg, S.; Jashina, L.; Telysheva, G. Wheat straw lignin extraction with bio-based solvents using enabling technologies. *Comptes Rendus Chim.* **2018**, *21* (6), 563–571.
- (209) Green, A.; Marshall, J. S.; Ma, D.; Wu, J. Acoustic streaming and thermal instability of flow generated by ultrasound in a cylindrical container. *Phys. Fluids* **2016**, *28* (10).
- (210) Morschhäuser, R.; Krull, M.; Kayser, C.; Boberski, C.; Bierbaum, R.; Püschner, P. A.; Glasnov, T. N.; Kappe, C. O. Microwave-assisted continuous flow synthesis on industrial scale. *Green Process. Synth.* **2012**, *1* (3), 281–290.
- (211) Oliverio, M.; Procopio, A.; Glasnov, T. N.; Goessler, W.; Kappe, C. O. Microwave-assisted grafting to MCM-41 silica and its application as catalyst in flow chemistry. *Aust. J. Chem.* **2011**, *64* (11), 1522–1529.
- (212) Rahimi, M.; Shahhosseini, S.; Sobati, M. A.; Movahedirad, S.; Khodaei, B.; Hassanzadeh, H. A novel multi-probe continuous flow ultrasound assisted oxidative desulfurization reactor; experimental investigation and simulation. *Ultrason. Sonochem.* **2019**, *56* (January), 264–273.
- (213) Rahimi, M.; Shahhosseini, S.; Movahedirad, S. Continuous-flow ultrasound assisted oxidative desulfurization (UAOD) process: An efficient diesel treatment by injection of the aqueous phase. *Ultrason. Sonochem.* **2017**, *39* (April), 611–622.
- (214) Gedye, R.; Smith, F. Erste MW-Reaktion Gedye. *Tetrahedron Lett.* **1986**, *27* (3), 279–282.
- (215) Giguere, R. J.; Bray, T. L.; Duncan, S. M.; Majtich, G. Erste MW-Reaktion Giguere. *Tetrahedron Lett.* **1986**, *27* (41), 4945–4948.
- (216) Organic, A.; Caddick, S. Tetrahedron. *Nature* **1957**, *179* (4572), 1222–1223.
- (217) S. Varma, R. Solvent-free organic syntheses . using supported reagents and microwave irradiation. *Green Chem.* **1999**, *1* (1), 43–55.
- (218) Pitchai, K.; Birla, S. L.; Subbiah, J.; Jones, D.; Thippareddi, H. Coupled electromagnetic and heat transfer model for microwave heating in domestic ovens. *J. Food Eng.* **2012**, *112* (1–2), 100–111.
- (219) Diaz-Ortiz, A.; de la Hoz, A.; Alcazar, J.; Ramon Carrillo, J.; Antonia Herrero, M.; Fontana, A.; de Mata Munoz, J. Reproducibility and Scalability of Solvent-Free Microwave-Assisted Reactions: From Domestic Ovens to Controllable Parallel Applications. *Comb. Chem. High Throughput Screen.* **2007**, *10* (3), 163–169.
- (220) Díaz-Ortiz, Prieto, P.; de la Hoz, A. A Critical Overview on the Effect of Microwave Irradiation in Organic Synthesis. *Chem. Rec.* **2019**, *19* (1), 85–97.
- (221) Tierney, J. P.; Lidström, P. Microwave Assisted Organic Synthesis. *Microw. Assist. Org. Synth.* **2009**, *57* (589), 1–280.
- (222) Nüchter, M.; Ondruschka, B.; Bonrath, W.; Gum, A. Microwave assisted synthesis – a critical technology overview. *Green Chem.* **2004**, *6* (3), 128–141.
- (223) Polshettiwar, V.; Nadagouda, M. N.; Varma, R. S. Microwave-Assisted Chemistry: a Rapid and Sustainable Route to Synthesis of Organics and Nanomaterials. *Aust. J. Chem.* **2009**, *62* (1), 16.
- (224) Kokel, A.; Schäfer, C.; Török, B. Application of microwave-assisted heterogeneous catalysis in sustainable synthesis design. *Green Chem.* **2017**, *19* (16), 3729–3751.
- (225) Whittaker, A. G.; Sb, D. M. P. M. Powders t. *J. Chem. Soc.* **1995**, 2073–2079.
- (226) Tsukahara, Y.; Higashi, A.; Yamauchi, T.; Nakamura, T.; Yasuda, M.; Baba, A.; Wada, Y. In situ observation of nonequilibrium local heating as an origin of special effect of microwave on chemistry. *J. Phys. Chem. C* **2010**, *114* (19), 8965–8970.
- (227) Gutmann, B.; Schwan, A. M.; Reichart, B.; Gspan, C.; Hofer, F.; Kappe, C. O. Activation and deactivation of a chemical

transformation by an electromagnetic field: Evidence for specific microwave effects in the formation of grignard reagents. *Angew. Chemie - Int. Ed.* **2011**, *50* (33), 7636–7640.

- (228) Horikoshi, S.; Osawa, A.; Abe, M.; Serpone, N. On the generation of hot-spots by microwave electric and magnetic fields and their impact on a microwave-assisted heterogeneous reaction in the presence of metallic Pd nanoparticles on an activated carbon support. *J. Phys. Chem. C* **2011**, *115* (46), 23030–23035.
- (229) Barnett, S. B.; Ter Haar, G. R.; Ziskin, M. C.; Rott, H. D.; Duck, F. A.; Maeda, K. International recommendations and guidelines for the safe use of diagnostic ultrasound in medicine. *Ultrasound Med. Biol.* **2000**, *26* (3), 355–366.
- (230) Mason, T. J. Chapter 16 : Sonochemistry; 2015.
- (231) Suslick, K. S.; Eddingsaas, N. C.; Flannigan, D. J.; Hopkins, S. D.; Xu, H. The Chemical History of a Bubble. *Acc. Chem. Res.* **2018**, *51* (9), 2169–2178.
- (232) Storey, A. A.; Ramírez, J. M.; Quiroz, D.; Burley, D. V.; Addison, D. J.; Walter, R.; Anderson, A. J.; Hunt, T. L.; Athens, J. S.; Huynen, L.; et al. Radiocarbon and DNA evidence for a pre-Columbian introduction of Polynesian chickens to Chile. *Proc. Natl. Acad. Sci. U. S. A.* **2007**, *104* (25), 10335–10339.
- (233) Frederick, J. R. *Ultrasonic engineering*; J. Wiley: New York, 1965.
- (234) Brown, B.; Goodman, J. B. *High-intensity ultrasonics: industrial applications*; Iliffe Books; D. Van Nostrand Co.: London; Princeton, N.J., 1965.
- (235) Tao, Y.; Sun, D. W. Enhancement of Food Processes by Ultrasound: A Review. *Crit. Rev. Food Sci. Nutr.* **2015**, *55* (4), 570–594.
- (236) Bonrath, W.; A. Paz Schmidt, R. Ultrasound in Synthetic Organic Chemistry. *Adv. Org. Synth. (Volume 1)* **2010**, *26*, 81–117.
- (237) Suslick, K. S.; Casadonte, D. J. Heterogeneous sonocatalysis with nickel powder. *J. Am. Chem. Soc.* **1987**, *109* (11), 3459–3461.
- (238) Cravotto, G.; Fokin, V. V.; Garella, D.; Binello, A.; Boffa, L.; Barge, A. Ultrasound-promoted copper-catalysed azide - alkyne cycloaddition. *J. Comb. Chem.* **2010**, *12* (1), 13–15.
- (239) Bertram, A. K.; Liu, M. T. H. Cycloaddition of arylchlorocarbenes using ultrasound. *J. Chem. Soc. Chem. Commun.* **1993**, No. 5, 467–468.
- (240) Cravotto, G.; Cintas, P. The combined use of microwaves and ultrasound: Improved tools in process chemistry and organic synthesis. *Chem. - A Eur. J.* **2007**, *13* (7), 1902–1909.
- (241) Cintas, P.; Carnaroglio, D.; Rinaldi, L.; Cravotto, G. Complementary and synergic effects. **2012**, *30* (June), 3–5.
- (242) Cravotto, G.; Beggiato, M.; Penoni, A.; Palmisano, G.; Tollari, S.; Lévêque, J. M.; Bonrath, W. High-intensity ultrasound and microwave, alone or combined, promote Pd/C-catalysed aryl-aryl couplings. *Tetrahedron Lett.* **2005**, *46* (13), 2267–2271.
- (243) Palmisano, G.; Bonrath, W.; Boffa, L.; Garella, D.; Barge, A.; Cravotto, G. Heck reactions with very low ligandless catalyst loads accelerated by microwaves or simultaneous microwaves/ultrasound irradiation. *Adv. Synth. Catal.* **2007**, *349* (14–15), 2338–2344.
- (244) Cravotto, G.; Orio, L.; Gaudino, E. C.; Martina, K.; Tavor, D.; Wolfson, A. Efficient synthetic protocols in glycerol under heterogeneous catalysis. *ChemSusChem* **2011**, *4* (8), 1130–1134.
- (245) Chemat, F.; Poux, M.; Martino, J.-L. Di; Berlan, J. An Original Microwave-Ultrasound Combined Reactor Suitable for Organic Synthesis: Application to Pyrolysis and Esterification. *J. Microw. Power Electromagn. Energy* **1996**, *31* (1), 19–22.
- (246) Cravotto, G.; Cintas, P. Power ultrasound in organic synthesis: Moving cavitation chemistry from academia to innovative and large-scale applications. *Chem. Soc. Rev.* **2006**, *35* (2), 180–196.
- (247) Friščić, T.; James, S. L.; Boldyreva, E. V.; Bolm, C.; Jones, W.; Mack, J.; Steed, J. W.; Suslick, K. S. Highlights from Faraday discussion 170: Challenges and opportunities of modern mechanochemistry, Montreal, Canada, 2014. *Chem. Commun.* **2015**, *51* (29), 6248–6256.
- (248) Do, J. L.; Friščić, T. Mechanochemistry: A Force of Synthesis. *ACS Cent. Sci.* **2017**, *3* (1), 13–19.
- (249) Howard, J. L.; Cao, Q.; Browne, D. L. Mechanochemistry as an emerging tool for molecular synthesis: What can it offer? *Chem. Sci.* **2018**, *9* (12), 3080–3094.
- (250) Suryanarayana, C. Mechanical alloying and milling. *Mech. Alloy. Milling* **2004**, *46*, 1–472.
- (251) Belenguer, A. M.; Friščić, T.; Day, G. M.; Sanders, J. K. M. Solid-state dynamic combinatorial chemistry: Reversibility and thermodynamic product selection in covalent mechanosynthesis. *Chem. Sci.* **2011**, *2* (4), 696–700.
- (252) Michalchuk, A. A. L.; Tumanov, I. A.; Drebuschak, V. A.; Boldyreva, E. V. Advances in elucidating mechanochemical

- complexities via implementation of a simple organic system. *Faraday Discuss.* **2014**, *170*, 311–335.
- (253) Içli, B.; Christinat, N.; Tönnemann, J.; Schüttler, C.; Scopelliti, R.; Severin, K. Synthesis of molecular nanostructures by multicomponent condensation reactions in a ball mill. *J. Am. Chem. Soc.* **2009**, *131* (9), 3154–3155.
- (254) Hernández, J. G.; Frišćić, T. Metal-catalysed organic reactions using mechanochemistry. *Tetrahedron Lett.* **2015**, *56* (29), 4253–4265.
- (255) Nielsen, S. F.; Peters, D.; Axelsson, O. The Suzuki reaction under solvent-free conditions. *Synth. Commun.* **2000**, *30* (19), 3501–3509.
- (256) Braga, D.; D'Addario, D.; Polito, M.; Grepioni, F. Mechanically induced expeditious and selective preparation of disubstituted pyridine/pyrimidine ferrocenyl complexes. *Organometallics* **2004**, *23* (11), 2810–2812.
- (257) Klingensmith, L. M.; Leadbeater, N. E. Ligand-free palladium catalysis of aryl coupling reactions facilitated by grinding. *Tetrahedron Lett.* **2003**, *44* (4), 765–768.
- (258) Tullberg, E.; Peters, D.; Frejd, T. The Heck reaction under ball-milling conditions. *J. Organomet. Chem.* **2004**, *689* (23), 3778–3781.
- (259) Zhu, X.; Liu, J.; Chen, T.; Su, W. Mechanically activated synthesis of (E)-stilbene derivatives by high-speed ball milling. *Appl. Organomet. Chem.* **2012**, *26* (3), 145–147.
- (260) Rak, M. J.; Saadé, N. K.; Frišćić, T.; Moores, A. Mechanochemistry of ultra-small monodisperse amine-stabilized gold nanoparticles with controllable size. *Green Chem.* **2014**, *16* (1), 86–89.
- (261) Declerck, V.; Colacino, E.; Bantreil, X.; Martinez, J.; Lamaty, F. Poly(ethylene glycol) as reaction medium for mild Mizoroki-Heck reaction in a ball-mill. *Chem. Commun.* **2012**, *48* (96), 11778–11780.
- (262) Thorwirth, R.; Stolle, A.; Ondruschka, B.; Wild, A.; Schubert, U. S. Fast, ligand- and solvent-free copper-catalysed click reactions in a ball mill. *Chem. Commun.* **2011**, *47* (15), 4370–4372.
- (263) Leonardi, M.; Villacampa, M.; Menéndez, J. C. Multicomponent mechanochemical synthesis. *Chem. Sci.* **2018**, *9* (8), 2042–2064.
- (264) Veverková, E.; Poláčková, V.; Liptáková, L.; Kázmerová, E.; Mečiarová, M.; Toma, Š.; Šebesta, R. Organocatalyst Efficiency in the Michael Additions of Aldehydes to Nitroalkenes in Water and in a Ball-Mill. *ChemCatChem* **2012**, *4* (7), 1013–1018.
- (265) Hernández, J. G.; Juaristi, E. Efficient ball-mill procedure in the “green” asymmetric aldol reaction organocatalysed by (S)-proline-containing dipeptides in the presence of water. *Tetrahedron* **2011**, *67* (36), 6953–6959.
- (266) Guillena, G.; del Carmen Hita, M.; Nájera, C.; Vióquez, S. F. Solvent-free asymmetric direct aldol reactions organocatalysed by recoverable (Sa)-binam-l-prolinamide. *Tetrahedron Asymmetry* **2007**, *18* (19), 2300–2304.
- (267) Rodríguez, B.; Rantanen, T.; Bolm, C. Solvent-free asymmetric organocatalysis in a ball mill. *Angew. Chemie - Int. Ed.* **2006**, *45* (41), 6924–6926.
- (268) Immohr, S.; Felderhoff, M.; Weidenthaler, C.; Schüth, F. An orders-of-magnitude increase in the rate of the solid-catalysed co oxidation by in situ ball milling. *Angew. Chemie - Int. Ed.* **2013**, *52* (48), 12688–12691.
- (269) Penteado, F.; Monti, B.; Sancineto, L.; Perin, G.; Jacob, R. G.; Santi, C.; Lenardão, E. J. Ultrasound-Assisted Multicomponent Reactions, Organometallic and Organochalcogen Chemistry. *Asian J. Org. Chem.* **2018**, *7* (12), 2368–2385.
- (270) Banerjee, B. Ultrasound and Nano-Catalysts: An Ideal and Sustainable Combination to Carry out Diverse Organic Transformations. *ChemistrySelect.* 2019, pp 2484–2500.
- (271) Ying, A.; Wang, L.; Qiu, F.; Hu, H.; Yang, J. Magnetic nanoparticle supported amine: An efficient and environmental benign catalyst for versatile Knoevenagel condensation under ultrasound irradiation. *Comptes Rendus Chim.* **2015**, *18* (2), 223–232.
- (272) Saadatjoo, N.; Golshekan, M.; Shariati, S.; Azizi, P.; Nemati, F. Ultrasound-assisted synthesis of β -amino ketones via a Mannich reaction catalysed by Fe₃O₄magnetite nanoparticles as an efficient, recyclable and heterogeneous catalyst. *Arab. J. Chem.* **2017**, *10*, S735–S741.
- (273) Haas, I.; Shanmugam, S.; Gedanken, A. Pulsed sonoelectrochemical synthesis of size-controlled copper nanoparticles stabilized by poly(N-vinylpyrrolidone). *J. Phys. Chem. B* **2006**, *110* (34), 16947–16952.
- (274) Wani, I. A.; Ganguly, A.; Ahmed, J.; Ahmad, T. Silver nanoparticles: Ultrasonic wave assisted synthesis, optical characterization and surface area studies. *Mater. Lett.* **2011**, *65* (3), 520–522.
- (275) Wu, S.; Sun, A.; Zhai, F.; Wang, J.; Xu, W.; Zhang, Q.; Volinsky, A. A. Fe₃O₄ magnetic nanoparticles synthesis from tailings by ultrasonic chemical co-precipitation. *Mater. Lett.* **2011**, *65* (12), 1882–1884.
- (276) Moghimi-Rad, J.; Zabihi, F.; Hadi, I.; Ebrahimi, S.; Isfahani, T. D.; Sabbaghzadeh, J. Effect of ultrasound radiation on the size and size distribution of synthesized copper particles. *J. Mater. Sci.* **2010**, *45* (14), 3804–3811.

- (277) Shui, A.; Zhu, W.; Xu, L.; Qin, D.; Wang, Y. Green sonochemical synthesis of cupric and cuprous oxides nanoparticles and their optical properties. *Ceram. Int.* **2013**, *39* (8), 8715–8722.
- (278) Microscope, O.; Laser, F.; Mdplan, O.; Ctc-, D. M.; Api, M. C.; Hene, M. G.; Electron, S.; Imaging, M.; Jsm-, J. perature during laser pruning has a lower bound of 1750 K, as suggested by the liquid-drop model for the size-dependent melting of nanoparticles. [11] The melting temperature of iron nanoparticles, T. *Adv. Mater.* **2003**, *0044* (3), 303–305.
- (279) Cerchier, P.; Dabalà, M.; Brunelli, K. Green synthesis of copper nanoparticles with ultrasound assistance. *Green Process. Synth.* **2017**, *6* (3), 311–316.
- (280) Ismail, N. A.; Shameli, K.; Wong, M. M. T.; Teow, S. Y.; Chew, J.; Sukri, S. N. A. M. Antibacterial and cytotoxic effect of honey mediated copper nanoparticles synthesized using ultrasonic assistance. *Mater. Sci. Eng. C* **2019**, *104* (January), 109899.
- (281) Horikoshi, S.; Abe, H.; Sumi, T.; Torigoe, K.; Sakai, H.; Serpone, N.; Abe, M. Microwave frequency effect in the formation of Au nanocolloids in polar and non-polar solvents. *Nanoscale* **2011**, *3* (4), 1697–1702.
- (282) Ding, T.; Zhu, J. J. Microwave heating synthesis of HgS and PbS nanocrystals in ethanol solvent. *Mater. Sci. Eng. B Solid-State Mater. Adv. Technol.* **2003**, *100* (3), 307–313.
- (283) Yu, W.; Tu, W.; Liu, H. Synthesis of Nanoscale Platinum Colloids by Microwave Dielectric Heating. *Langmuir* **2002**, *15* (1), 6–9.
- (284) Jhung, S. H.; Jin, T.; Hwang, Y. K.; Chang, J. S. Microwave effect in the fast synthesis of microporous materials: Which stage between nucleation and crystal growth is accelerated by microwave irradiation? *Chem. - A Eur. J.* **2007**, *13* (16), 4410–4417.
- (285) Baghbanzadeh, M.; Carbone, L.; Cozzoli, P. D.; Kappe, C. O. Microwave-assisted synthesis of colloidal inorganic nanocrystals. *Angew. Chemie - Int. Ed.* **2011**, *50* (48), 11312–11359.
- (286) Gerbec, J. A.; Magana, D.; Washington, A.; Strouse, G. F. Microwave-enhanced reaction rates for nanoparticle synthesis. *J. Am. Chem. Soc.* **2005**, *127* (45), 15791–15800.
- (287) Duan, H.; Wang, D.; Li, Y. Green chemistry for nanoparticle synthesis. *Chem. Soc. Rev.* **2015**, *44* (16), 5778–5792.
- (288) Rivas, R. by M. E. “Ball Milling Towards Green Synthesis: Applications, Projects, Challenges.” *Johnson Matthey Technol. Rev.* **2017**, *60* (2), 148–150.
- (289) James, S. L.; Adams, C. J.; Bolm, C.; Braga, D.; Collier, P.; Frišćic, T.; Grepioni, F.; Harris, K. D. M.; Hyett, G.; Jones, W.; et al. Playing with organic radicals as building blocks for functional molecular materials. *Chem. Soc. Rev.* **2012**, *41* (1), 413–447.
- (290) Lou, S. J.; Mao, Y. J.; Xu, D. Q.; He, J. Q.; Chen, Q.; Xu, Z. Y. Fast and Selective Dehydrogenative C-H/C-H Arylation Using Mechanochemistry. *ACS Catal.* **2016**, *6* (6), 3890–3894.
- (291) Jörres, M.; Aceña, J. L.; Soloshonok, V. A.; Bolm, C. Asymmetric carbon-carbon bond formation under solventless conditions in ball mills. *ChemCatChem* **2015**, *7* (8), 1265–1269.
- (292) Hermann, G. N.; Becker, P.; Bolm, C. Mechanochemical Iridium(III)-Catalysed C-H Bond Amidation of Benzamides with Sulfonyl Azides under Solvent-Free Conditions in a Ball Mill. *Angew. Chemie - Int. Ed.* **2016**, *55* (11), 3781–3784.
- (293) Jörres, M.; Mersmann, S.; Raabe, G.; Bolm, C. Organocatalytic solvent-free hydrogen bonding-mediated asymmetric Michael additions under ball milling conditions. *Green Chem.* **2013**, *15* (3), 612–616.
- (294) Martina, K.; Rotolo, L.; Porcheddu, A.; Delogu, F.; Bysouth, S. R.; Cravotto, G.; Colacino, E. High throughput mechanochemistry: Application to parallel synthesis of benzoxazines. *Chem. Commun.* **2018**, *54* (5), 551–554.
- (295) Porcheddu, A.; Colacino, E.; Cravotto, G.; Delogu, F.; De Luca, L. Mechanically induced oxidation of alcohols to aldehydes and ketones in ambient air: Revisiting TEMPO-assisted oxidations. *Beilstein J. Org. Chem.* **2017**, *13*, 2049–2055.
- (296) Mishra, A. K.; Moorthy, J. N. Mechanochemical catalytic oxidations in the solid state with: In situ -generated modified IBX from 3,5-di-tert-butyl-2-iodobenzoic acid (DTB-IA)/Oxone. *Org. Chem. Front.* **2017**, *4* (3), 343–349.
- (297) Grätz, S.; Borchardt, L. Mechanochemical polymerization-controlling a polycondensation reaction between a diamine and a dialdehyde in a ball mill. *RSC Adv.* **2016**, *6* (69), 64799–64802.
- (298) Jicsinszky, L.; Caporaso, M.; Tuza, K.; Martina, K.; Calcio Gaudino, E.; Cravotto, G. Nucleophilic Substitutions of 6I-O-Monosyl- β -cyclodextrin in a Planetary Ball Mill. *ACS Sustain. Chem. Eng.* **2016**, *4* (3), 919–929.
- (299) Huot, J.; Ravnsbæk, D. B.; Zhang, J.; Cuevas, F.; Latroche, M.; Jensen, T. R. Mechanochemical synthesis of hydrogen storage materials. *Prog. Mater. Sci.* **2013**, *58* (1), 30–75.
- (300) Hlova, I. Z.; Castle, A.; Goldston, J. F.; Gupta, S.; Prost, T.; Kobayashi, T.; Scott Chumbley, L.; Pruski, M.; Pecharsky, V. K. Solvent- and catalyst-free mechanochemical synthesis of alkali metal monohydrides. *J. Mater. Chem. A* **2016**, *4*

- (31), 12188–12196.
- (301) Naimi-Jamal, M. R.; Mokhtari, J.; Dekamin, M. G.; Kaupp, G. Sodium tetraalkoxyborates: Intermediates for the quantitative reduction of aldehydes and ketones to alcohols through ball milling with NaBH₄. *European J. Org. Chem.* **2009**, 4 (21), 3567–3572.
- (302) Sawama, Y.; Yasukawa, N.; Ban, K.; Goto, R.; Niikawa, M.; Monguchi, Y.; Itoh, M.; Sajiki, H. Stainless Steel-Mediated Hydrogen Generation from Alkanes and Diethyl Ether and Its Application for Arene Reduction. *Org. Lett.* **2018**, 20 (10), 2892–2896.
- (303) Menuel, S.; Léger, B.; Addad, A.; Monflier, E.; Hapiot, F. Cyclodextrins as effective additives in AuNP-catalysed reduction of nitrobenzene derivatives in a ball-mill. *Green Chem.* **2016**, 18 (20), 5500–5509.
- (304) Espinosa, J. C.; Navalon, S.; Alvaro, M.; Dhakshinamoorthy, A.; Garcia, H. Reduction of C=C Double Bonds by Hydrazine Using Active Carbons as Metal-Free Catalysts. *ACS Sustain. Chem. Eng.* **2018**, 6 (4), 5607–5614.
- (305) Li, L.; Li, L.; Cui, C.; Fan, H.; Wang, R. Heteroatom-doped Carbon Spheres from Hierarchical Hollow Covalent Organic Framework Precursors for Metal-Free Catalysis. *ChemSusChem* **2017**, 10 (24), 4921–4926.
- (306) Wang, H. C.; Li, B. L.; Zheng, Y. J.; Wang, W. Y. Mesoporous carbon as a metal-free catalyst for the reduction of nitroaromatics with hydrazine hydrate. *Bull. Korean Chem. Soc.* **2012**, 33 (9), 2961–2965.
- (307) Singh, S. K.; Xu, Q. Nanocatalysts for hydrogen generation from hydrazine. *Catal. Sci. Technol.* **2013**, 3 (8), 1889–1900.
- (308) Paveglio, G. C.; Longhi, K.; Moreira, D. N.; München, T. S.; Tier, A. Z.; Gindri, I. M.; Bender, C. R.; Frizzo, C. P.; Zanatta, N.; Bonaccorso, H. G.; et al. How mechanical and chemical features affect the green synthesis of 1 H -pyrazoles in a ball mill. *ACS Sustain. Chem. Eng.* **2014**, 2 (7), 1895–1901.
- (309) Nun, P.; Martin, C.; Martinez, J.; Lamaty, F. Solvent-free synthesis of hydrazones and their subsequent N-alkylation in a Ball-mill. *Tetrahedron* **2011**, 67 (42), 8187–8194.
- (310) Oliveira, P. F. M.; Baron, M.; Chamayou, A.; André-Barrès, C.; Guidetti, B.; Baltas, M. Solvent-free mechanochemical route for green synthesis of pharmaceutically attractive phenolhydrazones. *RSC Adv.* **2014**, 4 (100), 56736–56742.
- (311) Patil, N. M.; Sasaki, T.; Bhanage, B. M. Chemoselective transfer hydrogenation of α,β -unsaturated carbonyls using palladium immobilized ionic liquid catalyst. *Catal. Letters* **2014**, 144 (11), 1803–1809.
- (312) Ahammed, S.; Saha, A.; Ranu, B. C. Hydrogenation of azides over copper nanoparticle surface using ammonium formate in water. *J. Org. Chem.* **2011**, 76 (17), 7235–7239.
- (313) Gowda, S.; Abiraj, K.; Gowda, D. C. Reductive cleavage of azo compounds catalysed by commercial zinc dust using ammonium formate or formic acid. *Tetrahedron Lett.* **2002**, 43 (7), 1329–1331.
- (314) Rajagopal, S.; Spatola, A. F. Mechanism of Palladium-Catalysed Transfer Hydrogenolysis of Aryl Chlorides by Formate Salts. *J. Org. Chem.* **1995**, 60 (5), 1347–1355.
- (315) Jang, I. J.; Shin, H. S.; Shin, N. R.; Kim, S. H.; Kim, S. K.; Yu, M. J.; Cho, S. J. Macroporous-mesoporous alumina supported iridium catalyst for hydrazine decomposition. *Catal. Today* **2012**, 185 (1), 198–204.
- (316) Million-Picallion, L.; Berger, G.; Lefèvre, G.; Delaunay, S.; Mansour, C. Stability of hydrazine, morpholine and ethanolamine at 275 °C and in situ measurement of redox and acid-base properties. *J. Solution Chem.* **2015**, 44 (9), 1900–1919.
- (317) Olliaee, S. N.; Zhang, C.; Hwang, S. Y.; Cheung, H. M.; Peng, Z. Synthesis and property of a Helwingia-structured nickel nitride/ nickel hydroxide nanocatalyst in hydrazine decomposition. *RSC Adv.* **2016**, 6 (44), 38494–38498.
- (318) Navlani-García, M.; Mori, K.; Kuwahara, Y.; Yamashita, H. Recent strategies targeting efficient hydrogen production from chemical hydrogen storage materials over carbon-supported catalysts. *NPG Asia Mater.* **2018**, 10 (4), 277–292.
- (319) Karimi, B.; Mansouri, F.; Vali, H. A Highly Water-Dispersible/Magnetically Separable Palladium Catalyst: Selective Transfer Hydrogenation or Direct Reductive N-Formylation of Nitroarenes in Water. *Chempluschem* **2015**, 80 (12), 1750–1759.
- (320) Mocchi, R.; Murgia, S.; De Luca, L.; Colacino, E.; Delogu, F.; Porcheddu, A. Ball-milling and cheap reagents breathe green life into the one hundred-year-old Hofmann reaction. *Org. Chem. Front.* **2018**, 5 (4), 531–538.
- (321) Pathare, S. P.; Sawant, R. V.; Akamanchi, K. G. Sulfated tungstate catalysed highly accelerated N-formylation. *Tetrahedron Lett.* **2012**, 53 (26), 3259–3263.
- (322) Giovani, S.; Singh, R.; Fasan, R. Efficient conversion of primary azides to aldehydes catalysed by active site variants of myoglobin. *Chem. Sci.* **2016**, 7 (1), 234–239.
- (323) González-Calderón, D.; Morales-Reza, M. A.; Díaz-Torres, E.; Fuentes-Benites, A.; González-Romero, C. A straightforward and versatile protocol for the direct conversion of benzylic azides to ketones and aldehydes. *RSC Adv.* **2016**, 6 (87), 83547–83550.

- (324) Zhao, W.; Yuan, P.; She, X.; Xia, Y.; Komarneni, S.; Xi, K.; Che, Y.; Yao, X.; Yang, D. Sustainable seaweed-based one-dimensional (1D) nanofibers as high-performance electrocatalysts for fuel cells. *J. Mater. Chem. A* **2015**, *3* (27), 14188–14194.
- (325) Tao, C. Z.; Cui, X.; Li, J.; Liu, A. X.; Liu, L.; Guo, Q. X. Copper-catalysed synthesis of aryl azides and 1-aryl-1,2,3-triazoles from boronic acids. *Tetrahedron Lett.* **2007**, *48* (20), 3525–3529.
- (326) Gandeepan, P.; Kaplaneris, N.; Santoro, S.; Vaccaro, L.; Ackermann, L. Biomass-Derived Solvents for Sustainable Transition Metal-Catalysed C-H Activation. *ACS Sustainable Chemistry and Engineering*. 2019, pp 8023–8040.
- (327) Sudhakar, M.; Naresh, G.; Rambabu, G.; Anjaneyulu, C.; Hari, A. Crude bio-glycerol as a hydrogen source for the selective hydrogenation of aromatic nitro compounds over Ru / MgLaO catalyst. *CATCOM* **2016**, *74*, 91–94.
- (328) Dodekatos, G.; Schünemann, S.; Tüysüz, H. Recent Advances in Thermo-, Photo-, and Electrocatalytic Glycerol Oxidation. *ACS Catal.* **2018**, *8* (7), 6301–6333.
- (329) Santoro, F.; Psaro, R.; Ravasio, N.; Zaccheria, F. N-Alkylation of amines through hydrogen borrowing over a heterogeneous Cu catalyst. *RSC Adv.* **2014**, *4* (6), 2596–2600.
- (330) Cui, X.; Zhang, C.; Shi, F.; Deng, Y. Au/Ag-Mo nano-rods catalysed reductive coupling of nitrobenzenes and alcohols using glycerol as the hydrogen source. *Chem. Commun.* **2012**, *48* (75), 9391–9393.
- (331) Sutter, M.; Pehlivan, L.; Lafon, R.; Dayoub, W.; Raoul, Y.; Métay, E.; Lemaire, M. 1,2,3-Trimethoxypropane, a glycerol-based solvent with low toxicity: New utilization for the reduction of nitrile, nitro, ester, and acid functional groups with TMDS and a metal catalyst. *Green Chem.* **2013**, *15* (11), 3020–3026.
- (332) Chahdoura, F.; Favier, I.; Gómez, M. Glycerol as suitable solvent for the synthesis of metallic species and catalysis. *Chemistry - A European Journal*. Wiley-VCH Verlag August 25, 2014, pp 10884–10893.
- (333) Ghosh, A.; Meshram, N. K.; Saha, R. Glycerol-mediated synthesis of nanoscale zerovalent iron and its application for the simultaneous reduction of nitrate and alachlor. *Environ. Sci. Pollut. Res.* **2019**, *26* (12), 11951–11961.
- (334) Parveen, R.; Ullah, S.; Sgarbi, R.; Tremiliosi-Filho, G. One-pot ligand-free synthesis of gold nanoparticles: The role of glycerol as reducing-cum-stabilizing agent. *Colloids Surfaces A Physicochem. Eng. Asp.* **2019**, *565* (December 2018), 162–171.
- (335) Vinodhini, J.; Mayandi, J.; Atchudan, R.; Jayabal, P.; Sasirekha, V.; Pearce, J. M. Effect of microwave power irradiation on TiO₂ nano-structures and binder free paste screen printed dye sensitized solar cells. *Ceram. Int.* **2019**, *45* (4), 4667–4673.
- (336) Dang-Bao, T.; Pradel, C.; Favier, I.; Gómez, M. Making Copper(0) Nanoparticles in Glycerol: A Straightforward Synthesis for a Multipurpose Catalyst. *Adv. Synth. Catal.* **2017**, *359* (16), 2832–2846.
- (337) Duan, Z.; Ma, G.; Zhang, W. Preparation of copper nanoparticles and catalytic properties for the reduction of aromatic nitro compounds. *Bull. Korean Chem. Soc.* **2012**, *33* (12), 4003–4006.
- (338) Santhanalakshmi, J.; Parimala, L. The copper nanoparticles catalysed reduction of substituted nitrobenzenes: Effect of nanoparticle stabilizers. *J. Nanoparticle Res.* **2012**, *14*.
- (339) Fan, R.; Chen, C.; Han, M.; Gong, W.; Zhang, H.; Zhang, Y.; Zhao, H.; Wang, G. Highly Dispersed Copper Nanoparticles Supported on Activated Carbon as an Efficient Catalyst for Selective Reduction of Vanillin. *Small* **2018**, *14* (36), 1–11.
- (340) Štefane, B.; Požgan, F. Advances in catalyst systems for the asymmetric hydrogenation and transfer hydrogenation of ketones. *Catal. Rev. - Sci. Eng.* **2014**, *56* (1), 82–174.
- (341) Zhang, M.; Li, Z. Cu/Cu₂O-MC (MC = Mesoporous Carbon) for Highly Efficient Hydrogenation of Furfural to Furfuryl Alcohol under Visible Light. *ACS Sustain. Chem. Eng.* **2019**, *7*, 11485–11492.
- (342) Zhang, H. X.; Siegert, U.; Liu, R.; Cai, W. Facile fabrication of ultrafine copper nanoparticles in organic solvent. *Nanoscale Res. Lett.* **2009**, *4* (7), 705–708.
- (343) Van De Kruijs, B. H. P.; Dressen, M. H. C. L.; Meuldijk, J.; Vekemans, J. A. J. M.; Hulshof, L. A. Microwave-induced electrostatic etching: Generation of highly reactive magnesium for application in Grignard reagent formation. *Org. Biomol. Chem.* **2010**, *8* (7), 1688–1694.
- (344) Horikoshi, S.; Serpone, N. Role of microwaves in heterogeneous catalytic systems. *Catalysis Science and Technology*. 2014, pp 1197–1210.
- (345) Bowman, M. D.; Holcomb, J. L.; Kormos, C. M.; Leadbeater, N. E.; Williams, V. A. Approaches for Scale-Up of Microwave-Promoted Reactions Abstract : *Org. Process Res. Dev.* **2008**, No. 3, 41–57.
- (346) Ley, S. V.; Fitzpatrick, D. E.; Ingham, R. J.; Myers, R. M. Organic synthesis: March of the machines. *Angew. Chemie - Int. Ed.* **2015**, *54* (11), 3449–3464.
- (347) Gioiello, A.; Mancino, V.; Filippini, P.; Mostarda, S.; Cerra, B. Concepts and optimization strategies of experimental design in continuous-flow processing. *J. Flow Chem.* **2016**, *6* (3), 167–180.

- (348) Plutschack, M. B.; Pieber, B.; Gilmore, K.; Seeberger, P. H. The Hitchhiker's Guide to Flow Chemistry. *Chem. Rev.* **2017**, *117* (18), 11796–11893.
- (349) Dallinger, D.; Kappe, C. O. Why flow means green – Evaluating the merits of continuous processing in the context of sustainability. *Curr. Opin. Green Sustain. Chem.* **2017**, *7*, 6–12.
- (350) Riley, D. L.; Neyt, N. C. Approaches for Performing Reductions under Continuous-Flow Conditions. *Synth.* **2018**, *50* (14), 2707–2720.
- (351) Cossar, P. J.; Hizartidis, L.; Simone, M. I.; McCluskey, A.; Gordon, C. P. The expanding utility of continuous flow hydrogenation. *Org. Biomol. Chem.* **2015**, *13* (26), 7119–7130.
- (352) Hutchings, M.; Wirth, T. A Simple Setup for Transfer Hydrogenations in Flow Chemistry. *Synlett* **2016**, *27* (12), 1832–1835.
- (353) Jensen, R. K.; Thykier, N.; Enevoldsen, M. V.; Lindhardt, A. T. A High Mobility Reactor Unit for R&D Continuous Flow Transfer Hydrogenations. *Org. Process Res. Dev.* **2017**, *21* (3), 370–376.
- (354) Doherty, S.; Knight, J. G.; Backhouse, T.; Bradford, A.; Saunders, F.; Bourne, R. A.; Chamberlain, T. W.; Stones, R.; Clayton, A.; Lovelock, K. Highly efficient aqueous phase reduction of nitroarenes catalysed by phosphine-decorated polymer immobilized ionic liquid stabilized PdNPs. *Catal. Sci. Technol.* **2018**, *8* (5), 1454–1467.
- (355) Desai, B.; Kappe, C. O. Heterogeneous Hydrogenation Reactions Using a Continuous Flow High Pressure Device. *J. Comb. Chem.* **2005**, *7* (5), 641–643.
- (356) Artiukha, E. A.; Nuzhdin, A. L.; Bukhtiyarova, G. A.; Bukhtiyarov, V. I. Flow synthesis of secondary amines over Ag/Al₂O₃ catalyst by one-pot reductive amination of aldehydes with nitroarenes. *RSC Adv.* **2017**, *7* (72), 45856–45861.
- (357) Nuzhdin, A. L.; Moroz, B. L.; Bukhtiyarova, G. A.; Reshetnikov, S. I.; Pyrjaev, P. A.; Aleksandrov, P. V.; Bukhtiyarov, V. I. Selective Liquid-Phase Hydrogenation of a Nitro Group in Substituted Nitrobenzenes over Au/Al₂O₃ Catalyst in a Packed-Bed Flow Reactor. *Chempluschem* **2015**, *80* (12), 1741–1749.
- (358) Liu, Y.; Guerrouache, M.; Kebe, S. I.; Carbonnier, B.; Le Droumaguet, B. Gold nanoparticles-supported histamine-grafted monolithic capillaries as efficient microreactors for flow-through reduction of nitro-containing compounds. *J. Mater. Chem. A* **2017**, *5* (23), 11805–11814.
- (359) Sun, H. bin; Ai, Y.; Li, D.; Tang, Z.; Shao, Z.; Liang, Q. Bismuth iron oxide nanocomposite supported on graphene oxides as the high efficient, stable and reusable catalysts for the reduction of nitroarenes under continuous flow conditions. *Chem. Eng. J.* **2017**, *314*, 328–335.
- (360) Ai, Y.; Liu, L.; Jing, K.; Qi, L.; Fan, Z.; Zhou, J.; Sun, H. bin; Shao, Z.; Liang, Q. Noncovalently functionalized carbon nanotubes immobilized Fe–Bi bimetallic oxides as a heterogeneous nanocatalyst for reduction of nitroaromatics. *Nano-Structures and Nano-Objects* **2017**, *10* (2017), 116–124.
- (361) Moghaddam, M. M.; Pieber, B.; Glasnov, T.; Kappe, C. O. Immobilized iron oxide nanoparticles as stable and reusable catalysts for hydrazine-mediated nitro reductions in continuous flow. *ChemSusChem* **2014**, *7* (11), 3122–3131.
- (362) Combata, D.; Concepción, P.; Corma, A. Gold catalysts for the synthesis of aromatic azo compounds from nitroaromatics in one step. *J. Catal.* **2014**, *311*, 339–349.
- (363) Kumar, M.; Soni, K.; Yadav, G. D.; Singh, S.; Deka, S. Applied Catalysis A : General Surfactant directed Ag₁ – x Ni_x alloy nanoparticle catalysed synthesis of aromatic azo derivatives from aromatic amines. *Applied Catal. A, Gen.* **2016**, *525*, 50–58.
- (364) Wang, M.; Funabiki, K.; Matsui, M. Synthesis and properties of bis(hetaryl)azo dyes. *Dye. Pigment.* **2003**, *57* (1), 77–86.
- (365) Serna, P.; Corma, A. Transforming Nano Metal Nonselective Particulates into Chemoselective Catalysts for Hydrogenation of Substituted Nitrobenzenes. *ACS Catalysis.* 2015, pp 7114–7121.
- (366) Moglie, Y.; Vitale, C.; Radivoy, G. Synthesis of azo compounds by nanosized iron-promoted reductive coupling of aromatic nitro compounds. *Tetrahedron Lett.* **2008**, *49* (11), 1828–1831.
- (367) Redacing, T.; Part, A. The Redacing Action of Glycols in AZkaZi. Part I I . 627 126. The Reducing Action of Glycols. **1959**, *9*, 627–630.
- (368) Razus, A. C.; Birzan, L.; Cristea, M.; Tecuceanu, V.; Blanariu, L.; Enache, C. Dyes and Pigments Novel mono- and bis-azo dyes containing the azulene-1-yl moiety : Synthesis , characterization , electronic spectra and basicity. *Dye. Pigment.* **2009**, *80* (3), 337–342.
- (369) Buncl, E. Catalysis in Strongly Acidic Media and the Wallach Rearrangement. *Acc. Chem. Res.* **1975**, *8* (4), 132–139.
- (370) Liu, X.; Li, H. Q.; Ye, S.; Liu, Y. M.; He, H. Y.; Cao, Y. Gold-catalysed direct hydrogenative coupling of nitroarenes to synthesize aromatic azo compounds. *Angew. Chemie - Int. Ed.* **2014**, *53* (29), 7624–7628.

- (371) Yan, M.; Jin, T.; Ishikawa, Y.; Minato, T.; Fujita, T.; Chen, L. Y.; Bao, M.; Asao, N.; Chen, M. W.; Yamamoto, Y. Nanoporous gold catalyst for highly selective semihydrogenation of alkynes: Remarkable effect of amine additives. *J. Am. Chem. Soc.* **2012**, *134* (42), 17536–17542.
- (372) Van Laren, M. W.; Elsevier, C. J. Selective homogeneous palladium(0)-catalysed hydrogenation of alkynes to (Z)-alkenes. *Angew. Chemie - Int. Ed.* **1999**, *38* (24), 3715–3717.
- (373) Srimani, D.; Diskin-Posner, Y.; Ben-David, Y.; Milstein, D. Iron pincer complex catalysed, environmentally benign, E-selective semi-hydrogenation of alkynes. *Angew. Chemie - Int. Ed.* **2013**, *52* (52), 14131–14134.
- (374) La Pierre, H. S.; Arnold, J.; Toste, F. D. Z-selective semihydrogenation of alkynes catalysed by a cationic vanadium bisimido complex. *Angew. Chemie - Int. Ed.* **2011**, *50* (17), 3900–3903.
- (375) Long, R.; Li, Y.; Liu, Y.; Chen, S.; Zheng, X.; Gao, C.; He, C.; Chen, N.; Qi, Z.; Song, L.; et al. Isolation of Cu Atoms in Pd Lattice: Forming Highly Selective Sites for Photocatalytic Conversion of CO₂ to CH₄. *J. Am. Chem. Soc.* **2017**, *139* (12), 4486–4492.
- (376) Mazumder, V.; Chi, M.; Mankin, M. N.; Liu, Y.; Metin, Ö.; Sun, D.; More, K. L.; Sun, S. A facile synthesis of MPd (M = Co, Cu) nanoparticles and their catalysis for formic acid oxidation. *Nano Lett.* **2012**, *12* (2), 1102–1106.
- (377) Lu, Z. W.; Wei, S. H.; Zunger, A.; Frota-Pessoa, S.; Ferreira, L. G. First-principles statistical mechanics of structural stability of intermetallic compounds. *Phys. Rev. B* **1991**, *44* (2), 512–544.
- (378) Yang, S.; Cao, C.; Peng, L.; Zhang, J.; Han, B.; Song, W. A Pd-Cu₂O nanocomposite as an effective synergistic catalyst for selective semi-hydrogenation of the terminal alkynes only. *Chem. Commun.* **2016**, *52* (18), 3627–3630.
- (379) Da Silva, F. P.; Fiorio, J. L.; Gonçalves, R. V.; Teixeira-Neto, E.; Rossi, L. M. Synergic Effect of Copper and Palladium for Selective Hydrogenation of Alkynes. *Ind. Eng. Chem. Res.* **2018**, *57* (48), 16209–16216.
- (380) Fu, S.; Chen, N. Y.; Liu, X.; Shao, Z.; Luo, S. P.; Liu, Q. Ligand-Controlled Cobalt-Catalysed Transfer Hydrogenation of Alkynes: Stereodivergent Synthesis of Z- and E-Alkenes. *J. Am. Chem. Soc.* **2016**, *138* (27), 8588–8594.
- (381) Hauwert, P.; Boerleider, R.; Warsink, S.; Weigand, J. J.; Elsevier, C. J. Mechanism of Pd(NHC)-catalysed transfer hydrogenation of alkynes. *J. Am. Chem. Soc.* **2010**, *132* (47), 16900–16910.
- (382) Siva Reddy, A.; Kumara Swamy, K. C. Ethanol as a Hydrogenating Agent: Palladium-Catalysed Stereoselective Hydrogenation of Ynamides To Give Enamides. *Angew. Chemie - Int. Ed.* **2017**, *56* (24), 6984–6988.
- (383) Campaña, A. G.; Estévez, R. E.; Fuentes, N.; Rubles, R.; Cuerva, J. M.; Buñuel, E.; Cárdenas, D.; Oltra, J. E. Unprecedented hydrogen transfer from water to alkenes and alkynes mediated by TlIII and late transition metals. *Org. Lett.* **2007**, *9* (11), 2195–2198.
- (384) Li, H. C.; An, C.; Wu, G.; Li, G. X.; Huang, X. B.; Gao, W. X.; Ding, J. C.; Zhou, Y. B.; Liu, M. C.; Wu, H. Y. Transition-Metal-Free Highly Chemoselective and Stereoselective Reduction with Se/DMF/H₂O System. *Org. Lett.* **2018**, *20* (18), 5573–5577.
- (385) Jordan, A. J.; Lalic, G.; Sadighi, J. P. Coinage Metal Hydrides: Synthesis, Characterization, and Reactivity. *Chem. Rev.* **2016**, *116* (15), 8318–8372.
- (386) Kaicharla, T.; Zimmermann, B. M.; Oestreich, M.; Teichert, J. F. Using alcohols as simple H₂-equivalents for copper-catalysed transfer semihydrogenations of alkynes. *Chem. Commun.* **2019**, *55* (89), 13410–13413.
- (387) Bao, H.; Zhou, B.; Jin, H.; Liu, Y. Diboron-Assisted Copper-Catalysed Z-Selective Semihydrogenation of Alkynes Using Ethanol as a Hydrogen Donor. *J. Org. Chem.* **2019**, *84* (6), 3579–3589.
- (388) Gomez-Romero, P. Hybrid organic-inorganic materials - in search of synergic activity. *Adv. Mater.* **2001**, *13* (3), 163–174.
- (389) Parola, S.; Julián-López, B.; Carlos, L. D.; Sanchez, C. Optical Properties of Hybrid Organic-Inorganic Materials and their Applications. *Adv. Funct. Mater.* **2016**, *26* (36), 6506–6544.
- (390) Heo, J. H.; Im, S. H.; Noh, J. H.; Mandal, T. N.; Lim, C. S.; Chang, J. A.; Lee, Y. H.; Kim, H. J.; Sarkar, A.; Nazeeruddin, M. K.; et al. Efficient inorganic-organic hybrid heterojunction solar cells containing perovskite compound and polymeric hole conductors. *Nat. Photonics* **2013**, *7* (6), 486–491.
- (391) Cui, J.; Jia, S. Organic-inorganic hybrid nanoflowers: A novel host platform for immobilizing biomolecules. *Coord. Chem. Rev.* **2017**, *352* (29), 249–263.
- (392) Taleghani, S.; Mirzaei, M.; Eshtiagh-Hosseini, H.; Frontera, A. Tuning the topology of hybrid inorganic-organic materials based on the study of flexible ligands and negative charge of polyoxometalates: A crystal engineering perspective. *Coord. Chem. Rev.* **2016**, *309* (December), 84–106.
- (393) Wan, C.; Tian, R.; Kondou, M.; Yang, R.; Zong, P.; Koumoto, K. Ultrahigh thermoelectric power factor in flexible hybrid inorganic-organic superlattice. *Nat. Commun.* **2017**, *8* (1).
- (394) You, N.; Zhang, C.; Liang, Y.; Zhang, Q.; Fu, P.; Liu, M.; Zhao, Q.; Cui, Z.; Pang, X. Facile Fabrication of Size-Tunable

- Core/Shell Ferroelectric/Polymeric Nanoparticles with Tailorable Dielectric Properties via Organocatalysed Atom Transfer Radical Polymerization Driven by Visible Light. *Sci. Rep.* **2019**, *9* (1), 1–12.
- (395) Sanchez, C.; Soler-Illia, G. J. D. A. A.; Ribot, F.; Lalot, T.; Mayer, C. R.; Cabuil, V. Designed hybrid organic-inorganic nanocomposites from functional nanobuilding blocks. *Chem. Mater.* **2001**, *13* (10), 3061–3083.
- (396) Corma, A.; Díaz, U.; García, T.; Sastre, G.; Velty, A. Multifunctional hybrid organic-inorganic catalytic materials with a hierarchical system of well-defined micro- and mesopores. *J. Am. Chem. Soc.* **2010**, *132* (42), 15011–15021.
- (397) Mir, S. H.; Nagahara, L. A.; Thundat, T.; Mokarian-Tabari, P.; Furukawa, H.; Khosla, A. Review - Organic-inorganic hybrid functional materials: An integrated platform for applied technologies. *J. Electrochem. Soc.* **2018**, *165* (8), B3137–B3156.
- (398) Sanchez, C.; Julián, B.; Belleville, P.; Popall, M. Applications of hybrid organic-inorganic nanocomposites. *J. Mater. Chem.* **2005**, *15* (35–36), 3559–3592.
- (399) Mohammadi Ziarani, G.; Badiei, A.; Mousavi, S.; Lashgari, N.; Shahbazi, A. Application of amino-functionalized SBA-15 type mesoporous silica in one-pot synthesis of spirooxindoles. *Cuihua Xuebao/Chinese J. Catal.* **2012**, *33* (11), 1832–1839.
- (400) Shagufta; Ahmad, I.; Dhar, R. Sulfonic Acid-Functionalized Solid Acid Catalyst in Esterification and Transesterification Reactions. *Catal. Surv. from Asia* **2017**, *21* (2), 53–69.
- (401) Bied, C.; Gauthier, D.; Moreau, J. J. E.; Chi Man, M. W. Preparation and characterization of new templated hybrid materials containing a chiral diamine ligand. *J. Sol-Gel Sci. Technol.* **2001**, *20* (3), 313–320.
- (402) Bhanja, P.; Modak, A.; Chatterjee, S.; Bhaumik, A. Bifunctionalized Mesoporous SBA-15: A New Heterogeneous Catalyst for the Facile Synthesis of 5-Hydroxymethylfurfural. *ACS Sustain. Chem. Eng.* **2017**, *5* (3), 2763–2773.
- (403) Allain, C.; Favette, S.; Chamoreau, L. M.; Vaissermann, J.; Ruhlmann, L.; Hasenknopf, B. Hybrid organic-inorganic porphyrin-polyoxometalate complexes. *Eur. J. Inorg. Chem.* **2008**, No. 22, 3433–3441.
- (404) Du, J.; Chen, Y. Organic-inorganic hybrid nanoparticles with a complex hollow structure. *Angew. Chemie - Int. Ed.* **2004**, *43* (38), 5084–5087.
- (405) Bhar, S.; Ananthkrishnan, R. Ru(II)-Metal complex immobilized mesoporous SBA-15 hybrid for visible light induced photooxidation of chlorophenolic compounds in aqueous medium. *Photochem. Photobiol. Sci.* **2017**, *16* (8), 1290–1300.
- (406) Zare, M.; Moradi-Shoeili, Z.; Ashouri, F.; Bagherzadeh, M. Heterogeneous SBA-15-supported Oxoperoxomolybdenum(VI) complex for enhanced olefin epoxidation. *Catal. Commun.* **2017**, *88*, 9–12.
- (407) Al-Rehili, S.; Fayli, K.; Hammami, M. A.; Moosa, B.; Patil, S.; Zhang, D.; Alharbi, O.; Hedhili, M. N.; Möhwald, H.; Khashab, N. M. Anisotropic Self-Assembly of Organic-Inorganic Hybrid Microtoroids. *J. Am. Chem. Soc.* **2017**, *139* (30), 10232–10238.
- (408) Barbe, J. M.; Canard, G.; Brandès, S.; Guilard, R. Organic-inorganic hybrid sol-gel materials incorporating functionalized cobalt(III) corroles for the selective detection of CO. *Angew. Chemie - Int. Ed.* **2005**, *44* (20), 3103–3106.
- (409) Wei, X. L.; Lu, X. H.; Ma, X. T.; Peng, C.; Jiang, H. Z.; Zhou, D.; Xia, Q. H. Synthesis and catalytic activity of organic-inorganic hybrid catalysts coordinated with cobalt(II) ions for aerobic epoxidation of styrene. *Catal. Commun.* **2015**, *61*, 48–52.
- (410) Song, B. Q.; Wang, X. L.; Sun, C. Y.; Zhang, Y. T.; Wu, X. S.; Yang, L.; Shao, K. Z.; Zhao, L.; Su, Z. M. An organic-inorganic hybrid photocatalyst based on sandwich-type tetra-Co-substituted phosphotungstates with high visible light photocatalytic activity. *Dalt. Trans.* **2015**, *44* (31), 13818–13822.
- (411) Reck, B. K.; Graedel, T. E. Challenges in metal recycling. *Science (80-.)* **2012**, *337* (6095), 690–695.
- (412) Parmeggiani, C.; Cardona, F. Transition metal based catalysts in the aerobic oxidation of alcohols. *Green Chem.* **2012**, *14* (3), 547–564.
- (413) Hickman, A. J.; Sanford, M. S. High-valent organometallic copper and palladium in catalysis. *Nature* **2012**, *484* (7393), 177–185.
- (414) Zhang, K.; Lu, L. Q.; Yao, S.; Chen, J. R.; Shi, D. Q.; Xiao, W. J. Enantioconvergent Copper Catalysis: In Situ Generation of the Chiral Phosphorus Ylide and Its Wittig Reactions. *J. Am. Chem. Soc.* **2017**, *139* (36), 12847–12854.
- (415) Hojoh, K.; Ohmiya, H.; Sawamura, M. Synthesis of α -Quaternary Formimides and Aldehydes through Umpolung Asymmetric Copper Catalysis with Isocyanides. *J. Am. Chem. Soc.* **2017**, *139* (6), 2184–2187.
- (416) Wang, D.; Zhu, N.; Chen, P.; Lin, Z.; Liu, G. Enantioselective Decarboxylative Cyanation Employing Cooperative Photoredox Catalysis and Copper Catalysis. *J. Am. Chem. Soc.* **2017**, *139* (44), 15632–15635.
- (417) Chen, Z.; Meyer, T. J. Copper(II) catalysis of water oxidation. *Angew. Chemie - Int. Ed.* **2013**, *52* (2), 700–703.

- (418) Maity, R.; Naskar, S.; Das, I. Copper(II)-Catalysed Reactions of α -Keto Thioesters with Azides via C-C and C-S Bond Cleavages: Synthesis of N-Acylureas and Amides. *J. Org. Chem.* **2018**, *83* (4), 2114–2124.
- (419) Zhang, G.; Han, X.; Luan, Y.; Wang, Y.; Wen, X.; Xu, L.; Ding, C.; Gao, J. Copper-catalysed aerobic alcohol oxidation under air in neat water by using a water-soluble ligand. *RSC Adv.* **2013**, *3* (42), 19255–19258.
- (420) Kitanosono, T.; Xu, P.; Kobayashi, S. Heterogeneous versus homogeneous copper(II) catalysis in enantioselective conjugate-addition reactions of boron in water. *Chem. - An Asian J.* **2014**, *9* (1), 179–188.
- (421) Jiang, N.; Ragauskas, A. J. Cu(II)-catalysed selective aerobic oxidation of alcohols under mild conditions. *J. Org. Chem.* **2006**, *71* (18), 7087–7090.
- (422) Fedorov, A.; Liu, H. J.; Lo, H. K.; Copéret, C. Silica-Supported Cu Nanoparticle Catalysts for Alkyne Semihydrogenation: Effect of Ligands on Rates and Selectivity. *J. Am. Chem. Soc.* **2016**, *138* (50), 16502–16507.
- (423) Zou, Y.; Wang, X.; Ai, Y.; Liu, Y.; Ji, Y.; Wang, H.; Hayat, T.; Alsaedi, A.; Hu, W.; Wang, X. β -Cyclodextrin modified graphitic carbon nitride for the removal of pollutants from aqueous solution: Experimental and theoretical calculation study. *J. Mater. Chem. A* **2016**, *4* (37), 14170–14179.
- (424) Kaboudin, B.; Abedi, Y.; Yokomatsu, T. Cu(II)- β -cyclodextrin complex as a nanocatalyst for the homo- and cross-coupling of arylboronic acids under ligand- and base-free conditions in air: Chemoselective cross-coupling of arylboronic acids in water. *European J. Org. Chem.* **2011**, No. 33, 6656–6662.
- (425) Gupta, D.; Mishra, A.; Kundu, S. Cu(II)- β -CD as Water-Loving Catalyst for One-Pot Synthesis of Triazoles and Biofuels Intermediate at Room Temperature without Any Other Additive. *ChemistrySelect* **2017**, *2* (10), 2997–3008.
- (426) Kaboudin, B.; Abedi, Y.; Yokomatsu, T. One-pot synthesis of 1,2,3-triazoles from boronic acids in water using Cu(II)- β -cyclodextrin complex as a nanocatalyst. *Org. Biomol. Chem.* **2012**, *10* (23), 4543–4548.
- (427) Yao, Y.-G.; Ye, R.-P.; Lin, L.; Liu, C.-Q.; Chen, C.-C. One-Pot Synthesis of Cyclodextrin-Doped Cu-SiO₂ Catalysts for Efficient Hydrogenation of Dimethyl Oxalate to Ethylene Glycol. *ChemCatChem* **2017**, *9*.
- (428) Duan, Z.; Ding, X.; Wang, Y.; Zhu, L.; Xia, D. A New Strategy for Fuel Desulfurization by Molecular Inclusion with Copper(II)- β -cyclodextrin@SiO₂@Fe₃O₄ for Removing Thiophenic Sulfides. *Energy and Fuels* **2018**, *32* (11), 11421–11431.
- (429) Bahadorikhali, S.; Ma'mani, L.; Mahdavi, H.; Shafiee, A. Copper supported β -cyclodextrin functionalized PEGylated mesoporous silica nanoparticle-graphene oxide hybrid: An efficient and recyclable nano-catalyst for straightforward synthesis of 2-arylbenzimidazoles and 1,2,3-triazoles. *Microporous Mesoporous Mater.* **2018**, *262* (September 2017), 207–216.
- (430) Starzewski, J.; Malczyk, M.; Lorenc, Z.; Nolewajka, E.; Ziółkowski, G. Registration of hospital infections: effects of 5 years observation of peritonitis. *Wiad. Lek.* **2000**, *53* (1–2), 60–64.
- (431) Wu, Z.; Borretto, E.; Medlock, J.; Bonrath, W.; Cravotto, G. Effects of Ultrasound and Microwaves on Selective Reduction: Catalyst Preparation and Reactions. *ChemCatChem* **2014**, *6* (10), 2762–2783.
- (432) Luche, J.-L. Effect of ultrasound on heterogeneous systems. *Ultrason. Sonochem.* **1994**, *1* (2), S111–S118.
- (433) Varma, R. S. "Greener" chemical syntheses using mechanochemical mixing or microwave and ultrasound irradiation. *Green Chem. Lett. Rev.* **2007**, *1* (1), 37–45.
- (434) Shaabani, A.; Sepahvand, H.; Hooshmand, S. E.; Borjian Boroujeni, M. Design, preparation and characterization of Cu/GA/Fe₃O₄@SiO₂ nanoparticles as a catalyst for the synthesis of benzodiazepines and imidazoles. *Appl. Organomet. Chem.* **2016**, *30* (6), 414–421.
- (435) Hsu, Y. W.; Wu, C. C.; Wu, S. M.; Su, C. C. Synthesis and properties of carbon nanotube-grafted silica nanoarchitecture-reinforced poly(lactic acid). *Materials (Basel)*. **2017**, *10* (7).
- (436) Gorbachuk, V. V.; Ziatdinova, R. V.; Evtugyn, V. G.; Stoikov, I. I. Stabilization of silica nanoparticles dispersions by surface modification with silicon derivative of thiacalix[4]arene. *J. Nanoparticle Res.* **2015**, *17* (3).
- (437) Martina, K.; Baricco, F.; Berlier, G.; Caporaso, M.; Cravotto, G. Efficient green protocols for preparation of highly functionalized β -cyclodextrin-grafted silica. *ACS Sustain. Chem. Eng.* **2014**, *2* (11), 2595–2603.
- (438) Martina, K.; Baricco, F.; Caporaso, M.; Berlier, G.; Cravotto, G. Cyclodextrin-Grafted Silica-Supported Pd Nanoparticles: An Efficient and Versatile Catalyst for Ligand-Free C-C Coupling and Hydrogenation. *ChemCatChem* **2016**, *8* (6), 1176–1184.
- (439) Mohanazadeh, F.; Amini, H. Silica chloride mediated alkylation of electron-rich aromatics by benzyl or tert-butyl chloride. *Bull. Korean Chem. Soc.* **2010**, *31* (10), 3038–3040.
- (440) Khalafi-Nezhad, A.; Panahi, F. Immobilized palladium nanoparticles on a silica-starch substrate (PNP-SSS): As an efficient heterogeneous catalyst for Heck and copper-free Sonogashira reactions in water. *Green Chem.* **2011**, *13* (9), 2408–2415.

- (441) Bagabas, A. A.; Frasconi, M.; Iehl, J.; Hauser, B.; Farha, O. K.; Hupp, J. T.; Hartlieb, K. J.; Botros, Y. Y.; Stoddart, J. F. γ -Cyclodextrin cuprate sandwich-type complexes. *Inorg. Chem.* **2013**, *52* (6), 2854–2861.
- (442) Matsui, Y.; Kurita, T.; Yagi, M.; Okayama, T.; Mochida, K.; Date, Y. The Formation and Structure of Copper(II) Complexes with Cyclodextrins in an Alkaline Solution. *Bulletin of the Chemical Society of Japan*. 1975, pp 2187–2191.
- (443) Sadeghzadeh, S. M.; Zhiani, R.; Moradi, M. KCC-1 Supported Cu(II)- β -Cyclodextrin Complex as a Reusable Catalyst for the Synthesis of 3-Aryl-2-oxazolidinones from Carbon Dioxide, Epoxide, Anilines. *ChemistrySelect* **2018**, *3* (12), 3516–3522.
- (444) Jiaju Liu, Peng He, Ligu Wang, Hui Liu, Yan Cao, H. L. An efficient and stable Cu/SiO₂ catalyst for the syntheses of ethylene glycol and methanol via chemoselective hydrogenation of ethylene carbonate. *chinese J. Catal.* **2018**, *39* (8), 1283–1293.
- (445) Velasco, M. I.; Krapacher, C. R.; De Rossi, R. H.; Rossi, L. I. Structure characterization of the non-crystalline complexes of copper salts with native cyclodextrins. *Dalt. Trans.* **2016**, *45* (26), 10696–10707.
- (446) Kreye, O.; Wald, S.; Meier, M. A. R. Introducing catalytic lossen rearrangements: Sustainable access to carbamates and amines. *Adv. Synth. Catal.* **2013**, *355* (1), 81–86.
- (447) Sharma, U.; Kumar, P.; Kumar, N.; Kumar, V.; Singh, B. Highly chemo- and regioselective reduction of aromatic nitro compounds catalysed by recyclable copper(II) as well as cobalt(II) phthalocyanines. *Adv. Synth. Catal.* **2010**, *352* (11–12), 1834–1840.
- (448) Liu, J.; Qiu, X.; Huang, X.; Luo, X.; Zhang, C.; Wei, J.; Pan, J.; Liang, Y.; Zhu, Y.; Qin, Q.; et al. From alkylarenes to anilines via site-directed carbon–carbon amination. *Nat. Chem.* **2019**, *11* (1), 71–77.
- (449) Sharma, S.; Yamini; Das, P. Hydrogenation of nitroarenes to anilines in a flow reactor using polystyrene supported rhodium in a catalyst-cartridge (Cart-Rh@PS). *New J. Chem.* **2019**, *43* (4), 1764–1769.
- (450) Yue, H.; Guo, L.; Liao, H. H.; Cai, Y.; Zhu, C.; Rueping, M. Catalytic Ester and Amide to Amine Interconversion: Nickel-Catalysed Decarbonylative Amination of Esters and Amides by C–O and C–C Bond Activation. *Angew. Chemie - Int. Ed.* **2017**, *56* (15), 4282–4285.
- (451) Sharma, S.; Bhattacharjee, D.; Das, P. Supported Rhodium Nanoparticles Catalysed Reduction of Nitroarenes, Arylcarbonyls and Aryl/Benzyl Sulfoxides using Ethanol/Methanol as In Situ Hydrogen Source. *Adv. Synth. Catal.* **2018**, *360* (11), 2131–2137.
- (452) Albert-Soriano, M.; Pastor, I. M. Metal–Organic Framework Based on Copper and Carboxylate-Imidazole as Robust and Effective Catalyst in the Oxidative Amidation of Carboxylic Acids and Formamides. *European J. Org. Chem.* **2016**, *2016* (30), 5180–5188.
- (453) Ji, P.; Manna, K.; Lin, Z.; Feng, X.; Urban, A.; Song, Y.; Lin, W. Single-Site Cobalt Catalysts at New Zr₁₂(μ ₃-O)₈(μ ₃-OH)₈(μ ₂-OH)₆ Metal-Organic Framework Nodes for Highly Active Hydrogenation of Nitroarenes, Nitriles, and Isocyanides. *J. Am. Chem. Soc.* **2017**, *139* (20), 7004–7011.
- (454) Yu, J.; Zhang, P.; Wu, J.; Shang, Z. Metal-free C–N bond-forming reaction: Straightforward synthesis of anilines, through cleavage of aryl C–O bond and amide C–N bond. *Tetrahedron Lett.* **2013**, *54* (24), 3167–3170.
- (455) Maejima, T.; Shimoda, Y.; Nozaki, K.; Mori, S.; Sawama, Y.; Monguchi, Y.; Sajiki, H. One-pot aromatic amination based on carbon-nitrogen coupling reaction between aryl halides and azido compounds. *Tetrahedron* **2012**, *68* (6), 1712–1722.
- (456) Mofford, D. M.; Reddy, G. R.; Miller, S. C. Aminoluciferins extend firefly luciferase bioluminescence into the near-infrared and can be preferred substrates over d-luciferin. *J. Am. Chem. Soc.* **2014**, *136* (38), 13277–13282.
- (457) Saneyoshi, H.; Ochikubo, T.; Mashimo, T.; Hatano, K.; Ito, Y.; Abe, H. Triphenylphosphinecarboxamide: An effective reagent for the reduction of azides and its application to nucleic acid detection. *Org. Lett.* **2014**, *16* (1), 30–33.
- (458) Xie, Y.; Pan, H.; Xiao, X.; Li, S.; Shi, Y. Organocatalytic asymmetric biomimetic transamination of aromatic ketone to optically active amine. *Org. Biomol. Chem.* **2012**, *10* (45), 8960–8962.
- (459) Saavedra, J. Z.; Resendez, A.; Rovira, A.; Eagon, S.; Haddenham, D.; Singaram, B. Reaction of InCl₃ with various reducing agents: InCl₃-NaBH₄-mediated reduction of aromatic and aliphatic nitriles to primary amines. *J. Org. Chem.* **2012**, *77* (1), 221–228.
- (460) Reddy, B. N.; Reddy, S. M.; Pathak, M. Synthesis of primary amines by one-pot reductive amination of aldehydes. *Der Pharma Chem.* **2015**, *7* (1), 1–4.
- (461) Jones, B. G.; Branch, S. K.; Thompson, A. S.; Threadgill, M. D. Synthesis of a series of trifluoromethylazoles and determination of pK_a of acidic and basic trifluoromethyl heterocycles by ¹⁹F NMR spectroscopy. *J. Chem. Soc. Perkin Trans. 1* **1996**, *53* (22), 2685.
- (462) Liu, S.; Yang, Y.; Zhen, X.; Li, J.; He, H.; Feng, J.; Whiting, A. Enhanced reduction of C–N multiple bonds using sodium borohydride and an amorphous nickel catalyst. *Org. Biomol. Chem.* **2012**, *10* (3), 663–670.

- (463) Huang, W. H.; Zavalij, P. Y.; Isaacs, L. Folding of long-chain alkanediammonium ions promoted by a cucurbituril derivative. *Org. Lett.* **2008**, *10* (12), 2577–2580.
- (464) Kita, Y.; Higuchi, T.; Mashima, K. Hydrogenation of amides catalysed by a combined catalytic system of a Ru complex with a zinc salt. *Chem. Commun.* **2014**, *50* (76), 11211–11213.
- (465) Cao, R.; Zhou, J.; Wang, W.; Feng, W.; Li, X.; Zhang, P.; Deng, P.; Yuan, L.; Gong, B. Oligoamide duplexes as organogelators. *Org. Lett.* **2010**, *12* (13), 2958–2961.
- (466) Kim, J. H.; Park, J. H.; Chung, Y. K.; Park, K. H. Ruthenium nanoparticle-catalysed, controlled and chemoselective hydrogenation of nitroarenes using ethanol as a hydrogen source. *Adv. Synth. Catal.* **2012**, *354* (13), 2412–2418.
- (467) Gholinejad, M.; Jeddi, N.; Pullithadathil, B. Agarose functionalized phosphorus ligand for stabilization of small-sized palladium and copper nanoparticles: Efficient heterogeneous catalyst for Sonogashira reaction. *Tetrahedron* **2016**, *72* (19), 2491–2500.
- (468) Tian, Z. Y.; Wang, S. M.; Jia, S. J.; Song, H. X.; Zhang, C. P. Sonogashira reaction using arylsulfonium salts as cross-coupling partners. *Org. Lett.* **2017**, *19* (19), 5454–5457.
- (469) Hu, H.; Yang, F.; Wu, Y. Palladacycle-catalysed deacetonative sonogashira coupling of aryl propargyl alcohols with aryl chlorides. *J. Org. Chem.* **2013**, *78* (20), 10506–10511.
- (470) Gallop, C. W. D.; Chen, M. T.; Navarro, O. Sonogashira couplings catalysed by collaborative (N-heterocyclic carbene)-copper and -palladium complexes. *Org. Lett.* **2014**, *16* (14), 3724–3727.
- (471) Wardrop, D. J.; Komenda, J. P. Dehydrative fragmentation of 5-hydroxyalkyl-1 H -tetrazoles: A mild route to alkylidene-carbenes. *Org. Lett.* **2012**, *14* (6), 1548–1551.
- (472) Liu, R.; Giordano, L.; Tenaglia, A. Ruthenium-Catalysed [2+2+2] Cycloaddition of 1,6-Enynes and Unactivated Alkynes: Access to Ring-Fused Cyclohexadienes. *Chem. - An Asian J.* **2017**, *12* (17), 2245–2257.
- (473) Yang, X.; Yan, R. A method for accessing sulfanylfurans from homopropargylic alcohols and sulfonyl hydrazides. *Org. Biomol. Chem.* **2017**, *15* (17), 3571–3574.
- (474) Krauss, J.; Wetzels, C.; Thiel, J.; Neudert, C.; Bracher, F. Synthesis and biological evaluation of new niphathesin analogues. *Arch. Pharm. (Weinheim)*. **2007**, *340* (3), 154–158.
- (475) Yabe, Y.; Yamada, T.; Nagata, S.; Sawama, Y.; Monguchi, Y.; Sajiki, H. Development of a palladium on boron nitride catalyst and its application to the semihydrogenation of alkynes. *Adv. Synth. Catal.* **2012**, *354* (7), 1264–1268.
- (476) Gieshoff, T. N.; Welther, A.; Kessler, M. T.; Prechtel, M. H. G.; Jacobi Von Wangelin, A. Stereoselective iron-catalysed alkyne hydrogenation in ionic liquids. *Chem. Commun.* **2014**, *50* (18), 2261–2264.
- (477) Li, S. S.; Tao, L.; Wang, F. Z. R.; Liu, Y. M.; Cao, Y. Heterogeneous Gold-Catalysed Selective Semireduction of Alkynes using Formic Acid as Hydrogen Source. *Adv. Synth. Catal.* **2016**, *358* (9), 1410–1416.
- (478) Fabry, D. C.; Ronge, M. A.; Rueping, M. Immobilization and continuous recycling of photoredox catalysts in ionic liquids for applications in batch reactions and flow systems: Catalytic alkene isomerization by using visible light. *Chem. - A Eur. J.* **2015**, *21* (14), 5350–5354.
- (479) Ceyhan, S.; Cetinkaya, Y.; Akdag, A.; Balci, M. Regioselectivity observed in manganese(III) acetate mediated addition of acetylacetone to various alkenes: mechanistic and theoretical studies. *Tetrahedron* **2016**, *72* (43), 6815–6824.
- (480) Zhang, H.; Huang, X. Ligand-Free Heck Reactions of Aryl Iodides: Significant Acceleration of the Rate through Visible Light Irradiation at Ambient Temperature. *Adv. Synth. Catal.* **2016**, *358* (23), 3736–3742.
- (481) Denmark, S. E.; Kallemeyn, J. M. Stereospecific palladium-catalysed cross-coupling of (E)- and (Z)-alkenylsilylanolates with aryl chlorides. *J. Am. Chem. Soc.* **2006**, *128* (50), 15958–15959.
- (482) Das, M.; Manvar, A.; Jacolot, M.; Blangetti, M.; Jones, R. C.; O'Shea, D. F. Stereoselective peterson olefinations from bench-stable reagents and N-phenyl imines. *Chem. - A Eur. J.* **2015**, *21* (24), 8737–8740.
- (483) Rao, S.; Prabhu, K. R. Stereodivergent Alkyne Reduction by using Water as the Hydrogen Source. *Chem. - A Eur. J.* **2018**, *24* (52), 13954–13962.
- (484) Jia, Y.; Qin, H.; Wang, N.; Jiang, Z. X.; Yang, Z. Fe₂O₃-Promoted Intermolecular Chlorotrifluoromethylthiolation of Alkenes. *J. Org. Chem.* **2018**, *83* (5), 2808–2817.
- (485) Cornella, J.; Martin, R. Ni-catalysed stereoselective arylation of inert C-O bonds at low temperatures. *Org. Lett.* **2013**, *15* (24), 6298–6301.
- (486) Werner, E. W.; Sigman, M. S. Operationally simple and highly (E)-styrenyl-selective heck reactions of electronically nonbiased olefins. *J. Am. Chem. Soc.* **2011**, *133* (25), 9692–9695.